Bridge Engineering Handbook

SECOND EDITION

FUNDAMENTALS

EDITED BY

Wai-Fah Chen and Lian Duan

CRC Press
Taylor & Francis Group

Bridge Engineering Handbook

SECOND EDITION

FUNDAMENTALS

Bridge Engineering Handbook, Second Edition

Bridge Engineering Handbook, Second Edition: Fundamentals

Bridge Engineering Handbook, Second Edition: Superstructure Design

Bridge Engineering Handbook, Second Edition: Substructure Design

Bridge Engineering Handbook, Second Edition: Seismic Design

Bridge Engineering Handbook, Second Edition: Construction and Maintenance

Bridge Engineering Handbook

SECOND EDITION

FUNDAMENTALS

EDITED BY

Wai-Fah Chen and Lian Duan

CRC Press
Taylor & Francis Group
Boca Raton London New York

CRC Press is an imprint of the
Taylor & Francis Group, an **informa** business

CRC Press
Taylor & Francis Group
6000 Broken Sound Parkway NW, Suite 300
Boca Raton, FL 33487-2742

Version Date: 20130923

International Standard Book Number-13: 978-1-4398-5234-7 (eBook - PDF)

Contents

Foreword

Throughout the history of civilization bridges have been the icons of cities, regions, and countries. All bridges are useful for transportation, commerce, and war. Bridges are necessary for civilization to exist, and many bridges are beautiful. A few have become the symbols of the best, noblest, and most beautiful that mankind has achieved. The secrets of the design and construction of the ancient bridges have been lost, but how could one not marvel at the magnificence, for example, of the Roman viaducts?

The second edition of the *Bridge Engineering Handbook* expands and updates the previous edition by including the new developments of the first decade of the twenty-first century. Modern bridge engineering has its roots in the nineteenth century, when wrought iron, steel, and reinforced concrete began to compete with timber, stone, and brick bridges. By the beginning of World War II, the transportation infrastructure of Europe and North America was essentially complete, and it served to sustain civilization as we know it. The iconic bridge symbols of modern cities were in place: Golden Gate Bridge of San Francisco, Brooklyn Bridge, London Bridge, Eads Bridge of St. Louis, and the bridges of Paris, Lisbon, and the bridges on the Rhine and the Danube. Budapest, my birthplace, had seven beautiful bridges across the Danube. Bridge engineering had reached its golden age, and what more and better could be attained than that which was already achieved?

Then came World War II, and most bridges on the European continent were destroyed. All seven bridges of Budapest were blown apart by January 1945. Bridge engineers after the war were suddenly forced to start to rebuild with scant resources and with open minds. A renaissance of bridge engineering started in Europe, then spreading to America, Japan, China, and advancing to who knows where in the world, maybe Siberia, Africa? It just keeps going! The past 60 years of bridge engineering have brought us many new forms of bridge architecture (plate girder bridges, cable stayed bridges, segmental prestressed concrete bridges, composite bridges), and longer spans. Meanwhile enormous knowledge and experience have been amassed by the profession, and progress has benefitted greatly by the availability of the digital computer. The purpose of the *Bridge Engineering Handbook* is to bring much of this knowledge and experience to the bridge engineering community of the world. The contents encompass the whole spectrum of the life cycle of the bridge, from conception to demolition.

The editors have convinced 146 experts from many parts of the world to contribute their knowledge and to share the secrets of their successful and unsuccessful experiences. Despite all that is known, there are still failures: engineers are human, they make errors; nature is capricious, it brings unexpected surprises! But bridge engineers learn from failures, and even errors help to foster progress.

The *Bridge Engineering Handbook*, second edition consists of five books:

Fundamentals
Superstructure Design
Substructure Design
Seismic Design
Construction and Maintenance

Fundamentals, Superstructure Design, and *Substructure Design* present the many topics necessary for planning and designing modern bridges of all types, made of many kinds of materials and systems, and subject to the typical loads and environmental effects. *Seismic Design* and *Construction and Maintenance* recognize the importance that bridges in parts of the world where there is a chance of earthquake occurrences must survive such an event, and that they need inspection, maintenance, and possible repair throughout their intended life span. Seismic events require that a bridge sustain repeated dynamic load cycles without functional failure because it must be part of the postearthquake lifeline for the affected area. *Construction and Maintenance* touches on the many very important aspects of bridge management that become more and more important as the world's bridge inventory ages.

The editors of the *Bridge Engineering Handbook*, Second Edition are to be highly commended for undertaking this effort for the benefit of the world's bridge engineers. The enduring result will be a safer and more cost effective family of bridges and bridge systems. I thank them for their effort, and I also thank the 146 contributors.

Theodore V. Galambos, PE
Emeritus professor of structural engineering
University of Minnesota

Preface to the Second Edition

In the approximately 13 years since the original edition of the *Bridge Engineering Handbook* was published in 2000, we have received numerous letters, e-mails, and reviews from readers including educators and practitioners commenting on the handbook and suggesting how it could be improved. We have also built up a large file of ideas based on our own experiences. With the aid of all this information, we have completely revised and updated the handbook. In writing this Preface to the Second Edition, we assume readers have read the original Preface. Following its tradition, the second edition handbook stresses professional applications and practical solutions; describes the basic concepts and assumptions omitting the derivations of formulas and theories; emphasizes seismic design, rehabilitation, retrofit and maintenance; covers traditional and new, innovative practices; provides over 2500 tables, charts, and illustrations in ready-to-use format and an abundance of worked-out examples giving readers step-by-step design procedures. The most significant changes in this second edition are as follows:

- The handbook of 89 chapters is published in five books: *Fundamentals, Superstructure Design, Substructure Design, Seismic Design,* and *Construction and Maintenance*.
- *Fundamentals,* with 22 chapters, combines Section I, Fundamentals, and Section VI, Special Topics, of the original edition and covers the basic concepts, theory and special topics of bridge engineering. Seven new chapters are Finite Element Method, High-Speed Railway Bridges, Structural Performance Indicators for Bridges, Concrete Design, Steel Design, High Performance Steel, and Design and Damage Evaluation Methods for Reinforced Concrete Beams under Impact Loading. Three chapters including Conceptual Design, Bridge Aesthetics: Achieving Structural Art in Bridge Design, and Application of Fiber Reinforced Polymers in Bridges, are completely rewritten. Three special topic chapters, Weigh-In-Motion Measurement of Trucks on Bridges, Impact Effect of Moving Vehicles, and Active Control on Bridge Engineering, were deleted.
- *Superstructure Design,* with 19 chapters, provides information on how to design all types of bridges. Two new chapters are Extradosed Bridges and Stress Ribbon Pedestrian Bridges. The Prestressed Concrete Girder Bridges chapter is completely rewritten into two chapters: Precast–Pretensioned Concrete Girder Bridges and Cast-In-Place Posttensioned Prestressed Concrete Girder Bridges. The Bridge Decks and Approach Slabs chapter is completely rewritten into two chapters: Concrete Decks and Approach Slabs. Seven chapters, including Segmental Concrete Bridges, Composite Steel I-Girder Bridges, Composite Steel Box Girder Bridges, Arch Bridges, Cable-Stayed Bridges, Orthotropic Steel Decks, and Railings, are completely rewritten. The chapter Reinforced Concrete Girder Bridges was deleted because it is rarely used in modern time.
- *Substructure Design* has 11 chapters and addresses the various substructure components. A new chapter, Landslide Risk Assessment and Mitigation, is added. The Geotechnical Consideration chapter is completely rewritten and retitled as Ground Investigation. The Abutments and

Retaining Structures chapter is divided in two and updated as two chapters: Abutments and Earth Retaining Structures.

- *Seismic Design,* with 18 chapters, presents the latest in seismic bridge analysis and design. New chapters include Seismic Random Response Analysis, Displacement-Based Seismic Design of Bridges, Seismic Design of Thin-Walled Steel and CFT Piers, Seismic Design of Cable-Supported Bridges, and three chapters covering Seismic Design Practice in California, China, and Italy. Two chapters of Earthquake Damage to Bridges and Seismic Design of Concrete Bridges have been rewritten. Two chapters of Seismic Design Philosophies and Performance-Based Design Criteria, and Seismic Isolation and Supplemental Energy Dissipation, have also been completely rewritten and retitled as Seismic Bridge Design Specifications for the United States, and Seismic Isolation Design for Bridges, respectively. Two chapters covering Seismic Retrofit Practice and Seismic Retrofit Technology are combined into one chapter called Seismic Retrofit Technology.
- *Construction and Maintenance* has 19 chapters and focuses on the practical issues of bridge structures. Nine new chapters are Steel Bridge Fabrication, Cable-Supported Bridge Construction, Accelerated Bridge Construction, Bridge Management Using Pontis and Improved Concepts, Bridge Maintenance, Bridge Health Monitoring, Nondestructive Evaluation Methods for Bridge Elements, Life-Cycle Performance Analysis and Optimization, and Bridge Construction Methods. The Strengthening and Rehabilitation chapter is completely rewritten as two chapters: Rehabilitation and Strengthening of Highway Bridge Superstructures, and Rehabilitation and Strengthening of Orthotropic Steel Bridge Decks. The Maintenance Inspection and Rating chapter is completely rewritten as three chapters: Bridge Inspection, Steel Bridge Evaluation and Rating, and Concrete Bridge Evaluation and Rating.
- The section on Worldwide Practice in the original edition has been deleted, including the chapters on Design Practice in China, Europe, Japan, Russia, and the United States. An international team of bridge experts from 26 countries and areas in Africa, Asia, Europe, North America, and South America, has joined forces to produce the *Handbook of International Bridge Engineering, Second Edition*, the first comprehensive, and up-to-date resource book covering the state-of-the-practice in bridge engineering around the world. Each of the 26 country chapters presents that country's historical sketch; design specifications; and various types of bridges including girder, truss, arch, cable-stayed, suspension, and so on, in various types of materials—stone, timber, concrete, steel, advanced composite, and of varying purposes—highway, railway, and pedestrian. Ten benchmark highway composite girder designs, the highest bridges, the top 100 longest bridges, and the top 20 longest bridge spans for various bridge types are presented. More than 1650 beautiful bridge photos are provided to illustrate great achievements of engineering professions.

The 146 bridge experts contributing to these books have written chapters to cover the latest bridge engineering practices, as well as research and development from North America, Europe, and Pacific Rim countries. More than 80% of the contributors are practicing bridge engineers. In general, the handbook is aimed toward the needs of practicing engineers, but materials may be re-organized to accommodate several bridge courses at the undergraduate and graduate levels.

The authors acknowledge with thanks the comments, suggestions, and recommendations made during the development of the second edition of the handbook by Dr. Erik Yding Andersen, COWI A/S, Denmark; Michael J. Abrahams, Parsons Brinckerhoff, Inc.; Dr. Xiaohua Cheng, New Jersey Department of Transportation; Joyce E. Copelan, California Department of Transportation; Prof. Dan M. Frangopol, Lehigh University; Dr. John M. Kulicki, Modjeski and Masters; Dr. Amir M. Malek, California Department of Transportation; Teddy S. Theryo, Parsons Brinckerhoff, Inc.; Prof. Shouji Toma, Horrai-Gakuen University, Japan; Dr. Larry Wu, California Department of Transportation; Prof. Eiki Yamaguchi, Kyushu Institute of Technology, Japan; and Dr. Yi Edward Zhou, URS Corp.

We thank all the contributors for their contributions and also acknowledge Joseph Clements, acquiring editor; Jennifer Ahringer, project coordinator; and Joette Lynch, project editor, at Taylor & Francis/CRC Press.

Preface to the First Edition

The *Bridge Engineering Handbook* is a unique, comprehensive, and state-of-the-art reference work and resource book covering the major areas of bridge engineering with the theme "bridge to the twenty-first century." It has been written with practicing bridge and structural engineers in mind. The ideal readers will be MS-level structural and bridge engineers with a need for a single reference source to keep abreast of new developments and the state-of-the-practice, as well as to review standard practices.

The areas of bridge engineering include planning, analysis and design, construction, maintenance, and rehabilitation. To provide engineers a well-organized, user-friendly, and easy-to-follow resource, the handbook is divided into seven sections. Section I, Fundamentals, presents conceptual design, aesthetics, planning, design philosophies, bridge loads, structural analysis, and modeling. Section II, Superstructure Design, reviews how to design various bridges made of concrete, steel, steel-concrete composites, and timbers; horizontally curved, truss, arch, cable-stayed, suspension, floating, movable, and railroad bridges; and expansion joints, deck systems, and approach slabs. Section III, Substructure Design, addresses the various substructure components: bearings, piers and columns, towers, abutments and retaining structures, geotechnical considerations, footings, and foundations. Section IV, Seismic Design, provides earthquake geotechnical and damage considerations, seismic analysis and design, seismic isolation and energy dissipation, soil–structure–foundation interactions, and seismic retrofit technology and practice. Section V, Construction and Maintenance, includes construction of steel and concrete bridges, substructures of major overwater bridges, construction inspections, maintenance inspection and rating, strengthening, and rehabilitation. Section VI, Special Topics, addresses in-depth treatments of some important topics and their recent developments in bridge engineering. Section VII, Worldwide Practice, provides the global picture of bridge engineering history and practice from China, Europe, Japan, and Russia to the U.S.

The handbook stresses professional applications and practical solutions. Emphasis has been placed on ready-to-use materials, and special attention is given to rehabilitation, retrofit, and maintenance. The handbook contains many formulas and tables that give immediate answers to questions arising from practical works. It describes the basic concepts and assumptions, omitting the derivations of formulas and theories, and covers both traditional and new, innovative practices. An overview of the structure, organization, and contents of the book can be seen by examining the table of contents presented at the beginning, while the individual table of contents preceding each chapter provides an in-depth view of a particular subject. References at the end of each chapter can be consulted for more detailed studies.

Many internationally known authors have written the chapters from different countries covering bridge engineering practices, research, and development in North America, Europe, and the Pacific Rim. This handbook may provide a glimpse of a rapidly growing trend in global economy in recent years toward international outsourcing of practice and competition in all dimensions of engineering.

In general, the handbook is aimed toward the needs of practicing engineers, but materials may be reorganized to accommodate undergraduate and graduate level bridge courses. The book may also be used as a survey of the practice of bridge engineering around the world.

The authors acknowledge with thanks the comments, suggestions, and recommendations during the development of the handbook by Fritz Leonhardt, Professor Emeritus, Stuttgart University, Germany; Shouji Toma, Professor, Horrai-Gakuen University, Japan; Gerard F. Fox, Consulting Engineer; Jackson L. Durkee, Consulting Engineer; Michael J. Abrahams, Senior Vice President, Parsons, Brinckerhoff, Quade & Douglas, Inc.; Ben C. Gerwick, Jr., Professor Emeritus, University of California at Berkeley; Gregory F. Fenves, Professor, University of California at Berkeley; John M. Kulicki, President and Chief Engineer, Modjeski and Masters; James Chai, Senior Materials and Research Engineer, California Department of Transportation; Jinrong Wang, Senior Bridge Engineer, URS Greiner; and David W. Liu, Principal, Imbsen & Associates, Inc.

We thank all the authors for their contributions and also acknowledge at CRC Press Nora Konopka, acquiring editor, and Carol Whitehead and Sylvia Wood, project editors.

Editors

Dr. Wai-Fah Chen is a research professor of civil engineering at the University of Hawaii. He was dean of the College of Engineering at the University of Hawaii from 1999 to 2007, and a George E. Goodwin Distinguished Professor of Civil Engineering and head of the Department of Structural Engineering at Purdue University from 1976 to 1999.

He earned his BS in civil engineering from the National Cheng-Kung University, Taiwan, in 1959, MS in structural engineering from Lehigh University in 1963, and PhD in solid mechanics from Brown University in 1966. He received the Distinguished Alumnus Award from the National Cheng-Kung University in 1988 and the Distinguished Engineering Alumnus Medal from Brown University in 1999.

Dr. Chen's research interests cover several areas, including constitutive modeling of engineering materials, soil and concrete plasticity, structural connections, and structural stability. He is the recipient of several national engineering awards, including the Raymond Reese Research Prize and the Shortridge Hardesty Award, both from the American Society of Civil Engineers, and the T. R. Higgins Lectureship Award in 1985 and the Lifetime Achievement Award, both from the American Institute of Steel Construction. In 1995, he was elected to the U.S. National Academy of Engineering. In 1997, he was awarded Honorary Membership by the American Society of Civil Engineers, and in 1998, he was elected to the Academia Sinica (National Academy of Science) in Taiwan.

A widely respected author, Dr. Chen has authored and coauthored more than 20 engineering books and 500 technical papers. His books include several classical works such as *Limit Analysis and Soil Plasticity* (Elsevier, 1975), the two-volume *Theory of Beam-Columns* (McGraw-Hill, 1976 and 1977), *Plasticity in Reinforced Concrete* (McGraw-Hill, 1982), and the two-volume *Constitutive Equations for Engineering Materials* (Elsevier, 1994). He currently serves on the editorial boards of more than 15 technical journals.

Dr. Chen is the editor-in-chief for the popular *Civil Engineering Handbook* (CRC Press, 1995 and 2003), the *Handbook of Structural Engineering* (CRC Press, 1997 and 2005), the *Earthquake Engineering Handbook* (CRC Press, 2003), the *Semi-Rigid Connections Handbook* (J. Ross Publishing, 2011), and the *Handbook of International Bridge Engineering* (CRC Press, 2014). He currently serves as the consulting editor for the *McGraw-Hill Yearbook of Science & Technology* for the field of civil and architectural engineering.

He was a longtime member of the executive committee of the Structural Stability Research Council and the specification committee of the American Institute of Steel Construction. He was a consultant for Exxon Production Research on offshore structures, for Skidmore, Owings, and Merrill in Chicago on tall steel buildings, and for the World Bank on the Chinese University Development Projects, among many others. Dr. Chen has taught at Lehigh University, Purdue University, and the University of Hawaii.

Dr. Lian Duan is a senior bridge engineer and structural steel committee chair with the California Department of Transportation (Caltrans). He worked at the North China Power Design Institute from 1975 to 1978 and taught at Taiyuan University of Technology, China, from 1981 to 1985.

He earned his diploma in civil engineering in 1975, MS in structural engineering in 1981 from Taiyuan University of Technology, China, and PhD in structural engineering from Purdue University in 1990.

Dr. Duan's research interests cover areas including inelastic behavior of reinforced concrete and steel structures, structural stability, seismic bridge analysis, and design. With more than 70 authored and coauthored papers, chapters, and reports, his research focuses on the development of unified interaction equations for steel beam-columns, flexural stiffness of reinforced concrete members, effective length factors of compression members, and design of bridge structures.

Dr. Duan has over 35 years experience in structural and bridge engineering. He was lead engineer for the development of Caltrans *Guide Specifications for Seismic Design of Steel Bridges*. He is a registered professional engineer in California. He served as a member for several National Highway Cooperative Research Program panels and was a Transportation Research Board Steel Committee member from 2000 to 2006.

He is the coeditor of the *Handbook of International Bridge Engineering,* (CRC Press, 2014). He received the prestigious 2001 Arthur M. Wellington Prize from the American Society of Civil Engineers for the paper, "Section Properties for Latticed Members of San Francisco-Oakland Bay Bridge," in the *Journal of Bridge Engineering,* May 2000. He received the Professional Achievement Award from Professional Engineers in California Government in 2007 and the Distinguished Engineering Achievement Award from the Engineers' Council in 2010.

Contributors

Erik Yding Andersen
COWI A/S
Lyngby, Denmark

Baidar Bakht
University of Manitoba
Winnipeg, Manitoba, Canada

Steve C.S. Cai
Louisiana State University
Baton Rouge, Louisiana

Wai-Fah Chen
University of Hawaii
Honolulu, Hawaii

Robert J. Dexter
University of Minnesota
Minneapolis, Minnesota

Lian Duan
California Department of Transportation
Sacramento, California

John W. Fisher
Lehigh University
Bethlehem, Pennsylvania

Dan M. Frangopol
Lehigh University
Bethlehem, Pennsylvania

Kenneth J. Fridley
University of Alabama
Tuscaloosa, Alabama

Frederick Gottemoeller
Bridgescape, LLC
Columbia, Maryland

Lars Hauge
COWI A/S
Lyngby, Denmark

Susan E. Hida
California Department of Transportation
Sacramento, California

Dietrich L. Hommel
COWI A/S
Lyngby, Denmark

Jeder Hseih
Continental Engineering Corporation
New Taipei City, Taiwan
Republic of China

Norimitsu Kishi
Kushiro National College of Technology
Kushiro, Japan

Alexander Krimotat
SC Solutions, Inc.
Sunnyvale, California

John M. Kulicki
Modjeski and Masters, Inc.
Mechanicsburg, Pennsylvania

Honggang Lei
Taiyuan University of Technology
Taiyuan, China

Fritz Leonhardt
Stuttgart University
Stuttgart, Germany

Xila Liu
Shanghai Jiao Tong University
Shanghai, China

Ward N. Marianos, Jr.
Consulting Engineer
Woodlands, Texas

Serge Montens
Jean Muller International
St.-Quentin-en-Yvelines, France

Aftab Mufti
University of Manitoba
Winnipeg, Manitoba, Canada

Sougata Roy
Lehigh University
Bethlehem, Pennsylvania

Duygu Saydam
Lehigh University
Bethlehem, Pennsylvania

Hassan Sedarat
SC Solutions, Inc.
Sunnyvale, California

Monte Smith
Sargent Engineers, Inc.
Olympia, Washington

Donald F. Sorgenfrei
Modjeski and Masters, Inc.
New Orleans, Louisiana

Dagmar Svecova
University of Manitoba
Winnipeg, Manitoba, Canada

James A. Swanson
University of Cincinnati
Cincinnati, Ohio

Robert A.P. Sweeney
Consulting Engineer
Montreal, Quebec, Canada

Man-Chung Tang
T.Y. Lin International
San Francisco, California

Shouji Toma
Hokkai-Gakuen University
Sapporo, Japan

Fu-Hsiang Wu
Chung Hua University
Taoyuan, Taiwan
Republic of China

Eiki Yamaguchi
Kyushu Institute of Technology
Tobata, Japan

Leiming Zhang
Shanghai Jiao Tong University
Shanghai, China

Wei Zhang
University of Connecticut
Storrs, Connecticut

1

Conceptual Design

Man-Chung Tang
T.Y. Lin International

1.1 Introduction

The basic purpose of a bridge is to carry traffic over an opening or discontinuity in the landscape. Various types of bridge traffic can include pedestrians, vehicles, pipelines, cables, water, and trains, or a combination thereof. An opening can occur over a highway, a river, a valley, or any other type of physical obstacle. The need to carry traffic over such an opening defines the function of a bridge. The design of a bridge can only commence after its function has been properly defined. Therefore, the process of building a bridge is not initiated by the bridge engineer. Just like roads or a drainage system, or other types of infrastructure, a bridge is a part of a transportation system and a transportation system is a component of a city's planning efforts or its area development plan. The function of a bridge must be defined in these master plans.

A bridge should be "safe, functional, economical, and good looking." Safety cannot be compromised. A bridge must be safe under all of the loads it is designed for. Otherwise, the bridge cannot be opened to traffic. Functionality should not be compromised. If four lanes are required, for example, it must provide four lanes. But in certain cases, it may still be acceptable if some lane widths are slightly different from the standard width recommended in the specifications, as long as this does not affect safety. As well, economy and aesthetics do not have absolute standards. There is no such thing as a "correct cost" of a bridge. It varies from place to place, time to time, and situation to situation. The cost of a bridge in

Florida may be vastly different from the cost of the same bridge if built in New York, or in Shanghai, even though the structures are exactly the same. So what is economical is clearly a relative term.

Aesthetics are even harder to define. For example, the Firth of Forth Bridge in Scotland was often criticized as the world's most ugly structure by some and at the same time lauded as a spectacularly beautiful landmark by others. The Eiffel Tower in Paris was mercilessly attacked by many architects, engineers, philosophers, and other intellectuals alike, as an eyesore at the time of its construction. But now, it has become the most beloved tourist attraction in France. Nevertheless, people do admire the beauty of some bridges and dislike others. If a bridge is deemed beautiful by most people, then we may be allowed to say that it is beautiful. So, at least at a given time and in a given place, it is possible to say whether a bridge is beautiful or not, based on popular opinion.

Thus, the mission of a bridge design may be defined as "to design a safe, functional, and beautiful bridge within the given budget."

Because both economy and aesthetics are relative, there is no "perfect" design, but only a "suitable" design for a bridge. Although it is unrealistic to strive for perfection in a bridge design, the engineer must ascertain whether the design is "appropriate." To be appropriate we must also consider durability, sustainability, life cycle performance, and effects on the environment. These topics are not discussed here because they will be addressed in later chapters of this book.

1.2 Four Stages of a Bridge Design

The design process of a bridge can be divided into four basic stages: conceptual, preliminary, detailed, and construction design. The purpose of the conceptual design is to come up with various feasible bridge schemes and to decide on one or more final concepts for further consideration (Nagai et al., 2004; Xiang, 2011). The purpose of the preliminary design is to select the best scheme from these proposed concepts and then to ascertain the feasibility of the selected concept and finally to refine its cost estimates. The purpose of the detailed design is to finalize all the details of the bridge structure so that the document is sufficient for tendering and construction. Finally, the purpose of the construction design is to provide step-by-step procedures for building the bridge. Each of the earlier design stages must carefully consider the requirements of subsequent stages. For example, the detailed design must consider how the bridge is to be built; the preliminary design must consider, in addition, what structural details will look like; and, the conceptual design must consider, in addition to all the above, what information the preliminary design will require. This means that a conceptual design must sufficiently consider what is required to complete the bridge in the given environment, including providing a general idea of costs and construction schedule as well as aesthetics.

By "consider" we do not mean that we have to actually perform detailed studies on the aforementioned issues during the conceptual design stage, although accumulated engineering experience can help us understand the feasibility of many basic ideas. For example, we do not have to conduct a calculation to ascertain that a 150-m span prestressed concrete box girder bridge is feasible, if we assume the girder depth to be approximately 7.50-m deep. Rather, our experience accumulated from working on many other bridges shows a medium span prestressed concrete box girder with a depth of 1/20th of the span length can work. By contrast, if we want to build a girder that is only 5.00 m deep, this would require a detailed study during the conceptual design stage because it is far less than the conventional girder depth of 1/20th of the span. Experience is of the utmost importance during the conceptual design stage. For this reason, only an experienced engineer should be appointed to perform a conceptual design.

Thus, a conceptual design is a process that must consider all details of the bridge in all phases from beginning to completion, at least based on experience if not in actual analysis. This is to ascertain that the proposed concept is feasible under the given conditions. Here, "feasibility" should not be restricted merely to structural stability and constructability; it must also satisfy the four basic requirements of a bridge: safety, functionality, economy, and aesthetics.

From another point of view, the conceptual design stage initiates the design of a bridge. It is a "conceiving" stage that begins with a blank slate—a creative process that tests the innovative abilities of the engineer.

Unfortunately, the importance of a conceptual design is typically misunderstood and even underestimated. In many instances, because the time assigned to completing a conceptual design is very limited, this can lead to immature concepts that can cause problems in the future. One way to improve the quality of a conceptual design is to assign a senior, more experienced staff to undertake this difficult and important task.

1.3 Establishing the Criteria

1.3.1 Codes and Specifications

Specifications and codes are legal documents. This means the design of a bridge must satisfy all provisions in the relevant specifications and codes, such as the "LRFD Bridge Design Specifications" published by the American Association of State Highway and Transportation Officials (AASHTO) (AASHTO, 2012). But specifications and codes are not always up to date. In our rapidly evolving world, many new ideas and developments may not be reflected in the prevailing specifications and codes because it takes time to modify them, or to introduce new provisions. Oftentimes, there are circumstances that require special attention.

The late Professor T.Y. Lin (Lin and Burns, 1981) advised engineers "not to just follow specifications and codes, but to follow the rules of nature." To this we may add that the responsibility of the bridge engineer is not merely to satisfy the requirements of the specifications, but to properly consider the actual conditions including the locality and the people it is designed to serve.

There are also circumstances that the prevailing specifications simply cannot cover. One example is the actual weight of trucks. Overloaded trucks are not uncommon in some localities. Overloaded trucks can cause overstress in the structure and reduce the fatigue life of the bridge. For example, the fatigue life of a welded steel detail is approximately inversely proportional to the cube of the stress range. If trucks are regularly overloaded to 150% of their design axle loads, this may reduce the service life of a steel detail to $< 30\%$ of its design life. Consequently, a 100-year design life may be reduced to 30 years.

Certainly, we must satisfy the specifications' demands but we must also go further to consider real conditions.

1.3.2 Project-Specific Design Criteria

A bridge is designed to satisfy a given function under given environmental conditions and constraints. The design must also follow the prevailing specifications and codes. They may collectively be called the design criteria of the bridge. These include, but are not limited to the following:

1. Type, volume, and magnitude of traffic to be carried by the bridge
2. Clearances required by the type of traffic on the deck
3. Navigation clearance under the bridge
4. Environmental effects such as earthquake, wind, flood, and other possible natural phenomena
5. Geological formation and soil characteristics at the site
6. Economic conditions or available project funding
7. Expectations of the stakeholders on form and aesthetics

Every one of these conditions can influence the design. And likewise, a violation of any one of these conditions can render the design concept unacceptable. Therefore, the conditions must be clearly defined before an engineer begins to conceptualize a new bridge. Certainly, the bridge we build must satisfy the functions it is designed for, including safely carrying the loads acting on it. In addition, there is always a budget that limits how much we are allowed to spend. Last but not least, it is critically important how well the bridge fits into its physical environment aesthetically.

These design criteria represent the constraints of the bridge we want to build. The function determines the width and elevation of the deck, although the navigational and other types of clearances determine the height and span length. Together with limitations created by the geological and topographic

conditions at the site, these criteria determine the basic geometry of the structure. The aim of the conceptual design is to come up with the most suitable bridge scheme that can satisfy all the given design criteria. Here, suitability is based on the requirements of "safety, functionality, economy, and aesthetics."

1.4 Characteristics of Bridge Structures

1.4.1 Bridge Types

Our first step is to consider the most suitable bridge type. We can group all bridges in the world into four basic types: girder bridge, arch bridge, cable-stayed bridge, and suspension bridge (see Figure 1.1). There are also varying possible combinations, such as the cable-stayed and suspension scheme proposed by Franz Dishinger, and the "partially cable-supported girder bridge" (Tang, 2007). For simplicity, we can drop the word "partially" in this name and call it cable-supported girder bridge. It is a combination of a girder bridge and any one of the aforementioned bridge types. The extra dosed bridge is a special subset of the cable-supported girder bridge.

Common wisdom suggests that girder bridges and arch bridges are good for short to medium spans, whereas cable-stayed bridges are good for medium to longer spans, and suspension bridges are good for very long spans. Based on this assumption, some engineers established rules to assign a span range for each of these bridge types. For example, in the 1960s, the reasonable maximum span length of a cable-stayed bridge was thought to be approximately 450 m and that of a girder bridge was thought to be approximately 250 m. These previously held theories did not last long as cable-stayed bridges with spans of over 1000 m have been completed since then.

Over time, with improvements in construction materials and advancements in construction equipment and technique, the reasonable span length of each bridge type has significantly increased. But in relative terms, the above mentioned comparisons are still valid. Only the numerical values of the span ranges have changed.

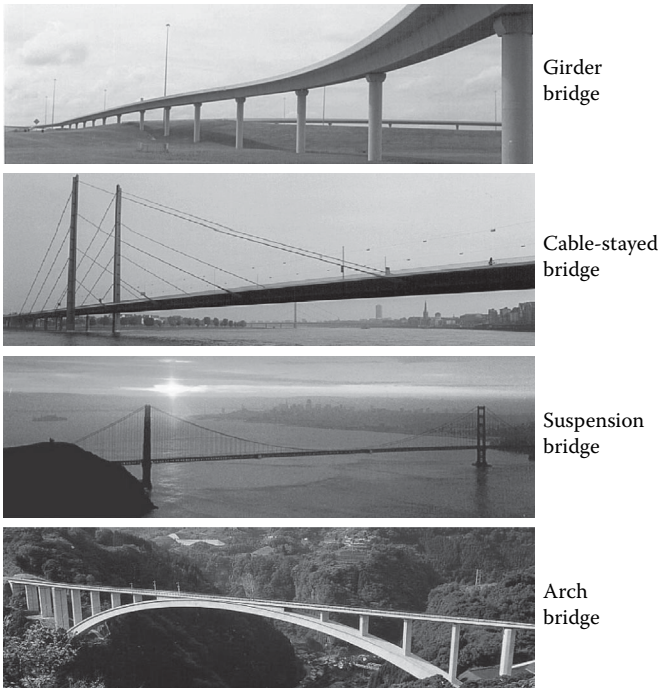

FIGURE 1.1 Four basic types of bridges.

However, an engineer should not be restricted by these assumptions. Instead, it is important for engineers to understand what the actual limits of each bridge type are, based on his or her understanding of the latest construction materials and equipment available at the time of construction. When a better material is available in the future, the engineer should be able to re-estimate these limitations using the same logic. To be able to do this, the engineer must have a good understanding of the characteristics of structures. We can begin by looking at the very basic elements of structures.

1.4.2 Basic Structural Elements

Some structures may look very simple and some structures may look very complex, but every structure is made up of only four basic types of structural elements, and each one is dominated by one type of function. They are axial force elements (A elements), bending elements (B elements), curved elements (C elements), and torsional elements (T elements), which can be abbreviated as the ABCT of structures. The first three types of elements are sufficient to compose almost all structure types (see Figure 1.2). Most torsional elements can be established using a combination of the first three element types. But, for convenience, having torsional elements will simplify our thinking process.

As an example, in a cable-stayed bridge, the predominant function of the cables, the girder, and the towers is to carry axial forces. These are mainly A elements. The same is true for a truss bridge. There are local effects that may cause bending moment in these elements, but they are less dominant and can be considered secondary. A girder bridge, however, carries the loads mainly by bending, so it is considered a B element.

When an axial force element changes direction, it creates a force component lateral to the axial force (see Figure 1.3). So each change of direction will create a lateral component. These lateral components can be used to resist lateral loads. If the lateral loads are sufficiently closely spaced, the structural element becomes a curve, resulting in a curved structural element, the C element. There are two major

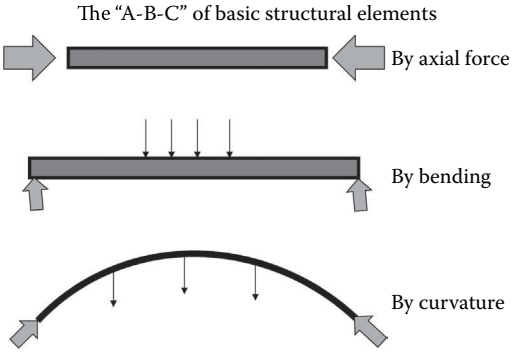

FIGURE 1.2 Structural elements A, B, and C.

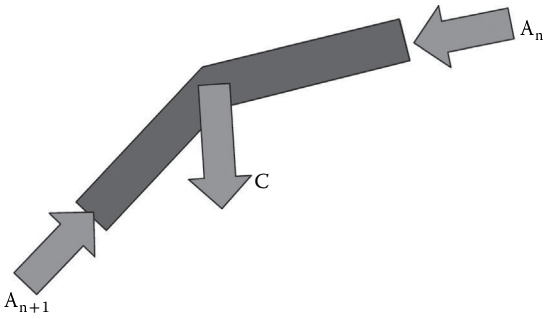

FIGURE 1.3 Formation of curve element.

types of curved elements: if the axial force is compression, the structure is similar to an arch. If the axial force is tension, the element is similar to a suspended cable such as the main cable of a suspension bridge.

Thus, with A, B, and C elements, we can create the framework of almost all major types of bridges known to us today. Torsion is usually a locally occurring phenomenon. It mainly coexists with one of the A, B, or C elements. An eccentrically loaded girder bridge, for example, will have torsion besides bending moment. Although both of them must be considered in the design, the predominant factor is still the bending moment and it therefore can be characterized as a B element.

In a design, we proportion the structural elements to remain within the allowable stress limits. Figure 1.4 shows the stress distribution of the A element and the B element. In an A element, the entire cross section can be utilized to its fullest extent because the entire cross section can reach the allowable stress at the same time. By contrast, in a B element, only the extreme fiber can reach the allowable stress, while the stress in the rest of the cross section is less than the allowable stress. So in a B element, most of the cross sectional area is not fully utilized and is consequently less efficient. The C element is similar to the A element and it is more efficient than the B element.

When a portion of the element is not participating in carrying loads, or if it is not used to its fullest extent, more material is required to carry the same load, thus increasing its dead weight, which is a big disadvantage in bridges, especially in long-span bridges. Currently, the world record span for each of these four types of bridges are the following: the 330-m span Shibanpo Bridge in Chongqing, China is the longest girder bridge span; the 552-m span Chaotianmen Bridge, also in Chongqing, China is the longest arch bridge span; the 1104-m Vladivostok Bridge in Russia is the longest cable-stayed bridge span; and the 1991-m span Akashi Kaikyo Bridge in Japan is the longest suspension bridge span. The Shibanpo Bridge (Figure 1.5), which is a girder bridge, over the Yangtze River in Chongqing is the smallest among world record spans of the four bridge types. The girder bridge is the only bridge type that relies

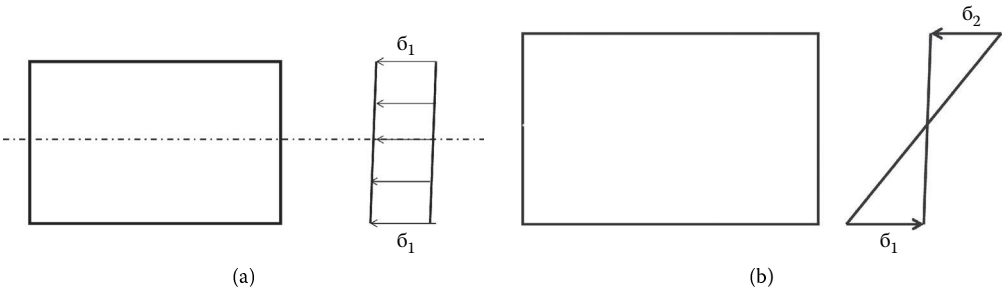

FIGURE 1.4 Stress distribution in A and B elements.

FIGURE 1.5 Shibanpo Bridge.

mainly on bending to carry the loads. It is a B element. B elements are less efficient. Therefore, a bridge that consists mainly of a B element is less efficient and thus its maximum span is smaller.

1.4.3 Know the Limits

Before we conceptualize a bridge, it is important to understand what problems may lie ahead. We must also know the limitations, or the boundaries within which we must remain. There are many different kinds of boundaries such as environmental, financial, social, historical, and technical boundaries. All these boundaries are project specific, which means they cannot be applied universally, with the exception of technical problems.

Through the course of designing a bridge, engineers must deal with many technical problems that fall into two categories: technical difficulties and technical limitations. Technical difficulties are problems that can be solved, even though the solution may cost time and money. A limitation is an upper bound that cannot be exceeded. One important example of a technical problem is the span length. What is the maximum possible span length for each of the four types of bridges mentioned above? We will try to answer this question with the following analysis.

When a bridge span is very long, we will face various technical problems. The most prominent problems are the following:

1. Girder stiffness in the transverse direction
2. Reduction in cable efficiency of very long cables in a cable-stayed bridge
3. Torsional stiffness of the main girder
4. Allowable stresses of the construction materials

All of these problems are, in some way, related to the construction materials we are going to use for the structure and they must be addressed when identifying maximum span lengths. Currently, for long-span bridges, the predominant materials used are steel and concrete, as has been the case in the past 150 years. Other materials, such as fibers and composites, even though available, are not ready for extensive use in the construction of major long-span bridges yet. Therefore, in the following analysis, we will only consider steel and concrete as the main materials for construction. As far as very long-span bridges are concerned, concrete only plays a secondary role, and steel is the predominant construction material to be used, with the exception of girder bridges.

Steel was introduced into widespread commercial application only from the mid-nineteenth century onward. Before that, iron was used for a short period of time. And further back, bridges were built mainly using stones and bricks. Stones and bricks have good compressive strength but almost no tensile strength, so the only type of bridge that can be built using stones and bricks is an arch bridge. This is evident in the historical record. For several thousands of years until the nineteenth century, basically all longer span bridges were built with stones and bricks. Moreover, they are all arch bridges.

In order to estimate the maximum possible span of each bridge type, we must address the above-mentioned problems first.

1.4.3.1 Lateral Stiffness of the Main Girder

The minimum width of a bridge is determined by its specified traffic pattern. As an example, the deck width of a regular six-lane bridge with pedestrian paths is usually approximately 34 m. Thus, for a 1000-m span, six-lane bridge, the span to width ratio is approximately 29.4, and the bridge should have little problem resisting lateral loads caused by wind, earthquakes, and other natural phenomena or manmade effects. However, if the span is increased to 2000 m, the ratio increases to 59, and the bridge may have a problem resisting lateral loads. If the span is even longer, the problem becomes more serious. To increase the bridge's stability, the simplest solution is to increase the width of the bridge (see Figure 1.6). A good

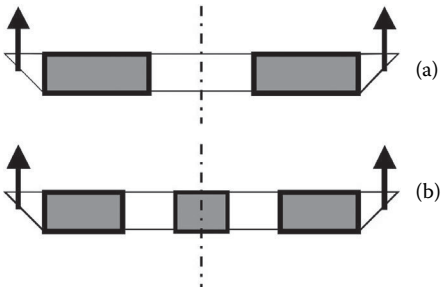

FIGURE 1.6 Separating bridge deck to increase girder width.

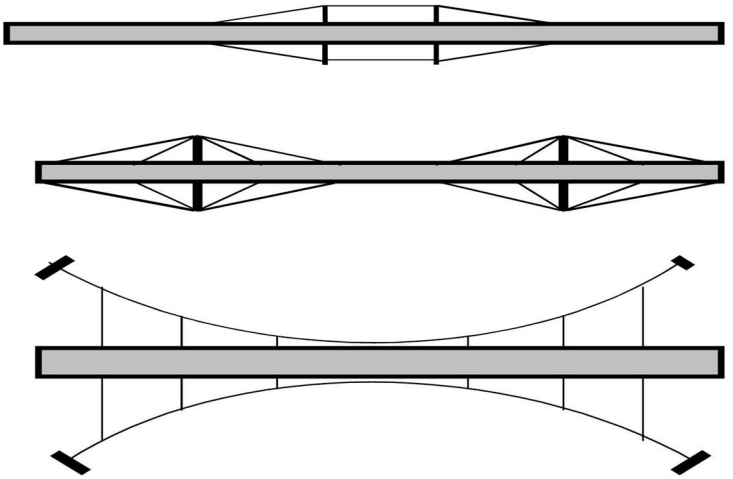

FIGURE 1.7 Cable strengthening.

example of this is the Messina Strait Bridge in Italy, which is currently under construction. There are other ways to increase the lateral stiffness of a bridge girder as well (see Figure 1.7). So, this problem is solvable.

1.4.3.2 Effectiveness of a Long Stay Cable

A cable that sags under its own weight will decrease the efficiency of the cable. The effective stiffness, $(EA)_{eff}$, of a cable with a horizontal projection of L can be estimated by the Ernst formula (see Figure 1.8).

$$(EA)_{eff} = r \times (E_{steel} \times A_{steel})$$

and

$$r = 1/\left[1 + (\gamma \times L)^2 \times E_{steel} / (12 \times f^3)\right]$$

where r is defined as the effective ratio of the cable; γ is the unit weight of the cable, which is equal to the total weight of the cable, including the covering pipes and other protection materials applied to the cable divided by the cable steel cross section; L is the horizontal projection length of the cable; and f is the average stress in the cable. Here r is an instantaneous value at cable stress equal to f. In reality, the stress in the cables changes when the bridge is loaded with live loads or other types of loads. Thus, if the cable stress changes from f_1 to f_2, the effective ratio, r_v will be

$$r_v = 1/\left[1+(\gamma \times L)^2 \times E_{steel} \times (f_1 + f_2)/(24 \times f_1^2 \times f_2^2)\right]$$

In a cable-stayed bridge, the allowable stress in the cables is usually specified as 45% of the breaking strength of the cable steel, or, 0.45 fu. There are two types of cables commonly used today, parallel wire cables with a breaking strength of 240 ksi and seven-wire strands with a breaking strength of 270 ksi. For a super long-span cable-stayed bridge, either type of cable is acceptable. For the purposes of this analysis, we will choose the seven-wire strands that have a higher strength. The effective ratio r varies mainly with L, which, for a very long span, can be assumed as half of the span length.

As shown in Figure 1.9, r may fall way below 1.0 if the cable is very long. This is what some engineers used to limit the maximum span length of a cable-stayed bridge. However, engineers must solve technical problems as they arise in the design, not succumb to them! As is evident from the equation, if we can shorten the cable span, L, the sag will be reduced. Thus, we will be able to avoid this problem. Figure 1.10 shows a few ways to reduce the effective span of a long cable. Therefore, this problem can be solved and it does not pose a limitation to the span length.

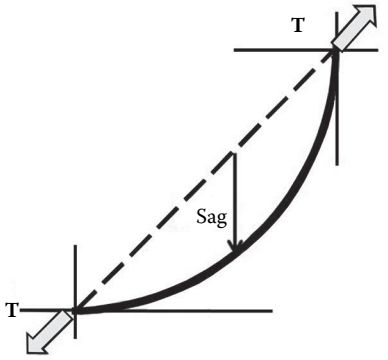

FIGURE 1.8 Form of a stay cable under its own weight.

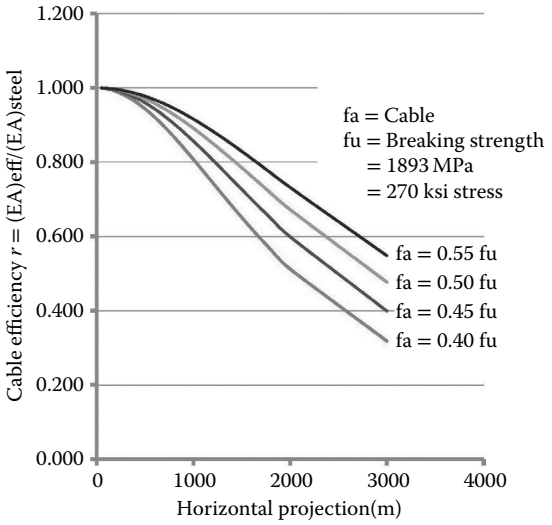

FIGURE 1.9 Cable efficiency.

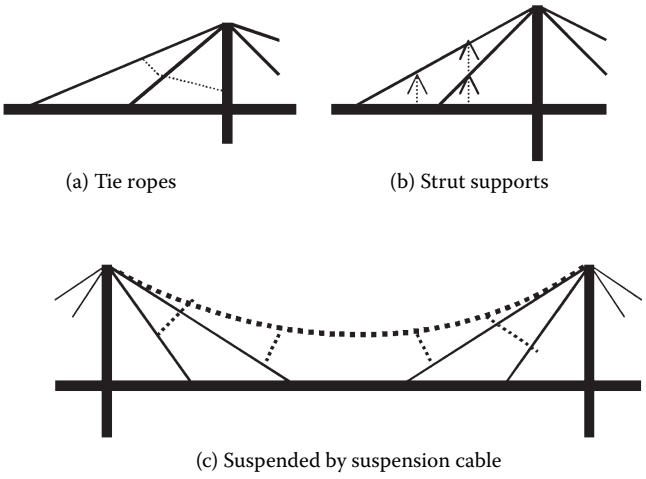

FIGURE 1.10 Various ways to increase cable efficiency.

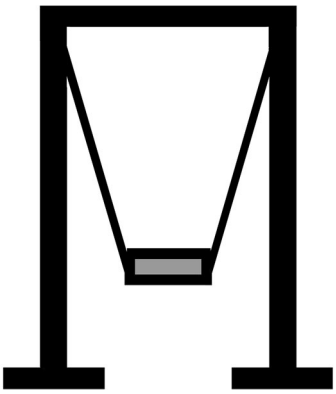

FIGURE 1.11 Spatial cable arrangement.

1.4.3.3 Torsional Stiffness

The torsional stiffness is important under eccentric loads and aerodynamic actions. In most cases, the use of a box cross section for the girder will provide sufficient torsional stiffness to resist eccentric loads. Otherwise, increasing the distance between the two cable planes of the bridge is one way to increase the torsional rigidity of the girder. The spatial arrangement of the cables (Figure 1.11) will also help. Another solution is to use a local cable stay system to stiffen up the girder. At worst, it is possible to install dampers to suppress the torsional oscillations. This problem, too, is solvable.

In short, these three problems discussed above are solvable technical problems and they do not pose any limitations to the span length.

1.4.3.4 Allowable Stresses

The allowable stress of construction materials is a technical limitation. For very long-span bridges, steel is the main construction material used. There are two kinds of steel for bridge construction—the regular steel and cold-drawn steel wires. Wire has a much higher strength than regular steel plates. Various countries may have different steel products. The yield strength, the breaking strength, and consequently, the allowable stress, may vary. Nevertheless, the allowable stress for any specific steel is fixed and is proportional to its yield strength or breaking strength. It is not possible for us to increase its strength, likewise impossible to increase the allowable stress of that same steel. Certainly, the quality of the steel

we use in construction today is continuously being improved; the allowable stress of steel has significantly increased in the last century. Therefore, the maximum possible span of bridges has also increased.

1.4.4 Maximum Possible Spans

Research on the maximum feasible span length of various types of bridges has been presented by various authors [4–6]. Obviously, with different assumptions the conclusions may differ. Based on the assumption that the limiting factor in the span length of a bridge is the allowable stress, we can proceed to estimate the maximum possible span length of the four types of bridges.

1.4.4.1 Suspension Bridges

The critical members with respect to allowable stress in a suspension bridge are the main cables. For a uniformly loaded bridge, the shape of the main cable is close to a parabola. For suspension bridges, the sag, d (Figure 1.12), is usually equal to approximately 1/12 to 1/8 of the span length, L. The deck is suspended from the main cables with hangers and its weight changes little regardless of the span length. If we assume the sag to be 1/8 of the span, for a uniform load of w (load per unit length), the total horizontal component, H, of the cable force, T, in the main cables will be (Figure 1.12)

$$H = w \times L \text{ and } T_{\max} = 1.12 \times w \times L$$

$$\text{or}, T_{\max} = 1.12 \times \left(wc + wg + w_{LL}\right) \times L = Ac \times fa$$

$$\text{and } L = fa \times Ac / [1.12 \times (wc + wg + w_{LL})] = fa \times Ac / \left[1.12 \times (1+\alpha) \times wc\right],$$

where wg is the weight of the girder and hangers and w_{LL} is the live load on the deck, and wc is the weight of the cables, $wc = Ac^{*}\gamma$, Ac is the total cross-sectional area of the cables, fa is the allowable stress of the cable, and γ is the unit weight of the cable. For an extremely long-span bridge, the live load is negligible compared with the dead load, and the girder weight is also relatively small compared with the weight of the cable itself. Thus, it is feasible to allow a higher stress in the cables because fatigue is less of a problem. In addition, we can use a wire with higher breaking strength, which is available today, for instance, $fu =$ 1890 MPa. With a safety factor of 2.2, the allowable stress fa will be 860 MPa. Thus, if we assume $wg+w_{LL}$ to be approximately equal to 20% of wc, that is, $\alpha = 0.20$, we can solve the equation and the maximum span length would be approximately 8000 m.

With the cable weight being the predominant weight of the bridge, the cable takes on the shape of a catenary as versus a parabola. But for our purposes, this deviation is not significant.

We can go back and verify the validity of this assumption by using real numbers. Let us assume that the weight of the girder, plus eight lanes of traffic would be approximately 350 kN/m, and the cable weight, wc = 17,500 kN/m, so $\alpha = 0.20$, the maximum cable force would be approximately 18,816 MN

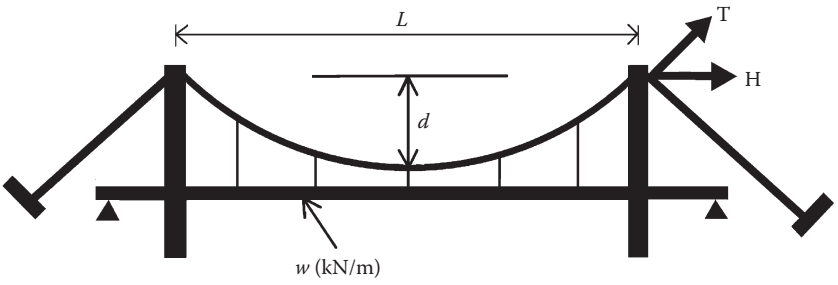

FIGURE 1.12 The main cable of a suspension bridge.

for a span of 8000 m. With an allowable stress of 860 MN/m^2, the cable cross section should be approximately 22 m^2, which should weigh approximately 1750 kN/m including accessories. Thus, our assumption of 8000 m being the maximum possible span of a suspension bridge is acceptable. If two cables are used, the diameter of each cable would be approximately 2.2 m assuming a compact factor of 0.80.

Currently, the world's longest span suspension bridge, Akashi Kaikyo Bridge in Japan, has a 1991-m span. It is <30% of the maximum possible span of 8000 m. The Messina Strait Bridge in Italy, which is under construction, will have a center span of 3300 m; it is still <50% of the 8000 m, so we do not have to worry about span length when we conceptualize a long-span suspension bridge.

1.4.4.2 Arch Bridges

An arch rib (Figure 1.13) is the reverse of a suspension cable. There are three distinct differences between an arch rib and a suspension cable even though they are both "curve" elements. First, the arch is a compression member and requires stiffness to be stable. It cannot use wires; rather, it employs steel plates, so the allowable stress is lower. The allowable stress of the steel plates we commonly use in bridge construction, is less than half of the allowable stress of the wires. As the allowable stress in the arch rib is smaller, the proportion of girder weight and live load will be higher, which may rise to approximately 30% of wc, or $\alpha = 0.3$, where wc denotes the weight of the arch rib for a super-long arch span. Second, because the arch rib is in compression instead of tension, the arch requires additional steel for bracing to ensure its stability. In effect, the effectiveness of the steel is reduced. Third, the arch usually has a rise to span ratio between 1/5 and 1/8, which is more efficient than a suspension cable.

Let us assume the rise to span ratio is 1/5 in a parabolically shaped arch. The maximum force, N_{max}, in the arch will be

$$N_{\max} = 0.76 \times w \times L$$

$$L_{\max} = f\mathrm{a} \times A\mathrm{c} / [0.76 \times (w\mathrm{c} + w\mathrm{g} + w_{\mathrm{LL}})] = f\mathrm{a} \times A\mathrm{c} / [0.76 \times (1+\alpha) \times w\mathrm{c}]$$

If we use steel with a yield strength of 75 ksi (560 MPa), which is currently available, the allowable stress should be approximately 336 MPa. Assuming $\alpha = 0.3$, the maximum span of an arch should be approximately 4200 m.

The current world record span of arch bridges is the 552-m span Ciaotianmen Bridge in Chongqing, China. This span length is only approximately 13% of the maximum possible span of 4200 m.

The above analysis assumes that the cross section of the arch is constant. In reality, the cross section of the arch ribs may vary according to the axial force. As a result, the maximum span could be slightly longer. The maximum force in the arch rib is located at both ends of the arch. It is not much larger than the minimum force located at the crown of the arch rib. The effect is therefore, not significant. In fact, practical limitations in an arch span are a function of their construction. Because the arch rib itself is not

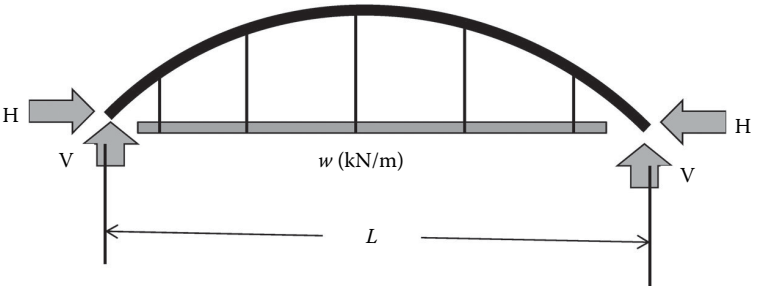

FIGURE 1.13 An arch.

stable until it is completely built, the structure is more difficult to build as the span gets longer. Therefore, even though the arch is very efficient in terms of the quantity of materials, very long-span arch bridges are still too expensive to build. This explains why much longer span arches have not been built to date.

1.4.4.3 Cable-Stayed Bridges

In both the suspension bridge and the arch bridge, the girder is not a main load carrying member of the entire structure. It only carries the local loads and transfers them to the suspension cables or the arch ribs. Therefore, in the above analysis, we only deal with the main load carrying members of the bridge—the suspension cables or the arch ribs. This is not the case with a cable-stayed bridge (Xie et al., 1998). The critical member that determines the maximum possible span is the girder, the compressive stress of which is the limiting factor. Even though the towers, the cables, and the girder are all main load carrying members in a cable-stayed bridge, the allowable stress in the towers and the cables does not pose a limitation to span length. Only the girder does.

The cables in a cable-stayed bridge can be arranged in a harp, fan, star, or a radial pattern (see Figure 1.14a). The harp pattern cable arrangement will result in the highest possible compression force in the girder, which is not suitable for long spans, whereas the radial pattern cable arrangement will leave the lower portion of the tower un-braced. A fan pattern is usually preferred in a long-span cable-stayed bridge because it is a compromise of the other two extremes, with less axial force in the girder while providing cable supports for the tower legs. However, in the present analysis, we will assume a radial pattern just for simplicity.

The maximum axial compression force in the girder, $H_{\max}$ (Figure 1.14b), of a cable-stayed bridge under a uniform load of w (kN/m) is

$$H_{\max} = (w\mathrm{p} + w\mathrm{g}) \times L/2$$

where wg is the structural dead weight of the girder, which is equal to $Ag^{*}\gamma$, where Ag is cross-sectional area of the girder, and γ is the unit weight of the girder including bracings and other structural accessories that are necessary but may not be fully participating in carrying the axial force in the girder, such as the floor beams in a box girder. If we assume this to be 30% in weight, the effective unit weight of the girder would be $1.30 \times 78 = 101.4$ kN/m^3; wp is a summation of live load and superimposed dead load on the deck, such as wearing surface and railings. For this calculation, we assume $w\mathrm{p} = 0.2\ w\mathrm{g}$.

Here, the maximum stress in the cross section is comprised of two components: the axial stress $H_{\max}/Ag$ and a flexural stress due to the local bending moment in the girder. For a very long-span cable-stayed bridge, the stress because of local bending is not significant and may be assumed to be approximately 20% of the allowable stress. Thus, for an allowable stress of 336 MPa, the maximum possible span length would be approximately 5500 m for a cable-stayed bridge.

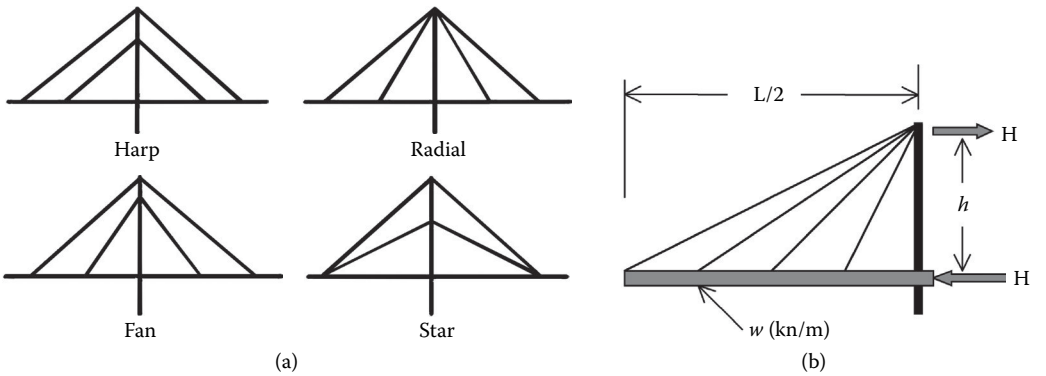

FIGURE 1.14 (a) Cable configurations. (b) Force diagram of a cable-stayed bridge.

Currently there are three super-long cable-stayed bridge spans in the world: the 1104-m span Vladivostok Bridge in Russia, 1088-m span Sutong Bridge in Jiangsu, China, and the 1018-m span Stonecutters Bridge in Hong Kong, China. Those spans are only approximately 20% of the maximum possible span length or less.

Similar to the arch calculation, the above calculation is based on the assumption that the girder cross section is constant along the entire span. In a cable-stayed bridge, the axial force in the girder is close to zero at mid span and increases to its maximum near the tower. Thus, if we increase the girder cross section of the girder as the axial force increases, the allowable axial force in the girder can be increased and, consequently, the maximum span can also be increased. This way, the theoretical maximum span length could be increased by almost 100%, to more than 10,000 m. For the present discussion, however, we will keep the girder constant for simplicity sake.

1.4.4.4 Girder Bridges

There is no clear cut criterion for estimating the maximum span of a girder bridge. Presently, girder bridges are the only bridge type in which some of the longest spans were entirely or partially built with concrete. The current longest span steel girder bridge is the 300-m span Rio Niteroi Bridge in Brazil, which was completed in 1974. Longer spans have not been built since then. The current longest span concrete girder bridge is the 301-m span Stolmasunde Bridge in Norway, completed in 1998. It appears that these are more or less the "reasonable" maximum spans. Currently, the world's longest girder span is the 330-m span Shibanpo Bridge, in Chongqing, China (Tang, 2010). This is a hybrid structure with a 103-m steel box section in the middle of the 330-m span that reduces weight. The rest of the bridge is a prestressed concrete box girder. By itself, pure steel or pure concrete would be difficult to reach this kind of span length. Experience from designing the Shibanpo Bridge (Figure 1.15) indicates that extending the steel portion to 250 m and the concrete portion on each side to approximately 150 m is possible, making a 550-m span a feasible solution. By itself, span length would not be considered a limitation here. Rather, issues of practicality such as weight and fabrication are determining factors. A very long-span concrete girder is excessively heavy and a very long-span steel bridge will require very thick flange plates that are extremely difficult to fabricate. The long-term deformation due to creep and shrinkage of concrete is still hard to predict, making very long-span concrete bridges vulnerable to excessive deflections.

Table 1.1 shows the current world record span and the maximum possible span of each type of bridge as we have explored above. This gives us an idea of how long spans can reach. With improvements in the quality of steel, the allowable stress can be increased in the future and likewise, the maximum possible span length can also increase.

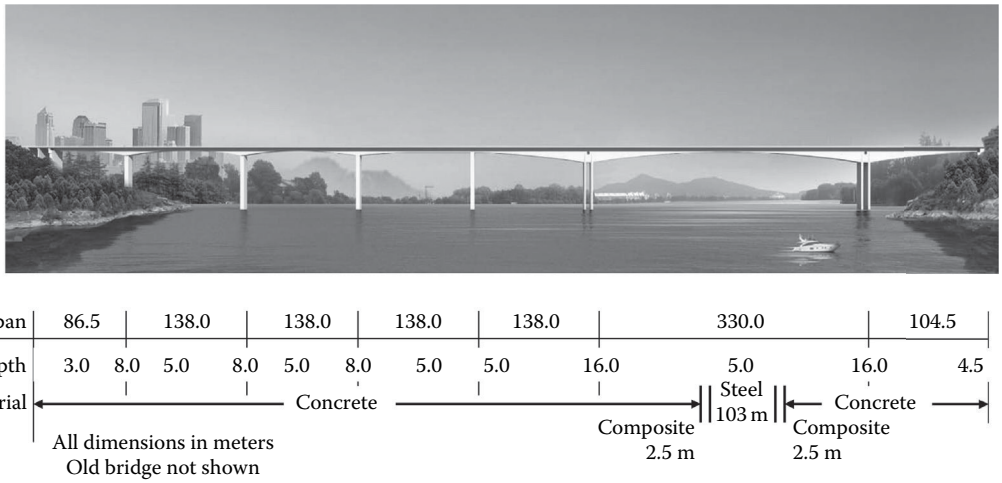

FIGURE 1.15 Shibanpo Bridge—steel and concrete hybrid construction.

TABLE 1.1 World's Longest Bridge Spans

Bridge Type	Bridge Name and Location	Maximum Span, m (ft)	Feasible Span, m (ft)
Girder bridge	Shibanpo Bridge, Chongqing, China	330 (1,083)	550 (1,805)
Arch bridge	Chaotianmen Bridge, Chongqing, China	552 (1,811)	4,200 (13,800)
Cable-stayed bridge	Vladivostok Bridge, Russia	1,104 (3,622)	5,500 (18,045)
Suspension bridge	Akashi Kaikyo Bridge, Japan	1,991 (6,532)	8,000 (26,247)

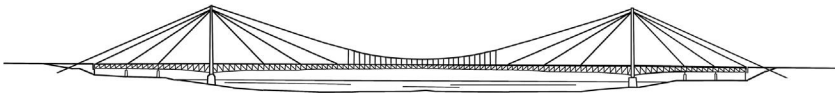

FIGURE 1.16 Dishinger's proposed combination of cable-stayed and suspension bridge.

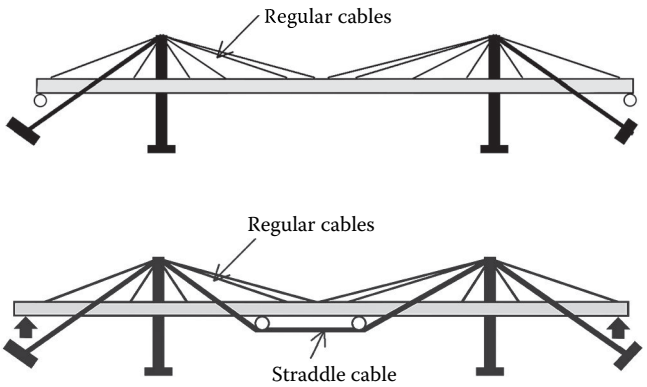

FIGURE 1.17 Cable-stayed bridge with earth-anchored cables.

1.4.4.5 Combination of Suspension and Cable-Stayed Bridges

The above analysis shows that, in a suspension bridge, the maximum span length is limited by the allowable tensile stress in the cables and in a cable-stayed bridge, compressive stress in the girder is the limiting factor. Thus the span length can be increased if we create a hybrid of these two bridge types, which was suggested by F. Dishinger (see Figure 1.16). Another way to increase the maximum span length of a cable-stayed bridge is to use an earth anchor for some of the cables (see Figure 1.17). The earth-anchored cables do not contribute to the maximum compression force in the girder. They are similar to the suspension cables. Consequently, the span length of a cable-stayed bridge can be extended. Since the maximum possible span lengths of the suspension bridge and cable-stayed bridge are way more than we need, these measures that effectively increase the span length are not important for our discussion.

The purpose of determining maximum possible span lengths is to assure ourselves that, technically, span length is not a concern in a conceptual design. Rather, the cost of a bridge increases rapidly with the span length, and we must be careful in selecting span lengths that are much longer than what is actually required. This also serves as a message that striving for world record spans is not necessarily a wise or practical endeavor. It is only a waste of money if the span is made unnecessarily longer than required.

1.4.4.6 Self-Anchored and Earth-Anchored Bridge Structures

A self-anchored bridge is a bridge that does not need additional horizontal anchorages, as in the case of a girder bridge or a cable-stayed bridge. The main cables of a suspension bridge, however, must be anchored in some way at both ends in order to resist the horizontal force from the cables. There are two ways to address the horizontal force problem: either the cables can be anchored to anchor blocks in the ground or the cables can be anchored to the girder at both ends. The latter arrangement creates a self-anchored suspension bridge system.

FIGURE 1.18 New eastern spans of the San Francisco-Oakland Bay Bridge.

Because the cable of a self-anchored suspension bridge is anchored to the girder at both ends and the cable force transferred to the girder, the girder must be constructed first before the cables can be strung, making the construction more difficult. The cables also introduce a large axial force into the bridge girder that, depending on the span length, causes the girder cross section to require strengthening; this, in turn, increases cost. This explains why self-anchored suspension bridge spans tend to be smaller.

The 385-m span of the new San Francisco–Oakland Bay Bridge's Eastern Spans (SFOBB) in California (Figure 1.18) has the world's longest span for self-anchored suspension bridges. This span length is very small compared to the longest earth-anchored suspension bridge, the 1991-m span Akashi Kaikyo Bridge in Japan. But there are situations in which a self-anchored suspension bridge is the proper choice, especially when soil conditions make anchoring a large horizontal force very difficult. This is exactly why the new SFOBB was designed as a self-anchored suspension bridge. Even though one end of the main bridge has good rock foundation, the other end is founded on 100 m of mud, which makes anchoring any cable into the ground practically impossible.

An arch has similar characteristics to those of a suspension bridge. Only in an arch, the horizontal reaction is acting inward toward the bridge, whereas in a suspension bridge the reaction is acting outward, away from the bridge. A tied arch is a type of a self-anchored structure because it does not require the foundation to resist horizontal force. An earth-anchored arch, usually called a true arch, similar to a suspension bridge, should not be built in poor soil conditions. A tied arch is an appropriate solution in that case.

1.5 Design Process

1.5.1 Load Path

Any load acting on the deck must be finally transferred to the foundation. The route that the load is being transferred from the point of application to the foundation is called the load path. For example, in a cable-stayed bridge with floor beams and edge girders, the load of a truck on the deck is transferred from the location directly under the wheels to the deck plate and floor beams to the edge girders, then through the cables to the tower, and further through the tower to the foundation. This is a load path.

In all cases, when the load is transferred from one member to the next member, it must go through a joint, or the linkage, that connects these two members together. These linkages must be properly constructed. Usually the linkages are more vulnerable than the main members. The cable anchorage that links a cable to the tower, for instance, is usually a weaker point on the load path. It is weaker than the cable and it is weaker than the tower. Thus, in a conceptual design, the load path must be very clearly defined, and all linkages must be properly established.

1.5.2 Taking Advantage of Redundancy: Permanent Load Condition

For a long time, and as is still often the case today, a bridge is analyzed as a two-dimensional structure. Thus, it has only to satisfy three basic equations according to applied mechanics:

$$\sum Fx = 0; \sum Fy = 0; \sum M = 0.$$

Any structure that can fully satisfy these three equations is a stable structure. Any structure that cannot fully satisfy these three equations is not structurally stable.

This seemingly simple criterion is a very powerful tool in a conceptual design. Although it is not possible to alter the stress distribution in a statically determinate structure, there are numerous possible patterns of stress distributions in a statically indeterminate structure. This can be illustrated by a simple example of a two-span bridge (see Figure 1.19). If the two spans are not continuous, the bridge consists of two statically determinate, simply supported beams. If it is continuous, it is a one degree statically indeterminate structure, which means there is one unknown when we try to calculate the forces and bending moments in the structure using the three equations above. This allows us to assign any value to the unknown and still satisfy these three equations, thus creating a stable structure.

For simplicity's sake, let us assume the bending moment at the middle support, M_b, is the unknown. If we set M_b to zero, the bending moment in the bridge will be the same as two simply supported beams. However, we can assign any other value to M_b, and for each value we assume, we will get a different bending moment diagram in the bridge. Thus, by varying the value of M_b, we can optimize the efficiency of the bridge girder.

There are many ways to accomplish the desired value of M_b in actual construction. One simple method is to adjust the reaction at the center support. This can be done by using hydraulic jacks. By adjusting this reaction, any value of M_b can be achieved.

A three-span continuous girder is a two degree statically indeterminate structure with two unknowns, the value of which we can assume as we prefer. Accordingly, an *N* degree statically indeterminate structure will have *N* unknowns, the values of which we can also assume. Thus, for the permanent load condition, we should be able to calculate the stress distribution of the entire bridge simply using the three basic equations mentioned in Section 1.5.2. This should be a rather simple calculation even for a highly redundant structure, such as a cable-stayed bridge with many cables.

Obviously, a bridge is not a two-dimensional structure. But often a two-dimensional analysis is sufficient for global design. If a three-dimensional analysis is necessary, we will have six equations to deal with instead of the three basic equations of mechanics above:

$$\sum Fx = 0; \sum Fy = 0; \sum Fz = 0; \sum Mx = 0; \sum My = 0; \sum Mz = 0.$$

However, the principle is the same. We can assign any desirable value to every unknown in the structure, so in the end we can solve the entire force distribution in the structure using these six equations.

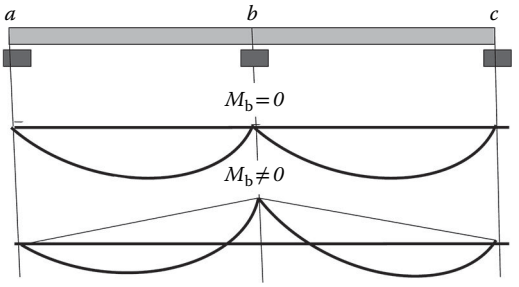

FIGURE 1.19 A two-span bridge.

For most bridges, the permanent load is the dominant load for the structure. The live load usually amounts to <20% of the total load. This means that, for most bridges, a major portion of the stresses in the structure can be calculated in this relatively simple manner as described above in this section .

It is important to note that this calculation does not take into account the stiffness of the bridge, so it can be done before we have determined the size of the members in the bridge.

1.5.3 Prestressing and Load Balancing

Prestressing can introduce various types of artificial forces into a structure. A parabolic prestressing tendon (Figure 1.20) for example, can produce a uniform load opposite to its curvature. A parabolically shaped prestressing tendon is not much different from the main cables of a suspension bridge, although it is of a smaller scale. If properly arranged, we can use prestressing to fully or partially balance the dead weight of a bridge girder. The degree of balancing can be properly controlled to achieve the best result. Other shapes of a prestressing tendon profile other than the parabolic shape can be used as well.

As a matter of fact, the stays of a cable-stayed bridge can be seen as a special case of prestressing. By specifying the force in each cable, we can produce a variety of moment diagrams in the girder.

Certainly, the original idea of prestressing was to precompress the concrete so that it could overcome the tensile stresses it experienced under service loads. The introduction of this idea has allowed us to build many long-span concrete bridges in the last century. However, when we design prestress concrete bridges, we cannot ignore the effects of long-term deformation of the structure due to creep and shrinkage of concrete and the relaxation of steel. For long-span prestressed concrete bridges, these effects can be quite significant.

The application of prestressing is not limited to concrete. We can prestress a steel bridge too. Prestressing introduces artificial forces into the structure, no matter what the structural materials are.

1.5.4 Live Load and Other Loads

Once the bridge is complete and open to traffic, it is not possible to modify the structure. Live loads and other loads are then applied to the structure after the bridge is complete so that the stresses must be calculated based on the actual stiffness of the members. The effects of these loads on the structure must be anticipated to get an estimate of their magnitude in a conceptual design. All these loads are either contained in the specifications or they are to be obtained through site-specific studies. However, as in Section 1.3.1, specifications are not always up to date. There are special circumstances that require special considerations.

1.5.5 Earthquake and Wind

Earthquake and wind represent two different types of loads a bridge has to endure.

Earthquake induces displacements to the bridge foundations. The bridge structure is forced to follow these displacements and thus must deform. The deformation creates stresses in the structure. The seismic displacements are cyclic movements with a finite magnitude. The duration of an earthquake

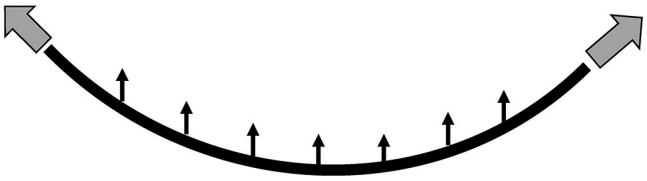

FIGURE 1.20 A prestressing tendon profile.

is relatively short, in most cases <1 minute. Consequently, the respond of the structure to these cyclic movements depends on how well the structure can accommodate these movements. Thus a flexible structure is more suitable for bridges in high seismic areas. Because the foundation displacements are the same, beefing up the structure by increasing the stiffness of the structure does not help, it only attracts higher responses.

Wind, on the contrary, induces aerodynamic forces on the bridge structure. These forces are influenced by the shape of the structural members, such as the cross section of the girder and the towers, as well as their stiffness. In general, increasing the stiffness of the structure will reduce the response of the bridge to aerodynamic forces.

Thus, earthquake and wind impose two opposing requirements on the structural stiffness of a bridge. Luckily, long-span bridges are inherently flexible and less susceptible to earthquake but more to wind, whereas short-span bridges are stiffer structures and more susceptible to earthquake and less to wind. In both cases, ductility is important to assure safety of the structure.

1.6 Conceptualization

As mentioned earlier, the task of a conceptual design of a bridge is to find the best solution for a given set of conditions and the goal is to conceive a bridge that will be safe, functional, and aesthetically pleasing within the given budget. The best solution typically presents itself in two different ways, either by derivation of a new concept based on the given conditions, or by applying an idea that may have long been held in the engineer's mind.

1.6.1 Deriving a New Bridge Concept

Deriving a new bridge concept to fit the given boundary conditions is a very common way to arrive at a new bridge concept. For example, if an 800-m span is required according to the navigational or other criteria, then the structure should be either a cable-stayed bridge or a suspension bridge. If the soil conditions are not good for anchoring large horizontal forces at either end of the bridge, then a cable-stayed bridge is the natural choice. Currently, our experience indicates that a concrete cable-stayed bridge is too heavy and thus not economical for such a span length. The solution would be to choose between steel or composite (steel frame with a concrete deck) girder based on economy and local construction experience. Local construction experience is very important because it directly affects the cost of construction. Then, we have to decide what the cross section of the girder should be. Should it be a box girder or a truss? Should it be streamline shaped, trapezoidal, or rectangular? Throughout the process, aesthetics is a concern. How should the towers look? What material should be used for the towers? What color combination will look best for the structural components? How should the aesthetic lighting be arranged? Also important are such technical issues as aerodynamic effects, seismic movements, foundation settlements, and thermal movements. Due consideration should also be given to durability, maintainability, constructability, life cycle costs, and environmental requirements. Little by little, we make selections among possible options and we finally arrive at a concept that satisfies all of the conditions imposed upon the structure.

The Dagu Bridge in Tianjin, China is a good example of this type of derivative process (Tang, 2012a). The bridge is over the Haihe, a river running diagonally across Tianjin, a city with a population of approximately 11 million. The bridge is located at the center of the city in an area designated for recreation and entertainment. The owner desired a signature bridge that could be symbolic of the city. The river is approximately 96 m wide at the bridge location, so a 106-m span was chosen to keep the piers out of the river. The bridge carries six lanes of traffic and two pedestrian paths with a minimum width of approximately 32 m. The deck connects to local streets in both ends so the elevation is fixed. The navigation clearance of the river thus limits the girder depth to approximately 1.4 m. It is also located in

a high seismic zone and the soil is relatively soft—a condition that precludes an earth-anchored suspension bridge or a true arch bridge. A tied-arch was selected after the owner had excluded girder bridges, suspension bridges, and cable-stayed bridges. From there on, the process of derivation proceeded as follows (Figure 1.21):

- Owing to navigation requirements of the river, the arches must be placed above the deck.
- A regular arch bridge would have two arch ribs, one each side of the deck. They would have been over 32 m apart.
- The girder is <1.4 m deep, which is not sufficient to span a 32 m-wide deck transversely. So, the two arches are moved to the edges of the traffic lanes. They are then about 24 m apart.
- If the two arch ribs are not connected to each other, they would have to be quite bulky in order to avoid lateral buckling. This is aesthetically not acceptable; two vertical arch ribs appear mundane.
- Tying the two arch ribs together with struts can stabilize the arch ribs so they can be relatively slender. But this would look too messy for a small span. It is aesthetically not acceptable.
- For the 106-m span, a basket-handle configuration would appear too flat.
- In the end, a three-dimensional structural system is used by having two planes of hangers for each arch rib. This solves the lateral buckling problem. Thus, the ribs can be made very slender indeed.
- With two planes of cables stabilizing each arch rib, it is possible to tilt the arch ribs outwards so passengers on the bridge deck will have a very open view.
- The surrounding landscape is asymmetrical; the height of one arch is made higher than the other to mimic the asymmetrical landscape and make the bridge look more intriguing. The taller arch has a steeper inclination so that it does not lean too far outward.
- And, this becomes the Dagu Bridge (see Figure 1.22).

It is evident that the process was partially driven by the constraints placed upon the bridge. But along the way, aesthetics were properly considered. This was a step-by-step process in which the final unique concept was derived from a simple preference by the owner for an arch bridge.

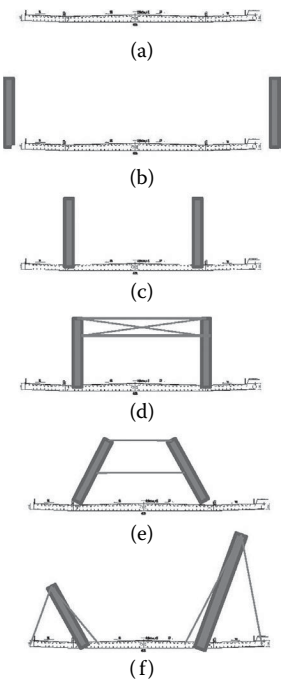

FIGURE 1.21 Development of the Dagu Bridge concept.

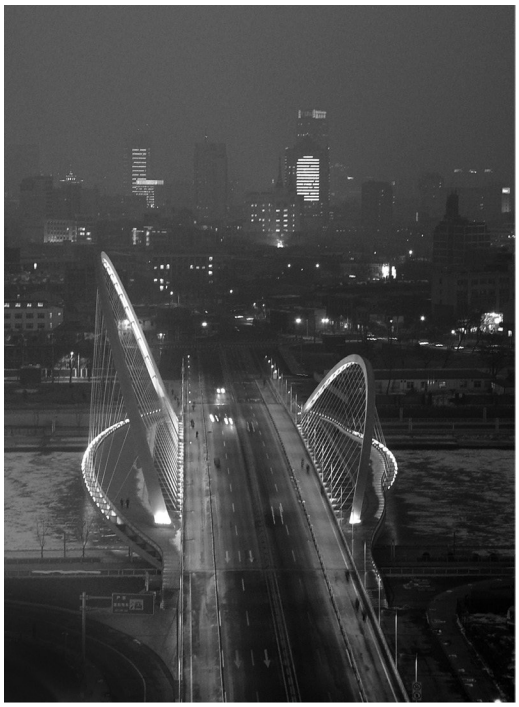

FIGURE 1.22 The Dagu Bridge in Tianjin, China.

As well, during the conceptual design stage we considered construction methods. The river was not navigable at the time of construction so false work was used to build the deck girder. The girder sections were welded together while being supported by piles. Another set of false work was set up on the completed deck to support the arch ribs. This construction method is straight forward and economical. Otherwise, it would have been difficult to build the inclined arch ribs.

1.6.2 Application of a Preexisting Concept

As engineers, we may have in our minds any number of bridge concepts we have found interesting but have not been able to find an opportunity to utilize. Or, it may be an existing bridge that, by making certain modifications, would be excellent structures for a certain landscape. Or, still yet, it may be an innovative concept that has been a long held idea. When the opportunity avails itself, it just suddenly clicks in our mind that this is the right choice. Simply put, this is not really developing a new bridge concept, but rather finding a suitable opportunity to apply an existing bridge concept. Minor modifications to the idea may be needed because it is unlikely to find a situation where everything falls exactly into place. But minor modifications are comparably insignificant.

The concept of the Twin River Bridges, a combined name for the Dongshuimen Bridge over the Yangtze River and the Qianshimen Bridge over the Jialing River in Chongqing, China, is a good example of this (see Figure 1.23). The configuration of the towers is very "Chinese" in the sense that it looks like the shuttle of an ancient Chinese weaving machine. To obtain a better visual effect, at the top of the towers is a gap between the two halves of the tower legs with only anchoring plates connecting them together, thus allowing sunlight to shine through. In China, we always wanted to design a more distinctive bridge tower. For a long period we worked to develop and to perfect such a tower shape. But a majority of Chinese bridges are six-lane bridges with pedestrian paths that require a deck width of approximately 34 m. Such a tower shape is not suitable for these wide bridge girders because it would

FIGURE 1.23 The Twin River Bridge—Dongshuimen Bridge and Qianshimen Bridge.

look too fat and loose its gracefulness. The Twin River Bridges have four lanes on the upper deck and two transit tracks on the lower deck. The deep girder and the narrower deck are perfect for such a tower shape. So, we have been waiting for the opportunity to apply this concept for a long time.

Obviously, this tower shape is more expensive because the curved formwork is more difficult to build. But, because these two bridges are very visibly located near the juncture of the two rivers that surround the city, like the front gate of the city, the owner placed a high emphasis on aesthetics for this project and a slightly higher cost was not a primary concern. The transit on the lower level has very stringent restrictions on deformations. The 13-m-deep truss girder is a good solution. It not only provides the required stiffness, but the truss structure with large openings will also offer transit passengers an excellent view of the river valleys. Because the bridge is relatively narrow, a single plane of cables was chosen to make the bridge look more transparent so as not to disturb the view of the city. In addition, the bridge was designed according to the concept of a cable-supported girder bridge. In this way, fewer cables were required, which rendered the bridge even more transparent. To simplify the formwork, the curvature of the exterior surface of the tower shafts was made constant for the entire height of the tower. The two bridges have a total of three towers. The shape of all three towers is the same except that the bottom portion of tower shafts are longer in some cases because the ground level varies at different towers. This makes the design of the formwork more efficient.

This is a rare instance in which a pre-existing idea was applied to a new bridge.

The two examples above exemplify two different approaches to the concept development for a given bridge. However, in many cases, the process is more of a combination of both approaches, like modifying an existing concept to fit the local conditions, or changing a part of a bridge to improve on economy and aesthetics.

1.7 Aesthetics

A bridge can be charming and graceful; a bridge can also be spectacular and emit excitement. Regardless, a bridge must be attractive. Aesthetics are a basic requirement of bridge design.

Engineers are used to following rules: rules in books, in specifications, or those rules proposed by other engineers. When it comes to aesthetics, there are no rules. Three thousand years ago, the Greeks paid an extraordinary amount of attention to aesthetics. They were rigorous and meticulous in their attention to the structural details of their buildings. The Parthenon, for example, has been recognized by many as the most perfect building in world history. Careful investigation indicated that every detail in the building was meticulously refined to create a specific visual impression to the human eye. For example, all horizontal lines are curved upwards to make them look horizontal. The spacing between columns is not the same, so that it appears the same. The diameter of the columns is also not uniform in order to make it look uniform. But, these are details, not rules of aesthetics.

Many scholars have tried to establish rules for structural beauty, but no one has ever succeeded. For instance, the "golden section" states that a rectangle that has a proportion of the two sides of Φ (= 1.6318)

is the best-looking rectangle. The golden section has been studied by many scholars for centuries. But it is debatable that such a rectangle looks better than a square under all circumstances.

In general, aesthetics is about proportion, balance, and harmony. The Italian Renaissance architect, Alberti, defined beauty as "a harmony of all the parts." In perceiving an object, we do not use logical derivations to determine whether it is beautiful or not. Rather, our reaction is more emotive. A beautiful bridge can be dramatic and daring. It can also be graceful and poetic. In sum, the fundamental idea is to elicit an emotional response from the audience and to get a visceral response from them. How we achieve this is an art in and of itself.

Generally, a bridge should be natural, simple, original, and harmonious with its surroundings (Tang, 2006a). A bridge can be a highly visible object in a city. It should look natural and fit well into its surroundings. In general, it should also be simple and not made to look superficial. A structure looks more natural if it can immediately convey its function and use to the general public.

Uniqueness is an important element in any piece of art. Likewise, a bridge should be unique. In other words, no two bridges should be the same. Each structure has its own particular requirements and site-specific features. All of these factors should be taken into consideration in order for the bridge to be original, and to have its own style, its own character and ultimately, its own design. Just like a painting, the original is the most valuable. So too, with bridge design, its uniqueness determines its subjective value.

Nature endorses simplicity. Even the most important equations of nature are extremely simple, like $F = ma$, or $E = mc^2$. The human mind, which is a product of nature, is accustomed to simplicity. Time and again, the simplest bridge configuration has been proven to be the best-looking and most popular solution. It has been said that to arrive at the most beautiful structure, the best method is to remove any and all elements that would not affect its function—this is a process of simplification! Obviously, this requires experience and a good understanding of structure and aesthetics.

In addition, a well-designed, aesthetically pleasing bridge is usually more economical because it is more natural and simple and follows nature's intentions. But, sometimes a more beautiful bridge may also be more expensive. Then, we may have to evaluate the benefit of beauty versus cost. Is it worthwhile to spend that extra money? Obviously, again, there are no rules to follow. It depends on the circumstances. Besides the functional value of carrying traffic, a bridge can also have symbolic meaning and aesthetic properties. If it is determined that the bridge should be a signature structure, for instance, then the additional cost may be well worthwhile.

Actually, we make these kinds of decisions all the time. Buying a house or clothes requires similar decision making. The majority of us do not live in the cheapest or the most expensive house, but rather, we live in a house that is both affordable and suits our needs and our aesthetic taste. In essence, we balance cost and taste to arrive at an appropriate choice.

Keep in mind, too, that a bridge, once complete, will be on prominent display for hundreds of years. This creates a clear need for the community to build an aesthetically pleasing bridge. A community cannot escape the negative effects of a poor-looking bridge. Although no bridge has ever been built solely with aesthetics in mind, nonetheless, a bridge can be an integral part of a city. And no beautiful city can accommodate an ugly bridge!

Developing the most aesthetically pleasing bridge requires significant time and effort. But once this becomes routine in design, this effort is not as taxing. It will always be the responsibility of the bridge engineer to pay attention to aesthetics. A bad-looking bridge can be akin to a kind of pollution to a community. Needless to say, this kind of pollution cannot be eradicated easily or quickly.

Aesthetic Lighting: Employing aesthetic lighting enhances a bridge especially at night. There are many ways to light a bridge. Most suspension bridges have lace lighting, where a series of lights are attached to the main cables. This type of lighting is convenient for a suspension bridge because the main cables are large enough to walk on, making maintenance of the lights relatively simple. For a cable-stayed bridge, the cables are too small so it is more convenient to install lights on the bridge deck. Figure 1.24 shows various schemes for aesthetic lighting.

FIGURE 1.24 Examples of aesthetic lighting.

Decorations: Decoration is like cosmetics. A real beauty does not need cosmetics. The most successful bridge is one that fully expresses itself through its structural form. Touching up small details, like adding covers to enclose cable anchorages is not decoration. Installing statues and flowerpots is decoration.

Most bridges are large structures. In such cases, the magnitude and the form of the bridge itself is so powerful that decoration only makes it look less impressive. However, if a bridge is made to be a symbol, to convey a certain meaning, or to commemorate an event, decorations may be appropriate.

In general, bridges in cities tend to be smaller in size and are more suited for decorating, which can create more harmony with the bridge's surroundings. A bridge in a natural setting should strive to maintain its connection to nature and be simple so decoration is usually not desirable.

1.8 Innovation

1.8.1 Experience and Precedents

Decision-making is derived from two information sources: the first is experience and prior knowledge and the second is actual analysis. Experience comes from precedents. Knowing what has been done before and its consequence gives an engineer a foundation for understanding what is possible in bridge design. This is important because we cannot analyze everything every time we design a bridge, especially at the conceptual design stage. This foundational knowledge can only come from direct or indirect experience, that is, either from something the engineer has done before or something the engineer knows that someone else has successfully done before. There are ample examples of successful bridge details available for the engineer to reference to. But in the case where the engineer deviates from existing examples, then an analysis is required to ascertain the concept's validity. If the deviation can be supported by engineering logic, then analysis is not required. Engineering logic is comprised of rules based on an accumulation of successful precedents. If the deviation cannot be supported by logic, then an analysis will be needed to ascertain its validity.

The drawback of heavily relying on precedents is that it can be detrimental to innovation. At worst, duplicating a precedent is, in essence, just copying an old idea.

1.8.2 Innovations

Engineering is an art, not a science! Science deals with all kinds of truth. Truth is unique and preexisting! Scientists only discover them. They can neither create truth nor modify the truth they discover. Therefore, there is no good science or bad science. However, engineers create things! Bridge engineers

build bridges where there was no bridge before. Through the course of designing a bridge, the engineer has to study many alternatives and make many decisions. Making decisions is an artistic process. As with any type of art, engineering can be good or bad as perceived by the public and it is subject to critique. But, because engineering is a creative undertaking, innovation should be inherent in the design.

For bridge engineers, the conceptual design stage is our first and best opportunity for innovation! This is the time when an engineer can think out-of-the-box to introduce new ideas!

Engineering is based on an accumulation of experience. Not everything in engineering is explainable by science. Most formulas in engineering specifications do not originate from scientific derivation but from experience. If no precedent exists, engineers perform laboratory experiments to confirm its validity. Thus, in developing bridge concepts, the engineer should not be limited by what has been done before. Imagination has no limits!

Innovation can be described as finding answers to three questions: "Why?," "Why not?," and "What if?" (Tang, 2006b). These are the three "Ws" of innovation! We ask why to challenge the status quo! Previously, we estimated that the maximum possible span of a suspension bridge is about 8000 m. If we accepted this as common wisdom, we would never venture further. But if we ask why, we would discover that the allowable stress is the limiting factor in this case. Understanding the "why" of things helps us to find solutions to problems and push the boundaries of what is possible. In this instance, finding a material that has a higher allowable stress can increase the maximum span length. This is where the question, "Why not?" comes in. Why not use a higher strength material? The question, "Why not?" allows us to introduce our new idea. Now, to assure that the new idea is safe and appropriate, we must ask many "what if" questions. In a case where we have used a higher strength wire, we must ask, "What if the increased strength may increase the brittleness of the wires?," "What if the higher strength steel is more susceptible to hydrogen embrittlement or other problems?," and so on until we are satisfied that the new idea is acceptable and safe.

During the conceptual design stage of the new SFOBB, the owner desired a single-pole tower configuration, which was deemed unacceptable by earthquake engineers for a bridge located in such a high seismic zone (Tang et al., 2000). Our question, "Why?" lets us understand that the reason this was unacceptable was because a single-pole tower is nonredundant, which is inappropriate for bridges in high seismic areas. The prevailing choice would have been a portal type tower with cross beams (Figure 1.25a) so that during an earthquake, plastic hinges can form in the cross beams, leaving the columns in an elastic state so the tower does not destabilize. We then ask, "Why can't we make the portal frame narrower and place the bridge deck outside of the tower shafts?" The final configuration, as shown in Figure 1.25b, is a compressed portal frame with short cross beams connecting the vertical columns. The final tower is even better than the conventional portal frame because it allows installation of any number of cross beams because they do not interfere with the traffic on the bridge deck. Now comes the third group of questions, the "What if's:" "*What* would happen *if* plastic hinges do not form in the cross beams during an earthquake? *What* would happen *if* the plastic hinges do not deform enough? *What*

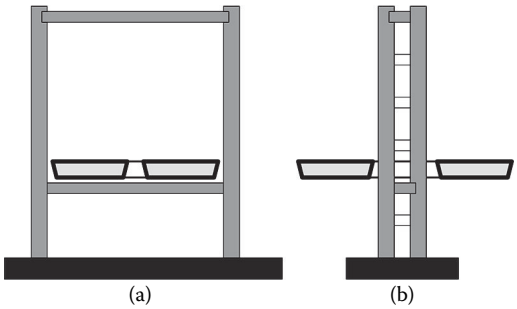

FIGURE 1.25 Development of the SFOBB tower.

would happen *if* the movement because of an earthquake was higher than anticipated?," and so on. To answer these questions, we have also conducted experiments to ascertain that plastic hinges will work. The final configuration of the bridge tower represents an innovative solution to a seemingly impossible-to-solve problem (see Figure 1.26). This new concept will be very useful for future bridges located in high seismic areas.

Innovation can break grounds and stretch the horizons of bridge engineering. In the case of the new SFOBB, following traditional thinking would have led us to design a portal frame tower. It was the nontraditional thinking, the asking of "why, why not, and what if," that led us to discover the new tower configuration. The concept of a "cable-supported girder bridge" is another example of nontraditional thinking. In the traditional design of a cable-stayed bridge, an arch bridge, or a suspension bridge, the deck girder is typically assumed as a secondary load carrying member and it is not expected to assist in carrying global bending moment. This makes sense when the bridge span is long and the girder is weak. But for some medium to short bridges, the girder does have a useful capacity to carry external loads. The cable-supported girder bridge reverses the roles and assigns the girder the role of being the primary load carrying member and the cable system the role of being the secondary load carrying member of the bridge. The cable system of a cable-supported girder bridge is only designed to supplement the girder capacity in carrying the loads. This gives us two advantages in the design: first, the capacity of both the girder and the cable system is fully utilized, and second, the cable system can be much smaller and therefore more economical. Figure 1.27 shows various alternatives of cable-supported girder bridges.

Another example of nontraditional thinking is the evolution arch bridges described in (Tang, 2012b). Traditional arch bridges include the through arch bridge, deck arch bridge, and half-through arch bridge. But an arch can be employed in very different ways in bridges. Figure 1.28 shows the derivation of five different arch configurations in bridge structures, beginning with a traditional basket-handle arch bridge and then evolving into very different forms thereafter. For the Caiyuanba Bridge, the arch ribs of the basket-handle arch incline inward so that the bracing between the two arch ribs are shorter and the two arch ribs stabilize each other. For the Dagu Bridge, the two arch ribs are pushed outwards to offer motorists an open view while driving on the bridge. Because the arch ribs have no struts connecting to each other, a three-dimensional hanger arrangement acts to stabilize the arch ribs. The Huihai Road Bridge concept was evolved by pushing these two outward inclining arch ribs to the center line of the bridge, while keeping the three-dimensional hanger configuration. The next variation is to twist the two arch ribs in that same design 90° to get the Sanhao Bridge configuration. The Taijiang Bridge

FIGURE 1.26 The new SFOBB tower configuration.

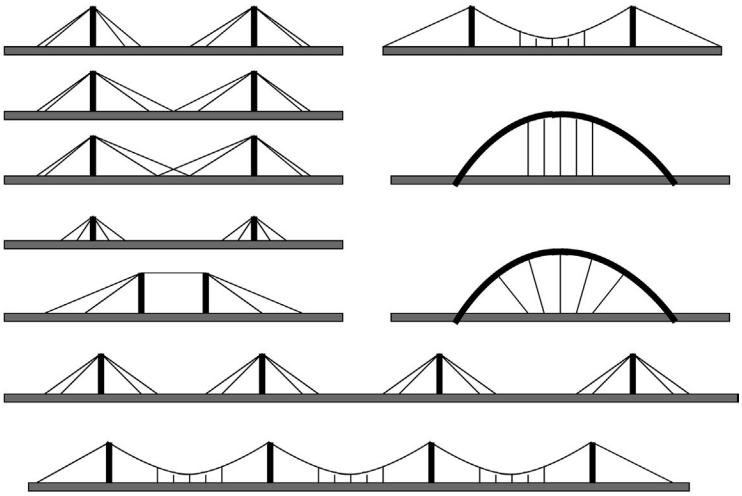

FIGURE 1.27 Various alternatives of a cable-supported girder bridge.

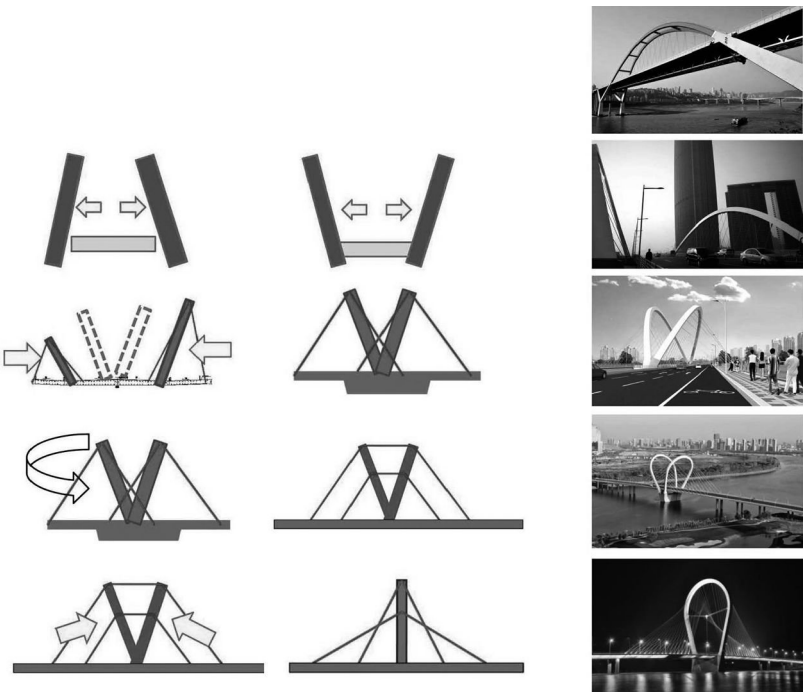

FIGURE 1.28 Arch bridges.

concept evolved when we rotated the two arch ribs to a vertical position until they merged together into one single-arch tower.

Certainly, each of these five bridge configurations has its own distinct characteristics and each requires special attention to assure its structural integrity. But these examples show that there are many ways to conceptualize a bridge—only our imaginations can limit us!

1.9 Summary

Conceptual design is where bridges are conceived. A good conceptual design must properly consider what may be required in the preliminary, detailed, and construction design stage; it must assure that the proposed concept is safe, functional, economical, and pleasing to the eye. Because every bridge is unique, the conceptual design must begin by being unique. The conceptual design is our best opportunity for innovative thinking and this is where new ideas are conceived!

Obviously, a bridge concept can be very distinguished or very mundane depending on how much effort the engineer is willing to spend in the pursuit of a better solution. Take the conceptualization of the Dagu Bridge (Figure 1.21) as an example. The process could have stopped at stage c, which had provided a workable solution for the bridge; or at any stage thereafter because each of them would be a workable solution for the bridge. Only through extra effort was it possible to arrive at the more distinctive final concept that was built.

A bridge is built for the public; we must be conservative in the design to assure safety and functionality. But during conceptualization, we must strive to be as innovative as possible. Only by pushing the boundaries of what we perceive as possible can we extend the horizons of engineering and thus improve our civilization. "Conservative Innovation" is the path to follow in the conceptual design of a bridge!

References

AASHTO. 2012. *AASHTO LRFD Bridge Design Specifications,* Customary U.S. Units. 2012. American Association of State Highway and Transportation Officials, Washington, DC.

Lin, T. Y. and Burns, N. H. 1981. *The Design of Prestressed Concrete Structures*. Wiley, New York, NY.

Nagai, M., Fujino, Y., Yamaguchi, H., and Iwasaki, E. 2004. Feasibility of a 1,400 m span steel cable-stayed bridge. *Journal of Bridge Engineering* 9(5), 444–452.

Tang, M. C., Manzanarez, R., Nader, M., Abbas, S., and Baker, G. 2000. Replacing the East Bay Bridge. *Civil Engineering Magazine of the American Society of Civil Engineers* 70(9), 38–43.

Tang, M. C. 2006a. *Bridge Forms and Aesthetics*. In: Proceedings of the Third International Conference on Bridge Maintenance, Safety and Management, July 16–19, Porto, Portugal, International Association for Bridge Maintenance and Safety.

Tang, M. C. 2006b. "*Why, Why Not, What…if*". Keynote speech, In: Proceedings of the International Conference on Bridge Engineering—Challenges in the 21st Century, November 1–3, Hong Kong.

Tang, M. C. 2007. Rethinking bridge design—A new configuration. *Civil Engineering Magazine of the American Society of Civil Engineers* 77(7), 28–45.

Tang, M. C. 2010. The New Shibanpo Bridge, Chongqing, China. *Structural Engineering International* 20(2), 157–160.

Tang, M. C. 2012a. *Bridge Thoughts*. Tsinghua University Press, Beijing, China (in Chinese).

Tang, M. C. 2012b. *The Art of Arches*. In: Conference of the International Association of Bridge Maintenance and Safety, July 8–12, Stresa, Lake Maggiore, Italy.

Xiang, H. F. 2011. *Conceptual Design of Bridges*. China Communications Press, Beijing, China (in Chinese).

Xie, X., Nagai, M., and Yamaguchi, H. 1998. Ultimate strength analysis of long-span cable-stayed bridge. *Journal of Structural Mechanics and Earthquake Engineering*, JSCE, 598(I-44), 171–181, (in Japanese).

2

Aesthetics: Basics*

Fritz Leonhardt
Stuttgart University

2.1 Introduction

Aesthetics falls within the scope of philosophy, physiology, and psychology. How then, you may ask, can I as an engineer presume to express an opinion on aesthetics, an opinion that will seem to experts to be that of a layman? Nevertheless, I am going to try.

For over 50 years I have been concerned with, and have read a great deal about, questions concerning the aesthetic design of building projects and judgment of the aesthetic qualities of works in areas of the performing arts. I have been disappointed by all but a few philosophical treatises on aesthetics. I find the mental acrobatics of many philosophers—whether, for example, existence is the existence of existing—difficult to follow. Philosophy is the love of truth, but truth is elusive and hard to pin down. Books by great building masters are full of observations and considerations from which we can learn in the same way that we study modern natural scientists.

My ideas on aesthetics are based largely on my own observations, the results of years of questioning—why do we find this beautiful or that ugly?—and on innumerable discussions with architects who also were not content with the slogans and "isms" of the times, but tried to think critically and logically.

The question of aesthetics cannot be understood purely by critical reasoning. It reaches to emotion, where logic and rationality lose their precision. Undaunted, I will personally address these questions, so pertinent to all of us, as rationally as possible. I will confine myself to the aesthetics of building works,

* Much of the material of this chapter was taken from Leonhardt, F., *Bridges—Aesthetics and Design*, Chapter 2: The basics of aesthetics, Deutsche Verlags-Anstalt, Stuttgart, Germany, 1984, with permission.

of man-made objects, although from time to time a glance at the beauty of nature as created by God may help us reinforce our findings.

I would beg you to pardon the deficiencies that have arisen because of my outside position as a layman. This work is intended to encourage people to study questions of aesthetics using the methods of the natural scientist (observation, experiment, analysis, hypothesis, and theory) and to restore the respect and value that it enjoyed in many cultures.

2.2 Terms

The Greek word *aisthetike* means the science of sensory perception and early on was attributed to the perception of the beautiful. Here we will define it as follows:

Aesthetics: The science or study of the quality of beauty an object possesses, and communicates to our perceptions through our senses (expression and impression according to Klages [1]).

Aesthetic: In relation to the qualities of beauty or its effects, aesthetic is not immediately beautiful but includes the possibility of nonbeauty or ugliness. Aesthetic is not limited to *forms*, but includes surroundings, light, shadows, and color.

2.3 Do Objects Have Aesthetic Qualities?

Two different opinions were expressed in old philosophical studies of aesthetics:

1. Beauty is not a quality of the objects themselves, but exists only in the imagination of the observer and is dependent on the observer's experience [2]. Smith said in his "Plea for Aesthetics," [3] "Aesthetic value is not an inborn quality of things, but something lent by the mind of the observer, an interpretation by understanding and feeling." But how can we interpret what does not exist? Some philosophers went so far as questioning the existence of objects at all, saying they are only vibrating atoms and everything we perceive is subjective and only pictured by our sensory organs. This begs the question, then, is it possible to picture the forms and colors of objects on film using a camera? These machines definitely have no human sensory organs.
2. The second school of thought maintains that objects have qualities of beauty. Kant [4] in his *Critique of Pure Reason* said, "Beauty is what is generally and without definition, pleasing." It is not immediately clear what is meant by "without definition," perhaps without explaining and grasping the qualities of beauty consciously. What is "generally pleasing" must mean that the majority of observers "like" it. Paul [5] expressed similar thoughts in his *Vorschule der Aesthetik* and remarked that Kant's constraint "without definition" is unnecessary. Thomas Aquinas (1225–1274) said, "A thing is beautiful if it pleases when observed. Beauty consists of completeness, in suitable proportions, and in the luster of colors." At another time, Kant said that objects may arouse pleasure independent of their purpose or usefulness. He discussed "disinterested pleasure," a pleasure free from any interest in objects: "When perceiving beauty, I have no interest in the existence of the object." This emphasizes the subjective aspect of aesthetic perception, but nonetheless bases the origin of beauty in the object.

Is one right? Most would side with Kant and grant that all objects have aesthetic qualities, whether we perceive them or not. Aesthetic value is transmitted by the object as a message or simulation and its power to ourselves depends on how well we are tuned for reception. This example drawn from modern technology should be seen only as an aid to understanding. If a person is receptive to transmissions of beauty, it then depends very largely on how sensitive and developed are the person's senses for aesthetic messages, whether the person has any feeling for quality at all. We will look at this question more closely in Section 2.4.

On the other hand, Schmitz, in his *Neue Phänomenologie* [6], sees in this simple approach "one of the worst original sins in the theory of cognition." This *physiologism* limits the information for human

perception to messages that reach the sensory organs and the brain in the form of physical signals and are therefore metaphysically raised to consciousness in a strangely transformed shape. We must see the relationships between the object and circumstances, associations, and situations. More important is the situation and observer's background and experience. The observer is "affectively influenced," [6] that is, the effect depends on the health of the observer's senses, mood, and mental condition; the observer will have different perceptions when sad or happy. The observer's background experience arouses concepts and facts for which the observer is prepared subconsciously or that are suggested by the situation. Such "protensions" [6] influence the effects of the object perceived, and include prejudices that are held by most people and that are often a strong and permanent hindrance to objective cognition and judgment. However, none of this phenomenology denies the existence of the aesthetic qualities of objects.

Aesthetic quality is not limited to any particular fixed value by the characteristics of the object, but varies within a range of values dependent on a variety of characteristics of the observer. Judgment occurs in a process of communication. Bahrdt [7], the sociologist, said, "As a rule aesthetic judgment takes place in a context of social situations in which the observers are currently operating. The observers may be a group, a public audience, or individuals who may be part of a community or public. The situation can arise at work together, during leisure time, or during a secluded break from the rush of daily life. In each of these different situations the observer has a different perspective and interpretation, and thus a different aesthetic experience [impression]."

Aesthetic characteristics are expressed not only by form, color, light, and shadow of the object, but also by the immediate surroundings of the object and thus are dependent on object environment. This fact is well known to photographers who can make an object appear much more beautiful by careful choice of light and backdrop. Often a photograph of a work of art radiates a stronger aesthetic message than the object itself (if badly exhibited) in a gallery. With buildings, the effect is very dependent on the weather, position of the sun, and on the foreground and background. It remains undisputed that there is an infinite number and variety of objects (which all normal healthy human beings find beautiful). Nature's beauty is a most powerful source of health for humans, giving credence to the suggestion that we have an inborn aesthetic sense.

The existence of aesthetic qualities in buildings is clearly demonstrated by the fact that there are many buildings, groups of buildings, or civic areas that are so beautifully designed that they have been admired by multitudes of people for centuries, and that today, despite our artless, materialistic attitudes to life, are still visited by thousands and still radiate vital power. We speak of classical beauty. All cultures have such works, and people go to great lengths to preserve and protect them; substantial assistance has come from all over the world to help preserve Venice, whose enchanting beauty is so varied and persuasive.

We can also give negative evidence for the existence of aesthetic qualities in objects in our man-made environment. Think of the ugliness of city slums, or depressing monotonous apartment blocks, or huge blocky concrete structures. These products of the "brutalist" school have provoked waves of protest. This affront to our senses prompted the Swiss architect Rolf Keller to write his widely read book *Bauen als Umweltzerstörung* [8].

All these observations and experiences point to the conclusion that objects have aesthetic qualities. We must now look at the question of how humans receive and process these aesthetic messages.

2.4 How Do Humans Perceive Aesthetic Values?

Humans as the receivers of aesthetic messages use all of their senses: they see with their eyes, hear with their ears, feel by touch, and perceive temperature and radiation by sensors distributed in the body, sensors for which there is no one name. Our sensory organs receive different waveforms, wavelengths, and intensities. We read shapes by light rays, whose wavelengths give us information about the colors of objects at the same time. The wavelength of visible light ranges from 400 μm (violet) to 700 μm (red) (1 μm = 1 millionth of 1 mm). Our ears can hear frequencies from approximately 2 to 20,000 Hz.

The signals received are transmitted to the brain and there the aesthetic reaction occurs—satisfaction, pleasure, enjoyment, disapproval, or disgust. In modern Gestalt psychology, Arnheim [9] explained the processes of the brain as the creation of electrochemical charge fields that are topologically similar to the observed object. If such a field is in equilibrium, the observer feels aesthetic satisfaction; in other cases the observer may feel discomfort or even pain. Much research needs to be done to verify such explanations of brain functions, but they do seem plausible. However, for most of us we do not need to know brain functions exactly.

During the course of evolution, which we assume to have taken many millions of years, the eye and ear have developed into refined sensory organs with varied reactions to different kinds of waveforms. Special tone sequences can stimulate so much pleasure that we like to hear them—they are consonant or in harmony with one another. If, however, the waveforms have no common nodes (Figure 2.1) the result will be dissonance or beats, which can be painful to our ear. Dissonances are often used in music to create excitement or tension.

The positive or negative effects are a result of not only the charge fields in the brain, but also the anatomy of our ear, a complex structure of drum oscular bones, spiral cochlea, and basilar membrane. Whether we find tones pleasant or uncomfortable would seem to be physiological and thus genetically conditioned. There are naturally individual differences in the sense of hearing, differences that occur in all areas and in all forms of plant and animal life.

There are also pleasant and painful messages for the eye. The effects are partly dependent on the condition of the eye, as, for example, when we emerge from a dark room into light. Color effects of a physiological nature were described in much detail by Goethe in his color theory [10]. In the following, we will discuss the effects of physical colors on the rested, healthy eye, and will not address color effects caused by the refraction or reflection of light.

Some bright chemical colors cause painful reactions, but most colors occurring naturally seem pleasant or beautiful. Again, the cause lies in waves. The monotonous waves of pure spectral colors have a weak effect. The eye reacts more favorably to superimposed waves or to the interaction of two separate colors, especially complementary colors.

We feel that such combinations of complementary colors are harmonious, and speak of "color harmony." Great painters have given us many examples of color harmony, such as the blue and yellow in the coat of Leonardo da Vinci's *Madonna of the Grotto*.

We all know that colors can have different psychological effects: red spurs aggression; green and blue have a calming effect. There are whole books devoted to color psychology and its influence on human moods and attitudes.

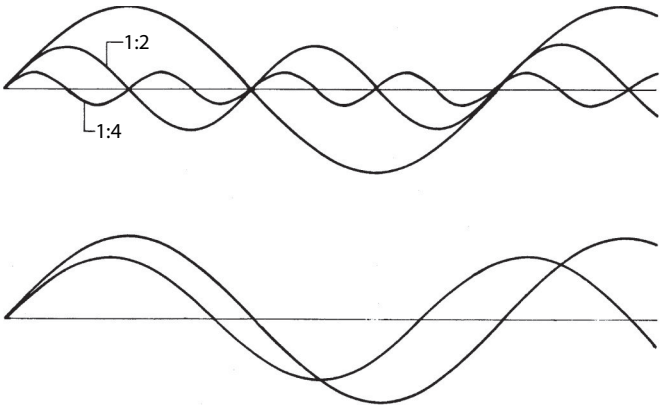

FIGURE 2.1 Wave diagrams for consonant and dissonant tones.

We can assume that the eye's aesthetic judgment is also physiologically and genetically controlled, and that harmonic waveforms are perceived as more pleasant than dissonant ones. Our eyes sense not only color but can form images of the three dimensional, spatial characteristics of objects, which is vital for judging the aesthetic effects of buildings. We react primarily to proportions of objects, to the relationships between width and length and between width and height, or between these dimensions and depth in space. The objects can have unbroken surfaces or be articulated. Illumination gives rise to interplay of light and shadow, whose proportions are also important.

Here the question of whether there are genetic reasons for perceiving certain proportions as beautiful or whether upbringing, education, or habit play a role cannot be answered as easily as for those of acoustic tone and color. Let us first look at the role proportions play.

2.5 Cultural Role of Proportions

Proportions exist not only between geometric lengths, but also between the frequencies of musical tones and colors. Interplay between harmonic proportions in music, color, and geometric dimensions was discovered early, and has preoccupied the thinkers of many different cultural eras.

Pythagoras of Samos, a Greek philosopher (571–497 BC) noted that proportion between small whole numbers (1:2, 2:3, 3:4, or 4:3, and 3:2) has a pleasing effect for tones and lengths. He demonstrated this with the monochord, a stretched string whose length he divided into equal sections, comparing the tones generated by the portions of the string at either side of an intermediate support or with the open tone [11–13].

In music these harmonic or consonant tone intervals are well known, for example,

String Length	Frequencies	
1:2	2:1	Octave
2:3	3:2	Fifth
3:4	4:3	Fourth
4:5	5:4	Major third

The more the harmonies of two tones agree, the better their consonance; the nodes of the harmonies are congruent with the nodes of the basic tones. Later, different tone scales were developed to appeal to our feelings in a different way depending on the degree of consonance of the intervals; think of major and minor keys with their different emotional effects.

A correspondence between harmonic proportions in music and good geometric proportions in architecture was suggested and studied at an early stage. In Greek temples many proportions corresponding with Pythagoras's musical intervals can be identified. Kayser [14] has recorded these relationships for the Poseidon temple of Paestum.

H. Kayser (1891–1964) dedicated his working life to researching the "harmony of the world" For him, the heart of the Pythagorean approach is the coupling of the tone of the monochord string with the lengths of the string sections, which relates the qualitative (tone perception) to the quantitative (dimension). The monochord may be compared with a guitar. If you pull the string of a guitar, it gives a tone; the height of the tone (quality) depends on the length (dimension = quantity) and the tension of the string. Kayser considered the qualitative factor (tones) as judgment by emotional feeling. It is from this coupling of tone and dimension, of perception and logic, of feeling and knowledge, that the emotional sense for the proportions of buildings originates—the tones of buildings, if you will.

Kayser also had shown that Pythagorean harmonies can be traced back to older cultures such as Egyptian, Babylonian, and Chinese, and that knowledge of harmonic proportions in music and building are approximately 3000 years old. Kayser's research has been continued by R. Haasse at the Kayser Institute for Harmonic Research at the Vienna College of Music and Performing Arts.

Let us return to our historical survey. In his famous 10 books *De Architectura,* Marcus Vitruvius Pollio (84–14 BC) noted the Grecian relationships between music and architecture and based his theories of proportion on them.

Wittlkower [12] mentions an interesting text by the monk Francesco Giorgio of Venice. Writing in 1535 on the design of the Church of S. Francesco della Vigna in Venice (shortened extract):

> To build a church with correct, harmonic proportions, I would make the width of the nave nine double paces, which is the square of three, the most perfect and holy number. The length of the nave should be twenty-seven, three times nine, that is an octave and a fifth…. We have held it necessary to follow this order, whose master and author is God himself, the great master builder…. Whoever should dare to break these rules, he would create a deformity, he would blaspheme against the laws of Nature.

So strictly were the laws of harmony, God's harmony, obeyed.

In his book *Harmonia,* Francesco Giorgio represented his mystic number analogies in the form of the Greek letter Λ. Thimus [15] revised this "Lambdoma" for contemporary readers (Figure 2.2).

"Rediscovered" for curing the ills of today's architecture, Andea di Piero da Padova—known to us as *Palladio* [16], was a dedicated disciple of harmonic proportions. He wrote, "The pure proportions of tones are harmonious for the ear, the corresponding harmonies of spatial dimensions are harmonious for the eye. Such harmonies give us feelings of delight, but no one knows why—except he who studies the causes of things."

Palladio's buildings and designs prove that beautiful structures can be created using these harmonic proportions when they are applied by a sensitive master. Palladio also studied proportions in spatial perspective, where the dimensions are continuously reduced along the line of vision. He confirmed the view already stated by Brunelleschi (1377–1446) that objective laws of harmony also apply to perspective space.

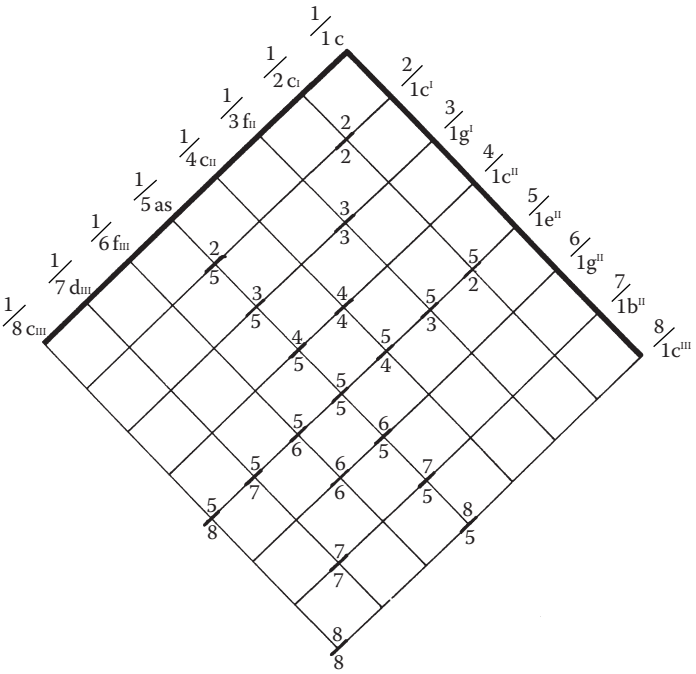

FIGURE 2.2 Giorgio numerical analogy in Λ-shape.

Even before Palladio, Leon Batista Alberti (1404–1472), had written about the proportions of buildings, Pythagoras had said

> The numbers that thrill our ear with the harmony of tones are entirely the same as those that delight our eye and understanding…. [We] shall thus take all our rules for harmonic relationships from the musicians who know these numbers well, and from those particular things in which Nature shows herself so excellent and perfect.

We can see how completely classical architecture, particularly during the Renaissance, was ruled by harmonic proportions. In the Gothic age master builders kept their canon of numbers secret. Not until a few years ago did the book *Die Geheimnisse der Kathedrale von Chartres* (The Secrets of Chartres Cathedral) by the Frenchman L. Charpentier appear [13], in which he deciphered the proportions of this famous work. It reads like an exciting novel. The proportions correspond with the first Gregorian scale, based on *re* with the main tones of *re-fa-la*. Relationships to the course of the sun and the stars are demonstrated.

Ancient philosophers spent much of their time attempting to prove that God's sun, moon, stars, and planets obeyed these harmonic laws. In his work *Harmonice Mundi* Johannes Kepler (1571–1630) showed that there are a great number of musical harmonies. He discovered his third planetary law by means of harmonic deliberations, the so-called octavoperations. Some spoke of "the music of the spheres" (Boethius, Musica mundana).

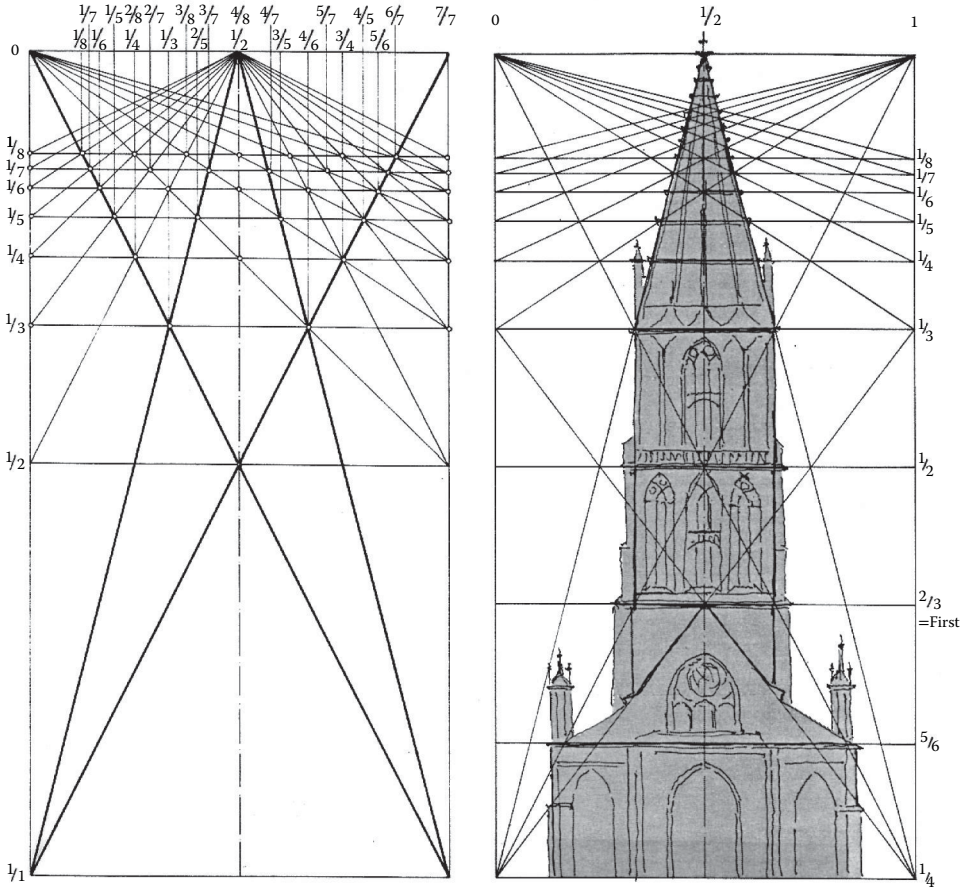

FIGURE 2.3 The Villard diagram for rectangle 2:1.

Villard de Honnecourt, the thirteenth-century cathedral builder from Picardy, gave us an interesting illustration of harmonic canon for division based on the upper tone series 1–½–⅓–¼, and so on. For Gothic cathedrals he started with a rectangle of 2:1. This Villard diagram (Figure 2.3) [13, 17] was probably used for the design of the Bern cathedral. Whole-number proportions of the fourth and third series can be seen in the articulation of the tower of Ulm Cathedral. A Villard diagram can be drawn for a square, and it then, for example, fits the cross section of the earlier basilica of St. Peter's Cathedral in Rome.

When speaking of proportion, many think of the golden mean, but this does not form a series of whole-number relationships and does not play the important role in architecture that is often ascribed to it (Equations 2.1 and 2.2). This proportion results from the division of a length $a + b$ where $b < a$ so that

$$\frac{b}{a} = \frac{a}{a+b} \tag{2.1}$$

This is the case if

$$a = \frac{\sqrt{5}+1}{2} b = 1.618\ b \tag{2.2}$$

the reciprocal value is $b = 0.618a$, which is close to the value of the minor sixth at ⅝ = 0.625 or = 1.6. The golden mean is a result of the convergence of the Fibonacci series, which is based on the proportion of

$$a : b = 1 : 2 = 0.500 = \text{octave}$$

$$b : (a+b) = 2 : 3 = 0.667 = \text{fifth}$$

$$3 : 5 = 0.600 = \text{major sixth}$$

$$5 : 8 = 0.625 = \text{minor sixth}$$

$$8 : 13 = 0.615$$

$$13 : 21 = 0.619$$

$$21 : 34 = 0.618 = \text{golden mean}$$

This numerical value is interesting in that

$$\frac{1.618}{1.618-1} = \frac{1.618}{0.618} = 2.618$$

and

$$2.168(6/5) = 3.1416 = \pi$$

The golden mean thus provided the key to squaring the circle, as can be found in Chartres Cathedral. It can be constructed by dividing the circle into five (Figure 2.4).

The Fibonacci series is also used to construct a logarithmic spiral, which occurs in nature in snail and ammonite shells, and which is considered particularly beautiful for ornaments. Le Corbusier (1887–1965) used the golden mean to construct his "Modulor" based on an assumed body height of 1.829 m but the Modulor is in itself not a guarantee of harmony.

An interesting proportion is $a : b = 1 : \sqrt{3} = 1 : 1.73$. It is close to the golden mean but for technical applications has the important characteristic that the angles to the diagonals are 30° or 60° (equilateral triangle) and the length of the diagonal is $2a$ or $2b$ (Figure 2.5). A grid with sides in the ratio of $1 : \sqrt{3}$ was patented on July 8, 1976 by Johann Klocker of Strasslach. He used this grid to design carpets, which were awarded prizes for their harmonious appearance.

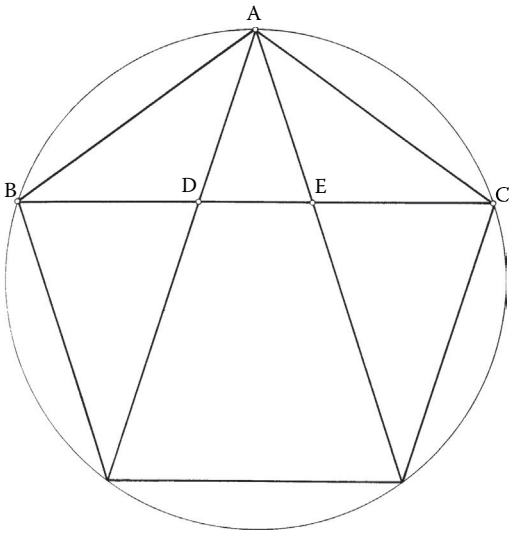

FIGURE 2.4 The golden mean in a pentagon.

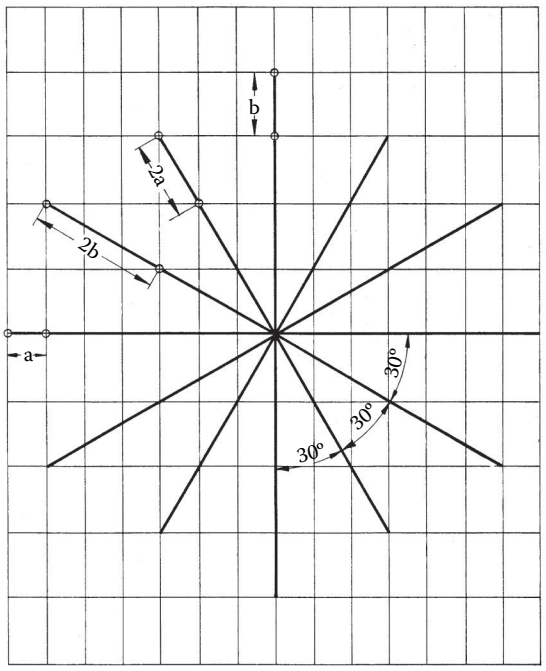

FIGURE 2.5 The Kloecker grid with $a{:}b = 1{:}\sqrt{3}$.

During the past 50 years architects have largely discarded the use of harmonic proportions. The result has been a lack of aesthetic quality in many buildings where the architect did not choose good proportions intuitively as a result of his artistic sensitivity. There were exceptions, as always. The Swiss architect Andre M. Studer [18] and the Finn Aulis Blomstdt consciously built "harmonically." One result of the

wave of nostalgia of the 1970s is a return in many places to such aesthetics. Kayser [14] and P. Jesberg in the *Deutsche Bauzeitschrift* DBZ 9/1977 gave a full description of harmonic proportions.

2.6 How Do We Perceive Geometric Proportions?

In music we can assert plausibly that a feeling and sense for harmonic tone series is controlled genetically and physiologically through the inborn characteristics of the ear. What about the proportions of lengths, dimensions of objects and volumes? Helmcke [19], of the Technical University of Berlin, wholeheartedly supported the idea of a genetic basis for the aesthetic perception of proportions and he argued as follows:

> During the evolution of animals and Man the choice of partner has undoubtedly always played an important role. Since ancient times men have chosen women as partners, who in their eyes were the most beautiful and well proportioned and equally women have chosen men as partners the strongest and most well-built in their eyes. Through natural selection [Darwin] during the evolution of a species this must have led to the evolution of aesthetic perception and feeling and resulted in the development in Man of a genetically coded aesthetic ideal for human partners, passed on from generation to generation. We fall in love more easily with a beautiful partner; love at first sight is directed mostly by an instinctive feeling for beauty, and not by logic. Nobody who knows Man and his history will doubt that there is an inherited human ideal of beauty. Every culture has demonstrated its ideal of human beauty, and if we study the famous sculptures of Greek artists we recognize that the European ideal of beauty in female and male bodies has not changed in the last 3000 years.

For the Greeks, the erotic character of the beauty of the human body played a dominant role. At the Symposium of Xenophon (ca. 390 BC) Socrates made a speech in praise of Eros. According to Grassi [20], the term *beautiful* is used preferentially for the human body.

The Spanish engineer Eduardo Torroja (1899–1961), whose structures were widely recognized for their beauty, wrote in his book *The Logic of Form* [21] that "truly the most perfect and attractive work of Nature is woman." Helmcke said that "Man's aesthetic feeling, while perceiving certain proportions of a body, developed parallel to the evolution of Man himself and is programmed genetically in our cells as a hereditary trigger mechanism."

According to this the proportions of a beautiful human body would be the basis of our hereditary sense of beauty. This view is too narrow because thousands of other natural objects radiate beauty, but let us continue to study "Man" for the time being.

Fortunately, all humans differ in their hereditary, attributes, and appearance, although generally only slightly. This means that our canons of beauty cannot be tied to strictly specific geometric forms and their proportions. There must be a certain range of scatter. This range covers the differences in the ideals of beauty held by different races. It ensures that during the search for a partner each individual's ideal will differ, keeping the competition for available partners within reasonable bounds.

We can also explain this distribution physiologically. Our eyes have to work much harder than our ears. The messages received by the eye span a range about a thousand times wider than the scale of tones to be processed by the ear. This means that with colors and geometric proportions harmony and disharmony are not so sharply defined as with musical tones. The eye can be deceived more easily and is not as quickly offended or aggravated as the ear, which reacts sensitively to the smallest dissonance.

More evidence for a hereditary sense of beauty is provided by the fact that even during their first year, children express pleasure at beautiful things and are offended, even to the point of weeping, by ugly objects. How children's eyes sparkle when they see a pretty flower.

Evidence against the idea that we have a hereditary sense of beauty is suggested by the fact that people argue so much about what is beautiful or ugly, demonstrating a great deal of insecurity in the judgment of aesthetic qualities. We will give this further thought in Section 2.7.

Our ability to differentiate between good and bad using our senses of taste and smell has also developed genetically and with certain variations is the same for most people [22]. With this background of genetic development, it is understandable that the proportions of those human bodies considered beautiful have been studied throughout the ages. A Greek sculptor Polyklet of Kikyon (465–420 BC) defined the following proportions:

two handbreadths = height of the face and height of the breast, distance breast to navel, navel to end of trunk
three handbreadths = height of skull, length of foot
four handbreadths = distance shoulder to elbow, elbow to fingertips
six handbreadths = ear to navel, navel to knee, length of trunk, length of thigh

Polyklet based his "canon for the ideal figure" on these relationships. These studies had the greatest influence on art during the age of humanism, for example, through the *Vier Büecher von menschlicher Proportione* 1528 by Albrecht Dürer (1471–1528).

Vitruvius also dealt with the human body in his books *De Architectura* and used the handbreadth as a unit of measure. Leonardo da Vinci followed Vitruvius's theories when drawing his image of man inscribed in a square (Figure 2.6).

Leonardo's friend, the mathematician Luca Pacioli (ca. 1445–1514) began his work *De Divina Proportione,* 1508, with the words:

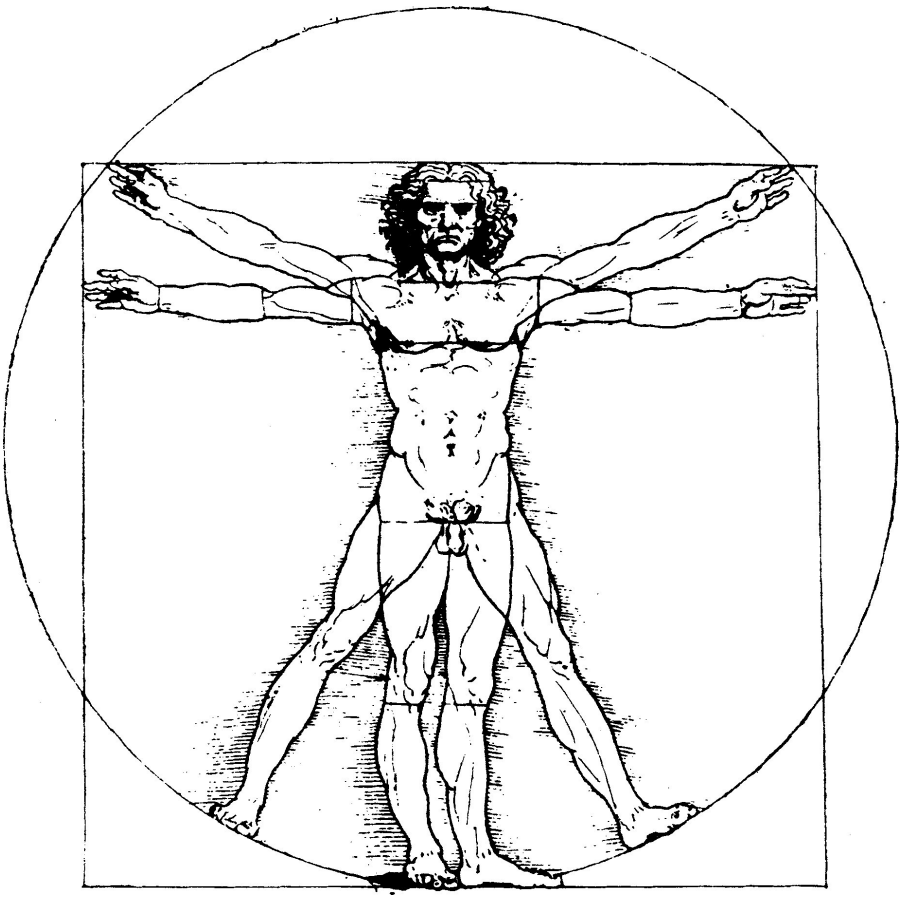

FIGURE 2.6 Image of man in circle and square according to Leonardo da Vinci.

> Let us first speak of the proportions of Man because all measures and their relationships are derived from the human body and here are to be found all numerical relationships, through which God reveals the innermost secrets of Nature. Once the ancients had studied the correct proportions of the human body they proportioned all their works, particularly the temples, accordingly. (Quoted by Wittlkower [12].)

The human body with outstretched arms and legs inscribed in a square and circle became a favorite emblem for humanistically oriented artists right up to Le Corbusier and Ernst Neufert. Let us close this section with a quotation from one of Helmcke's [19] works:

> The intellectual prowess of earlier cultures is revealed to us whenever their artists, architects, and patrons succeeded in incorporating, consciously or unconsciously, our hereditary, genetically programmed canon of proportions in their works; in achieving this they come close to our genetically controlled search for satisfaction of our sense of aesthetics. It reveals the spiritual pauperism of today's artists, architects and patrons when, despite good historical examples and despite advances in the natural sciences and the humanities they do not know of these simple biologically, anatomically based relationships or are too ungifted to perceive, understand, and realize them. Those who deprecate our search for the formal canons of our aesthetic feelings as a foolish and thus unnecessary pastime must expect to have their opinion ascribed to arrogant ignorance and to the lack of a sure instinctive sense of beauty, and already ethnologically known as a sign of decadence due to domestication.

The only criticism that, in my (Helmcke's) opinion can be leveled at the thousands of years' old search for universally valid canons of form, lies in the assumption that these canons shall consist of fixed proportions and shall thus be valid for all mankind.

What is needed is experience of and insight into the range of scatter of proportional relations and insight into the limits within our hereditary aesthetic sense reacts positively, and beyond which it reacts negatively.

2.7 Perception of Beauty in the Subconscious

We are not generally aware of how strongly our world of feelings, our degree of well-being, comfort, disquiet, or rejection is dependent on impressions from our surroundings. Neurologists know that parts of our brain are capable of reacting to external stimuli without reference to the conscious mind and of processing extensive amounts of information. This takes place in the limbic system of the primitive structures of the midbrain and the brain stem. For all those activities of the subconscious that deal with the processing of aesthetic messages, Smith [3] used the phrase "limbic aesthetics" and dedicated a whole chapter of his very readable book to them.

Our subconscious sense of beauty is almost always active, whether we are at home, in the city marketplace, in a church, in a beautiful landscape, or in the desert. Our surroundings affect us through their aesthetic characteristics even if our conscious thoughts are occupied with entirely different matters and impressions.

Smith wrote of the sensory appetite of these primitive parts of the brain for pleasant surroundings, for the magic of the city, and for the beauty of nature. The limbic system reacts to an oversupply of stimuli with rejection or anxiety.

Symbolic values connected with certain parts of our environment also act on the subconscious. The home, the church, school, garden, and so on have always possessed symbolic values created by learning and experience. These are related mostly to basic human situations and cause emotional reactions, without ever reaching the conscious level.

This perception of beauty at the subconscious level plays a particularly strong role in city dwellers. Their basic feeling of well-being is doubtless influenced by the aesthetic qualities of their environment in this way. This has social consequences (see Section 2.10) and underlines our responsibility to care about the beauty of the environment.

2.8 Aesthetic Judgment and Taste

When two observers are not agreed in their judgment of a work of art, the discussion is all too often ended with the old proverb, "De gustibus non disputandum est." We like to use a little Latin to show our classical education, which, as we know, is supposed to include an understanding of art. This "there's no accounting for taste" is an idle avoidance tactic, serving only to show that the speaker has never really made a serious effort to study aesthetics and thus has educational deficiencies in the realm of assessing works of art.

Of course, taste is subject to continual change, which in turn depends on current ideals, fashions, and is dependent on historical and cultural background. The popular taste in any given period of time or even the taste of single individuals is never a reliable measure of aesthetic qualities.

However, genetic studies have shown that we have a certain basic hereditary sense of beauty. Smith [3] said that this aesthetic perception has developed into one of the highest capabilities of our central nervous system and is a source of deep satisfaction and joy.

The judgment of aesthetic characteristics is largely dependent on feelings that are derived from our sensory perceptions. Beauty, then, despite some theories (Bense, Maser) cannot be rationally measured. When looking at the nature of feelings we must admit the fact that despite all our research and science, we know very little about humanity or about ourselves. We can, however, call upon observations and experiences that are helpful.

We repeatedly experience that the majority of people agree that a certain landscape, great painting, or building is beautiful. When entering a room, for example, in an old church, or while wandering through a street, feelings are aroused that are pleasant, comfortable, even elevating, if we sense a radiation of beauty. If we enter a slum area, we feel revulsion or alarm, as we perceive the disorder and decay. We can be more or less aware of these feelings, depending on how strongly our thoughts are occupied elsewhere. Sensitivities and abilities to sense beauty naturally differ from person to person, as is true of our other talents. This sensitivity is influenced by impressions from our environment, by experience, by relationships with our companions at home, at school, and with our friends. Two people judging the qualities of beauty of an object are likely to give different opinions.

Beautiful surroundings arouse feelings of delight in almost all people, but an ugly, dirty environment causes discomfort. Only the degree of discomfort will differ. In our everyday life such feelings often occur only at a subconscious level and often their cause is only perceived after subsequent reflection.

We can develop a clear capacity for judging aesthetic qualities only when we study the message emanated by an object consciously and ask ourselves whether or not we like a building or a room. Next, we must ask ourselves Why? Why do I like this and not that? Only by frequent analysis, evaluation, and consideration of consciously perceived aesthetic values can we develop that capacity of judgment that we commonly call taste—taste about which we must argue, so that we can strengthen and refine it. Taste, then, demands self-education, which can be cultivated by critical discussion with others or by guidance from those more experienced. Good judgment of aesthetic values requires a broad education. It can be compared to an art and requires skill, and like art it takes not only talent, but a lot of work.

We need not be afraid that such analysis will weaken our creative skills; in fact, the opposite is true: the goal of analysis is the discovery of the truth through creative thinking [23]. People have different talents and inclinations since they grow up in different circles with different cultural backgrounds and therefore their tastes will always differ. In any given culture, however, there is a certain polarity on the judgment of beauty. Psychologists call this agreement "normal behavior," "a normal reaction of the majority." This again corresponds with Kant's view that beauty is what is generally thought to be beautiful by the majority of people.

Beauty cannot be strictly proved, however; so we must be tolerant in questions of taste and must give freedom to what is generally felt to be beautiful and what is ugly. That there is a generally recognized concept of beauty is proved by the consistent judgment of the classical works of art of all great cultures, visited

year after year by thousands of people. Think of the popularity of exhibitions of great historic art today. It is history that has the last word on the judgment of aesthetic values, long after fashions have faded.

Fashions: Artistic creation will never be entirely free from fashion. The drive to create something new is the hallmark of creative beings. If the new becomes popular, it is soon copied, and so fashions are born. They are born of the ambition and vanity of humans and please both. The desire to impress often plays a role. Up to a certain point, fashions are necessary; in certain new directions true art may develop through the fashionable, acquiring stability through a maturing process and enduring beyond the original fashion. Often, such new developments are rejected, because we are strongly influenced by the familiar, by what we are used to seeing, and only later realize the value of the new. Again, history pronounces a balanced judgment.

Confusion is often caused in our sense of judgment by modern artists who deliberately represent ugliness in order to mirror the warped mental state of our industrial society. Some of this work has no real quality, but is nonetheless acclaimed as modern art. The majority dares not question this for fear of rejection, slander, and peer pressure.

Although some works that consciously display ugliness or repulsiveness may well be art, we must seriously question the sanity and honesty of the patrons of primitive smearings, tangles of scrap iron, or old baby baths covered in Elastoplast strips (J. Beuys) when such efforts are exhibited as works of art. Happily, the courage to reject clearly such affronts and to put them in their place is on the increase. We only need to read Claus Borgeest's book, *Das Kunsturteil,* [24], in which he wrote, "the belief in such 'art' is a modern form of self-inflicted immaturity, whose price is the self-deprivation of reason, man's supreme attribute."

In any case, it would be wrong to describe as beautiful works those haunted by ugliness, even if they have the quality of art. The artist intends to provoke and to encourage deliberation. However, the educational effects of such artistic creations are questionable, because we usually avoid their repeated study. Painters and sculptors, however, should be free to paint and sculpt as hatefully and repulsively as they wish—we do not have to look at their works. It is an entirely different case with buildings; they are not a private affair, but a public one. It follows that the designer has responsibility to the rest of humankind and a duty to produce beautiful buildings so that the designer does not give offence. Rightly, the ancient Greeks forbade public showings of ugliness, because their effects are largely negative.

We seldom find anyone who will hang ugly works of art in his or her home. It is beyond doubt that in the long term we feel comfortable only in beautiful surroundings and that beauty is a significant requirement for the well-being of our soul; this is much more important for people's happiness than we today care to admit.

2.9 Characteristics of Aesthetic Qualities Lead to Guidelines for Designing

The search for explanations and the analysis of aesthetic values are bound to lead to useful results, at least for man-made buildings and structures. We will now try to subject matters of feelings, emotions, to the clear light of recognition and understanding.

If we do this, we can certainly find answers to the question, "Why is this beautiful and this ugly?" For recognized masterpieces of architecture generally considered beautiful, there have been answers since ancient times, many of which are given in the quoted literature on proportions. Such buildings reveal certain characteristics of quality and from these we can deduce guidelines for design, such as certain proportions, symmetry, rhythm, repeats, contrasts, and similar factors. The master schools of old had such rules or guidelines, such as those of Vitruvius and Palladio. Today, these rules are surely valid and must be rediscovered for the sake of future architecture. They can prove a valuable aid in the design of building structures and at the very least contribute toward avoiding gross design errors.

Many architects and engineers reject rules, but in their statements about buildings we still find references to harmony, proportion, rhythm, dominance, function, and so on. Torroja [21] rejected rules, but he said "the enjoyment and conscious understanding of aesthetic pleasure will without doubt be much greater if, through a knowledge of the rules of harmony, we can enjoy all the refinements and perfections

of the building in question." Rules of harmony are based on rules of proportion, and somehow the striving for individual artistic freedom prevents us from recognizing relationships often imposed upon us by ethics.

Let us then attempt to formulate such characteristics, rules, or guidelines as they apply to building structures, particularly bridges.

2.9.1 Fulfillment of Purpose: Function

Buildings or bridge structures are erected for a purpose. The first requirement is that the buildings and bridges be designed to optimally suit this purpose. To meet the specific purpose, a bridge may have different structural types: arches, beams, or suspensions. The structure should reveal itself in a pure, clear form and impart a feeling of stability. We must seek simplicity here. The form of the basic structure must also correspond to the materials used. Brick and wood dictate different forms from those for steel or concrete. We speak of form justified by the material, or of "logic of form" [21]. This reminds us of the architect Sullivan's rule "form follows function" that became an often-misunderstood maxim for building design. The function of a building is not only that it stand up. One must fulfill all the various requirements of the people that inhabit the building. These include hygiene, comfort, shelter from weather, beauty, even coziness. The fulfillment of the functional requirements of buildings includes favorable thermal, climatic, acoustic, and aesthetic qualities. Sullivan undoubtedly intends for us to interpret his rule in this sense. For buildings the functional requirements are very complex, but in engineering structures, functions besides load-carrying capacity must be fulfilled, such as adequate protection against weather, limitation of deformation and oscillation, among others, and all these factors affect design. Quality and beauty must be united, and quality takes first priority!

2.9.2 Proportion

An important characteristic necessary to achieve beauty of a building is good, harmonious proportions, in three-dimensional space. Good proportions must exist between the relative sizes of the various parts of a building, between its height, width, and breadth; between masses and voids; closed surfaces and openings; and between the light and dark caused by sunlight and shadow. These proportions should convey an impression of balance. Tassios [25] preferred "expressive proportions" that emphasize the desired character of a building (see Section 2.9.8).

For structures it is not sufficient that their design is "statically correct." A ponderous beam can be as structurally correct as a slender beam, but it expresses something totally different. Not only are the proportions of the geometric dimensions of individual parts of the building important, but also those of the masses of the structure. In a bridge, for instance, these relationships may be between the suspended superstructure and the supporting columns, between the depth and the span of the beam, or between the height, length, and width of the openings. Harmony is also achieved by the repetition of the same proportions in the entire structure or in its various parts. This is particularly true in buildings.

Sometimes contrasting proportion can be a suitable element. The detailed discussion is referred to Chapter 4 of my book [26], which shows what good proportions can mean for bridges.

2.9.3 Order

A third important rule is the principle of order in the lines and edges of a building, an order achieved by limiting the directions of these lines and edges to only a few in space.

Too many directions of edges, struts, and the like create disquiet, confuse the observer, and arouse disagreeable emotions. Nature offers us many examples of how order can lead to beauty; just think of the enchanting shapes of snow crystals and of many flowers [27, 28]. Good order must be observed between the proportions occurring in a building; for instance, rectangles of 0.8:1 should not be placed next to

slim rectangles of 1:3. Symmetry is a well-tried element of order whenever the functional requirements allow symmetry without constraint.

We can include the repetition of equal elements under the rule of order. Repetition provides rhythm, which creates satisfaction. Too many repetitions, however, lead to monotony, which we encounter in the modular architecture of many high-rise buildings. Where too many repetitions occur, they should be interrupted by other design elements.

The selection of one girder system throughout the structure provides an element of good order. Interrupting a series of arches with a beam gives rise to aesthetic design problems. Under the principle of order for bridges we may include the desire to avoid unnecessary accessories. The design should be so refined that we can neither remove nor add any element without disturbing the harmony of the whole.

2.9.4 Refining the Form

In many cases, bodies formed by parallel straight lines appear stiff and static, producing uncomfortable optical illusions. Tall bridge piers or towers with parallel sides appear from below to be wider at the top than at the bottom, which would be unnatural. Nor does this uniform thickness conform to our concept of functionality, because the forces decrease with increasing height. For this reason, the Egyptians and Greeks gave the columns of their temples a very slight taper, which in many cases is actually curved. Towers are built tapered or stepped. On high towers and bridge piers, a parabolic taper looks better than a straight taper.

The spans of a viaduct crossing a valley should become smaller on the slopes and even the depth of the girders or edge fascia can be adjusted to the varying spans. Long beams of which the bottom edge is exactly horizontal look as if they are sagging, and so we give them a slight camber.

We must also check the appearance of the design from all possible vantage points of the future observer. Often the pure elevation on the drawing board is entirely satisfactory, but in skew angle views of unpleasant overlapping are found. We must also consider the effects of light and shadow. A wide cantilever deck slab can throw bridge girders into shadow and make them appear light, whereas similar shadows break the expressive character of an arch. Models are strongly recommended for checking a design from all possible viewpoints.

These refinements of form are based on long experience and must be studied with models from case to case.

2.9.5 Integration into the Environment

As the next rule, we recognize the need to integrate a structure or a building into its environment, landscape, or cityscape, particularly where its dimensional relationships and scale are concerned. In this respect many mistakes have been made during the past decades by placing massive concrete blocks in the heart of old city areas. Many factories and supermarkets also show this lack of sensitive integration. Sometimes long-span bridges with deep, heavy beams spoil lovely valley landscapes or towns with old houses lining the riverbank.

The dimensions of buildings must also be related to the human scale. We feel uneasy and uncomfortable moving between gigantic high-rise buildings. Heavy, brutal forms are often deliberately chosen by architects working with prefabricated concrete elements, but they are simply offensive. It is precisely their lack of scale and proportion that has led to the revolt against the brutality of this kind of architecture.

2.9.6 Surface Texture

When integrating a building with its surroundings, a major role is played by the choice of materials, the texture of the surfaces, and particularly by color. How beautiful and vital a natural stone wall can appear if we choose the right stone. By contrast, how repulsive are many concrete facades; not only do they have

a dull gray color from the beginning, but they weather badly, producing an ugly patina and appear dirty after only a few years. Rough surfaces are suitable for piers and abutments; smooth surfaces work well on fascia-beams, girders, and slender columns. As a rule, surfaces should be matte and not glossy.

2.9.7 Color

Color plays a significant role in the overall aesthetic effect. Many researchers have studied the psychological effects of color. Here, too, ancient rules of harmonious color composition apply, but today successful harmonious color schemes are rare. Often, we find the fatal urge for sensation, for startling aggressive effects, which can be satisfied all too easily with the use of dissonant colors, especially with modern synthetic pop—or shocking—colors. We can find, however, many examples of harmonious coloring, generally in town renovation programs. Bavaria has provided several examples where good taste has prevailed.

2.9.8 Character

A building and a bridge should have character; it should have a certain deliberate effect on people. The nature of this desired effect depends on the purpose, the situation, the type of society, and on sociological relationships and intentions. Monarchies and dictatorships try to intimidate by creating monumental buildings, which make people feel small and weak. We can hope this belongs to the past. Only large banks and companies still make attempts to impress their customers with monumentalism. Churches should lead inward to peace of mind or convey a sense of release and joy of life as in the Baroque or Rococo. Simple dwellings should radiate safety, shelter, comfort, and warmth. Beautiful houses can stimulate happiness.

Buildings of the last few decades express an air of austere objectivity, monotony, coldness, confinement, and, in cities, confusion, restlessness, and lack of composition; there is too much individuality and egoism. All this dulls people's senses and saddens them.

We seem to have forgotten that people also want to meet with joy in their man-made environment. Modern buildings seem to lack entirely the qualities of cheerfulness, buoyancy, charm, and relaxation. We should once again become familiar with design features that radiate cheerfulness without lapsing into Baroque profusion.

2.9.9 Complexity: Stimulation by Variety

Smith [3] postulated a "second aesthetic order," suggested by findings made by biologists and psychologists [29]. According to this, beauty can be enhanced by the tension between variety and similarity, between complexity and order. Baumgarten expressed this as early as 1750, "Abundance and variety should be combined with clarity. Beauty offers a twofold reward: a feeling of well being both from the perception of newness, originality, and variation as well as from coherence, simplicity, and clarity." Leibniz in 1714 demanded for the achievement of perfection as much variety as possible, but with the greatest possible order.

Berlyne [30] considered the sequence of tension and relaxation to be a significant characteristic of aesthetic experience. Venturi [31], a rebel against the "rasteritis" (modular disease) architecture of Mies van der Rohe said, "A departure from order—but with artistic sensitivity—can create pleasant poetic tension."

A certain amount of excitement caused by a surprising object is experienced as pleasant if neighboring objects within the order ease the release of tension. If variety dominates our orientation, reflex is overtaxed and feelings ranging from distaste to rejection are aroused. Disorder is not beautiful.

This complexity doubtless requires artistic skill to be successful. It can be used well in bridge design if, for instance, in a long, multi-span bridge the main span is accented by a variation in the girder

form. The interplay of complexity and order is important in architecture, particularly in city planning. Palladio was one of the first to extend the classical understanding of harmony by means of the complexity of architectural elements and ornamentation.

2.9.10 Incorporating Nature

We will always find the highest degree of beauty in nature, in plants, flowers, animals, crystals, and throughout the universe in such a variety of forms and colors that awe and admiration make it extremely difficult to begin an analysis. As we explore deeper into the realm of beauty we also find in nature rules and order, but there are always exceptions. It must also remain possible to incorporate such exceptions in the masterpieces of art made by creative humans [28].

The beauty of nature is a rich source for the needs of the soul, and for humans' psychic well being. All of us know how nature can heal the effects of sorrow and grief. Walk through beautiful countryside—it often works wonders. As human beings we need a direct relationship with nature, because we are a part of her and for thousands of years have been formed by her.

This understanding of the beneficial effects of natural beauty should lead us to insist that nature again be given more room in our man-made environment. This is already happening in many of our cities, but we must introduce many more green areas and groups of trees. Here we must mention the valuable work of Seifert [32] during the building of the first autobahns in Germany.

2.9.11 Closing Remarks on the Rules

We must not assume that the simple application of these rules will in itself lead to beautiful buildings or bridges. The designer must still possess imagination, intuition, and a sense for both form and beauty. Some are born with these gifts, but they must be practiced and perfected. The act of designing must always begin with individual freedom, which in any case will be restricted by all the functional requirements, by the limits of the site, and not least by building regulations that are usually too strict. The rules, however, provide us with a better point of departure and help us with the critical appraisal of our design, particularly at the model stage, thus making us aware of design errors.

The artistically gifted may be able to produce masterpieces of beauty intuitively without reference to any rules and without rational procedures. However, the many functional requirements imposed on today's buildings and structures demand that our work must include a significant degree of conscious, rational, and methodical reasoning.

2.10 Aesthetics and Ethics

Aesthetics and ethics are in a sense related; by ethics we mean our moral responsibility to humanity and nature. Ethics also infers humility and modesty, virtues that we find lacking in many designers of the last few decades and that have been replaced by a tendency toward the spectacular, the sensational, and the gigantic in design. Owing to exaggerated ambition and vanity and spurred by the desire to impress, unnecessary superlatives of fashions were created, lacking true qualities of beauty. Most of these works lack the characteristics needed to satisfy the requirements of the users of these buildings.

As a responsibility, ethics requires a full consideration of all functional requirements. In our man-made environment we must emphasize the categories of quality and beauty. In his *Acht Todsünden der Menschheit,* Loreanz [33] once said that "the senses of aesthetics and ethics are apparently very closely related, so that the aesthetic quality of the environment must directly affect Man's ethical behavior." He said further, "The beauty of Nature and the beauty of the man-made cultural environment are apparently both necessary to maintain Man's mental and psychic health. Total blindness of the soul for all that is beautiful is a mental disease that is rapidly spreading today and that we must take seriously because it makes us insensitive to the ethically obnoxious."

In one of his last important works, in *To Have or to Be* [34] Erich Fromm also said that the category of "goodness" must be an important prerequisite for the category "beauty," if beauty is to be an enduring value. Fromm goes so far as to say that "the physical survival of mankind is dependent on a radical spiritual change in Man." The demand for aesthetics is only a part of the general demand for changes in the development of "Man." These changes have been called for at least in part and at intervals by humanism, but their full realization in turn demands a new kind of humanism, as well expressed in the appeal by Peccei [35].

2.11 Summary

In order to reach a good capacity of judging aesthetic qualities of buildings or bridge structures, it is necessary to go deep into our human capacities of perception and feelings. The views of many authors who treated aesthetics may help to come to some understanding, which shall help us to design with good aesthetic quality.

References

1. Klages, L. 1970. *Grundlagen der Wissenschaft vom Ansdruck*, Auflage, Bonn, Germany.
2. HUME, D. 1882. 'Of the Standard of Taste', in his *Essays, Moral, Political and Literary*. London, UK. (Also available online at: http://pm.nlx.com)
3. Smith, P. F. 1981. *Architecktur und Aesthetik*, Stuttgart, Germany. [Original: Architecture and the Human Dimension, George Godwin, London, U.K. 1979.]
4. Kant, I. 1991. *Kritik der Urteilskraft*, Reklam, Stuttgart, Germany.
5. Paul, J. 1974. *Vorschule der Aesthetik*, München, Germany.
6. Schmitz, H. 1980. *Neue Phänomenologie*, Bonn, Germany.
7. Bahrdt, H. P. 1979. *Vortrag Hannover*, Stiftung FVS, Hamburg, Germany.
8. Keller, R. 1973. *Bauen als Umweltzerstörung*, Zürich, Switzerland.
9. Arnheim, R. 1978. *Art and Visual Perception*, Berkeley, CA, 1954. [German: Kunst und Sehen, Berlin, Germany.]
10. Goethe, J. W. 1979. *Farbenlehre*, Freies Geistesleben, Stuttgart, Germany.
11. Szabo, Á. 1969. *Anfänge der griechischen Mathematik*, R. Oldenbourg, München, Germany.
12. Wittlkower, R. 1969. *Architectural Principles in the Age of Humanism*, W. W. North & Company Ltd, London, U.K. [German: Grundlagen der Architecktur im Zeitalter des Humanismus, München, Germany.]
13. Charpentier, L. 1972. *Die Geheimnisse der Kathedrale von Chartres*, Gaia, Köln, Germany.
14. Kayser, H. 1958. *Paestum*, Heidelberg, Germany.
15. Thimus, A. von. 1968–1976. *Die Harmonische Symbolik des Altertums*, Köln, Germany.
16. Puppi, L. 1973. *Andrea Palladio*, New York Graphic Society, Waterbury, CT.
17. Strübin, M. 1947. *Das Villard-Diagramm, ein Schlüssel zur Bauweise der Gotik?* W. Jegher & A. Ostertag, Zürich, Switzerland, 527.
18. Studer, A. M. 1965. *Architektur, Zahlen und Werte*, Dtsch Bauz., Stuttgart, Germany.
19. Helmcke, J. G. 1976. *Ist das Empfinden von Aesthetisch Schoenen Formen Angeboren oder Anerzogen*, Heft 3 des SFB 64 der Universität Stuttgart, Germany, 59. [See also Grenzen menschlicher Anpassung, IL 14, Universität Stuttgart, Germany, 1975.]
20. Grassi, E. 1980. *Die Theorie des Schönen in der Antike*, DuMont, Köln, Germany.
21. Torroja, E. 1961. *Logik der Form*, Callwey, München, Germany.
22. Tellenbach, H. 1968. *Geschmack und Atmosphaere*, O. Müller, Salzburg, Austria.
23. Grimm, C. T. 1975. Rationalized esthetics in civil engineering, *J. Struct. Div.,* 101(ST9), *ASCE*, 1813–1822.
24. Borgeest, C. 1979. *Das Kunsturteil*, Fischer-Taschenbuch-Verlag, Frankfurt, Germany. [Also: Das sogenannte Schöne, Frankfurt, Germany.]

25. Tassios, T. P. 1980. *Relativity and Optimization of Aesthetic Rules for Structures*, IABSE Congr. Rep., Zürich, Switzerland.
26. Leonhartdt, F. 1984. *Bridges—Aesthetics and Design*, Deutsche Verlags-Anstalt, Stuttgart, Germany.
27. Heydemann, B. 1980. Auswirkungen des Angeborenen Schönheitssinnes bei Mensch und Tier, *Natur Umweltmagazin,* Ringer Verlag, München, Germany, 33–39.
28. Kayser, H. 1943. *Harmonia Plantarum*, B. Schwabe & Co., Basel, Switzerland. [Also: H. Akroasis, Die Lehre von der Harmonik der Welt, Stuttgart, Germany, 1976.]
29. Humphrey, N. 1973. The illusion of beauty, *Perception Bd.*, 2, 429–439.
30. Berlyne, D. E. 1971. *Aesthetics and Psycho-Biology*, Appleton-Century-Crofts, New York, NY.
31. Venturi, R. 1966. *Complexity and Contradiction in Architecture*, The Museum of Modern Art, New York, NY.
32. Seifert, A. 1962. *Ein Leben für die Landschaft*, Diederichs, Düsseldorf-Köln, Germany.
33. Lorenz, K. 1973. *Acht Todsünden der zivilisierten Menschheit*, R. Piper, München, Germany.
34. Fromm, E. 1976. *Haben oder Sein*, Dt. Taschenbuch Verl., Stuttgart, Germany.
35. Peccei, A. 1981. *Die Zukunft in unserer Hand*, Molden, München, Germany.

3

Bridge Aesthetics: Achieving Structural Art in Bridge Design

Frederick Gottemoeller
Bridgescape, LLC

> It so happens that the work which is likely to be our most durable monument, and to convey some knowledge of us to the most remote posterity, is a work of bare utility; not a shrine, not a fortress, not a palace but a bridge.
>
> **Montgomery Schuyler**
> *Writing about John Roebling's Brooklyn Bridge, 1883*

3.1 Introduction

3.1.1 Why Consider Aesthetics

People know intuitively that civilization forms around civil works for water, transportation, and shelter. The quality of the public life depends, therefore, on the quality of such civil works as aqueducts,

bridges, towers, terminals, meeting halls: their efficiency of design, their economy of construction, and the appearance of their completed forms. At their best, these civil works function reliably, cost the public as little as possible, and when sensitively designed, become works of art. The public is becoming ever more aware of this potential, and demanding an ever higher standard for the appearance of the bridges in their communities.

If civil works are to become works of art, engineers cannot just worry about the structure and leave the appearance to someone else. If a decision affects the size, shape, color, or surface texture of a visible part of the bridge, it affects how people will feel about the bridge. The shapes and sizes of the structural members themselves dominate people's impressions of a bridge. They are the largest elements of the bridge, therefore the first elements people see as they approach and the most strongly remembered. It is impossible to correct the appearance of a poorly proportioned or detailed structure by the application of "aesthetic treatments" involving color, texture, or ornamentation, though many have tried.

Since engineers control the shapes and sizes of the structural components, they must acknowledge that they are ultimately responsible for the appearance of their structures. Thus, to meet their obligations as professionals, engineers must respond to the public's concern. For the same reason engineers would not build a bridge that is unsafe, they should not build one that is ugly. All engineers are accustomed to dealing with issues of performance, efficiency, and cost. Now, they must also deal with issues of appearance, something the most accomplished have always done.

3.1.2 Frequent Objections to Considering Aesthetics

- It always adds cost.

  Not true. Simply paying attention to proportions and details can result in an attractive bridge with no increase in cost (Figure 3.1). Indeed, there are times when the search for economy also results in an improvement in appearance (Figure 3.2). Whether there is additional cost varies widely depending on region of the country, owner preferences and practices, contractor capabilities, span length, size of project, community aspirations, and other project specifics.

  If there is an increased cost, then the relevant question becomes: does the aesthetic improvement justify the additional cost? Few people automatically buy the cheapest car or living room

FIGURE 3.1 Often simply paying attention to proportions and details can result in an attractive bridge with no increase in cost. Canyon Creek Bridge, Anchorage, Alaska. (From AASHTO, *Bridge Aesthetics Sourcebook*, American Association of State Highway and Transportation Officials, Washington, DC, 2010. With permission.)

FIGURE 3.2 A conceptual engineering study for the Seattle LRT viaduct produced a design that both reduced cost and improved appearance compared to a standard design. (From AASHTO, *Bridge Aesthetics Sourcebook*, American Association of State Highway and Transportation Officials, Washington, DC, 2010. With permission.)

sofa no matter what it looks like. We make decisions every day to spend additional money to get a better quality product. We can make the same kind of judgments about bridges, keeping in mind that the bridges we build today will be prominent features in our communities for the next 80 years or more. If the affected community is involved, as it should be, we can take advantage of their concerns and insights as well.

- People can't agree on what looks better.

  Also not true. People have agreed for centuries on which paintings look better, which symphonies sound better, and which buildings are more attractive. A consensus on which bridges look better and why has existed since at least 1812 as articulated in the writings of Thomas Telford. That consensus has been recognized by artists and others. For example, Robert Maillert's Salginatobel Bridge (Figure 3.3) was formally recognized by New York's Museum of Modern Art in 1949 and by many others since. That consensus is embodied in this chapter.
- My client/boss won't let me.

  Show your client/boss this chapter.
- I don't know how.

  Read this chapter and you will.

3.1.3 What Is the Goal?

The purpose of this chapter is to help bridge designers improve the elegance of their bridges by examining actual examples and discussing the principles on which they are based. The ultimate goal is to make every bridge efficient, economical, and elegant by giving meaningful visual expression to loads, equilibrium, and forces. With this as a goal every bridge will become an asset to its community and environment.

The American Association of Highway and Transportation Officials (AASHTO) formally recognized this ultimate goal in 2010 when its Standing Committee on Bridges and Structures adopted a *Bridge Aesthetics Sourcebook* based on these principles. The *Sourcebook* was prepared by the Bridge Aesthetic Subcommittee of the Transportation Research Board.

Both this chapter and the *Sourcebook* are inspired by David Billington's work illuminating the history of structural art in bridge design. The next two sections of the chapter are a summary of that work.

FIGURE 3.3 Robert Maillert's Salginotobel Bridge.

The later portions of this chapter are based on the *Sourcebook* with specific quotations identified. The full *Sourcebook* is available from AASHTO at www.bookstore.transportation.org.

3.2 Engineer's Aesthetic and Structural Art

3.2.1 Aesthetic Tradition in Engineering

"Aesthetics" is a mysterious subject to most engineers, not lending itself to the engineer's usual tools of analysis, and rarely taught in engineering schools. Many contemporary engineers are not aware that many famous engineers have made aesthetics an explicit component of their work, beginning with the British engineer Thomas Telford. In 1812, Telford defined structural art as the personal expression of structure within the disciplines of efficiency and economy. Efficiency here meant reliable performance with minimum materials. Economy implied construction with competitive costs and minimal maintenance expenses. Within these bounds, engineer/structural artists find the means to choose forms and details that express their own vision, as Telford did in his Craigellachie Bridge (Figure 3.4). The arch is shaped to be an efficient structural form in cast iron, whereas the diamond pattern of spandrel bars, at a place in the bridge where structural considerations permit many options, is clearly chosen with an eye to its appearance.

Those engineers who were most conscious of the centrality of aesthetics for structure have also been regarded as the best in a technical sense. Starting with Thomas Telford (1757–1834), we can identify Gustave Eiffel (1832–1923), and John Roebling (1806–1869) as the undisputed leaders in their fields during the nineteenth century. They designed the largest and most technically challenging structures and they were leaders of their professions. Telford was the first president of the first formal engineering society, the Institution of Civil Engineers, and remained president for 14 years until his death. Eiffel directed his own design-construction-fabrication company and created the longest spanning arches and the highest tower of the time. Roebling founded his large scale wire rope manufacturing organization while building the world's longest spanning bridges (Figure 3.5).

In reinforced concrete, Robert Maillart (1872–1940) was the major structural artist of the early twentieth century. Maillart, first in his 1905 Tavanasa Bridge and later with the 1930 Salginatobel (Figure 3.3) and others, imagined a new form for three-hinged arches that included his own invention of the hollow box in reinforced concrete. The Swiss engineer Christian Menn (1927) has demonstrated how a deep understanding of arches, prestressing, and cable-stayed forms can lead to structures worthy of

FIGURE 3.4 Thomas Telford's Craigellachie Bridge.

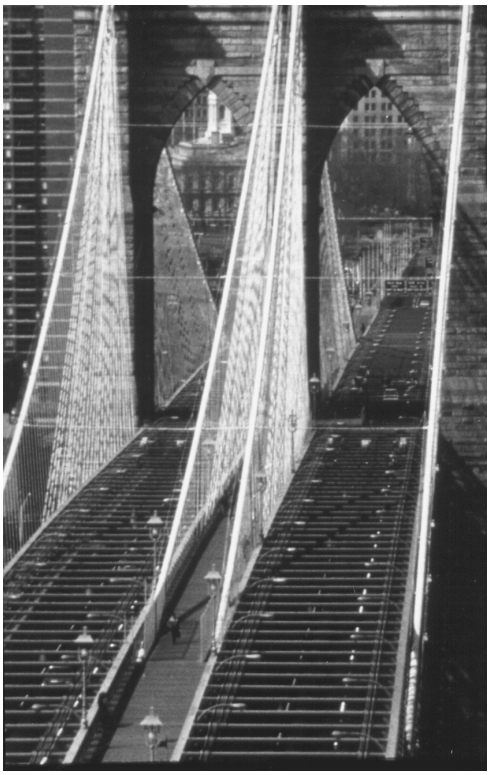

FIGURE 3.5 John Roebling's Brooklyn Bridge.

exhibition in art museums; for example, his 1964 Reichenau Arch (Figure 3.6) and his 1992 bridge at Sunniberg (Figure 3.7).

The engineers' aesthetic results from the conscious choice of form by engineers who seek the aesthetic expression of structure within the disciplines of efficiency and economy. Their forms are not the unconscious result of the search for economy nor the product of supposedly optimizing calculations. Instead, the engineer chooses a form from among several options with similar structural and economic

FIGURE 3.6 Rock foundations permit arch bridges. Christian Menn's Reichenau Bridge, Switzerland. (From AASHTO, *Bridge Aesthetics Sourcebook*, American Association of State Highway and Transportation Officials, Washington, DC, 2010. With permission.)

FIGURE 3.7 Christian Menn's Sunniberg Bridge.

characteristics because of its superior aesthetic potential. In seeking such aesthetic expression the engineers above and many other of the best structural engineers have recognized the possibility for structural engineering to be an art form parallel to but independent from architecture. These people have, over the last two centuries, defined a new tradition, structural art, which we take here to be the ideal for an engineer's aesthetic.

These works of structural art provide evidence that the common life flourishes best when the goals of freedom and discipline are held in balance. The disciplines of structural art are efficiency and economy, and its freedom lies in the potential it offers to the individual designer for the expression of a personal style motivated by the conscious aesthetic search for engineering elegance. These are the three leading ideals of structural art—efficiency, economy, and elegance.

3.2.2 Three Dimensions of Structure

Structure's first dimension is a scientific one. Each working structure must perform in accordance with the laws of nature. In this sense, then, technology becomes part of the natural world. Methods of analysis useful to scientists for explaining natural phenomena are often useful to engineers for describing the behavior of their artificial creations. It is this similarity of method that helps to feed the fallacy that engineering is applied science. But scientists seek to discover preexisting form and explain its behavior by inventing formulas, whereas engineers seek to invent forms, using preexisting formulas to check their designs. This scientific dimension is measured by efficiency.

Technological forms live also in the social world. Their forms are shaped by the patterns of politics and economics as well as by the laws of nature. Thus, the second dimension of structure is a social one. In the past completed structures might, in their most elementary forms, be the products of a single person: in the civilized modern world, however, these technological forms, although at their best designed by one person, are the products of a society. The public must support them, either through public taxation or through private commerce. The social dimension of structure is measured by Economy.

Technological objects visually dominate our industrial, urban landscape. They are among the most powerful symbols of the modern age. Structures and machines define our environment. The locomotive of the nineteenth century has given way to the automobile and airplane of the twentieth century. Large-scale complexes that include structures and machines become major public issues. Power plants, weapons systems, refineries, river works, transportation systems, and bridges—all have come to symbolize the promises and problems of industrial civilization.

Bridges such as the Golden Gate, the George Washington, and the Sunshine Skyway (Figure 3.8) serve to function for our time and carry on the traditions set by the Brooklyn Bridge. Nearly every American knows something about these immense structures, and modern cities repeatedly publicize themselves by visual reference to these works. So it is that the third dimension of technology is symbolic, and it is, of course, this

FIGURE 3.8 The Sunshine Skyway.

dimension that opens up the possibility for the new engineering to be structural art. Although there can be no measure for a symbolic dimension, we recognize a symbol by its expressive power and its elegance.

The designer must think aesthetically for structural form to become structural art. All of the leading structural artists thought about the appearance of their designs. These engineers consciously made aesthetic choices to arrive at their final designs. Their writings about aesthetics show that they did not base design only on the scientific and social criteria of efficiency and economy. Within those two constraints, they found the freedom to invent form. It was precisely the austere discipline of minimizing materials and costs that gave them the license to create new images that could be built and would endure.

3.2.3 Structural Art and Architecture

The modern world tends to classify towers, stadiums, and even bridges as "architecture," creating an important, but subtle, fallacy. The visible forms of the Eiffel Tower and the Brooklyn Bridge result directly from technological ideas and from the experience and imagination of individual structural engineers. Sometimes the engineers have worked with architects just as with mechanical or electrical engineers, but the forms have come from structural engineering ideas.

Structural designers give the form to objects that are of relatively large scale and of single use, and these designers see forms as the means of controlling the forces of nature to be resisted. Architectural designers, on the other hand, give form to objects that are of relatively small scale and of complex human use, and these designers see forms as the means of controlling the spaces to be used by people. The prototypical engineering form—the public bridge—requires no architect. The prototypical architectural form—the private house—requires no engineer. Structural engineers and architects learn from each other and sometimes collaborate fruitfully, especially when, as with tall buildings, large scale goes together with complex use. But the two types of designers act predominately in different spheres, and the results of their efforts deserve to have different names. Christian Menn's Sunniberg Bridge is an example of structural art arising solely from structural considerations. No architect was involved. "Architecture" is what architects do. "Structural art" is what engineers do.

3.3 Structural Art and the Design Process

3.3.1 Design Versus Analysis

Today many engineers see themselves as a type of applied scientist, analyzing structural forms established by others. Seeing oneself as an applied scientist is an unfortunate state of mind for a design engineer. It eliminates the imaginative half of the design process and forfeits the opportunity for the integration of form and structural requirements that can result in structural art. Design must start with the selection of a structural form. It is a decision that can be made well only by the engineer because it must be based on a knowledge of structural forms and how they control forces and movements.

Many engineers focus on analysis in the mistaken belief that the form (shape and dimensions) will be determined by the forces as calculated in the analysis. But, in fact, there are a large number of forms that can be shown by the analysis to work equally well. It is the engineer's option to choose among them, and in so doing, to determine the forces by means of the form, not the other way around.

Take the simple example of a two-span continuous girder bridge, using an existing structure, MD 18 over U.S. 50 (Figure 3.9). Here the engineer has a wide range of possibilities such as a girder with parallel flanges, or with various haunches having a wide range of proportions (Figure 3.10). The moments will depend on the stiffness at each point, which in turn will depend on the presence or absence of a haunch and its shape (Figure 3.11). The engineer's choice of shape and dimensions will determine the moments at each point along the girder. The forces will follow the choice of form. Within limits, the engineer can direct the forces as he chooses.

Now, let's examine which form the engineer should choose. All of them can support the required load. Depending on the specifics of the local contracting industry, many of them will be essentially

FIGURE 3.9 MD 18 over U.S. 50.

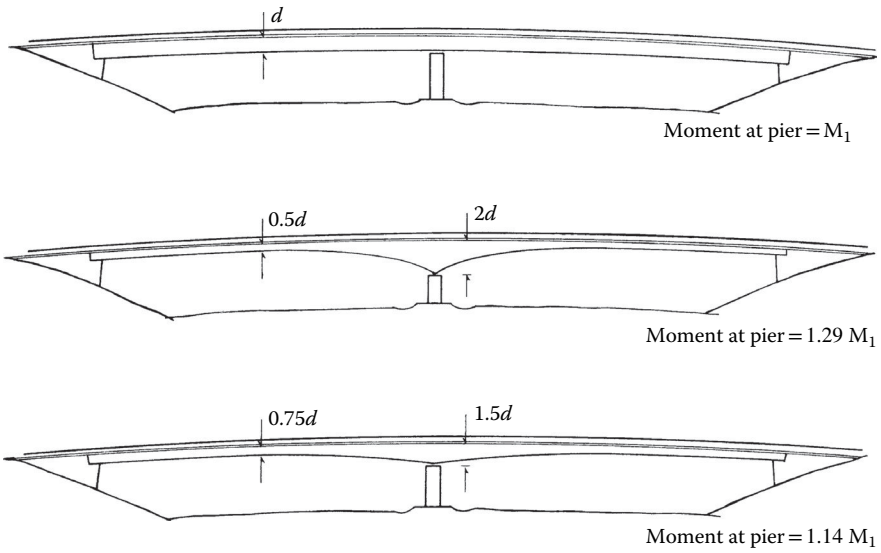

FIGURE 3.10 Forces determined by the engineer's choice of form.

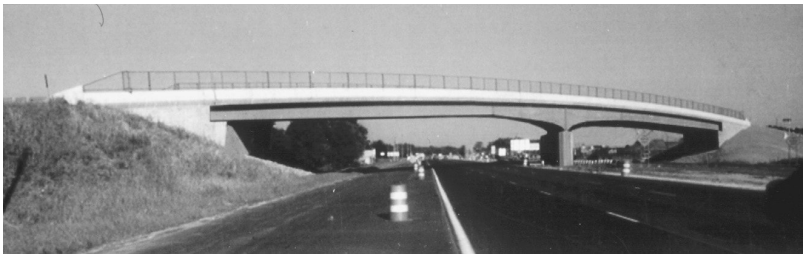

FIGURE 3.11 Another possibility for MD 18 over U.S. 50.

equal in cost. That leaves the engineer a decision that can only be made on aesthetic grounds. Why not pick the one that the engineer believes looks best?

That, in a nutshell, is the process that all of the great engineers have followed. Maillart's development of the three-hinged concrete box arch (Figure 3.3), for example, shows that the engineer cannot choose form as freely as a sculptor, but he is not restricted to the discovery of preexisting forms as the scientist is. The engineer invents form, and Maillart's career shows that such invention has both a visual and a rational basis. For Maillart, the dimensions were not to be determined by the calculations alone, and even the calculations' results could be changed (by adjusting the form) because a designer rather than an analyst is

at work. Analysis is the servant of design, not the source of it. Design, the development of the form, is by far the more important of the two activities. Before there is any analysis, there must be a form to analyze.

3.3.2 Role of Case Studies in Bridge Design

Looking at built bridges is a good way for engineers to improve their skills. Bridge design, especially of highway overpasses, often involves standard problems but always in different situations. Case studies can help designers with standard problems by showing models and points of comparison for a large number of bridges without implying that each such bridge be mere imitation.

The primary goal is to look carefully at all major aspects of the completed bridge, to understand the reasons for each design decision, and to discuss alternatives, all to the end of improving future designs. Such cases help to define more general ideas or principles. Case studies are well recognized by engineers when designing for acceptable performance and low cost; they can be useful when considering appearance as well. The parts of a case study for a typical highway overpass are as follows:

1. An *overall evaluation* of the bridge as a justification for studying it. Is it a good example that can be better? Is it a model of near perfection? Is it a bad example to be avoided?, and so on.
2. A *description* of the complete bridge, divided into parts roughly coinciding with easily identifiable costs and including modifications to each part as suggested improvements. In this major description there is an order to the parts that implies a priority for the structural engineer.
   a. The *Concept and Form* of the completed bridge goes together with a summary of the bridge performance history (including maintenance) and of its construction cost, usually given per square foot of bridge. Required clearances, foundation conditions, hydraulic requirements, traffic issues, and other general requirements would be covered here.
   b. The *Superstructure* includes primarily the main horizontal spanning members such as continuous girders, arches, trusses, and so on. In continuous steel girder bridges, the cost is primarily identified with the fabricated steel cost. Modification in design by haunching, changing span lengths, or making girders continuous with columns would be discussed including their influence on cost.
   c. The *Piers* are most frequently columns or frames either in the median or outside the shoulders or at both places in highway overpasses. These are normally highly visible elements and can have many possible forms. Different designs for the relationship among steel girder, bearings, and columns can make major improvements in appearance without detriment to cost or performance.
   d. The *Abutments* are also highly visible parts of the bridge that include bearings, cantilever walls, cheek walls, wing walls, and so on.
   e. The *Deck* includes the concrete slab, overhangs, railings, parapets, provisions for drainage, and so on, all of which have an influence on performance as well as on the appearance either when seen in profile or from beneath the bridge.
   f. The *Color* is especially significant for steel structures that are painted and texture can be important for concrete surfaces of piers, abutments, and deck.
   g. *Other Features* include lighting, signing, plantings, guardrail, and other elements and their transitions onto the bridge, all of which can have important visual consequences to the design.

   The order of these parts is significant because it focuses attention on the engineering design. The performance of a weak structural concept cannot be saved by good deck details. An ugly form cannot be salvaged by color or landscaping. The first four parts are structural, the fifth is in part structural, whereas the last two, while essential for the bridge engineer to consider, involve primarily nonstructural ideas.
3. A *comparison* to other similar bridges or bridge designs for similar conditions as a critique of the concept and form. Including bridges with very different forms creates a useful stimulus to design imagination.

4. A *conclusion* with a discussion of the relationship of this study to a theory of bridge design. Clearly any such discussion must be based upon a set of ideas about design that implicitly bias the writer, who should make these potential biases explicit. This conclusion should show how the case study illustrates a theory and even at times forces a modification of it. General ideas form only out of specific examples.

   The images of the MD 18 bridge (Figures 3.9 through 3.11) shows how a case study can be used to improve future designs. Understanding costs is always important, but breaking them down by components often identifies opportunities to make changes that significantly improve appearance without materially increasing cost. In this case recognizing that the cost of the steel girders was a relatively small part of the total bridge cost suggested improving the bridge's appearance by haunching the girder. Indeed, depending on the practices in a given state and the capabilities of local fabricators, the added fabrication cost of the haunch might be offset by the savings in steel, resulting in no cost increase at all. Any increase in girder cost might seem like a significant amount when measured relative to the cost of the girders by themselves. But seen relative to the cost of the bridge as a whole it could be a very small increase. Thus, a change in this one component can make a significant improvement in the appearance of the bridge but have little impact on the cost of the bridge as a whole.

3.4 Conceptual Engineering, the Neglected Phase of Design

3.4.1 Creating the Concept and Form

Creative engineering design consists neither in applying free visual imagination alone nor in applying rigorous scientific analysis alone nor in applying careful cost analysis alone, but of applying all three together at the same time. Creative engineering design starts with a vision of what might be. Development of the structural vision requires what many engineers call conceptual engineering. Conceptual engineering is the stage when the basic concept and form of the bridge is determined.

Conceptual engineering is the most important part of design. All that follows, including the aesthetic impression the bridge makes, will depend on the quality of the concept and form selected. Unfortunately, it is a stage that is often ignored or foreclosed by the application of unwarranted assumptions, preconceived ideas, or prior experience that may not in fact apply.

Reasons given for short changing this stage include "Everybody knows that (steel plate girders, precast concrete girders, cast in place concrete) are the most economical structure for this location," or "Lets use the same design as we did for the _____bridge last year." Or the selection of form is based largely on precedents and standards established by the bridge-building agency. For example, the form of a highway overpass may be predetermined by the client agency to be (steel plate girders, precast concrete girders cast in place concrete), because that is what the agency is used to or what local contractors are used to or even because the (steel plate girders, precast concrete girders, cast in place concrete) industry is a dominant political force in the state. Or the decision to forgo conceptual engineering may be simply habit—either the engineer's or the client's—often expressed in the phrase "We've always done it that way." The assumption underlying all of the above is that the current bridge cannot benefit from changes in ideas, practices, or materials that might have occurred since previous designs were done.

Some will protest conceptual engineering is unnecessary because costs will indeed differentiate and determine the form. Such beliefs often rely too much on unit costs from past projects, ignoring changing conditions, or unique aspects of the current bridge that might result in different unit costs. Or, the engineer might be assigning unwarranted precision to the results of his cost calculations. The cost of the bridge will not be the cost the engineer calculates; it will be whatever cost a contractor is willing to build it for. Rarely do engineer's estimates get within 5% of the contractor's bid. Given the engineer's lack of knowledge about the precise cost, differences of 5% or less might as well be treated as cost—neutral.

Perhaps the most insidious reason conceptual engineering is shortchanged is the practice of bridge building agencies to budget design separately from construction. This leads to pressure to minimize the cost of design, and the design phase most likely to be cut is conceptual engineering. Such decisions are usually based on the types of unexamined assumptions listed above. Thus, potential savings of hundreds of thousands of dollars in construction are foregone in order to save tens of thousands of dollars on design, the ultimate example of penny/wise—pound/foolish thinking.

Accepting these assumptions and beliefs places an unfortunate and unnecessary limitation on the quality of the resulting bridge. It often results in hammering a square peg into a round hole, creating a suboptimal bridge and unnecessary construction cost that far outweighs the cost of conceptual engineering. It also sacrifices the chance for innovation for, by definition, improvements must come from the realm of ideas not tried before. As Captain James B. Eads put it in the preliminary report on his great arch bridge over the Mississippi River at St. Louis:

> Must we admit that, because a thing has never been done, it never can be, when our knowledge and judgment assure us that it is entirely practicable?*

Unless these assumptions are challenged, no design will occur. Instead, there will be a premature assumption of the bridge form, and the engineer will move immediately into the analysis of the assumed type. That is why so many engineers mistake analysis for design. Design is more correctly the selection of the concept and form in the first place, which many engineers have not been permitted to do.

3.4.2 Doing Conceptual Engineering

Conceptual engineering should be the stage when all of the plausible options, and some not so plausible, are considered. Thus the engineer's first job is to question all limiting assumptions and beliefs. From that questioning will come the open mind that is necessary to develop a vision of what each structure can be at its best. Unless such questioning is the starting point it is unlikely that the most promising ideas will ever appear.

The options are then examined at a rough level of precision, with consideration of the design intent (see Section 3.5.2.2), various materials, size and form of major members, constructability, project cost, life cycle economics, and appearance. The most promising ideas are then taken to greater levels of refinement. Solutions will emerge that fit the requirements of the site and that are roughly equivalent in terms of structural efficiency and economics. The form of the bridge can then be selected based on which of these solution best appeals to the aesthetic sensibilities of the designer, the owner, and the public.

3.5 Application to Design

3.5.1 Ten Determinants of Appearance

"How people react to an object depends on what they see and the order in which they see it. This means the largest parts of the bridge—the superstructure, piers and abutments—have the greatest impact. Surface characteristics (color/texture) come next, then details (*Sourcebook*, p. 15)." This underlies the idea of a hierarchy of design as introduced in Section 3.3 and laid out in more detail here. In summary, design decisions should be approached in the following order of importance:

* James B. Eads 1868. Report of the Engineer-in-Chief of the Illinois and St. Louis Bridge Company, St. Louis, Missouri Democrat Book and Job Printing House; as reprinted in Engineers of Dreams, Henry Petroski, 1995, New York, Alfred A. Knopf, p. 54.

1. Horizontal and vertical geometry
2. Superstructure type
3. Pier/support placement and span arrangements
4. Abutment placement and height
5. Superstructure shape (including parapets, overhangs, and railings)
6. Pier shape
7. Abutment shape
8. Color
9. Texture, ornamentation, and details
10. Lighting, signing, and landscaping

It is the last five elements that are usually considered the "aesthetic" elements, but they are the least important in determining the final result. The aesthetic impact of the first five elements must be considered from the very beginning, or the resulting bridge will be a disappointment.

3.5.2 Thinking about Aesthetics in Design

Before a designer can start on the bridge itself, he or she must understand what the bridge is expected to accomplish, functionally as part of a transportation system and socially, visually and symbolically as part of a living community and environment. The designer must have an idea of all of the criteria that the structure must meet and all of the concerns that will act on the structure. In recent years, the Federal Highway Administration (FHWA) and many other transportation agencies have recognized that this is a broad task, requiring the coordination of many, often competing, interests. This process has been given the name Context Sensitive Design. (*Sourcebook*, p. 5; see the *Sourcebook* for more detail on how to use Context Sensitive Design techniques to address all of the concerns involved in a project.)

3.5.2.1 Understand the Goals and the Site

3.5.2.1.1 Owner Requirements

These requirements begin, of course, with the transportation goals that must be met. These include the widths and design speeds of the roadways being carried or traversed, what types of traffic will the bridge be expected to carry or traverse, and whether that includes pedestrians and/or transit. Among other things, these requirements will determine clearance envelopes the bridge must provide.

The owner may have conducted or be bound by a previous feasibility study, Environmental Assessment, Environmental Impact Study or other document, or there may be a formal project purpose and need statement that defines what the intended result of the project is. Other owner requirements will include design standards and policies, including in many cases existing aesthetic design guidelines. Finally, the owner may have established cost limitations that have to be considered.

3.5.2.1.2 The Community and Other Stakeholder Requirements

Potential stakeholders include communities, elected officials, businesses, public review agencies, and the people that will live with the bridge after it is constructed. All concerned parties should be involved from the very beginning, before putting pencil to paper. If people know that they have been included from the beginning, and that the designers have no preconceived notions, the process will run more smoothly, the final result will address the most strongly held desires of the community (Figure 3.12) and it will meet with their approval.

FIGURE 3.12 Community uses under a bridge may be as important as transportation uses. 17th Street Causeway, Ft. Lauderdale, Florida. (From AASHTO, *Bridge Aesthetics Sourcebook*, American Association of State Highway and Transportation Officials, Washington, DC, 2010. With permission.)

3.5.2.1.3 The Site

The obvious concerns are the physical features. Bridges over canyons or deep cuts will require a structural type that may be inappropriate for a highway crossing. Rivers have a certain width that must be crossed. Geology may favor a certain type of foundation or substructure layout.

Aesthetically, the site establishes the visual field or background against which the bridge will be seen and the context within which it will be judged. Some examples are as follows:

- A bridge on a high profile crossing a canyon or deep valley or a side hill alignment will be visible from a distance. The relationship of the bridge form to the sides of the canyon/valley will likely define the aesthetic impact.
- A bridge located at the top of a crest on a ridgeline will frame views of the distant landscape (Figure 3.13).
- A bridge on a flat coastal plain or over open water is often seen from a distance and in silhouette. The overall composition of its forms and its parts may be the most defining visual image.
- A bridge over a depressed highway will usually be the most prominent feature in the driver's visual field. The form and proportions of the superstructure, piers, and abutments will be critical to its aesthetic impact.

A rural site will have a background of natural features; an urban site will have a background of adjacent buildings and structures with their own architectural features.

How all of this looks will be affected by the daily movement of the sun and the change of seasons. The viewpoints and areas from which the bridge will be seen and by whom need to be understood and, in many case prioritized. It is not always possible to make a bridge look good from all angles.

The best way to understand the visual field is to go to the site at different times of day, at night and in as many different seasons as possible, and take lots of photos. For both aesthetic and technical reasons, there is no substitute for first-hand familiarity with the bridge site.

FIGURE 3.13 Genesee Mountain Interchange, I-70, Colorado. As motorists travel west from Denver on I-70, this bridge frames their first view of the Rocky Mountain peaks along the Continental Divide. (From AASHTO 2010, *Bridge Aesthetics Sourcebook*, American Association of State Highway and Transportation Officials, Washington, DC, 2010. With permission.)

3.5.2.1.4 Corridors and Interchanges

If the bridge is part of a larger project, an interchange or corridor, where multiple structures will be seen at the same time or in quick succession, the relationships between them needs to be considered. This situation often leads to the establishment of a theme that mandates similar forms for similar parts of the bridges in order to reduce the visual cacophony that results when bridges with different forms and details are seen together (Figure 3.14).

3.5.2.2 Develop a Design Intention

The *Sourcebook* describes this step as a written list of all of the factors that will influence the design of the bridge in their order of importance. The designer should solicit comments from all involved parties, make appropriate revisions, and then get it approved by the owner. This will be the basis of all future design work.

This step may have already been taken as part of an Environmental Impact Statement or planning study, which often result in a "purpose and need statement" or similar document. However, such statements need to be carefully reviewed to insure that they fully incorporate all of the bridge design issues and that no important component is missing.

3.5.2.3 Do a Conceptual Engineering Study

The importance of conceptual engineering is discussed in Section 3.4. Here are some techniques for making a conceptual engineering study successful.

1. Involve All Stakeholders in Identifying Options

> "Communities and review agencies will have opinions about what types of bridges are appropriate. Testing their ideas in the conceptual engineering phase will avoid the need to go back and look at their options later when they object that their ideas are not being considered. It will also encourage their support of the final decision. It may even result in the adoption of a superior but previously unconsidered bridge type (*Sourcebook*, p. 12)".

FIGURE 3.14 Albuquerque's Big I interchange has a theme covering pier shapes, MSE walls, standard details, and colors, the latter developed with community input. (From AASHTO, *Bridge Aesthetics Sourcebook*, American Association of State Highway and Transportation Officials, Washington, DC, 2010. With permission.)

2. Make sure all involved stakeholders know all of the implications of the alternatives, including comparative costs. Knowing all of the facts, they will be more likely to support the final decision.
3. Test promising options with 3D views taken from the important viewpoints. Even seasoned design professionals have a hard time anticipating all of the visual implications of a design from 2D engineering drawings. For nonprofessionals it is almost impossible. Showing 3D views of a planned bridge gives all participants a common image of each option to work from (Figure 3.15).
4. Evaluate the options and make the selection based on efficiency, economy, and elegance. Only by applying all three criteria of efficiency, economy, and elegance to multiple alternatives can the process narrow down to the concept that best satisfies all of the requirements.
5. Produce the Conceptual Engineering report. Many agencies call the product of conceptual engineering the type, size, and location report.

3.5.2.4 Proceed to Detailed Analysis and Design

Section 3.6 provides practical ideas for the detailed design of aesthetically pleasing bridges.

3.5.3 Working with Architects, Landscape Architects, and Artists

Gifted engineers working without the assistance of architects, artists, or other visual professionals have produced masterpieces. Thus, it is not necessary for all bridge design teams to include visual professionals. The engineer should seek to develop his or her skills in this area. However, for reasons of time or personal inclination, this is not always possible. Accordingly, engineers have often sought the advice of

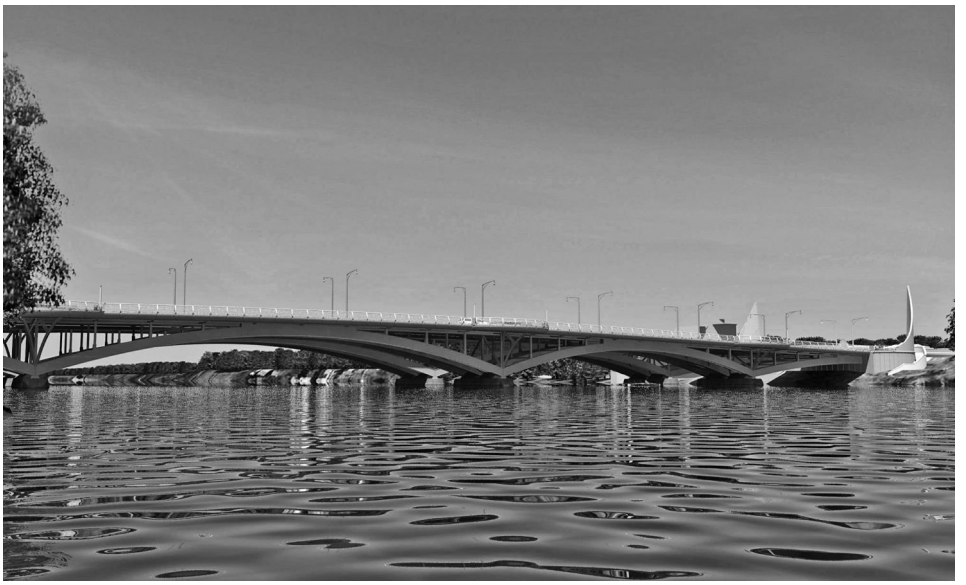

FIGURE 3.15 A photo simulation showing how a proposed bridge will affect an existing recreational lake and nearby commercials trip. Proposed Ken Burns Bridge over Lake Quinsigamond, Worchester, Massachusetts.

other visual professionals—experts in aesthetics who are consulted in the same way as experts in soils, traffic, and wind. Many memorable bridges illustrate the potential success of this approach. The Golden Gate Bridge is a famous example.

Such collaboration does not relieve the engineer of the responsibility to be knowledgeable about aesthetics. As the leader of the design team, he or she remains responsible for the final result. Many overdecorated and expensive failures have been created when the collaboration was done poorly or when someone other than the engineer took over the lead role. The visual professional's role should be as aesthetic advisor and critic, making comments and suggestions for the engineer's consideration. In this role a landscape architect, urban designer, architect, or artist can have a positive impact, but the engineer must have the last word (*Sourcebook*, p. 48).

Figure 3.16, for example, shows a successful collaboration between an engineer and architect.

If the involvement of aesthetic advisors is to be successful, the engineer must be sure that they understand the basic issues involved in bridge design. Most visual professionals are used to dealing with buildings and their immediate surroundings, but bridges are significantly different than buildings. They are much larger, they are often seen at high speeds, and they typically have few surfaces that are flat and level. The architect/landscape architect needs to take the time to understand these differences, and the engineer needs to insist that he or she does. Effectively working with other visual professionals also requires that the engineer develop sufficient knowledge about aesthetics and sufficient self-confidence to recognize valuable ideas and reject inappropriate ideas.

Some have observed that the public seems to more readily accept bridges designed by teams that include architects, urban designers, or landscape architects than those that do not. People sometimes feel that more of their goals will be met when such professionals are involved, in part because most people in these professions are skilled at discussing and responding to community concerns. Unfortunately, engineers have a reputation for being insensitive to community wishes, due in part to many engineers' inability to speak clearly and knowledgeably in this area.

The engineer needs to develop the vocabulary and knowledge to remain the project's spokesman to the client and community groups, even concerning aesthetic ideas. Gaining the vocabulary and

FIGURE 3.16 An example of a successful collaboration between an engineer and an architect/urban designer which considers nearby land uses and views as well as technical requirements. Clearwater Memorial Causeway, Clearwater, Florida. (From AASHTO, *Bridge Aesthetics Sourcebook*, American Association of State Highway and Transportation Officials, Washington, DC, 2010. With permission.)

knowledge to respond to a community's aesthetic concerns allows an engineer to fulfill the leadership role and retain the community's confidence.

3.5.4 Replacing Historic Bridges/Designing Bridges in Historic Places

Some communities see themselves as historic enclaves and view a bridge as a chance to restate local architectural traditions (Figure 3.17). In those situations a formal historic review process may be in place. The result is often pressure to build a new bridge that looks just like a previous bridge or matches a nearby architectural style. These projects are seldom an aesthetic success. Indeed, in situations governed by the National Commission for Historic Preservation, such an approach violates the Secretary of Interior Standards for Historic Preservation. A better approach is to develop new designs which respect and emulate elements of the previous bridge and any surrounding historic district. More detail on handling these concerns can be found in the *Sourcebook*.

FIGURE 3.17 Two existing traditional bridges, both eligible for the National Register of Historic Places, were replaced by bridges of innovative contemporary design in tune with the community's aspirations and self-image. Rich Street and Main Street Bridges, Civic Center, Columbus, Ohio.

3.6 Design Guidelines

The following section presents a quick outline of the practical ideas for developing an aesthetically successful bridge. The full details can be found in the *Sourcebook*. Ideas are presented for the Ten Determinants of Appearance in the order of their importance as discussed above.

3.6.1 Horizontal and Vertical Geometry

Before there is a concept for a bridge, the roadway geometry creates a ribbon in space that in itself can be either attractive or unattractive. The geometry establishes the basic lines of the structure, to which all else must react. A graceful geometry will go a long way toward fostering a successful bridge, while an awkward or kinked geometry will be very difficult to overcome. The structural engineer must work interactively with the project's highway engineers during development of the project geometry. A proactive approach is highly recommended since it is extremely difficult to change the project geometry during later stages (*Sourcebook*, p. 15).

This is a topic that particularly benefits from 3D studies, especially if the geometry can be overlaid on the topography through photos or digital terrain models.

3.6.2 Superstructure Type

The superstructure type refers to the structural system used to support the bridge. It can be an arch, girder, rigid frame, truss, or cable-supported type structure. Because of their size and prominence, the most memorable aspect of the structure will be provided by its structural members. The following are few highlights from the *Sourcebook* (pp. 17 and 18):

- Generally, thinner structures with longer spans are more visually transparent and pleasing than deeper structures or structures with shorter spans (see Figure 3.15).
- The superstructure can be shaped to respond to the forces on it so that the bridge visually demonstrates how it works. For example, haunched girders demonstrate the concentration of forces and moments over the piers. They also reduce the midspan structure depth and provide a more visually interesting opening beneath the structure (see Figure 3.18).
- Use of different structure types over the length of a bridge should be avoided as it usually interrupts the visual line created by the superstructure and is contrary to developing a sense of unity and integrity. If different structural types are unavoidable then a common parapet profile or other feature needs to be found to tie them together.

FIGURE 3.18 The haunch gives this girder a more interesting and attractive shape that also tells a story about the flow of moments and forces in the structure. The stiffener is utilitarian but its placement and curvature make it ornamental as well, so that it reinforces the story told by the haunch. I-81, Virginia. (From AASHTO, *Bridge Aesthetics Sourcebook*, American Association of State Highway and Transportation Officials, Washington, DC, 2010. With permission.)

- For multispan girder bridges, it is preferable to use the same depth of girder for the entire bridge length and not change girder depths based on the length of each individual span except for haunches at the piers.
- The underside of the bridge or soffit as a ceiling will be important for bridges over pedestrian traffic or recreational trails, where the underside will be readily visible because of the slow speed and close proximity of the observers.

3.6.3 Pier/Support Placement and Span Arrangements

Most bridges are linear frameworks of relatively slender columns and girders. A bridge viewed from its side will appear as a transparent silhouette (Figure 3.19). A bridge viewed looking along its length will appear to be a collection of massive structural forms. Pier placement will largely determine how attractive these views are.

The success of the visual relationship between the structure and its surrounding topography will depend heavily on the apparent logic of the pier placement. For example, a pier placed at the deepest point in a valley will seem unnecessarily tall. A pier placed in the water near the shore will seem less logical than one placed on the shore.

Pier placement establishes not only the points at which the structure contacts the topography but also the size and shape of the openings framed by the piers and superstructure. It is desirable to keep constant the height/span ratio of these openings.

3.6.4 Abutment Placement and Height

The abutment is the location where a bridge reaches the ground and the transparency of the structure transitions to the mass of the adjoining roadway or topography. Abutments may become visually massive structures (Figure 3.20) or practically disappear (Figure 3.21), depending on their height and the nature of the grading at the bridge ends. Abutment placement is visually more important on shorter bridges than on longer bridges, since an observer is more likely to view a short bridge in its entirety. Shorter abutments placed farther up on the slope widen the opening below the bridge and allow a more inclusive view of the landscape beyond. Taller abutments placed closer to an undercrossing roadway more strongly frame the opening and create a gateway effect. Passage through the bridge seems more of an event.

The abutment placement also influences the attractiveness of the space below the bridge for pedestrians. The abutment needs to be set back far enough to allow for a decent sidewalk width and shaped to avoid niches and offsets that might become hiding places or maintenance headaches.

FIGURE 3.19 The substructure for this high-level crossing with slender piers is virtually transparent. Meadows Parkway over Plum Creek, Castle Rock, Colorado (*Sourcebook* 3.6). (From AASHTO, *Bridge Aesthetics Sourcebook*, American Association of State Highway and Transportation Officials, Washington, DC, 2010. With permission.)

FIGURE 3.20 This full-height abutment frames a portion of the landscape beyond the bridge. Meadows Parkway Railroad Overpass, Castle Rock, Colorado (*Sourcebook* 2.8). (From AASHTO, *Bridge Aesthetics Sourcebook,* American Association of State Highway and Transportation Officials, Washington, DC, 2010. With permission.)

FIGURE 3.21 These minimum-height abutments essentially disappear behind the trees, maximizing the opening under the bridge and the view through to the area beyond. It is also a good example of the values to be gained by thinness and simplicity. I-95 over Pulaski Highway, Baltimore, Maryland (*Sourcebook* 1–4). (From AASHTO, *Bridge Aesthetics Sourcebook,* American Association of State Highway and Transportation Officials, Washington, DC, 2010. With permission.)

3.6.5 Superstructure Shape (Including Parapets, Overhangs, and Railings)

The superstructure elements such as deck overhangs, parapets, and railings establish and enhance the form of the structural members. The shapes of these elements and the shadows they cast will strongly influence the aesthetic interest of the structure. For example, the overhang dimension between the edge of the bridge deck and the girder fascia can range between two extremes.

- A wide overhang can create a deep shadow. When used in conjunction with a thin deck slab line and a relatively transparent barrier, the bridge is perceived as being slender and lighter.
- A narrower overhang will put the face of the parapet closer to the face of the fascia girder, making them look like one surface and making the superstructure seem thicker.

Railings and parapets are among the most visually prominent elements of a bridge (Figure 3.22). They are located at the highest point, are usually visible from a distance, and are the bridge components that are closest in proximity to drivers and pedestrians. From a cost perspective, modifications to railings and parapets

FIGURE 3.22 This pedestrian fence uses standard chain link, but the arched top edge, carefully designed details and distinctive color improve the appearance of the bridge without a significant increase in cost, I-235 Reconstruction, Des Moines, Iowa (*Sourcebook* 4–24). (From AASHTO, *Bridge Aesthetics Sourcebook*, American Association of State Highway and Transportation Officials, Washington, DC, 2010. With permission.)

are often less expensive than modifications to girders or other bridge components. Thus improvements to the railings and parapets can be a cost-effective way to improve the appearance of a bridge (*Sourcebook*, p. 21).

3.6.6 Pier Shape

The pier shape refers to the form and details of the piers. From many viewpoints, particularly those at oblique angles to the structure, the shapes of the piers will be the most prominent element of the bridge.

The majority of piers for many bridges are structural frames consisting of circular or rectangular columns with a cap beam that supports the superstructure girders. They look like an assembly of different parts rather than a unified form. Improving their appearance requires integrating the parts by, for example, aligning exterior columns with the outside end of the cap. This eliminates the cap cantilevers, integrates the columns with the cap and thus simplifies the overall appearance of the pier (as shown in Figure 3.22).

A major improvement can be obtained by integrating the pier cap within the plane of the superstructure. This type of cap is commonly used for concrete box girder bridges, and is an important reason for their visual appeal. It can also be used on other bridge types, such as steel plate girders. With this design the pier cap is invisible. The pier appears much simpler because the transverse lines of the cap are eliminated (see Figure 3.14). This change is particularly helpful on skewed bridges, where the length of a dropped pier cap makes it a sizable and distracting element.

3.6.7 Abutment Shape

As we saw in the section on abutment placement, abutments may become visually massive structures or practically disappear. Much depends on the height of the abutment together with the grading around it. Mid height and full height abutments create large surfaces that strongly influence how the bridge is perceived. Abutment shapes are typically more important visually on shorter bridges than on longer bridges, since an observer is more likely to view a short bridge in its entirety. For structures involving pedestrians, either on the bridge or below it, the provisions made for them at the ends of the bridge can be among the most memorable aspects of the structure for them.

Abutments may also have an important symbolic function, as these are the points where travelers begin and end their passage over a bridge. The abutment shape and/or elements placed on it can also be used to emphasize the bridge as a gateway to communities, parks, or other significant places (as in Figure 3.20). These elements need to be visually consistent with the bridge itself and large enough to have an effect when seen at the distances from which the bridge is usually observed. This is particularly necessary for elements

that will be seen from a multi-lane high speed roadway. Such elements will need to be on the order of 50 feet high and at least 10 feet wide in order to be noticed at all (note height of abutment feature in Figure 3.15).

3.6.8 Color

Color has a long history of application on bridges because of its strong visual impact at a low cost. Color, or lack thereof, will influence the effect of all the decisions that have gone before. It provides an economical vehicle to add an additional level of interest. The colors of uncoated structural materials as well as coated elements and details need to be considered.

Since bridges are almost always relatively small elements within the visual field of which they are a part, it is necessary to select color in relation to the surroundings. This can be done by means of colored photographs taken at various times of the day and at various seasons, or, better yet, by actually going to the site. There are several plausible strategies outlined in the *Sourcebook* (p. 27), such as

- Integrate the bridge into the surrounding landscape by selecting colors similar to nearby vegetation, rock formations, and so on. Many designers select shades of green, red, or brown with this in mind.
- Create a strong identity for the bridge by visually contrasting it with its surroundings. This may be particularly appropriate in the case of sites with little vegetation where the bridge can be viewed from a distance. The Golden Gate is a famous example of this strategy.
- Identify the bridge with a geographic region or culture through the use of colors that will form this association. For example, New Mexico has a tradition of coloring bridge surfaces to relate to its distinctive Native American culture.

Selection of a strategy should be an outgrowth of the vision statement.

It is foolhardy to select a color for something as large as a bridge or wall by looking at Federal Standard color chips in the office. At the very least, take the chips out to the site. Better yet, require the contractor to provide large (at least 4' x 8') sample panels on site on which candidate colors can be tested and a final selection made (*Sourcebook*, p. 27).

Color choices are complex decisions requiring specialized technical knowledge and refined visual sensibility. Architects and especially landscape architects frequently make color selections for outdoor environments. They can be helpful consultants.

3.6.9 Texture, Ornamentation, and Details

Ornamentation, texture, and details are elements that can add visual interest and emphasis. Structural elements themselves, such as stiffeners and bearings, can serve this function. Indeed, traditional systems of architectural ornament started from a desire to visually emphasize points where force is transferred, such as from beam to column through an ornamental capital.

Patterns of grooves or insets and similar details are other examples. Surface texturing, often produced by formliners, can be used to create patterns, add visual interest and introduce subtle surface variations and shading, which in turn soften or reduce the scale or visual mass of abutments, piers, and walls (*Sourcebook*, p. 27).

Ornament is best used sparingly. Less is generally better than more (Figure 3.23). As bridge engineer J.B. Johnson put it in 1912:

> In bridge building…to overload a structure or any part thereof with ornaments… would be to suppress or disguise the main members and to exhibit an unbecoming wastefulness. The plain or elaborate character of an entire structure must not be contradicted by any of its parts.

Above all, do not use false arches or other fake structural elements as cosmetic "make up" to disguise an inappropriate or uninteresting design. Aside from requiring additional costs to construct and maintain, adding false structure will rarely improve a design and is often viewed as extraneous clutter.

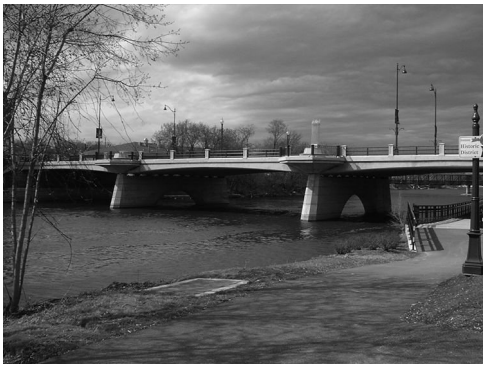

FIGURE 3.23 Rather than pasting bulky, vaguely historical ornament on a conventional structure, the designers of the Wilson Street Bridge in Batavia, Illinois have dealt with a historic setting in a different way. They have combined a structure of amazing thinness, only possible because of modern high strength concrete and post tensioning, with traditional details that reflect the nature of its setting. Both the past and the future are expressed, whereas views up and down the river are reopened that had been blocked for decades by the previous earth-filled concrete arch.

Using formliners that mimic other materials is particularly tricky. Using one material to simulate another creates a type of visual dishonesty that is always a problem in aesthetics. Some highlights from the *Sourcebook* (pp. 27 and 28):

- When using formliners to simulate another material, avoid suggesting a material that would not be utilized in that application. For example, stone texturing on the surfaces of a cantilevered pier cap creates visual disharmony because a cantilever could not in fact be constructed with stone.
- When simulating traditional material, such as stone or brick, formliner-created surfaces should be made as realistic as possible. For example, "mortar lines" should line up when the pattern turns a corner, just as they would on real masonry. Use color in addition to texture to assist in the simulation by, for example, differentially staining the "stones" of a simulated stone wall to reflect the variations in color found within and between actual stones (see Figure 3.20).
- The use of horizontal lines in patterns requires special attention to avoid conflict with the profiles of roadways and bridges, which are rarely straight or level. For example, the lines produced on a bridge parapet by a formliner with a strong horizontal pattern are likely to conflict with the top and bottom edges of the girder and/or parapet.
- Consider the speed and position of the observer. When texture is viewed up close and at slow speeds, the depth of relief and the details of the pattern can be fully appreciated. However, on a bridge over a rural freeway, finely textured surfaces and complicated patterns will not be perceptible to travelers moving at high speeds. In freeway conditions features with minimum dimensions of 3 or 4 inches and textures with a minimum relief of 2–3 inches are necessary to create a visible effect.
- The use of textures needs to be closely monitored in construction, since poor detailing or construction can severely affect the appearance. For example, the contractor should be required to align features of formliners between one formliner panel and the next so that no construction joints interrupt the overall pattern.

Utilitarian details, such as electrical conduits or bridge drainage, often create major and unforeseen visual impacts on bridge appearance (Figure 3.24). Every visible element of the bridge, no matter how utilitarian or seemingly inconsequential, must be anticipated and integrated into the concept. If it is visible, it must be designed to be seen.

FIGURE 3.24 This drainage system and blocky pier clash with an otherwise attractive overall aesthetic scheme. Union Pacific Railroad Bridge over I-25, Castle Rock, Colorado. (From AASHTO, *Bridge Aesthetics Sourcebook,* American Association of State Highway and Transportation Officials, Washington, DC, 2010. With permission.)

3.6.10 Lighting, Signing, and Landscaping

Though not actually part of the structural system, these elements can have great influence on the aesthetic impression a bridge makes.

3.6.10.1 Lighting

Roadway lighting is governed by the illumination requirements of the owner, but still requires multiple choices of pole type, height, and spacing as well as fixture and lamp type. Although an individual pole may not seem to be much of a visual element, a row or array of them on a bridge will exert surprising influence on the appearance of the bridge. Close coordination with the lighting engineer is necessary to make sure that this influence is positive.

The most important step is to simplify the array. For example, place all of the poles on either the median or the sidewalk, but not both. Another goal is to coordinate the pole location with bridge features by, for example, lining the poles up with pier locations or, at the very least, centering the longitudinal pattern of pole placement at the midpoint of the bridge.

Lighting of the bridge itself is a good way to draw attention to the bridge and make it an asset to the nighttime environment (Figure 3.25). Such lighting must be sensitive to motorists, pedestrians, boaters,

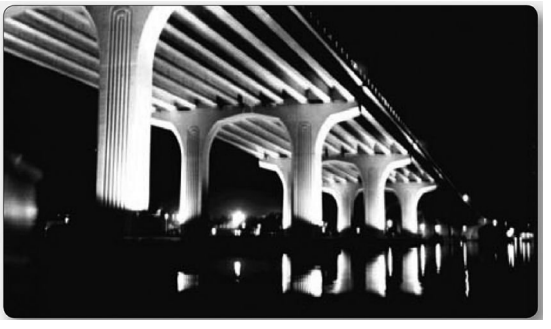

FIGURE 3.25 The Merrill Barber Bridge is located in Vero Beach, Florida. The pier flood lighting consists of high pressure sodium-type fixtures that are mounted 12' above the waterline pile caps. The lighting illuminates the piers and the bottom-side of the superstructure. The piers themselves are worth lighting because they incorporate several good design ideas. The vertical shafts are widely spaced and relatively thin; they are made to appear thinner by their vertical grooves. The cap is partially integrated into the plane of the girders so it appears thinner, and its bottom is gracefully curved to make it even thinner in the center and at its ends. (From AASHTO, *Bridge Aesthetics Sourcebook*, American Association of State Highway and Transportation Officials, Washington, DC, 2010. With permission.)

and other users. It should be selected and located to enhance and highlight the structure, yet minimize glare and unnecessary distraction. The lighting must respond appropriately to the context, both in terms of surrounding structures and environmental conditions. Considerations of impact on wildlife and light pollution in the night sky should be weighed together with those of aesthetics. Aesthetic lighting design for bridges requires specialized technical knowledge and refined visual sensibility beyond the capabilities of many lighting engineers. It is a consulting specialty of its own. Engineers should consider including such specialists when developing an aesthetic lighting design.

3.6.10.2 Signing

There are two types of signs mounted on bridges. The first and most common is where the bridge itself is used as a support for a sign serving the under passing roadway. The second is when a sign structure is erected on a bridge to serve the bridge's own roadway. This is often necessary on long viaducts and ramps. In both situations the sign usually blocks and/or complicates the lines of the bridge itself. The result is rarely attractive. Thus, the most desirable option is to keep signing off bridges. Saddling a bridge with an unattractive sign or sign structure defeats the purpose of creating an attractive aesthetic bridge design. The first goal should be to seek alternate locations for signs away from bridges. This will inevitably mean more specialized structures for the signs themselves (*Sourcebook*, p. 32).

The *Sourcebook* makes suggestions for what to do when signs must be mounted on bridges.

3.6.10.3 Landscaping

Landscaping is defined here to include planted areas and hardscape: stone, brick, or concrete paving, often colored and/or patterned, used primarily for erosion control or pedestrian circulation. Landscaping should enhance an already attractive structure. It should not be relied upon to cover up an embarrassment or hide some unfortunate detail. Conversely, it should not be allowed to grow up to hide some important feature that is crucial to the visual form of the bridge. Landscaping can be a more economical and effective way to add richness and interest to a design rather than special surface finishes or materials (see Figure 3.26). For example, a large, plain concrete abutment can be effectively enhanced by well-chosen landscaping (*Sourcebook*, p. 32).

FIGURE 3.26 Well-integrated landscaping at a bridge over I-5 in Olympia, Washington.

3.7 The Engineer's Challenge

The design guidelines just outlined will improve most everyday structures, but they will not guarantee structural art. There are no hard and fast rules or generic formulas that will guarantee outstanding visual quality. Each bridge is unique and should be studied individually, always taking into consideration all the issues, constraints, and opportunities of its particular setting or environment. Nevertheless, observing the successes and failures of other bridges and using design guidelines can improve an engineer's aesthetic abilities and help avoid visual disasters.

Society holds engineers responsible for the quality of their work. No one has the right to build an ugly bridge. Bridge designers must consider visual quality as fundamental a criterion in their work as performance, cost, and safety. Engineers can learn what makes bridges visually outstanding and develop their abilities to make their own bridges attractive. They can achieve outstanding visual quality in bridge design without compromising structural integrity or significantly increasing costs.

The ideal bridge is structurally straightforward and elegant, providing safe passage and visual delight for drivers, pedestrians, and people living or working nearby. It is an asset to its community and its environment. The engineer's challenge is not just to find the least costly solution. The engineer's challenge is to bring forth elegance from utility: we should not be content with bridges that just move cars and trucks and trains; they should move our spirits as well.

Acknowledgments

As mentioned in Section 3.1, the concepts in this chapter are inspired by the works of David Billington, professor of engineering at Princeton University. Through his descriptions and analyses of the works of outstanding engineers such as Thomas Telford, John Roebling, Christian Menn, and particularly Robert Maillert, he has reminded us all of the role that aesthetics has always played in the design of bridges of the highest quality. Indeed, Sections 3.2 and 3.3 are largely his work, adapted from the previous edition of this chapter that he and the author composed together. The later parts of the chapter are based on the *Bridge Aesthetics Sourcebook* prepared by the Bridge Aesthetic Subcommittee of the Transportation Research Board (TRB) and edited by the author. The author would particularly like to thank Joseph Showers, chair of the subcommittee, and members Robert Shulock, Dean van Landuyt, Eric Yermack, Mary McCahon, Ken Wilson, and all of the other members of the subcommittee who worked on the project, and acknowledge as well the support of TRB's General Structures Committee and the TRB staff. Bruce Johnson, Chief Bridge Engineer for the Oregon Department of Transportation, and Bob Healy, Deputy Chief Engineer, Structures for the Maryland Highay Adminstration must also be recognized for their efforts in securing adoption of the *Sourcebook* by the Standing Committee on Bridges and Structures of the American Association of State Highway and Transportation Officials (AASHTO). Finally, the author would like to thank AASHTO and particularly AASHTO staff member Kelly Rehm for publishing the *Sourcebook* and for allowing parts of the text and some of the images to appear in this chapter.

Bibliography

As described in the Introduction, much more discussion of the guidelines in this chapter and much additional discussion of related topics are contained in following:

AASHTO. 2010. *Bridge Aesthetics Sourcebook*. American Association of State Highway and Transportation Officials, Washington, DC.

Much more detail and background on the discussion and ideas in this chapter can be found in the following book by the author:

Gottemoeller, F. 2004. *Bridgescape, The Art of Designing Bridges*. 2nd Ed. John Wiley & Sons, Inc., New York, NY.

The following should be part of the reference library of any engineer interested in bridge aesthetics, in alphabetical order:

Allen, E. and Zalewski, W. 2010. *Form and Forces, Designing Efficient, Expressive Structures*. John Wiley & Sons, Inc., New York, NY.

Leonhardt, F. 1983. *Brucken*. MIT Press, Cambridge, MA.

Pye, D. 1999. *The Nature and Aesthetics of Design. 5th Reprinting*. Cambium Press, Bethel, CT.

Schlaich, J. and Bergermann, R. 2003. *Light Weight Structures*. Prestel Publishing, New York, NY.

Tang, M. C. 2001. *36 Years of Bridges*. Tango International, New York, NY.

A complete discussion of the topics in Sections 3.2, 3.3, and 3.34 can be found in the following three books by David Billington:

Billington, D. P. 1983. *The Tower and The Bridge: The New Art of Structural Engineering*. Basic Books, Inc., New York, NY.

Billington, D. P. 1989. *Robert Maillart and The Art of Reinforced Concrete*. The MIT Press, The Massachusetts Institute of Technology, Cambridge, MA.

Billington, D. P. 2003. *The Art of Structural Design, a Swiss Legacy*. Princeton University Art Museum, Princeton, NJ.

4

Planning of Major Fixed Links

Erik Yding Andersen
COWI A/S

Lars Hauge
COWI A/S

Dietrich L. Hommel
COWI A/S

4.1 Introduction

4.1.1 Characteristics of Fixed Links

Within the infrastructure of land transportation, "fixed links" are defined as permanently installed structures allowing for uninterrupted passage of a certain volume and composition of traffic with adequate safety, efficiency, and comfort. The fixed links often cross large stretches of water, but may also comprise significant land works, for example, when circumventing congested city areas.

4.1.2 Cost-Benefit Evaluations

Existing traffic services are often provided by ferries before a fixed link is established and a fixed link offers shorter traveling times and higher traffic capacities than the existing services and the establishment

of a fixed link usually have a strong, positive impact on the industrial and economic development of the areas to be served by the link. The beneficial effects shall be assessed against costs, impacts, and constraints given for the project, as described further in Section 4.2, in order to reach decisions for project development. This is a task that shall be managed directly by the responsible authority, though some of the practical work may be left to independent entities.

4.1.3 Project Procurement

The future owner must also consider how to procure the project, that is how the project can be managed, financed, and owned; how the physical infrastructure can be designed, contracted, constructed, operated, and eventually how risks shall be shared among the parties involved. The procurement aspects are addressed in Section 4.3.

4.1.4 Technical Development

In parallel with development of the above political aspects of a potential fixed link, the technical aspects of the project must also be developed. This comprises establishment of the basic conditions on which the project shall be prepared, design development, contracting, construction, and operation and maintenance as described in Section 4.4, and further detailed in subsequent Sections 4.5 through 4.9.

4.1.5 Fixed Link Examples

Generally the term fixed link is associated with highway or rail sections of considerable length and a fixed link might comprise a combination of different civil engineering structures like tunnels, artificial islands, causeways, and different types of bridges (Figure 4.1). Table 4.1 lists major fixed links in the world established since early 1990s.

Examples of major Scandinavian fixed links are described in Section 4.10 (also see Figure 4.4 later in the chapter).

FIGURE 4.1 Rendering of the proposed multi-span suspension bridge connecting Yemen and Djibouti. (Courtesy of Dissing+Weitling architecture.)

TABLE 4.1 Recent Major Fixed Links

Name of Link	Length Total	Types of Structures	Opened (Plan)	Traffic Mode
Gibraltar Fixed Link, Spain–Morocco	>14 km	Bridge and tunnel solutions investigated	(>2025)	Road and/or rail
Bridge of the Horns Yemen–Djibouti	29 km	High-level multi-span suspension bridges	(>2020)	Road and rail
Tiran Strait Fixed Link, Egypt–Saudi Arabia	6 km	High-level suspension bridge	(>2020)	Road
Sunda Strait Crossing, Indonesia	> 26 km	High-level suspension bridge and viaducts	(>2020)	Road
Fehmarnbelt Fixed Link, Denmark–Germany	19 km	Immersed tunnel and approach ramps	2020	Road and rail
Qatar–Bahrain Causeway, Qatar–Bahrain	40 km	Arch bridge, viaducts, and artificial islands	2019	Road and rail
Messina Strait Crossing, Italy	5.1 km	High-level suspension bridge—triple steel box girder	2017	Road and rail
Hong Kong–Zhuhai–Macau Fixed Link, China–Macau	50 km	Cable-stayed bridges, viaducts, artificial islands, and immersed tunnel	2016	Road
Sheikh Jaber Al Ahmed Al Sabah Causeway, Kuwait	22 km	High-level cable-stayed bridge and viaducts	2016	Road
Puente Nigale, Maracaibo, Venezuela	10 km	High-level cable-stayed bridges and viaducts	2016	Road Rail—opt.
Mumbai Trans-Harbor Link, India	22 km	High-level bridge	2014	Road and metro
Penang Second Bridge, Malaysia	23.4 km	High-level cable-stayed bridge	2012	Road
Jiaozhou Bay Bridge, China	42.5 km	Cable-stayed bridge and viaducts	2011	Road
Louisiana Highway 1 Bridge, United States of America	29 km	Low and medium-level bridges	2011	Road
Busan Geoje Fixed Link, Korea	8.2 km	Two cable-stayed bridges, immersed tunnel and rock tunnels	2010	Road
Stonecutters Bridge, Hong Kong, China	1.6 km	High-level twin-box cable-stayed bridge	2009	Road
Incheon Grand Bridge, Korea	18.4 km	High-level cable-stayed bridge and viaducts	2009	Road
Hangzhou Bay Bridge, China	35.7 km	Cable-stayed bridge and concrete viaducts	2007	Road
Rion–Antirion Bridge, Greece	2.9 km	High-level cable-stayed bridge, viaducts	2004	Road
Rosario–Victoria Bridge, Argentina	12.2 km	High-level cable-stayed bridge and viaducts	2003	Road
Seohae Bridge, Korea	7.3 km	High-level cable-stayed bridge, viaducts	2000	Road
Øresund Link, Sweden–Denmark	16 km	Immersed tunnel, artificial island, high-level cable-stayed bridge, viaducts	2000	Road and rail

(*Continued*)

TABLE 4.1 (Continued) Recent Major Fixed Links

Name of Link	Length Total	Types of Structures	Opened (Plan)	Traffic Mode
Honshu–Shikoku Connection, Japan				
• Kojima-Sakaide Route/ Centre	37.3 km	High-level suspension and cable-stayed bridges	1988	Road and rail Road
• Kobe-Naruto Route/East	89.6 km	High-level suspension bridges	1998	
• Onomichi-Imabari Route/West	59.4 km	High-level suspension and cable-stayed bridges	1999	Road
Vasco da Gama Bridge, Portugal	12.3 km	Viaducts and high-level cable-stayed bridge	1998	Road
Great Belt Link, Denmark	17.5 km		1998	Road and rail
• West Bridge		Low-level concrete bridge		Road
• East Bridge		High-level suspension bridge		Rail
• East Tunnel		Bored tunnel		
Lantau Fixed Crossing, Hongkong	3.4 km			Road and rail Road and rail
• Tsing Ma Bridge		High-level suspension bridge	1997	
• Kap Shui Mun Bridge		High-level cable-stayed bridge	1997	
Confederation Bridge, Canada	12.9 km	High-level concrete box girder bridge	1997	Road
Trans-Tokyo Bay Crossing, Japan	15.1 km	Bored tunnel, artificial islands, high and low-level steel box girder bridges	1997	Road
Second Severn Bridge, Great Britain	5.1 km	Viaducts and high-level cable-stayed bridge	1996	Road

4.2 Feasibility

Major fixed links represent important investments for the society and have considerable influence on the development potentials of the areas they serve.

Common to major infrastructure projects is that the responsible authority or political entity for infrastructure development must rank the items in the portfolio of potential projects. And often the task also comprises a ranking between alternatives for the individual projects. The ranking process is based upon cost-benefit assessments with content as lined out in Table 4.2.

In order to carry out the feasibility studies comprising the elements in Table 4.2, it is necessary to have a description of the project in question, that is the design must be developed in parallel—to a detailing level depending on the progression of the project discussions—as described separately in Sections 4.4 through 4.9.

4.2.1 Political Aspects

For most of the issues listed in Table 4.2, the associated analyses can be performed according to well-established methods and knowledge—as briefly described in the remaining part of this section—and the results of the analyses can be expressed in terms that are generally accepted in professional environments.

When it comes to the importance associated with the individual results from a societal point of view, the evaluations used for the decision making will be very dependent upon the weight given to various political aspects. Decision-making related to major fixed links can be very complex and heavily influenced by political agenda and decisions may take decades or even centuries to make.

The political circumstances for major fixed links may vary enormously and how the political process is best organized is left for discussion elsewhere. In the following, focus is directed toward the technical aspects of the required feasibility analysis.

TABLE 4.2 Main Elements in Typical Cost-Benefit Assessments for Infrastructure Projects

Benefit	Improved traffic capacity and reduced travel times	
	Improved safety for users and third parties	
	Socio-economic benefits	
	Project revenue from tolling	
	Landmarks and monuments	
Cost/Impact	Construction cost	Direct costs and land acquisition
		Capitalization
	Operational cost	Operation and emergency
		Inspection and maintenance
	Environmental	Human adverse impacts
		Flora and fauna
	Land acquisition requirements	
	Societal	Settlement patterns
		Migration potentials
		Labor market impact
Constraints	Laws / agreements	(regional/national/federal)
	Conventions	International
	Environmental preservation areas	
	Existing structures and infrastructure	
	Existing traffic	(ship/air/road/rail)

4.2.2 Benefits

4.2.2.1 Improved Traffic Capacity

In order to assess the beneficial impact of a new fixed link the demand for the improved traffic capacity must be assessed and used to model the future traffic patterns and volumes. In case a tolled link is considered the willingness to pay for use of the link must be included in the assessments. Such traffic analyses may be performed at an early stage where the design development of the link is at a sketch level only. The results will be crucial to the evaluations of the beneficial socio-economic effects.

4.2.2.2 Project Revenue from Tolling

The estimated revenue from tolling may be decisive for a positive decision to establish a new fixed link. Assessment of the revenue potential is closely related to the traffic analyses and the assessments of the users' willingness to pay. In cases where a new fixed link replaces, for example, a ferry link this willingness has already been tested to some extent and the uncertainty on the assessment of the revenue potential will hence be closely linked to the uncertainty associated with the future traffic volumes.

4.2.2.3 Improved Safety

Establishment of a new fixed link may also have a beneficial effect on the safety of both users of the link (compared to present situation) and third parties (e.g., neighbors, shipping traffic, etc.). This aspect may be included as a positive socio-economic effect.

4.2.2.4 Socio-Economic Benefits

Society may benefit from a new fixed link in many respects: commercial collaboration may be easier, potential customer basis may be expanded, labor force mobility may be enhanced, settlement patterns may change positively, and so on. Both benefits and potential negative impacts will have to be studied in an overall analysis of the planning impacts of a new link.

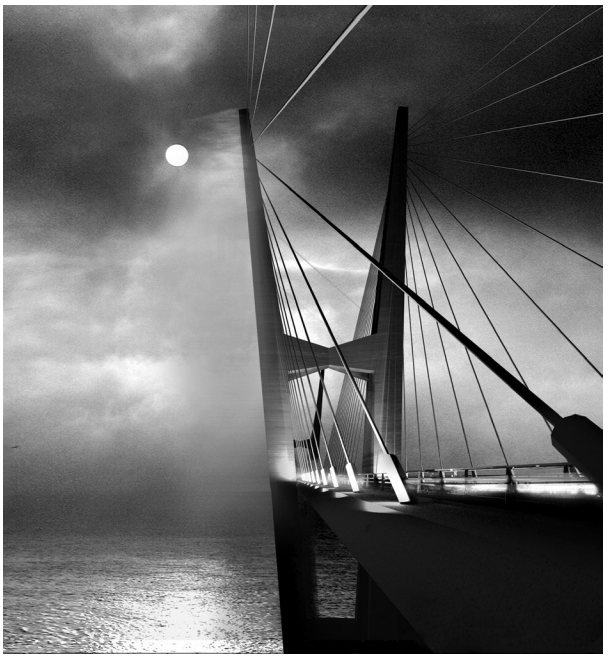

FIGURE 4.2 Fehmarnbelt conceptual design for cable-stayed bridge for road and rail. Example of project with landmark quality. (Courtesy of Dissing+Weitling architecture.)

4.2.2.5 Landmarks and Monuments

A special beneficial effect may be the establishment of a new landmark structure that may attract positive attention to a city or a region and have a positive influence on, for example, tourism (a similar but negative effect may arise if the fixed link is becoming a historical monument for political influential persons or groups) (see Figure 4.2).

4.2.3 Impacts

4.2.3.1 Costs

The estimated cost is decisive for the decision on undertaking the construction of the link, for selection of solution models, and for the selection of concepts for tendering. The cost estimate may also be important for decisions of detailed design items on the bridge.

4.2.3.1.1 Costing Basis

The principles for establishing an estimate for the construction cost and operation and maintenance costs may vary significantly and be politically sensitive and hence it will be advisable early in major fixed link projects to establish a well-documented description of principles for and methods to be used for building up a price estimate. An important aspect is to decide how uncertainties in the basis for the costing shall be treated.

4.2.3.1.2 Cost Uncertainty Estimation

In order to define the cost uncertainty it may be helpful to divide into two contributions that may be partly overlapping: (1) the uncertainties of the basic data, quantities, construction processes, and time in the estimation and (2) risk of supplementary costs because of unwanted events.

The uncertainty is in principle to be defined for each single input to the cost model. The uncertainty is taken as the Bayesian understanding of the contribution, in which the variations because of lack of knowledge is allowed to be included. Especially, early in the planning, unsettled basis for the design may be part of the uncertainty.

The risks for construction cost add-ons can in principle be taken from a construction risk analysis. Furthermore, it shall be noted that only the part of the construction risk that has impact on the construction cost shall be included. The risk for operational cost add-ons can in principle be taken from an operational risk analysis.

The risk estimation will result in a best estimate of the contribution from risk items to the cost, the so-called risk add-on, and this value will be associated with uncertainty. The other uncertainties may also influence the best estimate of the cost, but their main purpose is to illustrate the distribution of the cost estimate.

4.2.3.1.3 Life Cycle Costs

The life cycle cost is an integration of the entire amount of costs for the bridge from the first idea to the final demolition and hence comprises operational aspects too. The life cycle costs are normally expressed as a present value figure. Hence, the interest rate used will be very important as it is a weighting of future expenses against initial expenses.

It shall be defined whether the lifetime costs are considered from an owner point of view or from a societal point of view. For example, the disturbance of the traffic resulting in waiting time for the users can be regarded as an operational cost from a societal point of view, whereas it is only a cost for the owner if it influences the users' behavior so that the income will be less.

Important contributors to the life cycle cost for bridges are as follows:

- The total construction cost, including costs for the owner's organization, land acquisition, and so on.
- Construction risk add-ons
- Operational and emergency services expenses
- Operational risk add-ons for unwanted events
- Inspection and maintenance costs
- Future modifications or expansion of the bridge
- Demolition costs

4.2.3.1.4 Cost Estimates at Different Project Phases

Cost estimates are made repeatedly during the planning of a project. In the first instance the aim is to investigate whether the cost of the project is of a realistic magnitude and whether it is worthwhile to continue with feasibility studies. Later the cost estimates are used to compare solution concepts, evaluate designs, and design modification. The final cost estimate before the tender is used to evaluate the overall profitability of the project and to benchmark the received bids.

Different degrees of detailing of the estimates will be needed in these stages. In the early phases a top-down "overall unit cost" approach may be the only realistic method for estimating a price, whereas in the later phases it is necessary to have a detailed breakdown of the cost items and the associated risks and uncertainties.

4.2.3.2 Environmental Impacts

Infrastructure projects like fixed links will make significant footprints in the environment—both in the temporary construction phase and the operational phase. The infrastructure may have impacts on many different aspects: human beings, surrounding environments, aesthetics, flora, fauna, hydraulic conditions, and so on.

It is required to have an environmental impact assessment prepared that addresses all these issues. It is a quite significant task to carry out and often it will touch upon issues that may be politically sensitive in the region where the fixed link is established. As a solid baseline description of the conditions before establishment of the fixed link has to be established before construction commences, the environmental

investigations and assessments shall take place early in the project period—and may occasionally be on the critical path of fast track projects.

4.2.3.2.1 CO_2 Footprint

The carbon dioxide footprint of infrastructure projects attracts increasing focus in the climate debate and it is expected that a CO_2 account will be required for all major infrastructure projects in order for the public to assess the climatic impact of the project. The list of contributors to the CO_2 account is long; however, the dominating contributors are expected to be from production of the constituent materials of an infrastructure project, which is mainly steel and concrete.

It may be valuable just to document that attention has been given to the CO_2 footprint, for example, by specifying work methods and design solutions with a small or minimum contribution.

4.2.3.2.2 Environmental Protection Areas

One particular aspect of environmental legislation and administration that may influence infrastructure projects significantly is cases where the only mitigating action accepted is to "re-establish nature," that is it is not sufficient to make compensating actions. In this situation, cost is not considered (by the environmental authorities) and the cost impact for an infrastructure project can be prohibitive. Such administrative practice has been met in relation to Nature2000 or EU-habitat areas in Europe.

4.2.3.3 Land Take

For fixed links across water stretches, land take issues are normally not a significant problem offshore, although it may often be difficult to find suitable solutions for the land works and connecting roads and railway lines.

4.2.3.4 Societal Impacts

The beneficial and negative socio-economic impacts will have to be treated together in one analysis.

4.2.4 Constraints and Legal Requirements

In addition to the many physical constraints that may apply to infrastructure projects, attention should be devoted also to legal and regulatory constraints.

Protection of habitats for flora and fauna and regulatory requirements from national authorities and international organizations may impose severe environmental constraints on projects. It may be crucial to the success of a project that such constraints are identified early in the project development and attention is given on a continuous basis to assure that requirements are fulfilled and that any potential violation of constraints and regulations be addressed immediately.

4.2.5 Decision Making

In the development of a project, numerous situations are encountered in which comparisons and rankings must be made as basis for decisions. It is starting with the ideas of a project and continuing with the concept phase, the evaluation of feasibility, to the different levels of detailing of the design, the construction, the commissioning, operation, and so on. The decisions that should be made may be of different nature, conditions will be developing, and the decision maker may change.

4.2.5.1 Alternatives and Their Characteristics

All possible alternatives including the "do-nothing" option should in principle be identified during the decision-making process. The most obviously nonconforming alternatives may be excluded quickly from the study. In complex cases, a continued process of detailing of analysis and reduction of number

of alternatives may be pursued. The selection of parameters for which it is most appropriate to make more detailed analyses can be made on the basis of a sensitivity analysis of the parameters with respect to the utility. Risks may be regarded as uncertain events with adverse consequences. Of particular interest are the different risk pictures of the alternatives. These risk pictures shall be quantified by the use of preferences so that they can be part of the comparison.

4.2.5.2 Comparison Analysis

The final decision will be based on a comparison analysis once the various elements of the cost-benefit analysis framework have all been detailed to a satisfactory level. And in order to reach this situation, the scope of the comparison must be defined: do we aim at the technically best solution, the solution with minimum environmental impact, the socio-economically best solution, the most profitable or the cheapest solution? In most cases the decision maker's scope is a combination of a number of these goals.

The main components of the comparison analysis will hence comprise many of the elements from Table 4.2 and can be

- Establishment of decision alternatives
- Criteria to be used for evaluation of the alternatives
- Quantitative assessment of impacts of the various alternatives utilizing an evaluation grid
- Preference patterns for one or more decision makers with associated importance of criteria
- Assessment of uncertainties

A quantitative assessment of all criteria must be made. Some of the criteria can be expressed in economical terms. The relative importance of the criteria in noneconomical terms must be determined through a determination of the preference pattern of the decision maker. This process results in quantification in terms comparable with economical terms of all criteria, also for matters that are claimed "priceless." However, a decision must eventually be made, and decisions are made also in situations where risk of environment, risk of lives, aesthetics and other "priceless" matters are at stake.

Provided the criteria are quantified and weighted according to the preference of the decision maker, the final decision may better reflect the general objectives of the decision maker and the quantified model makes furthermore the decision process more transparent. The impact of the preferences can be illustrated through sensitivity studies. It may be helpful as the basis for communication of the results to test for preference patterns of different decision makers or other interested parties.

It is very important to base the comparisons and the derived decisions on planning and management tools, which can rationalize, support, and document the decision making. Rational decision-making theories are formulated mathematically in the economical science. However, no details will be given here, as the general idea is intuitively understandable: Among the possible decisions, the best decision is the one with the highest expected utility to the decision maker, and the highest utility is often also described as the best cost-benefit relationship. It is of great importance to quantify the uncertainties of the parameters describing the alternatives. The expectation value of the utility is determined in the final ranking. With representation of the uncertainties and with the use of modern mathematical tools/software, a complete sensitivity analysis can be achieved.

4.2.5.3 Comparisons at Different Project Stages

After the initial identification of possible alternatives, the purpose of the first comparison may be to reduce the number of alternatives, alternative design concepts, to be investigated in the later phases.

In this first ranking the detail of the analysis should be adequate to determine the least attractive solutions with an appropriate certainty. This will in most cases imply that a relatively crude model can be used at this stage. A semiqualitative assessment of some of the parameters, based on experienced professional's judgment, can be used.

At a later phase, decisions will have to be made on which models to select for tender design, and later in the tender evaluation, to which tenderer to award the contract. In these comparisons the basis and the input shall be well established, as the comparison here shall be able to select the single best solution with sufficient accuracy. A weighting of criteria is necessary. A strictly rational weighting and conversion of these criteria directly into terms of economical units may not be possible. It is normally regarded sufficient, if the weighting and selection process are indicated to the tenderers before the tender.

4.3 Procurement

4.3.1 Financing and Ownership

The responsible authority for infrastructure will be the long-term owner of the infrastructure projects. However—provided sufficient revenue can be generated from operation of the new infrastructure to finance the construction and operation in a certain period—the authority will have the option either to maintain ownership himself or to give a concession to a third party who will then finance, establish, own, and operate in a concession period until final transfer of the ownership to the responsible authority.

4.3.1.1 Ownership Maintained by Authority

4.3.1.1.1 Authority's Existing Organization

The authority will establish the infrastructure by conventional means—finance himself and maintain the ownership within own organization. Overall management of the fixed link will remain in-house. This approach can be considered the traditional—as used by state and regional governments around the world.

4.3.1.1.2 Publicly Owned Company

Occasionally authorities may opt for financing by acquiring external loans, which may be obtained favorably if guaranteed by public bodies, and then depreciate the loans by the revenue from the fixed link tolling in order to alleviate indirect tax burdens. In such cases the establishment and operation of the fixed link may be organized via a public-owned company—operating on market conditions. This approach has been applied by the Danish government to set up a publicly owned shareholding company Sund & Bælt A/S, which has been responsible for establishment of the Great Belt Fixed Link and subsequently operation and maintenance of the link as the final owner. Loans are obtained favorably on the market based upon a guarantee from the Danish state.

4.3.1.2 Public Private Partnerships

In cases where the authority opts for an approach where the financing and construction is provided by an external entity, a concession can be granted for establishment and operation of the fixed link for a period until eventual handing back to the responsible authority. This arrangement is often referred to as a public-private partnership and may be based upon a wide variety of terms and conditions, also including shadow tolling in case sufficient revenue cannot be generated to make the link feasible. Examples are the Busan–Geoje Fixed Link in Korea under concession to Daewoo and the Limerick Southern Ring Road crossing of the Limerick River in Ireland under concessions to a group of contractors and financers.

4.3.2 Procurement Strategy

Irrespective of the financing set-up, it will be of crucial importance to select a good procurement approach under the conditions given for the actual fixed link. The decision regarding the optimum procurement method should ideally be based on the demand that the work and activities at all times and phases are being distributed and executed by the most qualified party (owner, consultant, contractor) meeting the required quality level, at lowest overall cost and shortest time. The procurement strategy shall consider that tendering procedures shall be clarified with commercial and legal regulations for the region.

The following attempts to provide a short overview of various concepts that are to be considered in the definition of the procurement strategy for a fixed link project.

4.3.2.1 Contracting Concepts

Two main contracting concepts are as follows:

- Design Bid Build (DBB), a concept whereby an engineering consultant prepares the construction contract documents on behalf of the owner, who then retains a contractor for the construction
- Design-Build (DB), a concept that assigns both detailed engineering design and construction responsibilities to a single entity, normally the contractor

The DBB concept requires that the owner and his consultant participate actively during all phases and are in a position to influence and control the quality and performance capability of the completed facility. The main differences between the various forms of the DBB are the degree of detailing at the tender stage and whether alternatives will be permitted.

Completing the detailed design before inviting tenders is attractive if the strategy is to obtain lump sum bids in full compliance with the owner's conditions.

A "partial design"—often 60%–70%—represents a good compromise between initial design costs and definitions of owner's requirements to serve as a reference for alternative tenders. An advantage is that it is possible to achieve early start of the construction work, while completing the design work. This procedure normally allows contractors to submit alternatives in which case the tender design serves the important purpose of setting the quality standards that will be required by the owner and subsequently be applied by the owner's designer in completion of the design.

A hybrid approach can be met occasionally when a project is tendered as a DBB project, but changed into a DB project because it is deemed appropriate to let the contractor continue the design development by the bid design team. This approach was the result of the tendering of the West Bridge across Great Belt in Denmark, where a DB contract was awarded for a bid design that was completely different from the tendered solutions.

The DB concept assigns a high degree of autonomy to the contractor and as a consequence, the owner's possibilities for influencing quality and performance capability of the completed facility directly in the design process are reduced. In order to ensure that the contractor delivers a project that meets the expectations of the owner, it is hence necessary to specify these very carefully and complete in the tender documents. Aesthetical, functional, maintenance, durability, and other technical standards and requirements are to be defined. Also legal, environmental, financial, time, interface, and other more or less transparent constraints to the contractor's freedom of performance should be described in the tender documents in order to ensure comparable solutions and prices. Close supervision of the contractors during the design and construction phases is essential. The DB approach was chosen for the Øresund Fixed Link between Denmark and Sweden with the aim to benefit the most from the innovative capabilities of contractors.

For major bridges there is a risk that bids may be based on substandard or marginal designs or designs so radical and unusual that they may be difficult to comprehend during the tender evaluation. The owner then has the dilemma of either to reject a low bid or accept it and pay high additional costs for subsequent upgrading.

In order to mitigate this risk on the Øresund Fixed Link project, two illustrative designs were developed by the owner's team and floated with the tender specifications. Strict boundaries for the contractors' freedom to change visible geometrical dimensions of the project in combination with partly a comprehensive set of design requirements and specifications and partly a technically strong client organization, constituted the basis for a successful completion of the construction process—at quality, on budget, and in time. Adjustments to the contractor's project were negotiated after the bid was handed over to the owner.

A further development of this approach is the Competitive Dialogue Process applied by Transport Scotland in their preparations for contract award for the Forth Replacement Project construction.

Basically the contract is a DB contract for which two very detailed illustrative designs had been developed for tendering. After floating the tender, the owner carried through a Competitive Dialogue Process with the two tendering groups in which all significant design issues were raised and discussed between the owner and the contractor (but not disclosed to the competing group). The owner could reject solutions he would not accept and in certain cases adjust the employers' requirements in order to reach a full clarification. Such changes in the employers' requirements would be revealed to the competing group immediately. In this way the owner assured a close interaction with the tenderers in their development of the designs to his satisfaction. The final bid received from the tenderers would hence be fully compliant as all reservations should be clarified in advance. The Competitive Dialogue Process will of course require resources and time, but it may overall be cost efficient for the owner—even if he pays a significant amount for the tenderers' bid design development.

4.3.3 Contract Packaging

A major fixed link project is usually divided into several reasonable contracts based on the following:

- Vertical separation (e.g., main bridge, approach bridges, viaducts, and interchanges)
- Horizontal separation (e.g., substructure and superstructure)
- Disciplinary separation (e.g., concrete and steel works)

These general principles are to be applied to the specific situation of each project. Furthermore, view points as to the achievement of the intended quality level together with contract sizes allowing for competitive bidding are to be considered in the final choice.

4.3.4 Examples of Procurement Conditions

A few examples of the procurement conditions associated with selected major fixed link projects are listed in Table 4.3.

The brief list of examples above illustrates that the various aspects are combined in various ways according to the particular characteristics of each individual project and its circumstances (which

TABLE 4.3 Procurement Conditions for Selected Fixed Links

Fixed Link	Owner	Concession	Financing	Revenue	Contracting	Elements
Stonecutters	State	State	Own capital	None	Design-Bid-Build	Bridge
Höga Kusten	State	State	Own capital	None	Design-Bid-Build	Bridge
Pont de Normandie	State	State	Own capital	None	Design-Build	Bridge
Forth Replacement	State	State	Own capital	Tolled	Competitive Dialogue	Bridge
Qatar-Bahrain Causeway	State	State company	Own capital	Tolling	Design-Build	Bridge
Stretto di Messina	State	State company	Own capital	Tolling	Design-Build	Bridge
GB-East Bridge	State	State company	Loans	Tolling	Design-Bid-Build	Bridge
GB-West Bridge	State	State company	Loans	Tolling	Design-Build	Bridge
GB-Tunnel	State	State company	Loans	Fixed fee	Design-Bid-Build	Bored Tunnel
Øresund	State	State company	Loans	Tolling	Design-Build	Bridge & Tunnel
Fehmarn	States	State company	Loans	Tolling	Design-Build	Tunnel
Busan-Geoje	PPP	Private	Equity and Loans	Tolling	Design-Build	Bridges and Tunnel
Izmit	PPP	Private	Loans	Tolling	Design-Build	Bridge

may change during the process). The Scandinavian projects—Great Belt, Øresund and Fehmarn—are described in more detail in Section 4.10.

4.4 Technical Development

The technical development of a fixed link project will be described separately in the following sections, but in reality the first phases of the technical development will take place in parallel with the feasibility evaluations and the definition of the organization and the procurement strategy.

The technical development is traditionally split into the following:

- Establishment of basic conditions
- Design development and technical follow-up
- Tendering and contracting
- Construction and commissioning
- Operation, maintenance, and transfer

By nature the above split may indicate a sequence of activities. However, some may be overlapping and running in parallel. This may be illustrated as shown in Table 4.4, where the development over time for each area is shown in horizontal direction.

In this chapter, all areas are addressed although the main emphasis is put on the issues related to the planning phase.

4.5 Basic Conditions

4.5.1 Introduction

The project is based on all the information and all the requirements that are decisive in the planning and design of a fixed link. The project basis is normally developed simultaneously with the early design activities, and it is important to have the owner's main requirements defined as early as possible, and to be precise about what types of link solutions have to be included.

4.5.2 General Requirements

4.5.2.1 Functional and Geometrical Requirements

Most geometrical requirements for the design of fixed links stem from functional/operational requirements for traffic and all the important installations. However, geometrical requirements may also be necessary in order to mitigate accidents or needed for safety and emergency situations. Geometrical considerations should be addressed in the risk analyses.

TABLE 4.4 Components of Technical Development and the Related Time Phases (Not to Scale)

Basic Conditions	Functional Requirements/Site Data/Codes and Standards/ Constraints
Design development and technical follow-up	Alignment → concept → basic → detailed → execution → follow-up → supervision
Tendering and contracting	Tendering → bidding → evaluation → contract award → final pricing
Construction and commissioning	Selection → mobilization → construction → commissioning
Training, operation, and maintenance	Planning → training → operation and emergency Planning → training → inspection and maintenance

4.5.2.2 Structural Requirements

4.5.2.2.1 Design Basis

A main purpose of a design basis is to provide a set of requirements with the purpose to ensure an adequate structural layout, safety, and performance of the load-bearing structures and installations of a fixed link for the intended use.

4.5.2.2.2 Structural Design Codes

The structures must resist load effects from self-weight and a variety of external loads and environmental phenomena—climate and degradation effects. In order to obtain a fairly uniform level of structural safety, the statistical nature of the generating phenomena as well as the structural capacity shall be considered. A rational approach is to adapt probabilistic methods. However, these are generally not efficient for standard design situations and consequently it is recommended to apply a format as used in codes of practice. These codes such as European codes (Euro Codes, 2011) and American codes (AASHTO LRFD, 2012) are calibrated to achieve a uniform level of structural safety for ordinary loading situations, and probabilistic methods can subsequently be used to calibrate the safety factors for loads and/or design situations that are not covered by these codes of practice.

4.5.2.3 Environmental Requirements

Fixed links crossing environmentally sensible water stretches need to be developed with due attention to environmental requirements. Environmental strategies will be directed toward modification of the structural design to reduce any impact and to consider compensation or mitigation for unavoidable impacts, and thus the strategy will directly influence the cost efficiency of a project. Guidelines for environmental considerations in the structural layout and detailing, and the construction planning are to be developed by a specialized consultant and these will typically address areas such as the following:

- Geometry of structures affecting the hydraulic situation
- Space occupied by bridge structures, ramps, and depot areas—project footprint
- Amount and character of excavated soils—spill and waste materials
- Amount of external resources (raw materials sourcing)
- Methodology of earth works (dredging and related spill)
- Noise, vibration, and light pollution—both during construction and operation
- Air pollution and waste materials from construction and operation

Consequences of the environmental requirements are to be considered in the various project phases. Typical examples for possible improvements are selection of spans as large as possible or reasonable, shaping of the underwater part of foundations to reduce their blocking effect, orientation of structures parallel to the prevailing current direction, streamlining of protection structures and minimizing their size, reduction of embankment length, optimal layout of depot areas close to the shorelines, and reuse of excavated material to the largest extent.

The process should be started at the very early planning stages and continued until the link is completed and the impact on the environment has been monitored and assessed.

4.5.2.4 Risk Requirements

4.5.2.4.1 Types of Risk

Risk studies and risk management have gained a widespread application within the planning, design, and construction of fixed links. Risks are inherent to major transportation links, and therefore it is important for the owner and the society that risks are known, evaluated, and handled in a professional

way, that is included in the basis together with the technical and economical aspects. Risks are often studied separately according to the consequences of concern, for example:

- Economical risk (rate of interest, inflation, budget overrun, and changed traffic pattern)
- Operational risk (accidents, loss of lives, impact to environment, disruption of the traffic, loss of assets, and loss of income)
- Construction risks (failure to meet time schedule or quality standards, unexpected ground conditions, and accidents)

Economical risks in the project may be important for decisions on whether to initiate the project at all. The construction risk may have important implications on the selection of the structural concept and construction methods.

4.5.2.4.2 Risk Management Framework

Main risk management components are shown in Figure 4.3. The risk policy is formulated by the owner in few words, for example: The safety of the transportation link must be comparable with the safety for the same length of similar traffic on land.

The risk acceptance criteria are engineering formulations of the risk policy in terms of, for example, upper limits of risk. The risk policy also specifies the types of risk to be considered.

The risks typically considered are user fatalities and economical loss. In some cases other risks are specifically studied, for example risk of traffic disruption and risk of environmental damage, but these risks may conveniently be converted to economical losses.

The risk analysis consists of systematic hazard identification and an estimation of the two components of the risk, the likelihood and the consequence. Finally, the risk is evaluated against the acceptance criteria. If the risk is found unacceptable, risk-reducing measures are required. It is recommended

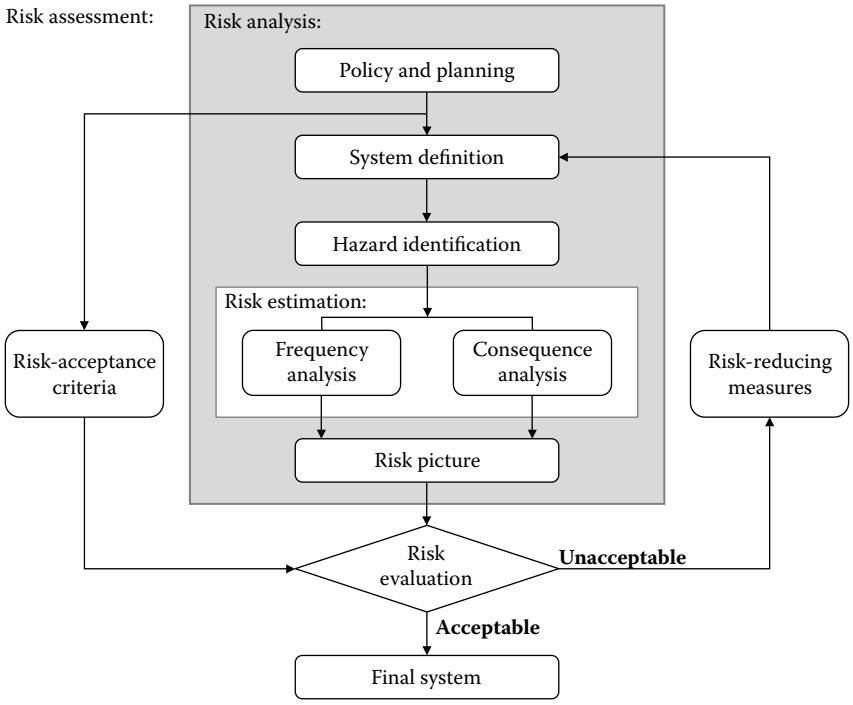

FIGURE 4.3 Risk management components. (Courtesy of COWI A/S.)

to develop and maintain an accurate accounting system for the risks and to plan to update the risk assessment in pace with the project development. It should be noted that any risk evaluation implies an inherent or direct assessment of preferences.

In the following, three common risk evaluation methods are discussed: fixed limits, cost efficiency, and ALARP.

Fixed limits are the classical form of acceptance criteria. Fixed limits are also known from legislation and it may easily be determined whether a determined risk is acceptable or not. However the determination of limits, which can ensure an optimal risk level, may be difficult.

With pure cost efficiency consideration an upper limit is not defined; but all cost efficient risk reducing measures are introduced. For this cost-benefit consideration, it is necessary to establish direct quantification of the consequences in units comparable to costs.

The ALARP method—As Low As Reasonably Practicable—applies a cost-benefit consideration in which it, however, is stated that the risk shall be reduced until the cost of the reduction measures is in disproportion with the risk reducing effect. This will result in a lower risk level than the pure cost efficiency. In ALARP a constraint of the acceptable risk is further introduced as an upper limit beyond which the risk is unconditionally unacceptable. This constraint will not be coincident with the upper limit in the fixed limit methodology.

Often it is claimed that society regards 1 accident with 100 fatalities as worse than 100 accidents with each 1 fatality. Such risk aversion attitude can be introduced in the risk policy and the risk acceptance criteria. The aversion against large accidents can also be modeled with aversion factors that are multiplied on the consequences of accidents with many fatalities; the more fatalities the higher the factor.

The sensitivity of the evaluations of risk should be considered by a due representation of the uncertainty of the information in the models.

4.5.2.4.3 Risk Studies in Different Project Phases

The general result of the risk management is a documentation of the risk level, basis for decisions, and risk communication. The specific aims and purpose for risk management will depend on the phase of the project. Here some few examples of the purpose of risk management are given in feasibility study, tender design, detailed design, construction, and operation.

In the early planning the risk will be crudely analyzed sometimes using more qualitative assessments of the risks. A risk management framework should be defined early in the design process. In the beginning of the project, work may also have to be initiated in order to have a basis for the more detailed work in later phases, as example can be mentioned vessel traffic observations to serve as basis for the estimation of vessel impact probability. In later phases detailed special studies on single probabilities or consequences may have to be undertaken.

In the feasibility study the most important activities are to identify all relevant events, focus on events with significant risk and risks with potential impact on geometry (safety, rescue, span length).

In the tender design phase risks are examined in more detail, in particular risks with potential impact on the project basis. Accidental loads are established based on the risk studies.

In the detailed design phase, the final documentation of the risk level should be established and required modifications to the design will be introduced. The draft operational procedures should be reviewed in the view of risks.

4.5.2.5 Aesthetic Requirements

The final structures and components of a fixed link are a result of a careful aesthetical appraisal and design of all the constituent elements, to obtain an optimal technical and sculptural form of individual elements, and to obtain an overall aesthetic quality and harmonious relation between the elements and the setting. Although difficult, it is recommended to establish guidelines for the attitude toward aesthetical questions.

4.5.3 Site Conditions

4.5.3.1 Soil Conditions

It is important to know the soil conditions at the site and hence it will be necessary to perform comprehensive site investigations and laboratory testing in order to establish a decent understanding of the geological and geotechnical conditions—and to derive the design soil parameters.

4.5.3.2 Navigation Conditions

The shipping routes and the proposed arrangement for a major bridge across navigable waters may be such that both substructure and superstructure could be exposed to vessel collisions. General examples of consequences of vessel collisions are as follows:

- Fatalities and injuries to users of the bridge and maybe to crew and vessel passengers
- Pollution of the environment, in case of accidental release of hazardous cargo
- Damage or total loss of bridge
- Damage or total loss of vessels
- Loss of income in connection with prolonged traffic disruption of the bridge link

A bridge design that is able to withstand worst case vessel impact loads on all exposed elements is normally not cost effective. Furthermore, such a deterministic approach does not reduce the risk to the environment and to the vessels. Therefore, a probabilistic approach addressing the main risks in a systematic and comprehensive way is recommended. This approach should include studies of safe navigation conditions, vessel collision risk analysis, and vessel collision design criteria, as outlined in Sections 4.5.3.2.1 through 4.5.3.2.3.

Navigation risks should be addressed as early as possible in the planning phases.

The general approach outlined here is in accordance with the IABSE Green Book (Larsen, 1993). The approach has been applied in the development of the three major Scandinavian fixed links described in Section 4.10.

4.5.3.2.1 Safe Navigation Conditions

Good navigation conditions are a prerequisite for safe passage of the bridge such that vessel collisions with the bridge or tunnel will not occur under normal conditions, but only as a result of navigation error or technical failure on board during approach.

The proposed bridge concept shall be analyzed in relation to the characteristics of the vessel traffic. The main aspects to be considered are as follows:

- Preliminary design of bridge
- Definition of navigation routes and navigation patterns
- Data on weather conditions, currents, and visibility
- Distribution of vessel movements with respect to type and size
- Information on rules and practice for navigation, including use of pilots and tugs
- Records of vessel accidents in the vicinity of the bridge
- Analysis of local factors influencing the navigation conditions
- Identification of special hazards from barges, long tows, and other special vessels
- Future navigation channel arrangements
- Forecast of future vessel traffic and navigation conditions to the relevant study period
- Identification of largest safe vessel and tow and of preventive measures for ensuring full control with larger passing vessels

Today all ships greater than 300 GT is required to carry an automatic transponder that will identify and locate the vessel and provide supplementary information about loading condition, departure port, destination, and so on—the AIS system—Automatic Identification System. As data are typically

acquired with a few minutes interval access to the data will provide extremely valuable information about sailing patterns, tonnages, and so on for use in a ship collision analysis.

4.5.3.2.2 Vessel Collision Analysis

An analysis should be used to support the selection of design criteria for vessel impact.

Frequencies of collisions and frequencies of bridge collapse should be estimated for each bridge element exposed to vessel collision. Different relevant types of hazards to the bridge shall be identified and modeled; for example, hazards from ordinary traffic that is laterally too far out of the ordinary route, hazards from vessels failing to properly turn at a bend near the bridge, and from vessels sailing more or less at random courses.

The frequencies of collapse depend on the design criteria for vessel impact. The overall design principle is that the design vessels are selected such that the estimated bridge collapse frequency fulfills an acceptance criterion.

In case unacceptable high risks for collapse or traffic disruption are encountered, the introduction of a VTS system (Vessel Traffic Service system) shall be considered.

4.5.3.2.3 Vessel Collision Design Criteria

Design criteria for vessel impact shall be developed. This includes selection of design vessels for the various bridge elements that can be hit. It also includes estimates of sizes of impact loads and rules for application of the loads. Both bow collisions and sideways collisions should be considered. Design capacities of the exposed girders against impact from a deck house shall be specified.

The vessel impact loads are preferably expressed as load indentation curves applicable for dynamic analysis of bridge response. Rules for application of the loads shall be proposed. Impact loads may be estimated on basis of general formulas established in (Larsen, 1993).

4.5.3.3 Wind Conditions

Bridges exposed to the actions of wind should be designed to be consistent with the type of bridge structure, the overall wind climate at the site and the reliability of site specific wind data. Wind effects on traffic could also be an important issue to be considered.

4.5.3.3.1 Susceptibility of Bridge Structures to Wind

Wind will, in general, introduce time variant actions on all bridge structures. The susceptibility of a given bridge to the actions of wind depends on a number of structural properties such as overall stiffness, mass, and shape of deck structure and support conditions.

Cable-supported bridges and long-span beam structures are often relatively light and flexible structures in which case wind actions may yield significant contributions to structural loading as well as to user comfort. Site specific wind data are desirable for the design. Engineering codes and standards will often provide useful information on mean wind properties, whereas codification of turbulence properties are rare. Guidelines for turbulence properties for generic types of terrain (sea, open farm land, moderately build up areas) may be found in specialized literature. In case the bridge is to be situated in complex hilly/mountainous terrain or in the proximity of large structures (buildings, bridges, dams) it is advisable to carry out field investigations of the wind climate at the bridge site. Important wind effects from isolated obstacles located near the planned bridge may often be investigated by means of wind tunnel model testing.

In general, it is recommended to include aerodynamic design studies in the design process. Traditionally aerodynamic design has relied extensively on wind tunnel testing for screening and evaluation of design alternatives. Today computational fluid dynamics methods are becoming increasingly popular because of speed and efficiency compared to experimental methods.

4.5.3.3.2 Wind Climate Data

The properties of turbulence in the atmospheric boundary layer change with latitude, season, and topography of the site, but must be known with certain accuracy in order to establish a bridge design

to a desired level of safety. The following wind climatic data should be available for a particular site for design of wind sensitive bridge structures.

Mean wind

- Maximum 10 minutes average wind speed corresponding to the design lifetime of the structure
- Vertical wind speed profile
- Maximum short duration wind speed (3 seconds gust wind speed)

Turbulence properties (along-wind, cross wind lateral, and cross-wind vertical):

- Intensity
- Spectral distribution
- Spatial coherence

The magnitude of the mean wind will govern the steady state wind load to be carried by the bridge structure and be determinant for the development of aeroelastic instability phenomena. The turbulence properties will govern the narrow band random oscillatory buffeting response of the structure, which is similar to the sway of trees and bushes in storm winds.

4.5.3.4 Hydraulic Conditions

Bridges and tunnels in marine environments are exposed to the effect of waves and currents and the design must consider these effects in order to provide structures with sufficient safety against detrimental responses. Vice versa the presence of the fixed link—being it bridge or tunnel—may also influence the environmental conditions at the site in a manner that should be considered carefully in both the loading conditions and in the evaluations of the environmental impacts; for example scour and blocking effects from bridge piers.

4.5.3.4.1 Current Conditions and Wave Climate

As for wind, basic data must be available for the design on current and wave conditions at the site. Based upon bathymetric maps and site data and observations on the hydraulic conditions (+ wind) hydraulic models can be established by which it is possible to assess the wave and current parameters that are needed in order to make a safe design of the structures.

4.5.3.5 Ice Conditions

The geographic location of a bridge site will define if ice loads are of concern for that structure. The ice loads will originate from either surface ice, ice ridges, or rafted ice and they may be defined as live loads or accidental loads (exceptional environmental loads that are not included in live loads).

From recent studies carried out for the Great Belt Link, the following main experience was obtained:

- Ice loads have a high dynamic component very likely to lock in the resonance frequencies of the bridge structure.
- Bearing capacity of the soil is dependent on number and type of load cycles, so advanced soil testing is a must with large ice forces.
- Damping in soil and change of stiffness cause important reductions in the dynamic response.
- If possible, the piers should be given an inclined surface at the water level, see Strait Crossing Bridge (2011)
- High ductility of the structure shall be achieved.

4.5.3.6 Earthquake Conditions

Structures should be able to resist regional seismic loads in a robust manner avoiding loss of human lives and major damages, except for the very rare but large earthquake. The design methods should be consistent with the level of seismicity and the amount of available reliable information. Available codes

and standards typically do not cover important lifeline structures such as a fixed link, but they may be used for inspiration for the development of a design basis. A site-specific seismic hazard analysis is usually carried out for a major bridge project and corresponding design criteria are developed.

4.6 Design Development and Technical Follow-Up

4.6.1 Screening Studies

The first step in the project development consists of a review of all information relevant to the link and includes a survey of the most likely and feasible technical solutions for the structures.

The transportation mode that is highway and rail traffic and the amount of traffic is taken from a traffic estimate. The prognosis of traffic is often associated with a considerable uncertainty as fixed links will not only satisfy the existing demands but may also create new demands because of the increased quality of the transport. It will have to be decided whether a railway line shall accommodate 1 or 2 tracks (or more). Similarly for the highway traffic, the traffic can either be transported on shuttle trains or the bridge can be accommodated with a carriageway designed to a variety of standards; the main characteristics being the number of lanes.

The decision on the expected traffic demands and the associated traffic solution models is often based on a mix of technical, economical, socio-economical, and political parameters. The decision may be confirmed at later stages of the planning, when more information is available on these parameters.

A fixed link concept study will review alignment possibilities and define an appropriate corridor for further studies. It will consider the onshore interchanges for the anticipated traffic modes and identify potential conflict areas. It will describe all feasible arrangements for the structures from coast to coast, and review the requirement for special structures onshore. Finally the study defines those concepts to be considered in more depth in the subsequent project phase.

An environmental condition review has the aim to identify potential effects of the structures to the environment and to review the environmental legal framework. It shall also identify important conflict areas and describe the project study area. It shall review the available information on the marine and onshore environment, and define the need for additional investigations.

A technical site condition study shall address the geological situation and the foundation conditions, assess potential seismicity, evaluate the navigation conditions, and study the climatic and hydraulic conditions. It shall review the topographic situation, and define additional studies or investigations for the following project phase.

A preliminary design basis study will review the statutory requirements, codes, and standards and identify the need for relevant safety and durability requirements.

Finally, a preliminary costing basis study shall define the cost estimation technique to be applied and provide first preliminary cost estimates.

Considering the results of these studies, a comprehensive investigation program for the next project step—the feasibility study—will be defined.

4.6.2 Feasibility and Concept Study

The feasibility study concentrates on the required preparatory studies, and describes and compares afterwards all viable solutions. After an interim selection process to reduce the number of solutions to be studied, concept studies are undertaken for each selected solution. Parallel to this study a geological and a sub-soil investigation should be carried out in the defined alignment corridor.

During the feasibility study the project basis is developed to cover the definition of functional requirements and review and define the navigational aspects. The basis for a risk policy and procedures for the risk management shall be included. The project basis shall also allow for the elaboration of a design basis and for the development of a more refined costing basis. Each of the solutions selected for investigation

shall be developed in a preliminary design and described through drawings and text. It is recommended to start an architectural study of the solutions in the feasibility studies. The feasibility study shall further include the definitions and constraints for operation and maintenance, and present the major construction stages.

Mechanical and electrical installations as well as utilities and access facilities have to be considered as early in the project phases as possible. These elements often have influence on the geometric layout and provide other constraints for the project. For instance is proper access, for example, through elevators in towers and inspection vehicles, vital for later operation and maintenance. The extent of these elements varies from project to project depending on the traffic modes and on the length of the link. Specific reference to these elements is not made in the following sections.

The feasibility study phase is concluded by a comparison analysis that provides the technical ranking of all solutions.

4.6.3 Tender Design

When a DBB approach is selected and a well defined fixed link is aimed for, the main purpose of a tender design to be floated by the owner is to describe the complexity of the structure and works and to determine the quantities, allowing the contractors to prepare a bid for the construction works. A major goal for a tender process is as low cost as possible within the given framework. This is normally identical to the lowest quantities and/or the most suitable execution method. However, other priorities may be relevant for the owner in certain cases,—for example construction time.

When a DB approach is selected, the owner is more open to variations and alternatives and hence a very important purpose of the tender documents and drawings is to describe as precisely as possible the expectations of the owner to the future fixed link in terms of functionality, appearance, safety, and so on. The tender design drawings and documents will have a more informative character in some instances, while in other areas detailed specifications may be given to the approval process for the design to be provided by the contractor.

It is important that the project basis is updated and completed prior to the commencement of the tender design. This will minimize the risk of contractual disputes. Aesthetics should be treated during the tender design.

It is vital that a common understanding of the works between consultant and owner is achieved. Especially assumptions regarding the physical conditions of the site are important; for instance sub-soil, wind, and earthquake conditions. Awareness, that these factors might have a significant influence on the design and thereby on the quantities and complexity, is important.

Normally the sub-soil conditions for the most important structures are determined before the tender design to minimize the uncertainty.

Further, the assumptions for the determination of the quantities are important. It shall be settled, if splice lengths in the reinforcement are included, if holes or cut-outs in the structure are included, what material strengths have been assumed. An estimate of the expected variation of quantities (global or local quantities) should be provided.

The tender design shall be buildable. In a DBB contract, the tender design should be based on a safe and well-known fabrication and erection scheme. In case of DB the tender design is carried out in close cooperation between consultant and contractor. This assures that the design accommodates contractor's methods and the available equipment.

A tender design is not fully detailed and should focus on elements with large cost impact and on elements with large uncertainties in order to arrive as close as possible to the actual quantities and to describe the complexity of the structure effectively from a costing point of view. A tender design normally comprises layout drawings of main structural elements, detailed drawings of typical details with a high degree of repetition, typical reinforcement arrangement, and mass distribution.

It is important that accidental loads, for instance vessel collision, train derailment, cable rupture, earthquake, and ice are considered in the tender design phase as they are often governing for the design.

Durability, operation, and maintenance aspects should be considered in the tender design. Experience from operation and maintenance of similar bridges is an advantage, because it allows a proper service life tender design to be carried out based on past experience. It is at the early design stages that the constructions methods are chosen that have a significant effect on further O&M costs.

It is not unusual that a tender design is prepared for more than one solution to arrive at the optimal solution. It could for instance be two solutions with different materials (concrete and steel) as for the Great Belt, East Bridge, two solutions with traffic arranged differently (one level versus two levels) as for the Øresund Link. Different structural layouts, such as cable-stayed or suspension bridge versus immersed or bored tunnel, could be relevant to investigate under certain conditions, such as for the Fehmarn Belt Fixed Link. After the designs have been prepared to a certain level, a selection can be carried out based on a preliminary pricing. Depending on the situation and owners preferences, only one solution or more solutions may be brought all the way to tender.

Tender documents to follow the drawings have to be prepared. The tender documents typically comprise bill of quantities, special specifications, and so on.

4.6.4 Detailed Design

The detailed design is either carried out before or partly before and after signing of the construction contact. In case completion of the detailed design is carried out in parallel with the construction work, the submission of the detailed design has to be planned and coordinated with the contractor. This is especially the case for a DB contract. The awareness of the fact that parts of the structure are completed, typically the foundation structures, before the calculations of the entire structure are completed, require a detailed planning of the design work.

The two types of design, design of permanent works and design of temporary works, are often carried out by different consultants. Design of temporary works is normally conducted in-house by the contractor, whereas the design of the permanent works is carried out by the consultant.

The purpose of the detailed design is to demonstrate that all the requirements are met, and to prepare drawings for the construction. Detailed design drawings define all measures and material qualities in the structure. Shop drawings for steel works will normally be prepared by the steel fabricator. Detailed reinforcement arrangements and bar schedules are either prepared by the contractor or the consultant. It is important that the consultant prescribes the tolerance requirements that the design has been based on that are in excess of what is required by the codes.

The detailed design should consider serviceability limit state (e.g., deflection and comfort), ultimate limit state (e.g., stress and stability), and accidental limit state (e.g., collapse of the structure). In order to demonstrate the adequacy of the design, substantial analyses, including 3D global Finite Element analyses, Local Finite Element analyses, and non linear analyses in geometry and/or materials are carried out. Dynamic calculations, typically response spectrum analyses, are performed to determine the response from wind and earthquake. The dynamic amplifications of traffic load and cable rupture are determined by time-history analysis, which are also used for ship collision, wind, and earthquake analysis.

For large slender bridge structures carrying railway traffic at high speed extensive dynamic analyses are required in order to demonstrate that safe and comfortable conditions can be achieved for the railway users.

For large cable-supported bridges, wind tunnel testing is conducted as part of the detailed design. Preliminary wind tunnel testing is often carried out in the tender design phase to demonstrate the aerodynamic stability of the structure. Other tests, such as scour protection tests and fatigue tests, such can also be carried out with the purpose to verify the design assumptions.

Detailed sub-soil investigations for all foundations are carried out before or in parallel with the detailed design.

The operation and maintenance objectives in the detailed design have to be implemented in a way that

- Give an overall cost-effective operation and maintenance
- Cause a minimum of traffic restrictions because of O&M works
- Provide optimal personnel safety
- Protect the environment
- Allow for an easy documentation of maintenance needs and results

In addition, the contractor has to provide a forecast schedule for the replacement of major equipment during the lifetime of the bridge.

4.6.5 Follow-Up during Construction

During construction the consultant's representative follows up to ensure that the construction is performed according to the consultant's intention of the project. The design follow up is an activity, carried out within the supervision organization as general supervision or technical services.

The general supervision follows up to ensure that the project intentions are followed by the contractor during construction. This activity is performed during review of the contractor's method statements, working procedures, and his design of temporary structures and equipment.

Important construction activities are followed by the general supervision by direct inspections on site. To follow the actual quality of the workmanship and materials used, spot review of contractor's quality control documentation is carried out on a random basis by the general supervision.

In cases where the work results in a nonconformity to the design or the specifications, the general supervision is consulted to evaluate the contractors' proposals to rectify the nonconformities or to use the structural element as built without any making good and where the contractor proposes changes to the design; the general supervision is consulted to evaluate the proposals and give recommendation whether to accept the changes or not.

To support the site supervision team, the general supervision prepares the instruction or manuals that the site supervision uses as basis for their work. The instructions and manuals are advantageously prepared by the consultant who knows where the difficulties during construction are expected, and where the critical points in the structure are, points where it is important that no mistakes are made during construction. The site supervision gives feedback to the general supervision on the instructions based on the experience gained. Often revision has to be carried out to suit actual performance of the contractor on site. The general supervision monitors the performance of the site supervision by interviews or audits.

The general supervision advises in which cases specialist assistance or special testing of materials or special investigations are required. The results of such activities are evaluated by the general supervision, and a final recommendation is given, based on all information available for the case in question.

Special testing institutes are often involved in third part controls that are normally carried out on a spot basis only. Examples are NDT of welds on steel structures or mechanical and chemical analyses of steel plate material. Third part testing of concrete constituents such as cement, aggregates, and admixtures is also carried out at official laboratories on a spot basis only.

The general supervision normally prepares the operation and maintenance procedures and instruction for the structural parts to be used during inspections and regular maintenance in the operation phase. Some instructions are based on detailed manuals, prepared by the contractor's suppliers; for example, for bearings, expansion joints, electrical installations or special equipment such as dehumidification systems or buffers. Preparation of these manuals by the suppliers is a part of the contractual obligations, and the manuals are prepared in the language of the country where the structure is located to facilitate the use by the maintenance staff.

Prior to the contractor's handing over of the structure, an inspection is carried out by the general supervision. The purpose of the inspection is to check for errors or omissions, which should be corrected by the contractor within the frames of the contract.

4.7 Tendering and Contracting

4.7.1 Tender Evaluation

4.7.1.1 Design-Bid-Build

The objective of tender evaluation is to make all tenders directly comparable via a rating system. The rating system is predefined by the owner, and should be part of the tender documents. The tender evaluation activities can be split into phases:

1. Preparation
2. Compilation and checking of tenders
3. Evaluation of tenders
4. Preparation for contract negotiations
5. Negotiation and award of contract

The preparation phase covers activities up to and including the receipt of tenders. The main activities are as follows:

- Define tender opening procedures and tender opening committee.
- Quantify the differences in present value because of function, operation, maintenance, and owner's risk for each of the tendered projects, using the owner's cost estimate.

After receipt of tenders a summary report, as a result of compilation and checking of tenders, should be prepared to summarize tender sums. The objective of this report is to collect the information supplied in different tenders into a single summarizing document and to present a recommendation of tenders for detailed review.

Typical activities among others are as follows:

- Check completeness of compliance of all tenders, including arithmetical correctness and errors or omissions.
- Identify possible qualifications and reservations.
- Identify parts of tenders where clarification is needed or more detailed examination required.
- Prepare a preliminary list of questions for clarification by the tenderers.
- Review compliance with requirements for alternative designs.
- Upgrade alternative tender design and pricing to the design basis requirements for tender design.

The evaluation of tenders in addition to activities already carried out among others, includes:

- Tender clarification by initial submission of questionnaires to tenderers, followed by clarification meetings and subsequent receipt of tenderers' written clarification answers
- Adjustment of tender prices to a comparable basis taking account of revised quantities because of modified tender design effects of combined tenders, alternatives, options, reservations, and differences in present value
- Appraisement of the financial components of the tenders
- Appraisement of owner's risk
- Technical review of alternatives and their effect on interfaces
- Appraisement of the proposed tender time schedule
- Appraisement of proposed subcontractors, suppliers, consultants, testing institutes, and so on
- Review of method statements and similar information
- Establishment of list of total project cost

The objective of evaluating owner's risk should be to assess possible overruns in cost and time. An evaluation of the split of economical consequences between contractor and owner should be carried out. Risk and uncertainty are inherent in all construction works, and especially in works of exceptional size.

Preparation for contract negotiations should be performed as late as possible allowing all aspects for the actual project type that can be taken into account. Typical activities should include the following:

- Modify tender design to take account of current status of the project development so as to establish an accurate contract basis.
- Modify tender design to accommodate alternatives.
- Liaise with third parties regarding contractual interfaces.
- Liaise with interfacing authorities.
- Establish strategies and recommendations for contract negotiations.

The probable extent and nature of the negotiations will become apparent from the tender evaluation. Typical activities during negotiations and award of contract are as follows:

- Preparation of draft contract documents
- Clarification of technical, economical, and legal matters
- Finalizing contract documents

4.7.1.2 Design-Build

The main goal is shared with the DBB approach to award a contract for construction of a fixed link. Many of the elements mentioned in the Section 4.7.1.1 will hence also be part of the tendering process for a DB contract. The approach selected by owners for carrying through the tendering process for a DB contract cannot be described quite as schematic as the sequence of DBB tender evaluation activities.

Common to all approaches is that the owner wishes to open up for the contractors' participation in and response for the design process in order to gain benefits from the special skills and qualifications of the individual contractor. Hence a common characteristic of tender documents for a DB contract is that functional and geometrical requirements are very well described, the design basis is extensive, and eventually great effort has been placed on definition of the work process to follow until a contract is awarded and the rules of this game condensed into the employers' requirements.

4.8 Construction and Commissioning

Development of contract conditions will relate to the selected procurement method, checking of design, construction, and so on.

No further details will be given here, but it is appropriate to emphasize the importance of these aspects for the planning of the overall project development.

4.9 Operation, Maintenance, and Transfer

Operation and maintenance conditions will have a significant influence on the life cycle costs of the fixed link elements and as such should be considered carefully in the planning phases in order to achieve structural solutions that are also optimized in respect to operation and maintenance costs and demolition!

4.9.1 Very Long Fixed Links

Over the last decades very long fixed links have been completed or many more have been planned. Construction-wise, the length will imply more extensive works and the distances between production facilities on land and the construction site will pose a logistic challenge to the contractors, which is evident.

The larger lengths will also pose increasing demands on operation and maintenance of the fixed link.

4.9.1.1 Operation and Emergency

Users will experience long lengths of very uniform views amplifying any tendencies of sleepiness, which may pose a safety problem for the traffic in general. Attention should be given to achieving variation of the user experience along such long fixed links. And rest facilities for users may be considered along the fixed link.

Situations may arise where users need to turn around and return to the origin of the fixed link. Facilities for such situations should be evaluated.

The situation is of special importance in case of emergencies where time is critical, as it would be detrimental to injured traffic victims if rescue vehicles should run the whole length of the fixed link. Facilities for turn around for emergency vehicles should be considered as well as the option to approach an emergency area opposite the normal traffic flow—provided pertinent traffic control systems are in place. Also helicopter-pads for efficient transport of injured persons should be considered.

4.9.1.2 Inspection and Maintenance

Experience from fixed links in operation shows that operation and maintenance staff working on carriageway areas poses a risk to both the operation and maintenance staff itself and to the users of the fixed link that may collide. On long fixed links operation and maintenance is a continuous activity and it must be considered how the user traffic and the O&M activities can be separated. This may require special facilities for access for the O&M staff that would not be required for shorter links with structures of similar type. The issues have been addressed for the Fehmarn Belt Fixed Link—approximately 18 km long—where, for the bridge concept, parking areas were arranged for O&M vehicles at all expansion joints completely outside the carriageway and for the tunnel concept the same considerations led to special operation and maintenance elements, every approximately 2 km.

4.10 Fixed Link Examples

The activities within establishment of fixed links in Denmark are illustrative examples of different approaches to procurement, different combinations of fixed link elements along the length of the fixed link. The major fixed links comprise the 18 km long Great Belt Fixed Link completed in 1998, the 16 km long Øresund Fixed Link completed in 2000, and the 18 km long Fehmarn Belt Fixed Link planned for inauguration in 2020. All fixed link carry both road and railway traffic (see Figure 4.4).

FIGURE 4.4 Denmark with the national Great Belt Link, the Øresund Link to Sweden and the Fehmarn Belt Link to Germany. (Courtesy of COWI A/S.)

4.10.1 Great Belt Link

The first tender design for a combined railway and motorway bridge across Great Belt/Storebælt was prepared in 1977–1978. However, only one and a half months short of issuing tender documents and call for bids, the progress of the project was temporarily stopped by the government in August 1978. Several state-of-the-art investigation such as vessel impact, fatigue, and wind loads had been carried out for two selected record-breaking navigation spans; a 780 m main span cable-stayed bridge and a 1416 m main span suspension bridge, both designed for a heavy duty double track railway and a six-lane motorway.

The construction of the present fixed link is based on a political agreement of June 12, 1986, where the main principles for the fixed link were set out. The link should consist of a low-level bridge for combined railway and highway traffic, the West Bridge from Funen to a small island in the middle of the Belt, from where the link should continue to Zealand in a bored or an immersed tunnel for the railway, the East Tunnel, and a high-level bridge for the highway traffic, the East Bridge (see Figure 4.5).

4.10.1.1 Organization

The company A/S Storebæltsforbindelsen was established January 23, 1987 on the basis of an agreement of June 12, 1986 between political parties, forming a majority in the Danish Parliament. The company was registered as a limited company with the Danish State as sole shareholder. The purpose of the company was to plan, design, implement, and operate the fixed link.

The management of the company was organized in accordance with the Danish Company Act and consisted of a supervisory board, appointed by the shareholder, and management, appointed by the supervisory board. The management consisted of three directors: the managing director, the technical director, and the finance director.

The line organization consisted of a number of project organizations, each headed by a project director who was responsible to the management for planning, design, and construction of his specific part of the link.

FIGURE 4.5 The Great Belt Fixed Link. Combined road and rail low-level West Bridge in foreground, East Bridge suspension road bridge, and ramp to the East Tunnel for railway. (Courtesy of Sund & Bælt Holding A/S.)

The project is financed by government guaranteed commercial loans to be paid back via user tolls. The pay-back period for the highway part is estimated to 15 years, whereas the railway crossing is to be paid by the Danish State Railways over 30 years in fixed installments per year.

4.10.1.2 East Bridge

In 1987 the conceptual design was carried out for the high-level highway bridge. The main objectives were to develop a global optimization with regard to the following:

- Alignment, profile, and navigation clearance
- Position of vessel lanes
- Navigation span solutions, based on robust and proven design and construction technology
- Constructible and cost-competitive solutions for the approach spans, focusing on repetitive industrialized production methods onshore
- Master time schedule
- Master budget

From 1989 to 1990 outline design, tender design, and tender documents were prepared with the main focus on navigation safety and environmental considerations. Comparative studies of four alternative main bridge concepts were carried out to thoroughly evaluate the technical, economical, and environmental effects of the range of main spans:	
Cable-stayed bridge	916 m main span
Cable-stayed bridge	1204 m main span
Suspension bridge	1448 m main span
Suspension bridge	1688 m main span

Navigation risk studies found only the 1688 m main span adequate to cross the existing navigation route without affecting the navigation conditions negatively.

A 1624 m main span suspension bridge with side spans of 535 m across a 78° relocated navigation route was chosen for tender and construction.

The pylons were tendered in both steel and concrete. For the approach bridges' superstructure, 124 m long concrete spans and 168 m long steel spans as well as composite steel/concrete concepts were developed. Although an equally competitive economy was found, it was decided to limit the tender designs to concrete and steel spans. However, the tenderers were free to propose hybrid solutions.

The tender documents were subdivided into four packages to be priced by the contractors; superstructure and substructure inclusive pylons for the suspension bridge, and superstructures and substructures for the approach bridges. The tender documents were released to prequalified contractors and consortia in June 1990.

In December 1990 the tenders were received. Eight consortia submitted 32 tenders, and four alternatives to the basic tender design.

In October 1991 construction contracts were signed with two international consortia; a German, Dutch, and Danish joint venture for the substructures, inclusive concrete pylons, and an Italian contractor for an alternative superstructure tender where high strength steel where applied to a more or less unchanged basic cross section, thereby increasing the span length for the approach bridges from 168 to 193 m (see Figure 4.6).

The suspension span is designed with a main cable sag corresponding to 1/9 x span length. The steel bridge girder hangs from 80 cm diameter main cables in hangers each 24 m.

The girder is continuous over the full cable-supported length of 2.7 km between the two anchor blocks. The traditional expansion joints at the tower positions are thus avoided. Expansions joints are arranged in four positions only—at the anchor blocks and at the abutments of the approach bridges.

FIGURE 4.6 Great Belt, East Bridge, Denmark. (Courtesy of Sund & Bælt Holding A/S.)

The concrete pylons rise 254 m above sea level. They are founded on caissons placed directly on crushed stone beds.

The anchor blocks shall resist cable forces of 600,000 tons. They are founded on caissons placed on wedge-shaped foundation bases suitable for large horizontal loading. An anchor block caisson covers an area of 6100 m^2.

The caissons for the pylons, the anchor blocks, and the approach spans as well as the approach span pier shafts have been constructed at a prefabrication site established by the contractor 30 nautical miles from the bridge site. The larger caissons have been cast in two dry docks, and the smaller caissons and the pier shafts for the approach bridges on a quay area, established for this purpose.

A pylon caisson weighed 32,000 tons and an anchor block caisson 36,000 tons when they were towed from the dry dock by tug boats to their final position in the bridge alignment.

The two approach bridges, 2530 m and 1538 m, respectively, are continuous from the abutments to the anchor blocks.

Both the suspension bridge girder and the approach bridge girders are designed as closed steel boxes and constructed of few basic elements: flat panels with trough stiffeners and transverse bulkhead trusses. The suspension bridge girder is 31.0 m wide and 4.0 m deep; the girder for the approach bridges is 6.7 m deep. They are fabricated in sections, starting in Italy. In Portugal, on their way by barge to Denmark, a major preassembly yard was established for girder sections to be assembled, before they were finally joined to full span girders in Denmark.

The East Bridge was inaugurated on June 14, 1998.

4.10.1.3 West Bridge

The 6.6 km West Bridge was tendered in three alternative types of superstructure: a double deck composite girder, triple independent concrete girders side by side, and a single steel box girder. All three bridge solutions shared a common gravity-founded sand-filled caisson substructure, topped by pier shafts of varying layout.

Tenders were handed out to six prequalified consortia in April 1988, and 13 offers on the tender solutions as well as three major alternatives and nine smaller alternatives were received from five groups.

Tender evaluation resulted in selecting an alternative design: two haunched concrete box girders with a typical span length of 110.4 m reduced to 81.75 m at the abutments and the expansion joints. The total length was subdivided into six continuous girders, requiring seven expansion joints.

Altogether 324 elements, comprising 62 caissons, 124 pier shafts, and 138 girders have been cast in five production lines at a reclaimed area close to the bridge site. All the elements were cast, moved, stored, and loaded out on piled production lines without use of heavy gantry cranes or dry-docks. The maximum weight of an element was 7400 tons. The further transportation and installation was carried out by The Swan, a large purpose-built catamaran crane vessel (see Figure 4.7).

By this concept, which was originally presented in the tender design, but further developed in the contractor's design, the entire prefabrication system was optimized in regard to resources, quality, and time.

The bridge was handed over January 26, 1994.

4.10.1.4 East Tunnel

Two immersed tunnel solutions as well as a bored tunnel were considered for the 9 km wide eastern channel. After tender, the bored tunnel was selected for economical and environmental reasons.

The tunnel consists of two 7.7 m internal diameter tubes, each 7412 m long and 25 m apart. At the deepest point, the rails are 75 m below the sea level.

Four purpose-built tunnel boring machines of the earth balance pressure types have bored the tunnels, launched from each end of both tubes.

The tunnel tubes are connected at about 250 m intervals by 4.5 m diameter cross passages, which provide safe evacuation of passengers and are the location for all electrical equipment.

About 250 m of reinforced concrete cut-and-cover tunnels are built at each end of the bored tubes (see Figure 4.8).

The tunnel is lined with precast concrete segmental rings, bolted together with synthetic rubber gaskets. Altogether 62,000 segments have been produced. A number of protective measures have been taken to secure 100 years service life design.

On April 7, 1995, the final tunnel lining segment was installed. Thus the construction of the tunnel tubes was completed, almost five years after work commenced.

The tunnel was handed over in mid-1997.

FIGURE 4.7 Great Belt, West Bridge, Denmark. (Courtesy of Sund & Bælt Holding A/S.)

FIGURE 4.8 Great Belt, East Tunnel, Denmark. (Courtesy of Sund & Bælt Holding A/S.)

4.10.2 Øresund Link

The 16 km fixed link for combined railway and motorway traffic between Denmark and Sweden consists of three major projects: a 3.7 km immersed tunnel, a 7.8 km bridge, and an artificial island that connects the tunnel and the bridge.

The tunnel contains a four-lane motorway and two railway tracks. The different traffic routes are separated by walls, and a service tunnel is placed between the motorway's two carriageways (lanes). The tunnel is 40 m wide and 8 m high. The 20 reinforced concrete tunnel elements, 174 m long and weighing 50,000 tons, were being prefabricated at the Danish side, and towed to the alignment.

4.10.2.1 Organization

The Øresund Link's Owner is Øresundskonsortiet, established as a consortium between the Danish company A/S Øresundsforbindelsen and the Swedish company Svensk–Danska Broförbindelsen in January 27, 1992. The two parties each own 50% of the consortium.

The purpose of the consortium is to own, plan, design, finance, construct, and operate the fixed link across Øresund.

The management of the consortium is similar to the Storebælt organization with a supervisory board that has appointed a managing director, a technical director, and a finance director.

The project is financed by commercial loans, guaranteed jointly and severally between the Danish and the Swedish governments. The highway part will be paid by user tolls, whereas the two countries' railway companies will pay fixed installments per year. The pay-back period is estimated to 24 years. The revenue also has to cover the construction work expenses for the Danish and Swedish land-based connections.

4.10.2.2 Øresund Bridge

In July 1994, the Øresundskonsortiet prequalified a number of contractors to built the bridge on a design and construct basis.

The bridge was tendered in three parts: the approach bridge from Sweden, the high-level bridge with a 490 m main span and a vertical clearance of 57 m, and the approach bridge toward Denmark. Two solutions for the main bridge were suggested: primarily a two-level concept with the highway on the

top deck and the two-track railway on the lower deck; secondary a one-level bridge. Both concepts were based on cable-stayed main bridges.

Five consortia were prequalified to participate in the competition for the high-level bridge, and six consortia for the approach bridges.

In June 1995, the bids for the Øresund Bridge were delivered. Although all four consortia had elaborated tenders for the two-level bridge, only two tenders were received for the one-level bridge, and only one consortium suggested to built the approach bridges in one level. The two-level concept was clearly the economically most favorable solution.

In November 1995 the contract for the entire bridge was awarded to a Danish–Swedish–German consortium (see Figure 4.9).

The 7,8 km bridge includes a 1090 m cable-stayed bridge with a main span of 490 m. The 3013 m and 3739 m approach bridges have spans of 141 m. The entire superstructure is a composite structure with steel truss girders between the four-lane motorway on the upper concrete deck and the dual track railway on the lower deck.

Fabrication of the steel trusses as well as casting of the concrete deck was carried out in Spain. The complete 140 m long girder sections, weighing up to 7000 tons, were tugged on flat barges to the bridge site and lifted into position on the piers.

On the cable-stayed bridge the girder was erected in 140 m sections on temporary supports before being suspended by the stays. This method is unusual for a cable-stayed bridge, but it is attractive because of the availability of the heavy lift vessel, and it reduces the construction time and limits vessel traffic disturbance.

The cable system consists of two vertical cable planes with parallel stays, the so-called harp shaped cable system. In combination with the flexural rigid truss girder and an efficient pier support in the side spans, a high stiffness is achieved.

The module of the truss remains 20 m both in the approach and in the main spans. This results in stay cable forces of up to 16,000 tons, which is beyond the range of most suppliers of prefabricated cables. Four prefabricated strands in a square configuration have therefore been adopted for each stay cable.

FIGURE 4.9 Øresund Link, cable-stayed bridge, Denmark–Sweden. (Courtesy of Søren Madsen/Øresundsbron.)

The concrete pylons are 203.5 m high and founded on limestone. Caissons, prefabricated on the Swedish side of Øresund, have been placed in 15 m water depth, and the cast-in-place of the pylon shafts is progressing. Artificial islands have been established around the pylons and near-by piers to protect against vessel impact.

All caissons, piers, and pier shafts are being prefabricated on shore to be assembled offshore.

The bridge was opened for traffic in July 2000.

4.10.3 Fehmarn Belt Link

4.10.3.1 Feasibility Study

In 1995 the Danish and German Ministry of Transport invited eight consulting consortia to tender for the preliminary investigations for a fixed link across the 19 km wide Fehmarn Belt.

Two Danish/German consortia were selected: one to carry out the geological and geotechnical investigations, and the other to investigate technical solution models, the environmental impact, and to carry out the day-to-day coordination of the investigations.

In the first phase, seven different technical solutions were investigated, and in the second five recommended solutions were the basis for a concept study:

- A bored railway tunnel with and without shuttle services
- An immersed railway tunnel with and without shuttle services
- A combined highway and railway bridge
- A combined highway and railway bored tunnel
- A combined highway and railway immersed tunnel

With a set of more detailed and refined functional requirements, various concepts for each of the five solution models have been studied in more detail than in the first phase. To provide an adequate basis for a vessel collision study and the associated part of the risk analysis, vessel traffic observations were carried out by the German Navy. In parallel, the environmental, the geological, and the geotechnical investigations were continued.

The feasibility study was concluded with the final reporting early 1999 where the technical study recommended a cable-stayed bridge as the main solution and an immersed tunnel as an alternative solution. The environmental study resulted in a comparable ranking of the solutions. The total construction costs for these two solutions amounted to 2.426 MEURO and 3.079 MEURO, respectively (cost level June 1996). These solutions were 4+2 models, for example they were planned for 4 roadway lanes and 2 railway tracks.

The results of the technical and environmental studies have been supplemented by economical studies and constituted the basis for public discussions and political decisions on the preferred procurement model, whether to establish a fixed link, and also which solution model should be preferred.

4.10.3.2 Conceptual Design Phase

Based upon an intergovernmental agreement entered into between Denmark and Germany in September 2008, Denmark was entrusted to develop, construct, finance, and operate the future Fehmarn Belt Fixed Link. Under the ministry of transport, a state owned organization was set up with the name Femern A/S to develop the project.

The treaty defines a cable-stayed bridge as the preferred and an immersed tunnel as the alternative solution of a link for a dual carriageway roadway and a twin track railway connection. Femern A/S appointed in April 2009 two independent consultant teams to develop the bridge and tunnel solution in parallel.

The final concept designs of the competing link structures (status November 2010) encompass the following:

1. Cable-stayed main bridge with 2 main spans of 724 m each and a total length of 2414 m, two approach bridges with lengths of 5748 m and 9412 m, respectively consisting of 200 m spans typically, and reclaimed peninsulas to connect to the shorelines. The superstructure carries road and rail in 2 levels and uses a steel cross section for the main bridge and a composite section for the approach spans. Land works to connect to the road and rail on land are part of the project, too.
2. Immersed tunnel with total length of approximately 18 km with large reclaimed areas in front of the shore lines. The tunnel comprises in one section 2 roadway tubes, a central gallery between the roadway tubes, and 2 railway tubes. Standard elements of 217 m length are planned and special elements of 42 m length are arranged where technical equipment will be placed. These special elements are deeper (2 stories) than the normal ones and 10 of these elements will be used. Land works to connect to the road and rail on land are part of the project too (see Figure 4.10).

Femern A/S has, on the basis of the completed concept designs and an initial environmental evaluation, found that the tunnel offers slight advantages with respect to the marine environment and thus recommended in November 2010 to develop the immersed tunnel as the preferred solution in the future. This recommendation was confirmed by the Danish Transport Minister in February 2011 and constitutes the present working basis. The final decision between the 2 solutions has to await the conclusion from the ongoing EIA (Environmental Impact Analysis) or VVM (Danish equivalent to EIA) studies.

Here it shall be noted that Femern A/S's published cost evaluation has derived at construction costs of 3800 MEURO for both technical solutions—a quite unusual result.

Alternatives to the 2 main solutions are studied and evaluated too, and they cover a suspension bridge with a large, single span and a bored tunnel solution with 3 bored tubes.

The future steps in the project development are confirmation of the preferred solution by final EIA/VVM, submission for plan approval in Germany and Denmark, start of the tendering procedures, and ending up in a construction act to be passed by the Danish Parliament. The actual construction start is envisaged in 2014 and the opening of the link planned for 2020.

FIGURE 4.10 Fehmarnbelt Link, concept bridge design, Denmark–Germany. (Courtesy of Dissing+Weitling architecture.)

References

AASHTO. 2012. *LRFD Bridge Design Specifications.* 6th Edition, American Association of State Highway and Transportation Officials, Washington, DC.

Euro Codes. 2011. *Basis of Structural Design.* European Committee for Standardization, Brussels, Eurocode EN 1990, Related Design volumes EN 1991—EN 1999.

Larsen, O. D. 1993. *Ship Collision with Bridges. The Interaction between Vessel Traffic and Bridge Structures.* Structural Engineering Document no. 4. IABSE Green Book, ISBN 3-85748-079-3, International Association for Bridge and Structural Engineering, Zürich, Switzerland.

Strait Crossing Bridge. 2011. Homepage for the Confederation Bridge by Strait Crossing Bridge Ltd (http://www.confederationbridge.com/en/).

5

Highway Bridge Design Specifications

John M. Kulicki
Modjeski and Masters, Inc.

5.1 Introduction

Several bridge design specifications will be referred to repeatedly herein. In order to simplify the references, the "Standard Specifications" means the *AASHTO Standard Specifications for Highway Bridges* (AASHTO, 2002), the 17th edition will be referenced unless otherwise stated. The "LRFD Specifications" means the *AASHTO LRFD Bridge Design Specifications* (AASHTO, 2012), and the 6th edition will be referenced, unless otherwise stated. The 1st edition of this latter document was developed in the period 1988–1993 when statistically-based probability methods were available, and that became the basis of quantifying safety. Because this is a more modern philosophy than either the load factor design (LFD) method or the allowable stress design (ASD) method, both of which are available in the Standard Specifications, and neither of which have a mathematical basis for establishing safety, much of the chapter will deal primarily with the LRFD Specifications (AASHTO, 2012).

There are many issues that comprise a design philosophy. For example, the expected service life of a structure, the degree to which future maintenance should be assumed to preserve the original resistance of the structure or should be assumed to be relatively nonexistence, how brittle behavior can be avoided, how much redundancy and ductility are needed, the degree to which analysis is expected to accurately represent the force effects actually experienced by the structure, the extent to which loads are thought to be understood and predictable, the degree to which the designers' intent will be upheld by vigorous material testing requirements and thorough inspection during construction, the balance between the need for high-precision during construction in terms of alignment and positioning compared to allowing for misalignment and compensating for it in the design, and, perhaps most fundamentally, the basis for establishing safety in the design specifications. It is this last issue, the way that specifications seek to establish safety, with which this chapter deals.

5.2 Philosophy of Safety

5.2.1 Introduction

A review of the philosophy used in a variety of specifications resulted in three possibilities, ASD, LFD, and reliability-based design, a particular application of which is referred to as load and resistance factor design (LRFD). These philosophies are discussed in Sections 5.2 through 5.5.

5.2.2 Allowable Stress Design

ASD is based on the premise that one or more factors of safety can be established based primarily on experience and judgment that will assure the safety of a bridge component over its design life, for example, this design philosophy for a steel member resisting moments is characterized by design criteria as mentioned in Equation 5.1.

$$\sum M/S \leq F_y/1.82 \tag{5.1}$$

where

Σm = sum of applied moments
F_y = specified yield stress
S = elastic section modules

The constant 1.82 is the factor of safety.

The "allowable stress" is assumed to be an indicator of the resistance and is compared to the results of stress analysis of loads. Allowable stresses are determined by dividing the elastic stress at the onset of some assumed undesirable response, for example, yielding of steel or aluminum, crushing of concrete, a loss of stability, by a safety factor. In some circumstances, the allowable stresses were increased on the basis that more representative measures of resistance, usually based on inelastic methods, indicated that some behaviors are stronger than others. For example, the ratio of fully yielded cross-sectional resistance (no consideration of loss of stability) to elastic resistance based on first yield is approximately 1.12–1.15 for most rolled shapes bent about their major axis. For a rolled shape bent about its minor axis, this ratio is 1.5 for all practical purposes. This increased plastic strength inherent in weak axis bending was recognized by increasing the basic allowable stress for this illustration from 0.55 to 0.60 F_y and retaining the elastic calculation of stress.

The specified loads are the working basis for stress analysis. Individual loads, particularly environmental loads, such as wind forces or earthquake forces, may be selected based on some committee-determined recurrence interval. This philosophy treats each load in a given load combination on the structure as equal from the view point of statistical variability. A "common sense" approach may be taken to recognize that some combinations of loading are less likely to occur than others, for example, a load combination involving a 100 mph (160 kph) wind, dead load, full shrinkage, and temperature may be thought to be far less likely than a load combination involving the dead load and the full design live load. For example, in ASD the former load combination is permitted to produce a stress equal to four-thirds of the latter. There is no consideration of the probability of both a higher than expected load and a lower than expected strength occurring at the same time and place. There is little or no direct relationship between the ASD procedure and the actual resistance of many components in bridges, or to the probability of events actually occurring.

These drawbacks notwithstanding, ASD has produced bridges that, for the most part, have served very well. Given that this is the historic basis for bridge design in the United States, it is important to proceed to other, more robust design philosophies of safety with a clear understanding of the type of safety currently inherent in the system.

5.2.3 Load Factor Design

In LFD a preliminary effort was made to recognize that the live load, in particular, was more highly variable than the dead load. This thought is embodied in the concept of using a different multiplier on dead and live load, for example, a design criteria may be expressed, as shown in Equation 5.2.

$$1.3M_{\mathrm{D}} + 2.17\left(M_{\mathrm{L+I}}\right) \leq \varphi M_{\mathrm{u}} \tag{5.2}$$

where

M_{D} = moment from dead loads
$M_{\mathrm{L+I}}$ = moment from live load and impact
M_{u} = resistance
φ = a strength reduction factor

Resistance is usually based on attainment of either loss of stability of a component or the attainment of inelastic cross-sectional strength. Continuing the rolled beam example mentioned in Section 5.2.2, the distinction between weak axis and strong axis bending would not need to be identified because the cross-sectional resistance is the product of yield strength and plastic section modulus in both cases. In some cases, the resistance is reduced by a "strength reduction factor," which is based on the possibility that a component may be undersized, the material may be understrength, or the method of calculation may be more or less accurate than typical. In some cases, these factors have been based on statistical analysis of resistance itself. The joint probability of higher than expected loads and less than that expected resistance occurring at the same time and place is not considered.

In the Standard Specifications(AASHTO, 2002), the same loads are used for ASD and LFD. In the case of LFD, the loads are multiplied by factors greater than unity and added to other factored loads to produce load combinations for design purposes.

The drawback to LFD as seen from the viewpoint of probabilistic design is that the load factors and resistance factors were not calibrated on a basis that takes into account the statistical variability of design parameters in nature. In fact, the factors for steel girder bridges were established for one correlation at a simple-span of 40 ft (12.2 m). At that span, both LFD and service load design are intended to give the same basic structure. For shorter spans, LFD is intended to result in slightly more capacity, whereas for spans over 40 ft (12.2 m), it is intended to result in slightly less capacity with the difference increasing with span length. The development of this one point calibration for steel structures is given by Vincent (1969).

5.2.4 Probability and Reliability-Based Design

Probability-based design seeks to take into account directly the statistical mean resistance, the statistical mean loads, the nominal or notional value of resistance, the nominal or notional value of the loads, and the dispersion of resistance and loads as measured by either the standard deviation or the coefficient of variation, that is, the standard deviation divided by the mean. This process can be used directly to compute probability of failure for a given set of loads, statistical data, and the designer's estimate of the nominal resistance of the component being designed. Thus, it is possible to vary the designer's estimated resistance to achieve a criterion that might be expressed in terms such as the component (or system) must have a probability of failure of less than 0.0001, or whatever variable is acceptable to society. Design based on probability of failure is used in numerous engineering disciplines, but its application of bridge engineering has been relatively small. The AASHTO Guide Specification and Commentary for Vessel Collision Design of Highway Bridges (AASHTO, 2010) is one of the few codifications of probability of failure in U.S. bridge design.

Alternatively, the probabilistic methods used to develop a quantity known as the "reliability index," is somewhat, but not completely, relatable to the probability of failure. Using a reliability-based code in the

purest sense, the designer is asked to calculate the value of the reliability index provided by his or her design and then compare that to a code-specified minimum value. Through a process of calibrating load and resistance factors to reliability indices in simulated trial designs, it is possible to develop a set of load and resistance factors, so that the design process looks very much like the existing LFD methodology. The concept of the reliability index and a process for reverse-engineering load and resistance factors is discussed in Section 5.2.5.

In the case of the LRFD Specifications, some loads and resistances have been modernized as compared to the Standard Specifications. In many cases, the resistances are very similar. Most of the load and resistance factors have been calculated using a statistically-based probability method, which consider the joint probability of extreme loads and extreme resistance. In the parlance of the LRFD Specifications, "extreme" encompasses both maximum and minimum events.

5.2.5 Probabilistic Basis of the LRFD Specifications

5.2.5.1 Introduction to Reliability as a Basis of Design Philosophy

A consideration of probability-based reliability theory can be simplified considerably by initially considering that natural phenomena can be represented mathematically as normal random variables, as indicated by the well-known bell-shaped curve. This assumption leads to closed form solutions for areas under parts of this curve, as given in many mathematical handbooks and programmed into many hand calculators.

Accepting the notion that both load and resistance are normal random variables, we can plot the bell-shaped curve corresponding to each of them in a combined presentation dealing with distribution as the vertical axis against the value of load, Q, or resistance, R, as shown in Figure 5.1 from Kulicki et al. (1994). The mean value of load ($\overline{Q}$) and the mean value of resistance ($\overline{R}$) are also shown. For both the load and the resistance, a second value somewhat offset from the mean value, which is the "nominal" value, or the number that designers calculate the load or the resistance to be is also shown. The ratio of the mean value divided by the nominal value is called the "bias." The objective of a design philosophy based on reliability theory, or probability theory, is to separate the distribution of resistance from the distribution of load, such that the area of overlap, that is, the area where load is greater than resistance, is tolerably small. In the particular case of the LRFD formulation of a probability-based specification, load factors and resistance factors are developed together in a way that forces the relationship between the resistance and load to be such that the area of overlap in Figure 5.1 is less than or equal to the value that a code-writing body accepts. Note in Figure 5.1 that is the nominal load and the nominal resistance, not the mean values, that are factored.

A conceptual distribution of the difference between resistance and loads, combining the individual curves discussed above, is shown in Figure 5.2, where the area of overlap from Figure 5.1 is shown as negative values, that is, those values to the left of the origin.

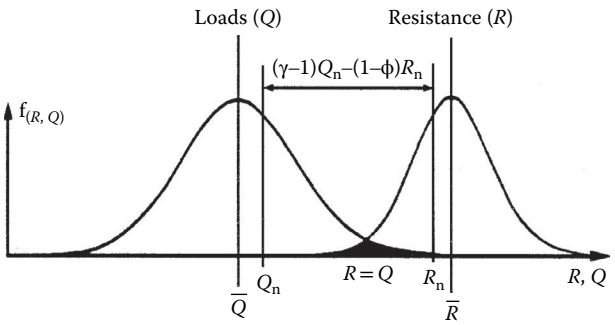

FIGURE 5.1 Separation of loads and resistance.

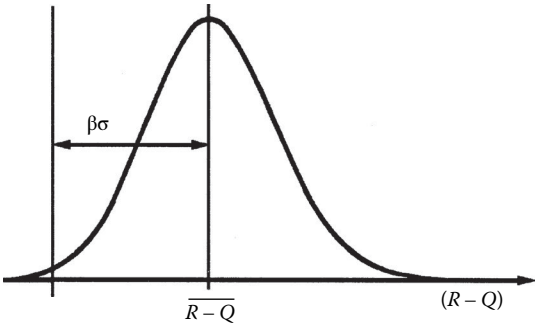

FIGURE 5.2 Definition of reliability index β.

It now becomes convenient to define the mean value of resistance minus load as some number of standard deviations, βσ, from the origin. The variable "β" is called the "reliability index" and "σ" is the standard deviation of the Quantity *R*−*Q*. The problem with this presentation is that the variation of the Quantity *R*−*Q* is not explicitly known. Much is already known about the variation of loads by themselves or resistances by themselves, but the difference between these has not yet been quantified. However, from the probability theory, it is known that if load and resistance are both normal and random variables, then the standard deviation of the difference is shown in Equation 5.3.

$$\sigma_{(R-Q)} = \sqrt{\sigma_R^2 + \sigma_Q^2} \tag{5.3}$$

Given the standard deviation and considering Figure 5.2 and the mathematical rule that the mean of the sum or difference of normal random variables if the sum or difference of their individual means, we can now define the reliability index, β, shown in Equation 5.4.

$$\beta = \frac{\overline{R} - \overline{Q}}{\sqrt{\sigma_R^2 + \sigma_Q^2}} \tag{5.4}$$

Comparable closed-form equations can also be established for other distributions of data, for example, log-normal distribution. A "trial and error" process is used for solving for β when the variable in question does not fit one of the already existing closed-form solutions.

The process of calibrating load and resistance factors starts with Equation 5.4 and the basic design relationship; the factored resistance must be greater than or equal to the sum of the factored loads as shown in Equation 5.5.

$$\varphi R = Q = \sum \gamma_i x_i \tag{5.5}$$

Solving for the average value of resistance yields:

$$\overline{R} = \overline{Q} + \beta\sqrt{\sigma_R^2 + \sigma_Q^2} = \lambda R = \frac{1}{\varphi}\lambda \sum \gamma_i x_i \tag{5.6}$$

Using the definition of bias, indicated by the symbol λ, Equation 5.6, leads to the second equality in Equation 5.6. A straightforward solution for the resistance factor φ is as shown in Equation 5.7.

$$\varphi = \frac{\lambda \sum \gamma_i x_i}{\overline{Q} + \beta \sqrt{\sigma_R^2 + \sigma_Q^2}} \tag{5.7}$$

Unfortunately, Equation 5.7 contains three unknowns, that is the resistance factor φ, the reliability index β, and the load factors γ.

The acceptable value of the reliability index β, must be chosen by a code-writing body. Although not explicitly correct, we can conceive of β as an indicator of the fraction of times that a design criterion will be met or exceeded during the design life, analogous to using standard deviation as an indication of the total amount of population included or not included by a normal distribution curve. Utilizing this analogy, a β of 2.0 corresponds to approximately 97.3% of the values being included under the bell-shaped curve, or 2.7 of 100 values not included. When β is increased to 3.5, for example, now only two values in approximately 10,000 are not included.

It is more technically correct to consider the reliability index to be a comparative indicator. One group of bridges having a reliability index that is greater than a second group of bridges also has more safety. Thus, this can be a way of comparing a new group of bridges designed by some new process to a database of existing bridges designed by either ASD or LFD. This is, perhaps, the most correct and most effective use of the reliability index. It is this use that formed the basis for determining the target, or code specified, reliability index, and the load and resistance factors in the LRFD Specifications, as will be discussed in the next two sections.

The probability-based LRFD for bridge design may be seen as a logical extension of the current LFD procedure. ASD does not recognize that various loads are more variable than others. The introduction of the LFD methodology brought with it the major philosophical change of recognizing that some loads are more accurately represented than others. The conversion to probability-based LRFD methodology could be thought of as a mechanism to more systematically and rationally select the load and resistance factors than was done with the information available when LFD was introduced.

5.2.5.2 Calibration of Load and Resistance Factors

Assuming that a code-writing body has established a target value reliability index β, usually denoted β_T, Equation 5.7 still indicates that both the load and resistance factors must be found. One way to deal with this problem is to select the load factors and then calculate the resistance factors. This process has been used by several code-writing authorities (AASHTO, 2012; CAS, 2006; OMTC, 1994). The steps in the process are as follows:

1. Factored loads can be defined as the average value of load, plus some number of standard deviation of the load, as shown as the first part of Equation 5.8.

$$\gamma_i x_i = \overline{x_i} + n\sigma_i = \overline{x_i} + nV_i\overline{x_i} \tag{5.8}$$

Defining the "variance," V_i, as being equal to the standard deviation divided by the average value, leads to the second-half of Equation 5.8. Utilizing the concept of bias one more time, Equation 5.8 can now be condensed into Equation 5.9.

$$\gamma_i = \lambda(1 + nV_i) \tag{5.9}$$

Thus, it can be seen that load factors can be written in terms of the bias and the variance. This gives rise to the philosophical concept that load factors can be defined so that all loads have the same probability of being exceeded during the design life. This is not to say that the load factors are identical, just that the probability of the loads being exceeded is the same.

2. Using Equation 5.7, for a given set of load factors, the value of resistance factor can be assumed for various types of structural members and for various load components, for example, shear, moment, and so on the various structural components. Computer simulations of a representative body of structural members can be done, yielding a large number of values for the reliability index.
3. Reliability indices are compared to the target reliability index. If close clustering results, a suitable combination of load and resistance factors has been obtained.
4. If close clustering does not result, a new trial set of load factors can be used and the process repeated until the reliability indices do cluster around, and acceptably close to, the target reliability index.
5. The resulting load and resistance factors taken together will yield reliability indices close to the target value selected by the code-writing body as acceptable.

The outline above assumes that suitable load factors are assumed. If the process of varying the resistance factors and calculating the reliability indices does not converge to a suitable narrowly grouped set of reliability indices, then the load factor assumptions must be revised. In fact, several sets of proposed load factors may have to be investigated to determine their effect on the clustering of reliability indices.

The process described earlier is very general. To understand how it is used to develop data for a specific situation, the rest of this section will illustrate the application to calibration of the load and resistance factors for the LRFD Specifications. The basic steps were as follows:

- Develop a database of sample current bridges.
- Extract load effects by percentage of total load.
- Develop a simulation bridge set for calculation purposes.
- Estimate the reliability indices implicit in current designs.
- Revise loads-per-component to be consistent with the LRFD Specifications.
- Assume load factors.
- Vary resistance factors until suitable reliability indices result.

Approximately 200 representative bridges were selected from various regions of the U.S. by requesting sample bridge plans from various states. The selection was based on structural type, material, and geographic location to represent a full-range of materials and design practices as they vary around the country. Anticipated future trends should also be considered. In the particular case of the LRFD Specifications, this was done by sending questionnaires to various departments of transportation asking them to identify the types of bridges they are expecting to design in the near future.

For each of the bridges in the database, the load indicated by the contract drawings was subdivided by the following characteristic components:

- The dead load due to the weight of factory-made components
- The dead load of cast-in-place components
- The dead load due to asphaltic wearing surfaces where applicable
- The dead weight due to miscellaneous items
- The live load due to the HS20 loading
- The dynamic load allowance or impact prescribed in the 1989 AASHTO Specifications

Full tabulations for all these loads for the full set of bridges in the database are presented in Nowak (1993).

Statistically projected live load and the notional values of live load force effects were calculated. Resistance was calculated in terms of moment and shear capacity for each structure according to the prevailing requirements, in this case the AASHTO Standard Specifications for LFD.

Based on the relative amounts of the loads identified above for each of the combination of span and spacing and type of construction indicated by the database, a simulated set of 175 bridges was developed that was comprised of the following:

- Twenty-five noncomposite steel girder bridge simulations for bending moments and shear with spans of 30, 60, 90, 120 and 200 ft (9, 18, 27, 36, and 60 m) and for each of those spans, spacing of 4, 6, 8, 10, and 12 ft (1.2, 1.8, 2.4, 3.0, and 3.6 m)
- Representative composite steel girder bridges for bending moments and shear having the same parameters as those identified above
- Representative reinforced concrete T-beam bridges for bending moments and shear having spans of 30, 60, 90, and 120 ft (9, 18, 27, and 36 m), with spacing of 4, 6, 8, 10, and 12 ft (1.2, 1.8, 2.4, 3.0, and 3.6 m) in each span group
- Representative prestressed concrete I-beam bridges for moments and shear having the same span and spacing parameters as those used for the steel bridges

Full tabulations of these bridges and their representative amounts of the various loads are presented in Nowak (1993).

The reliability indices were calculated for each simulated and each actual bridge for both shear and moment. The range of reliability indices that resulted from this phase of the calibration process is presented in Figure 5.3 from Kulicki et al. (1994). It can be seen that a wide-range of values were obtained using the current specifications, but this was anticipated based on previous calibration work done for the Ontario Highway Bridge Design Code (Nowak and Lind, 1979).

These calculated reliability indices, as well as past calibration of other specifications, serve as a basis for the selection of the target reliability index, β_T. A target reliability index of 3.5 was selected for the OHBDC and is under consideration for other reliability-based specifications. A consideration of the data shown in Figure 5.3 indicates that a β of 3.5 is representative of past LFD practice. Hence, this value was selected as a target for the calibration of the LRFD Specifications.

5.2.5.3 Load and Resistance Factors

The parameters of bridge load components and various sets of load factors, corresponding to different values of the parameter "*n*" in Equation 5.9 are summarized in Table 5.1 from Nowak (1993).

Recommended values of load factors correspond to $n = 2$. For simplicity of the designer, one factor is specified for shop- and field-built components, $\gamma = 1.25$. For D_3, weight of asphalt and utilities, $\gamma = 1.50$. For live load and impact, the value of load factor corresponding to $n = 2$ is $\gamma = 1.60$. However, a more conservative value of $\gamma = 1.75$ is utilized in the LRFD Specifications.

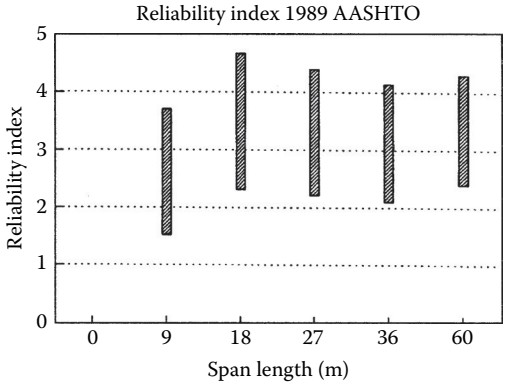

FIGURE 5.3 Reliability indices inherent in the 1989 AASHTO standard specifications.

TABLE 5.1 Parameters of Bridge Load Components

Load Component	Bias Factor	Coefficient of Variation	Load Factor		
			$n = 1.5$	$n = 2.0$	$n = 2.5$
Dead load, shop built	1.03	0.08	1.15	1.20	1.24
Dead load, field built	1.05	0.10	1.20	1.25	1.30
Dead load, asphalt and utilities	1.00	0.25	1.375	1.50	1.65
Live load (with impact)	1.10–1.20	0.18	1.40–1.50	1.50–1.60	1.60–1.70

TABLE 5.2 Considered Resistance Factors

Load Component	Limit State	Resistance Factors (φ)	
Noncomposite steel		Lower	Upper
	Moment	0.95	1.00
	Shear	0.95	1.00
Composite steel	Moment	0.95	1.00
	Shear	0.95	1.00
Reinforced concrete	Moment	0.85	0.90
	Shear	0.90	0.90
Prestressed concrete	Moment	0.95	1.00
	Shear	0.90	0.95

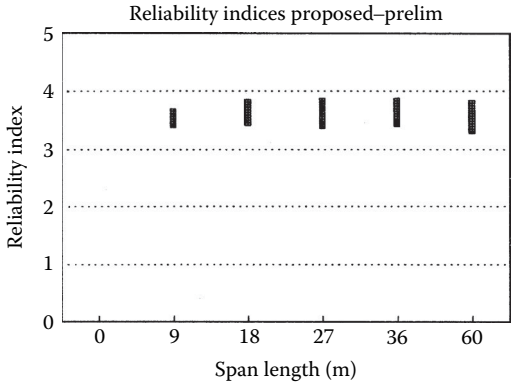

FIGURE 5.4 Reliability indices inherent in LRFD specifications.

The acceptance criterion in the selection of resistance factors is how close the calculated reliability indices are to the target value of the reliability index, β_T. Various sets of resistance factors, φ, are considered. Resistance factors used in the code are rounded off to the nearest 0.05.

Calculations were performed using the load components for each of the 175 simulated bridges. For a given resistance factor, material, span, and girder spacing, the reliability index is computed. Values of β were calculated for live load factors, $\gamma = 1.75$. For comparison, the results are also shown for live load factor, $\gamma = 1.60$. The calculations are performed for the resistance factors, φ, listed in Table 5.2 from Nowak (1993).

Reliability indices were recalculated for each of the 175 simulated cases and each of the actual bridges from which the simulated bridges were produced. The range of values obtained using the new load and resistance factors is indicated in Figure 5.4 (Kulicki et al. 1994).

Figure 5.4 shows that the new calibrated load and resistance factors, and new load models and load distribution techniques work together to produce very narrowly clustered reliability indices. This was the objective of developing the new factors. Correspondence to a reliability index of 3.5 is something that can now be altered by AASHTO. The target reliability index could be raised or lowered as may be advisable in the future and the factors can be recalculated accordingly. This ability to adjust the design parameters in a coordinated manner is one of the strengths of a probabilistically-based reliability design.

5.3 Limit States

All comprehensive design specifications are written to establish an acceptable level of safety. There are many methods of attempting to provide safety and the method inherent in many modern bridge design specifications, including the LRFD Specifications, the Ontario Highway Bridge Design Code (OMTC, 1994) and the Canadian Highway Bridge Design Code (CAS, 2006), is probability-based reliability analysis. The method for treating safety issues in modern specifications is the establishment of "limit states" to define groups of events or circumstances that could cause a structure to be unserviceable for its original intent.

The LRFD Specifications are written in a probability-based limit state format requiring examination of some, or all, of the four limit states defined below for each design component of a bridge:

- The service limit state deals with restrictions on stress, deformation, and crack width under regular service conditions. These provisions are intended to ensure the bridge to perform acceptably during its design life.
- The fatigue and fracture limit state deals with restrictions on stress range under regular service conditions reflecting the number of expected stress range excursions. These provisions are intended to limit crack growth under repetitive loads to prevent fracture during the design life of the bridge.
- The strength limit state is intended to ensure that strength and stability, both local and global, are provided to resist the statistically significant load combinations that a bridge will experience in its design life. Extensive distress and structural damage may occur under strength limit state conditions, but overall structural integrity is expected to be maintained.
- The extreme event limit state is intended to ensure the structural survival of a bridge during a major earthquake, or when collided by a vessel, vehicle or ice flow, or where the foundation is subject to the scour that would accompany a flood of extreme recurrence, usually considered to be 500 years. These provisions deal with circumstances considered to be unique occurrences whose return period is significantly greater than the design life of the bridge. The joint probability of these events is extremely low, and, therefore, they are specified to be applied separately. Under these extreme conditions, the structure is expected to undergo considerable inelastic deformation by which locked-in force effects because of temperature effects, creep, shrinkage, and settlement will be relieved.

5.4 Design Objectives

5.4.1 Safety

Public safety is the primary responsibility of the design engineer. All other aspects of design, including serviceability, maintainability, economics, and aesthetics are secondary to the requirement for safety. This does not mean that other objectives are not important, but safety is paramount.

5.4.1.1 Equation of Sufficiency

In design specifications the issue of safety is usually codified by an application of the general statement the design resistances must be greater than or equal to the design load effects. In ASD, this requirement can be formulated as shown in Equation 5.10.

$$\Sigma Q_i \leq \frac{R_E}{FS} \tag{5.10}$$

where

Q_i = a load
R_E = elastic resistance
FS = factor of safety

In LFD, the formulation as shown in Equation 5.11.

$$\Sigma \gamma_i Q_i \leq \varphi R \tag{5.11}$$

where

γ_i = a load factor
Q_i = a load
R = resistance
φ = a strength reduction factor

In LRFD, the formulation as shown in Equation 5.12.

$$\Sigma \eta_i \gamma_i Q_i \leq \varphi\, R_n = R_r \tag{5.12}$$

where

$\eta_i = \eta_D \eta_R \eta_I$: limited such that $\eta = \eta_D \eta_R \eta_I \geq 0.95$ for loads for which a maximum value of γ_i is appropriate, and, $\eta_i = \dfrac{1}{\eta_I \eta_D \eta_R} = 1.0$ for loads for which a minimum value of γ_i is appropriate
γ_i = load factor: a statistically-based multiplier on force effects
φ = resistance factor: a statistically-based multiplier applied to nominal resistance
η_i = load modifier
η_D = a factor relating to ductility
η_R = a factor relating to redundancy
η_I = a factor relating to operational importance
Q_i = nominal force effect: a deformation, stress, or stress resultant
R_n = nominal resistance: based on the dimensions as shown on the plans and on permissible stresses, deformations, or specified strength of materials
R_r = factored resistance: φR_n

Equation 5.12 is applied to each designed component and connection as appropriate for each limit state under consideration.

5.4.1.2 Special Requirements of the LRFD Specifications

Comparison of the equation of sufficiency as it was written above for ASD, LFD, and LRFD shows that as the design philosophy evolved through these three stages, more aspects of the component under design and its relation to its environment and its function to society must be expressly considered. This is not to say that a designer using ASD necessarily considers less than a designer using LFD or LRFD. The specification provisions are the minimum requirements and prudent designers often consider additional aspects. However, as specifications mature and become more reflective of the real world, additional criteria are often needed to assure adequate safety that may have been provided, albeit non-uniformly, by simpler provisions. Therefore, it is not surprising to find that the LRFD Specifications require explicit consideration of ductility, redundancy, and operational importance in Equation 5.12, whereas the Standard Specifications does not.

Ductility, redundancy, and operational importance are significant aspects affecting the margin of safety of bridges. Although the first two directly relate to the physical behavior, the last concerns the consequences of the bridge being out of service. The grouping of these aspects is, therefore, arbitrary; however, it constitutes a first effort of codification. In the absence of more precise information, each effect, except that for fatigue and fracture, is estimated as ±5%, accumulated geometrically, a clearly subjective approach. With time, improved quantification of ductility, redundancy, and operational importance, and their interaction, may be attained.

5.4.1.2.1 Ductility

The response of structural components or connections beyond the elastic limit can be characterized by either brittle or ductile behavior. Brittle behavior is undesirable because it implies the sudden loss of load-carrying capacity immediately when the elastic limit is exceeded, or even before that in some cases. Ductile behavior is characterized by significant inelastic deformations before any loss of load-carrying capacity occurs. Ductile behavior provides warning of structural failure by large inelastic deformations. Under cyclic loading, large reversed cycles of inelastic deformation dissipate energy and have a beneficial effect on structure response.

If, by means of confinement or other measures, a structural component or connection made of brittle materials can sustain inelastic deformations without significant loss of load-carrying capacity, this component can be considered ductile. Such ductile performance should be verified by experimental testing.

Behavior that is ductile in a static context, but which is not ductile during dynamic response, should also be avoided. Examples of this behavior are shear and bond failures in concrete members, and loss of composite action in flexural members.

The ductility capacity of structural components or connections may either be established by full- or large-scale experimental testing, or with analytical models that are based on realistic material behavior. The ductility capacity for a structural system may be determined by integrating local deformations over the entire structural system.

Given proper controls on the innate ductility of basic materials, proper proportioning and detailing of a structural system are the key considerations in ensuring the development of significant, visible, inelastic deformations before failure at the strength and extreme event limit states.

For the fatigue and fracture limit state for fracture-critical members and for the strength limit state for all members:

$\eta_D \geq 1.05$ for nonductile components and connections

$= 1.00$ for conventional designs and details complying with these specifications

≥ 0.95 for components and connections for which additional ductility enhancing measures have been specified beyond those required by these specifications

For all other limit states:

$\eta_D = 1.00$

5.4.1.2.2 Redundancy

Redundancy is usually defined by stating the opposite; for example, a nonredundant structure is one in which the loss of a component results in collapse, or, a nonredundant component is one whose loss results in complete or partial collapse. Multiple load path structures should be used unless there are compelling reasons to the contrary. The LRFD Specifications require additional resistance in order to reduce probability of loss of nonredundant component, and to provide additional resistance to accommodate load redistribution.

For the strength limit state:

$\eta_R \geq 1.05$ for nonredundant members

$= 1.00$ for conventional levels of redundancy

≥ 0.95 for exceptional levels of redundancy

For all other limit states:

$\eta_R = 1.00$

The factors currently specified were based solely on judgment and were included to require more explicit consideration of redundancy. Research by Ghosn and Moses (2001) provided a more rational requirement based on reliability indices thought to be acceptable in damaged bridges that must remain in service for a period of about two years. The "reverse engineering" concept is being applied to develop values similar in intent to η_R.

5.4.1.2.3 Operational Importance

The concept of operational importance is applied to the strength and extreme-event limit states. The owner may declare a bridge or any structural component or connection, thereof, to be of operational importance. Such classification should be based on social/survival and/or security/defense requirements. If a bridge is deemed of operational importance, η_I is taken as ≥ 1.05. Otherwise, η_I is taken as 1.0 for typical bridges and may be reduced to 0.95 for relatively less important bridges.

5.4.1.3 Design Load Combinations in the LRFD Specifications

The following permanent and transient loads and forces listed in Table 5.3 are considered in the AASHTO LRFD Specifications (AASHTO, 2012).

TABLE 5.3 Load Designations

Name of Load	LRFD Designation
Downdrag	DD
Dead load of structural components attachments	DC
Dead load of wearing surfaces and utilities	DW
Dead load of earth fill	EF
Horizontal earth pressure	EH
Locked-in force effects from construction	EL
Earth surcharge load	ES
Vertical earth pressure	EV
Vehicular braking force	BR
Vehicular centrifugal force	CE
Creep	CR
Vehicular collision force	CT
Vessel collision force	CV
Earthquake	EQ
Friction	FR
Ice load	IC
Vehicular dynamic load allowance	IM
Vehicular live load	LL
Live load surcharge	LS
Pedestrian live load	PL
Secondary forces from post-tensioning	PS
Settlement	SE
Shrinkage	SH
Temperature gradient	TG
Uniform temperature	TU
Water load and stream pressure	WA
Wind on live load	WL
Wind load on structure	WS

Source: AASHTO, *AASHTO LRFD Bridge Design Specifications*. Customary U.S. Units, 2012, American Association of State Highway and Transportation Officials, Washington, DC, With permission.

The vehicular live load HL93 consisting of either one or, for force effects at interior supports of continuous beams, two of the truck loads with three axles or the tandem load, combined with the uniform lane load will be discussed in Chapter 6.

The load factors for various loads, comprising a design load combination, are indicated in Tables 5.4, 5.5 and 5.6 for LRFD. All of the load combinations are related to the appropriate limit state. Any, or all, of the four limit states may be required in the design of any particular component and those that are the minimum necessary for consideration are indicated in the Specifications where appropriate. Thus, a design might involve any load combination in Table 5.4.

All relevant subsets of the load combinations in Table 5.4 should be investigated. The factors should be selected to produce the total factored extreme force effect. For each load combination, both positive and negative extremes should be investigated. In load combinations where one force effect decreases the effect of another, the minimum value should be applied to load reducing the force effect. For each load combination, every load that is indicated, including all significant effects because of distortion, should be multiplied by the appropriate load factor.

It can be seen in Table 5.4 that some of the load combinations have a choice of two load factors. The larger of the two values for load factors shown for TU, TG, CR, SH, and SE are to be used when calculating deformations; the smaller value shall be used when calculating all other force effects. Where movements are calculated for the sizing of expansion dams, the design of bearing, or similar situations where consideration of unexpectedly large movements is advisable, the larger factor should be used. When considering the effect of these loads on forces that are compatibility generated, the lower factor may be used. This latter use requires structural insight.

Consideration of the variability of loads in nature indicates that loads may be either larger or smaller than the nominal load used in the design specifications. The LRFD Specifications recognizes the variability of permanent loads by providing both maximum and minimum load factors for the permanent loads, as indicated in Table 5.5. For permanent force effects, the load factor that produces the more critical combination shall be selected from Table 5.5. In the application of permanent loads, force effects for each of the specified load types should be computed separately. Assuming variation of one type of load by span, length, or component within a bridge is not necessary. For each force effect, both extreme combinations may need to be investigated by applying either the high or the low load factor as appropriate. The algebraic sums of these products are the total force effects for which the bridge and its components should be designed. This reinforces the traditional method of selecting load combinations to obtain realistic extreme effects.

When the permanent load increases the stability or load-carrying capacity of a component or bridge, the minimum value of the load factor for that permanent load shall also be investigated. Uplift, which is treated as a separate load case in past editions of the AASHTO Standard Specifications for Highway Bridges, becomes a Strength I load combination. For example, when the dead load reaction is positive and live load can cause a negative reaction, the load combination for maximum uplift force would be 0.9 DC + 0.65 DW + 1.75 (LL+IM). If both reactions were negative, the load combination would be 1.25 DC + 1.50 DW + 1.75 (LL+IM).

The load combinations for various limit states shown in Table 5.4 are described below.

Strength I: Basic load combination relating to the normal vehicular use of the bridge without wind

Strength II: Load combination relating to the use of the bridge by permit vehicles without wind. If a permit vehicle is traveling unescorted, or if control is not provided by the escorts, the other lanes may be assumed to be occupied by the vehicular live load herein specified. For bridges longer than the permit vehicle, addition of the lane load, preceding, and following the permit load in its lane, should be considered.

Strength III: Load combination relating to the bridge exposed to maximum wind velocity that prevents the presence of significant live load on the bridge.

Strength IV: Load combination relating to very high dead load to live load force effect ratios. This calibration process had been carried out for a large number of bridges with spans not exceeding 200 ft

TABLE 5.4 Load Combinations and Load Factors in AASHTO LRFD

	DC	LL								Use One of These at a Time			
	DD	IM											
	DW	CE											
	EH	BR											
	EV	PL											
	ES	LS											
	EL												
	PS												
	CR												
Load Combination Limit State	SH		WA	WS	WL	FR	TU	TG	SE	EQ	IC	CT	CV
Strength I (unless noted)	γ_p	1.75	1.00	—	—	1.00	0.50/1.20	γ_{TG}	γ_{SE}	—	—	—	—
Strength II	γ_p	1.35	1.00	—	—	1.00	0.50/1.20	γ_{TG}	γ_{SE}	—	—	—	—
Strength III	γ_p	—	1.00	1.40	—	1.00	0.50/1.20	γ_{TG}	γ_{SE}	—	—	—	—
Strength IV	γ_p	—	1.00	—	—	1.00	0.50/1.20	—	—	—	—	—	—
Strength V	γ_p	1.35	1.00	0.40	1.0	1.00	0.50/1.20	γ_{TG}	γ_{SE}	—	—	—	—
Extreme event I	γ_p	γ_{EQ}	1.00	—	—	1.00	—	—	—	1.00	—	—	—
Extreme event II	γ_p	0.50	1.00	—	—	1.00	—	—	—	—	1.00	1.00	1.00
Service I	1.00	1.00	1.00	0.30	1.0	1.00	1.00/1.20	γ_{TG}	γ_{SE}	—	—	—	—
Service II	1.00	1.30	1.00	—	—	1.00	1.00/1.20	—	—	—	—	—	—
Service III	1.00	0.80	1.00	—	—	1.00	1.00/1.20	γ_{TG}	γ_{SE}	—	—	—	—
Service IV	1.00	—	1.00	0.70	—	1.00	1.00/1.20	—	1.0	—	—	—	—
Fatigue I—*LL*, *IM*, and *CE* only	—	1.50	—	—	—	—	—	—	—	—	—	—	—
Fatigue I II— *LL*, *IM*, and *CE* only	—	0.75	—	—	—	—	—	—	—	—	—	—	—

Source: AASHTO, *AASHTO LRFD Bridge Design Specifications*. Customary U.S. Units, 2012, American Association of State Highway and Transportation Officials, Washington, DC, With permission.

TABLE 5.5 Load Factors for Permanent Loads, γ_p, in AASHTO LRFD

Type of Load, Foundation Type, and Method Used to Calculate Downdrag		Load Factor	
		Maximum	Minimum
DC: Component and attachments		1.25	0.90
DC: Strength IV only		1.50	0.90
DD: Downdrag	Piles, α Tomlinson method	1.4	0.25
	Piles, λ method	1.05	0.30
	Drilled shafts, O'Neill and Reese (1999) method	1.25	0.35
DW: Wearing surfaces and utilities		1.50	0.65
EH: Horizontal earth pressure			
Active		1.50	0.90
At-rest		1.35	0.90
AEP for anchored walls		1.35	N/A
EL: Locked-in construction stresses		1.00	1.00
EV: Vertical earth pressure			
Overall stability		1.00	N/A
Retaining walls and abutments		1.35	1.00
Rigid buried structure		1.30	0.90
Rigid frames		1.35	0.90
Flexible buried structures			
Metal box culverts and structural plate culverts with deep corrugations		1.5	0.9
Thermoplastic culverts		1.3	0.9
All others		1.95	0.9
ES: Earth surcharge		1.50	0.75

Source: AASHTO, *AASHTO LRFD Bridge Design Specifications*. Customary U.S. Units, 2012, American Association of State Highway and Transportation Officials, Washington, DC, With permission.

TABLE 5.6 Load Factors for Permanent Loads Due to Superimposed Deformations, γ_p, in AASHTO LRFD

Bridge Component	PS	CR, SH
Superstructures—Segmental	1.0	See γ_p for DC, Table 3.4.1–3.4.2
Concrete substructures supporting segmental Superstructures (see 3.12.4, 3.12.5)		
Concrete superstructures—nonsegmental	1.0	1.0
Substructures supporting nonsegmental superstructures		
using I_g	0.5	0.5
using $I_{effective}$	1.0	1.0

(60 m). Spot checks had also been made on a few bridges up to 590 ft (180 m) spans. For the primary components of large bridges, the ratio of dead and live load force effects is rather high, and could result in a set of resistance factors different from those found acceptable for small and medium-span bridges. It is believed to be more practical to investigate one more load case, rather than requiring the use of two sets of resistance factors with the load factors provided in Strength I, depending on other permanent loads present. This Load Combination IV is expected to govern when the dead load to live load force effect ratio exceeds approximately 7.0.

Strength V: Load combination relating to normal vehicular use of the bridge with wind of 55 mph (90 kmph) velocity.

Extreme Event I: Load combination relating to earthquake. The designer supplied live load factor signifies a low probability of the presence of maximum vehicular live load at the time when the earthquake occurs. In ASD and LFD the live load was ignored when designing for earthquake.

Extreme Event II: Load combination relating to reduced live load in combination with a major ice event, or a vessel collision, or a vehicular impact.

Service I : Load combination relating to the normal operational use of the bridge with 55 mph (90 kmph) wind. All loads are taken at their nominal values and extreme load conditions are excluded. This combination is also used for checking deflection of certain buried structures, the investigation of slope stability, and investigation of transverse bending stresses in segmental concrete girders.

Service II: Load combination whose objective is to prevent yielding of steel structures because of vehicular live load, approximately halfway between that used for Service I and Strength I limit state, for which case the effect of wind is of no significance. This load combination corresponds to the overload provision for steel structures in past editions of the AASHTO Standard Specifications for the Design of Highway Bridges.

Service III: Load combination relating only to prestressed concrete structures with the primary objective of crack control. The addition of this load combination followed a series of trial designs done by 14 states and several industry groups during 1991 and early 1992. Trial designs for prestressed concrete elements indicated significantly more prestressing would be needed to support the loads specified in the proposed specifications. There is no nationwide physical evidence that these vehicles used to develop the notional live loads have caused detrimental cracking in existing prestressed concrete components. The statistical significance of the 0.80 factor on live load is that the event is expected to occur about once a year for bridges with two design lanes, less often for bridges with more than two design lanes, and about once a day for the bridges with a single design lane.

Service IV: Load combination used to investigate tension in prestressed concrete columns to control cracking.

Fatigue I: Infinite life fatigue and fracture load combination relating to gravitational vehicular live load and dynamic response.

Fatigue II: Finite life fatigue load case for which the load factor reflects a load level that has been found to be representative of the truck population.

5.4.2 Serviceability

The LRFD Specification treats serviceability from the view points of durability, inspectibility, maintainability, rideability, deformation control, and future widening.

Contract documents should call for high quality materials and require that those materials that are subject to deterioration from moisture content and/or salt attack be protected. Inspectibility is to be assured through adequate means for permitting inspectors to view all parts of the structure that have structural or maintenance significance. The provisions related to inspectibility are relatively short, but as all departments of transportation have begun to realize, bridge inspection can be very expensive and is a recurring cost because of the need for biennial inspections. Therefore, the cost of providing walkways and other access means and adequate room for people and inspection equipment to be moved about on the structure is usually a good investment.

Maintainability is treated in the specification in a similar manner to durability; there is a list of desirable attributes to be considered.

The subject of live load deflections and other deformations remains a very difficult issue. However, there is very little direct correlation between live load deflection and premature deterioration of bridges. There is much speculation that "excessive" live load deflection contributes to premature deck deterioration, but, to-date (late 2012), no causative relationship has been statistically established.

Rider comfort is often advanced as a basis for deflection control. Studies in human response to motion have shown that it is not the magnitude of the motion, but rather the acceleration that most

people perceive, especially in moving vehicles. Many people have experienced the sensation of being on a bridge and feeling a definite movement, especially when traffic is stopped. This movement is often related to the movement of floor systems, which are really quite small in magnitude, but noticeable nonetheless. There being no direct correlation between magnitude (not acceleration) of movement and discomfort has not prevented the design profession from finding comfort in controlling the gross stiffness of bridges through a deflection limit. As a compromise between the need for establishing comfort levels and the lack of compelling evidence that deflection was cause of structural distress, the deflection criteria, other than those pertaining to relative deflections of ribs of orthotropic decks and components of some wood decks, were written as voluntary provisions to be activated by those states that so chose. Deflection limits, stated as span divided by some number, were established for most cases, and additional provisions of absolute relative displacement between planks and panels of wooden decks and ribs of orthotropic decks were also added. Similarly, optional criteria were established for a span-to-depth ratio for guidance primarily in starting preliminary designs, but also as a mechanism for checking when a given design deviated significantly from past successful practice.

5.4.3 Constructability

Several new provisions were included in the LRFD Specification related to the following:

- The need to design bridges so that they can be fabricated and built without undue difficulty and with control over locked-in construction force effects
- The need to document one feasible method of construction in the contract documents, unless the type of construction is self-evident
- A clear indication of the need to provide strengthening and/or temporary bracing or support during erection, but not requiring the complete design thereof

References

AASHTO. 2002. *Standard Specifications for Highway Bridges.* 17th Edition. American Association of State Highway and Transportation Officials, Washington, DC.

AASHTO. 2012. *AASHTO LRFD Bridge Design Specifications.* Customary U.S. Units, 2012, American Association of State Highway and Transportation Officials, Washington, DC.

AASHTO. 2010. *Guide Specifications and Commentary for Vessel Collision Design of Highway Bridges.* 2nd Edition with 2010 Interim. American Association of State Highway and Transportation Officials, Washington, DC.

CAS. 2006. *Canadian Highway Bridge Design Code,* with supplements. Canadian Standards Association. Rexdale, Ontario, Canada.

Ghosn, M., and Moses, F. 2001. Redundancy in Highway Bridge Superstructures. *NCHRP Report 458*. Transportation Research Board, National Research Council, Washington, DC.

Kulicki, J. M., Mertz, D. R., and Wassef, W. G. 1994. *LRFD Design of Highway Bridges*. NHI Course 13061. Federal Highway Administration, Washington, DC.

Nowak, A. S. 1993. *Calibration of LRFD Bridge Design Code.* Department of Civil and Environmental Engineering Report UMCE 92-25. University of Michigan, Ann Arbor, MI.

Nowak, A. S., and Lind, N. C. 1979. Practical Bridge Code Calibration, ASCE. *Journal of the Structural Division.* 105(ST12), 2497–2510.

OMTC. 1994. *Ontario Highway Bridge Design Code.* Ontario Ministry of Transportation and Communications, Toronto, Ontario, Canada.

Vincent, G. S. 1969. *LFD of Steel Highway Bridges. AISI Bulletin 15*. American Iron and Steel Institute, Washington, DC.

6

Highway Bridge Loads and Load Distribution

Susan E. Hida
California Department of Transportation

6.1 Introduction

Highway bridge loads and load distribution as specified in the AASHTO LRFD (Load and Resistance Factor Design) Bridge Design Specifications (AASHTO, 2012) are discussed in this chapter. Stream flow, ice loads, vessel collision loads, loads for barrier design, loads for anchored and mechanically stabilized walls, seismic forces, and loads due to soil-structure interaction will be addressed in proceeding chapters. Load combinations are discussed in Chapter 5.

When proceeding from one component to another in bridge design, the controlling load and the controlling factored load combination will change. For example, permit vehicles, factored and combined for one load group, may control girder design for bending in one location. The standard design vehicular live load, factored and combined for a different load group, may control girder design for shear in another location. Still other loads, such as those due to seismic events, may control column and footing design.

Note that in this chapter, superstructure refers to the deck, beams or truss elements, and any other appurtenances above the bridge soffit. Substructure refers to those components that support loads from the superstructure and transfer load to the ground, such as bent caps, columns, pier walls, footings, piles, pile extensions, and caissons. Longitudinal refers to the axis parallel to the direction of traffic. Transverse implies the axis perpendicular to the longitudinal axis.

6.2 Permanent Loads

The LRFD Specifications refer to the weights of the following as "permanent loads":

- The structure
- Formwork that becomes part of the structure

- Utility ducts or casings and contents
- Signs
- Concrete barriers
- Wearing surface and/or potential deck overlay(s)
- Other elements deemed permanent loads by the design engineer and owner
- Earth pressure, earth surcharge, and downdrag

The permanent load is distributed to the girders by assigning to each all loads from superstructure elements within half the distance to the adjacent girder. This includes the dead load of the girder itself and in the case of box girder structures, the soffit. Added dead loads including traffic barriers, sidewalks and curbs, and soundwalls, may be equally distributed to all girders. Wide structures may warrant a more exact approach.

6.3 Vehicular Live Loads

6.3.1 Design Vehicular Live Load

The AASHTO "design vehicular live load," HL93, is a combination of a "design truck" or "design tandem," and a "design lane." Both the design truck and design lane are from AASHTO Standard Specifications, but combined. A shorter, but heavier, design tandem is combined with the design lane and the force effects used if a worse condition is created than with the design truck. Superstructures with very short spans, especially those less than 20 ft (12 m) in length, are often controlled by the tandem combination.

The design vehicular live load was replaced in 1993 because of heavier gross vehicle weights and axle loads compared to the design live load in previous Specifications (AASHTO, 2002), and because a statistically representative, notional load was needed to achieve a "consistent level of safety." The notional load that was found to best represent "exclusion vehicles" that is trucks with loading configurations greater than allowed, but, routinely granted permits by agency bridge rating personnel, was the HL93. It is notional in that it does not represent any specific vehicle (FHWA, 1993). The mean and standard deviation of truck traffic was determined and used in the calibration of the load factors for HL93.

The AASHTO "design truck" is shown in Figure 6.1. The variable axle spacing between the 32 k (145 kN) loads is adjusted to create a critical condition for the design of each location in the structure. In the transverse direction, the design truck is 10 ft (3 m) wide and may be placed anywhere in the standard 12 ft (3.6 m) wide lane. The wheel load, however, may not be positioned any closer than 4 ft (0.6 m) from the lane line, or 2 ft (0.3 m) from the face of curb, barrier, or railing. The AASHTO "design tandem" is similar to the design truck in the transverse direction, but consists of two 25 k (110 kN) axles spaced at 4 ft (1.2 m) on center.

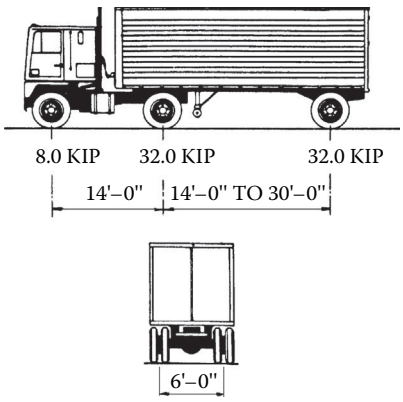

FIGURE 6.1 AASHTO-LRFD design truck.

The AASHTO "design lane" loading is equal to 0.64 k/ft (9.3 N/mm) and emulates a caravan of trucks. Similar to the truck loading, the lane load is spread over a 10 ft (3 m) wide area in the standard 12 ft (3.6 m) lane. The lane loading is not interrupted except when creating an extreme force effect such as in "patch" loading of alternate spans.

When checking an extreme reaction at an interior pier or negative moment between points of contraflexure in the superstructure, two design trucks with a 14 ft (4.3 m) spacing between the 145 kN axles are to be placed on the bridge with a minimum of 50 ft (15 m) between the rear axle of the first truck and the lead axle of the second truck. Only 90% of the truck and lane load is used.

6.3.2 Permit Vehicles

Some states in the USA have developed their own "Permit Design Vehicle" to account for vehicles routinely granted permission to travel a given route, and to accommodate larger permit truck requests. California (Caltrans, 2013) uses a 15-axle design vehicle with a variable axle spacing in the center of 54 k axle loads (shown in Figure 6.2). The truck was created to envelop recent heavier axle loads particularly on short trucks, double-wide permits, and long-span wheel configurations.

The permit vehicular live load is combined with other loads in the Strength Limit State II as discussed in Chapter 5. The commentary to the LRFD Specifications suggests that the design permit vehicle is to be both side-by-side another vehicle, and preceded and proceeded by a lane load—unless escorted to prohibit other truck traffic on the bridge simultaneously.

6.3.3 Fatigue Loads

For fatigue loading, the LRFD Specifications use the design truck alone with a constant axle spacing of 30 ft (9 m). The load factors vary for finite and infinite fatigue life as discussed in Chapter 5. The load is placed to produce extreme force effects. In lieu of more exact information, the frequency of the fatigue load for a single lane may be determined by multiplying the average daily truck traffic by "*p*" where "*p*" is 1.00 in the case of one lane available to trucks, 0.85 in the case of two lanes available to trucks, and 0.80 in the case of three or more lanes available to trucks. If the average daily truck traffic is not known, 20% of the average daily traffic may be used on rural interstate bridges, 15% for other rural and urban interstate bridges, and 10% for bridges in urban areas.

California has created an additional fatigue truck and fatigue load combo to account for frequent permit vehicles. The design vehicle is shown in Figure 6.3 and is factored by 1.0.

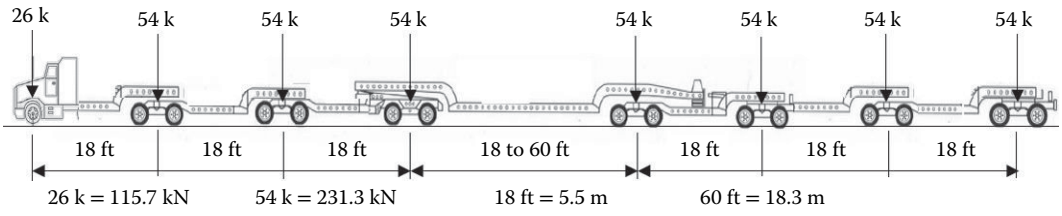

FIGURE 6.2 Caltrans permit truck—Strength II.

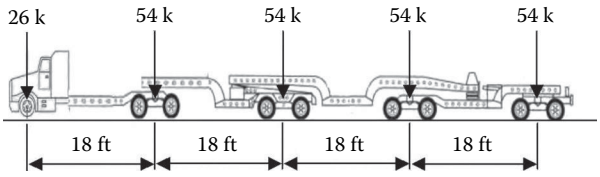

FIGURE 6.3 Caltrans permit truck—Fatigue II.

6.3.4 Load Distribution for Superstructure Design

Superstructures are generally analyzed first in the longitudinal direction, and then in the transverse direction. Live load distribution in the longitudinal direction is simply a matter of structural analysis and is best understood with the aid of influence lines. Note that, by definition of the vehicular design live load, no more than one truck can be in one lane simultaneously, except as previously described to generate maximum reactions or negative moments. Figure 6.4 summarizes live load distribution for design of a longitudinal superstructure element—an interior gired. The "lever rule" is sometimes called for and implies consideration of the slab between two girders as simply supported. The reaction is determined by summing the reactions from the slabs on either side of the beam under consideration. Additional

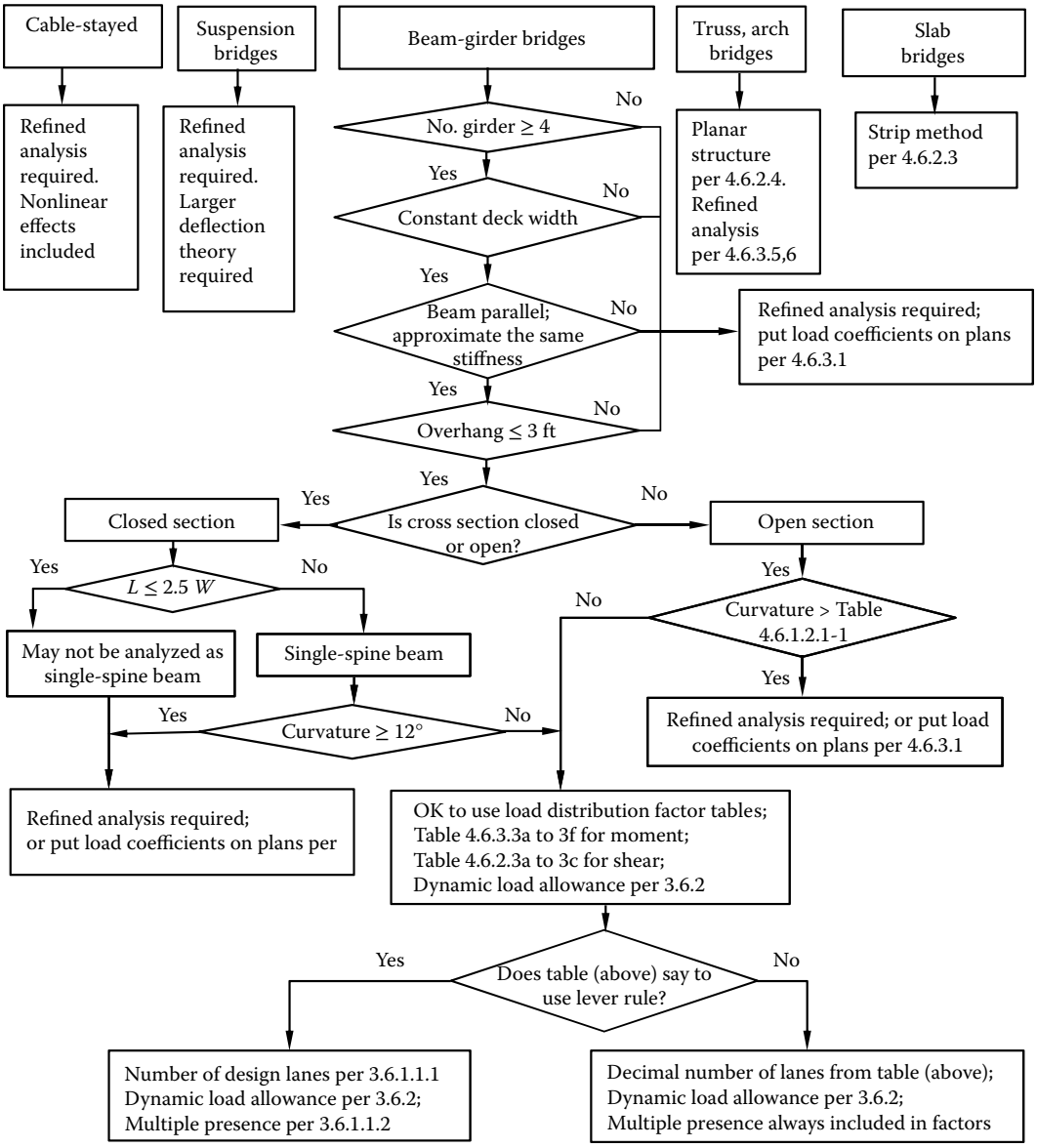

FIGURE 6.4 Live load distribution for an interior girder design.

expressions are provided to account for skew as shown in Tables 6.1 and 6.2. Those for bending can result in values less than one, a reduction that is not taken by some owners.

"Refined analysis" refers to a three-dimensional (3D) consideration of the loads and is to be used on more complex structures. Choices include: classical force and displacement, finite difference, finite element, folded plate, finite strip, grillage analogy, series/harmonic, or yield line methods.

6.3.4.1 Beam-Slab Bridges

Approximate methods for live load distribution on beam-slab bridges are appropriate for the types of cross-sections shown in Table 4.6.2.2.1-1 of the AASHTO LRFD Specifications. Load distribution factors are generated from expressions found in AASHTO LRFD Tables 4.6.2.2.2a-f and Tables 4.6.2.2.3a-c, and result in a decimal number of lanes for girder design. These expressions are based on a study by Zokaie et al. (1991) and a function of: beam area, beam width, beam depth, overhang width, polar moment of inertia, St. Venant's torsional constant, stiffness, beam span, number of beams, number of cells, beam spacing, depth of deck, and deck width. Limitations on girder spacing, span length, and span depth reflect the limitations of the data set used in development. Note that load distribution factors are not used in 3D analysis. Skew factors also are not used because the skewed supports in a 3D model cause the resultant force effects to capture the skew effects.

6.3.4.2 Decks

Decks may be designed for vehicular live loads using empirical methods, or, by distributing loads on to "effective strip widths," and analyzing the strips as continuous or simply-supported beams. Empirical methods rely on transfer of forces by arching of the concrete and shifting of the neutral axis. The AASHTO Specifications require design for a 16 k point load.

6.3.4.3 Slab-Type Bridges

Cast-in-place concrete slabs or voided slabs, stressed wood decks, and glued/spiked wood panels with spreader beams are designed for an equivalent width of longitudinal strip per lane for both shear and moment. That width, E, is determined from the formula (see Equations 6.1 and 6.2):

TABLE 6.1 Reduction of Load Distribution Factors for Moment in Longitudinal Beams on Skewed Supports

Type of Superstructure	Applicable Cross-Section from Table 4.6.2.2.1-1	Any Number of Design Lanes Loaded	Range of Applicability
Concrete deck, filled grid, or partially filled or unfilled grid deck composite with reinforced concrete slab on steel or concrete beams	a,e, k and also i, j if sufficiently connected to act as a unit	$1 - c_1(\tan\theta)^{1.5}$ $c_1 = 0.25\left(\frac{K_g}{12.0Lt_s^3}\right)^{0.25}\left(\frac{S}{L}\right)^{0.50}$	$30° \le \theta \le 60°$ 3.5 ft $\le S \le$16 ft
Concrete beams, concrete T-beams, T- and double T-sections		if $\theta < 30°$ then $c_1 = 0$ if $\theta > 60°$ use $\theta = 60°$	20 ft $\le L \le$ 240 ft $N_b \ge 4$
Concrete deck on concrete spread box beams, multi-cell concrete box girders, concrete box beams, and double T-sections used in multi-beam decks	b,c,d,f,g	$1.05 - 0.25 \tan\theta \le 1.0$ if $\theta > 60°$ use $\theta = 60°$	$0 \le \theta \le 60°$

TABLE 6.2 Correction Factors for Load Distribution Factors for Support Shear of the Obtuse Corner

Type of Superstructure	Applicable Cross-Section from Table 4.6.2.2.1-1	Correction Factor	Range of Applicability
Concrete deck, filled grid, or partially filled or unfilled grid deck composite with reinforced concrete slab on steel or concrete beams; Concrete beams, concrete T-beams, T- and double T-sections	a,e, k and also i, j if sufficiently connected to act as a unit	$1.0+0.20\left(\frac{12.0Lt_s^3}{K_g}\right)^{0.3}\tan\theta$	$0° \le \theta \le 60°$ 3.5 ft $\le S \le$16.0 ft 2.0 ft $\le L \le$ 240 ft $N_b \ge 4$
Cast-in-place concrete multi-cell box	D	$1.0+\left[0.25+\frac{12.0L}{70d}\right]\tan\theta$	$0° \le \theta \le 60°$ 6.0 ft $\le S \le$ 13.0 ft 20 ft $< L <$ 140 ft 35 ft $< d <$ 110 ft $N_b \ge 3$
Concrete deck on spread concrete box beams	b, c	$1.0+\frac{\sqrt{\frac{Ld}{12}}}{6S}\tan\theta$	$0° \le \theta \le 60°$ 6.0 ft $< S <$ 11.5 ft 20 ft $< L <$ 140 ft 18 ft $< d <$ 65 ft $N_b \ge 3$
Concrete box beams used in multibeam decks	f, g	$1.0+\frac{12.0L\sqrt{\tan\theta}}{90d}$	$0° \le \theta \le 60°$ 20 ft $< L <$ 120 ft 17 $< d <$ 60 ft 35 ft $< b <$ 60 ft $5 \le N_b \le 20$

$$E = 10.0 + 5.0\sqrt{L_1 W_1} \quad \text{(ft)}$$

$$E = 250 + 0.42\sqrt{L_1 W_1} \quad \text{(mm)} \tag{6.1}$$

when one lane is loaded, and

$$E = 84.0 + 1.44\sqrt{L_1 W_1} \le 12.0W/N_L \quad \text{(ft)}$$

$$E = 2100 + 0.12\sqrt{L_1 W_1} \le W / N_L \quad \text{(mm)} \tag{6.2}$$

when more than one lane is loaded. L_1 is the lesser of the actual span or 60 ft (18,000 mm), W_1 is the lesser of the edge-to-edge width of bridge and 30 ft (9,000 mm) in the case of single-lane loading, and 60 ft (18,000 mm) in the case of multi-lane loading.

6.3.5 Load Distribution for Substructure Design

Bridge substructure includes bent caps, columns, pier walls, pile caps, spread footings, caissons, and piles. These components are designed by placing one or more design vehicular live loads on the traveled way as previously described for maximum reaction and negative bending moment, not exceeding the maximum number of vehicular lanes permitted on the bridge. This maximum may be determined by dividing the width of the traveled way by the standard lane width 12.0 ft (3.6 m), and "rounding down" that is disregarding any fractional lanes. Note that the traveled way need not be measured from the edge-of-deck if curbs or traffic barriers will restrict the traveled way for the life of the structure, and the

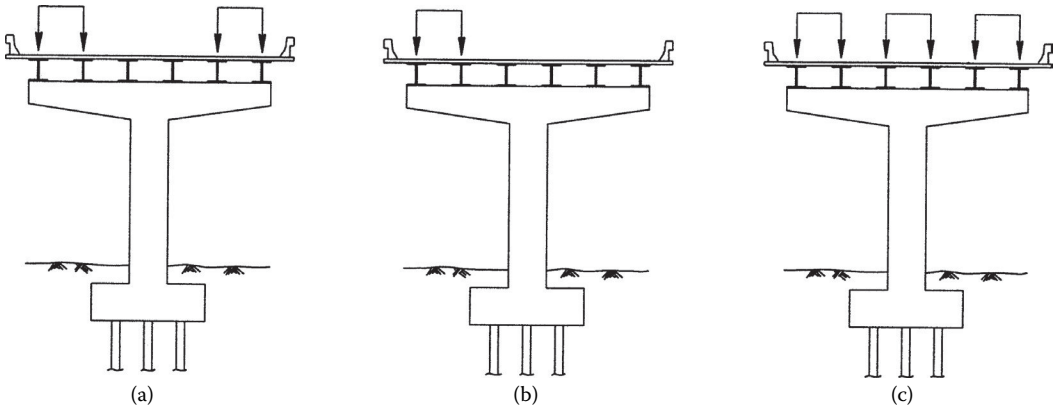

FIGURE 6.5 Various load configurations for substructure design.

fractional number of lanes determined using load distribution charts for girder design are not used for substructure design.

Figure 6.5 shows selected load configurations for substructure elements. A critical load configuration may result from not using the maximum number of lanes permissible. For example, Figure 6.5a shows a load configuration that may generate the critical loads for bent cap design and Figure 6.5b shows a load configuration that may generate the critical bending moment for column design. Figure 6.5c shows a load configuration that may generate the critical compressive load for design of the piles. Other load configurations will be needed to complete design of a bridge footing. Note that girder locations are often ignored in determination of substructure design moments and shears: loads are assumed to be transferred directly to the structural support, disregarding load transfer through girders in the case of beam-slab bridges. Adjustments are made to account for the likelihood of fully loaded vehicles occurring side-by-side simultaneously. This "multiple presence factor" is discussed in the next section.

In the case of rigid frame structures, bending moments in the longitudinal direction will also be needed to complete column (or pierwall) as well as foundation designs. Skew effects in both the transverse and longitudinal directions must also be included.

Load configurations that generate these three cases must be checked:

1. Maximum/minimum axial load with associated transverse and longitudinal moments
2. Maximum/minimum transverse moment with associated axial load and longitudinal moment
3. Maximum/minimum longitudinal moment with associated axial load and transverse moment

If a permit vehicle is also being designed for, then these three cases must also be checked for the load combination associated with Strength Limit State II (discussed in Chapter 5).

6.3.6 Multiple Presence of Live Load Lanes

Multiple presence factors modify the vehicular live loads for the probability that vehicular live loads occur together in a fully loaded state. The factors are shown in Table 6.3.

These factors should be applied prior to analysis or design only when using the lever rule or doing three-dimensional analysis. Sidewalks should be treated as a fully loaded lane. If a two-dimensional girder line analysis is being done and distribution factors are being used for a beam-and-slab type of bridge, multiple presence factors are not used because the load distribution factors already consider three-dimensional effects. For the fatigue limit state, the multiple presence factors are also not used.

TABLE 6.3 Multiple Presence Factors

Number of Loaded Lanes	Multiple Presence Factors
1	1.20
2	1.00
3	0.85
>3	0.65

6.3.7 Dynamic Load Allowance

Vehicular live loads are assigned a "dynamic load allowance" load factor of 1.75 at deck joints, 1.15 for all other components in the fatigue and fracture limit state, and 1.33 for all other components and limit states. This factor accounts for hammering effects when riding surface discontinuities exist, and long undulations when settlement or resonant excitation occurs. If a component such as a footing is completely below grade, or, a component such as a retaining wall is not subject to vertical reactions from the superstructure, this increase is not taken. Wood bridges or any wood component is factored half as much as the above values, that is, 1.375 for deck joints, 1.075 for fatigue, and 1.165 typical. Buried structures such as culverts are subject to the dynamic load allowance but are a function of depth of cover (see Equation 6.3):

$$IM = 33(1.0 - 0.125D_E) \geq 0\% \quad (D_E \text{ in ft})$$

$$IM = 40(1.0 - 4.1\times10^{-4}D_E) \geq 0\% \quad (D_E \text{ in mm}) \tag{6.3}$$

6.3.8 Horizontal Loads Because of Vehicular Traffic

Substructure design of vertical elements requires that horizontal effects of vehicular live loads be designed for. Centrifugal forces and braking effects are applied horizontally at a distance 6 ft (1.80 m) above the roadway surface. The centrifugal force is determined by multiplying the design truck or design tandem—alone—by the following factor (see Equation 6.4):

$$C = f\frac{v^2}{gR} \tag{6.4}$$

Highway design speed, v, is in ft/s (m/s); gravitational acceleration, g, is 32.2 ft/s^2 (9.807 m/s^2); radius of curvature in traffic lane, R, is in ft (m); and f is 4/3 for load combinations other than fatigue and 1.0 for fatigue. Likewise, the braking force is determined by multiplying the design truck or design tandem from all lanes likely to be unidirectional in the future by 0.25. In this case, the lane load is not used because braking effects would be damped out on a fully loaded lane.

6.4 Pedestrian Loads

Live loads are also created by pedestrians and bicycles. The LRFD Specifications call for a 0.075 k/ft (73.6×10^{-3} MPa) load simultaneous with highway loads on sidewalks wider than 2 ft (0.6 m). "Pedestrian- or bicycle-only" bridges are to be designed for 0.090 k/ft (4.1×10^{-3} MPa). If the pedestrian- or bicycle-only bridge is required to carry maintenance or emergency vehicles, these vehicles are designed for, omitting the dynamic load allowance. Potential resonance of the structure with pedestrian foot fall also needs to be checked as directed in the AASHTO LRFD Guide Specification for Design of Pedestrian Bridges (AASHTO, 2009).

6.5 Wind Loads

The LRFD Specifications provide wind loads as a function of base design wind velocity, V_B equal to 100 mph (160 km/h); and base pressures, P_B, corresponding to wind speed V_B. Values for P_B are listed in Table 6.4. The design wind pressure, P_D, is then calculated as (see Equation 6.5):

$$P_D = P_B\left(\frac{V_{DZ}}{V_B}\right)^2 = P_B\frac{V_{DZ}^2}{10{,}000} \quad \left(\text{k/f}^2\right)$$

$$P_D = P_B\left(\frac{V_{DZ}}{V_B}\right)^2 = P_B\frac{V_{DZ}^2}{25{,}600} \quad (\text{MPa}) \tag{6.5}$$

where V_{DZ} is the design wind velocity at design elevation Z in mph (km/hr). V_{DZ} is a function of the friction velocity, V_0 mph (km/hr) multiplied by the ratio of the actual wind velocity to the base wind velocity both at 30 ft (10 m) above grade, and the natural logarithm of the ratio of height to a meteorological constant length for given surface conditions (see Equation 6.6):

$$V_{DZ} = 2.5V_0\left(\frac{V_{10}}{V_B}\right)\ln\left(\frac{Z}{Z_0}\right) \tag{6.6}$$

Values for *V*o and *Z*o are shown in Table 6.5.

The resultant design pressure is then applied to the surface area of the superstructure as seen in elevation. Solid-type traffic barriers and sound walls are considered as part of the loading surface. If the product of the resultant design pressure and applicable loading surface depth is less than a lineal load of 0.30 k/ft (4.4 N/mm) on the windward chord, or 0.15 k/ft (2.2 N/mm) on the leeward chord, minimum loads of 0.30 (4.4) and 0.15 (2.2) k/ft (N/mm), respectively, are designed for.

Wind loads are combined with other loads in Strength Limit States III and V, and Service Limit State I, as defined in Chapter 5. Wind forces because of the additional surface area from trucks is accounted for by applying a 0.10 k/ft (1.46 N/mm) load 6 ft (1800 mm) above the bridge deck.

Wind loads for substructure design are of two types: loads applied to the substructure, and those applied to the superstructure and transmitted to the substructure. Loads applied to the superstructure are as previously described. A base wind pressure of 40 psf (2×10^{-3} MPa) force is applied directly to the substructure, and is resolved into components (perpendicular to the front and end elevations) when the structure is skewed.

In absence of live loads, an upward load of 0.02 k/ft² (9.6×10^{-4} MPa) is multiplied by the width of the superstructure and applied at the windward quarterpoint simultaneously with the horizontal wind

TABLE 6.4 Base Wind Pressures, $\boldsymbol{P}_B$, corresponding to $\boldsymbol{V}_B = 100$ mpr (160 km/h)

Structural Component	Windward Load, k/ft² (MPa)	Leeward Load, k/ft² (MPa)
Trusses, columns, and arches	0.050 (0.0024)	0.025 (0.0012)
Beams	0.050 (0.0024)	NA
Large flat surfaces	0.040 (0.0019)	NA

TABLE 6.5 Values of $\boldsymbol{V}_o$ and $\boldsymbol{Z}_o$ for Various Upstream Surface Conditions

Condition	Open Country	Suburban	City
V_o mph (km/h)	8.20 (13.2)	10.90 (15.2)	12.0 (19.4)
Z_o ft (mm)	0.23 (70)	3.28 (300)	8.20 (800)

loads applied perpendicular to the length of the bridge. This uplift load may create a worst condition for substructure design when seismic loads are not of concern.

For bridges in locations vulnerable to coastal storms, hurricane forces, or storm surge, the reader is referred to the AASHTO Guide Specifications for Bridges Vulnerable to Coastal Storms (AASHTO, 2008).

6.6 Effects due to Superimposed Deformations

Elements of a structure may change dimension and or position because of settlement, shrinkage, creep, or temperature. Changes in geometry cause additional stresses that are of particular concern at bearings, connections, and in rigid-framed structures. Segmentally constructed structures require use of time-dependent software to precisely calculate time-dependant properties and resultant deformations in order to minimize construction-induced stresses. Determining effects from foundation settlement are a matter of structural analysis. Temperature effects are dependent on the maximum potential temperature differential from the temperature at time of erection. Upper and lower bounds are shown in Table 6.6, where "moderate" and "cold" climates are defined as having fewer, or, more than 14 days with an average temperature below 32°F (0°C), respectively.

Using appropriate coefficients of thermal expansion, effects from temperature changes are calculated using basic structural analysis. More refined analysis will consider the time lag between the surface and internal structure temperatures. The LRFD Specification identifies four zones in the United States and provides a linear relationship for the temperature gradient in steel and concrete (see Table 6.7 and Figures 6.6 and 6.7).

6.7 Exceptions to Code-Specified Design Loads

The designer is responsible not only for providing plans that accommodate design loads per the referenced design specifications, but also for any loads unique to the structure and bridge site. It is also the designer's responsibility to indicate all loading conditions designed for in the contract documents—preferably the construction plans. History seems to indicate that construction plans survive longer than construction specifications—and that the next generation of bridge engineers will indeed be given the task of "improving" today's new structure.

TABLE 6.6 Temperature Ranges

Climate	Steel or Aluminum	Concrete	Wood
Moderate	0 to 12°F (−18 to 50°C)	10 to 80°F (−12 to 27°C)	10 to 75°F (−12 to 24°C)
Cold	−30 to 12.0°F (−35 to 50°C)	0 to 80°F (−18 to 27°C)	0 to 75°F (−18 to 24°C)

TABLE 6.7 Basis of Temperature Gradients

	Concrete		50 mm Asphalt		100 mm Asphalt	
Zone	T_1 F (°C)	T_2 F (°C)	T_1 (°C)	T_2 (°C)	T_1 (°C)	T_2 (°C)
1	54 (30)	14 (7.8)	24	7.8	17	5
2	46 (25)	12 (6.7)	20	6.7	14	5.5
3	41 (23)	11 (6)	18	6	13	6
4	38 (21)	9 (5)	16	5	12	6

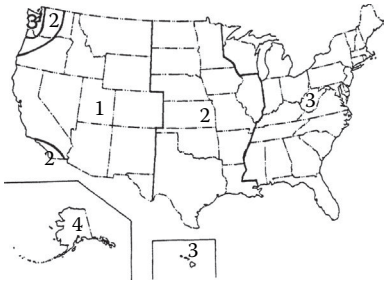

FIGURE 6.6 Solar radiation zones for the United States.

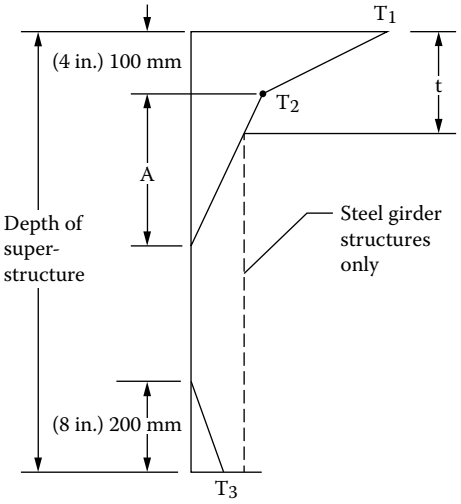

FIGURE 6.7 Positive vertical temperature gradient in concrete and steel superstructures.

References

AASHTO. 2002. *Standard Specifications for Highway Bridges*. 17th Edition. American Association of State Highway and Transportation Officials, Washington, DC.

AASHTO. 2008. *Guide Specifications for Bridges Vulnerable to Coastal Storms*. American Association of State Highway and Transportation Officials, Washington, DC.

AASHTO. 2009. *LRFD Guide Specifications for Design of Pedestrian Bridges*. 2nd Edition. American Association of State Highway and Transportation Officials, Washington, DC.

AASHTO. 2012. *AASHTO LRFD Bridge Design Specifications*. Customary US Units. American Association of State Highway and Transportation Officials, Washington, DC.

Caltrans. 2013. *California Amendments to the AASHTO LRFD Highway Bridge Design Specifications, Customary US Units, 2012*. 6th Edition. California Department of Transportation, Sacramento, CA.

FHWA. 1993. *LRFD Design of Highway Bridges, Training Course*. Vol. 1. Federal Highway Administration, Washington, DC.

Zokaie, T., Osterkamp, T. A., and Imbsen, R. A. 1991. *Distribution of Wheel Loads on Highway Bridges*, NCHRP Report 12-2611. Transportation Research Board, National Research Council, Washington, DC.

7

Railroad Bridge Design Specifications*

Donald F. Sorgenfrei
Modjeski and Masters, Inc.

Ward N. Marianos, Jr.
Consulting Engineer

Robert A.P. Sweeney
Consulting Engineer

7.1 Introduction

7.1.1 Railroad Network

The United States railroad network consists predominantly of privately owned freight railroad systems classified according to operating revenue, the government owned National Railroad Passenger Corporation (Amtrak), and numerous transit systems owned by local agencies and municipalities.

Since the deregulation of the railroad industry brought about by the Staggers Act, there have been numerous railway system mergers. The Federal Register (FRA, 2010) lists 693 Railroad entries, some of them subsidiaries of larger railroads. Based on the Association of American Railroads (AAR) data (AAR, 2010), there are 7 class 1 (major) railroads, 23 regional railroads, and 533 local railroads operating over approximately 140,000 miles of track. Amtrak operates approximately 23,000 miles of railroad. The 7 class 1 railroads comprise only 1.25% of the number of railroads in the United States but account for 67.5% of the trackage and 93.3% of the freight revenue. Most railroads in North America are standard gauge, 4 ft. 8.5 in.

By far the leading freight commodity is coal, which accounts for 26% of all the car loads. Other leading commodities in descending order by carloads are: chemicals and allied products, farm products, motor vehicles and equipment, food and sundry products, and nonmetallic minerals. Freight equipment has drastically changed over the years in container type, size and wheelbase, and carrying capacity. The most predominant freight car is the hopper car used with an open top for coal loading and the

* Much of the material in this chapter was developed for the American Railway Engineering and Maintenance of Way Association (AREMA) Manual for Railway Engineering and is used with permission.

covered hopper car used for chemicals and farm products. In recent years special cars have been developed for the transportation of trailers, box containers, and automobiles.

The average freight car capacity (total number of freight cars in service divided by the aggregate capacity of those cars) has risen approximately 10 tons each decade with the tonnage ironically matching the decades; that is, 1950s—50 tons, 1960s—60 tons up to the end of the 1990s. In the first decade of this century rail lines were capable of handling 111 tons to 125 tons net per car with gross weights of 286,000 and 315,000 lbs each car, often in dedicated units. Trains with trailing tonnage approaching 23,000 tons and up to 150 cars are beginning to occur.

In 1929 there were 56,936 steam locomotives in service. By the early 1960s they were totally replaced by diesel electric units. The number of diesel electric units has gradually decreased as available locomotive horsepower has increased. The earlier freight trains were commonly mixed freight of generally light railcars, powered by heavy steam locomotives. In recent years that has given way to heavy railcars, unit trains of common commodity (coal, grain, containers, etc.) with powerful locomotives. Newer heavy haul locomotives generally have 6 axles, generate 4,300–4,400 HP and weight 415,000–420,000 lbs with a few topping out at 435,000 lbs.

These changes in freight hauling have resulted in concerns for railroad bridges, many of which were not designed for these modern loadings. The heavy, steam locomotive with steam impact governed in design considerations. Present bridge designs are still based on the steam locomotive wheel configuration with diesel impact but fatigue cycles from the heavy carloads are of major importance.

The railroad industry records annual route tonnage referred to as "million gross tons" (MGT). An experienced railroader can fairly well predict conditions and maintenance needs for a route based on knowing the MGT for that route. It is common for class 1 railroads to have routes of 30–50 MGT with some coal routes in the range of 150 MGT.

Passenger trains are akin to earlier freight trains, with one or more locomotives (electric or diesel) followed by relatively light cars. Likewise, transit cars are relatively light.

7.1.2 Basic Differences between Railroad and Highway Bridges

A number of differences exist between railroad and highway bridges:

1. The ratio of live load to dead load is much higher for a railroad bridge than for a similarly sized highway structure. Generally serviceability issues such as fatigue and deflection control govern designs rather than strength. For this reason and because of the cost to switch to load factor design, design of North American bridges continues to be based on working stress criteria except for some parts dealing with concrete.
2. Robustness is essential to deal with the harsh railway environment.
3. The design impact load on railroad bridges is higher than on highway structures.
4. Simple span structures are typically preferred over continuous structures for railroad bridges. Many of the factors that make continuous spans attractive for highway structures are not as advantageous for railroad use. Continuous spans are also more difficult to replace in emergencies than simple spans.
5. Interruptions in service are typically much more critical for railroads than for highway agencies. Therefore, constructability and maintainability without interruption to traffic are crucial for railroad bridges.
6. Since the bridge supports the track structure, the combination of track and bridge movement cannot exceed the tolerances in track standards. Interaction between the track and bridge should be considered in design and detailing.
7. Seismic performance of highway and railroad bridges can vary significantly. Railroad bridges have performed well during seismic events.
8. Railroad bridge owners typically expect a longer service life from their structures than highway bridge owners expect from theirs.

7.1.3 Regulatory Environment

The Federal Railway Administration (FRA) in the United States has issued rules that affect the design, evaluation, inspection, and management of railway bridges. FRA states that the present standard references for railroad bridge design and analysis are found in the "Manual for Railway Engineering" of the American Railway Engineering and Maintenance-of-Way Association (AREMA, 2012).

7.1.4 Manual for Railway Engineering, AREMA

The base document for railroad bridge design, construction, and inspection is AREMA's Manual for Railway Engineering (AREMA, 2012). The recommended practice in this manual is revised annually and only the latest edition is valid.

Early railroads developed independent specifications governing the design loadings, allowable strains, quality of material, fabrication, and construction of their own bridges. There was a proliferation of specifications written by individual railroads, suppliers, and engineers. One of the earliest general specifications is titled *Specification for Iron Railway Bridges and Viaducts*, by Clarke, Reeves, and Company (Phoenix Bridge Company). By 1899 private railroads joined efforts in forming AREMA. Many portions of those original individual railroad specifications were incorporated into the first manual titled *Manual of Recommended Practice for Railway Engineering and Maintenance of Way* published in 1905. In 1911 the Association dropped "Maintenance of Way" from its name and became the American Railway Engineering Association (AREA); however, in 1997 the name reverted back to the original name with the consolidation of several railroad associations.

The Manual is not deemed a specification but rather a recommended practice. Certain provisions naturally are standards by necessity for the interchange of rail traffic, such as track gage, track geometrics, clearances, basic bridge loading, and locations for applying loadings. Individual railroads may, and often do, impose more stringent design requirements or provisions because of differing conditions peculiar to that railroad or region of the country, but basically all railroads subscribe to the provisions of the manual.

Although the Manual is a multi-volume document, bridge engineering provisions are grouped in the structural volume and subdivided into applicable chapters by primary bridge material and special topics, as listed:

Chapter 7 Timber Structures
Chapter 8 Concrete Structures and Foundations (includes waterproofing for all structures)
Chapter 9 Seismic Design for Railway Structures
Chapter 10 Structures, Maintenance and Construction
Chapter 15 Steel Structures (includes bridge bearing requirements for all structures)

The primary structural chapters each address bridge loading (dead load, live load, impact, wind, seismic, etc.) design, materials, fabrication, construction, maintenance/inspection, and capacity rating. There is uniformity among the chapters in the configuration of the basic live load, which is based on the Cooper E-series steam locomotive. The present live load configuration is two locomotives with tenders followed by a uniform live load, as shown in Figure 7.1. There is no uniformity in the chapters in the location and magnitude of many other loads because of differences in the types of bridges built with different materials

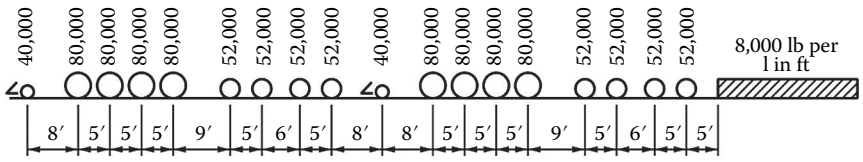

FIGURE 7.1 Cooper E80 live load.

and differences in material behavior. Also it is recognized that each chapter has been developed and maintained by separate committee groups of railroad industry engineers, private consulting engineers, and suppliers. These committees readily draw from railroad industry experiences, research, and from work published by other associations such as American Association of State Highway and Transportation Officials (AASHTO), American Institute of Steel Construction (AISC), American Concrete Institute (ACI), American Welding Society (AWS), American Public Works Association (APWA), and so on.

7.2 Railroad Bridge Philosophy

Railroad routes are well established and the construction of new railroad routes is not common; thus, the majority of railroad bridges built or rehabilitated are on existing routes and on existing right-of-way. Simply stated, the railroad industry first extends the life of existing bridges as long as economically justified. It is not uncommon for a railroad to evaluate an 80- or 90-year-old bridge, estimate its remaining life, and then rehabilitate it sufficiently to extend its life for some economical period of time.

Bridge replacement generally is determined as a result of a lack of load carrying capacity, restrictive clearance, or deteriorated physical condition. If bridge replacement is necessary, then simplicity, cost, future maintenance, and ease of construction without significant rail traffic disruptions typically governs the design. Types of bridges chosen are most often based on the capability of a railroad to do its own construction work. Low maintenance structures, such as ballasted deck prestressed concrete box girder spans with concrete caps and piles, are preferred by some railroads. Others may prefer weathering steel elements.

In review of the existing railroad industry bridge inventory, the majority of bridges by far are simple span structures over streams and roadways. Complex bridges are generally associated with crossing major waterways or other significant topographical features. Signature bridges are rarely constructed by railroads. The enormity of train live loads generally preclude the use of double leaf bascule bridges and suspension and cable-stay bridges because of bridge deflection and shear load transfer, respectively. Railroads, where possible, avoid designing skewed or curved bridges, which also have inherent deflection problems.

When planning the replacement of smaller bridges, railroads first determine if the bridge can be eliminated using culverts. A hydrographic review of the site will determine if the bridge opening needs to be either increased or can be decreased.

The manual provides complete details for common timber structures and for concrete box girder spans. Many of the larger railroads develop common standards, which provide complete detailed plans for the construction of bridges. These plans include piling, pile bents, abutments, and wing walls, spans (timber, concrete, and steel), and other elements in sufficient detail for construction by in-house forces or by contract. Only site-specific details such as permits, survey data, and soil conditions are needed to augment these plans.

Timber trestles are most often replaced by other materials rather than in-kind. However, it is often necessary to renew portions of timber structures to extend the life of a bridge for budgetary reasons. Replacing pile bents with framed bents to eliminate the need to drive piles or the adding of a timber stringer and recentering a chord to increase capacity is common. The replacement of timber trestles is commonly done by driving either concrete or steel piling through the existing trestle, at twice the present timber span length and offset from the existing bents. This is done between train movements. Either precast or cast-in-place caps are installed atop the piling beneath the existing timber deck. During a track outage period, the existing track and timber deck is removed and new spans (concrete box girders or rolled steel beams) are placed. In this type of bridge renewal, key factors are: use of prefabricated bridge elements light enough to be lifted by railroad track mounted equipment (piles, caps, and spans), speed of installation of bridge elements between train movements, bridge elements that can be installed in remote site locations without outside support, and overall simplicity in performing the work.

The railroad industry has a large number of 150–200 ft. span pin connected steel trusses, many with worn joints, restrictive clearances, and low carrying capacity, for which rehabilitation cannot be economically justified. Depending on site specifics, a common replacement scenario may be to install an

intermediate pier or bent and replace the span with two girder spans. Railroad forces have perfected the technique of laterally rolling out old spans and rolling in new prefabricated spans between train movements.

Railroads frequently will relocate existing bridge spans to other sites in lieu of constructing new spans, if economically feasible. This primarily applies to beam spans and plate girder spans up to 100 ft. in length. For this reason the requirement for heavy and densely loaded lines are generally applied to all new bridges as the bridge span could end up anywhere at some time in the future. Furthermore, a new industry may locate on a line and completely change the traffic volume.

In general, railroads prefer to construct new bridges on-line rather than relocating or doglegging to an adjacent alignment. Where site conditions do not allow ready access for direct span replacement, a site by-pass, or run-around, called a "shoo-fly" is constructed that provides a temporary bridge while the permanent bridge is constructed.

The design and construction of larger and complex bridges is done on an individual basis.

7.3 Railroad Bridge Types

Railroad bridges are nearly always simple span structures. Listed below in groupings by span length are the more common types of bridges and materials used by the railroad industry for those span lengths.

Short spans to 16 ft.-Timber stringers
-Concrete slabs
-Rolled steel beams
to 32 ft.-Conventional and prestressed concrete box girders and beams
-Rolled steel beams
to 50 ft.-Prestressed concrete box girders and beams
-Rolled steel beams, deck and thru girders
Medium spans from 80 to 125 ft.-Prestressed concrete beams
-Deck and thru plate girders
Long spans-Deck and thru trusses (simple, cantilever, and arches)

Suspension bridges are not used by freight railroads because of excessive deflection.

7.4 Bridge Deck

7.4.1 General

The engineer experienced in highway bridge design may not think of the typical railroad bridge as having a deck. However, it is essential to have a support system for the rails. Railroad bridges typically are designed as either open deck or ballast deck structures. Some bridges, particularly in transit applications, use direct fixation of the rails to the supporting structure.

7.4.2 Open Deck

Open deck bridges have ties supported directly on load carrying elements of the structure (such as stringers or girders). The dead loads for open deck structures can be significantly less than for ballast deck structures. Open decks, however, transfer more of the dynamic effects of live load into the bridge than ballast decks. In addition, the bridge ties required are both longer and larger in cross-section than the standard track ties. This adds to their expense. Bridge tie availability has declined, and their supply may be a problem, particularly in the better grades of structural timber. Disposal of creosoted timber is also a concern. AAR is examining the feasibility of alternative materials that provide similar cushioning and structural performance.

7.4.3 Ballast Deck

Ballast deck bridges have the track structure supported on ballast, which is carried by the structural elements of the bridge. Typically, the track structure (rails, tie plates, and ties) is similar to track constructed on grade. Ballast deck structures offer advantages in ride and maintenance requirements. Unlike open decks, the track alignment on ballast deck spans can typically be maintained using standard track maintenance equipment. If all other factors are equal, most railroads currently prefer ballast decks for new structures.

In ballast deck designs, an allowance for at least 6 in. of additional ballast is prudent. Specific requirements for additional ballast capacity may be provided by the railroad. In addition, the required depth of ballast below the tie should be verified with the affected railroad. Typical values for this range from 8 in. to 12 in. or more. The tie length used will have an effect on the distribution of live load effects into the structure. Ballast decks are also typically waterproofed. The weight of waterproofing should be included in the dead load. Provisions for selection, design, and installation of waterproofing are included in Chapter 8 of the AREMA Manual.

7.4.4 Direct Fixation

Direct fixation structures have rails supported on plates anchored directly to the bridge structure. Direct fixation decks are much less common than either open decks or ballast decks, and are rare in freight railroad service. Although direct fixation decks eliminate the dead load of ties and ballast, and can reduce total structure height, they transfer more dynamic load effects into the bridge. Direct fixation components need to be carefully selected and detailed. Since attenuation properties are proprietary in nature, the manual does not give any guidance on their design in the structural volume.

7.4.5 Deck Details

Walkways are frequently provided on railroad bridge decks. They may be on one or both sides of the track. Railroads and various governments have their own policies and details for walkway placement and construction.

Railroad bridge decks on curved track should allow for super elevation. With ballast decks, this can be accomplished by adjusting ballast depths. With open decks, it can require the use of beveled ties or building the superelevation into the superstructure.

Continuous welded rail (CWR) is frequently installed on bridges. This can affect the thermal movement characteristics of the structure. Check with the affected railroad for their policy on anchorage of CWR on structures. Long-span structures may require the use of rail expansion joints.

7.5 Design Criteria

7.5.1 Geometric Considerations

Railroad bridges have a variety of geometric requirements. The AREMA Manual has clearance diagrams showing the space required for passage of modern rail traffic. It should be noted that lateral clearance requirements are increased for structures carrying curved track.

Track spacing on multiple track structures should be determined by the affected railroad. Safety concerns are leading to increased track spacing requirements.

If possible, skewed bridges should be avoided. Skewed structures, however, may be required by site conditions. A support must be provided for the ties perpendicular to the track at the end of the structure. This is difficult on open deck structures. An approach slab below the ballast may be used on skewed ballast deck bridges.

7.5.2 Proportioning

Typical depth to span length ratios for steel railroad bridges are 1:9–1:12. Guidelines for girder spacing are given in Chapter 15 of the Manual (AREMA 2012).

7.5.3 Bridge Design Loads

7.5.3.1 Dead Load

Dead load consists of the weight of the structure itself, the track it supports, and any attachments it may carry. Dead loads act because of gravity and are permanently applied to the structure.

Unit weights for calculation of dead loads are given in the Manual Chapters 7, 8, and 15. The table in Chapter 15 is reproduced here as Table 7.1.

Dead load is applied at the location it occurs in the structure, typically as either a concentrated or distributed load.

The Manual states that track rails, inside guard rails, and rail fastenings shall be assumed to weigh 200 plf of track. The 60 lb/ft^3 weight given for timber should be satisfactory for typical ties. Exotic woods may be heavier. Concrete ties are sometimes used, and their heavier weight should be taken into account if their use is anticipated.

In preliminary design of open deck structures, a deck weight of 600–650 plf of track can be assumed. This should be checked with the weight of the specific deck system used, for final design. Example calculations for track and deck weight are shown for simple open deck bridges in Table 7.2 and for similar

TABLE 7.1 Unit Weights for Dead Load Stresses

Type	Pounds per Cubic Foot
Steel	490
Concrete	150
Sand, gravel, and ballast	120
Asphalt-mastic and bituminous macadam	150
Granite	170
Paving bricks	150
Timber	60

TABLE 7.2 Minimum Weight of Rail, Inside Guard Rails, Bridge Ties, Guard Timbers, and Fastenings for Typical Open Deck (Walkway Not Included)

Item	Weight (plf of track)
Rail (140 RE): (140 lb/yd. × 2 rails/track × lin. yd./3 lin. ft.)	93
Inside guard rails: (115 lb/yd × 2 rails/track × lin. yd/3 lin. ft)	77
Ties (10 in. × 10 in. × 10 ft. bridge ties, minimum size): (10 in. × 10 in. × 10 ft. × 1 ft.^{2} × 60 lb/ft.^{3} × 1 tie/14 in. × 12 in./ft.)	357
Guard timbers (4 × 8 in.) (4 in. × 8 in. × 1 ft.^{2}/144 in.^{2} × 60 lb/ft.^{2} × 2 guard timbers/ft.)	27
Tie Plates (7 3/4 × 16 in. for rail with 6 in. base) (30.72 lb/plate × 1 tie/14 in. × 12 in./ft. × 2 tie plates/tie)	53
Spikes (5/8 × 5/8 in. × 6 in. reinforced throat) (0.828 lb/spike × 18 spikes per tie × 1 tie/14 in. × 12 in./ft.)	13
Miscellaneous fastenings (hook bolts and lag bolts) (approximately 2.25 lb/hook bolt + 1.25 lb/lag screw × 2 bolts/tie × 1 tie/14 in. × 12in./ft.)	6
Total weight	626

TABLE 7.3 Minimum Weight of Rail, Inside Guard Rails, Guard Timbers, and Fastenings for Typical Ballast Deck (Walkway and Ballast Supports Not Included)

Item	Weight (plf of track)
Rail (140 RE): (140 lb/yd. × 2 rails/track × lin. yd./3 lin. ft.)	93
Inside guard rails: (115 lb/yd. × 2 rails/track × lin. yd./3 lin. ft.)	77
Ties (neglect, since included in ballast weight):	- -
Guard timbers (4 × 8 in.) (4 in. × 8 in. × 1 ft.^{2}/144 in.^{2} × 60 lb/ft.^{2} × 2 guard timbers/ft.)	27
Tie plates (7 3/4 × 16 in. for rail with 6 in. base) (30.72 lb/plate × 1 tie/14 in. × 12 in./ft. × 2 tie plates/tie)	53
Spikes (5/8 × 5/8 in. × 6 in. reinforced throat) (0.828 lb/spike × 18 spikes per tie × 1 tie/14 in. × 12 in./ft.)	13
Ballast (assume 6 in. additional over time) (Approximately 120lb/ft. × 27 in. depth/12 in./ft. × 20 ft.)	4320
Waterproofing (Approximately 150lb/ft. × 0.75 in. depth/12 in./ft. × 20 ft.)	188
Total weight	4752

ballast deck bridges in Table 7.3. These tables show minimum weights as example calculations and the standards of a particular railroad may be significantly different.

Railroad bridges frequently carry walkways and signal and communication cables, and may be used by utilities. Provisions (both in dead load and physical location) may need to be made for these additional items. Some structures may even carry ornamental or decorative items.

7.5.3.2 Live Load

Historically, freight railroads have used the Cooper E load configuration as a live load model. Cooper E80 is currently the minimum design live load recommended by AREMA for new structures. The E80 load model is shown in Figure 7.1. The 80 in E80 refers to the 80 kip weight of the locomotive drive axles. An E60 load has the same axle locations, but the loads are factored by 60/80. Most of the larger railroads are designing new structure to carry E90 or E100 loads.

The designated steel bridge design live load also includes an "Alternate E80" load, consisting of four 100 kip axles. This is shown in Figure 7.2. This load controls over the regular Cooper load on shorter spans and is factored for other E loads in a similar manner.

The Cooper live load model does not match the axle loads and spacing of locomotives currently in service. It did not even reflect all locomotives at the turn of the twentieth century, when it was introduced by Theodore Cooper, an early railroad bridge engineer. Nevertheless, it has remained in use throughout the last century. One of the reasons for its longevity is the wide variety of rail rolling stock that has been and is currently in service. The load effects of this equipment on given span lengths must be compared, as discussed in Section 7.6. The Cooper live load model gives a universal system with which all other load configurations can be compared. Engineering personnel of each railroad calculate how the load effects of each piece of equipment compare to the Cooper loading.

A table of maximum load effects over various span lengths is included in Chapter 15, Part 1 of the AREMA Manual (AREMA, 2012).

7.5.3.3 Impact

Impact is the dynamic amplification of the live load effects on the bridge caused by the movement of the train across the span. Formulas for calculation of impact are included in Chapters 8 and 15 of the Manual (AREMA, 2012). The design impact values are based on an assumed train speed of 60 mph.

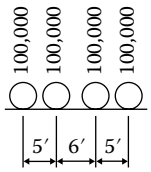

FIGURE 7.2 Alternate live load.

It should be noted that the steel design procedure allows reduction of the calculated impact for ballast deck structures. Different values for impact from steam and diesel locomotives are used. The steam impact values are significantly higher than diesel impact over most span lengths.

Impact is not applied to timber structures, since the capacity of timber under transient loads is significantly higher than its capacity under sustained loads. Allowable stresses for timber design are based on the sustained loads.

7.5.3.4 Centrifugal Force

Centrifugal force is the force a train moving along a curve exerts on a constraining object (track and supporting structure) that acts away from the center of rotation. Formulas or tables for calculation of centrifugal force are included in Chapters 7, 8, and 15 of the Manual (AREMA, 2012). The train speed required for the force calculation should be obtained from the railroad.

Although the centrifugal action is applied as a horizontal force, it can produce overturning moment because of its point of application above the track. Both the horizontal force and resulting moment must be considered in design or evaluation of a structure.

The horizontal force tends to displace the structure laterally:

- For steel structures (deck girders, for example), it loads laterals and cross frames.
- For concrete structures (box girders, for example), the superstructure is typically stiff enough in the transverse direction that the horizontal force is not significant for the superstructure.

For all bridge types, the bearings, anchor bolts, and substructure must be able to resist the centrifugal horizontal force.

The overturning moment tends to increase the live load force in members on the outside of the curve and reduce the force on inside members. However, interior members are not designed with less capacity than exterior members.

Substructures must be designed to resist the centrifugal overturning moment. This will increase forces toward the outside of the curve in foundation elements.

The centrifugal force is applied at the location of the axles along the structure, 6 ft. above the top of rail, at a point perpendicular to the center of a line connecting the rail tops. The effect of track super elevation may compensate somewhat for centrifugal force. The plan view location of the curved track on the bridge (since railroad bridge spans are typically straight, laid out along the curve chords) can also be significant.

Rather than applying the centrifugal force at each axle location, some railroads simply increase the calculated live load force by the centrifugal force percentage, factor in the effect of the force location above the top of rail, and use the resulting value for design.

7.5.3.5 Lateral Loads from Equipment

This item includes all lateral loads applied to the structure due to train passage, other than centrifugal force. These are largely because of "nosing"—the tendency of the train to bear laterally against the rails as it travels down the track.

The magnitude and application point of these loads varies among Chapters 7, 8, and 15 of the Manual (AREMA, 2012). For timber, a load of 20 kips is applied horizontally at the top of rail. For steel, a load of one quarter of the heaviest axle of the specified live load is applied at the base of rail. In both cases,

the lateral load is a moving concentrated load that can be applied at any point along the span in either horizontal direction. It should be noted that lateral loads from equipment are not included in design of concrete bridges. However, if concrete girders are supported on steel or timber substructures, lateral loads should be applied to the substructures.

Lateral loads from equipment are applied to lateral bracing members, flanges of longitudinal girders or stringers without a bracing system, and to chords of truss spans.

Experience has shown that very high lateral forces can be applied to structures because of lurching of certain types of cars. Wheel hunting is another phenomenon, which applies lateral force to the track and structure. Damaged rolling stock can also create large lateral forces.

It should be noted that there is not an extensive research background supporting the lateral forces given in the Manual (AREMA, 2012). However, the lateral loads in the Manual (AREMA, 2012) have historically worked well when combined with wind loads to produce adequate lateral resistance in structures.

7.5.3.6 Longitudinal Force from Live Load

Longitudinal forces are typically produced from starting or stopping trains (acceleration or deceleration) on the bridge. They can be applied in either longitudinal direction. These forces are transmitted through the rails and distributed into the supporting structure.

In the Manual (AREMA, 2012), Chapter 7 takes the longitudinal force because of breaking to be 15% of the vertical live load, without impact, applied at 6 ft. above top of rail. Chapters 9 and 15 use a formula that is easier to apply that produces roughly the same values with the load placed 8 ft. above the top of rail. Similarly, Chapter 7 uses 25% of the drive axle loads for traction at 6 ft. above top of rail, whereas Chapters 8 and 15 use a formula with the load applied at 3 ft. above top of rail.

Recent research performed by the AAR has shown that little of the longitudinal force is distributed by the rails. The heavy axle loads currently used in service make the entire rail and supporting bridge structure act as a unit with little or no slippage even in ballast deck structures. Previous editions of the AREMA Manual permitted reduction in longitudinal force based on tests on much lighter vehicles. These reductions are no longer valid. Longitudinal forces are distributed to the various components of the supporting structure according to their relative stiffness. Care must be taken to ensure these forces are taken out of the structure preferably without inducing torsion.

Chapter 15 of the Manual (AREMA, 2012) states that the longitudinal force on multiple track structures is to be applied in the same manner as the impact factors. Chapters 7 and 8 of the Manual (AREMA, 2012) are silent on this matter.

Longitudinal force is particularly significant in long structures, such as viaducts, trestles, or major bridges. Large bridges may have internal traction or braking trusses to carry longitudinal forces to the bearings. Viaducts frequently have braced tower bents at intervals to resist longitudinal force. Transit equipment can have high acceleration and deceleration rates (higher than conventional freight), which can lead to high longitudinal force on transit structures.

7.5.3.7 Wind Loading

Wind loading is the force on the structure because of wind action on the bridge and train.

For all materials the wind on the train is taken as 300 plf, applied 8 ft. above top of rail.

Chapters 7, 8, and 15 of the Manual (AREMA, 2012) deal with wind on the structure differently:

1. Timber: Use 30 psf as a moving horizontal load acting in any direction.
2. Concrete: Use 45 psf as a horizontal load perpendicular to the track centerline.
3. Steel: As a moving horizontal load
   a. Use 30 psf on loaded bridge.
   b. Use 50 psf on unloaded bridge.

The application areas of the wind on structure vary as well:

1. Timber: For trestles, the affected area is 1.5 times the vertical projection of the floor system. For trusses, the affected area is the full vertical projection of the spans, plus any portion of the leeward trusses not shielded by the floor system. For trestles and tower substructures, the affected area is the vertical projections of the components (bracing, posts, and piles).
2. Steel: Similar to timber, except that for girder spans, 1.5 times the vertical projection of the span is used.
3. Concrete: Wind load is applied to the vertical projection of the structure. (Note that 45 psf = 1.5 [30 psf].)

The 30 psf wind force on a loaded structure and 50 psf force on an unloaded structure used in Chapter 15 of the Manual (AREMA, 2012) reflect assumptions on train operations. It was assumed that the maximum wind velocity under which train operations would be attempted would produce a force of 30 psf. Hurricane winds, under which train operations would not be attempted, would produce a wind force of 50 psf.

For stability of spans and towers against overturning because of wind on a loaded bridge, the live load is reduced to 1200 plf, without impact being applied. This value represents an unloaded, stopped train on the bridge.

It should be noted that Chapter 15 has a minimum wind load on loaded bridges of 200 plf on the loaded chord or flange and 150 plf on the unloaded chord or flange.

Virtually every bridge component can be affected by wind. However, wind is typically most significant in design of the following:

1. Lateral bracing and cross-frames
2. Lateral bending in flanges
3. Vertical bending in girders and trusses due to overturning
4. Tower piles or columns
5. Foundations

7.5.3.8 Stream Flow, Ice, and Buoyancy

These loads are experienced by a portion of the structure (usually a pier) because of its location in a body of water.

These topics are only specifically addressed in Chapter 8 of the Manual (AREMA, 2012). This is because they apply almost entirely to bridge substructures, which typically consist of concrete.

Buoyancy, stream flow, and ice pressure are to be applied to any portion of the structure that can be exposed to them. This typically includes piers and other elements of the substructure. Buoyancy can be readily calculated for immersed portions of the structure.

Chapter 8 of the AREMA Manual gives formulas for use in design for forces due to stream flow and ice pressure.

Spans may be floated off of piers because of buoyancy, stream flow, and ice pressure. Loaded ballast cars are sometimes parked on bridges during floods or ice build-up to resist this.

Drift or debris accumulation adjacent to bridges can be a significant problem, reducing the flow area through the bridge and effectively increasing the area exposed to force from stream flow.

Two other factors concerning waterways must be considered. The first is vessel collision (or, more correctly) allision with piers. Pier protection is covered in Part 23, Spans over Navigable Streams, of Chapter 8. These requirements should be addressed when designing a bridge across a navigable waterway.

The second factor to be considered is scour. Scour is a leading cause of bridge failure. AREMA addresses these concerns in Part 1, Track, Section 3.4. Hydraulic studies to determine required bridge openings should be performed when designing new structures or when hydrologic conditions upstream of a bridge change.

7.5.3.9 Volume Changes

Volume changes in structures can be caused by thermal expansion or contraction or by properties of the structural materials, such as creep or shrinkage. Volume changes in themselves, if unrestrained, have relatively little effect on the forces on the structure. Restrained volume changes, however, can produce significant forces in the structure. The challenge to the designer is to provide a means to relieve volume changes or to provide for the forces developed by restrained changes.

Chapter 7 of the Manual (AREMA, 2012) does not specifically state thermal expansion movement requirements. Owing to the nature of the material and type of timber structures in use, it is unlikely that thermal stresses will be significant in timber design. Chapter 15 requires an allowance of 1 in. of length change because of temperature per every 100 ft. of span length in steel structures. Chapter 8 of the Manual (AREMA, 2012) provides the following table for design temperature rise and fall values for concrete bridges:

Climate	Temperature Rise	Temperature Fall
Moderate	30°F (17°C)	40°F (22°C)
Cold	35°F (20°C)	45°F (25°C)

It should be noted that the tabulated values refer to the temperature of the bridge concrete. A specific railroad may have different requirements for thermal movement.

Expansion bearings are the main design feature typically used to accommodate volume changes. Common bearing types include the following:

1. Sliding steel plates
2. Other sliding bearings
3. Rocker bearings
4. Roller bearings (cylindrical and segmental)
5. Elastomeric bearing
6. Multi-rotational bearings

Provision should be made for span length change because of live load. For spans longer than 300 ft., provision must be made for expansion and contraction of the bridge floor system.

For concrete structures, provisions need to be made for concrete shrinkage and creep. Specific guidelines are given in Chapter 8, Parts 2 and 17 for these properties. It is important to remember that creep and shrinkage are highly variable phenomena, and allowance should be made for higher than expected values. It also should be noted the AREMA Manual requires 0.25 $in.^2$/ft. minimum of reinforcing steel in exposed concrete surfaces as shrinkage and temperature reinforcement.

Chapter 8 also requires designing for longitudinal force because of friction or shear resistance at expansion bearings. This is in recognition of the fact that most expansion bearings have some internal resistance to movement. This resistance applies force to the structure as the bridge expands and contracts. The AREMA Manual contains procedures for calculating the shear force transmitted through bearing pads. Loads transmitted through fixed or expansion bearings should be included in substructure design.

Bearings must also be able to resist wind and other lateral forces applied to the structure.

Chapter 15, part 10 of the AREMA Manual covers bridge bearings and should be used for bearing design and detailing.

It should be noted that movement of bridge bearings affects the tolerances of the track supported by the bridge. This calls for careful selection of bearings for track with tight tolerances (such as high-speed rail). Maintenance requirements are also important when selecting bearings, since unintended fixity due to freezing of bearings can cause significant structural damage.

7.5.3.10 Seismic Loads

Seismic design for railroads is covered in Chapter 9 of the Manual (AREMA, 2012).

The philosophical background of Chapter 9 recognizes that railroad bridges have historically performed well in seismic events. This is because of the following factors:

1. The track structure serves as an effective restraint (and dampening agent) against bridge movement.
2. Railroad bridges are typically simple in their design and construction.
3. Trains operate in a controlled environment, which makes types of damage permissible for railroad bridges that might not be acceptable for structures in general use by the public.

Item 3 above is related to the post-seismic event operation guidelines given in Chapter 9. These guidelines give limits on train operations following an earthquake. The limits vary according to earthquake magnitude and distance from epicenter. After an earthquake all trains within 100 miles of the area where an earthquake has been reported are ordered to run at restricted speed until the magnitude and location of the epicenter have been determined. Once the details of an earthquake are known, then for magnitudes above 5 on the Richter scale, Chapter 9 gives recommended responses differentiated for California and elsewhere with various operating radii and either restricted speed or no movement.

For example, following an earthquake of magnitude 6.0 or above, all trains within a 100-mile radius of the epicenter for a California earthquake must stop until the track and bridges in the area have been inspected and cleared for use. (Note that specific railroad policies may vary.)

Three levels of ground motion are defined in Chapter 9:

- Level 1—Motion that has a reasonable probability of being exceeded during the life of the bridge
- Level 2—Motion that has a low probability of being exceeded during the life of the bridge
- Level 3—Motion for a rare, intense earthquake

Three performance limit states are given for seismic design of railroad bridges. The serviceability limit state requires that the structure remain elastic during Level 1 ground motion. Only moderate damage and no permanent deformations are acceptable.

The ultimate limit state requires that the structure suffer only readily detectable and repairable damage during Level 2 ground motion, although economic considerations may permit the railroad to allow more damage where there is no passenger traffic, and so on.

The survivability limit state requires that the bridge not collapse during Level 3 ground motion. Extensive damage may be allowed. For some structures, the railroad may elect to allow for irreparable damage and plan to replace the bridges following a Level 3 or in some cases for a Level 2 event as mentioned above.

The return period used for each performance limit state depends on a number of factors:

- Immediate safety (based on volume of passenger use, hazardous materials traffic, and effect on community life lines)
- Immediate value of the structure (expressed in term of volume of traffic)
- Replacement value (based on span length, bridge length, and/or bridge height)

An in-depth discussion of seismic analysis and design is beyond the scope of this section. Guidelines are given in Chapter 9 of the AREMA Manual and in Unsworth (2010). Base acceleration coefficient maps for various return periods are included in the AREMA Manual Chapter 9.

Even if no specific seismic analysis and design is required for a structure, it is good practice to detail structures for seismic resistance if they are in potentially active areas. Specific concerns are addressed in Chapter 9. Provisions of adequate bearing areas and designing for ductility are examples of inexpensive seismic detailing.

7.5.3.11 Stability Check

Chapter 15 of the Manual (AREMA, 2012) has a stability check to ensure that simple spans will not topple over in the case of a minor derailment. The application of the eccentric load recommended is not expected to eliminate damage to the structure.

7.5.4 Load Combinations

A variety of loads can be applied to a structure at the same time. For example, a bridge may experience dead load, live load, impact, centrifugal force, wind, and stream flow simultaneously. The AREMA Manual (AREMA, 2012) chapters on structure design recognize that it is unlikely that the maximum values of all loads will be applied concurrently to a structure. Load combination methods are given to develop maximum credible design forces on the structure.

Chapter 7, in Section 2.3.5.5, Combined Stresses, states: "For stresses produced by longitudinal force, wind or other lateral forces, or by a combination of these forces with dead and live loads and centrifugal force, the allowable working stresses may be increased 50%, provided the resulting sections are not less than those required for dead and live loads and centrifugal force."

Chapter 15, in Section 1.3.14.3, Allowable Stresses for Combinations of Loads or Wind Forces only, states the following:

1. Members subject to stresses resulting from dead load, live load, impact load, and centrifugal load shall be designed so that the maximum stresses do not exceed the basic allowable stresses of Section 1.4, of Basic Allowable Stresses, and the stress range does not exceed the allowable fatigue stress range of Article 1.3.13.
2. The basic allowable stresses of Section 1.4, Basic Allowable Stresses, shall be used in the proportioning of members subject to stresses resulting from wind loads only, as specified in Article 1.3.8.
3. Members, except floor beam hangers, which are subject to stresses resulting from lateral loads, other than centrifugal load, and/or longitudinal loads, may be proportioned for stresses 25% greater than those permitted by paragraph 1, but the section of the member shall not be less than that required to meet the provisions of paragraph a or paragraph 2 alone.
4. Increase in allowable stress permitted by paragraph 3 shall not be applied to allowable stress in high strength bolts.

Chapter 8 of the Manual (AREMA, 2012), in Part 4 on Pile Foundations, defines primary and secondary loads. Primary loads include dead load, live load, centrifugal force, earth pressure, buoyancy, and negative skin friction. Secondary (or occasional) loads include wind and other lateral forces, ice and stream flow, longitudinal forces, and seismic forces. Section 4.2.2.b allows a 25% increase in allowable loads when designing for a combination of primary and secondary loads, as long as the design satisfies the primary load case at the allowable load.

These three load combination methods are based on service load design. Chapter 8, in Part 2, Reinforced Concrete Design, addresses both service load and load factor design with 8 load combinations for service load design and 9 load combinations for load factor design.

Chapter 8, Section 2.2.4 gives several limitations on the load combination tables. For example, load factor design is not applicable to foundation design or for checking structural stability. In addition, load factors should be increased or allowable stresses adjusted if the predictability of loads is different than anticipated in the chapter.

For stability of towers, use the 1200 plf vertical live load as described in the Wind Loading section.

As a general rule, the section determined by a load combination should never be smaller than the section required for dead load, live load, impact, and centrifugal force.

It is important to use the appropriate load combination method for each material and component in the bridge design. Combination methods from different sections and chapters should not be mixed.

7.5.5 Serviceability Considerations

7.5.5.1 Fatigue

Fatigue resistance is a critical concern in design of steel structures. It is also a factor, though of less significance, in the design of concrete bridges. A fatigue design procedure, based on allowable stresses, impact values, number of cycles per train passage, fracture criticality of the member, and type of details, is applied to steel bridges. Fatigue can be the controlling design case for many new steel bridges.

7.5.5.2 Deflection

Live load deflection control is a significant serviceability criterion. Track standards limit the amount of deflection in track under train passage. The deflection of the bridge under the live load accumulates with the deflection of the track structure itself. This total deflection can exceed the allowable limits if the bridge is not sufficiently stiff. The stiffness of the structure can also affect its performance and longevity. Less stiff structures may be more prone to lateral displacement under load and out-of-plane distortions. Specific deflection criteria are given in Chapter 15 for steel bridges. Criteria for concrete structures are given in Chapter 8, Table 8.2.8.

Long-term deflections should also be checked for concrete structures under the sustained dead load to determine if any adverse effects may occur because of cracking or creep.

7.5.5.3 High Speed Railway Considerations

The Manual (AREMA, 2012) does not as yet have criteria for high speed rail. These are under development and because of the need to meet higher crash worthiness Standards in North America are likely to be different than those developed in Europe or Asia. Clearly additional attention will be made to the dynamics inherent in such operations.

7.5.5.4 Others

Other serviceability criteria apply to concrete structures. Reinforced concrete must be checked for crack control. Allowable stress limits are given for various service conditions for prestressed concrete members.

7.6 Capacity Rating

7.6.1 General

Rating is the process of determining the safe capacity of existing structures. Specific guidelines for bridge rating are given in Chapters 7, 8, and 15 of the AREMA Manual.

Ratings are typically performed on both as-built and as-inspected bridge conditions. The information for the as-built condition can be taken from the bridge as-built drawings. However, it is important to check the current condition of the structure. This is done by performing an inspection of the bridge and adjusting the as-built rating to include the effects of any deterioration, damage, or modifications to the structure since its construction. Material property testing of bridge components may be very useful in the capacity rating of an older structure.

Structure ratings are normally presented as the Cooper E value live load that the bridge can safely support. The controlling rating is the lowest E value for the structure (based on a specific force effect on a critical member or section.) For example, a structure rating may be given as E74, based on moment at the termination of a flange cover plate.

As discussed in the Live Load section, there are a wide variety of axle spacings and loadings for railroad equipment. Each piece of equipment can be rated to determine the maximum force effects it produces for a given span length. The equipment rating is given in terms of the Cooper load that would

produce the equivalent force effect on the same span length. Note that this equivalent force effect value will probably be different for shear and moment on each span length.

In addition to capacity ratings, fatigue evaluations can be performed on structures to estimate their remaining fatigue life. These are typically only calculated for steel structures. Guidelines for this can be found in the AREMA Manual, Chapter 15.

7.6.2 Normal Rating

The normal rating of the structure is the load level that can be carried by the bridge for an indefinite time period. This indefinite time period can be defined as its expected service life. The allowable stresses used for normal rating are the same as the allowable stresses used in design. The impact effect calculation, though, is modified from the design equation. Reduction of the impact value to reflect the actual speed of trains crossing the structure (rather than the 60 mph speed assumed in the design impact) is allowed. Formulas for the impact reduction are included in the rating sections of the AREMA Manual chapters.

7.6.3 Maximum Rating

The maximum rating of the structure is the maximum load level that can be carried by the bridge at infrequent intervals. This rating is used to check if extra-heavy loads can cross the structure. Allowable stresses for maximum rating are increased over the design allowable values.

The impact reduction for speed can be applied as for a normal rating. In addition, "slow orders" or speed restrictions can be placed on the extra-heavy load when crossing the bridge. This can allow further reduction of the impact value, thus increasing the maximum rating of the structure (note that this maximum rating value would apply only at the specified speed).

References

AAR. 2010. *Railroad Facts*. 2010 Edition. Association of American Railroads, Washington, DC.

AREMA. 2012. *Manual for Railway Engineering*, American Railway Engineering and Maintenance of Way Association, Lanham, MD.

FRA. 2010. *Bridge Safety Standards*. Final Rule, July 15, 2010. Department of Transportation. Federal Railway Administration, Federal Register pages 41282–41309. Government Printing Office, Washington, DC.

Unsworth, J. F. *Design of Modern Steel Railway Bridges*. 2010. CRC Press, Boca Raton, FL.

8

High-Speed Railway Bridges

Jeder Hseih
Continental Engineering Corporation

Fu-Hsiang Wu
Chung Hua University

8.1 Introduction

8.1.1 High-Speed Rail Network

Since Japan launched its first bullet train from Tokyo to Osaka (Tokaido Sinkansen) in October 1964, although its maximum operation speed was only 210 km/h (130.3 mph) at the time, it has moved the railway transportation into a high-speed era. Many countries started to develop high-speed rail technology and high-speed rail networks. Although many countries have built high-speed rail, there are three major high-speed rail train systems available in the world—the Japanese SKS, French TGV, and German ICE systems. China has recently developed its own high-speed rail train running on its newly developed high-speed rail network.

In general, "high speed" for a railway system is defined as speeds greater than 200 km/h (124.3 mph). Many efforts have been made by each high-speed train system to upgrade their speed. Although testing speed has reached more than 500 km/h (310.7 mph), maximum operating speed has been maintained at 300 km/h (186.4 mph) for all existing high-speed rail systems, until recently. For the newly finished high-speed rail line from Wuhan to Guangzhou in China, the maximum operating speed is 350 km/h (217.5 mph). The 1318 km long high-speed line from Beijing to Shanghai, with 86.5% of elevated bridge structures and a maximum speed up to 380 km/h (236.1 mph), just opened June 30, 2011 [1].

In the more than 40 years of operation, high-speed rail has proven that it is the choice for the future. Currently, many countries have built high-speed rail line/networks, including Japan, Korea, Taiwan, and China in Asia and France, Germany, Spain, the United Kingdom, the Netherlands, Belgium, and Turkey in Europe. Not only are these countries expanding their high-speed rail networks, but also many other countries are planning to build high-speed rail.

Because of the "high speed" factor, there are different considerations for planning and design of civil works for a high-speed rail system compared to other infrastructure projects. This chapter focuses only on the major bridge-design criteria required specifically for the high-speed rail system.

8.1.2 System Assurance

A complete high-speed rail system will have many subsystems:

- Core system
  - Rolling stocks
  - Power supply system
  - Signaling system
  - Communication system
- Civil work
- Stations
- Depots
- Track

How to deal with the interfaces and to integrate all of the above to be a complete, safe, and reliable high-speed rail system is a challenge. Because of the complexity in planning and implementation of a high-speed rail system, a systematic approach—system assurance—has been adopted recently by many project owners.

The objective of system assurance is to achieve the targets of RAMS (reliability, availability, maintainability, and safety) for the operation. Although the planning and design process for a high-speed rail bridge will not be much different from that for a highway bridge, function requirements for the high-speed rail operation must be identified first in order to develop the requirements for high-speed rail bridges.

8.1.3 Taiwan High-Speed Rail

The Taiwan High-Speed Rail project (THSRP) is one of the largest build-operation-transfer (BOT) projects in the world. The route runs from Taipei in the north to Kaoshiung in the south, with eight stations and a total length of 345 km (214.4 miles). There are 252 km (156.6 miles) of elevated viaducts/bridges, 62 km (38.5 miles) of tunnels, and 31 km (19.3 miles) of earthworks (cut and fill). The section from central Taiwan to the southern end of the route is all elevated viaducts with a total length of 157.3 km (98.3 miles), which made it the longest continuous viaduct in the world by the time it was completed in 2004 (Figure 8.1).

FIGURE 8.1 Arial photo of Taiwan high-speed rail elevated viaduct.

The construction and operation agreement (C&OA) was signed in July 1998. After more than 18 months preparation, 12 design and build civil contracts were awarded by the project company, Taiwan High-Speed Rail Corporation (THSRC), in March–May, 2000. Before end of 2004, in under than 5 years, all civil work construction was completed and handed over to the subsequent contractors for the construction of track work and installation of the E&M system. Commencement of operation began on January 5, 2007.

By August 2010, after 3 years and 8 months of operation, traffic had reached 100 million passengers. It has also survived a Richter scale 6.4 earthquake that occurred on March 4, 2010, the largest earthquake in southern Taiwan in 100 years. The seismic warning system was immediately triggered and the emergency brake system of six trains in the affected area was activated automatically. Although one bogie (24 bogies for a 12-car train) in one train derailed, all six trains were safely stopped and stayed on the viaducts. The most important thing is that no one got hurt. There was damage on the track and the overhead catenary system because of derailment, but all civil structures were safe and sound without any damage.

In terms of construction duration and operation performance, THSRP is considered one of the most successful high-speed projects in recent years. In August 2010, THSRP was selected as the outstanding civil project by the Asian Civil Engineering Coordinating Council (ACECC) and the award was presented at its 5th International Civil Engineering Conference in Sydney, Australia.

The information presented in this chapter is mainly based on the THSRP and may serve as a guideline for reference only. Engineers who work for planning and design of a high-speed rail bridge must recognize any unique requirements by the project owner as well as requirements from the local regulations and local conditions.

8.2 Requirements

8.2.1 General Requirements

In term of travel time, high-speed rail systems are very competitive in the range of 300–800 km (186.4–497.1 mph) among available transportation systems, based on past records. When the speed is upgraded, the competitiveness will also increase. However, a new high-speed rail system usually requires a very large investment. The cost benefit of this investment not only depends on the cost effectiveness of the engineering construction, but also depends on the system's operation performance in the future. Therefore, all engineering planning and design of the project shall be driven by operation requirements.

In general, the project owner assesses and defines the project basic data or the operation requirements, subjected to the available technology, in the early stage of the project in order to proceed with engineering planning. These basic project data typically include expected passengers in target year, expected travel time, maximum operation speed, maximum design speed, minimum service hours, train capacity, and so on. Technical requirements for the infrastructures shall be developed accordingly.

Using THSRP as an example, the basic project data are as follows:

- Taipei–Kaoshiung travel time
  - 90 minutes (one stop at Taichung for 3 minutes)
  - 120 minutes (4 intermediate stops, 2 min/stop)
- Minimum services: 18 h/day
- Continuous train services with 4-minute interval for 2 hours
- Minimum 800 seats/train
- Maximum operation speed 300 km/h (186.4 mph)
- Design speed for civil work of 350 km/h (217.5 mph)

In general, the functional requirement for the bridges is to "fit for purpose" of high-speed railway operation. This implies that design of alignment, track, tunnel, bridge, and earthwork, and so on. shall allow the train running safely and comfortably at high speed. This applies not only under normal conditions but also under abnormal conditions.

Furthermore, any facilities required to implement the emergency plan after an incident need to be considered for design of the infrastructure.

8.2.2 Safety Requirements

Because of the "high speed" aspect, safety is the highest priority to be considered for the operation of a high-speed rail system. In general, the project owner needs to develop technical safety requirements in accordance with the operation plan. This safety technical requirement not only specifies the safety for the normal condition but also takes into consideration the worst condition.

For the design of high-speed railway bridge, important safety requirements are as follows:

- Design life is 100 years (depending on the project owner).
- To allow a train running safely at maximum operation speed as well as the maximum design speed.
- The structure needs to resist natural disasters—earthquake, typhoon, flooding, etc.—in accordance with local regulations or as specified by the project owner.
- It must be easy to evacuate passengers under abnormal conditions.
- To provide emergency staircases at least every 3000 m (1.86 miles) on both sides of the routes.
- To provide safety walkways on both sides of the tracks to allow passenger evacuation.
- To contain the train on the viaduct in case of derailment.
- To provide derailment protection walls on both sides of tracks.

8.2.3 Maintenance Requirements

Because of "high speed," no one shall be allowed on the permanent way during normal operation. In case of emergency, should there be any need to carry out necessary work on the permanent way, speed restrictions shall be applied. Therefore, in order not to interrupt the operation services, no maintenance is allowed during normal operation periods. In general, the maintenance period for most high-speed rail operators is from midnight to 6:00 AM. Owing to limited maintenance time, maintainability is a very important factor to be considered in the design of the infrastructure for the high-speed rail system.

8.2.3.1 Maintainability

- Drainage system shall allow for easy cleaning.
- Any components without 100 years of design life shall be replaceable—expansion joints, bearings, and so on.
- Components such as bearings, which may impact the operation, shall be able to be replaced within 4 hours.
- During the replacement of the bearings, the girder is allowed to be lifted only by 1 cm without impact to the track.

8.2.3.2 Durability

- To provide adequate concrete protection layer.
- To provide waterproofing layer on the deck.
- Steel or steel components shall have adequate corrosion protection, galvanized, or painting.
- First maintenance shall be within 25 years (depending on the project owner).

8.2.3.3 Accessibility

- Maintenance walkway must be provided on both sides of the tracks (also used as the safety walkway).
- In case of box girders, a manhole shall be provided at bottom of the girder every 100 m.
- A manhole shall be provided at the bottom of the girder for a river bridge to allow access to the top of the pier cap.

- Inside the box girder, minimum clearance of 2.0 × 1.8 m shall be maintained to be used as the walkway.
- In case of other types of girder, proper access should be provided for inspection of the girder.

8.2.4 Environmental Requirements

Environmental protection is becoming a more and more important issue for every infrastructure project. In most countries, government regulation would require an environment impact analysis (EIA) report to be approved before the infrastructure project is allowed to proceed. During the course of implementation, all commitments for environmental protection made in the EIA report as well as the government regulation shall be followed. For high-speed rail bridges, two major issues that need to be considered are noise and vibration.

8.2.4.1 Noise

Noise for high-speed rail mainly comes from four different sources—interaction between wheel and rail, engine noise, aerodynamic effect of the car body, and pantograph. There is also a sonic boom issue at the tunnel portal because of the micro pressure wave when trains come out of the tunnel at high speed. Providing a buffer zone between the high-speed line and residences might be the best mitigation measure to solve the noise issue. However, when required land cannot be provided, other mitigation measures need to be considered. Although different technologies are available, a noise barrier is still considered as the easiest and most cost effective mitigation for noise problems.

8.2.4.2 Vibration

The main concern is the vibration of adjacent buildings/residences caused by the dynamic response of the structure through the ground when the train is passing by at high speed. In general, vibration should comply with government regulation, which defines the acceptable vibration level to be tolerable to people. However, any special requirements for a high-tech microchip manufacturing plant, if located nearby, need to be identified and treated with special care.

Use THSRP as an example, the general requirements for the noise and vibration are as follows:

- Noise and vibration need to comply with EIA report.
- Noise level shall comply with noise control regulation.
- To provide 1.25 m (4.1 ft) high (from top of rail) reinforced concrete noise barrier on both sides of viaduct.
- To provide additional metal noise barrier up to 4 m (13.1 ft) high (from top of rail), if necessary, depending on the estimated noise level and local conditions.
- Design needs to consider the loading of the noise barrier up to 4 m (13.1 ft) high to allow installation of noise barrier in the future.
- Vibration level shall comply with German DIN4150 (no domestic regulation).

8.2.5 Special Requirements

Although the design process for a high-speed rail bridge will not be too much different than that of a highway bridge, there are still certain special factors that need to be considered in design.

8.2.5.1 Track and Structure Interaction

Continuous welded rail (CWR) is commonly used in the modern railway system now to improve riding quality. However, when CWR is placed on a bridge, there will be additional stress in the rail at structure expansion joints because of movement of the bridge girders due to temperature change. The amount

of the stress will depend on the range of temperature change and the expansion length of the girder. The rail may be broken or buckled depending on stress in tension or in compression, should stress level exceed its limitation.

Therefore, this temperature effect, because of track and structure interaction, shall be properly considered in the design of the bridge. Otherwise, risk for running safety due to deformation of track would be much higher and subsequently cost for maintenance of the track will be increased. Rail expansion joints may be installed to cope with this temperature effect, however rail expansion joint is not only expensive but also very costly to maintain and therefore rail expansion joint shall be avoided as much as possible. In THSRP, there is only one location along the entire 345 km (214.4 miles) route where the rail expansion joint has to be installed because a long-span steel bridge at that location could not be avoided.

Temperature variation between day and night, as well as the seasonal change of temperature, are different depending on the area. Allowable expansion length of the girder depends on the temperature range to be considered. Each project owner shall define his project-specific criteria for temperature to be the basis for design.

In THSRP, maximum temperature of 40°C (104°F) and minimum temperature of 0°C (32°F) are used. It also generally requires that the maximum limit from a fixed point to a free end of a structure permitted without a rail expansion joint is 100 m (328.1 ft).

Track turnout is very sensitive to movement. In general, turnout should be avoided to be located on the bridge. However, in THSRP, more than 70% of the route is elevated viaducts/bridge and most of the stations are also elevated such that turnout on bridge could not be avoided. A special requirement is that turnout shall avoid the free end (expansion joint) of the structure and comply with minimum distance between the structural movement joint and the turnout. Therefore, all turnouts shall be located on the continuous deck.

Furthermore, differential movement between track and girder will be induced by other loading, such as traction force, braking force, earthquake force, and so on. Effects under these loading conditions shall also be considered properly in the design.

8.2.5.2 Dynamic Effect because of Moving Train

A high-speed rail bridge has to be designed for the dynamic effects of the train loading to avoid excessive structural response in terms of strength as well as displacement due to possible resonance. Dynamic effects of the structures will depend on the type of train system used (axle load, axle spacing, number of cars, etc.), running speed, and type of structures (material, cross section, span length, etc.) adopted. It should be noted that the maximum dynamic effect may not necessarily occur at the maximum speed. If possible, the structure shall be designed such that structural nature frequency shall be different from the natural frequency of the train in order to avoid resonance.

In general, a static design load, with appropriate impact factors following international standard, is determined by the project owner depending on the train systems (passenger train, maintenance vehicle, or freight train if any) used for the project. Detailed dynamic analyses shall be carried out using the actual train loading configuration to check the impact factor. Whichever is critical shall be used for design.

The response of the structure to the actual train depends on the train speed and the natural frequency of the structure. The calculation shall be made using a computer program for the dynamic analysis of structures under the action of moving loads. Unless otherwise justified, structural damping of 2% for steel structures, 2.5% for prestressed concrete structures, and 4% for reinforced concrete structures shall be used in conducting the dynamic analyses.

A fatigue damage assessment shall also be carried out for all structural elements that are subjected to fluctuations of stress. This fatigue assessment shall be assessed over the required structural life as determined by the project owner.

8.2.5.3 Deflection Control

The main objective for the design of a bridge for the high-speed railway is to allow the high-speed running safely and comfortably, which would depend on the track conditions. Therefore, any movement or displacement of the structure that may impact the track geometry shall be minimized and properly controlled in the design of bridge.

The most important factor to be considered is the deflection of superstructures during the passing of the high-speed train. This includes not only the vertical deflection at mid-span but also the rotation at structural expansion joints. Twisting of superstructure girders due to eccentric train loading because of off center track or the centrifugal force at curve section needs to be considered also. The allowable deflection limits are given in Section 8.4.2.3.

When a train is running across a bridge with multiple spans, especially with equal span length, significant deflection, even fulfilling the safety requirement may cause a horse riding situation and thus a comfort problem. Therefore, the longer the total length of bridge, the smaller girder deflection should be required.

Movement of girders due to temperature effect, especially for a bridge with continuous span, shall also be carefully reviewed. Effect of creep and shrinkage for the prestressed concrete girders may also induce vertical deformation of girders. The long-term impact because of creep and shrinkage shall be carefully evaluated.

8.2.5.4 Vertical Settlement

Vertical settlement of foundation induces permanent deformation of the track geometry unless track is adjusted accordingly to maintain its quality. Impact on the structure because of vertical settlement of the foundation shall be considered in the design of bridge. But limitations on the residual settlement shall be defined to minimize the impact to the track and to ensure the required adjustment of the track is within allowable limit. These limitations will depend on the alignment criteria and type of track adopted for the project.

In the design of a bridge, estimation of vertical settlement of the foundation shall account for all superimposed dead loads, including trackwork, to ensure required structure elevation is met upon completion of construction.

As for residual vertical settlement, the concern is the differential vertical settlement between adjacent piers, which would cause a slope change in the track alignment. For THSRP, the limitations on maximum differential settlement are (measured by change in slope) as follows:

- For simply supported multi-spans, a change in slope of 1 in 1000
- For continuous spans, a change in slope of 1 in 1500

8.2.6 Interface Requirements

High-speed rail shall be an integrating system including civil, track, stations, depots, and the core systems (including rolling stock system, power supply system, signaling system, communication system, and wayside E & M system). Therefore, design of high-speed rail bridges shall take into account all requirements for those systems. In general, all these interface requirements need to be identified before the design of bridge can be carried out.

8.2.6.1 Safety

Based on general safety requirements, a detailed interface requirement for safety shall be developed.

8.2.6.1.1 Safety Walkway

Walkway shall be provided along the outside of the two outside tracks. Minimum width of safety walkway shall be based on local regulations. Minimum clearance from the track shall be based on project-specific requirements.

Specific requirement for nonslip walking surface shall be developed. Handrail shall be provided along the walkway. Detailed requirements (location, height, sizes) for handrail shall be developed.

Walkway crossing the tracks shall be provided where necessary to allow the walkway to be continuous. Requirements for crossing of the track shall be developed.

8.2.6.1.2 Emergency Exit

Egress and access stairs from the safety walkway on each side shall be provided in accordance with project-specific safety requirements.

Requirements for the minimum width of the stairway, landing, and railing shall be in accordance with local regulations. Width and length of the landing shall provide adequate space to turn a stretcher. Additional platform at top of the stairs shall be provided for queuing and for storage of rail transport devices in accordance with the project-specific requirements.

Emergency exits shall be located near the public road and adequate safety area shall be provided at ground level in accordance with project-specific safety requirements and local regulations. Access road with minimum width connecting the safety area and public road shall be provided in accordance with local regulations.

Lighting, power, emergency telephone, CCTV, security device, and other monitoring devices shall be provided in accordance with the project-specific requirements. Designer is required to make provision in the detailed design for the fitting of this equipment.

Fence with minimum height and gate at the bottom of the stairs shall be provided in accordance with project-specific safety requirements. Detailed security provisions for the key of the gates shall be defined by the project owner.

8.2.6.1.3 Derailment Protection

Derailment is a risk for any railway. Railway operators always make the best effort to maintain the railway and to set up the operating rules to prevent from derailment to minimize the risk. However, the design of bridges still needs to consider the condition in case of a derailment.

Different protections need to be considered to contain the train on the bridge in case of derailment to prevent the train from falling off the bridge. For THSRP, derailment containment walls are mandatory for all mainline on the bridge. The derailment containment walls are located outside of the track with 2 m (6.6 ft) from the center of the track. The height of the wall is 0.2 m (0.66 ft) above the level of the adjacent track's lower rail.

High-speed rail bridges shall be designed and constructed in such a way that in the event of a derailment, the resulting damage to the bridge will be minimal. Overturning or collapse of the structure as a whole shall not be allowed, but local damage could be tolerated. At least two design situations shall be considered for derailment on bridges:

1. Derailment with the derailed vehicles remaining in the track area
2. Derailment with the vehicles remaining balanced on the edge of the bridge

For through and semi-through type bridges, the impact from the derailed train shall be considered for all structural elements that are within 5.0 m (16.4 m) of the track centerline. In addition, through truss type bridges shall be designed such that the sudden rupture of one vertical or diagonal member of the truss will not cause collapse of the structure.

8.2.6.2 Trackwork

Both ballast track and ballastless track has been used for high-speed rail. In general, ballast track has the advantage of lower initial cost, shorter construction period, and easier adjustment if needed. But ballast track requires frequent maintenance and thus the maintenance cost will be higher. On the other hand, slab track requires higher initial investment and construction speed is much slower. It also has limitations on the adjustment. However, slab track is basically maintenance free other than regular

inspection. Therefore, most recent high-speed rail systems have adopted the slab track system because of lower lifecycle cost.

The interface requirements for the track shall be developed before the design of bridge is carried out. The interface related to track includes the following:

- Type of track form
- Weight of track
- Stiffness of track
- Turnout and switch locations
- Fixing between track and deck
- Locations of horizontal curves as well as the vertical curves
- Radius of the curves and required cants

8.2.6.3 System-Wide Interface

8.2.6.3.1 Power Supply Facilities

The main components of the power supply system are the overhead catenary line (OCL), the bulk substations (BSS), paralleling points (PP), sectioning points (SP), and the power supervisory control and data acquisition (SCADA) system.

Interface for design for bridges related to power supply facilities are mainly the overhead catenary system, facilities required to feed in the power from BSS and cable connections to the PP and SP, transformers to be located on the bridge, and cables required for the SCADA system. Detailed requirements will depend on the system adopted and shall be defined by the project owner or provided by the core system supplier.

In general, an overhead catenary system will be laid out by sections (between 1000 to 1500 m) and with a neutral zone between the sections. Each section will have catenary poles to support the catenary suspension system and a tensioning system for the suspended catenary cables.

Pole foundations shall be properly designed to minimize the deflection under different loading conditions that may impact the performance of overhead catenary system. Required plinths with preembedded anchor bolts or other facilities for the erection of catenary poles on bridges shall be identified.

8.2.6.3.2 Signaling and Communication Facilities

Many signaling and communication devices or equipment will be installed on the bridges. The requirements such as spacing, locations, weight, embedded conduits, and fixing details shall be defined by the project owner or system supplier. Design of the bridge shall consider the impact of this equipment and the required foundations provided as required. This equipment will include but is not limited to the following:

- Feed-in device (FID) equipment cases
- Disaster warning systems and location cases
  - Equipment for handling strong winds, heavy rain, floods (track level), and earthquake
- Emergency phones
- Hot box detectors
- Dragging detectors
- Track crossing devices
- Emergency train stopping buttons
- Protection switches
- Intrusion detection devices
- Broken-rail detection equipment
- Route and block markers
- Worker protection equipment
  - Zone elementary protection equipment
  - Block section protection equipment

  - Tunnel elementary protection equipment
  - Locking cancellation switch
- Antenna masts
- Embedded cableways

8.2.6.3.3 Wayside E&M Services

Requirements for wayside E&M service shall be defined by the project owner or provided by the supplier. Equipment includes but is not limited to the following:

- Lighting on bridges, at viaduct/bridge emergency access, and egress locations
- Power receptacles
- Emergency exit signs
- General signage
- Emergency telephones
- Intruder alarm systems at emergency exit
- Fire services provisions
- Power supply for all wayside E&M services
- Earthing/grounding and bonding requirements for all wayside E&M services

8.2.6.3.4 Miscellaneous

1. Cable troughs
   Cable troughs are required along each side of the high-speed rail mainline to carry the signaling, power, and communications cables required to operate the high-speed rail. Required dimensions shall be defined by the project owner or provided by the E&M system supplier.

   If the covers of the cable trough are considered to form part of the walkway surface, the cable trough covers shall be designed for the minimum live load in accordance with the project-specific requirements. As the cable troughs will also act as part of the emergency walkway, they shall provide an even, stable walking surface without creating a tripping hazard and have a nonslip surface.

   Connection boxes with adequate space shall be provided at 600 m intervals (or determined by the project owner or cable supplier), and be nearby the signaling FID cases. All cable troughs and connection boxes shall be drained.

   The cable trough cover shall be physically fixed to the cable trough or shall have sufficient weight to prevent it from blowing away because of suction caused by the passing high-speed vehicle.
2. Earthing and bonding provisions
   Normally, a high-speed rail system will be an AC electrified railway with an overhead catenary, where the running rails, negative feeders, earth wires, and dedicated reinforcement in structure are to be used as the traction current return path. Also the earthing and bonding requirements are necessary for other electrical systems to ensure:
   - The safety of passengers and operating personnel from electrical shock
   - That there is minimum electromagnetic interference between electrical systems
   - That the effects of electrolytic corrosion arising from outside DC stray currents are minimized

   Detailed requirements for earthing and bonding shall be defined by project owner or in accordance with the local regulation. In general, a bridge shall be built with a earthing system providing earthing terminals for electrical equipments and metallic components.
3. The earth electrode rods shall be installed in the ground and connected to the reinforcement of foundation. The number of electrode rods shall depend on the earth resistance.
4. The reinforcement of the foundation and pile caps shall be electrically connected to the reinforcement of the column and the bridge girder.

5. Dedicated welded rebars or copper wire shall be used. Number of dedicated rebars or size of copper wire shall depend on the required conductivity capacity.
6. Welded connection shall be made between the reinforcements and dedicated rebars in pile cap and column.
7. Electrical connection by cable between earthing points of column and girder shall be provided if monolithic construction is not used.
8. Earthing point terminals shall be provided on the column, at base of girder, and on top of the bridge deck. The number of terminals provided shall be defined by the project owner.

8.3 Planning

The objective of the design is not only to satisfy all the project requirements to be fit for the purpose of high-speed rail operation, but also to produce the most economic design with the lowest lifecycle cost. Therefore, good planning is the key to achieve this objective.

8.3.1 Material

Modern construction of bridges normally uses reinforced concrete, prestressted concrete, or steel. The choice depends on availability of materials, construction period, cost of construction, or preference of project owner and engineer. In general, prestressed concrete has been adopted for high-speed rail bridges in most recent projects, except bridges with shorter spans where reinforced concrete is used or longer span lengths where steel is used. However, even if steel construction is used, reinforced concrete deck is still required.

Although there is no preference technically for the material used, the engineer shall carefully evaluate the performance under various loadings such as seismic load, dynamic effects, fatigue, noise, and so on. Durability and maintainability such as cracking and corrosion protection shall also be considered.

High-strength concrete has been developed in recent years and has proven to have better performance. Use of high strength concrete will, no doubt, have the advantage of reducing the weight of the structure and thus reduce cost. However, it may cause larger deflection under the live load, which needs to be carefully considered in design. In addition, lighter structures, especially high speed-railway bridges, that are subjected to severe impact load may have a significantly larger dynamic effect. Therefore, selection of grade of high-strength concrete shall be carefully evaluated to achieve the best results.

8.3.2 Structural Type

In general, railway bridges have normally adopted a simple span structure, mainly because of track structure interaction issues. When span length gets longer (normally up to 30–40 m [98.4 ft – 131.2 ft]), simple span structure may not be economical and a continuous bridge may need to be adopted to save materials and costs. However, a continuous bridge has a longer expansion length. The engineer must carefully evaluate track-structure interaction effect to ensure no impact to the track.

In general, a simple span bridge is easier to construct than a continuous bridge. However, a continuous bridge with monolithic type construction is more efficient in performance, especially under seismic load because the ductility is better. However, for a simple span bridge, seismic load in the longitudinal direction will be resisted by each pier uniformly, whereas for the continuous bridge, fixed supported piers have to resist all the longitudinal seismic force and movable supported pier would not be subjected to any longitudinal seismic force. For continuous bridges with longer spans, certain special devices such as a lock-up device may be considered to help to distribute the seismic force more uniformly to each pier. It should also be noted that temperature change will have larger impact on the vertical profile of the deck for the continuous bridge than the simple span bridge. In addition, if monolithic-type construction is adopted, residual vertical settlement of the foundation needs to be

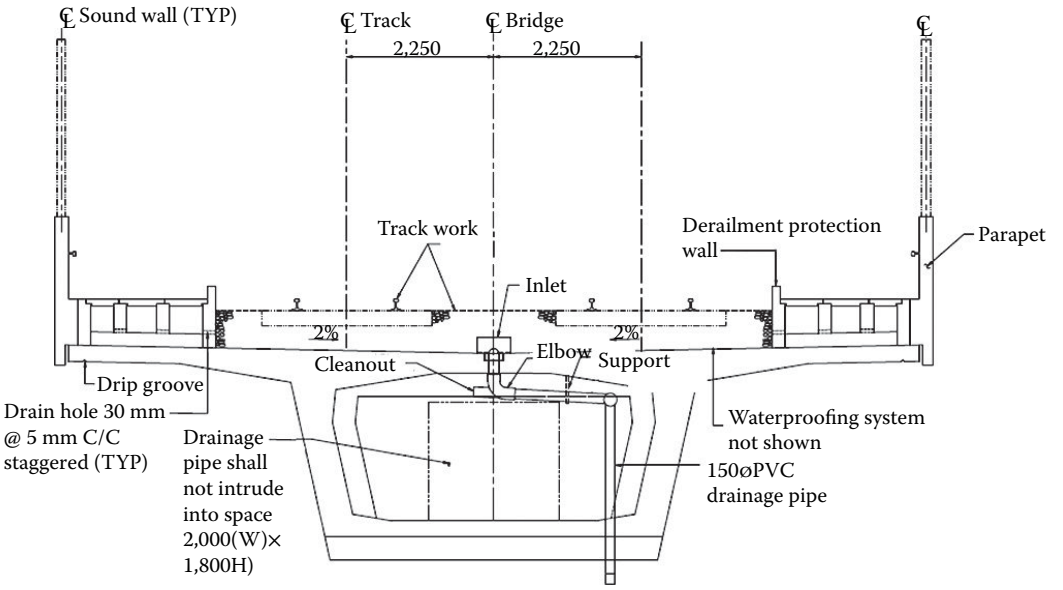

FIGURE 8.2 Typical section of viaduct.

properly controlled in the design. Otherwise, no repair other than track adjustment could be done if significant vertical settlement occurred. Therefore, the engineer shall carefully evaluate this to choose the best solution.

A unique type of bridge, mostly adopted by the Japanese SKS, is called rigid-frame structure. This is a simple space frame structure built with reinforced concrete. This type of bridge consists of a series of reinforced concrete frame units with a reinforced concrete deck in between. Each unit has 4–5 bays of columns with each bay of 8–10 m (26.2–32.8 ft) spacing and total length of 40–50 m (131.2–160.0 ft). This type of construction is easier to standardize, both in design and construction. It has had good performance during earthquakes in the past. But it would induce clearance limitations for the highways or local roads passing under it because of the small interval between columns.

There are varieties of cross sections used for modern bridge construction, especially highway bridges. However, railway bridges in general carry heavier live loads with greater impact than highway bridges and those cross sections used for a highway bridge may not necessarily be good for the railway bridge. The selection of cross sections shall be evaluated based on the necessary structural performance, functionality, safety, serviceability, maintainability, and economical and aesthetic considerations.

Prestressed concrete box girder bridges have been commonly used in most recent high-speed railway projects for its better performance mainly in terms of torsional resistance. Prestressed concrete I girders are also used in certain areas where irregular structure is required. However, torsional resistance shall be carefully considered in design. A typical box girder cross section is shown in Figure 8.2.

8.3.3 Typical Span Length

High-speed railway normally has dedicated right of way and no level crossing will be allowed for safety and security considerations. Therefore, a high percentage of high-speed railway construction is elevated viaducts/bridges except in remote areas. The cost of the bridge depends on type of structure and material adopted, considering all the technical requirements. With this long stretch of bridges, standard typical design is normally developed where it is possible to ease the construction and to be cost effective. Then, typical span length adopted is the key for the overall construction cost.

In general, shorter spans are lighter, easier to transport but require more small foundations. However, longer spans are heavier, more difficult to transport, and require fewer but larger foundations. In other words, the cost of superstructure increases with span length increases and cost of substructure decreases with span length increases. The optimized span length will be the balance point where total cost is minimum.

Although standard design with typical length is preferred to reduce the cost, it should be noted that there is a disadvantage when a series of multiple spans with same span length for a section is used. For a standard design with same span length, not only the vertical natural frequency and deflection, because creep and shrinkage for each span is identical, but also the dynamic effect and deflection response is the same when a high-speed train is passing at a constant speed. This will create a harmonic motion for a passing high-speed train in this section and resonance will occur at a certain critical speed that vertical response of bridge will be amplified. This may induce a horse-riding situation and thus a comfort issue for passengers. Therefore, riding quality shall be carefully evaluated and, if possible, two or more typical designs should be developed and the bridge should be laid out with alternate different span lengths unless the deflection is controlled to absolute minimum.

8.3.4 Construction Method

Traditionally, construction method is the choice of the contractor for an employer design contract. Whatever construction method is adopted, it is the decisive factor for the final cost and construction time. However, for a high-speed railway project with long length of bridges involving mass production, careful planning should be carried out on the project level to consider overall project cost, construction program, and construction package arrangement. Recently, many project owners have adopted a design-and-build contract approach for the infrastructure In this case, construction method to be adopted is even more important to be considered in the design.

In general, no matter what construction method is used for the superstructures, construction method for the substructure, including the piles, pile caps, spread footings, pier columns, and pier caps, will remain the same without too much difference in cost and construction time. However, choice of construction methods for the superstructure will make a big difference in terms of cost and time.

Conventionally, bridge girders are constructed by the cast-in-place method, which require temporary shoring, false work, as well as the space required for the temporary shoring and false work. Such a method is typically slow and requires large labor efforts. When mass production is required, this method is definitely not fit for schedule required, except for the special isolated case.

The advance shoring method, with self-launching shoring equipment, is one of the mature methods that could be considered for the mass production of girders. The shoring equipment could be designed to accommodate variations in span length of girders. The commonly used equipment is for single span only. However, equipment for double spans has also been used before, which will require higher cost for equipment but provide faster construction speed (2 spans at the same time). The cycle time for each span is 7–14 days. This method will be a cost-effective solution for multiple spans with lengths exceeding at least more than 2–3 km (1.24–1.86 miles). It should be noted that construction should be planned carefully if encountering a nontypical span, which has to use other method to ensure smooth construction. Otherwise, equipment has to be removed and reassembled again to skip the nontypical span.

One other method for mass production is the full span precast launching method. The girder is precast in the precast yard, lifted to the girder carry vehicle at top of bridge, transported to the site using the completed decks, and the girder launched in place. This method requires large investment for the precast yards and launching equipment, including heavy lifting cranes, girder carried vehicles, and self-launching overhead gantry. The cycle time is 1–2 span/day depending on transport distance and number of launching overhead gantry. This method will be cost-effective solution for multiple spans with lengths exceeding a certain scale (normally more than 10–12 km [6.21–7.46 miles] minimum) since the cost for such equipment and the precast yard will be offset by a shorter construction schedule.

Similarly, nontypical spans need to be planned and constructed earlier to allow the launching gantry to pass through. Otherwise, the launching operation will be interrupted and delayed.

Construction method for other nontypical span varies. The balanced cantilever method is mostly commonly adopted, especially for prestressed concrete bridges with longer span length. But these nontypical span bridges are usually considered as project-specific cases and do not have a significant impact on the overall project cost.

8.3.5 THSRP Planning

Taiwan High-Speed Rail is more than 70% elevated viaducts/bridges, with total length of 252 km (152.6 miles). The typical simple span prestressed concrete box girder bridge was used where possible (the typical box girder is shown in Figure 8.2). The typical simple span ranges between 25 and 35 m (82.0–114.8 ft). For the locations where a longer span was required to overpass the highways, conventional railway, or other obstacles, 3-spans continuous prestressed concrete girder bridges with monolithic construction were used. Typical 3-spans continuous girder bridges were 30 m + 50 m + 30 m (98.4 ft + 164.0 ft + 98.4 m), 40 m + 60 m + 40 m (131.2 ft + 196.9 ft + 131.2 ft) and 60 m + 100 m + 60 m (131.2 ft + 328.1 ft + 131.2 ft). At locations where even longer span length was required or vertical clearance was limited, steel truss bridges were used. There was a total nine steel truss bridges where the maximum span length is up to 140 m (459.3 ft).

There were 12 design and build contracts awarded for the civil works of THSRP. Among these contracts, there were seven contracts in which the scope is either all, or at least more than 20 km (12.4 miles), of viaducts/bridges. Five out of these seven contractors adopted the full-span precast launching method. The other two contractors used the advance shoring method. The typical span length selected was 30 m (98.4 ft) except two contracts where 35 m (114.6 ft) span was used.

8.4 Design Criteria

The requirements for planning and design of the bridges for high-speed rail have been presented to allow engineers to understand the overall considerations for the high-speed rail bridges. This section will provide the detailed criteria specifically for the design of high-speed railway bridges. However, most of the criteria are project-specific and may also depend on the area where high-speed railway is to be built. Therefore, criteria given in this section are the criteria used for the THSRP and are intended for reference only [2]. Project owners needs to develop their project-specific criteria.

8.4.1 Loadings

8.4.1.1 Dead Loads (D)

8.4.1.1.1 Self Weight

The self weight consists of the weight of the entire main body of the structure that is carrying the loads. The density of the various materials shall be specified by the project owner.

8.4.1.1.2 Superimposed Dead Load

Superimposed dead load shall include the weight of the components other than the main body stated above. It shall include at least, but not be limited to, waterproofing membrane, parapets, walkway, lighting, signal masts, catenary poles, noise barriers, cable troughs, sleepers and ballast or slab track as appropriate, running rails, fastening devices, track bed, and cables in the cable troughs. The unit weight of the various materials shall be specified by the project owner.

The self weight of the track shall be based on the track form either ballast track or slab track adopted for the project considering possible future variation due to maintenance. If ballast track form is used, ballast shall be considered in the following combinations with partial variable loads:

1. Double-track bridges
   a. Two tracks with full ballast
   b. Two tracks with full ballast plus 30% increase
   c. One track with full ballast plus the other track with half ballast (for transverse section design)
   d. One track with full ballast plus the other track with all ballast removed over a 15-meter length, this length being selected to give the most critical condition
2. Single-track bridges
   a. One track with full ballast or full ballast plus 30% increase

8.4.1.2 Railway Load

8.4.1.2.1 High-Speed Rail Train Loading (L)

The high-speed rail train loading shall depend on the rolling stock system adopted for the project. It also depends on the purpose of traffic intended, that is, passenger train service only or mixing traffic with both freight service and passenger train service. The design train load shall also cover the maintenance vehicle used for the project. There are well established international standards that may be adopted. However, it is up to the project owner to determine the design train loading to be used to best fit for the purpose of the project.

THSRP is intended only for the passenger service. After careful evaluation of different scenarios with different rolling stock systems, speeds, structural types with various span length, it was decided to follow the UIC standards (including impact factors) but with slight modification of the high-speed rail load, as shown in Figure 8.3.

The designer shall consider the loading arrangement cases that will produce the worst condition in terms of stress or displacement.

For structures with one or two tracks, high-speed rail train loading shall be applied to one and both tracks. For structures with more than two tracks, train loads shall be arranged as follows, whichever produces the greater stress:

1. Two tracks loaded with full train loading, the third one with 50% of train loading and all other tracks unloaded
2. All tracks loaded with 75% of full train loading

8.4.1.2.2 Nosing (Hunting) Effect (NE)

The nosing effect (the lateral force resulting from wheel-rail contact) is a concentrated load of 10 t (98.1 kN, 22 kips), applied horizontally at the top of the low rail, perpendicular to the track centerline at the most unfavorable position. This effect must be considered for elements in direct contact with rail fastenings when slab track is used. It is not applicable for the design of bridge decks with ballasted track.

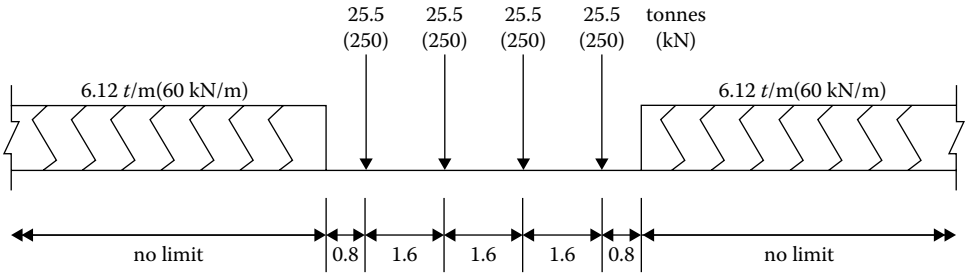

FIGURE 8.3 HSR design load.

8.4.1.2.3 Cant Effect (CE)

For structures on curved tracks, cant effect shall be considered. This effect moves the centroid of the train laterally. The effect of the cant on the ballast thickness shall be taken into account.

Three cases shall be considered:

1. Train at rest
2. Train running at 120 km/h (74.5 mph)
3. Train running at design speed

In the train-running cases, centrifugal forces shall be taken into account.

8.4.1.2.4 Centrifugal Force (CF)

For a track on curve, centrifugal force shall be considered as a horizontal load applied toward the outside of the curve at 1.8 m (5.9 ft) above the running surface. The centrifugal force shall always be combined with the vertical load.

Two cases shall be considered:

1. $V = 120$ km/h (74.5 mph)
2. $V =$ maximum design speed

When computing centrifugal force, the HSR loading shall be placed on the portion of curved track on the bridge, which is the most critical for the design of the particular part of the bridge.

Centrifugal forces and the nosing force shall be applied simultaneously for slab track structures.

For structures on curves carrying two tracks, the centrifugal forces shall be applied simultaneously with the corresponding HSR train loading to both tracks.

For structures on curves carrying more than two tracks, the centrifugal forces shall be applied simultaneously with the corresponding HSR train loading in the following two cases, whichever produces greater stress:

1. Two tracks loaded with full HSR train loadings and centrifugal forces, the third one with 50% of the HSR train loadings and centrifugal forces, and all other tracks unloaded
2. All tracks loaded with 75% of the HSR train loadings and centrifugal forces

8.4.1.2.5 Traction and Braking Forces (LF)

Traction and braking forces act at the top of the rails in the longitudinal direction of the track. They shall be considered as uniformly distributed over the influence length L of the action effect of the structural element considered.

Their characteristic values shall follow recognized international railway code or determined by the project owner.

The traction and braking forces are applicable to all types of track construction, that is, long welded rails or jointed rails, with or without expansion devices.

Traction and braking forces shall be combined with the corresponding vertical train loads.

For a double-track bridge, one track in traction and one track in braking shall be considered simultaneously.

8.4.1.2.6 Fatigue Loading

A fatigue damage assessment shall be carried out for all structural elements that are subjected to fluctuations of stress. The fatigue assessment shall follow the recognized international railway code. For structures carrying multiple tracks the fatigue loading shall be applied to a maximum of two tracks in the most unfavorable positions. The fatigue damage shall be assessed over the required structural life of 100 years.

8.4.1.2.7 Slipstream Effects from Passing Trains

For the design of the bridge structure, loading due to the slipstream effects of passing trains shall be applied to the bridge parapet and noise barrier, if any. The slipstream effect is when a structure situated near the track is subjected to a travelling wave of alternating pressure and suction due to passing of rail traffic.

Loading because of the slipstream effects of passing trains shall be considered to occur in combination with wind load W_2.

The actions may be approximated by equivalent loads at the head and rear end of the train. Study shall be carried out to determine the proper loading to be considered for different types of structure adjacent to the track and for the different configurations of the streamlined HSR rolling stock.

The loading given in the following was used for THSRP and is intended for information only:

1. Simple vertical surfaces parallel to the track
   The values of the pressure (q) are given in Figure 8.4. If the height of the trackside structure is less than or equal to 1.0 m (3.3 ft), or if the width is less than or equal to 2.5 m (8.2 ft.), the value of q shall be increased by a factor $k_2 = 1.3$.
2. Simple horizontal surface above the track

The values of the pressure (q) are given in Figure 8.5. The loaded width of the structural member under consideration extends up to 10 m (32.8 ft) either side of the centerline of the track. For trains passing each other in opposite directions the actions shall be added. Only two tracks need be considered.

8.4.1.3 Environmental Loads

8.4.1.3.1 Wind Load (W)

Bridges shall be designed to withstand a wind load of the following:

1. The maximum wind load for nonoperating condition (W_1)
   The maximum wind load considered shall follow the local code. The wind shielding area shall include the exposed area of all bridge elements. In the case of three or more tracks, one train load with wind load (W_1) on the train shall be added. The exposed area of train shall be as specified in 2.

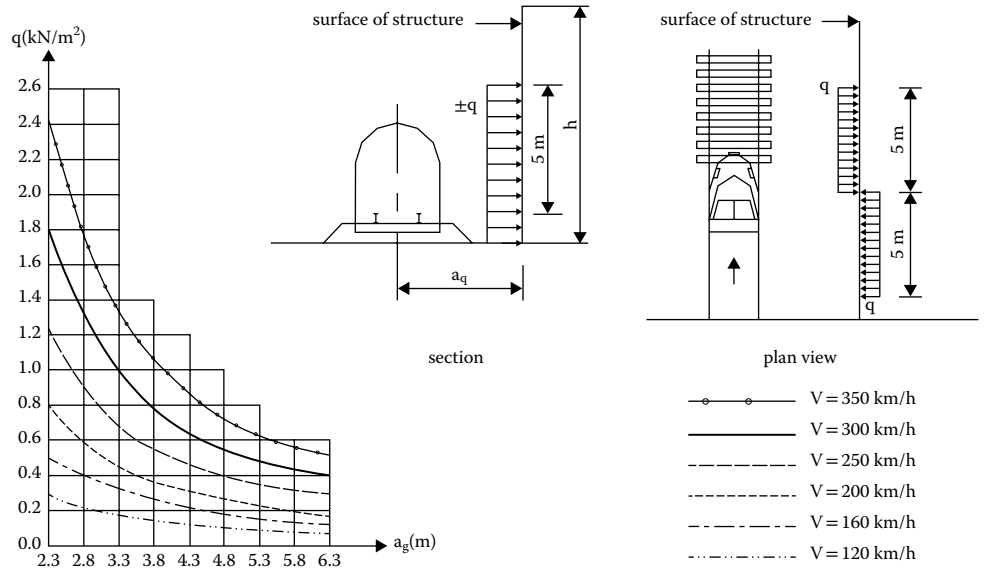

FIGURE 8.4 Slipstream effects on vertical surface.

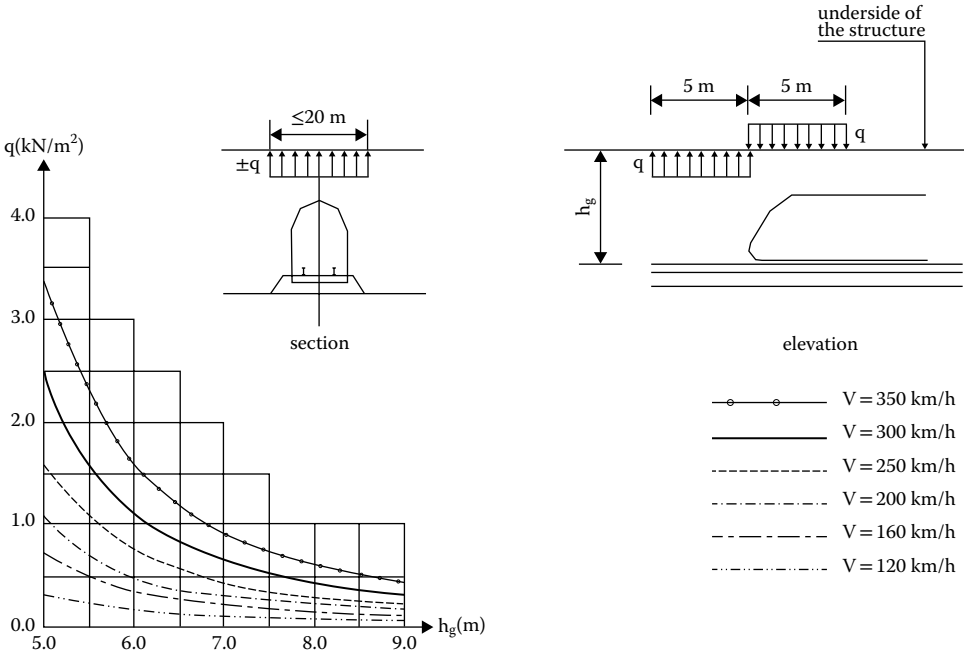

FIGURE 8.5 Slipstream effects on horizontal surface.

2. The maximum wind load under permissible operation (W_2)
   The maximum wind speed under which the operation of high-speed train is allowed shall depend on the rolling stock used and the safety regulation imposed on the high-speed train operation. The proper maximum wind load considered under the operation condition shall be determined by the project owner. Under the operation conditions, the wind shielding area shall include the exposed area of all bridge elements and the area of the trains.

   A rolling train may be considered as a box of projected area above the low rail and its length such as to produce the most critical loading condition for the design.
3. Overturning force
   In addition to the horizontal wind loads, with or without trains, there shall be an upward load applied at the windward quarter point of the transverse width of the superstructure. This vertical load considered shall follow the local bridge design code.

Wind effects on local members such as noise barriers shall be considered. Special bridges shall be given particular consideration.

8.4.1.3.2 Temperature Effects (T)

Provisions shall be made for stresses and movements resulting from temperature variations. The expected temperature rise and fall and the coefficients of thermal expansion shall follow the local condition and the material used for the bridge construction.

1. Uniform temperature change
   Bridge design shall consider any possible thermo expansion/contraction and temperature restrain force because of seasonal change of temperature. The maximum temperature range considered shall be determined from local conditions. For considering uniform temperature effects, the effective flexural rigidity the pier and foundation shall follow the local bridge design code.

2. Temperature gradients
   In the vertical direction, the temperature drops between top and bottom surfaces because of direct exposure to the sun shall be considered in design of the bridge. In the horizontal direction, the temperature difference from one edge of the bridge to the other shall also be considered. However, the horizontal temperature gradient is normally only applied to steel structures and combination of vertical and horizontal gradients need not be considered. The temperature gradient range considered shall be based on local condition.
   For THSRP, the vertical temperature gradient is considered as
   - 5°C (41°F) for bridges with ballast
   - 10°C (50°F) for bridges without ballast

   And 10°C (50°F) difference between one edge of bridge to the other is considered for the horizontal temperature gradient.

When temperature effects are considered, the effects of 1 and 2 above shall be combined.

8.4.1.3.3 Rail Force Because of Temperature (RF)

The rail-induced loads on the structure because of temperature will depend on type of track, rail fastener system, stiffness of rail, rail expansion device, variation of temperature, and layout of the bridge structure. Track–structure interaction analysis shall be carried out to determine the maximum forces to be considered for the design.

For THSRP, for the simply supported structure with a fixed point at one end, the rail force at the structure expansion end is specified as follows:

1. For ballasted track
   a. $f = \pm 0.3$ t/m/rail when there is no rail expansion device
   b. $f = \pm 50$ t/rail when there is a rail expansion device
2. For slab track
   a. $f = \pm 0.5$ t/m/rail when there is no rail expansion device
   b. $f = \pm 100$ t/rail when there is a rail expansion device

In other cases, a special analysis shall be undertaken.

8.4.1.4 Exceptional Loads

8.4.1.4.1 Collision Force from Highway Vehicles (CL)

Any pier liable to be damaged by a highway vehicle shall be designed for a force of 100 t (981 kN, 220 kips,) acting horizontally in any direction at 1.20 m (3.9 ft) above road level. For these piers, pier protection structures shall be considered and designed in accordance with the relevant design code.

Any deck liable to suffer collision from a highway vehicle shall be designed to resist a force 50 t (490 kN, 110 kips) vertically upward and 100 t (980 kN, 220 kips) horizontally applied simultaneously. These forces are applied on the bottom edge of the bridge deck in the most unfavorable position.

8.4.1.4.2 Derailment Load (DR)

High-speed rail bridges shall be constructed in such a way that in the event of a derailment, the resulting damage to the bridge will be minimal. Overturning or collapse of the structure as a whole shall not be allowed.

Two design situations shall be considered for derailment on bridges:

1. Derailment with the derailed vehicles remaining in the track area
   Collapse of any major part of the structure shall not be allowed, but local damage can be tolerated.
   For THSRP, the structure is required to be designed using load factor design with two vertical line loads each of 5 t/m (49 kN/m, 3.36 kip/ft) over a length of 6.4 m (21.0 ft) and 1.4 m (4.6 ft) apart. These loads shall be parallel to the track in the most unfavorable position inside

an area of width 1.5 times the gauge on either side of the track centerline, or as limited by any derailment containment wall.

2. Derailment with the vehicles remaining balanced on the edge of the bridge
   Overturning or collapse of the bridge shall not be allowed. For THSRP, it is required that a vertical line of 60 kN/m (4.11 kip/ft) over a length of 20.0 m (65.6 ft) to be applied on the edge of the structure.

The derailment load shall be combined with 60% of temperature load together for design of the structure. For multiple tracks bridge, the railway loads on other tracks shall be considered as appropriate if operation on other tracks is allowed.

For THSRP, derailment containment walls as a protection in case of derailment are required for all mainline at locations 2 m (6.6 ft) from the center of the track. The height of the wall is 0.2 m (0.66 ft) above the level of the adjacent track's lower rail. The walls are required to be designed for a transverse horizontal concentrated load of 15 t applied at the top of the wall and at the most unfavorable position.

8.4.1.4.3 Earthquake Loads (EQ)

The primary purpose of earthquake design is to safeguard against major failures and loss of life. The use of seismic isolation devices may be considered. The design base earthquake loads shall be in accordance with local regulations.

For THSRP, two levels of earthquake are required to be considered for the high-speed rail bridge:

1. Design for repairable damage (Type I earthquake)
   This earthquake level is the ground acceleration corresponding to a return period of 950 years, which has a 10% probability of exceedance in 100 years. Under this, earthquake structures are allowed to respond into the inelastic range with a ductility ratio not exceeding the allowable ductility demand so that all damage is repairable.
2. Design for safe operation at maximum speed and no yielding (Type II earthquake)
   The design ground acceleration for this earthquake level is equal to one-third of the maximum ground acceleration for Type I earthquake. Structures shall be designed for a serviceability limit state in which yielding of reinforcement or structural steel is not permitted under Type II earthquakes.
   Displacement of the deck shall be checked to ensure that it remains within the allowable values for this type of earthquake so that trains can brake safely to a stop from the full design speed of 350 km/h (217.5 mph).

The capacity design procedure shall be used for bridges of ductile behavior. This is to ensure the hierarchy of strengths of the various structural components necessary for leading to the intended configuration of plastic hinges and for avoiding brittle failure modes. With this procedure, the bridge can be designed so that a dependably stable plastic mechanism can form in the structure through the formation of flexural plastic hinges, normally in the piers. The foundation shall be designed for the plastic moment capacity of the pier such that the damage of the structure will always be above the foundation at a plastic-hinge location. The location of plastic hinges shall be at points accessible for inspection and repair. In general, the bridge deck shall remain in the elastic range.

Regular viaduct/bridges may be analyzed by the equivalent static analysis method. Bridges that are irregular shall be analyzed with dynamic analysis methods, multi-model response spectrum analysis, or time history analysis.

A regular viaduct/bridge has six or fewer spans, no abrupt or unusual changes in mass, stiffness or geometry, and no large changes in these parameters from span to span or pier to pier. Lengths of viaduct/bridge with more than six simply supported spans may be considered to be regular, provided that the maximum pier stiffness ratio (including foundation stiffness) from span to span is not > 2. Any viaduct/bridge not satisfying these requirements shall be considered to be irregular.

For long viaducts, it is recommended that the bridge model shall consist of at least eight spans in addition to the boundary spans and/or an abutment. Each multi-span analytical model should be overlapped

by at least one useable span from the proceeding model. Boundary spans are end spans modeled on either side of the bridge section from which element forces or joint displacements are of interest. They serve as redundant spans in the sense that analytical results are ignored. The use of at least one boundary span coupled with mass-less springs at the "dead" end of the model is recommended.

A combination of orthogonal horizontal seismic forces with vertical seismic force shall be used to account for the directional uncertainty of earthquake motions and the simultaneous occurrences of earthquake forces in three perpendicular directions. The method of combination shall be based on local code.

To prevent bridge girder from falling off the abutment or pier table, the minimum distance between the girder end and the edge of the supporting substructure shall be provided following the local code. In addition, the length of support provided must accommodate displacement resulting from the overall inelastic response of the bridge structure, possible independent movement of different parts of the substructure, and out of phase rotations of piers resulting from travelling surface wave motions. As an alternative, set-up to prevent loss-of-span failure may be used that may consist of shear key arrangement, buffers, dampers, and/or linkage bolts or cables. Friction connections are not acceptable. Hold-down devices shall be provided at all supports or hinges, where the vertical seismic force opposes and exceeds 50% of the dead load reaction.

To warrant the formation of plastic hinges in a Type I earthquake to dissipate energies of the earthquake without any brittle failure modes such as shear failure, member design such as shear design of column, and strength design of foundation members shall be based upon internal forces resulting from the formation of plastic hinges in the columns.

8.4.1.5 Other Loadings

Other loadings such as earth pressure, buoyancy, stream flow, creep and shrinkage, live load on walkway, loads from maintenance gantry if any, construction loads, and so on are not given here. These loads shall be either based on relevant local codes or defined by the project owner as appropriate. Loading from E&M equipment shall be based on system design and obtained from system suppliers or defined by the project owner.

8.4.2 Load Combinations

A variety of loads can be applied to a structure at the same time. Different scenarios need to be considered properly to ensure the structure is safe under normal condition or extreme condition. In general, various recognized international codes provide basic consideration for load combinations, which can be referenced or used. However, the project owner must review carefully to ensure project-specific requirements have been properly covered.

Load combinations to be considered also depend on the design methods used, that is service load design or load factor design. The following are the load combinations used for the THSRP project. The groups represent various combinations of loads and forces to which a structure may be subjected. Each component of the structure shall be considered with the group of loads that produces the most critical design condition.

8.4.2.1 Service Load Design

		% Allowable Stress
Group I	$D + L + I + CF + E + B + SF$	100
Group II	$D + E + B + SF + W_1$	125
Group III	Group I $+ W_2 + LF + F$	125
Group IV	Group I $+ OF + T$	125
Group V	Group II $+ OF + T$	140
Group VI	Group II $+ OF + T$	140
Group VII	$D + E + B + SF + EQ_{II} + L_1 + LF_1$	125
Group VIII	Group I + additional or reduced ballast	125

where

D = Dead load + superimposed dead load (SDL)
L = Live load (modified UIC train loading)
I = Impact
L_1 = One train live load
I_1 = Impact for one train
CF = Centrifugal force
CF_1 = One train centrifugal force
E = Earth pressure
B = Buoyancy
SF = Maximum design base stream flow
SF_1 = Stream flow with 1 year return period
W_1 = Maximum wind load for nonoperation condition
W_2 = Maximum wind load under permissible operation (including slipstream effects from passing trains)
LF = Longitudinal force from live load (braking and acceleration forces)
LF_1 = Longitudinal force from one train live load (braking)
F = Longitudinal force because of friction or shear resistance at expansion bearings
OF = Other forces (shrinkage (SH) and creep (CR), settlement of supports, nosing, rail force (RF), loads from maintenance gantry and increase in SDL because of ponding)
EQ_I = Type I earthquake
EQ_{II} = Type II earthquake
T = Temperature effects (including uniform temperature change and temperature gradient)
DR = Derailment load case
CL = Collision force highway vehicle to pier

8.4.2.2 Load Factor Design and Load Combination

Group I	1.4 (D + 5/3(L +I) + CF + E + B + SF)
Group II	1.8 (D + L + I + CF + E + B + SF)
Group III	1.4 (D + E + B + SF + W_1)
Group IV	1.4 (D + L + I + CF + E + B + SF + W_2 + LF + F)
Group V	1.4 (D + L + I + CF + E + B + SF + T + OF)
Group VI	Group III + 1.4 OF + 1.4T
Group VII	Group IV + 1.4 OF + 1.4T
Group VIII	1.3 (or 0.9*) (D + E + B) + L_1+ EQ_I + SF_1
Group IX	D + L + 0.6T + DR
Group X	D + L + 0.6T + CL

8.4.2.3 Deflection Control

The vertical and lateral angular deformation of the HSR structures shall be checked for running safety under the following loading combinations:

Group I	L + I + CF + SF
Group II	L_1 + I_1 + CF_1 + SF + W_2
Group III	L_1 + I_1 + CF_1 + EQ_{II}

The allowable angular changes are given in Table 8.1

The deck relative displacement in the longitudinal direction shall be checked for running safety under the following loading combinations:

Group IV	L + I + LF
Group V	L_1 + I_1 + LF_1 + EQ_{II}

TABLE 8.1 Allowable Angular Change

Span m (ft)	Vertical Angle (θ/1000)	Horizontal Angle (θ/1000)
10 (32.8)	1.7	1.7
20 (65.6)	1.7	1.7
30 (98.4)	1.5	1.7
40 (131.2)	1.3	1.3
≧50 (164.0)	1.3	1.3

For normal operation (Group IV) and under Type II earthquake (Group V), the relative displacement between bridge decks, or between deck and abutment, shall be 7 mm and 25 mm, respectively.

For passenger comfort, considering one train of modified UIC loading with impact factor, the deflection of the bridge shall be less than the allowable, as given in the following:

Δ = maximum deflection of the bridge with 1 train on the bridge
L = span length in meters
L_T = total bridge/viaduct length (from abutment to abutment)

	Span/deflection ratio L/Δ
	$15 \le L \le 120$ m
1 to 5 spans	2200
5 spans and $L_T < 800$ m	$\dfrac{2200}{\left(\dfrac{5\times L+167}{L_T+167}\right)^{1/2}}$
$L_T \ge 800$ m	$\dfrac{2200}{\left(\dfrac{5\times L+167}{967}\right)^{1/2}}$

Under dynamic condition, deformations of the structure because of the passing train at high speed shall be less than the criteria given below. The dynamic analysis of structure under the action of actual moving train load with different speeds shall be carried out to determine the dynamic response. Only one train needs to be considered.

1. Vertical acceleration of the bridge ≤ 0.35 g
2. The variation of cant induced ≤ 0.4 mm/m by transverse rotation of the bridge (upon a base of 3 m longitudinally)
3. End rotations of bridge at the expansion join shall not exceed

$$\theta = \left[\frac{8\times10^{-3}}{h(\text{m})}\text{radians}\right] \text{ for transition between the deck and abutment}$$

$$\theta_1 + \theta_2 = \left[\frac{8\times10^{-3}}{h(\text{m})}\text{radians}\right] \text{ between two consecutive decks with same girder height}$$

$$\theta_1 + \theta_2 = \left[\frac{4\times10^{-3}}{h_1(\text{m})}\text{radians}\right] + \left[\frac{4\times10^{-3}}{h_2(\text{m})}\text{radians}\right] \text{ between two consecutive decks}$$

with different girder height

where

h (m) the distance between the top of rail and the center of the bridge bearing
h_1(m) the distance between the top of rail and the center of the first bridge bearing
h_2(m) the distance between the top of rail and the center of the second bridge bearing

8.4.3 Other Considerations

8.4.3.1 Bearings

Pot bearings shall be used for structures supporting the HSR main line. Elastomeric bearing may be considered elsewhere where permitted by the appropriate design requirements.

Bearings shall comply with the Eurocode design, testing, and installation specification. Cast iron and cast steel shall not be used for the pot and piston of bearings. The pot wall and base shall be monolithic. Welded and bolted fabrication of the pot shall not be allowed. Bearings carrying vertical load shall be installed in a horizontal plane.

Fixed bearings may be used in combination with other methods of restraint, such as shear keys or stoppers, to carry the Type I earthquake forces. Hold-down devices shall be provided at all supports or hinges where the vertical seismic force opposes and exceeds 50% of the dead load reaction.

Bearings shall be replaceable at any time during the life of the structure without any interference with the train operation. Access for jacking superstructures for replacing bearings shall be considered. The aging of bearings shall be taken into account for pier design. For elastomeric bearings, a 50% increase of stiffness shall be used to account for aging and low-temperature effect.

8.4.3.2 Structural Expansion Joints

Structural expansion joints shall be provided to accommodate the longitudinal movements of the bridge and to prevent overstress in the rails. Structural design shall interface with the trackwork design to ensure that structure arrangement is compatible with trackwork requirements. Maximum allowable displacement of expansion joints shall be determined in accordance with track work requirements. The designer shall verify the actual displacement required. If the actual displacement is larger than this maximum, the trackwork designer shall be consulted and a special design shall be provided.

The design of structural expansion joints shall provide free movement space in the bridge longitudinal direction for creep, shrinkage, temperature variation, braking and acceleration, and Type II earthquake. It shall also provide enough space between two adjacent structures to prevent unbuffered impact between them during a Type I earthquake.

A turnout or a crossover shall not be placed over any structure expansion joint. In THSRP, the minimum distance between the structural movement joint and the switch point end of the turnout shall be

- 10 m (32.8 ft), if the structural expansion length is < 60 m (196.9 ft)
- 20 m (65.6 ft), if the structural expansion length is between 60 m (196.9 ft) and 90 m (295.3 ft)
- 25 m (82.5 ft), if the structural expansion length is between 90 m (295.3 ft) and 100 m (328.1 ft)

The sizes and locations of the turnout shall be determined by the project owner based on operation requirements.

8.4.3.3 Special Requirements

1. Prestressing
   For prestressed bridges with continuous spans, the structure shall be arranged such that additional longitudinal prestressing may be added in the future. This additional prestress shall be 15% of the designed prestress, and shall be in the form of external tendons for which spare anchorages and deviator blocks shall be provided.

2. Truss Bridge
   For through and semi-through-type bridges, collision from high-speed rail train should be considered for all structural elements that are within 5.0 m (16.4 ft) of the track centerline. For through truss-type bridges, design shall consider that the sudden rupture of one vertical or diagonal member of the truss shall not cause collapse of the structure.
3. Box girder
   For the design of the side cantilevers of a prestressed concrete box girder box cross section, an additional factor of 20% shall be added to the dead loads on the slab overhang to account for dynamic effects.
4. Drainage
   Bridge and viaduct decks shall be designed to provide both longitudinal and transverse drainage.

   Rainwater shall be collected by a system of deck surface falls, inlets, longitudinal and transverse drains, and downspouts as necessary to ensure that ponding depths do not exceed the maximum allowed by the trackwork design.

   Inlets, gratings, drains, and downspouts shall be rigid and rattle proof and made of noncorrosive material. They shall be maintainable and replaceable throughout with minimum interruption to train operations and shall be provided with suitable cleanouts and splashbacks.

   Movement joints shall be provided in pipes to accommodate corresponding movements in the structure and these joints shall be waterproof and maintainable.
5. Noise Barrier
   Design for noise barriers shall be capable of resisting the wind load W_1. In addition, the noise barriers shall also be capable of resisting the slipstream effects from passing trains combined with wind loads (W_2). The actual height of the noise barrier required shall be determined by a noise level control study.
6. Maintenance
   Special care shall be taken in the design in order to reduce maintenance requirements to an absolute minimum.

Access arrangements for maintaining all exterior surfaces or equipment attached thereto shall be considered. Access openings shall be provided for inspection and maintenance in the bottom slabs of box girders close to the piers. The interval and size of the opening shall be based on the maintenance requirements as determined by the project owner. At locations where access from the ground beneath is considered impractical, access to the inside of box girder decks shall be provided at abutments. A minimum opening shall be provided through box girder at diaphragms over all piers to allow a continuous walkway inside the box girder along the bridge.

If a pier is not accessible from the ground beneath, such as river crossing bridge, access opening shall be provided in the bottom slab of box girders so that the pier top can be reached from the inside of the box girder. If necessary a work platform shall be provided at the pier top for the maintenance of bearings.

A lifting hook shall be embedded in the underside of the superstructure top slab above each access opening if required by the maintenance. The requirements of the lifting hook shall be in accordance with the maintenance plan.

References

1. BSHSR. 2011. http://baike.baidu.com/view/141756.htm (In Chinese).
2. THSRC. 2000. *Taiwan High Speed Rail Project Civil Work Contract Documents: Volume 9 – Design Specifications*, Taiwan High Speed Rail Corporation, Taipei, Taiwan.

9

Structural Performance Indicators for Bridges

Dan M. Frangopol
Lehigh University

Duygu Saydam
Lehigh University

9.1 Introduction

Performance of bridge structures is highly affected by the time-dependent deterioration processes associated with aggressive environmental conditions (e.g., corrosion) and aging of the materials they are composed of. In order to avoid the consequences of structural failures, maintenance programs are carried out by the responsible authorities. It is necessary to predict the lifecycle performance of bridge structures accurately to establish a rational maintenance program. However, the prediction of lifecycle performance involves difficulties because of the complexity and uncertainties in loading and deterioration processes. Consequently, it is important to use proper indicators to evaluate the structural performance of bridges.

Significant research has been done on quantifying structural performance with deterministic and probabilistic indicators such as safety factor and reliability index, respectively. Recent bridge design codes consider uncertainty by including specific factors in the computation of structural resistance and load. However, the prediction of time-dependent bridge performance under uncertainty may require the use of several performance indicators. For example, system reliability measures (i.e., system probability of failure, system reliability index) are adequate for quantifying the safety of a structure

with respect to ultimate limit states, but the system redundancy index is required to evaluate the availability of warning before system failure. Moreover, performance indicators related to damage tolerance of structures, such as vulnerability and robustness are essential to consider for bridges under deterioration and local damage together with the indicators related to system safety. In order to provide acceptable safety levels of bridges, the values of performance indicators under consideration should not violate predefined threshold levels. However, lifecycle cost of a bridge structure is another measure that decision makers have to balance with the performance indicators. Nevertheless, it is evident that evaluating bridge performance requires considering multiple indicators simultaneously.

In this chapter, a review of structural performance indicators that can be used to evaluate the performance of bridge structures and methods of assessing structural performance is presented. The techniques of bridge performance evaluation are presented. The methods of establishing safety levels in bridge design codes are briefly summarized. The formulation of bridge performance indicators and several associated references are introduced. These indicators are categorized under four main groups being performance indicators regarding: (1) condition, (2) safety, (3) damage tolerance, and (4) cost. Finally, the role of inspection and structural health monitoring (SHM) on updating bridge performance assessment and prediction is discussed.

9.2 Levels of Performance Evaluation of Bridge Structures

Performance of bridge structures can be quantified at cross-section level, member (component) level, overall structure (system) level, and group of structures (network) level. The strength of a bridge component under different loading conditions can be expressed in terms of the capacity of its most critical cross-section when stability problems are not considered. Under consideration of stability problems, the performance is quantified at member level. In most of the current bridge design codes, strength requirements are based on component strength. Although such an approach may ensure an adequate level of safety of components, it does not provide the information about the overall performance of the bridge. However, performance at system level is of concern in performance-based design. Structural reliability theory offers a rational framework for quantification of system performance by including the uncertainties both in the resistance and the load effects and correlations. In this section, the very basics of probabilistic performance analysis (e.g., reliability analysis) of bridge structures at component level and system level are presented.

9.2.1 Component-Based Approach

Performance evaluation of bridge cross-sections, bridge members, and bridge structures is based on limit states defining the failure domain (FD) under specific loading conditions. The limit states defining the failure modes of components are included in design codes. The factors multiplying the load effects and nominal strength exist to ensure a predefined safety level of the component. However, if the purpose is to evaluate the performance of an existing bridge structure or design a bridge for different target performance levels, the equation defining limit states must be in the pure form. A general representation of a limit state that is used in reliability analysis in terms of a performance function $g(\mathbf{X})$ can be expressed as

$$g(\mathbf{X}) = g(X_1, X_2, ..., X_n) = 0 \tag{9.1}$$

where $\mathbf{X} = (X_1, X_2, \ldots, X_n)$ is a vector of random variables of the system, and the performance function $g(\mathbf{X})$ determines the state of the system as $[g(\mathbf{X}) > 0]$ = "Safe state," and $[g(\mathbf{X}) < 0]$ = "Failure state." For instance, the limit state for the mid-span (positive) flexural failure of a composite bridge girder can be expressed as

$$g_{\text{flexure+}} = R - L = M_{\text{u}} - (M_{\text{DLNC}} + M_{\text{DLC}} + M_{\text{LL+I}}) = 0 \tag{9.2}$$

where R and L are the resistance and load effect, respectively, and M_u, M_{DLNC}, M_{DLC}, and M_{LL+I} are the ultimate moment capacity, moment due to noncomposite dead loads, moment due to composite dead loads, and moment due to live load including impact, respectively.

9.2.2 System-Based Approach

Overall bridge performance with respect to the occurrence of a failure mode can be evaluated by modeling the bridge system failure as series or parallel or series–parallel combination of bridge component limit states (Hendawi and Frangopol, 1994). The FD, representing the violation of bridge system limit state can be expressed in terms of bridge component limit states as (Ang and Tang, 1984) the following:

1. For series system

$$FD \equiv \bigcup_{k=1}^{n} \{g_k(X) < 0\}$$

2. For parallel system

$$FD \equiv \bigcap_{k=1}^{n} \{g_k(X) < 0\}$$

3. For series–parallel system

$$FD \equiv \bigcup_{k=1}^{n} \bigcap_{i=1}^{c_n} \{g_{k,j}(X) < 0\}$$

where c_n is the number of components in the nth cut set.

In Figure 9.1, a simplified model for system reliability analysis of a bridge superstructure for flexural failure mode is illustrated. According to this model, the system failure will occur if slab fails, or any two adjacent girders fail, or both slab and any two adjacent girders fail. Therefore, the failure of two adjacent girders together is a parallel combination of the failures of two girders separately. The failure of slab and the failures of any two adjacent girders are in series since either yields system failure.

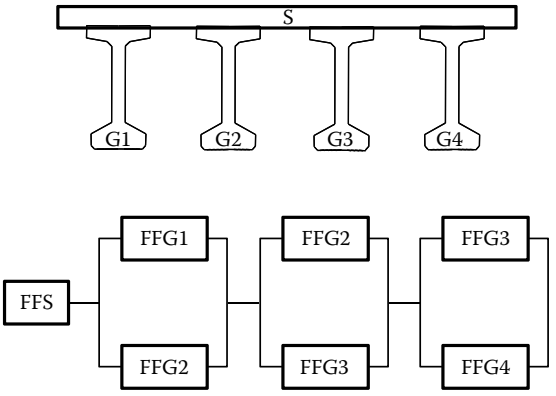

FFS : Flexural failure of slab
FFG1: Flexural failure of girder 1
FFG2: Flexural failure of girder 2
FFG3: Flexural failure of girder 3
FFG4: Flexural failure of girder 4

FIGURE 9.1 Bridge superstructure series-parallel system model for flexure.

The performance of a system, which consists of a number of subsystems, depends not only on the performance of the subsystems but also on the interaction among these subsystems. An example of a system of systems is a highway bridge network, where each bridge is a system itself and interacts with the other bridges for the performance of entire network by means of traffic flow.

9.3 Methods of Establishing Safety Levels

In the 1930s, when American Association of State Highway Officials (AASHO) started publishing the Standard Specifications for Highway Bridges, only one factor of safety was used to ensure adequate safety level of structural members. The design philosophy was called working stress design (WSD) or allowable stress design (ASD). Until early 1970s, WSD was embedded in the Standard Specifications. American Association of State Highway and Transportation Officials (AASHTO) adjusted WSD to reflect the variable predictability of certain load types by varying the factor of safety in 1970s. The design philosophy is called load factor design (LFD). WSD and LFD are embedded in the current edition of Standard Specification. Today, bridge engineering profession has moved toward a more rational methodology, called load and resistance factor design (LRFD), which accounts for the uncertainties in the structural resistance as well as the uncertainties in loads and their effects.

9.3.1 Working Stress Design

WSD establishes allowable stresses as a fraction or percentage of a given material's load-carrying capacity, and requires that calculated design stresses not exceed those allowable stresses. The limiting stress, which can be yield stress or stress at instability or fracture, is divided by a factor of safety to provide the allowable stress. The factor of safety is used to provide a design safety margin over the theoretical design capacity to allow for some consideration of uncertainties The condition of safety with respect to the occurrence of a specific failure mode including the factor of safety can be written as

$$\frac{R_n}{FS} \geq \sum Q_i \tag{9.3}$$

where R_n is the member nominal resistance, FS is the factor of safety, and Q_i is the load effect. The advantage of WSD is its simplicity. However, it lacks the adequate treatment of uncertainty. Factor of safety is not based on reliability theory and is chosen subjectively by the code writers. Furthermore, the stresses may not be a good measure of resistance.

9.3.2 Load Factor Design

In LFD, different types of loads have different load factors accounting for the uncertainties in these loads. The condition of safety with respect to the occurrence of specific failure mode including the load factors can be written as

$$R_n \geq \sum \gamma_i Q_i \tag{9.4}$$

where γ_i is the load factor. Even though LFD is more complex than WSD, it does not involve safety assessment based on reliability theory.

9.3.3 Load and Resistance Factor Design

Although considered to a limited extent in LFD, the design philosophy of LRFD takes uncertainty in the behavior of structural elements into account in an explicit manner. Load and resistance factors are used for design at cross-section and component levels. LRFD suggests the use of a resistance factor and

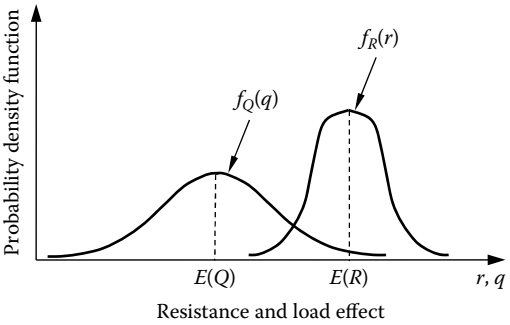

FIGURE 9.2 Probability density functions of resistance and load effect.

partial load factors to account for the uncertainties in the resistance and the load effect. The partial load factor approach was originally developed during the 1960s for reinforced concrete structures. It gives the opportunity for live and wind loads to have greater partial load factors than the dead load because of the fact that live loads and wind loads have greater uncertainty. The condition of safety with respect to the occurrence of specific failure mode including the reduced resistance and factored loads using resistance and partial load factors can be expressed as

$$\varphi R_n \geq \eta_i \sum \gamma_i Q_i \tag{9.5}$$

where φ is the resistance factor and η_i is the load modifier (AASHTO, 2012).

LRFD is based on the ultimate strength of critical member cross-sections or the load carrying capacity of members (Ellingwood et al., 1980). In LRFD, the resistance R and the load effect Q are usually considered as statistically independent random variables. If the resistance R is greater than the load effect Q, a margin of safety exists. However, since resistance and load effect are random variables, there is a probability that resistance is smaller than load effect. This probability is related to the overlap area of the frequency distributions of the resistance and load effect and their dispersions. Figure 9.2 illustrates the probability density functions (PDFs) of the resistance and load effect. In this figure $E(Q)$ and $E(R)$ represent the mean values of load effect and resistance, respectively.

9.4 Performance Indicators for Bridges

9.4.1 Performance Indicators Regarding Condition

The conditions of bridges in the United States are rated using two different methods based on visual inspection. The first method is using National Bridge Inventory (NBI) condition rating system (FHWA, 1995). According to NBI condition rating system, the evaluation is for the physical condition of the deck, superstructure, and substructure components of a bridge. The second method, Pontis (Cambridge Systematics, Inc, 2009), uses the element-level condition rating method to describe the conditions of bridges.

9.4.1.1 NBI Condition Ratings

Condition codes are properly used if they provide an overall characterization of the general condition of the entire component being rated. Conversely, they are improperly used if they attempt to describe localized damage. Correct assignment of a condition code should consider both the severity of the deterioration and the extent to which it is widespread throughout the component being rated. The load-carrying capacity of the structure has no influence on the condition ratings. NBI condition rating describes the conditions of bridge deck, superstructure, and substructure using a scale of 0–9

TABLE 9.1 NBI Condition Ratings for Deck, Superstructure, and Substructure

Code	Description
N	Not applicable
9	Excellent condition
8	Very good condition—no problems noted
7	Good condition—some minor problems
6	Satisfactory condition—structural elements show some minor deterioration
5	Fair condition—all primary structural elements are sound but may have minor section loss, cracking, spalling, or scour
4	Poor condition—advanced section loss, deterioration, spalling, or scour
3	Serious condition—loss of section, deterioration, spalling, or scour have seriously affected primary structural components
2	Critical condition—advanced deterioration of primary structural elements. Unless closely monitored it may be necessary to close the bridge until corrective action is taken
1	"Imminent" failure condition—major deterioration or section loss present in critical structural components or obvious vertical or horizontal movement affecting structure stability
0	Failed condition—out of service—beyond corrective action

Source: Adapted from FHWA, Report No. FHWA-PD 96-001, U.S. Department of Transportation, Washington, DC, 1995.

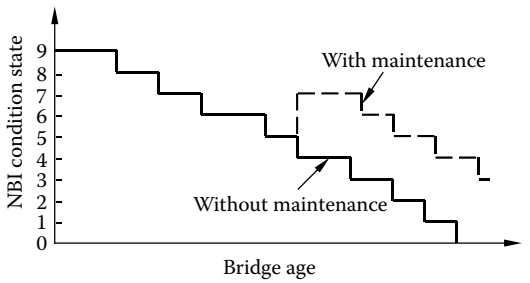

FIGURE 9.3 Lifetime profiles for NBI condition states.

(FHWA, 1995). These condition states are described in Table 9.1. The typical lifetime condition state profiles with and without maintenance activities, for a bridge structure, are presented in Figure 9.3. A highway bridge is classified as structurally deficient if the deck or superstructure or substructure has a condition rating of 4 or less in the NBI rating scale.

9.4.1.2 Pontis Condition Ratings

Pontis (Cambridge Systematics, Inc, 2009) is a bridge management system that assists transportation agencies in managing bridge inventories and making decisions about preservation and functional improvements for their structures. Based on visual inspection, Pontis assigns condition states for various bridge components among deck, superstructure, and substructure (CDOT, 1998). The condition states vary between 1 and 5 (or 4), with increasing condition state indicating higher damage level. To illustrate, the condition states for an open, painted steel girder are provided in Table 9.2. Applications of Pontis condition rating to bridges can be found in Estes and Frangopol (2003), Al-Wazeer (2007), and Saydam et al. (2013b)

TABLE 9.2 Pontis Condition Ratings for Open, Painted Steel Girder Element

Condition State	Description
1	There is no evidence of active corrosion and the paint system is sound and functioning as intended to protect the metal surface.
2	There is little or no active corrosion. Surface or freckled rust has formed or is forming. The paint system may be chalking, peeling, curling, or showing other early evidence of paint system distress, but there is no exposure of metal.
3	Surface or freckled rust is prevalent. The paint system is no longer effective. There may be exposed metal but there is no active corrosion that is causing loss of section.
4	The paint system has failed. Surface pitting may be present but any section loss due to active corrosion does not yet warrant structural analysis of either the element or the bridge.
5	Corrosion has caused section loss and is sufficient to warrant structural analysis to ascertain the impact on the ultimate strength and/or serviceability of either the element or the bridge

Source: Adapted from Colorado Department of Transportation (CDOT), Pontis Bridge Inspection Coding Guide, CDOT, Denver, Colorado, 1998.

9.4.2 Performance Indicators Regarding Safety

The failure models in time-dependent system reliability analysis are based on four common indicators. These are the PDF of time to failure, cumulative distribution function (CDF) of time to failure, survivor function, and failure (hazard) rate function. These measures are mostly used when studying the structural performance until the structural system fails for the first time (e.g., no repair). In this section, first probability of failure is defined, then the indicators mentioned above are presented, and finally the most common performance indicator for bridge structures, reliability index, is discussed.

9.4.2.1 Probability of Failure

The stochastic nature of the structural resistance and the load effects can be described by their PDFs. The probability of failure of any section, component or system is defined as the probability of occurrence of the event that resistance is smaller than the load effects and can be evaluated by solving the following convolution integral:

$$P_f = P(g \le 0) = \int_0^\infty F_R(s) f_Q(s) \mathrm{d}s \tag{9.6}$$

where g is the performance function, R is the resistance in a certain failure mode, Q is the load effect in the same failure mode, F_R is the CDF of R, and f_Q is the PDF of the load effect Q.

Probability of failure is the basis for most probabilistic performance indicators. It is used at all levels (cross-section, component, system, system of systems). In many cases, it is impossible or very demanding to evaluate P_f by analytical methods. Therefore, numerical methods such as Monte Carlo Simulations are used.

9.4.2.2 Probability Density Function of Time to Failure

The time elapsed from when the bridge structure is put into service until it fails is referred to as the time to failure, T. Since the time to failure exhibits uncertainty it is considered as a random variable. The appropriate unit of the time to failure for bridge structures is the calendar time units such as months and years. To illustrate PDF of time to failure, suppose a set of N_0 identical structures are put into service at time $t = 0$. As time progresses, some of the structures may fail. Let $N_S(t)$ be the number of survivors at time t. The PDF of time to failure can be expressed as (Ramakumar, 1993)

$$f(t) = \lim_{\Delta t \to 0}\left[\frac{1}{N_0}\frac{N_s(t) - N_s(t+\Delta t)}{\Delta t}\right] = -\frac{1}{N_0}\frac{\mathrm{d}}{\mathrm{d}t}N_s(t) \tag{9.7}$$

The PDF of time to failure is qualitatively illustrated in Figure 9.4.

9.4.2.3 Cumulative Distribution Function of Time to Failure

CDF of time to failure is also known as cumulative probability of failure. The probability of failure until a certain time represents the CDF of time to failure. It can be expressed as (Rausand and Høyland, 2004)

$$F(t) = P(T \le t) = \int_0^t f(u)\mathrm{d}u \quad \text{for } t > 0 \tag{9.8}$$

where $P(T \le t)$ is the probability of failure within time interval $(0, t]$, $f(t)$ is the PDF of the time to failure, and u is the integration variable. The CDF of time to failure is illustrated in Figure 9.5 qualitatively. $f(t)$ can be expressed in terms $F(t)$ as

$$f(t) = \frac{\mathrm{d}}{\mathrm{d}t}F(t) = \lim_{\Delta t \to 0}\left[\frac{F(t+\Delta t) - F(t)}{\Delta t}\right] = \lim_{\Delta t \to 0}\left[\frac{P(t \le T \le t+\Delta t)}{\Delta t}\right] \tag{9.9}$$

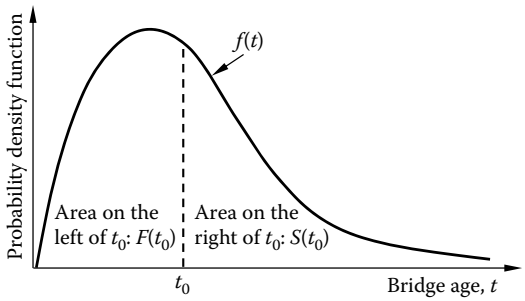

FIGURE 9.4 PDF of time to failure.

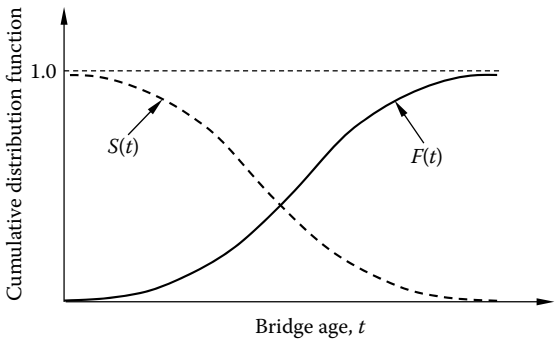

FIGURE 9.5 CDF of time to failure and survivor function.

For small Δt, this implies (Rausand and Høyland, 2004)

$$P(t \le T \le t+\Delta t) \approx f(t)\Delta t \tag{9.10}$$

9.4.2.4 Survivor Function

Survivor function is the probability that a component or system survived until time t and is still functioning at time t. It is also known as the reliability function. Survivor function is the complement of the cumulative time probability of failure and can be expressed as

$$S(t) = 1 - F(t) = P(T > t) = \int_t^{\infty} f(u)\,\mathrm{d}u \qquad for\ t > 0 \tag{9.11}$$

The time-variation of survivor function for a bridge structure is illustrated in Figure 9.5 qualitatively.

9.4.2.5 Failure (Hazard) Rate Function

Failure rate function is a measure of risk associated with an item at time t. It is also known as hazard rate or hazard function. Failure rate also can be defined as the conditional probability of failure in the time interval $(t, t+\Delta t]$, given that a component was functioning at time t (Ramakumar, 1993). It can be expressed as (Rausand and Høyland, 2004)

$$h(t) = \lim_{\Delta t \to 0}\left[\frac{P(t \le T \le t+\Delta t \mid T > t)}{\Delta t}\right] = \lim_{\Delta t \to 0}\left[\frac{F(t+\Delta t) - F(t)}{\Delta t}\frac{1}{S(t)}\right] = \frac{f(t)}{S(t)} \tag{9.12}$$

where $P(t \le T \le t+\Delta t \mid T > t)$ indicates the probability that the structure will fail in the time interval $(t, t+\Delta t]$, given that the structure had survived at time t. This implies for small Δt

$$P(t \le T \le t+\Delta t \mid T > t) \approx h(t)\Delta t \tag{9.13}$$

Failure rate function is a time-dependent performance indicator like the other reliability functions. The variation of failure rate function in time is illustrated qualitatively in Figure 9.6. Application of lifetime functions (e.g., PDF of time to failure, CDF of time to failure, survivor function, and failure rate function) to bridge components and systems can be found in van Noortwijk and Klatter (2004), Yang et al. (2004), Okasha and Frangopol (2010a), and Orcesi and Frangopol (2011).

9.4.2.6 Reliability Index

The reliability of a bridge structure can be expressed in terms of either probability of failure or its corresponding reliability index. As a measure of reliability, reliability index can be defined as the shortest

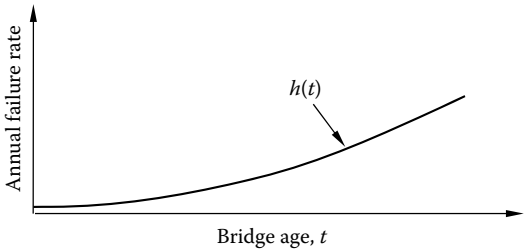

FIGURE 9.6 Typical failure (hazard) rate function for a bridge structure.

distance from the origin to the limit state surface in the standard normal space. For normally distributed independent variables, the reliability index β can be calculated as

$$\beta = \frac{E(R) - E(Q)}{\sqrt{\sigma^2(R) + \sigma^2(Q)}} \tag{9.14}$$

where $E(R)$ and $E(Q)$ are the mean values of the resistance and load effect, and $\sigma(R)$ and $\sigma(Q)$ are the standard deviations of the resistance and load effect, respectively. First and second order reliability methods (FORM and SORM), which approximately provide the reliability index by searching the most probable point on the failure surface ($g_j = 0$), are the most common methods to compute reliability index. The probability of failure and reliability index are approximately related to each other as follows:

$$P_f = 1 - \Phi(\beta) \tag{9.15}$$

where $\Phi(.)$ indicates the CDF of standard normal variate. Reliability index is one of the most common performance indicators for performance quantification of bridge structures. For instance, a reliability index level of 3.5 was targeted for establishing the safety levels in calibration of AASHTO LRFD Bridge Design Specification (AASHTO, 2012). In Figure 9.7a, the variation of bridge system reliability index due to only the corrosion, only increase in live load, and both the corrosion and increase in live load are illustrated hypothetically. In Figure 9.7b, the effect of sudden damage on reliability index is presented qualitatively. Application of reliability to bridge structures can be found in Enright and Frangopol (1999a, b), Estes and Frangopol (1999, 2001), and Akgül and Frangopol (2004a, b).

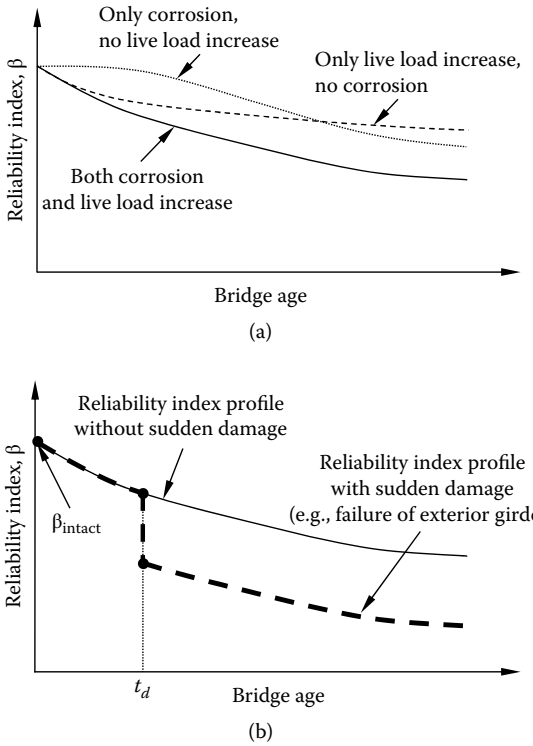

FIGURE 9.7 Variation of reliability index in time with (a) continuous deterioration, and (b) effect of sudden damage.

9.4.3 Performance Indicators Regarding Tolerance to Damage

9.4.3.1 Redundancy

There are several definitions and indicators for structural redundancy. A measure of redundancy, in the context of availability of warning before system failure, was proposed by Frangopol and Nakib (1991) as

$$RI_1 = \frac{P_{f(\text{dmg})} - P_{f(\text{sys})}}{P_{f(\text{sys})}} \tag{9.16}$$

where $P_{f(\text{dmg})}$ is the probability of damage occurrence to the system (e.g., first yielding of any member) and $P_{f(\text{sys})}$ is the probability of system failure (e.g., system collapse).

A measure of redundancy, as the availability of alternative load path after sudden local damage, was proposed by Frangopol and Curley (1987) as

$$RI_2 = \frac{\beta_{\text{intact}}}{\beta_{\text{intact}} - \beta_{\text{damaged}}} \tag{9.17}$$

where β_{intact} is the reliability index of the intact system and β_{damaged} is the reliability index of the damaged system. The variation of redundancy index, RI_2, in time is illustrated in Figure 9.8 qualitatively.

Redundancy is a system performance measure. However, it is also applicable at the cross-section and component levels as a measure of warning with respect to failure. AASHTO LRFD Bridge Design Specifications (2012) considers redundancy in bridge structures. The load modifier η_i in Equation 9.5, which accounts for redundancy level, is based on the redundancy definition in Frangopol and Nakib (1991). Application of redundancy concept to deteriorating bridge structures can be found in Ghosn et al. (2010), Okasha and Frangopol (2009, 2010b), and Saydam and Frangopol (2011).

9.4.3.2 Vulnerability and Damage Tolerance

Vulnerability is a performance measure used to capture the essential feature of damage tolerant structures. A probabilistic measure of vulnerability was proposed by Lind (1995), defined as the ratio of the failure probability of the damaged system to the failure probability of the undamaged system

$$V = \frac{P(r_{\text{d}}, Q)}{P(r_0, Q)} \tag{9.18}$$

where r_{d} indicates a particular damaged state, r_0 indicates a pristine system state, Q is the prospective loading, $P(r_{\text{d}}, Q)$ represents the probability of failure of the system in the damaged state, $P(r_0, Q)$

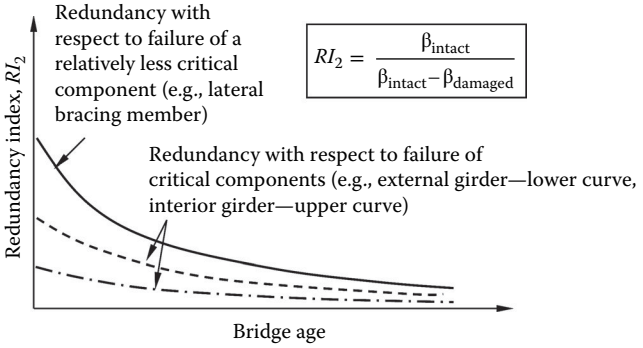

FIGURE 9.8 Variation of redundancy index in time.

represents the probability of failure of the system in the pristine state, and V refers to vulnerability of the system in state r_d for prospective loading Q. The vulnerability V is 1.0 if the probabilities of failure of the damaged and intact systems are the same. Lind (1995) also defined the damage tolerance of a structure as the reciprocal of vulnerability. Vulnerability and damage tolerance are system-level performance indicators. Figure 9.9 illustrates the variation of vulnerability for a bridge structure qualitatively. Application of time-dependent vulnerability concept to bridge structures can be found in Saydam and Frangopol (2011).

9.4.3.3 Robustness

Robustness is one of the key measures in the field of progressive collapse and damage tolerant structures. Although robustness is recognized as a desirable property in structures and systems, there is not a widely accepted theory on robust structures. Maes et al. (2006) defined robustness of a system as

$$ROI_1 = \min_i \frac{P_{f_0}}{P_{f_i}} \tag{9.19}$$

where P_{f_0} is the system failure probability of the undamaged system, and P_{f_i} is the system failure probability assuming one impaired member i. The time-variation of robustness index with respect to failure of bridge components, ROI_1, is illustrated in Figure 9.10 qualitatively.

Baker et al. (2008) stated a robust system to be one where indirect risks do not contribute significantly to the total system risk, and proposed a robustness index defined as follows:

$$ROI_2 = \frac{R_{\text{Dir}}}{R_{\text{Dir}} + R_{\text{Ind}}} \tag{9.20}$$

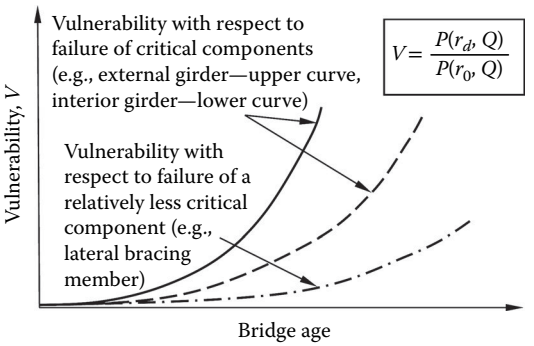

FIGURE 9.9 Variation of vulnerability in time.

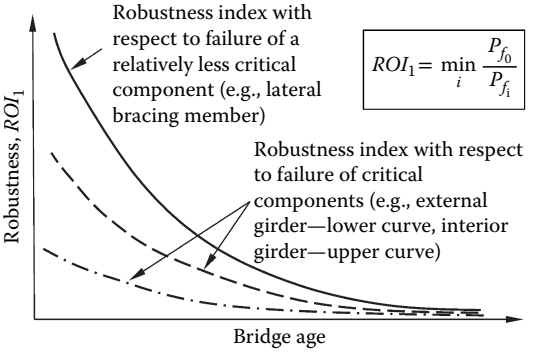

FIGURE 9.10 Variation of robustness in time.

where R_{Dir} and R_{Ind} are the direct and indirect risks, respectively. This index varies between 0 and 1.0 with larger values representing a larger robustness. Robustness is a system performance indicator. Additional robustness indicators and applications to bridge structures are indicated in Ghosn and Frangopol (2007), Biondini et al. (2008), Ghosn et al. (2010), Biondini and Frangopol (2010), and Saydam and Frangopol (2011).

9.4.3.4 Resilience

Bruneau et al. (2003) defined resilience as the ability of the system to reduce the chances of a shock, to absorb a shock if it occurs (abrupt reduction of performance), and to recover quickly after a shock (reestablish normal performance). According to their definition, a resilient system exhibits (1) reduced failure probabilities, (2) reduced consequences from failures in terms of lives lost, damage, and negative economic and social consequences, and (3) reduced time to recovery. The analytical definition of resilience is based on the concept of functionality, also called "serviceability" or "quality of infrastructure" (Bruneau et al., 2003; Cimellaro et al., 2010).

Resilience is a system performance indicator. Resilience is also applied to systems of systems such as highway bridge networks. Application of resilience concept to highway bridge networks can be found in Bocchini and Frangopol (2011), Frangopol and Bocchini (2011), and Bocchini et al. (2013). Bocchini and Frangopol (2011) defined resilience analytically as

$$RES = \frac{\int_{t_0}^{t_0+t_h} Q(t)\,dt}{t_h} \tag{9.21}$$

where t_0 is the time at which the extreme event occurs, t_h is the investigated time horizon, and $Q(t)$ is an indicator of the functionality level of the investigated system. Figure 9.11 illustrates the meaning of resilience graphically.

9.4.4 Performance Indicators Regarding Cost

9.4.4.1 Lifecycle Cost

One of the most important measures in evaluation of structural performance is lifecycle cost. The proper allocation of resources can be achieved by minimizing the total cost, whereas keeping structural safety at a desired level. The expected total cost during the lifetime of a bridge structure can be expressed as (Frangopol et al., 1997)

$$C_{ET} = C_T + C_{PM} + C_{INS} + C_{REP} + C_F \tag{9.22}$$

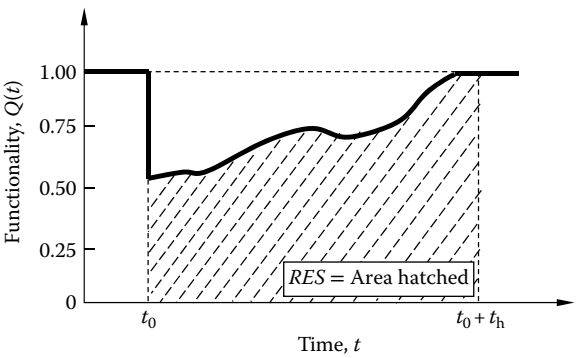

FIGURE 9.11 Graphical illustration of resilience. (Adapted from Bocchini, P. and Frangopol, D. M., *Journal of Bridge Engineering*, ASCE, 17(1), 2011.)

where C_T is the initial cost, C_{PM} is the expected cost of routine maintenance cost, C_{INS} is the expected cost of inspections, C_{REP} is the expected cost of repair, and C_F is expected failure cost.

Lifecycle cost and performance level of a bridge structure are two conflicting criteria. Much research has been done in the area of balancing cost and performance and optimum planning for lifecycle management of civil structures and infrastructures (Ang and De Leon, 1997; Ang et al., 1998; Chang and Shinozuka, 1996; Estes and Frangopol, 1999; Frangopol et al., 1997, 2001; Frangopol et al., 2001; Okasha and Frangopol, 2010c; Okasha and Frangopol, 2011; Frangopol, 2011; Frangopol and Bocchini, 2012; Kong and Frangopol, 2004). In Figure 9.12, various cases of hypothetical trade-off solutions are presented for balancing cost and performance level.

9.4.4.2 Risk

The most common formulation of risk in engineering is multiplication of probability of occurrence by the consequences of an event. Direct risk is the one associated with the damage occurrence itself, whereas indirect risk is associated with the system failure as a result of the damage. Direct and indirect risks are formulated as (Baker et al., 2008)

$$R_{\text{Dir}} = \int_x \int_y C_{\text{Dir}} f_{D|E}(y \mid x) f_E(x) \, \mathrm{d}y \, \mathrm{d}x \tag{9.23}$$

$$R_{\text{Indir}} = \int_x \int_y C_{\text{Indir}} P(F \mid D = y) f_{D|E}(y \mid x) f_E(x) \, \mathrm{d}y \, \mathrm{d}x \tag{9.24}$$

where C_{Dir} and C_{Indir} are the direct and indirect consequences, x and y are the random variables in the event tree, $f_X(x)$ and $f_Y(y)$ are used to denote the PDF of random variables x and y. E, D, and F represent the hazard occurrence, damage occurrence, and system failure, respectively. These integrals can be computed with numerical integration or Monte Carlo Simulation. Risk is applicable at component and

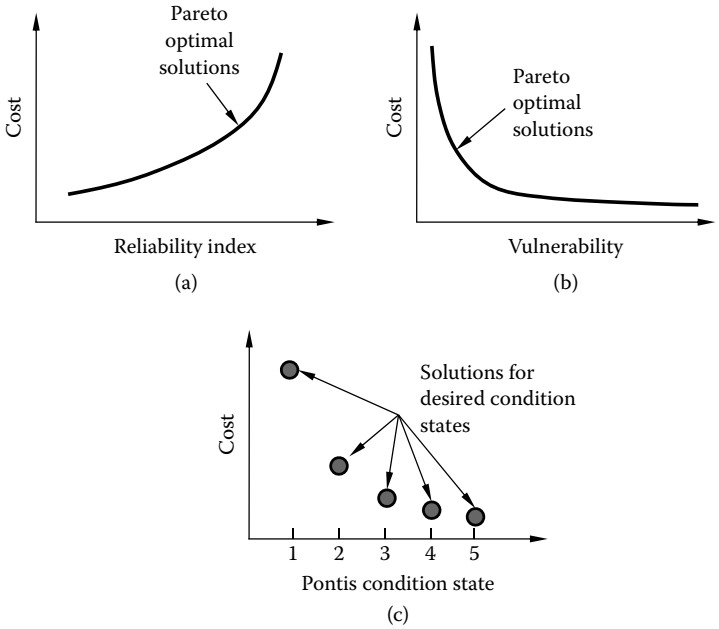

FIGURE 9.12 Conflicting objectives in balancing cost and performance, trade-off solutions for (a) cost and reliability index, (b) cost and vulnerability, and (c) cost and Pontis condition state.

system levels as well as system of systems level. Applications of risk concept to bridges can be found in Decò and Frangopol (2011), Saydam et al. (2013a, b), Zhu and Frangopol (2012, 2013).

9.5 Updating Bridge Performance

9.5.1 Role of Inspection and Structural Health Monitoring

Difficulties arise in prediction of lifecycle performance because of the complexity and high uncertainty of the deterioration process. Information from inspection and/or SHM can assist in accurate assessment of lifecycle performance of bridge structures. Figures 9.13a and b illustrate two possible cases of information that SHM can provide at an instance within the lifetime of a structure. The overlap of the PDFs can be actually more significant than the predicted (Figure 9.13a). In other words, the actual safety level of the structure can be less than the expected level. Vice versa, the overlap of the PDFs can be less significant than that predicted (Figure 9.13b). In this case, the actual safety level of the structure is higher than the expected level. This approach can be extended, in a lifecycle context, for the assessment of optimal maintenance intervention times. Figure 9.14a illustrates the case when performance prediction not supported with SHM leads to late maintenance intervention, which may lead to unacceptable safety levels, even catastrophic failure of the structure. However, Figure 9.14b represents the case when performance prediction not supported with SHM yields untimely and unnecessary maintenance intervention, reaching the performance threshold

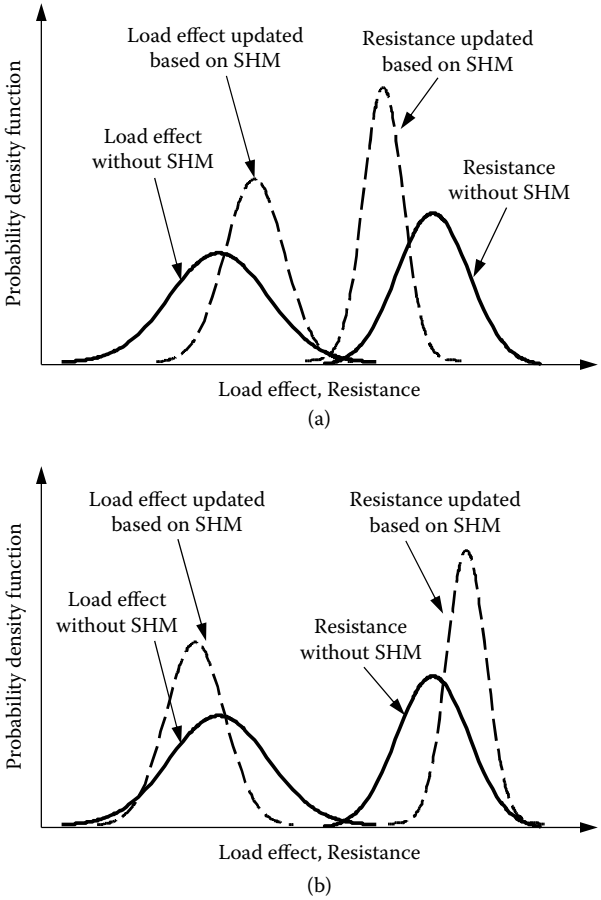

FIGURE 9.13 PDF load effect and resistance with and without SHM: actual safety level is (a) less, (b) larger than the predicted safety level.

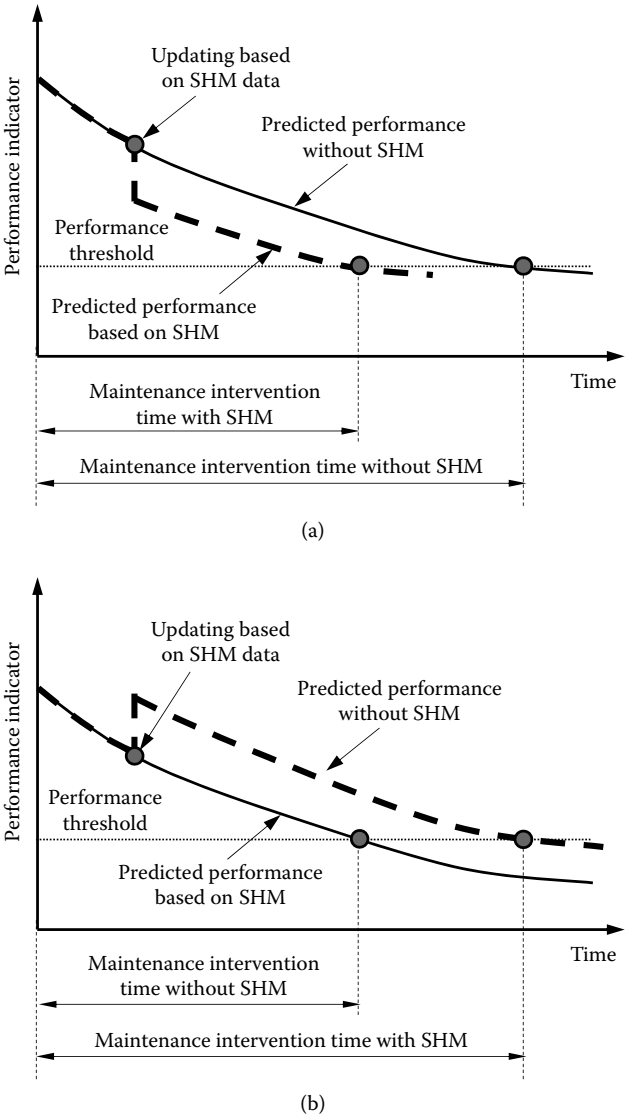

FIGURE 9.14 Role of SHM in a lifecycle context (a) late maintenance intervention without SHM (b) unnecessary maintenance intervention without SHM

earlier than the actual. Applications of SHM concepts on bridges can be found in Frangopol and Messervey (2009a, b, and 2011), Frangopol et al. (2008b), Kim and Frangopol (2011), Okasha and Frangopol (2012).

9.5.2 Bayesian Updating

In the case when there is information before the time of SHM, the new information obtained from SHM must be combined with the existing information in a reasonable manner. When the available information is in statistical form or contains variability, Bayesian approach is the proper tool for combining and updating the available data sets. The prior distribution $f'(\theta)$ can be combined with the observational data obtained from SHM data to find the posterior distribution $f''(\theta)$ as follows (Ang and Tang, 2007):

$$f''(\theta) = kL(\theta) f'(\theta) \tag{9.25}$$

where $L(\theta)$ is the likelihood function of θ, and k is the normalizing constant. Likelihood function, $L(\theta)$ is the conditional probability of observing a certain experimental outcome assuming that the value of the parameter is θ. The normalizing constant k, can be expressed as

$$k = \frac{1}{\int_{-\infty}^{\infty} L(\theta) f'(\theta) d\theta} \tag{9.26}$$

where $L(\theta)$ and $f'(\theta)$ are defined above. Applications of bridge performance updating can be found in Frangopol et al. (2008a) and Strauss et al. (2008).

9.6 Summary

In this chapter, levels of performance assessment, methods of establishing safety levels and common performance indicators for bridge structures are presented. Brief information about the role of SHM on performance assessment and prediction is introduced. Several indicators can be used to define performance at cross-section and component levels, whereas others are appropriate to be used to quantify performance of systems and groups of systems. The issue of which indicators should be considered depends on the priorities and objectives of the decision makers. In general, the main purpose of a design process is minimizing the lifecycle cost, while maintaining safety at an acceptable level. If time-dependent analysis is required, time-dependent indices such as cumulative probability of failure, survivor function, hazard function, or cumulative hazard function may be essential. Furthermore, structures are subjected to damage and deterioration during their lifetime. In this case, not only basic safety measures such as reliability index but also the measures related to damage tolerance of structures such as vulnerability, redundancy, and robustness may be beneficial. The performance indicators for bridge structures are not limited to those mentioned in this chapter. More effort should be placed on determination of bridge performance indicators and their use in risk communication and optimal decision making under uncertainty.

Acknowledgments

The support from (1) the National Science Foundation through grants CMS-0638728 and CMS-0639428, (2) the Commonwealth of Pennsylvania, Department of Community, and Economic Development, through the Pennsylvania Infrastructure Technology Alliance (PITA), (3) the U.S. Federal Highway Administration Cooperative Agreement Award DTFH61-07-H-00040, and (4) the U.S. Office of Naval Research Contract Numbers N00014-08-1-0188 and N 00014-12-1-0023 is gratefully acknowledged. The opinions and conclusions presented in this chapter are those of the authors and do not necessarily reflect the views of the sponsoring organizations.

Defining Terms

$f(t)$: probability density function of time to failure, T
f_Q : probability density function of Q
g : performance function
$h(t)$: failure (hazard) rate function
k : normalizing constant
r_0 : pristine system state
r_d : damaged system state
t : time
t_0 : the time at which an extreme event occurs

t_h : the investigated time horizon
ϕ : resistance factor
γ_i : load factor
η_i : load modifier
$\sigma(.)$: standard deviation
C_{Dir} : cost of the direct consequences
C_{ET} : total expected cost
C_F : expected failure cost
C_{Ind} : cost of the indirect consequences
C_{INS} : expected cost of inspections
C_{PM} : expected cost of routine maintenance cost
C_{REP} : expected cost of repair
C_T : initial cost
$E(.)$: mean value
FS : factor of safety
F_R : cumulative distribution function of R
$F(t)$: cumulative distribution function of time to failure T
L : load effect
$L(\theta)$: likelihood function of θ
M_{DLNC} : moment due to noncomposite dead load
M_{DLC} : moment due to composite dead load
M_{LL+I} : moment due to live load including impact
M_u : ultimate moment capacity
N_0 : initial number of items
$N_S(t)$: number of surviving items at time t
P_f : probability of failure
P_{f_0} : failure probability of the undamaged system
P_{f_i} : system failure probability assuming one impaired member i
$P_{f(dmg)}$: probability of damage occurrence to the system
$P_{f(sys)}$: probability of system failure
$Q(t)$: an indicator of the functionality level of the investigated system
Q_i : load effect in mode i
R : resistance
R_{dir} : direct risk
R_{ind} : indirect risk
R_n : member nominal resistance
RES : resilience
RI : redundancy index
ROI : robustness index
T : time to failure
$S(t)$: survivor function
V : vulnerability
β : reliability index
$\beta_{damaged}$: reliability index of the damaged system
β_{intact} : reliability index of the intact system
$\Phi(.)$: CDF of standard normal variate

References

Akgül, F., and Frangopol, D. M. 2004a. Computational platform for predicting lifetime system reliability profiles for different structure types in a network. *Journal of Computing in Civil Engineering*, ASCE, 18(2), 92–104.

Akgül, F., and Frangopol, D. M. 2004b. Bridge rating and reliability correlation: Comprehensive study for different bridge types. *Journal of Structural Engineering*, ASCE, 130(7), 1063–1074.

Al-Wazeer, A. A. R. 2007. *Risk-Based Bridge Management Strategies.* University of Maryland, College Park, PhD dissertation.

American Association of State Highway and Transportation Officials (AASHTO). 2012. *LRFD Bridge Design Specifications*, AASHTO 6th Ed., Washington, DC.

Ang, A. H-S., and De Leon, D. 1997. Target reliability for structural design based on minimum expected life-cycle cost. *Reliability and Optimization of Structural Systems.* In: D. M. Frangopol, R. B. Corotis, and R. Rackwitz (eds.). Pergamon, New York, NY, 71–83.

Ang, A. H-S., Lee, J-C., and Pires, J. A. 1998. Cost-effectiveness evaluation of design criteria. *Optimal Performance of Civil Infrastructure Systems*. In: D. M. Frangopol (ed.). ASCE, Reston, VA, 1–16.

Ang, A. H.-S., and Tang, W. H. 1984. *Probability Concepts in Engineering Planning and Design.* Vol. II, John Wiley & Sons, New York.

Ang, A. H-S., and Tang, W. H. 2007. *Probability Concepts in Engineering: Emphasis on Applications in Civil & Environmental Engineering.* John Wiley & Sons, NJ.

Baker, J. W., Schubert, M., and Faber, M. H. 2008. On the assessment of robustness. *Structural Safety.* Elsevier, 30, 253–267.

Biondini, F., and Frangopol, D. M. 2010. Structural robustness and redundancy of deteriorating concrete bridges. *Bridge Maintenance, Safety, Management, Health Monitoring and Optimization.* In: D. M. Frangopol, R. Sause, and C. S. Kusko (eds.). CRC Press/Balkema, Taylor & Francis Group plc, London, full paper on CD-ROM, Taylor & Francis Group plc, London, 2473–2480.

Biondini, F., Frangopol, D. M., and Restelli, S. 2008. On structural robustness, redundancy and static indeterminacy. *Proceedings of the ASCE Structures Congress.* Vancouver, BC, Canada, April 24–26. In: *Structures 2008: Crossing Borders,* ASCE, 2008, 10 pages on CD-ROM.

Bocchini, P., and Frangopol, D. M. 2012. Optimal resilience- and cost-based post-disaster intervention prioritization for bridges along a highway segment. *Journal of Bridge Engineering*, ASCE, 17(1), 117-129.

Bocchini, P., Frangopol, D. M., Ummenhofer, T., and Zinke, T. 2013. Resilience and sustainability of the civil infrastructure: Towards a unified approach. *Journal of Infrastructure Systems*, ASCE (in press), doi:10.1061/(ASCE)IS.1943-555X.0000177.

Bruneau, M. et al. 2003. A framework to quantitatively assess and enhance the seismic resilience of communities. *Earthquake Spectra*, EERI, 19(4), 733–752.

Cambridge Systematics, Inc. 2009. Pontis Release 4.5 User Manual, AASHTO, Washington, DC.

Chang, S. E., and Shinozuka, M. 1996. Lifecycle cost analysis with natural hazard risk. *Journal of Infrastructure Systems*, 2(3), 118–126.

Cimellaro, G. P., Reinhorn, A. M., and Bruneau, M. 2010. Seismic resilience of a hospital system. *Structure and Infrastructure Engineering*, Taylor & Francis, 6(1), 127–144.

Colorado Department of Transportation (CDOT) 1998. Pontis Bridge Inspection Coding Guide, Denver, Colorado.

Decò, A., and Frangopol, D. M. 2011. Risk assessment of highway bridges under multiple hazards. *Journal of Risk Research*, Taylor & Francis, 14(9), 1057–1089.

Ellingwood, B., Galambos, T. V., MacGregor, J. G., and Cornell, C. A. 1980. Development of a probability-based load criterion for American National Standard A58. *NBS Special Publication 577*, U.S. Dept of Commerce, Washington, DC.

Enright, M. P., and Frangopol, D. M. 1999a. Reliability-based condition assessment of deteriorating concrete bridges considering load redistribution. *Structural Safety*, Elsevier, 21, 159–195.

Enright, M. P., and Frangopol, D. M. 1999b. Condition prediction of deteriorating concrete bridges. *Journal of Structural Engineering*, ASCE, 125(10), 1118–1125.

Estes, A. C., and Frangopol, D. M. 1999. Repair optimisation of highway bridges using system reliability approach. *Journal of Structural Engineering*, ASCE, 125(7), 766–775.

Estes, A.C., and Frangopol, D. M. 2001. Bridge lifetime system reliability under multiple limit states. *Journal of Bridge Engineering*, ASCE, 6(6), 523–528.

Estes, A.C., and Frangopol, D. M. 2003. Updating bridge reliability based on bridge management systems visual inspection results. *Journal of Bridge Engineering*, ASCE, 8(6), 374–382.

Federal Highway Administration (FHWA). 1995. Recording and Coding Guide for Structure Inventory and Appraisal of the Nation's Bridge, Report No. FHWA-PD 96-001, U.S. Department of Transportation, Washington, DC.

Frangopol, D. M. 2011. Life-cycle performance, management, and optimization of structural systems under uncertainty: Accomplishments and challenges. *Structure and Infrastructure Engineering*, Taylor & Francis, 7(6), 389–413.

Frangopol, D. M., and Bocchini, P. 2011. Resilience as optimization criterion for the rehabilitation of bridges belonging to a transportation network subject to earthquake. *Proceedings of the 2011 Structures Congress*, ASCE, Las Vegas, NV, USA, April 14-16, CD-ROM, 2044–2055.

Frangopol, D. M., and Bocchini, P. 2012. Bridge network performance, maintenance, and optimization under uncertainty: Accomplishments and challenges. *Structure and Infrastructure Engineering*, Taylor & Francis, 8(4), 341–356.

Frangopol, D. M., and Curley, J. P. 1987. Effects of damage and redundancy on structural reliability. *Journal of Structural Engineering*, ASCE, 113(7), 1533–1549.

Frangopol, D. M., Strauss, A., and Kim, S. 2008a. Use of monitoring extreme data for the performance prediction of structures: General approach. *Engineering Structures*, Elsevier, 30(12), 3644-3653.

Frangopol, D. M., Strauss, A., and Kim, S. 2008b. Bridge reliability assessment based on monitoring. *Journal of Bridge Engineering*, ASCE, 13(3), 258–270.

Frangopol, D. M., Kong, J. S., and Gharaibeh, E. S. 2001. Reliability-based life-cycle management of highway bridges. *Journal of Computational Civil Engineering*, 15(1), 27–34.

Frangopol, D. M., and Messervey, T.B. 2009a. Maintenance principles for civil structures. Chapter 89 in *Encyclopedia of Structural Health Monitoring*, C. Boller, F-K. Chang, and Y. Fujino, eds., John Wiley & Sons Ltd, Chicester, UK, 4, 1533–1562.

Frangopol, D. M., and Messervey, T.B. 2009b. Life-cycle cost and performance prediction: Role of structural health monitoring. Chapter 16 in *Frontier Technologies for Infrastructures Engineering*, S-S, Chen and A.H-S. Ang, eds., *Structures and Infrastructures Book Series*, 4, D. M. Frangopol, Book Series Editor, CRC Press/Balkema, Boca Raton, London, New York, Leiden, 361–381.

Frangopol, D. M., and Messervey, T.B. 2011. Effect of monitoring on reliability of structures. Chapter 18 in *Monitoring Technologies for Bridge Management*, B. Bahkt, A.A. Mufti, and L.D. Wegner, eds., Multi-Science Publishing Co. Ltd., U.K., 515–560.

Frangopol, D. M., Lin, K-Y., and Estes, A. C., 1997. Life-cycle cost design of deteriorating structures. *Journal of Structural Engineering*, ASCE, 123(10), 1390–1401.

Frangopol, D. M., and Nakib, R. 1991. Redundancy in highway bridges. *Engineering Journal*, American Institute of Steel Construction, Chicago, IL, 28(1), 45–50.

Ghosn, M., and Frangopol, D. M. 2007. Structural redundancy and robustness measures and their use in assessment and design. *Applications of Statistics and Probability in Civil Engineering* In: J. Kanda, T. Takada, and H. Furuta (eds.). Taylor & Francis Group plc, London, 181–182, and full 7 page paper on CD-ROM.

Ghosn, M., Moses, F, and Frangopol, D. M. 2010. Redundancy and robustness of highway bridge superstructures and substructures. *Structure and Infrastructure Engineering*, Taylor & Francis, Boca Raton, FL, 6(1–2), 257–278.

Hendawi S., and Frangopol, D. M. 1994. System reliability and redundancy in structural design and evaluation. *Structural Safety*, Elsevier, 16(1–2), 47–71.

Kim, S., and Frangopol, D. M. 2011. Cost-effective lifetime structural health monitoring based on availability. *Journal of Structural Engineering*, ASCE, 137(1), 22–33.

Kong, J. S., and Frangopol, D. M. 2004. Cost-reliability interaction in life-cycle cost optimization of deteriorating structures. *Journal of Structural Engineering*, ASCE, 130(11), 1704–1712.

Lind, N. C. 1995. A measure of vulnerability and damage tolerance. *Reliability Engineering and System Safety*, Elsevier, 43(1), 1–6.

Maes, M. A., Fritzson, K. E., and Glowienka, S. 2006. Structural robustness in the light of risk and consequence analysis. *Structural Engineering International*, IABSE, 16(2), 101–107.

Okasha, N. M., and Frangopol, D. M. 2009. Lifetime-oriented multi-objective optimization of structural maintenance considering system reliability, redundancy and life-cycle cost using GA. *Structural Safety*, Elsevier, 31(6), 460–474.

Okasha, N. M., and Frangopol, D. M. 2010a. Advanced modeling for efficient computation of life-cycle performance prediction and service-life estimation of bridges. *Journal of Computing in Civil Engineering*, ASCE, 24(6), 548–556.

Okasha, N. M., and Frangopol, D. M. 2010b. Time-variant redundancy of structural systems. *Structure and Infrastructure Engineering*, Taylor & Francis, 6(1–2), 279–301.

Okasha, N. M., and Frangopol, D. M. 2010c. Novel approach for multi-criteria optimization of lifecycle preventive and essential maintenance of deteriorating structures. *Journal of Structural Engineering*, ASCE, 136(8), 1009–1022.

Okasha, N.M., and Frangopol, D. M. 2011. Computational platform for the integrated life-cycle management of highway bridges. *Engineering Structures*, Elsevier, 33(7), 2145–2153.

Okasha, N.M., and Frangopol, D. M. 2012. Integration of structural health monitoring in a system performance based life-cycle bridge management framework. *Structure and Infrastructure Engineering*, Taylor & Francis, 8(11), 999–1016.

Orcesi, A. D., and Frangopol, D. M. 2011. Use of lifetime functions in the optimization of nondestructive inspection strategies for bridges. *Journal of Structural Engineering*, ASCE, 137(4), 531–539.

Ramakumar, R. (1993). *Engineering Reliability: Fundamentals and Applications.* Prentice Hall, NJ, Englewood Cliffs, NJ.

Rausand, M., and Høyland, A. 2004. *System Reliability Theory: Models, Statistical Methods and Applications*. Wiley, NJ, Hoboken, NJ.

Saydam, D., Bocchini, P., and Frangopol, D. M. 2013a. Time-dependent risk associated with highway bridge networks. *Engineering Structures*, Elsevier, 54, 221–233.

Saydam, D., and Frangopol, D. M., 2011. Time-dependent performance indicators of damaged bridge superstructures. *Engineering Structures*, Elsevier, 33(9), 2458–2471.

Saydam, D., Frangopol, D. M., and Dong, Y. 2013b. Assessment of risk using bridge element condition ratings. *Journal of Infrastructure Systems*, ASCE (in press), doi:10.1061/(ASCE)IS.1943–555X.0000131.

Strauss, A., Frangopol, D. M., and Kim, S. 2008. Use of Monitoring Extreme Data for the Performance Prediction of Structures: Bayesian Updating. *Engineering Structures*, Elsevier, 30(12), 3654–3666.

van Noortwijk, J. M., and Klatter, H. E. 2004. The use of lifetime distributions in bridge maintenance and replacement modelling. *Computers & Structures*, Elsevier, 82(13–14), 1091–1099.

Yang, S-I., Frangopol, D. M., and Neves, L. C. 2004. Service life prediction of structural systems using lifetime functions with emphasis on bridges. *Reliability Engineering & System Safety*, Elsevier, 86(1), 39–51.

Zhu, B., and Frangopol, D. M. 2012. Reliability, redundancy and risk as performance indicators of structural systems during their life-cycle. Engineering Structures, Elsevier, 41, 34-49.

Zhu, B. and Frangopol, D. M. 2013. Risk-based approach for optimum maintenance of structures under traffic and earthquake loads. *Journal of Structural Engineering*, ASCE, 139(3), 422–434.

10

Structural Theory

Xila Liu
Shanghai Jiao Tong University

Leiming Zhang
Shanghai Jiao Tong University

10.1 Introduction

In this chapter, general forms of three sets of equations required in solving a solid mechanics problem and their extensions into structural theory are presented. In particular, more generally used procedures of the displacement method is expressed in more detail. Finite element method (FEM) is presented in Chapter 11 and structural modeling is discussed in Chapter 12.

10.1.1 Basic Equations: Equilibrium, Compatibility, and Constitutive Law

In general solving a solid mechanics problem must satisfy: equations of equilibrium (static or dynamic), conditions of compatibility between strains and displacements, and stress–strain relations or material constitutive law (see Figure 10.1). The initial and boundary conditions on forces and displacements are naturally included.

From consideration of equilibrium equations, one can relate the stresses inside a body to external excitations, including body and surface forces. There are three equations of equilibrium relating the six components of stress tensor σ_{ij} for an infinitesimal material element that will be shown later in

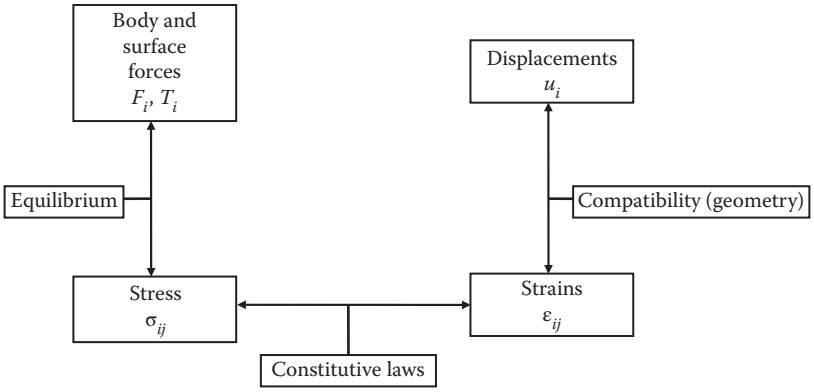

FIGURE 10.1 Relations of variables in solving a solid mechanics problem.

Section 10.2.1. In case of dynamics, the equilibrium equations are replaced by equations of motion, which contain second-order derivatives of displacement with respect to time.

In the same way, taking into account geometric conditions, one can relate strains inside a body to its displacements, by six equations of kinematics expressing the six components of strain (ε_{ij}) in terms of the three components of displacement (u_i). These are known as the strain-displacement relations (see Section 10.3.1).

Both the equations of equilibrium and kinematics are valid regardless of the specific material of which the body is made. The influence of the material is expressed by constitutive laws in six equations. In the simplest case, not considering the effects of temperature, time, loading rates, and loading paths, these can be described by relations between stress and strain only.

Six stress components, six strain components, and three displacement components are connected by three equilibrium equations, six kinematics equations, and six constitutive equations. The 15 unknown quantities can be determined from the system of 15 equations.

For convenience, small deformations and elastic materials are assumed in the following discussion and thus the principle of superposition is valid.

10.1.2 Three Levels: Continuous Mechanics, Finite Element Method, and Beam-Column Theory

In solving a solid mechanics problem, the most direct method solves the three sets of equations described in the previous section. Generally there are three ways to establish the basic unknowns, namely, the displacement components, the stress components, or a combination of both. The corresponding procedures are called the displacement method, the stress method, or the mixed method, respectively. But these direct methods are only practicable in some simple circumstances, such as those detailed in elastic theory of solid mechanics.

Many complex problems cannot be easily solved with conventional procedures. In other words, closed-form solution cannot be obtained for many complex problems. Complexities arise because of factors such as irregular geometry, nonhomogeneities, nonlinearity, and arbitrary loading conditions. An alternative now available is based on a concept of discretization. The FEM, a numerical technique for finding approximate solutions of partial differential equations, divides a body into many "small" bodies called finite elements. Formulations by the FEM on the laws and principles governing the behavior of the body usually result in a set of simultaneous equations that can be solved by direct or iterative procedures. And loading effects such as deformations and stresses can be evaluated within certain accuracy. Hitherto FEM has been the most widely used structural analysis

method. For more detailed discussion, references may be made to Chapter 11, Bathe and Wilson (1976), Desai (1979), and Cook et al. (2002).

In dealing with a continuous beam, the size of the three sets of equations is greatly reduced by assuming characteristics of beam members, such as plane sections remain plane. For framed structures or structures constructed using beam-columns, structural mechanics gives them a more pithy and practical analysis.

10.1.3 Theoretical Structural Mechanics, Computational Structural Mechanics, and Qualitative Structural Mechanics

Structural mechanics deals with a system of members or bars connected by joints that may be pinned, semirigid or rigid. Classical methods of structural analysis are based on principles such as the principle of virtual displacement, the minimization of total potential energy, the minimization of total complementary energy, which result in the three sets of governing equations. Unfortunately, conventional methods are generally intended for hand calculations and developers of the FEM took great pains to minimize the amount of calculations required, even at the expense of making the methods somewhat unsystematic. This made the conventional methods unattractive for translation to computer codes.

The digital computer called for a more systematic method of structural analysis, leading to computational structural mechanics. By taking great care to formulate the tools of matrix notation in a mathematically consistent fashion, the analyst achieved a systematic approach convenient for automatic computation: matrix analysis of structures. One of the hallmarks of structural matrix analysis is its systematic nature that renders digital computers even more important in structural engineering.

Of course, the analyst must maintain a critical, even skeptical, attitude toward computer results. In any event, computer results must satisfy our intuition of what is "reasonable." This qualitative judgment requires that the analyst possess a full understanding of structural behavior, both that being modeled by the program and that can be expected in the actual structures. Engineers should decide what approximations are reasonable for the particular structure and verify that these approximations are indeed valid, and know how to design the structure so that its behavior is in reasonable agreement with the model adopted to analyze it. This is the main task of structural analysis.

10.1.4 Matrix Analysis of Structures: Force Method and Displacement Method

Matrix analysis of structures was developed in the early 1950s. Although it was initially used on fuselage analysis, this method was proven to be pertinent to any complex structure. If internal forces are selected as basic unknowns, the analysis method is referred to as force method; in a similar way, the displacement method refers to the case where displacements are selected as the primary unknowns. Both methods involve obtaining the joint equilibrium equations in terms of the basic internal forces or joint displacements as primary unknowns and solving the resulting set of equations for these unknowns. Having done this, one can obtain internal forces by back substitution, since even in the case of displacement method the joint displacements determine each member's basic displacements, which are directly related to the internal forces and stresses in the member.

A major feature evident in structural matrix analysis is an emphasis on a systematic approach to the statement of the problem. This systematic characteristic together with matrix notation makes it especially convenient for computer coding. In fact, the displacement method, whose basic unknowns are uniquely defined, is generally more convenient than the force method. Most general purpose structural analysis programs are based on the displacement method. But there are still cases where it may be more desirable to use the force method.

10.2 Equilibrium Equations

10.2.1 Equilibrium Equation and Virtual Work Equation

For any volume V of a material body having A as the surface area, as shown in Figure 10.2, it has the following conditions of equilibrium:
at surface points

$$T_i = \sigma_{ji} n_j \tag{10.1a}$$

at internal points

$$\sigma_{ji,j} + F_i = 0 \tag{10.1b}$$

$$\sigma_{ji} = \sigma_{ij} \tag{10.1c}$$

where n_i represents the components of unit normal vector $\boldsymbol{n}$ of the surface; T_i is the stress vector at the point associated with $\boldsymbol{n}$; $\sigma_{ji,j}$ represents the first derivative of σ_{ij} with respect to x_j; and F_i is the body force intensity. Any set of stresses σ_{ij}, body forces F_i, and external surface forces T_i that satisfies Equations 10.1a through 10.1c is a statically admissible set.

Equations 10.1b and 10.1c may be written in (x,y,z) notation as

$$\begin{aligned}
\frac{\partial \sigma_x}{\partial x} + \frac{\partial \tau_{xy}}{\partial y} + \frac{\partial \tau_{xz}}{\partial z} + F_x = 0 \\
\frac{\partial \tau_{yx}}{\partial x} + \frac{\partial \sigma_y}{\partial y} + \frac{\partial \tau_{yz}}{\partial z} + F_y = 0 \\
\frac{\partial \tau_{zx}}{\partial x} + \frac{\partial \tau_{zy}}{\partial y} + \frac{\partial \sigma_z}{\partial z} + F_z = 0
\end{aligned} \tag{10.1d}$$

and

$$\tau_{xy} = \tau_{yx}, \text{ etc.} \tag{10.1e}$$

where σ_x, σ_y, and σ_z are the normal stress in (x,y,z) direction, respectively; τ_{xy}, τ_{yx}, and so on, are the corresponding shear stresses in (x,y,z) notation; F_x, F_y, and F_z are the body forces in (x,y,z) direction, respectively.

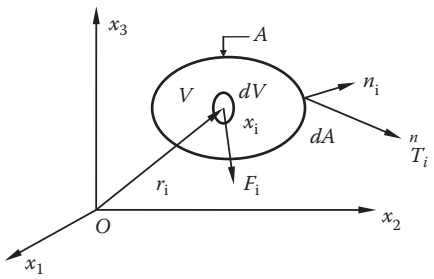

FIGURE 10.2 Derivation of equations of equilibrium.

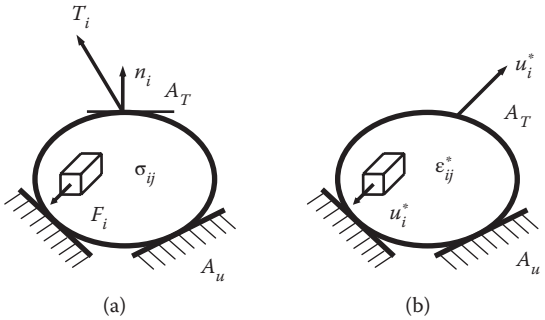

FIGURE 10.3 Two independent sets in the equation of virtual work.

The principle of virtual work has proved a very powerful technique of solving problems and providing proofs for general theorems in solid mechanics. The equation of virtual work uses two independent sets of equilibrium and compatible (see Figure 10.3, where A_u and A_T represent displacement and stress boundary respectively) as follows:

$$\int_A T_i u_i^* \, dA + \int_V F_i u_i^* \, dV = \int_V \sigma_{ij} \varepsilon_{ij}^* \, dV \tag{10.2}$$

or

$$\delta W_{\text{ext}} = \delta W_{\text{int}} \tag{10.3}$$

which states that the external virtual work (δW_{ext}) equals to the internal virtual work (δW_{int}).

Here the integration is over the whole area A, or volume V, of the body. The stress field σ_{ij}, body forces F_i, and external surface forces T_i are a statically admissible set that satisfy Equations 10.1a through 10.1c. Similarly, the strain field ε_{ij}^* and the displacement u_i^* are compatible kinematics sets that satisfy displacement boundary conditions and Equation 10.16 (see Section 10.3.1). This means the principle of virtual work applies only to small strain or small deformation.

The important point to keep in mind is that neither the admissible equilibrium set σ_{ij}, F_i, and T_i (Figure 10.3a) nor the compatible set ε_{ij}^* and u_i^* (Figure 10.3b) need be the actual state, also nor the equilibrium and compatible sets be related to each other in any way. In the other words, these two sets are completely independent of each other.

10.2.2 Equilibrium Equation for Elements

For an infinitesimal material element, equilibrium equations have been summarized in Section 10.2.1, which will transfer into specific expressions in different methods. As in ordinary FEM or displacement method, it will result in the following element equilibrium equations:

$$\left\{\overline{F}\right\}^e = \left[\overline{k}\right]^e \left\{\overline{d}\right\}^e \tag{10.4}$$

where $\left\{\overline{F}\right\}^e$ and $\left\{\overline{d}\right\}^e$ are the element nodal force vector and displacement vector respectively, whereas $\left[\overline{k}\right]^e$ is element stiffness matrix; the overbar here means in local coordinate system.

In the force method of structural analysis, which also adopts the idea of discretization, it is proved possible to identify a basic set of independent forces associated with each member, in that not only are these forces independent of one another, but also all other forces in that member are directly dependent

on this set. Thus, this set of forces constitutes the minimum set that is capable of completely defining the stressed state of the member. The relationship between basic and local forces may be obtained by enforcing overall equilibrium on one member, which gives

$$\left\{\overline{F}\right\}^e = [L]\{P\}^e \tag{10.5}$$

where $[L]$ = the element force transformation matrix; $\{P\}^e$ = the element primary forces vector. It is important to emphasize that the physical basis of Equation 10.5 is member of overall equilibrium.

Take a conventional plane truss member for exemplification (see Figure 10.4 from Meyers, 1983), one has

$$\left\{\overline{k}\right\}^e = \begin{bmatrix} EA/l & 0 & -EA/l & 0 \\ 0 & 0 & 0 & 0 \\ -EA/l & 0 & EA/l & 0 \\ 0 & 0 & 0 & 0 \end{bmatrix} \tag{10.6}$$

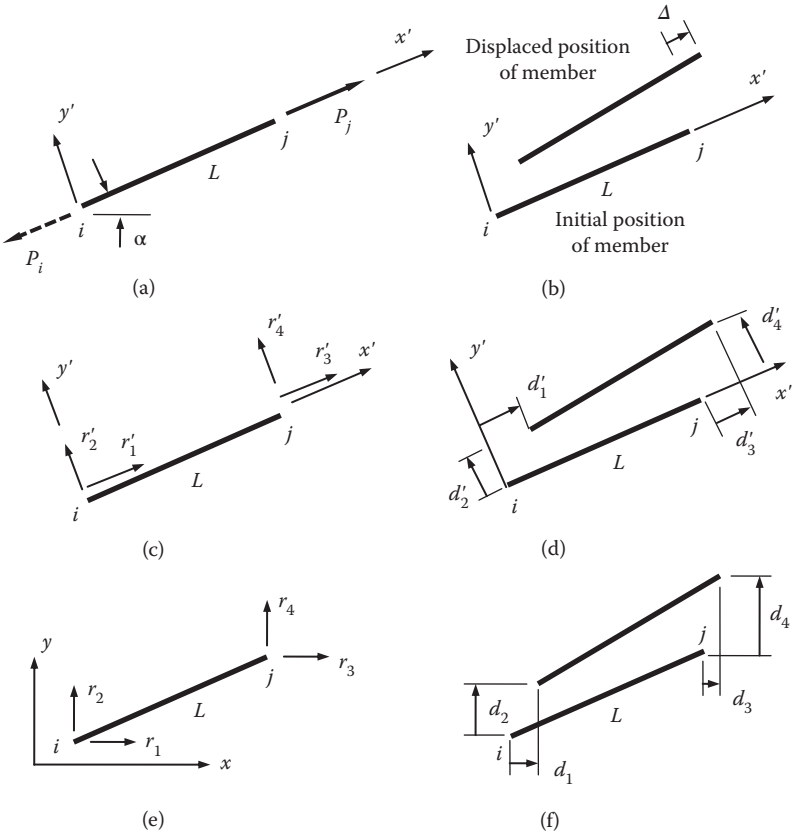

FIGURE 10.4 Plane truss member-end forces and displacements.

and

$$\begin{aligned}\left\{\overline{F}\right\}^e &= \left\{ r_1' \;\; r_2' \;\; r_3' \;\; r_4' \right\}^T \\ \left\{\overline{d}\right\}^e &= \left\{ d_1' \;\; d_2' \;\; d_3' \;\; d_4' \right\}^T \\ [L] &= \left\{ -1 \;\; 0 \;\; 1 \;\; 0 \right\}^T \\ \{P\}^e &= \{P\}\end{aligned} \tag{10.7}$$

where EA/l = axial stiffness of the truss member; P = axial force of the truss member.

10.2.3 Coordinate Transformation

The values of the components of vector $\boldsymbol{V}$, designated by v_1, v_2, and v_3 or simply v_i are associated with the chosen set coordinate axes. Often it is necessary to reorient the reference axes and evaluate the new values for the components of $\boldsymbol{V}$ in the new coordinate system. Assuming that $\boldsymbol{V}$ has components v_i and v_i' in two sets of right-handed Cartesian coordinate systems x_i (old) and x_i' (new) having the same origin (see Figure 10.5), and $\vec{e}_i$, $\vec{e}_i'$ are the unit vectors of x_i and x_i' respectively. Then

$$v_i' = l_{ij} v_j \tag{10.8}$$

where $l_{ji} = \vec{e}_j' \cdot \vec{e}_i = \cos(x_j', x_i)$ that is, the cosines of the angles between x_i' and x_j axes for i and j ranging from 1 to 3; and $[\alpha] = (l_{ij})_{3\times3}$ is called coordinate transformation matrix from old system to new system.

It should be noted that the elements of l_{ij} or matrix $[\alpha]$ are not symmetrical, $l_{ij} \neq l_{ji}$. For example, l_{12} is the cosine of angle from x_1' to x_2 and l_{21} is that from x_2' to x_1 (see Figure 10.5). The angle is assumed to be measured from the primed system to the untrimmed system.

For a plane truss member (see Figure 10.4), the transformation matrix from local coordinate system to global coordinate system may be expressed as

$$[\alpha] = \begin{bmatrix} \cos\alpha & -\sin\alpha & 0 & 0 \\ \sin\alpha & \cos\alpha & 0 & 0 \\ 0 & 0 & \cos\alpha & -\sin\alpha \\ 0 & 0 & \sin\alpha & \cos\alpha \end{bmatrix} \tag{10.9}$$

where α is the inclined angle of the truss member that is assumed to be measured from the global to the local coordinate system.

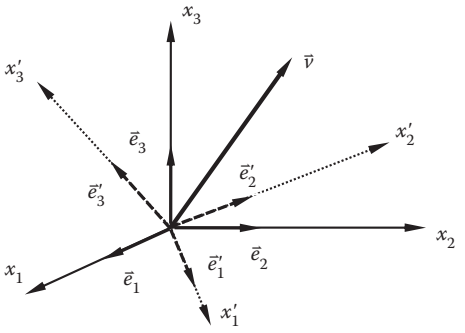

FIGURE 10.5 Coordinate transformation.

10.2.4 Equilibrium Equation for Structures

For discretized structure, the equilibrium of the whole structure is essentially the equilibrium of each joint. After assemblage, for ordinary FEM or displacement method

$$\{F\} = [K]\{D\} \tag{10.10}$$

for force method

$$\{F\} = [A]\{P\} \tag{10.11}$$

where $\{F\}$= nodal loading vector, $[K]$= total stiffness matrix, $\{D\}$= nodal displacement vector, $[A]$ = total forces transformation matrix, and $\{P\}$= total primary internal forces vector.

It should be noted that the coordinate transformation for each element from local coordinates to global coordinate system must be done before assembly.

In the force method, Equation 10.11 will be adopted to solve for internal forces of a statically determinate structure. The number of basic unknown forces is equal to the number of equilibrium equations available to solve for them and the equations are linearly independent. For statically unstable structures, analysis must consider their dynamic behavior. When the number of basic unknown forces exceeds the number of equilibrium equations, the structure is said to be statically indeterminate. In this case some of the basic unknown forces are not required to maintain structural equilibrium. These are "extra" or "redundant" forces. To obtain a solution for the full set of basic unknown forces, it is necessary to augment the set of independent equilibrium equations with elastic behavior of the structure, namely the force-displacement relations of the structure. Having solved for the full set of basic forces, we can determine the displacements by back substitution.

10.2.5 Influence Lines and Surfaces

In the design and analysis of bridge structures subjected to moving loads, it is necessary to study the effects intrigued by loads placed in various positions. This can be done conveniently by means of diagrams showing the effect of moving a unit load across the structures. Such diagrams are commonly called influence lines (for framed structures) or influence surfaces (for plates). Observe that a moment or shear diagram shows the variation in moment or shear along the structure because of some particular position of load; an influence line or surface for moment or shear shows the variation of moment or shear at a particular section because of a unit load placed anywhere along the structure.

Exact influence lines for statically determinate structures can be obtained analytically by statics alone. From Equation 10.11, the total primary internal forces vector $\{P\}$ can be expressed as

$$\{P\} = [A]^{-1}\{F\} \tag{10.12}$$

by which given a unit load at one node, the excited internal forces of all members will be obtained, and thus Equation 10.12 gives the analytical expression of influence lines of all member internal forces for discretized structures subjected to moving nodal loads.

For statically indeterminate structures, influence values can be determined directly from a consideration of the geometry of the deflected load line resulting from the imposing of unit deformation corresponding to the function under study, based on the principle of virtual work. This may better be demonstrated by a two-span continuous beam shown in Figure 10.6, where influence line of internal bending moment M_B at section B is required.

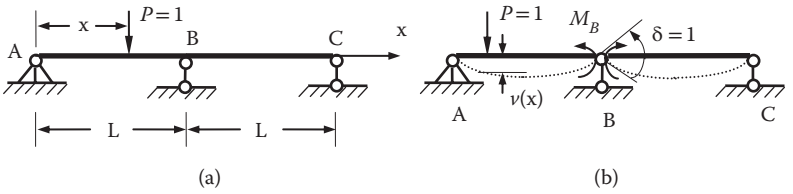

FIGURE 10.6 Influence line of a two-span continuous beam.

Cutting section B to expose M_B and give it a unit relative rotation $\delta = 1$ (see Figure 10.6), and employing the principle of virtual work gives

$$M_B \cdot \delta = -P \cdot v(x) \tag{10.13}$$

There,

$$M_B = -v(x) \tag{10.14}$$

which means the influence value of M_B equals to the deflection $v(x)$ of the beam subjected to a unit rotation at joint B (represented by dashed line in Figure 10.6b). Solving for $v(x)$ can be carried out easily referring to material mechanics.

10.3 Compatibility Equations

10.3.1 Large Deformation and Large Strain

Strain analysis is concerned with the study of deformation of a continuous body that is unrelated to properties of the body material. In general, there are two methods of describing the deformation of a continuous body, Lagrangian and Eulerian. The Lagrangian method employs the coordinates of each particle in the initial position as the independent variables. The Eulerian method defines the independent variables as the coordinates of each material particle at the time of interest.

Let the coordinates of material particle P in a body in the initial position be denoted by $x_i(x_1, x_2, x_3)$ referred to the fixed axes x_i as shown in Figure 10.10 later in the chapter. And the coordinates of the particle after deformation are denoted by $\xi_i(\xi_1, \xi_2, \xi_3)$ with respect to axes x_i. As for the independent variables, Lagrangian Formulation uses the coordinates (x_i), whereas Eulerian Formulation employs the coordinates (ξ_i). From motion analysis of line element PQ (see Figure 10.7), one has

For Lagrangian Formulation, the Lagrangian strain tensor is

$$\varepsilon_{ij} = \frac{1}{2}(u_{i,j} + u_{j,i} + u_{r,i}u_{r,j}) \tag{10.15}$$

where $u_{i,j} = \dfrac{\partial u_i}{\partial x_j}$ and all quantities are expressed in terms of (x_i).

For Eulerian Formulation, the Eulerian strain tensor is

$$E_{ij} = \frac{1}{2}(u_{i/j} + u_{j/i} + u_{r/i}u_{r/j}) \tag{10.16}$$

where $u_{i/j} = \dfrac{\partial u_i}{\partial \xi_j}$ and all quantities are described in terms of (ξ_i).

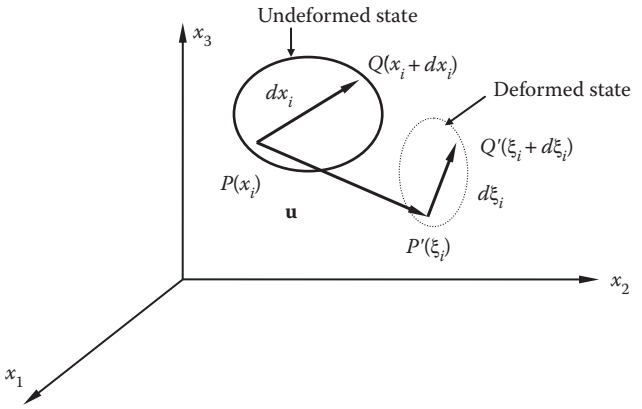

FIGURE 10.7 Deformation of a line element for Lagrangian and Eluerian variables.

If the displacement derivatives $u_{i,j}$ and $u_{i/j}$ are not so small that their nonlinear terms cannot be neglected, it is called large deformation, and the solving of u_i will be rather difficult since the nonlinear terms appear in the governing equations.

If both the displacements and their derivatives are small, it is immaterial whether the derivatives in Equations 10.15 and 10.16 are calculated using the (x_i) or the (ξ_i) variables. In this case both Lagrangian and Eulerian descriptions yield the same strain–displacement relationship:

$$\varepsilon_{ij} = E_{ij} = \frac{1}{2}(u_{i,j} + u_{j,i}) \tag{10.17}$$

which means small deformation, the most common in structural engineering.

For given displacements (u_i) in strain analysis, the strain components (ε_{ij}) can be determined from Equation 10.17. For prescribed strain components (ε_{ij}), some restrictions must be imposed on it in order to have single-valued continuous displacement functions u_i, since there are six equations for three unknown functions. Such restrictions are called compatibility conditions, which for a simple connected region may be written as

$$\varepsilon_{ij,kl} + \varepsilon_{kl,ij} - \varepsilon_{ik,jl} - \varepsilon_{ji,ik} = 0 \tag{10.18a}$$

or, expanding these expressions in the (x, y, z) notations, it gives

$$\begin{aligned}
\frac{\partial^2 \varepsilon_x}{\partial y^2} + \frac{\partial^2 \varepsilon_y}{\partial x^2} &= 2\frac{\partial^2 \varepsilon_{xy}}{\partial x \partial y} \\
\frac{\partial^2 \varepsilon_y}{\partial z^2} + \frac{\partial^2 \varepsilon_z}{\partial y^2} &= 2\frac{\partial^2 \varepsilon_{yz}}{\partial y \partial z} \\
\frac{\partial^2 \varepsilon_z}{\partial x^2} + \frac{\partial^2 \varepsilon_x}{\partial z^2} &= 2\frac{\partial^2 \varepsilon_{zx}}{\partial z \partial x} \\
\frac{\partial}{\partial x}\left(-\frac{\partial \varepsilon_{yz}}{\partial x} + \frac{\partial \varepsilon_{zx}}{\partial y} + \frac{\partial \varepsilon_{xy}}{\partial z}\right) &= \frac{\partial^2 \varepsilon_x}{\partial y \partial z} \\
\frac{\partial}{\partial y}\left(-\frac{\partial \varepsilon_{zx}}{\partial y} + \frac{\partial \varepsilon_{xy}}{\partial z} + \frac{\partial \varepsilon_{yz}}{\partial x}\right) &= \frac{\partial^2 \varepsilon_y}{\partial z \partial x} \\
\frac{\partial}{\partial z}\left(-\frac{\partial \varepsilon_{xy}}{\partial z} + \frac{\partial \varepsilon_{yz}}{\partial x} + \frac{\partial \varepsilon_{zx}}{\partial y}\right) &= \frac{\partial^2 \varepsilon_z}{\partial x \partial y}
\end{aligned} \tag{10.18b}$$

Any set of strains ε_{ij} displacements u_i that satisfies Equations 10.17 and 10.18a or 10.18b, and displacement boundary conditions, is a kinematics admissible set, or compatible set.

10.3.2 Compatibility Equation for Elements

For ordinary FEM, compatibility requirements are self-satisfied in the formulating procedure. As the same for equilibrium equations, a basic set of independent displacements can be identified for each member, and the kinematics relationships between member basic displacements and member-end displacements of one member can be given as follows:

$$\{\Delta\}^e = [L]^T \left\{\overline{d}\right\}^e \tag{10.19}$$

where $\{\Delta\}^e$ is element primary displacement vector, and $[L]$ and $\left\{\overline{d}\right\}^e$ have been shown in Section 10.2.2. For plane truss member, $\{\Delta\}^e = \{\Delta\}$, where Δ is the relative displacement of member (see Figure 10.5). It should also be noted that the physical basis of Equation 10.19 is overall compatibility of the element.

10.3.3 Compatibility Equation for Structures

For the whole structure, one has the following equation after assembly process:

$$\{\Delta\} = [A]^{\mathrm{T}} \{D\} \tag{10.20}$$

where $\{\Delta\}$ = total primary displacement vector; $\{D\}$ = total nodal displacement vector; and $[A]^{\mathrm{T}}$ = the transposition of $[A]$ described in Section 10.2.4.

A statically determinate structure is kinematically determinate. Given a set of basic member displacements, there are a sufficient number of compatibility relationships available to allow the structure nodal displacements to be determined. In addition to their application to settlement and fabrication error loading, thermal loads can also be considered for statically determinate structures. External forces on a structure cause member distortions and, hence, nodal displacements, but before such problems can be solved, the relationships between member forces and member distortions must be developed. These will be shown in Section 10.5.1.

10.3.4 Contragredient Law

During the development of the equilibrium and compatibility relationships, it has been noticed that various corresponding force and displacement transformations are the transposition to each other, as shown not only in Equations 10.5 and 10.19 of element equilibrium and compatibility relations, but also in Equations 10.11 and 10.20 of global equilibrium and compatibility relations, although each pair of these transformations was obtained independently of the other in the development. These special sets of relations are termed the contragredient law that was established on the basis of virtual work concepts. Therefore, after a particular force transformation matrix is obtained, the corresponding displacement transformation matrix would be immediately apparent, and it remains valid on the contrary.

10.4 Constitutive Equations

10.4.1 Elasticity and Plasticity

A material body will produce deformation when subjected to external excitations. If upon the release of applied actions the body recovers its original shape and size, it is called elastic material, or one can say the material has the characteristic of elasticity. Otherwise, it is a plastic material or a material with

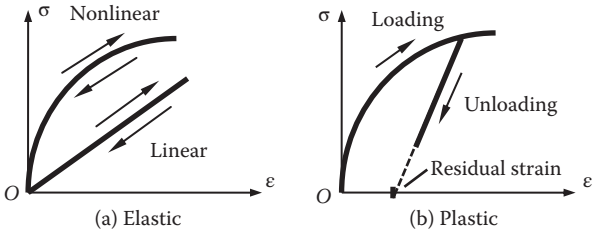

FIGURE 10.8 Sketches of behavior of elastic and plastic materials.

plasticity. For an elastic body, the current state of stress depends only on the current state of deformation; that is, the constitutive equations for elastic material are given by

$$\sigma_{ij} = F_{ij}(\varepsilon_{kl}) \tag{10.21}$$

where F_{ij} called the elastic response function. Thus the elastic material behavior described by Equation 10.21 is both reversible and path-independent (see Figure 10.8a), in which case the material is usually termed Cauchy elastic material.

Reversibility and path independence are not exhibited by plastic materials (see Figure 10.8b). In general, a plastic material does not return to its original shape; residual deformations and stresses remain inside the body even when all external tractions are removed. As a result, it is necessary for plasticity to extend the elastic stress–strain relations into the plastic range where permanent plastic stain is possible. It makes the solution of a solid mechanics problem more complicated. For more detailed discussion about constitutive equations, references are made to Chen and Saleeb (1982), Chen (1982), Chen and Han (2007).

10.4.2 Linear Elastic and Nonlinear Elastic Behavior

Just as the term linear implies, linear elasticity means the elastic response function F_{ij} of Equation 10.21 is a linear function, whose most general form for a Cauchy elastic material is given by

$$\sigma_{ij} = B_{ij} + C_{ijkl}\varepsilon_{kl} \tag{10.22}$$

where B_{ij} = components of initial stress tensor corresponding to the initial strain free state (i.e., $\varepsilon_{ij} = 0$), and C_{ijkl} = tensor of material elastic constants.

If it is assumed that $B_{ij} = 0$, Equation 10.22 will be reduced to

$$\sigma_{ij} = C_{ijkl}\varepsilon_{kl} \tag{10.23}$$

which is often referred to as the generalized Hook's Law.

For an isotropic linear elastic material, the elastic constants in Equation 10.23 must be the same for all directions and thus C_{ijkl} must be an isotropic fourth-order tensor, which means that there are only two independent material constants. In this case, Equation 10.23 will reduce to

$$\sigma_{ij} = \lambda\varepsilon_{kk}\delta_{ij} + 2\mu\varepsilon_{ij} \tag{10.24}$$

where λ and μ are the two material constants, usually called Lame's constants; δ_{ij} = Kronecker delta and ε_{kk} = the summation of the diagonal terms of ε_{ij} according to the summation convention, which means that whenever a subscript occurs twice in the same term, it is understood that the subscript is to be summed from 1 to 3.

If the elastic response function F_{ij} in Equation 10.21 is not linear, it is called nonlinear elastic, and the material exhibits nonlinear mechanical behavior even when sustaining small deformation. That is, the material elastic "constants" do not remain constant any more, whereas the deformation can still be reversed completely.

10.4.3 Geometric Nonlinearity

Based on the sources from which it arises, nonlinearity can be categories into material nonlinearity (including nonlinear elasticity and plasticity) and geometric nonlinearity. When the nonlinear terms in the strain-displacement relations cannot be neglected (see Section 10.3.1), or the deflections are large enough to cause significant changes in the structural geometry, it is termed geometric nonlinearity. It is also called large deformation and the principle of supper position derived from small deformations is no longer valid. It should be noted that for accumulated large displacements with small deformations, it could be linearized by a step-by-step procedure.

According to the different choice of reference frame, there are two types of Lagrangian Formulation: the Total Lagrangian Formulation that takes the original unstrained configuration as the reference frame, and the Updated Lagrangian Formulation based on the latest obtained configuration, which are usually carried out step-by-step. Whatever formulation one chooses, a geometric stiffness matrix or initial stress matrix will be introduced into the equations of equilibrium to take account of the effects of the initial stresses on the stiffness of the structure. These depend on the magnitude or conditions of loading and deformations, and thus cause the geometric nonlinearity. In beam-column theory, this is well known as the second order or the P-Δ effect. For detailed discussions, see Chapter 5 of *Bridge Engineering Handbook, Second Edition: Seismic Design.*

10.5 Displacement Method

10.5.1 Stiffness Matrix for Elements

In displacement method, displacement components are taken as primary unknowns. From Equations 10.5 to 10.19 the equilibrium and compatibility requirements on elements have been acquired. For a statically determinate structure, no subsidiary conditions are needed to obtain internal forces under nodal loading or the displaced position of the structure given the basic distortion such as support settlement, fabrication errors. For a statically indeterminate structure, however, supplementary conditions, namely the constitutive law of materials constructing the structure, should be incorporated for the solution of internal forces as well as nodal displacements.

From structural mechanics, the basic stiffness relationships for a member between basic internal forces and basic member-end displacements can be expressed as

$$\{P\}^e = [k]^e \{\Delta\}^e \tag{10.25}$$

where $[k]^e$ is the element basic stiffness matrix, which can be termed $[EA/l]$ for a conventional plane truss member (see Figure 10.4).

Substitution of Equations 10.19 and 10.25 with Equation 10.5 yields

$$\begin{aligned} \left\{\overline{F}\right\}^e &= [L][k]^e [L]^T \left\{\overline{d}\right\}^e \\ &= \left[\overline{k}\right]^e \left\{\overline{d}\right\}^e \end{aligned} \tag{10.26}$$

where

$$\left[\overline{k}\right]^e = [L][k]^e [L]^T \tag{10.27}$$

is called element stiffness matrix, as the same in Equation 10.4. It should be kept in mind that the element stiffness matrix $\left[\overline{k}\right]^e$ is symmetric and singular, since given the member-end forces, member-end displacements cannot be determined uniquely because the member may undergo rigid body movement.

10.5.2 Stiffness Matrix for Structures

Our final aim is to obtain equations that define approximately the behavior of the whole body or structure. Once the element stiffness relations of Equation 10.26 is established for a generic element, the global equations can be constructed by assembling process based on the law of compatibility and equilibrium, which are generally expressed in matrix notation as

$$\{F\} = [K]\{D\} \tag{10.28}$$

where $[K]$ is the stiffness matrix for the whole structure. It should be noted that the basic idea of assembly involves a minimization of total potential energy, and the assemblage stiffness matrix $[K]$ is symmetric and banded or sparsely populated.

Equation 10.28 tells us the capabilities of a structure to withstand applied loading rather than the true behavior of the structure if boundary conditions are not introduced. In other words, without boundary conditions there can be an infinite number of possible solutions since stiffness matrix $[K]$ is singular, that is, its determinant vanishes. Hence, Equations 10.28 should be modified to reflect boundary conditions and the final modified equations are expressed by inserting overbars as

$$\left\{\overline{F}\right\} = \left[\overline{K}\right]\left\{\overline{D}\right\} \tag{10.29}$$

10.5.3 Matrix Inversion

It has been shown that sets of simultaneous algebraic equations are generated in the application of both displacement method and force method in structural analysis, which are usually linear. The coefficients of the equations are constant and do not depend on the magnitude or conditions of loading and deformations, since linear Hook's law is generally assumed valid and small strains and deformations are used in the formulation. Solving Equation 10.29 is namely to invert the modified stiffness matrix $\left[\overline{K}\right]$. This requires tremendous computational efforts for large-scale problems. The equations can be solved by using direct, iterative, or other methods. Two steps of elimination and back-substitution are involved in the direct procedures, among which are Gaussian elimination and a number of its modifications. There are some of the most widely used sets of direct methods because of their better accuracy and small number of arithmetic operations.

10.5.4 Special Consideration

In practice, a variety of special circumstances, ranging from loading to internal member conditions, to supporting conditions, should be given due consideration in structural analysis.

Initially strains, which are not directly associated to stresses, result from two causes, thermal loading, or fabrication error. If the member with initial strains is unconstrained, there will be a set of initial member-end displacements associated with these initial strains, but nevertheless no initial member-end forces. For a member constrained to act as part of a structure, the general member force-displacement relationships will be modified as follows:

$$\left\{\overline{F}\right\}^e = \left[\overline{k}\right]^e \left(\left\{\overline{d}\right\}^e - \left\{\overline{d_0}\right\}^e\right) \tag{10.30a}$$

or

$$\left\{\overline{F}\right\}^e = \left[\overline{k}\right]^e \left\{\overline{d}\right\}^e + \left\{R_{F0}\right\}^e \tag{10.30b}$$

where

$$\left\{R_{F0}\right\}^e = -\left[\overline{k}\right]^e \left\{\overline{d}_0\right\}^e \tag{10.31}$$

are fixed-end forces, and $\left\{\overline{d}_0\right\}^e$ a vector of initial member-end displacements for the member.

It is interesting to note that a support settlement may be regarded as an initial strain. Moreover, initial strains including thermal loading and fabrication errors, as well as support settlements, can all be treated as external excitations. Hence the corresponding fixed-end forces as well as the equivalent nodal loading can be obtained that makes the conventional procedure described previously still practicable.

For a skewed support that provides a constraint to the structure in a nonglobal direction, the effect can be given due consideration by adapting a skewed global coordinate (see Figure 10.9) by introducing skewed coordinate at the skewed support. This can perhaps better be demonstrated by considering a specific example of a plane truss shown in Figure 10.9. For members jointed at skewed support, the coordinate transformation matrix will takes the form of

$$[\alpha] = \begin{bmatrix} \cos\alpha_i & -\sin\alpha_i & 0 & 0 \\ \sin\alpha_i & \cos\alpha_i & 0 & 0 \\ 0 & 0 & \cos\alpha_j & -\sin\alpha_j \\ 0 & 0 & \sin\alpha_j & \cos\alpha_j \end{bmatrix} \tag{10.32}$$

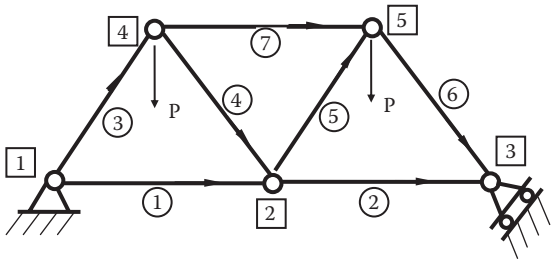

(a) Dimensions and loading

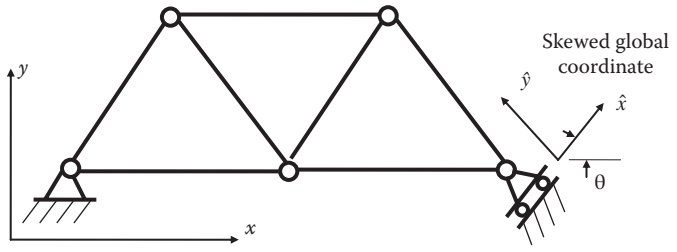

General global coordinate

(b) Mixed coordinate model

FIGURE 10.9 Plane truss with skewed support.

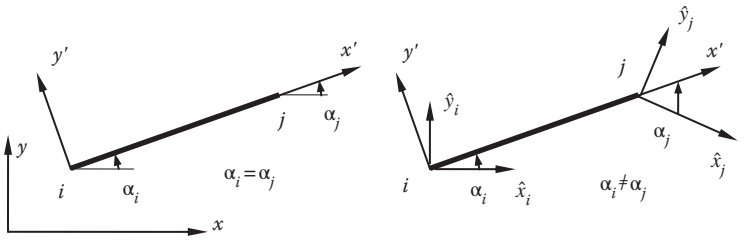

FIGURE 10.10 Plane truss member coordinate transformation.

where α_i and α_j are inclined angles of truss member in skewed global coordinate (see Figure 10.10). Say, for member 2 in Figure 10.9, $\alpha_i = 0$ and $\alpha_j = -\theta$.

For other special members such as inextensional or variable cross-section ones, it may be necessary or convenient to employ special member force–displacement relations in structural analysis. Although the development and programming of a stiffness method general enough to take into account all these special considerations is formidable, more important perhaps is the fact that the application of the method remains little changed.

10.6 Substructuring and Symmetry Consideration

For highly complex or large-scale structures, one will be required to solve a very large set of simultaneous equations, which are sometimes restricted by the computation resources available. In that case, special data handling schemes like static condensation are needed to reduce the number of unknowns by appropriately numbering nodal displacement components and disposition of element force–displacement relations. Static condensation is useful in dynamic analysis of framed structures since the rotatory moment of inertia is usually neglected.

Another scheme physically partitions the structure into a collection of smaller structures called "substructures," which can be processed by parallel computers. In static analysis, the first step of substructuring is to introduce imaginary fixed inner boundaries, and then release all inner boundaries simultaneously, which gives rise to a subsequent analysis of these substructure series in a smaller scale. It is essentially the patitioning of Equation 10.28, as follows. For *r*th substructure, one has
case (α): introducing inner fixed boundaries

$$\begin{bmatrix} K_{bb} & K_{bi} \\ K_{ib} & K_{ii} \end{bmatrix}^{(r)} \begin{Bmatrix} 0 \\ D_i^{\alpha} \end{Bmatrix}^{(r)} = \begin{Bmatrix} F_b^{\alpha} \\ F_i \end{Bmatrix}^{(r)} \tag{10.33}$$

case (β): releasing all inner fixed boundaries

$$\begin{bmatrix} K_{bb} & K_{bi} \\ K_{ib} & K_{ii} \end{bmatrix}^{(r)} \begin{Bmatrix} D_b \\ D_i^{\beta} \end{Bmatrix}^{(r)} = \begin{Bmatrix} F_b^{\beta} \\ 0 \end{Bmatrix}^{(r)} \tag{10.34}$$

where subscripts b and i denote inner fixed and free nodes, respectively.

Combining Equations 10.33 and 10.34 gives the force-displacement relations for enlarged elements—substructures that may be expressed as

$$\left[K_b\right]^{(r)} \left\{D_b\right\}^{(r)} = \left\{F_b\right\}^{(r)} \tag{10.35}$$

which is analogous to Equation 10.26 and $\{F_b\}^{(r)} = \{F_b^{(r)}\} - [K_{bi}^{(r)}][K_{ii}^{(r)}]^{-1}\{F_i^{(r)}\}$.

And thereby the conventional procedure is still valid.

Similarly, in the cases of structural symmetry of geometry and material, proper consideration of loading symmetry and antisymmetry can give rise to a much smaller set of governing equations.

For more details, please refer to other literature on structural analysis (Chen and Atsuta, 1976; Michalos, 1958; Wilson, 2009).

References

Bathe, K. J., and Wilson, E. L. 1976. *Numerical Methods in Finite Element Analysis*, Prentice-Hall, New York, NY.

Chen, W. F. 1982. *Plasticity in Reinforced Concrete.* McGraw-Hill, New York, NY.

Chen, W. F., and Atsuta, T. 1976. *Theory of Beam-Columns.* Volumes 1 and 2. McGraw-Hill, New York, NY.

Chen, W. F., and Han, D. J. 2007. *Plasticity for Structural Engineers.* J. Ross Publishing, Inc., Fort Lauderdale, FL.

Chen, W. F., and Saleeb, A. F. 1982. *Constitutive Equations for Engineering Materials.* Volume 1. Elasticity and Modeling. John Wiley & Sons, New York, NY.

Cook, R. D., David, S., Malkus, D. S., Plesha, M. E., and Witt, R. J. 2002. *Concepts and Applications of Finite Element Analysis.* 4th Edition. John Wiley & Sons, New York, NY.

Desai, C. S. 1979. *Elementary Finite Element Method.* Prentice-Hall, Englewood Cliffs, NJ.

Meyers, V. J. 1983. *Matrix Analysis of Structures.* Harper & Row, New York, NY.

Michalos, J. 1958. *Theory of Structural Analysis and Design.* Ronald Press, New York, NY.

Wilson, E. L. 2009. *Static and Dynamic Analysis of Structures*, Computers and Structures Inc., Berkeley, CA.

11

Finite Element Method

Eiki Yamaguchi
Kyushu Institute of Technology

11.1 Introduction

With the advancement of computer technology and commercial package, the finite element method (FEM) is now used exclusively for the analysis of structures including bridges. However, it should be well-understood that FEM is a numerical method and provides an approximate solution. The quality of the solution could vary from engineer to engineer responsible for the analysis. To conduct a good finite element analysis (FEA), the engineer should have a certain amount of knowledge of FEM, even though it is possible to get results with little knowledge of FEM itself from an FEM package.

This chapter intends to provide the fundamentals of FEM, the minimum knowledge that a bridge engineer is supposed to acquire if he/she conducts the FEA of structures. Closely related to the present chapter are Chapters 10 and 12; the former discusses the basic structural theory and the latter presents structural modeling, respectively.

Bridge engineering deals with so many physical phenomena. FEM is versatile and can be applied to a great variety of engineering problems. The advanced application of FEM is beyond the scope of this chapter and readers are advised to refer to technical books on FEM. There are a great many books on FEM published and available to date (e.g., Hughes, 2000; Cook et al., 2002; Zienkiewicz et al., 2005).

In the first section of the chapter, we present the essentials of FEM, making use of a one-dimensional boundary-value problem (BVP). We touch upon almost all the fundamental features of FEM in this section. In the subsequent section, we discuss the application of FEM to a solid mechanics problem. The linear problem is considered, as it is the base of the solid mechanics. The chapter then concludes with some other important remarks on FEM.

11.2 FEM for One-Dimensional Boundary-Value Problem

11.2.1 One-Dimensional Boundary-Value Problem

We consider the BVP described by the following equations:

$$EAu_{,xx} + p = 0 \qquad (0 < x < L) \tag{11.1}$$

$$u(0) = U_0 \tag{11.2}$$

$$EAu_{,x}(L) = P \tag{11.3}$$

where the comma indicates the derivative: $(\,)_{,x} = \mathrm{d}(\,)/dx$; $(\,)_{,xx} = \mathrm{d}^2(\,)/\mathrm{d}x^2$.

This set of equations governs the deformation of a bar shown in Figure 11.1. EA is the axial stiffness of the bar, p the distributed load, u the displacement, U_0 the displacement at $x = 0$, and P the force applied at $x = L$. For the sake of simplicity, we assume $L = 6$, $EA = 1$, $p = -2$, $U_0 = -1$, and $P = 7$. The above BVP is now written as

[BVP1]
Find $u(x)$ that satisfies Equations 11.4 through 11.6:

$$u_{,xx} - 2 = 0 \qquad (0 < x < 6) \tag{11.4}$$

$$u(0) = -1 \tag{11.5}$$

$$u_{,x}(6) = 7 \tag{11.6}$$

We can obtain the exact solution of the above BVP easily as

$$u(x) = x^2 - 5x - 1 \tag{11.7}$$

In this section, FEM is exemplified by this problem.

11.2.2 Strong Form and Weak Form

We combine Equations 11.4 through 11.6 as follows:

$$-\int_0^6 (u_{,xx} - 2)w\,\mathrm{d}x + (u_{,x}(6) - 7)w(6) = 0 \tag{11.8}$$

where $w(x)$ is a weight function, an arbitrary function that satisfies

$$w(0) = 0 \tag{11.9}$$

By conducting the integration by parts, we reach the following equation:

$$\int_0^6 u_{,x}\, w_{,x}\,\mathrm{d}x + \int_0^6 2w\,\mathrm{d}x - 7w(6) = 0 \tag{11.10}$$

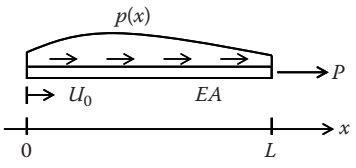

FIGURE 11.1 A bar problem.

Then we construct another BVP:

[BVP2]
Find $u(x)$ that satisfies Equations 11.5 and 11.10 for any function $w(x)$ that satisfies Equation 11.9.

In BVP2, the satisfaction of one boundary condition, Equation 11.5, is required explicitly, whereas the other, Equation 11.6, is imbedded in Equation 11.10. The former is of the Dirichlet boundary condition, giving the specific value on the boundary, and the latter the Neumann boundary condition, giving the gradient on the boundary. Note that the Dirichlet boundary condition is also called the essential boundary condition, whereas the Neumann boundary condition is called the natural boundary condition.

The exact solution of BVP2 is identical to that of BVP1, which we can prove without much difficulty (Hughes, 2000). The two BVPs are nothing but the same problem, just in different forms.

As for the derivative, BVP1 involves the second derivative of $u(x)$, whereas BVP2 has the integration of the first derivative of $u(x)$ only. Thus the requirement of $u(x)$ is weaker in BVP2. Therefore, BVP1 and BVP2 are called the strong form and the weak form of BVP, respectively.

11.2.3 Weighted-Residual Method

The exact solution does not always exist or it may be very difficult to obtain even if it exists. In such cases, we seek an approximate solution.

The exact solution satisfies all the equations that define the problem, whereas the approximate solution does not necessarily satisfy all of them or it satisfies even none of them. There are many approximate solutions for a BVP, the deviations of which from the exact solution can vary to a great degree.

Out of various methods for obtaining approximate solutions, the weighted residual method (WRM) is explained herein. FEM is classified into WRM, as explained later.

WRM deals with the weak form of BVP. And for the present BVP, whereas Equation 11.5 is imposed rigorously, Equations 11.10 is satisfied only approximately. Specifically, WRM takes the following steps:

Step 1. A trial function is constructed in such a way that Equation 11.5 is satisfied. It usually takes the following form:

$$u(x) = \sum_{j=1}^{m} a_j \varphi_j(x) + \sum_{j=m+1}^{n} \overline{a}_j \varphi_j(x) \tag{11.11}$$

where

a_j = unknown constant
$\overline{a}_j$ = known constant
$\varphi_j(x)$ = known function (base function)

Step 2. Equation 11.11 is substituted into Equations 11.10, leading to a set of simultaneous equations for a_j.

Step 3. The simultaneous equations are solved for a_j.

Equation 11.11 with a_j thus obtained yields an approximate solution.

To carry out the computations in the steps above, the weight function $w(x)$ needs be specific in a sense, whereas keeping its arbitrariness. The Galerkin method is often used in this conjunction: the same base functions as those of the trial function are employed. When Equation 11.11 is the trial function, the Galerkin method would give the following weight function:

$$w(x) = \sum_{j=1}^{m} b_j \varphi_j(x) \tag{11.12}$$

where

b_j = arbitrary constant

Needless to say, the weight function, Equation 11.12, must satisfy Equation 11.9, the requirement of the weight function.

Example Problem 1

Obtain an approximate solution of the present BVP. Employ the following trial function and apply the Galerkin method:

$$u(x) = a_1 x - 1 \tag{11.13}$$

where a_1 is an unknown constant.

It is noted that we can easily confirm that the trial function, Equation 11.13, satisfies the essential boundary condition, Equation 11.5, as it is supposed to.

SOLUTION

The Galerkin method gives the following weight function:

$$w(x) = b_1 x \tag{11.14}$$

where b_1 is an arbitrary constant. The weight function, Equation 11.14, satisfies its requirement of Equation 11.9.

Substitution of Equations 11.13 and 11.14 into Equations 11.10 leads to

$$b_1 (a_1 - 1) = 0 \tag{11.15}$$

Since b_1 is arbitrary, a_1 is obtained as

$$a_1 = 1 \tag{11.16}$$

yielding the following approximate solution:

$$u(x) = x - 1 \tag{11.17}$$

The solution thus obtained is plotted in Figure 11.2. It is trivial that WRM with the linear trial function cannot give the exact solution since the exact solution is a quadratic polynomial. If the quadratic polynomial is employed for the trial function instead of Equation 11.13, WRM would result in the exact solution. In general, a higher-degree function yields a better approximate solution, but the computational cost would be larger.

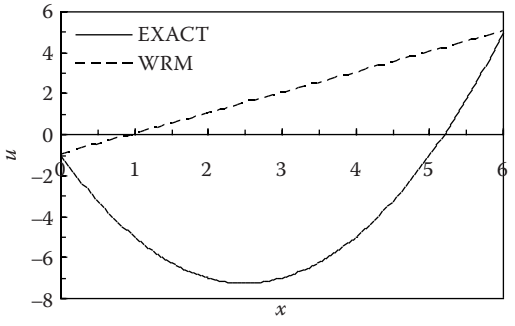

FIGURE 11.2 Solution by WRM.

11.2.4 FEM

FEM is a WRM and deals with the weak form of BVP. In FEM, the problem domain is decomposed into small regions. The small region is called a finite element. The trial function is defined in the element, whereas the trial function in the conventional WRM is for the entire problem domain. In FEM, the integration in Equation 11.10 is conducted over each element individually and the summation will be taken to evaluate the integration value over the entire domain. The finite element procedure for Equation 11.10 is therefore expressed formally as follows:

$$G = \sum_e G^e - 7w(6) = 0 \tag{11.18}$$

where

$$G^e = \int_{L^e} u_{,x}\, w_{,x}\, \mathrm{d}x + \int_{L^e} 2w\, \mathrm{d}x \tag{11.19}$$

$\sum_e$ indicates the summation of the contributions of all the elements, and L^e is the region (length) of each element.

When we employ the Galerkin method, the trial function and the weight function are given as

$$u(\xi) = \sum_{a=1}^{n} N^a(\xi)\, U^a \tag{11.20}$$

$$w(\xi) = \sum_{a=1}^{n} N^a(\xi)\, W^a \tag{11.21}$$

Both functions are defined in a specific element. To describe the functions, nodes are set up in the element and n in the above equations is the number of nodes in the element. U^a and W^a are the displacement at Node a and the weight at Node a, respectively. The displacement at the node is named the nodal displacement and the weight at the node is the nodal weight. $N^a(\xi)$ is the base function and is often called the shape function in FEM.

Figure 11.3 shows two bar elements: one is a 2-node element with a linear trial function and the other a 3-node element with a quadratic trial function. After their respective shape functions, the 2-node element is called a linear element, whereas the 3-node element a quadratic element. Each solid circle in

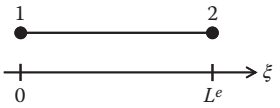

(a)

$$u(\xi) = \frac{L^e - \xi}{L^e} U^1 + \frac{\xi}{L^e} U^2$$

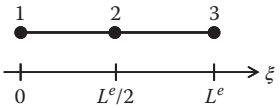

(b)

$$u(\xi) = \left(\frac{L^e - \xi}{L^e}\right)\left(\frac{L^e - 2\xi}{L^e}\right) U^1 + \frac{4\xi}{L^e}\left(\frac{L^e - \xi}{L^e}\right) U^2 - \frac{\xi}{L^e}\left(\frac{L^e - 2\xi}{L^e}\right) U^3$$

FIGURE 11.3 Bar element (a) 2-node bar element (linear element); (b) 3-node bar element (quadratic element).

the elements represents "node." The unknown coefficients of the trial function such as U^1 are the nodal displacements. Thus, the unknown has a specific physical/engineering meaning in FEM. Employing a different function for the trial function, a different element is established. There are some requirements for the trial function, the details of which are not discussed herein, but can be found in books on FEM.

We take the following steps in FEM:

Step 1. Decide the type of element and the element mesh for the analysis.
Step 2. Carry out the integration in Equation 11.19 for each element.
Step 3. Compute Equation 11.18, which leads to a set of simultaneous equations for the nodal displacements.
Step 4. Solve the set of simultaneous equations for the nodal displacements.

The simultaneous equations obtained in Step 3 may be called the finite element equations.

Example Problem 2

Obtain a solution of the present BVP by FEM.

SOLUTION

Step 1. It is decided that the 3 linear elements of the equal length are used as presented in Figure 11.4. The employed element type is the one shown in Figure 11.3a. Note that two numbers are assigned to each node: one is the global node number and the other the local node number. The latter is needed to describe the trial functions. In the present example, the node numbers 1–4 in Figure 11.4 are the global node numbers, whereas the node numbers 1 and 2 in Figure 11.3a are the local node numbers.

Step 2. **Element ①**

We have the following expressions for this element:

$$u(\xi)=\sum_{a=1}^{2}N^a(\xi)U^a=\frac{2-\xi}{2}U^1+\frac{\xi}{2}U^2 \tag{11.22}$$

$$w(\xi)=\sum_{a=1}^{2}N^a(\xi)W^a=\frac{2-\xi}{2}W^1+\frac{\xi}{2}W^2 \tag{11.23}$$

$$\xi=x \tag{11.24}$$

Therefore, we get

$$u_{,x}=-\frac{1}{2}U^1+\frac{1}{2}U^2 \tag{11.25}$$

$$w_{,x}=-\frac{1}{2}W^1+\frac{1}{2}W^2 \tag{11.26}$$

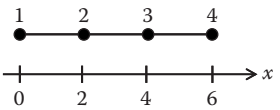

FIGURE 11.4 Finite element mesh.

$$G^1 = \int_0^2 u_{,x}\, w_{,x}\, dx + \int_0^2 2w\, dx$$
$$= \begin{bmatrix} W^1 & W^2 \end{bmatrix} \left(\begin{bmatrix} \frac{1}{2} & -\frac{1}{2} \\ -\frac{1}{2} & \frac{1}{2} \end{bmatrix} \begin{bmatrix} U^1 \\ U^2 \end{bmatrix} + \begin{bmatrix} 2 \\ 2 \end{bmatrix} \right) \tag{11.27}$$

The 2×2 matrix in Equation 11.27 is called an element stiffness matrix in FEM.

Element ②, Element ③
Similar computations yield

$$G^2 = \int_2^4 u_{,x}\, w_{,x}\, dx + \int_2^4 2w\, dx$$
$$= \begin{bmatrix} W^2 & W^3 \end{bmatrix} \left(\begin{bmatrix} \frac{1}{2} & -\frac{1}{2} \\ -\frac{1}{2} & \frac{1}{2} \end{bmatrix} \begin{bmatrix} U^2 \\ U^3 \end{bmatrix} + \begin{bmatrix} 2 \\ 2 \end{bmatrix} \right) \tag{11.28}$$

$$G^3 = \int_4^6 u_{,x}\, w_{,x}\, dx + \int_4^6 2w\, dx$$
$$= \begin{bmatrix} W^3 & W^4 \end{bmatrix} \left(\begin{bmatrix} \frac{1}{2} & -\frac{1}{2} \\ -\frac{1}{2} & \frac{1}{2} \end{bmatrix} \begin{bmatrix} U^3 \\ U^4 \end{bmatrix} + \begin{bmatrix} 2 \\ 2 \end{bmatrix} \right) \tag{11.29}$$

Step 3. Equation 11.18 then gives

$$G = \sum_{a=1}^{3} G^a - 7w(6)$$
$$= \begin{bmatrix} W^1 & W^2 & W^3 & W^4 \end{bmatrix} \left(\begin{bmatrix} \frac{1}{2} & -\frac{1}{2} & 0 & 0 \\ -\frac{1}{2} & 1 & -\frac{1}{2} & 0 \\ 0 & -\frac{1}{2} & 1 & -\frac{1}{2} \\ 0 & 0 & -\frac{1}{2} & 1 \end{bmatrix} \begin{bmatrix} U^1 \\ U^2 \\ U^3 \\ U^4 \end{bmatrix} + \begin{bmatrix} 2 \\ 4 \\ 4 \\ -5 \end{bmatrix} \right) \tag{11.30}$$
$$= 0$$

Since $U^1 = u(0) = -1$, $W^1 = w(0) = 0$ and $W^2 - W^3$ are arbitrary, Equation 11.30 leads to

$$\begin{bmatrix} 2 & -1 & 0 \\ -1 & 2 & -1 \\ 0 & -1 & 1 \end{bmatrix} \begin{bmatrix} U^2 \\ U^3 \\ U^4 \end{bmatrix} = \begin{bmatrix} -9 \\ -8 \\ 10 \end{bmatrix} \tag{11.31}$$

Step 4. Solving Equation 11.31, we arrive at

$$\begin{bmatrix} U^2 \\ U^3 \\ U^4 \end{bmatrix} = \begin{bmatrix} -7 \\ -5 \\ 5 \end{bmatrix} \tag{11.32}$$

Equation 11.31 is often written as

$$\boldsymbol{KU} = \boldsymbol{F} \tag{11.33}$$

where $\boldsymbol{K}$ is the stiffness matrix, $\boldsymbol{U}$ the nodal displacement vector, and $\boldsymbol{F}$ the nodal force vector.

$\boldsymbol{F}$ includes not only the concentrated forces at the nodes but also the effects of the distributed forces and the displacement boundary condition (the essential boundary condition). The latter effects are called the equivalent nodal forces when they need to be distinguished from the rigorous nodal forces, the concentrated forces applied literally at the nodal points.

11.2.5 Error

The FE results are shown in Figure 11.5a together with the exact solution. The solid squares are the nodal values obtained by FEM. They are connected by the straight broken lines because the shape functions of the element employed in this analysis are linear.

We can prove without much difficulty that the nodal displacements will be always exact for any values of p, U_0, and P, which, however, does not mean that nodal displacements are exact in other problems. In fact, nodal displacements are not necessarily exact. Nevertheless, the accuracy of the displacement is better at or in the neighborhood of the node in general.

Figure 11.5b presents the first derivative of the displacement. A distinct contrast to the displacement is observed: the deviation from the exact solution is larger at the node and smaller inside the element in the case of the first derivative of the displacement. Note that the first derivative of the displacement is nothing but the strain and that the observation herein is therefore valid for the strain and thus for the stress.

In fact, as for the error in FEM, we can show the following (Cook et al., 2002):

1. Displacements are most accurate at or in the neighborhood of the node, whereas strains (stresses) are most accurate inside the element.
2. The error in the displacement is proportional to the square of element size, whereas the error in the strain (stress) is proportional to element size.

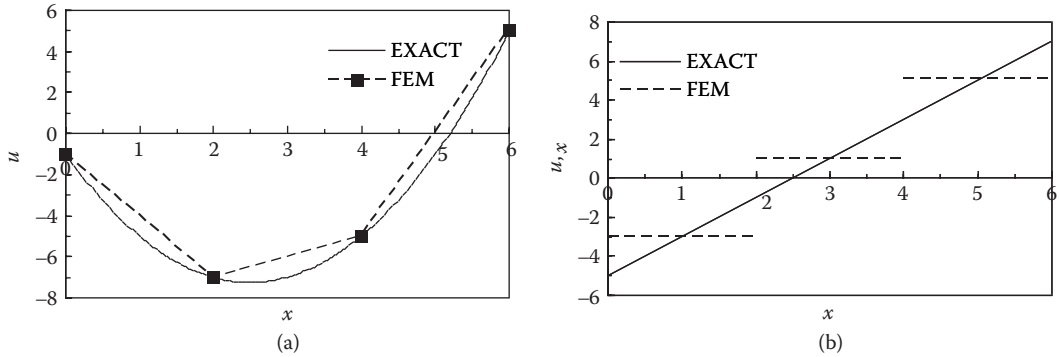

FIGURE 11.5 Solution by FEM (a) displacement; (b) derivative (strain).

TABLE 11.1 Element Length and Error

Number of Elements	Element Length	Maximum Error: Displacement $\max\lvert u-u_{\text{exact}}\rvert$	Maximum Error: Strain $\max\lvert u_{,x}-u_{,x\_\text{exact}}\rvert$
1	6	9	6
2	3	2.25	3
3	2	1	2

To illustrate the 2nd point above, we conduct the finite element analysis of the present BVP, employing different element sizes (lengths). The variation of the error is summarized in Table 11.1. The error decreases as the element size decreases in the way described above: the maximum error in the displacement $u(x)$ becomes 1/4 and 1/9 when the element length becomes 1/2 and 1/3, respectively; the maximum error in the strain $u_{,x}(x)$ becomes 1/2 and 1/3 when the element length becomes 1/2 and 1/3, respectively.

11.2.6 Isoparametric Element

A group of elements is called isoparametric. The isoparametric element is quite popular because of its versatility. Three isoparametric bar elements are presented in Figure 11.6, where r is a natural coordinate. The interval of the natural coordinate is (−1, 1) regardless of the physical length of the element, and the nodes are equally spaced in the natural coordinate system. The displacement $u(r)$ and the physical (global) coordinate $x(r)$ are expressed as

$$u(r)=\sum_{a=1}^{n} N^a(r)\,U^a \tag{11.34}$$

$$x(r)=\sum_{a=1}^{n} N^a(r)\,X^a \tag{11.35}$$

The same shape functions are used for both $u(r)$ and $x(r)$. This is why the term "isoparametric" is employed for the name.

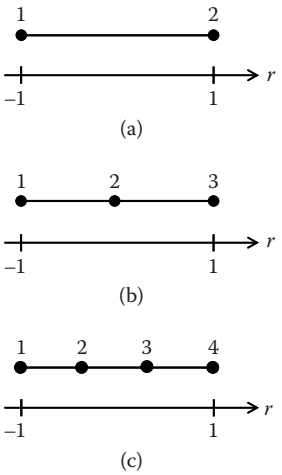

FIGURE 11.6 Isoparametric bar element. (a) 2-node element (linear element); (b) 3-node element (quadratic element); (c) 4-node element (cubic element).

The shape functions are given as follows:

2-node element ($n = 2$)

$$N^1 = \frac{1-r}{2}, N^2 = \frac{1+r}{2} \tag{11.36}$$

3-node element ($n = 3$)

$$N^1 = \frac{-r(1-r)}{2}, N^2 = 1-r^2, N^3 = \frac{r(1+r)}{2} \tag{11.37}$$

4-node element ($n = 4$)

$$N^1 = \frac{-(1-r)(1-9r^2)}{16}, N^2 = \frac{9(1-3r)(1-r^2)}{16}, N^3 = \frac{9(1+3r)(1-r^2)}{16}, N^4 = \frac{-(1+r)(1-9r^2)}{16} \tag{11.38}$$

It is noted that the superscript a in N^a indicates the association with Node a, whereas r^2 is the square of r. We can easily observe

$$N^a(r^a) = 1, N^a(r^b) = 0, \sum_{a=1}^{n} N^a(r) = 1 \tag{11.39}$$

where $a = b$. r^a and r^b are the natural coordinates at Node a and Node b, respectively.

Equations 11.39a and 11.39b ensure that Equations 11.34 and 11.35 can express the correct nodal values:

$$u(r^b) = \sum_{a=1}^{n} N^a(r^b)\, U^a = N^b(r^b)\, U^b = U^b \tag{11.40}$$

$$x(r^b) = \sum_{a=1}^{n} N^a(r^b)\, X^a = N^b(r^b)\, X^b = X^b \tag{11.41}$$

Equation 11.39c certifies that the rigid-body motion can be embodied: when the displacements at all the nodes are U_0, we get

$$u(r) = \sum_{a=1}^{n} N^a(r)\, U^a = U_0 \sum_{a=1}^{n} N^a(r) = U_0 \tag{11.42}$$

Example Problem 3

Obtain a solution of the present BVP by FEM using one 3-node isoparametric element.

SOLUTION

We assume Node 2 is located at the middle of the element. Then, we have $X^2 = (X^1 + X^3)/2$ and

$$u(r) = \sum_{a=1}^{3} N^a(r)\, U^a = \frac{-r(1-r)}{2} U^1 + (1-r^2) U^2 + \frac{r(1+r)}{2} U^3 \tag{11.43}$$

$$w(r) = \sum_{a=1}^{3} N^a(r)\, W^a = \frac{-r(1-r)}{2} W^1 + (1-r^2) W^2 + \frac{r(1+r)}{2} W^3 \tag{11.44}$$

$$x(r) = \sum_{a=1}^{3} N^a(r)\, U^a = \frac{1-r}{2} X^1 + \frac{1+r}{2} X^3 = 3(1+r) \tag{11.45}$$

Through the chain rule, we obtain the derivatives

$$u_{,x} = \frac{du}{dr}\frac{dr}{dx} = \left(\frac{-1+2r}{2}U^1 - 2rU^2 + \frac{1+2r}{2}U^3\right)\left(\frac{1}{3}\right)$$
$$= \frac{-1+2r}{6}U^1 - \frac{2r}{3}U^2 + \frac{1+2r}{6}U^3 \tag{11.46}$$

$$w_{,x} = \frac{dw}{dr}\frac{dr}{dx} = \left(\frac{-1+2r}{2}W^1 - 2rW^2 + \frac{1+2r}{2}W^3\right)\left(\frac{1}{3}\right)$$
$$= \frac{-1+2r}{6}W^1 - \frac{2r}{3}W^2 + \frac{1+2r}{6}W^3 \tag{11.47}$$

We take the same procedure as that in Example Problem 2, leading to

$$\begin{bmatrix} \frac{8}{9} & -\frac{4}{9} \\ -\frac{4}{9} & 7 \end{bmatrix}\begin{bmatrix} U^2 \\ U^3 \end{bmatrix} = \begin{bmatrix} -\frac{76}{9} \\ \frac{91}{18} \end{bmatrix} \tag{11.48}$$

The equation yields

$$\begin{bmatrix} U^2 \\ U^3 \end{bmatrix} = \begin{bmatrix} -7 \\ 5 \end{bmatrix} \tag{11.49}$$

Substituting the result into Equation 11.42, we get

$$u(r) = \frac{r(1-r)}{2} - 7(1-r^2) + \frac{5r(1+r)}{2} = 9r^2 + 3r - 7 \tag{11.50}$$

Using Equation 11.45, we can show that Equation 11.50 is equal to Equation 11.7, the exact solution.

Node 2 is not necessarily located at the middle of the element. We can assign Node 2 somewhere else. For example, we may locate Node 2 at $x = 2$ (Figure 11.7). We then have

$$x(r) = \frac{-r(1-r)}{2}X^1 + (1-r^2)X^2 + \frac{r(1+r)}{2}X^3 = 2(1-r^2) + 3r(1+r) = r^2 + 3r + 2 \tag{11.51}$$

$$x_{,r} = 2r + 3 \tag{11.52}$$

$$u_{,x} = \frac{du}{dr}\frac{dr}{dx} = \left(\frac{-1+2r}{2}U^1 - 2rU^2 + \frac{1+2r}{2}U^3\right)\left(\frac{1}{2r+3}\right)$$
$$= \frac{-1+2r}{2(2r+3)}U^1 - \frac{2r}{2r+3}U^2 + \frac{1+2r}{2(2r+3)}U^3 \tag{11.53}$$

$$w_{,x} = \frac{dw}{dr}\frac{dr}{dx} = \left(\frac{-1+2r}{2}W^1 - 2rW^2 + \frac{1+2r}{2}W^3\right)\left(\frac{1}{2r+3}\right)$$
$$= \frac{-1+2r}{2(2r+3)}W^1 - \frac{2r}{2r+3}W^2 + \frac{1+2r}{2(2r+3)}W^3 \tag{11.54}$$

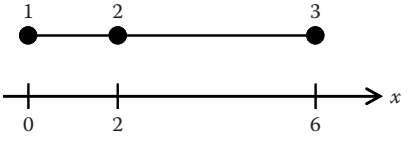

FIGURE 11.7 3-node element with Node 2 located at third point.

The derivatives are now much more involved, and FEM would not give the exact solution.

The lesson here is that the mid node had better be assigned at the midpoint of the element. Likewise, in the case of 4-node element (Figure 11.6c), it is better that all the nodes are equally spaced. If the nodes are not placed at these optimum points, we may say that the elements are distorted and need be prepared for less accuracy. In two- and three-dimensional problems, quadrilateral and hexahedral elements are often used. For a good accuracy, the elements had better be a square and a cube, respectively. If the shape is different, the element is said to be distorted and the accuracy would be lower.

11.3 FEM for Solid Mechanics Problem

The previous section covers almost all the essentials of FEM. The present section deals with the application to general solid-mechanics problems. The problem domain is in a higher dimension space, and therefore the element also becomes a two-dimensional shape such as a quadrilateral or a three-dimensional shape such as a hexahedron. Otherwise, the FE procedure is basically the same as that for the one-dimensional problem in the previous section. In short, we solve solid mechanics problems by the following procedure:

Step 1. Decide the type of element and the element mesh for the analysis.
Step 2. Compute the element stiffness matrix and the nodal force vector for each element.
Step 3. Assemble all the element contributions to form the FE equation, a set of simultaneous equations for nodal displacements.
Step 4. Solve the FE equation to obtain the nodal displacements.
Step 5. Compute strain and stress from the nodal displacements, if required.

11.3.1 Strong Form and Weak Form

We state BVP of the solid mechanics as

[Strong form]
Find the displacement u_i that satisfies the following three equations:

$$\text{Equilibrium equation} \quad \sigma_{ij,j} + b_i = 0 \quad \text{in } V \tag{11.55}$$

$$\text{Stress boundary condition} \quad t_i = \sigma_{ij} n_j \quad \text{on } S_\sigma \tag{11.56}$$

$$\text{Displacement boundary condition} \quad \overline{u}_i = u_i \quad \text{on } S_u \tag{11.57}$$

The stress σ_{ij} is linked to u_i through the strain ε_{ij} as

$$\text{Compatibility equation (strain} - \text{displacement relationship)} \quad \varepsilon_{ij} = \frac{1}{2}(u_{i,j} + u_{j,i}) \tag{11.58}$$

$$\text{Constitutive equation (stress} - \text{strain relationship)} \quad \sigma_{ij} = D_{ijkl}\varepsilon_{kl} \tag{11.59}$$

b_i, t_i, n_j, $\overline{u}_i$, and D_{ijkl} are the body force, the prescribed boundary surface force, the unit outward normal to the boundary surface, the prescribed boundary displacement and the elasticity coefficient; V is the elastic body to be analyzed; S_σ the boundary surface where the surface force is prescribed; S_u the boundary

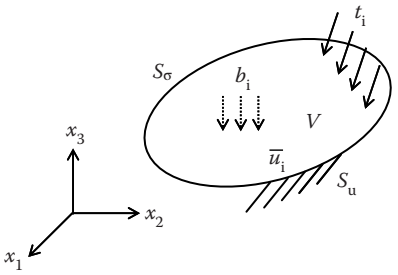

FIGURE 11.8 Solid mechanics problem.

surface where the displacement is prescribed. Note that there may be the mixed boundary surface where some components of the surface force and some components of the displacement are prescribed.

The problem is illustrated in Figure 11.8. For the given b_i, t_i, and $\overline{u}_i$, the deformation of the body V is to be obtained: u_i, ε_{ij}, and σ_{ij} are to be computed.

Using the weight function w_i that satisfies

$$w_i = 0 \qquad \text{on } S_u \tag{11.60}$$

and is arbitrary otherwise, we have from Equations 11.55 and 11.56

$$\int_V (\sigma_{ij,j} + b_i) w_i \, dV + \int_{S_\sigma} (t_i - \sigma_{ij} n_j) w_i \, dS = 0 \tag{11.61}$$

By the Gauss theorem together with Equation 11.60, the first term on the left-hand side becomes

$$\int_V \sigma_{ij,j} w_i \, dV = \int_{S_\sigma} \sigma_{ij} n_j w_i \, dS - \int_V \sigma_{ij} w_{i,j} \, dV \tag{11.62}$$

Then we can rewrite Equation 11.62 as

$$\int_V \sigma_{ij} w_{i,j} \, dV = \int_V b_i w_i \, dV + \int_{S_\sigma} t_i w_i \, dS \tag{11.63}$$

With Equation 11.63, we set up the weak form of BVP.

[Weak form]

Find the displacement u_i that satisfies Equation 11.63 for any function w_i. w_i satisfies Equation 11.60 and σ_{ij} is linked to u_i through Equations 11.58 and 11.59.

Incidentally, putting

$$\delta u_i = w_i \tag{11.64}$$

$$\delta \varepsilon_{ij} = \frac{1}{2}(\delta u_{i,j} + \delta u_{j,i}) \tag{11.65}$$

we get from Equation 11.63

$$\int_V \sigma_{ij} \, \delta \varepsilon_{ij} \, dV = \int_V b_i \, \delta u_i \, dV + \int_{S_\sigma} t_i \, \delta u_i \, dS \tag{11.66}$$

By viewing δu_i and $\delta \varepsilon_{ij}$ as the virtual displacement and the virtual strain, respectively, we may interpret Equation 11.66 as "internal virtual work = external virtual work." This is known as "Principle of Virtual Work" in mechanics. It is noted that Equation 11.66 holds good for any constitutive relationships as the derivation has nothing to do with the constitutive equation.

For the two-dimensional problem in a state of plane stress, we can write the fundamental equations in the weak form, Equations 11.58 through 11.60 and 11.63, more explicitly as

$$\{\varepsilon\} = \{\partial u\} \tag{11.67}$$

$$\{\sigma\} = [D]\{\varepsilon\} \tag{11.68}$$

$$\{w\} = \{0\} \qquad \text{on } S_u \tag{11.69}$$

$$\int_S \{\partial w\}^T \{\sigma\} a dS = \int_S \{w\}^T \{b\} a dS + \int_{C_\sigma} \{w\}^T \{t\} a dC \tag{11.70}$$

where

$$\{\varepsilon\} = \left\{ \varepsilon_x \;\; \varepsilon_y \;\; \gamma_{xy} \right\}^T \tag{11.71}$$

$$\{\partial u\} = \left\{ u_{x,x} \;\; u_{y,y} \;\; u_{x,y} + u_{y,x} \right\}^T \tag{11.72}$$

$$\{\sigma\} = \left\{ \sigma_x \;\; \sigma_y \;\; \sigma_{xy} \right\}^T \tag{11.73}$$

$$[D] = \frac{E}{1-\nu^2} \begin{bmatrix} 1 & \nu & 0 \\ \nu & 1 & 0 \\ 0 & 0 & \dfrac{1-\nu}{2} \end{bmatrix} \tag{11.74}$$

$$\{w\} = \left\{ w_x \;\; w_y \right\}^T \tag{11.75}$$

$$\{\partial w\} = \left\{ w_{x,x} \;\; w_{y,y} \;\; w_{x,y} + w_{y,x} \right\}^T \tag{11.76}$$

$$\{b\} = \left\{ b_x \;\; b_y \right\}^T \tag{11.77}$$

$$\{t\} = \left\{ t_x \;\; t_y \right\}^T \tag{11.78}$$

E and v in Equation 11.74 are Young's modulus and Poisson's ratio, respectively.

In the two-dimensional problem, the domain is planar, and the boundary is defined by a line segment or line segments. Therefore, the volume integration over V and the surface integration over S_σ in Equation 11.63 are reduced to the surface integration over the two-dimensional body S and the line integration over the stress-prescribed boundary line C_σ, respectively. In Equation 11.70, "a" is the thickness of the body, which is very small in the plane-stress problem.

Note that only one component of $\{t\}$ may be prescribed in some solid mechanics problems. In such a case, Equations 11.70 and 11.78 need be adjusted.

11.3.2 FEM

FEM deals with the weak form of BVP. We decompose the problem domain V into small regions, elements, and we conduct the integration in Equation 11.63 for each element. Then we sum up the element contributions to complete the computation of Equation 11.63. Mathematically the procedure is expressed as

$$\sum_e G^e = 0 \tag{11.79}$$

where

$$G^e = \int_{V^e} \sigma_{ij} w_{i,j}\, dV - \int_{V^e} b_i w_i\, dV - \int_{S_\sigma^e} t_i w_i\, dS \tag{11.80}$$

The superscript "e" stands for the association of the variable with the element, and Equation 11.79 is the summation of the contributions of all the elements.

In a one-dimensional problem, the element is a line segment. In two- and three-dimensional problems, the elements are planar and spatial, respectively. The one-dimensional isoparametric element is explained in the last section. In the next subsection, we go over the two-dimensional isoparametric element. When the isoparametric element is employed and the Galarkin method is applied, we have the following expressions:

$$u_i = \sum_{a=1}^{n} N^a U_i^a \tag{11.81}$$

$$w_i = \sum_{a=1}^{n} N^a W_i^a \tag{11.82}$$

n is the number of nodes in an element, N^a the shape function associated with Node a, and U_i^a the nodal displacement and W_i^a the nodal weight, respectively. For not only all the displacement and weight components but also all the coordinates, the same shape function is used, which is the feature of the isoparametric element.

In view of Equations 11.58, 11.59, 11.81, and 11.82, we can rewrite Equation 11.80 as

$$G^e = \sum_{b=1}^{n} W_i^b \left\{ \sum_{a=1}^{n} \left(\int_{V^e} D_{ijkl} N_{,j}^b N_{,l}^a\, dV \right) U_k^a - \int_{V^e} b_i N^b\, dV - \int_{S_\sigma^e} t_i N^b\, dS \right\} \tag{11.83}$$

The first term in the inner parenthesis on the right-hand side yields the element stiffness matrix. The second and third terms lead to the element nodal force vector. By the substitution of Equation 11.83 into Equation 11.79, we get

$$\{W\}^T \left([K]\{U\} - \{F\} \right) = 0 \tag{11.84}$$

$\{W\}$ is the nodal weight vector, $[K]$ the stiffness matrix, $\{U\}$ the nodal displacement vector, and $\{F\}$ the nodal force vector. The components of $\{W\}$ on S_u are zero, whereas the other components of $\{W\}$ are arbitrary. The components of $\{U\}$ on S_u are prescribed, whereas the other components of $\{U\}$ are unknown.

By the same manipulation as that in Example Problem 2, we arrive at the simultaneous equations

$$[K]\{U\} = \{F\} \tag{11.85}$$

$\{U\}$ in Equation 11.85 now contains only unknowns, and the numbers of components of $[K]$, $\{U\}$, and $\{F\}$ in Equation 11.85 are smaller than those of their respective counterparts in Equation 11.84. The set of simultaneous equations, Equation 11.85, are to be solved for $\{U\}$.

For the plane-stress problem, Equation 11.83 can be written more explicitly as

$$G^e = \{W^e\}^T \left([K^e]\{U^e\} - \{F^e\}\right) \tag{11.86}$$

where

$$\{W^e\} = \left\{ W_x^1 \; W_y^1 \; W_x^2 \; W_y^2 \; \cdots \; W_x^n \; W_y^n \right\}^T \tag{11.87}$$

$$[K^e] = \int_{V^e} [B]^T [D][B] dV = \int_{S^e} [B]^T [D][B] a dS \tag{11.88}$$

$$\{U^e\} = \left\{ U_x^1 \; U_y^1 \; U_x^2 \; U_y^2 \; \cdots \; U_x^n \; U_y^n \right\}^T \tag{11.89}$$

$$\begin{aligned} \{F^e\} &= \int_{V^e} [N]^T \{b\} dV + \int_{S_\sigma^e} [N]^T \{t\} dS \\ &= \int_{S^e} [N]^T \{b\} a dS + \int_{C_\sigma^e} [N]^T \{t\} a dC \end{aligned} \tag{11.90}$$

$$[B] = \begin{bmatrix} N_{,x}^1 & 0 & N_{,x}^2 & \cdots & N_{,x}^n & 0 \\ 0 & N_{,y}^1 & 0 & \cdots & 0 & N_{,y}^n \\ N_{,y}^1 & N_{,x}^1 & N_{,y}^2 & \cdots & N_{,y}^n & N_{,x}^n \end{bmatrix} \tag{11.91}$$

$$[N] = \begin{bmatrix} N^1 & 0 & N^2 & 0 & \cdots & N^n & 0 \\ 0 & N^1 & 0 & N^2 & \cdots & 0 & N^n \end{bmatrix} \tag{11.92}$$

In the two-dimensional problem, the elements are also planar: S^e in Equations 11.88 and 11.90 is a part of S that the element occupies and C_σ^e in Equation 11.90 is a part of C_σ that the element occupies. $[K^e]$, $\{U^e\}$, $\{F^e\}$, $[B]$, and $[D]$ are the element stiffness matrix, the element nodal displacement vector, the element nodal force vector, the strain-nodal displacement matrix, and the stress–strain matrix, respectively.

The number of equations in Equation 11.85 is very large in general. Because of this, for FEA we need to require a large memory capacity in a computer, and we need to consume a great part of computational time for the solution of this set of simultaneous equations. The issue of dealing with the simultaneous equations efficiently from a computational point of view, therefore, has attracted and still attracts many researchers. Various methods have been proposed. Basic strategy is to make use of the characteristics of the stiffness matrix

- Symmetric
- Sparse
- Banded

The stiffness matrix is not symmetric in some analyses, but generally so. "Sparse" means the stiffness matrix has many components the values of which are zero, and "banded" means many nonzero components are clustered near the diagonal terms.

We note that in the solution process of Equation 11.85 the inverse matrix of the stiffness matrix, $[K]^{-1}$, is never computed, even though some FEM textbooks may have the expression of $\{U\}=[K]^{-1}\{F\}$ for describing the FE procedure. This is simply because taking the inverse matrix is computationally very inefficient for the solution of simultaneous equations.

11.3.3 Isoparametric Elements

For illustration, the 4-node quadrilateral isoparametric element and the 8-node quadrilateral isoparametric element, both of which are popular in two-dimensional FEA, are explained in this subsection. The two elements are shown in Figure 11.9.

The isoparametric element is defined in the natural coordinate system. The two-dimensional isoparametric element is a square in the natural coordinate system with the side length of 2. The isoparametric element is then mapped onto the physical finite element in the physical (global) coordinate system. Their shape functions are given as follows:

4-node quadrilateral isoparametric element

$$N^a=\frac{1}{4}(1+rr^a)(1+ss^a)\quad(a=1-4) \tag{11.93}$$

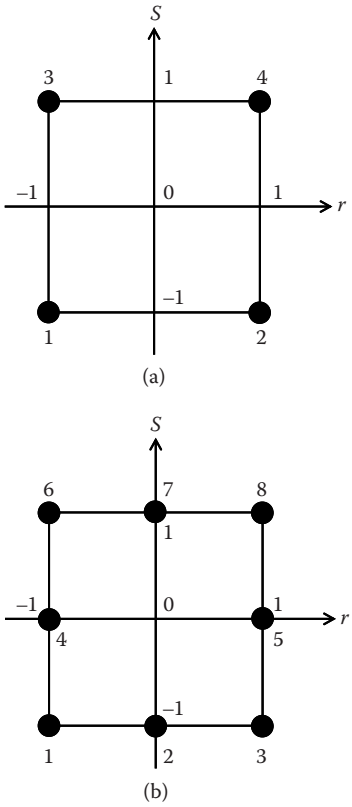

FIGURE 11.9 Two-dimensional isoparametric element. (a) 4-node quadrilateral isoparametric element (linear element); (b) 8-node quadrilateral isoparametric element (quadratic element).

8-node quadrilateral isoparametric element

$$N^a = \frac{1}{4}(1+rr^a)(1+ss^a)(rr^a+ss^a-1) \quad (a=1,3,6,8) \tag{11.94}$$

$$N^a = \frac{1}{2}(1-r^2)(1+ss^a) \quad (a=2,7) \tag{11.95}$$

$$N^a = \frac{1}{2}(1+rr^a)(1-s^2) \quad (a=4,5) \tag{11.96}$$

r^a and s^a are the nodal r-coordinate and the nodal s-coordinate at Node a, respectively. As realized in Figure 11.9, both r and s take the value between −1 and 1. After their respective shape functions, the 4-node quadrilateral isoparametric element is called a linear element, whereas the 8-node quadrilateral isoparametric element a quadratic element.

In either element, the following equalities hold:

$$N^a(r^a, s^a)=1, N^a(r^b, s^b)=0, \sum_{a=1}^{n} N^a(r,s)=1 \tag{11.97}$$

where $a \neq b$. Equations 11.97a and 11.97b ensure that the correct nodal values can be expressed. Equation 11.97c guarantees that the element embodies the rigid-body displacement.

The shape functions are defined in the natural coordinate system, whereas Equation 11.83 requires the derivatives of those functions with respect to the global coordinates. Making use of the chain rule, we compute the required derivatives as

$$\begin{Bmatrix} N^a_{,x} \\ N^a_{,y} \end{Bmatrix} = [J]^{-1} \begin{Bmatrix} N^a_{,r} \\ N^a_{,s} \end{Bmatrix} \tag{11.98}$$

where $[J]$ is the Jacobian matrix given by

$$[J] = \begin{bmatrix} \dfrac{\partial x}{\partial r} & \dfrac{\partial y}{\partial r} \\ \dfrac{\partial x}{\partial s} & \dfrac{\partial y}{\partial s} \end{bmatrix} \tag{11.99}$$

In the isoparametric element, the coordinates are interpolated by the same shape functions. Therefore, we can evaluate the components of the Jacobian matrix without much difficulty. For example, we get

$$\frac{\partial x}{\partial r} = \frac{\partial}{\partial r}\left(\sum_{a=1}^{n} N^a X^a\right) = \sum_{a=1}^{n} N^a_{,r} X^a \tag{11.100}$$

where X^a is the nodal x-coordinate at Node a.

11.3.4 Gauss Integration Scheme

As realized in Equation 11.83, we need to conduct integration many times in FEM. In practical problems, we cannot evaluate almost all those integrations analytically, and we have to make resort to numerical integration. The numerical integration takes the following form in general:

$$\int_a^b f(x)dx = \sum_{i=1}^{n} w_i f(x_i) \tag{11.101}$$

where w_i and x_i are constants. Various numerical-integration formulae are available and they employ different values of w_i and x_i. n is the number of reference points. The bigger n is, the better the accuracy becomes. However, the bigger n requires more computational time.

A popular integration method in FEM is the Gauss integration scheme, which is called also the Gauss integration for short. The reference points have been selected specifically. The points up to $n = 4$ are presented in Table 11.2, where the interval of integration is normalized so that it runs from −1 to 1. The reference point in the Gauss integration is called the Gauss integration point or simply the Gauss point.

With n Gauss points, the Gauss integration gives the exact integration value of a polynomial function up to $2n$-1 order. For example, with $n = 2$ we get

$$\begin{aligned}\int_{-1}^{1}\left(x^3+2x^2\right)\mathrm{d}x &= \sum_{i=1}^{2} w_i\left(x_i^3+2x_i^2\right)\\ &= 1.0\times\left\{\left(-1/\sqrt{3}\right)^3+2\times\left(-1/\sqrt{3}\right)^2\right\}+1.0\times\left\{\left(1/\sqrt{3}\right)^3+2\times\left(1/\sqrt{3}\right)^2\right\}\\ &= \frac{3}{4}\end{aligned} \tag{11.102}$$

We can easily verify that 3/4 is the exact value.

For the integration in two- or three-dimensional space, the numerical integration is conducted as

$$\int_{-1}^{1}\int_{-1}^{1} f(x,y)\,\mathrm{d}x\,\mathrm{d}y = \sum_{i=1}^{m}\sum_{j=1}^{p} w_i w_j f(x_i,y_j) \tag{11.103}$$

TABLE 11.2 Gauss Integration Points

n	I	x_i	w_i
1	1	0	2
2	1	$-\frac{1}{\sqrt{3}}$	1
	2	$+\frac{1}{\sqrt{3}}$	1
3	1	$-\sqrt{\frac{3}{5}}$	$\frac{5}{9}$
	2	0	$\frac{8}{9}$
	3	$+\sqrt{\frac{3}{5}}$	$\frac{5}{9}$
4	1	$-\sqrt{\frac{3+\sqrt{4.8}}{7}}$	$\frac{1}{2}-\frac{\sqrt{30}}{36}$
	2	$-\sqrt{\frac{3-\sqrt{4.8}}{7}}$	$\frac{1}{2}+\frac{\sqrt{30}}{36}$
	3	$+\sqrt{\frac{3-\sqrt{4.8}}{7}}$	$\frac{1}{2}+\frac{\sqrt{30}}{36}$
	4	$+\sqrt{\frac{3+\sqrt{4.8}}{7}}$	$\frac{1}{2}-\frac{\sqrt{30}}{36}$

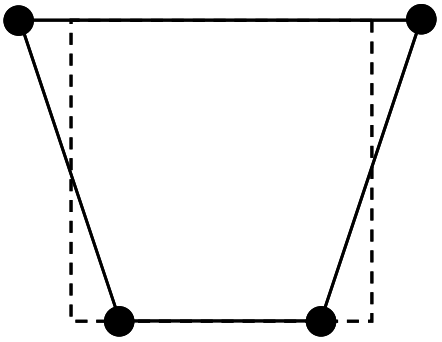

FIGURE 11.10 Mode with no deformation at center of element.

$$\int_{-1}^{1}\int_{-1}^{1}\int_{-1}^{1} f(x, y, z)\mathrm{d}x\mathrm{d}y\mathrm{d}z = \sum_{i=1}^{m}\sum_{j=1}^{p}\sum_{k=1}^{q} w_i w_j w_k f(x_i, y_j, z_k) \tag{11.104}$$

Equation 11.103 is often called the $m \times p$ Gauss integration and Equation 11.104 the $m \times p \times q$ Gauss integration.

With the greater number of Gauss points, we can obtain more accurate integration value. However, the better evaluation of the stiffness matrix does not necessarily improve the accuracy of FEA. The smaller number of Gauss points employed often yields better FE result. The scheme of the integration with the smaller number of Gauss points is known as the reduced integration. In general, FEM tends to overestimate the stiffness, whereas the reduced integration underestimates it, which justifies the employment of the reduced integration. The number of Gauss points directly influences computational time. The reduced integration is favorable from this viewpoint as well.

However, the small number of Gauss points might cause numerical instability. For example, if we employ the 1×1 Gauss integration, the deformation mode shown in Figure 11.10 cannot be evaluated appropriately, as there is no deformation at the element center that is the 1×1 Gauss point.

The condition that could cause such a problem has been derived. For a two-dimensional elastic problem, the deformation mode that has no strains at the Gauss points can exist if the following inequality is satisfied (Zienkiewicz et al., 2005):

$3 \times$ (the number of Gauss Points) < the number of total degrees-of-freedom

The determinant of the stiffness matrix vanishes under this condition. We need to note that even when the inequality is not met, the numerical instability may arise, yielding an unrealistic FE result.

The optimum number of Gauss points depends on the problem and the finite element mesh employed. Usually the 2×2 Gauss integration gives satisfactory result in two-dimensional analysis with the 4-node quadrilateral element or the 8-node quadrilateral element.

11.3.5 Stress Computation

Once nodal displacements are obtained, we can compute strain at any point in the element by the derivatives of the shape functions. Through the stress–strain relationships, we can then get stress. We express the stress computation formally as

$$\{\sigma\} = [D][B]\{U^e\} \tag{11.105}$$

As we have observed in the one-dimensional problem, the accuracy of the stress obtained by Equation 11.105 is better inside the element than at the nodes and the accuracy varies from point to point. Herein as an example, we discuss the optimum points for stress computation in the 8-node quadrilateral isoparametric element.

The shape functions of the 8-node quadrilateral isoparametric element are cubic polynomials, and the displacement in the element is expressed as

$$\left\{ u \; v \right\} = \left\{ 1 \; r \; s \; r^2 \; rs \; s^2 \; r^2 s \; rs^2 \right\} [e] \tag{11.106}$$

where $[e]$ is the 8×2 coefficient matrix. Only two cubic terms are involved. We next consider an element for which a complete cubic polynomial is employed. We can write the displacement in this element as

$$\left\{ u \; v \right\} = \left\{ 1 \; r \; s \; r^2 \; rs \; s^2 \; r^3 \; r^2 s \; rs^2 \; s^3 \right\} [f] \tag{11.107}$$

where $[f]$ is the 10×2 coefficient matrix. Since the nodal displacements are good in accuracy in general, we assume the two elements have the same nodal displacements. By substituting the nodal natural coordinates into Equations 11.106 and 11.107, we can get the nodal displacement, which is expressed as

$$\left[U_e^e \right] = [E][e] \tag{11.108}$$

$$\left[U_f^e \right] = [F][f] \tag{11.109}$$

where $\left[U_e^e \right]$ and $\left[U_f^e \right]$ are the nodal-displacement matrices. $\left[U_e^e \right] = \left[U_f^e \right]$ then leads to

$$\begin{aligned} [e] &= [E]^{-1}[F][f] \\ &= \begin{bmatrix} 1 & 0 & 0 & 0 & 0 & 0 & 0 & 0 & 0 & 0 \\ 0 & 1 & 0 & 0 & 0 & 0 & 1 & 0 & 0 & 0 \\ 0 & 0 & 1 & 0 & 0 & 0 & 0 & 0 & 0 & 1 \\ 0 & 0 & 0 & 1 & 0 & 0 & 0 & 0 & 0 & 0 \\ 0 & 0 & 0 & 0 & 1 & 0 & 0 & 0 & 0 & 0 \\ 0 & 0 & 0 & 0 & 0 & 1 & 0 & 0 & 0 & 0 \\ 0 & 0 & 0 & 0 & 0 & 0 & 0 & 1 & 0 & 0 \\ 0 & 0 & 0 & 0 & 0 & 0 & 0 & 0 & 1 & 0 \end{bmatrix} [f] \end{aligned} \tag{11.110}$$

The computation of the strain requires the derivatives of the displacement with respect to the global coordinates. Since the shape functions of the isoparametric element are given in terms of the natural coordinates, we need to take the following step:

$$\begin{bmatrix} \dfrac{\partial u}{\partial x} & \dfrac{\partial v}{\partial x} \\ \dfrac{\partial u}{\partial y} & \dfrac{\partial v}{\partial y} \end{bmatrix} = [J]^{-1} \begin{bmatrix} \dfrac{\partial u}{\partial r} & \dfrac{\partial v}{\partial r} \\ \dfrac{\partial u}{\partial s} & \dfrac{\partial v}{\partial s} \end{bmatrix} \tag{11.111}$$

The Jacobian matrix $[J]$ takes care of the mapping between the two coordinate systems, and the second matrix on the right-hand side of Equation 11.111 is more directly related to the strain. Using Equations 11.106 and 11.107, we can obtain the components of this matrix, the derivatives with respect to the natural coordinates:

$$\begin{bmatrix} \frac{\partial u}{\partial r} & \frac{\partial v}{\partial r} \\ \frac{\partial u}{\partial s} & \frac{\partial v}{\partial s} \end{bmatrix} = \begin{bmatrix} 0 & 1 & 0 & 2r & s & 0 & 2rs & s^2 \\ 0 & 0 & 1 & 0 & r & 2s & r^2 & 2rs \end{bmatrix} [e] \tag{11.112}$$

$$\begin{bmatrix} \frac{\partial u}{\partial r} & \frac{\partial v}{\partial r} \\ \frac{\partial u}{\partial s} & \frac{\partial v}{\partial s} \end{bmatrix} = \begin{bmatrix} 0 & 1 & 0 & 2r & s & 0 & 3r^2 & 2r & s^2 & 0 \\ 0 & 0 & 1 & 0 & r & 2s & 0 & r^2 & 2rs & 3s^2 \end{bmatrix} [f] \tag{11.113}$$

In view of Equations 11.110, 11.112, and 11.113, we can locate the points where the derivatives of the displacements with respect to the natural coordinates in the two elements, Equations 11.112 and 11.113, coincide with each other:

$$r = \pm\frac{1}{\sqrt{3}}, s = \pm\frac{1}{\sqrt{3}} \tag{11.114}$$

which are the 2 × 2 Gauss points. This indicates that the stress states at these points in the 8-node quadrilateral isoparametric element are as accurate as those in the element whose shape functions contain complete cubic polynomials. Thus, we may conclude that the optimum points for the stress computation in the 8-node quadrilateral isoparametric element are the 2 × 2 Gauss points.

When the element is not rectangular, the 2 × 2 Gauss points may not be the optimum points. However, since the distortion of the element needs be minimized for good FEA, the 2 × 2 Gauss points can be assumed as the optimum stress-computation points in practice.

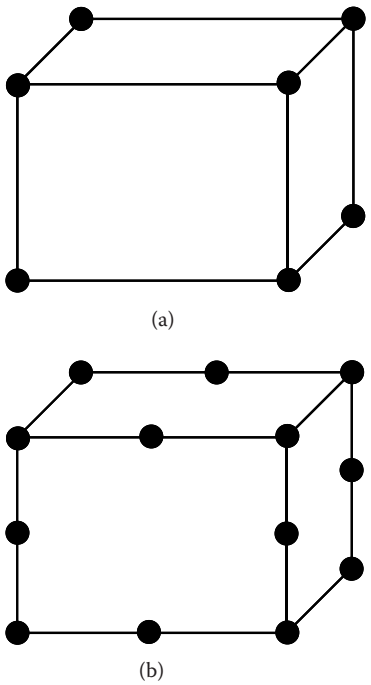

FIGURE 11.11 Three-dimensional isoparametric element. (a) 8-node hexahedron isoparametric element (linear element); (b) 20-node hexahedron isoparametric element (quadratic element).

Similarly, the optimum points have been obtained for other elements (Barlow, 1976). The optimum points in the one-dimensional quadratic element and in the three-dimensional quadratic element are the two-point Gauss points and the $2 \times 2 \times 2$ Gauss points, respectively. The optimum points in the one-dimensional linear element, in the two-dimensional linear element, and in the three-dimensional linear element are the one-point Gauss point, the 1×1 Gauss point, and the $1 \times 1 \times 1$ Gauss point, respectively. The three-dimensional elements are depicted in Figure 11.11.

Even when the stress states at the points other than the optimum points need be computed, we still had better not make resort to Equation 11.105. Instead, it is better to interpolate/extrapolate using the stress states at the optimum points. A well-known scheme is the stress-projection method in which the shape functions are utilized for the interpolation/extrapolation (Zienkiewicz et al., 2005).

11.4 Some Other Topics in Structural Mechanics

11.4.1 Structural Elements

As we have described in the previous sections, FEM is a powerful tool to solve BVPs. Different theories pose different BVPs, which then may lead to different finite elements.

In the field of structural mechanics, there are finite elements developed for specific structural theories. The beam element and the plate element are typical of that class. We also need to note that since, for example, various beam theories exist, such as the Bernoulli–Euler beam theory and the Timoshenko beam theory, there exist various finite elements only for the beam accordingly.

If a structure or a member is long whereas the height (thickness) h and the width b are small (Figure 11.12a), it is considered a beam. In Figure 11.13, we present a typical beam element for the analysis of bending behavior based on the Bernoulli–Euler beam theory. The nodal variables include not only the deflection w but also its derivative (the slope) $\theta = dw/dx$. The shape function for w is a cubic polynomial; it arises as the governing

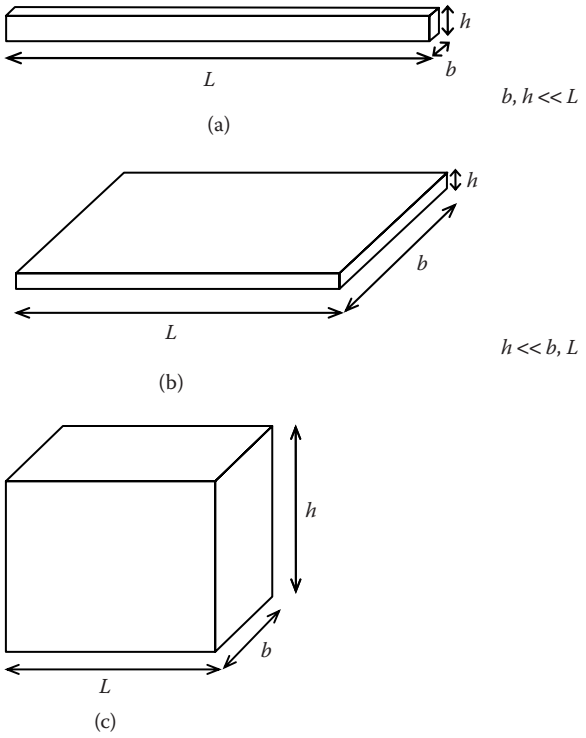

FIGURE 11.12 Structural body (a) beam; (b) plate; (c) continuum.

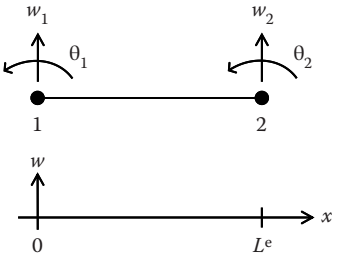

FIGURE 11.13 Beam element for analysis of bending behavior.

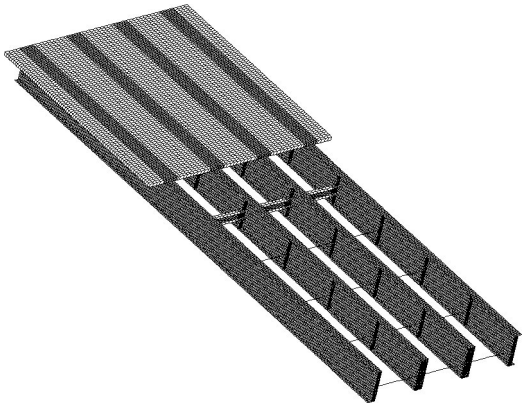

FIGURE 11.14 Finite element mesh of steel girder bridge with concrete slab.

differential equation in the Bernoulli–Euler beam theory has the term of the 4th-order derivative of the deflection d^4w/dx^4. The Bernoulli–Euler beam theory is good for a beam whose aspect ratio h/L is small.

If h/L is not so small, we need to apply the Timoshenko beam theory. The beam element based on the Timoshenko beam theory also has the rotational degree-of-freedom at the node. However, it is not the derivative of w.

When the magnitudes of b and L of the structure are comparable, the beam theory is not valid. If h is still small in comparison with b and L (Figure 11.12b), we can apply the plate theory instead. If all the three dimensions are similar (Figure 11.12c), it is just a solid.

In FEM, it is therefore important to take three steps before the actual computation: (1) capture the characteristics of the structure and the constituent members; (2) identify the applicable theory; and (3) pick up the relevant finite elements.

We show an example of the finite element mesh of a steel girder bridge with a concrete slab in Figure 11.14. Only a part of the slab is presented so that the steel girders are visible. The bridge is modeled by three types of finite element, depending on the features of the members and the purpose of the analysis; the concrete slab is modeled by solid elements, the main steel girders by plate elements, the cross girder at the mid span by plate elements, and the other cross girders by beam elements. The reason why the plate element is employed for the cross girder at the mid span of the bridge is that structural behavior near the mid span was of great interest in this particular analysis. Note that the plate element is applicable to a beam-like member and can give more information on its structural performance than the beam element. However, the plate-element analysis is usually much more costly.

11.4.2 Nonlinear Analysis

As deformation becomes large, the relationship between the displacement and the load deviates from linearity. The phenomenon is attributable to material nonlinearity, geometrical nonlinearity, or both.

A typical material nonlinearity is elastic–plastic behavior. The geometrical nonlinearity is significant when the difference in shape from the original configuration and the deformed configuration can no longer be neglected.

In day-to-day structural design, we usually do not have to conduct nonlinear analysis. However, in some countries such as Japan, seismic design requires nonlinear analysis since contained damage is permitted in the event of a large earthquake. Also, when the structural performance up to or beyond ultimate strength needs be evaluated, we carry out nonlinear analysis.

For a nonlinear problem, instead of Equation 11.85 we arrive at

$$\{K\} = \{F\} \tag{11.115}$$

where $\{K\}$ is a function of $\{U\}$.

This is a set of nonlinear simultaneous equations. In general, to obtain the solution, we need to resort to a numerical method, which usually involves iteration. A typical method is the Newton–Raphson method.

In a nonlinear structural problem, quite often an equilibrium path is of great interest. The equilibrium path is the relationship between the displacement and the load of the structure in a state of equilibrium. When Equation 11.115 consists of n equations, we need to prescribe the values of n components out of $2n$ components, the sum of n components of $\{U\}$ and n components of $\{F\}$. We then solve Equation 11.115 for the remaining n components in $\{U\}$ and $\{F\}$.

For instance, we prescribe all the n components of $\{F\}$ and solve Equation 11.115 for the n components of $\{U\}$. In a structural problem, a set of loads $\{F_0\}$ is usually given, and $\{F\}$ is expressed as $\alpha\{F_0\}$ where α is prescribed. In this case, we can rewrite Equation 11.115 as

$$\{K\} = \alpha\{F_0\} \tag{11.116}$$

The typical iteration procedure is as follows:

Step 1. The linearized equation of Equation 11.116 is constructed

$$[DK^{(m)}]\{\Delta U\} = \alpha\{F_0\} - \{K^{(m)}\} \tag{11.117}$$

where m is the number of iterations and $[DK^{(m)}]$ is a coefficient matrix and a function of $\{U^{(m)}\}$.

Step 2. Equation 11.117 is solved for $\{\Delta U\}$.

Step 3. The displacement is updated

$$\{U^{(m+1)}\} = \{U^{(m)}\} + \{\Delta U\} \tag{11.118}$$

Step 4. If convergence is achieved, we accept $\{U^{(m+1)}\}$ as the solution. Otherwise, go back to Step 1, replacing m with $m + 1$.

In the Newton–Raphson method, $[DK]$ is the tangent stiffness matrix defined by $[DK] = [\partial K/\partial U]$.

By increasing the value of α successively and computing $\{U\}$, we can obtain the equilibrium states that yield the equilibrium path. Since the load is a control parameter, this approach is called the load control method.

The load-carrying capacity of a structure is usually limited, as schematically illustrated in Figure 11.15a. Therefore, the value of α is limited, and the load control method fails after the limit point α_{max}. Thus, by the load control method we cannot fully trace the equilibrium path showing such a softening behavior.

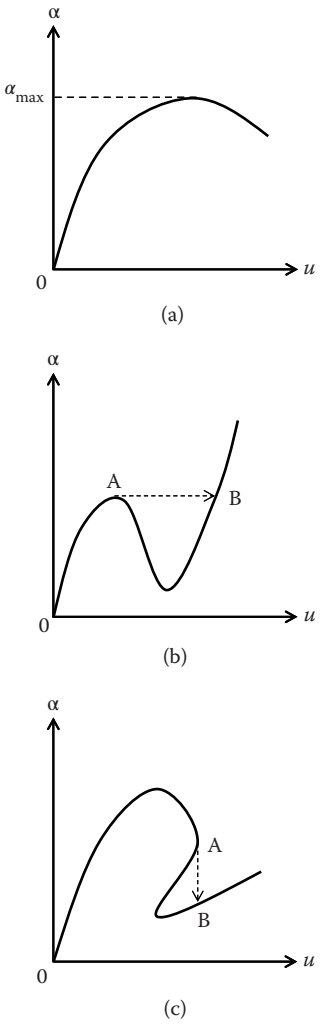

FIGURE 11.15 Equilibrium path (a) softening behavior; (b) snap-through phenomenon; (c) snap-back phenomenon.

Some structures exhibit the snap-through phenomenon (Figure 11.15b). We cannot trace this type of equilibrium path by the load control method, either: the FE result would jump from Point A to Point B, missing the equilibrium path between the two points.

To overcome the problem, we may control the displacement: one component of $\{U\}$ is prescribed and Equation 11.116 is solved for α and the remaining n-1 components of $\{U\}$. This is the so-called displacement control method. The displacement control method however fails if the structure shows the phenomenon known as the snap-back (Figure 11.15c): the FE result would jump from Point A to Point B, missing the equilibrium path between the two points.

More general methods have been developed by introducing an additional equation. The additional equation can take various forms. The generic form is given by

$$\sum_{i=1}^{n} a_i^2 \Delta U_i \Delta U_i + (b\Delta\alpha)^2 = (\Delta c)^2 \tag{11.119}$$

where a_i and b are the constants that adjust the contributions of the displacement increment ΔU_i and the load increment $\Delta\alpha$, whereas Δc is the parameter that controls the distance between two subsequent equilibrium states in the $a_i\Delta U_i$-$b\Delta\alpha$ space. Riks (1979) used the equation with $a_i = b = 1$ and Crisfield (1980) with $b = 0$.

We solve Equation 11.116 together with Equation 11.119 for $\{U\}$ and α, $n + 1$ unknowns in total.

References

Barlow, J. 1976. Optimal stress locations in finite element models. *Int. J. Num. Meth. Eng*, 10, 243–51.

Cook, R. D., Malkus, D. S., Plesha, M. E., and Witt, R. J. 2002. *Concepts and Applications of Finite Element Analysis* (4th edition). John Wiley & Sons, New York, NY.

Crisfield, M. A. 1980. Incremental/iterative solution procedures for nonlinear structural analysis. *Num. Meth. Nonlinear Prob.* C. Taylor, E. Hinton, D. R. J. Owen and E. Onate (Eds.), 261–90. Pinerideg Press, Swansea, UK.

Hughes, T. J. R. 2000. *The Finite Element Methods Linear Static and Dynamic Finite Element Analysis*. Dover Publications, Mineola, NY.

Riks, E. 1979. An incremental approach to the solution of snapping and buckling problems. *Int. J. Solids Struct*, 15, 529–51.

Zienkiewicz, O. C., Taylor, R. L., and Nithiarasu, P. 2005. *The Finite Element Method* (6th edition). Vol. 1. Elsevier, Oxford, UK.

12

Structural Modeling

Alexander Krimotat
SC Solutions, Inc.

Hassan Sedarat
SC Solutions, Inc.

12.1 Introduction

Structural systems can in most cases become too complex to be designed based solely on empirical data or experience. A more rational procedure, using a mathematical simulation of the structure, is needed to understand the performance of the structure under various loading. The response of the structure will become even more complex if the loading is time-dependent. An example of a time-dependent loading is ground motion excitation, during which the structure can be subjected to strong ground shaking and high accelerations in both horizontal and vertical directions. Another source of complexity to the structural system, for example, is when the interaction of structure with soil (foundation system or embedded structures) or with fluid (tanks or floating structures) becomes important. If the design criteria allows for limited and controlled damage, or when passive energy dissipation systems, isolation, or sliding systems are used in the structure, then nonlinear behavior of the elements need to be included, which in turn requires more attention to ensure that the mathematical model provide a reliable representation of the physical system.

The purpose of this chapter is to present basic modeling principles and suggest some guidelines and considerations that should be taken into account during the structural modeling process. Additionally, some examples of numerical characterizations of selected bridge structures and their components are provided. The outline of this chapter follows the basic modeling process. First, the selection of modeling methodology is discussed, followed by a description of the structural geometry, definition of the material and section properties of the components, comprising the structure, and description of the boundary conditions and loads acting on the structure.

12.2 Theoretical Background

Typically, during the analytical phase of any bridge design, finite element (FE) procedures and programs are used to evaluate the structural integrity of the bridge system. Most structural analysis programs employ sound, well-established FE methodologies, and algorithms to solve the analytical problem. It is of utmost importance for the users of these programs to understand the theories, assumptions, and

limitations of numerical modeling using the FE method, as well as limitations on the accuracy of the computer systems used to execute these programs. Many textbooks (Bathe, 1996; Priestley et al., 1996; and Zienkiewicz et al., 2005) are available to study the theories and application of FE methodologies to practical engineering problems. It is strongly recommended that examination of these textbooks be made before using FE-based computer programs for any project work. For instance, when choosing the types of elements to use from the FE library, the user must consider some important factors, such as the basic set of assumptions used in the element formulation, the types of behavior that each element type captures, and the limitations on the physical behavior of the system.

Other important issues to consider include numerical solution techniques used in matrix operations, computer numerical precision limitations, and solution methods used in a given analysis. There are many solution algorithms that employ direct or iterative methods, and sparse solver technology for solving the same basic problems; however, selecting these solution methods efficiently requires the user to understand the best conditions in which to apply each method and the basis or assumptions involved with each method. Understanding the solution parameters such as tolerances for iterative methods and how they can affect the accuracy of a solution are also important, especially during the nonlinear analysis process.

The first attempt to automate the structural analysis was to code the techniques that were being implemented in hand-calculations such as moment-distribution procedure. It did not take long for engineers to realize that the methods that are efficient for hand-calculations are not necessarily the best for computer analysis. Therefore, stiffness matrix approach using the virtual displacement procedure that involved assembling the stiffness of each element into a global stiffness matrix was adopted for numerical analysis. Although it is not practical for hand-calculations, this procedure can be automated rather efficiently. Before engaging in the modeling of the physical system of interest, it is essential that the engineer identifies the objectives of the analysis. These objectives can be translated into set of the parameters, or unknowns, that are computed as a part of the analysis execution. The basic parameters include only unknown degrees of freedoms of the mathematical system.

The mathematical process of this procedure is summarized below.

1. To analyze a structure, the first step is to select unknown global degrees-of-freedom (DOF). These are the basic unknowns and once they are computed the other unknowns, such as element forces and element deformations, can be obtained easily. Therefore, it is necessary to establish the relationship between displacements and element deformations.
2. Therefore, the next step is to formulate a relation between global DOF and element deformations. It is important to note that deformations do not contain rigid-body motions whereas, displacements often do. These are kinematics equations that relate the displacements to element deformations. These relations can be linear or nonlinear. For large displacements, the relation between the two is nonlinear. In some structures a linear relation between deformations and displacements may provide sufficient accuracy, whereas in other structures, such as suspension bridges, the relation between deformations and displacements is nonlinear.
3. Since the element deformations are related to the global displacements DOF through kinematics, the formulation of action-deformation element for each element will relate the element forces to element deformations and the global DOF. The stress–strain relation for each element defines the action-deformation. This requires that the sectional and material properties of the element be defined. The relation between element force and its deformation can be linear or nonlinear.
4. Having a clear definition of the relation between element forces and element deformations, they can be easily related to the external forces using virtual displacement principle. For structures with large displacements the equations of equilibrium should be solved in the deformed configuration. This means that the stiffness for each element and the structural stiffness should be updated as the structure deforms.
5. Finally the equations of equilibrium can be solved and the unknown global displacement can be obtained.

Therefore, there are three sources of nonlinearity in any structural engineering analysis as follows:

1. Kinematics (relation between deformation and displacement—or geometry)
2. Materials
3. Equations of equilibrium (equations of equilibrium can be solved in the deformed or the undeformed shape)

Any combination of the above three is possible, as described in the Table 12.1.

The key assumption in a linear analysis is the member stiffness and that it is assumed that the stiffness remains constant during the analysis. Although a linear analysis is performed to estimate strength demand, nonlinear analysis is performed to estimate deformations demands. In many cases strength demand is sufficient for force-based design. However, for damage prediction or performance-based design a nonlinear analysis is necessary. In a nonlinear analysis the main goal is to better estimate the deformations and forces using a better definition of the stiffness values. In a nonlinear analysis, kinematics, material, or both can be defined with nonlinear relationships to better formulate the behavior of the structure.

There are two methods that incorporate the large displacement in the analysis. The first method is an approximate method. In this method the stiffness matrix is assembled once in the undeformed configuration with no iteration. The displacements and deformations and element forces are computed in the undeformed geometry. Therefore, the stiffness matrix is first order. The geometric stiffness is computed based on the computed forces and based on the undeformed configuration. Therefore, this is an approximate correction only. The displacement, deformation, and element forces will be computed with the modified stiffness in the undeformed geometry. Note that there is only one cycle to compute the geometric stiffness. There is no iteration, nor any consideration for the deformed configuration. Therefore, this method is very simple to be added to linear elastic programs. In this method a linear shape function is assumed and equations of equilibrium are solved in the undeformed configurations. This method is sometimes called "second-order correction analysis." Note that in this method the equations of equilibrium will not be satisfied in the deformed configuration.

The other method is true large displacement analysis. In this method the equations of equilibrium are directly solved in the deformed configurations. In this case even if there is no material nonlinearity, there is a need for iteration to obtain equilibrium. At each step, the geometry of the structure changes. Therefore, the relations between displacement and deformation change. Note that this relation is not linear. Therefore, at each step a new stiffness matrix is generated based on the deformed configuration of the structure. Although nonlinear analyses can provide a more reliable response of the structure, more engineering judgment and validations are needed to ensure the validity of the analysis.

Dynamic analysis is increasingly being required by many codes today, especially in regions of high seismicity. Response spectrum analysis is frequently used and easily performed with today's analysis tools; however, a basic understanding of structural dynamics is crucial for obtaining the proper results efficiently and interpreting analysis responses. Basic linear structural dynamics theory can be found in many textbooks (Chopra, 2007; Clough and Penzien, 1993; Wilson, 2009). Although many analysis tools on the

TABLE 12.1 Sources of Nonlinearity

	Kinematics	Action-Deformation	Solve Equation of Equilibrium in
Small displacement with linear elastic material properties	Linear	Linear	Undeformed shape
Small displacement with nonlinear material properties	Linear	Nonlinear	Undeformed shape
Second order (P-Δ)—with linear elastic material properties	Linear	Linear	Deformed shape
Second order (P-Δ)—with nonlinear material properties	Linear	Nonlinear	Deformed shape
Large (finite) displacements with linear material properties	Nonlinear	Linear	Deformed shape
Large displacements with nonlinear material properties	Nonlinear	Nonlinear	Deformed shape

market today can perform very sophisticated analyses in a timely manner, the user too must be more savvy and knowledgeable to control the overall analysis effort and optimize the performance of such tools.

12.3 Modeling

In the modern engineering office, with the proliferation and increased power of personal computers, increasing numbers of engineers depend on structural analysis computer programs to solve their engineering problems. This modernization of the engineering design office, coupled with an increased demand placed on the accuracy and efficiency of structural designs, requires a more detailed understanding of the basic principles and assumptions associated with the use of modern structural analysis computer programs.

In any structural analysis, a real structure needs to be idealized to its mathematical representation. This requires discretization of the real structure, selection of the material and section properties, definition of the applied load and displacement, and boundary conditions. This is one of the steps in this process that engineering judgment becomes inevitable. Even with a good judgment, the developed FE model of the structure needs to be validated to make sure that its response provides a reasonable estimate of the actual bridge. The degree of accuracy needed and level of validation effort at this step are controlled by the complexity of the structure.

12.3.1 Available Computer Programs

In general, there are two types of computer programs, namely:

1. General purpose linear and nonlinear FE computer programs such as ADINA, ANSYS, NASTRAN, and ABAQUS. These FE computer programs can be used for both simple modeling using beams and truss elements and continuum modeling. FE discretization of continuum monitors the state of stress and strain at each FE element. A large library of elements and material properties are available in these FE programs. Geometric nonlinearity can be explicitly included in the analysis with a true large displacement solution (see Table 12.1). These FE programs are more expensive and not developed for structural engineers only. Therefore, there is a need for a more modeling effort as well computer resources. As the computers become more powerful, the use of these FE programs becomes more reasonable. However, the engineers need to be trained with the nonlinear behavior and dynamic analysis to be able to develop a reliable model.
2. Linear and nonlinear computer programs specifically developed for structural engineers, such as GTSTRUDL, STAADIII, SAP2000, and LARSA. These computer programs are written for structural engineering problems. Usually the element and material libraries are limited to beams, truss, springs, and sometimes shell elements. Lumped plasticity beam elements have been introduced in many computer programs with nonlinear capability. Approximate large displacement formulation (elastic second order P–Δ—see Table 12.1) is usually used in these computer programs, where the stiffness matrix is modified with linearized geometric stiffness, whereas the equation of equilibrium are solved and checked on the undeformed geometry.

The objective of the analysis effort is to investigate the most probable responses of a bridge structure because of a range of applied loads. The results of these investigations must then be converted to useful design data, thereby providing designers with the information necessary to evaluate the performance of the bridge structure and to determine the appropriate actions in order to achieve the most efficient design configuration. Additionally, calculation of the structural system capacities is an important aspect in determining the most reliable design alternative.

Every effort must be made to ensure that all work performed during any analytical activity enables designers to produce a set of quality construction documents including plans, specifications, and estimates.

12.3.2 Selection of Modeling Methodology

The technical approach taken by the engineer must be based on a philosophy of providing practical analysis in support of the design effort. Significant importance must be placed on the analysis procedures by the entire design team. All of the analytical modeling, analysis, and interpretation of results must be based on sound engineering judgment and a solid understanding of fundamental engineering principles. Ultimately, the analysis must validate the design.

Many factors contribute to the determination of the modeling parameters. These factors should reflect issues such as the complexity of the structure under investigation, types of loads being examined, and most importantly, the information needed to be obtained from the analysis in the most efficient and 'design-friendly' formats. This section presents the basic principles and considerations for structural modeling. It also provides examples of modeling options for the various bridge structure types.

Analysis and design should be treated as two very closely related and coupled processes, rather than separate activities. The design-analysis process is illustrated in a flow chart in Figure 12.1. The challenge in developing technically sound and cost/schedule efficient design-analysis solutions is in formulating the right design-analysis problem. Analysis process is not just an isolated activity, but it is "Computer" experiments that disclose the physical characteristics of the structure. The first step is to understand the physics of the problem and be able to formulate the structural system. A conceptual model will need to be developed next, to better understand the structural behavior. Once a good understanding of the structural system is gained, model development should always be accompanied by the validation of the model. After validation of the model, the analysis and interpretation of the results will start. From this flow chart, it becomes very clear that there are several steps before and after the analysis that needs direct engineering judgment. For a reliable analysis and design, therefore, it is important to have a sound understanding and knowledge of structural mechanics, structural analysis, structural dynamics,

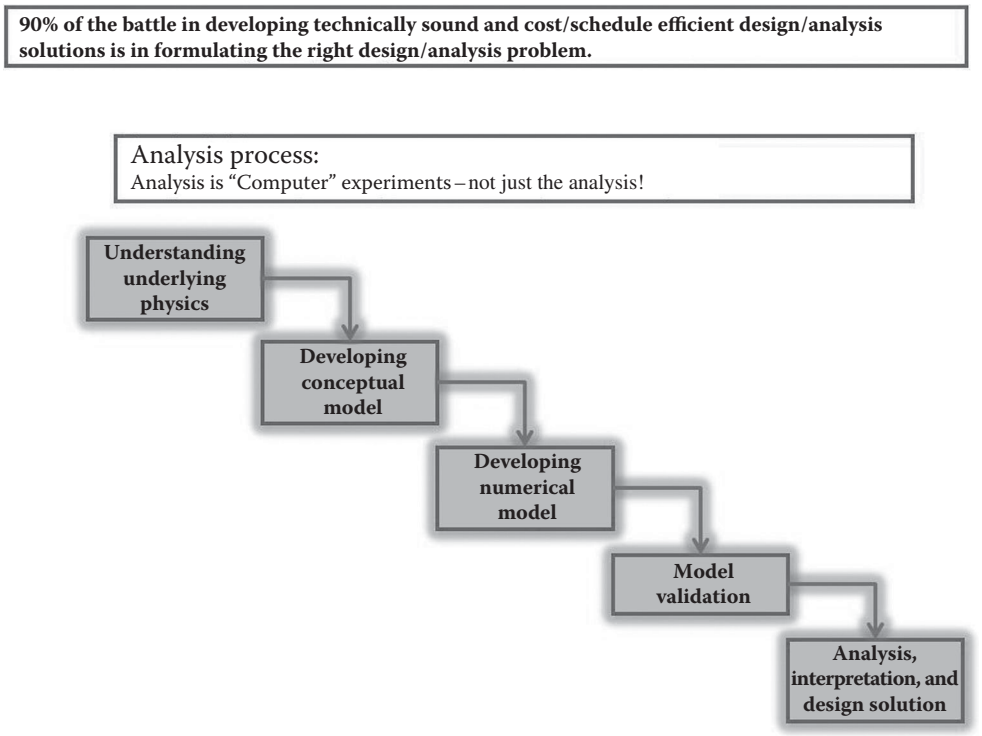

FIGURE 12.1 Design-analysis process.

nonlinear analysis, and nonlinear behavior of the structures even before performing any analysis. After analysis is complete, the engineer needs to be able to interpret and validate the results and identify possible mistakes or misrepresentations of the intentions of the modeling.

The model development process is shown in a flow chart in Figure 12.2. The technical approach to computer modeling is usually based on a logical progression. The first step in achieving a reliable computer model is to define a proper set of material and soil properties, based on published data and site investigations. In the second step, critical components are assembled and tested numerically where validation of these components' performances is considered important to the global model response. Closed form solutions or available test data are used for these validations. The next step is the creation and numerical testing of subsystems such as the bridge towers, superstructure elements, or individual frames. Again, as in the previous step, simple procedures are used in parallel to validate computer models. A full bridge model consisting of the bridge subsystems is assembled and exercised. This final global model should include appropriate representation of construction sequence, soil and foundation boundary conditions, structural component behavior, and connection details. In the last step, boundary condition definition and verification are essential parts of a modeling procedure.

The FE modeling and analysis process is further described in the flow chart shown in Figure 12.3. The assembled model will need to be subjected to applied load. The applied load can be static force or displacement or time-varying acceleration, force, or displacement. Following the analysis and after careful examination of the analytical results, the data is postprocessed and the demand values are extracted. An important part of the overall analytical procedure is the determination of the capacities of the structural members. A combination of engineering calculations, computer analyses, and testing is utilized in order to develop a comprehensive set of component and system capacities. The evaluation of the structural integrity of the bridge structure, its components, and their connections are then conducted by comparing capacities with the demands calculated from the structural analysis. If the demand values meet the requirement of the design criteria then the design can be finalized. Otherwise, the design needs to be adjusted and model needs to be updated for a new analysis. The entire process may be repeated to validate any modifications made, depending on the nature and significance of such modifications.

High order FEs such as three-dimensional solid elements or shell elements can be used in modeling of a structure depending on the complexity of the structure under investigation, and nature of the applied loads. More complex models, however, require a significantly higher degree of engineering experience and

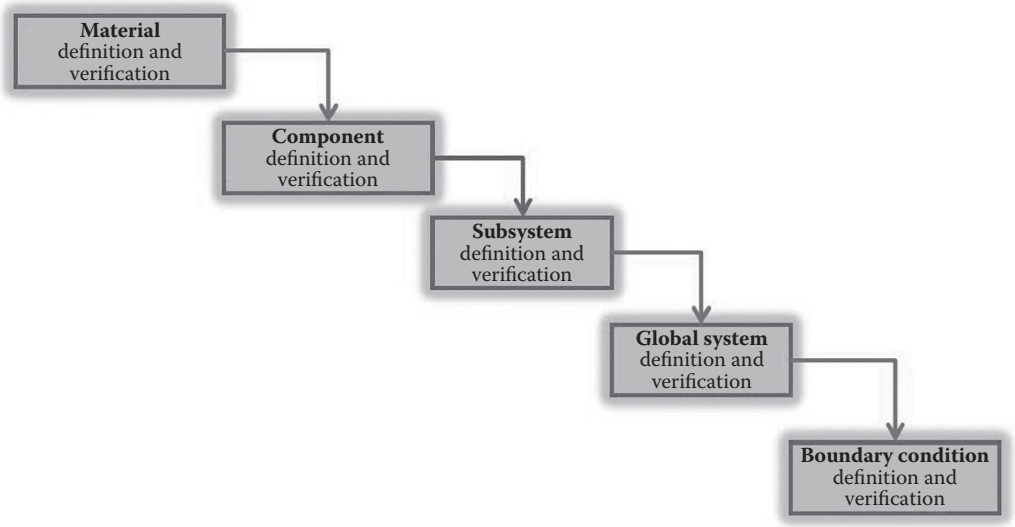

FIGURE 12.2 FE model development process.

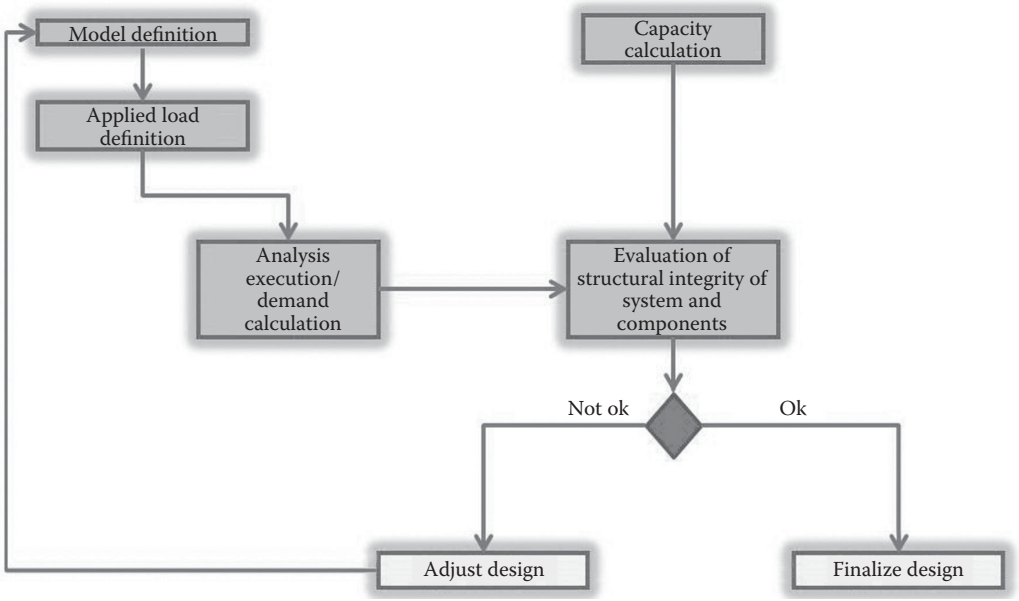

FIGURE 12.3 Modeling-analysis process.

expertise in the theory and application of the FE method. In the case of a complex model, the engineer must determine the degree of refinement of the model. This determination is usually made based on the types of applied loads as well as the behavioral characteristics of the structure being represented by the FE model. It is important to note that the format of the results obtained from detailed models (such as shell and 3-D continuum models) is quite different from the results obtained from beam (or stick) models. Stresses and strains are obtained for each of the bridge components at a much more detailed level therefore calculation of a total force applied to the superstructure, for example, becomes a more difficult, tedious task. However evaluation of local component behavior, such as cross frames, plate girder sections, or bridge deck sections can be accomplished directly from the analysis results of a detailed FE model. Some examples of FE modeling using high order FEs are shown in Figure 12.4 and 12.5. When high order FEs are implemented in a model, a mesh refinement study must be performed. An example of mesh refinement study is shown in Figure 12.6. The results of FE analysis can be inaccurate when very coarse mesh is used. A balance between mesh refinement and reasonable element aspect ratios must be maintained so that the behavioral characteristics of the computer model are representative of the structure it simulates.

An example of low-order FE modeling is shown in Figure 12.7. In this example the engineer, based on the requirement of the design criteria and project needs, has decided to simplify the continuum with elements such as beam, truss, or springs. The results of analysis in this type of modeling are usually forces and moments. These results are normally associated with individual element coordinate systems, thus simplifying the evaluations of these components. Normally, these force resultants describe axial, shear, torsion, and bending actions at a given model location. Therefore, it is very important during the initial modeling stages to determine key locations of interest, so the model can be assembled such that important results can be obtained at these locations. Although it is convenient to use element coordinate systems for the evaluation of the structural integrity of individual components, nodal results such as displacements and support reactions are usually generated for output in the global coordinate systems.

In many cases during model development, high order FEs can be mixed with low order elements such as beams and truss elements. This "hybrid" modeling procedure can result in an efficient and yet accurate FE model. The simple model shown in Figure 12.7 can be adjusted using hybrid modeling procedure as shown in Figures 12.8 and 12.9. For more complex structures with complicated geometric configurations,

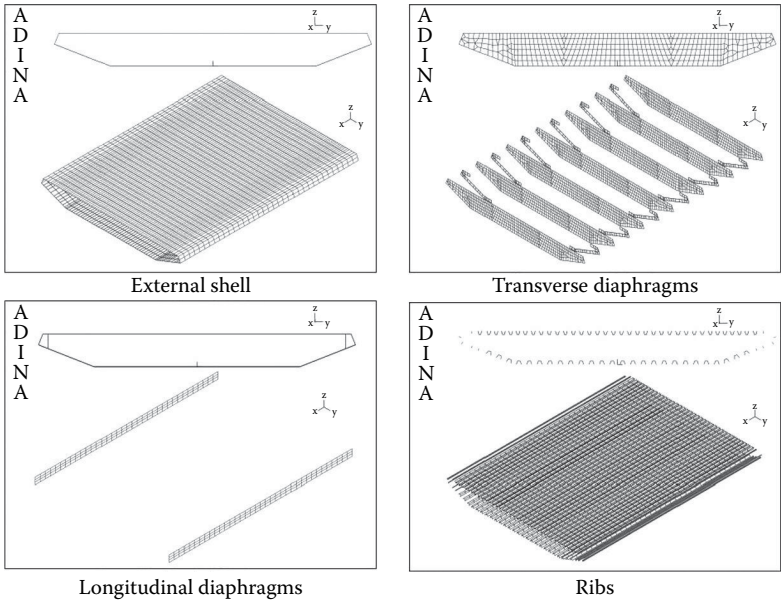

FIGURE 12.4 Typical FE model using high-order continuum elements.

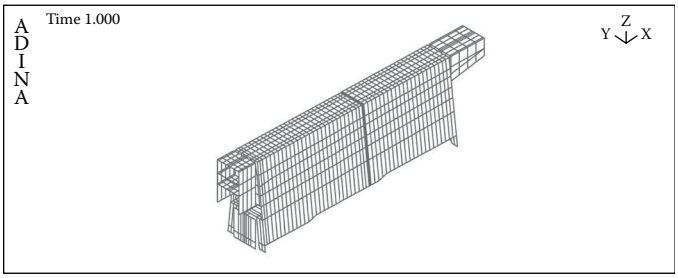

FIGURE 12.5 Typical FE model using high-order continuum elements.

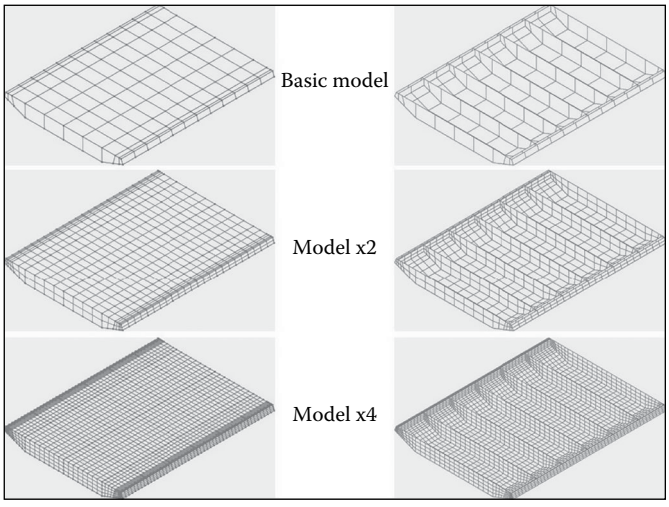

FIGURE 12.6 Mesh refinement study.

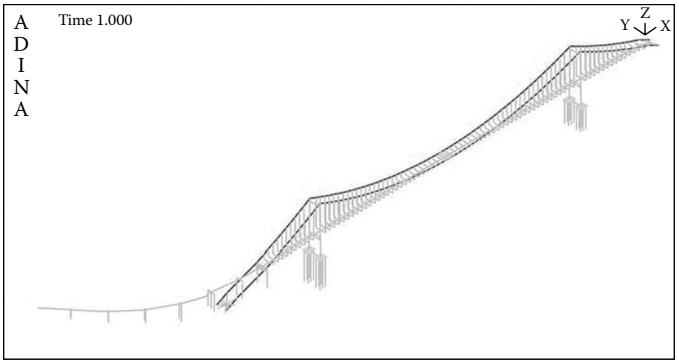

FIGURE 12.7 Typical beam model.

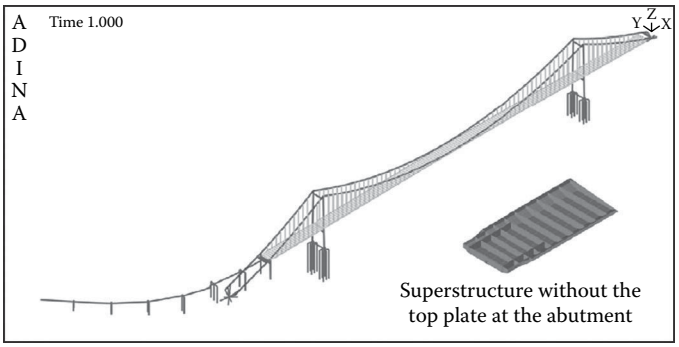

FIGURE 12.8 Combination of high and low-order finite element—typical hybrid modeling.

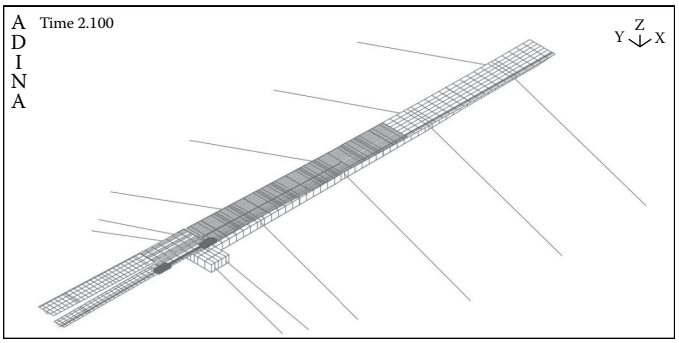

FIGURE 12.9 Combination of high and low-order finite element—typical hybrid modeling.

such as curved plate girder bridges (Figure 12.10), or bridges with highly skewed supports (Figure 12.11 and 12.12), more detailed FE models should be considered, especially if individual components within the superstructure need to be evaluated, which could not be facilitated with a beam superstructure representation. With the increasing speed of desktop computers, and advances in FE modeling tools, these models are becoming increasingly more popular. The main reason for their increased popularity is the improved accuracy, which in turn results in more efficient and cost-effective design. Higher orders of accuracy in modeling often come at a cost of analysis turnaround time and overall model efficiency.

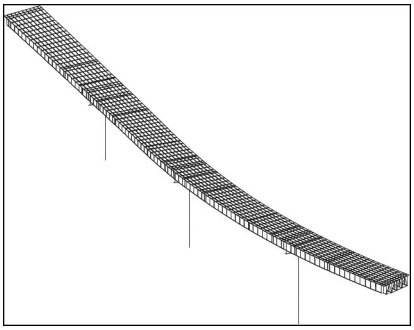

FIGURE 12.10 Steel plate girder bridge finite element model.

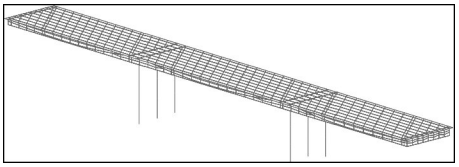

FIGURE 12.11 Concrete box girder with 45° skewed supports finite element model.

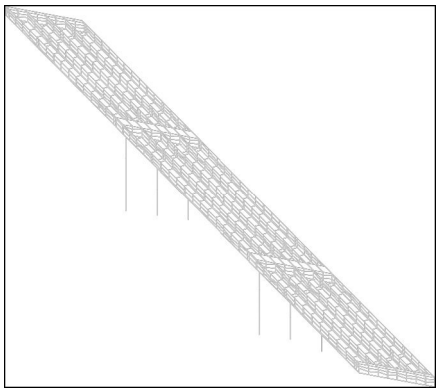

FIGURE 12.12 Concrete box girder modeling example (deck elements not shown).

The analyst must use engineering judgment to determine if the benefits of mesh refinement justify the costs. For example, for the convenience in design of bridge details such as reinforcement bar cut off, prestressing cable layouts, and section changes, the bridge superstructure is usually modeled with a high degree of refinement in the dead and live load analyses to achieve a well-defined force distribution. The same refinement may not be necessary in a dynamic analysis. Quite often coarser models are used in the dynamic analyses. These refinements are the minimum guidelines for discrete lumped mass models in dynamic analysis to maintain a reasonable mass distribution during the numerical solution process.

12.3.3 Geometry

After selecting an appropriate modeling methodology, serious considerations must be given to proper representation of the bridge geometric characteristics. These geometric issues are directly related to the behavioral characteristics of the structural components as well as the overall global structure.

The considerations must include not only the global geometry of the bridge structure, that is, horizontal alignment, vertical elevation, super-elevation of the roadway, and severity of the support skews, but local geometric characterizations of connection details of individual bridge components as well. Such details include representations of connection regions such as column to cap beam, column to box girder, column to pile cap, cap beam to superstructure, cross frames to plate girder, gusset plates to adjacent structural elements, as well as various bearing systems commonly used in the bridge engineering practice. Some examples of some modeling details are demonstrated in Figures 12.12 through 12.19. Specifically, Figure 12.12 demonstrates how a detailed model of a box girder bridge structure can be assembled via use of shell elements (for girder webs and soffit), truss elements (for posttensioning tendons), 3D solid elements (for internal diaphragms), and beam elements (for columns). Figure 12.13 illustrates some details of the web, deck, and abutment modeling for the same bridge structure. Additionally, spring elements are used to represent abutment support conditions for the vertical as well as back wall directions. An example of a column and its connection to the superstructure in an explicit FE model is presented in the Figure 12.14. Three elements are used to represent the full length of the column. A set of rigid links connects the superstructure to each of the supporting columns (Figures 12.15 and 12.16). It is necessary to properly transmit bending action of these components, since the beam elements (columns) are characterized by six DOF per node, whereas 3D solids (internal diaphragms) carry only three DOF per node (translations only). In this example posttensioning tendons are modeled explicitly, via truss elements with the proper drape shape (Figure 12.16). This was done so that accurate posttensioning load application was achieved and the effects of the skews were examined in detail. However, when beam models are used for the dynamic analysis (Figure 12.7), special attention must be given to the beam column joint modeling. For a box girder superstructure, since cap beams are monolithic to the superstructure, considerations must be given to capture proper dynamic behavior of this detail through modification of the connection properties. It is common to increase the section properties of the cap beam embedded in the superstructure to simulate high stiffness of this connection.

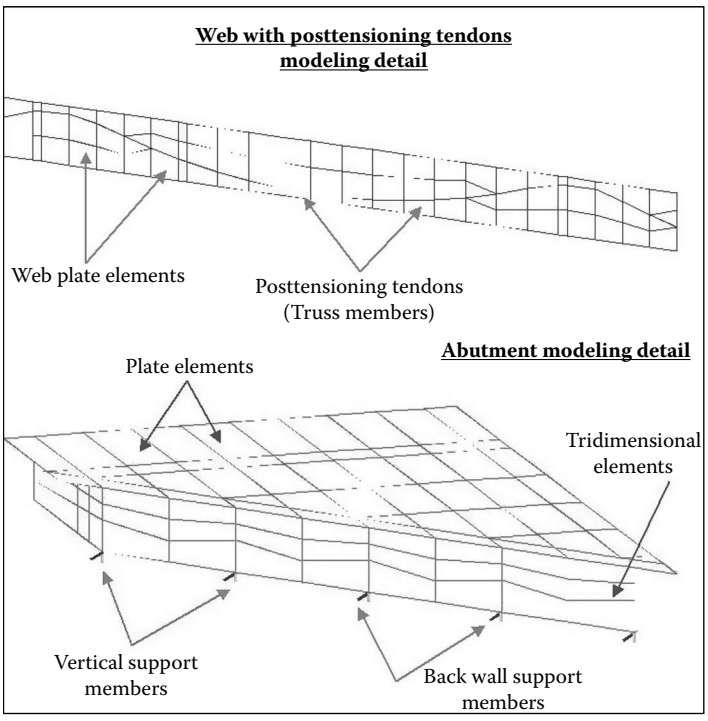

FIGURE 12.13 Selected modeling details.

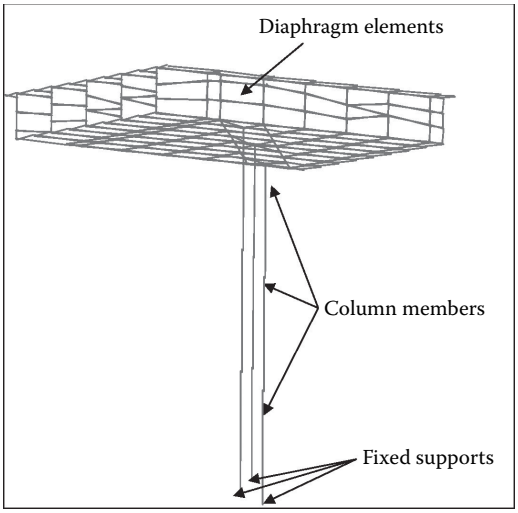

FIGURE 12.14 Bent region modeling detail.

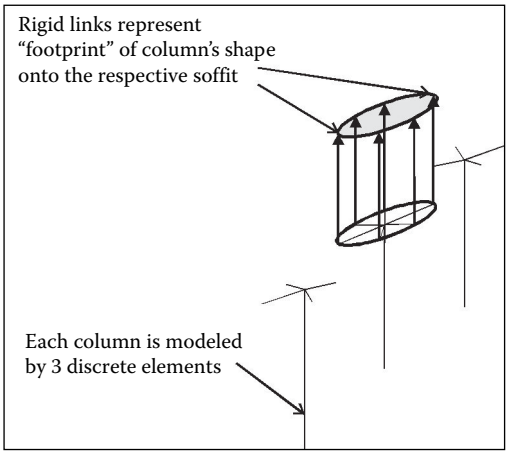

FIGURE 12.15 Column to superstructure connection modeling detail.

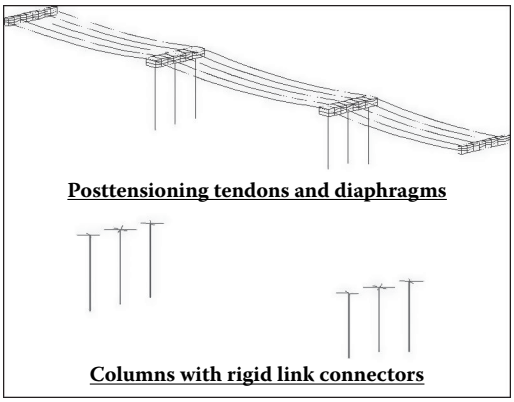

FIGURE 12.16 Posttensioning tendons, diaphragms, and column to diaphragm connection modeling examples.

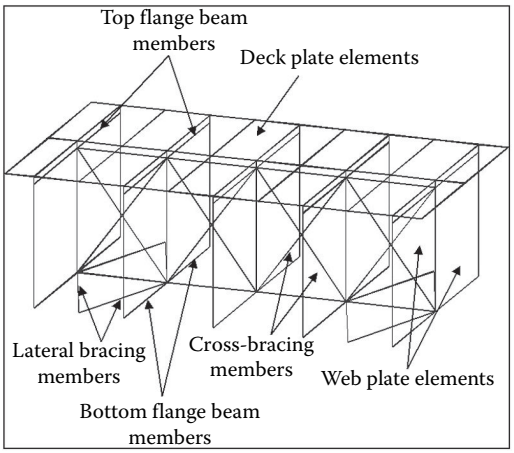

FIGURE 12.17 Plate girder superstructure modeling example.

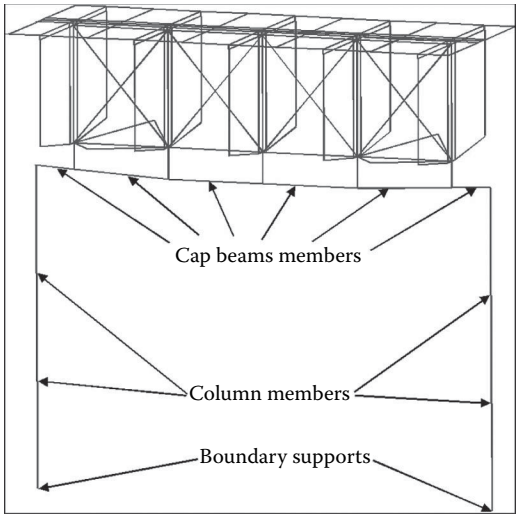

FIGURE 12.18 Plate girder bent region modeling example.

Figure 12.17 illustrates the plate girder modeling approach for a section of superstructure. Plate elements are used to model deck sections and girder webs, whereas beams are used to characterize flanges, haunches, cross frame members, as well as columns and cap beams (Figure 12.18). Proper offsets are used to locate the centerlines of these components in their proper locations.

12.3.4 Material and Section Properties

One of the most important aspects of capturing proper behavior of the structure is the determination of the material and section properties of its components. The Roark's Formulas for Stress and Strain (Young et al., 2011) is widely used for calculating section properties for a variety of cross-sectional geometry. For 3D solid FE, the material constitutive law is the only thing to specify, whereas other elements consideration of modification of material properties are needed to match the actual structural behavior. Most structural theories are based on homogenous material such as steel. Although this means structural behavior can be directly calculated using the actual material and section properties, it also indicates that nonhomogenous material such as reinforced concrete may subject certain limitation.

Because of its composite nonlinear performance nature of reinforced concrete, section properties need to be adjusted for the objective of analysis. For elastic analysis, if strength requirement is the objective, section properties are less important as long as relative stiffness is correct. Section properties become most critical when structure displacement and deformation are objectives. Since concrete cracks beyond certain deformation, section properties need to be modified for this behavior. In general, if ultimate deformation is expected, then effective stiffness should be the consideration in section properties. It is common to use half value of the moment of inertia for reinforced concrete and full value for prestressed concrete members. To replicate a rigid member behavior such as cap beams, section properties need to be amplified 100 times to eliminate local vibration problems in dynamic analysis.

Nonlinear behaviors are most difficult to handle in both complex and simple FE models. When solid elements are used, the constitutive relationships describing material behavior should be utilized. These properties should be calibrated by the data obtained from the available test experiments. For beam-column type elements however, it is essential that engineer properly estimates performance of the components either by experiments or theoretical detailed analysis. Once member performance is established, a simplified inelastic model can be used to simulate the expected member behavior. Depend on the complication of the member, bilinear, multi-linear also been used extensively. If member degradation needs to be incorporated in the analysis then Takeda model may be used. Although degrading model can correlate theoretical behavior with experimental result very well, elastic–plastic or bilinear models can give the engineer a good estimate of structural behavior without detailed material property parameters.

When a nonlinear analysis is performed, the engineer needs to understand the sensitivity issue raised by such analysis techniques. Without a good understanding of member behavior, it is very easy to fall into the "garbage in, garbage out" mode of operation. It is essential for the engineer to verify member behavior with known material properties before any production analyses are conducted. For initial design, all material properties should be based on the nominal values. However, it is important to verify design with expected material properties.

12.3.5 Boundary Conditions

Another key ingredient for the success of the structural analysis is the proper characterization of the boundary conditions of the structural system. Conditions of the columns or abutments at the support (or ground) points must be examined by engineers and properly implemented into the structural analysis model. This can be accomplished via several means based on different engineering assumptions. For example, during most of the static analysis, it is common to use a simple representation of supports (e.g., fixed, pinned, roller) without characterizations of the soil/foundation stiffness. However for a dynamic analysis, proper representation of the soil/foundation system is essential (Figure 12.19).

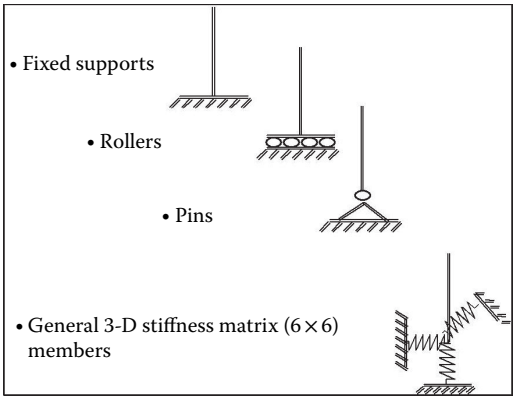

FIGURE 12.19 Examples of boundary conditions.

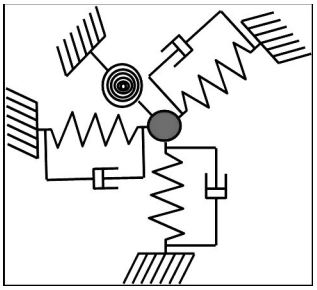

FIGURE 12.20 Nonlinear spring/damper model.

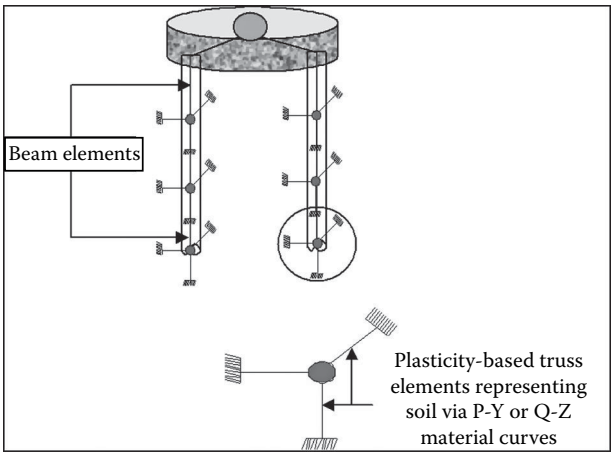

FIGURE 12.21 Soil/structure interaction modeling.

Usually, most FE programs will accept a (6 × 6) stiffness matrix input for such system. Other programs require extended (12 × 12) stiffness matrix input describing the relationship between the ground point and the base of the columns. before using these matrices, it is important that the user investigates the internal workings of the FE program, so the proper results are obtained by the analysis.

In some cases it is necessary to model the foundation/soil system with greater detail. Nonlinear modeling of the system can be accomplished via nonlinear spring/damper representation (Figure 12.20) or, in the extreme case, by explicit modeling of subsurface elements and plasticity based springs representing surrounding soil mass (Figure 12.21). It is important that if this degree of detail is necessary, the structural engineer works very closely with the geotechnical engineers to determine proper properties of the soil springs. As a general rule it is essential to set up small models to test behavior and check the results via hand calculations.

12.3.6 Loads

During engineering design activities, computer models are used to evaluate bridge structures for various service loads, such as traffic, wind, thermal, construction, and other service loads. These service loads can be represented by a series static load cases applied to the structural model. Some examples of application of the truck loads are presented in Figures 12.22 and 12.23.

In many cases, especially in high seismic zones, dynamic loads control many bridge design parameters. In this case, it is very important to understand the nature of these loads, as well as the theory that

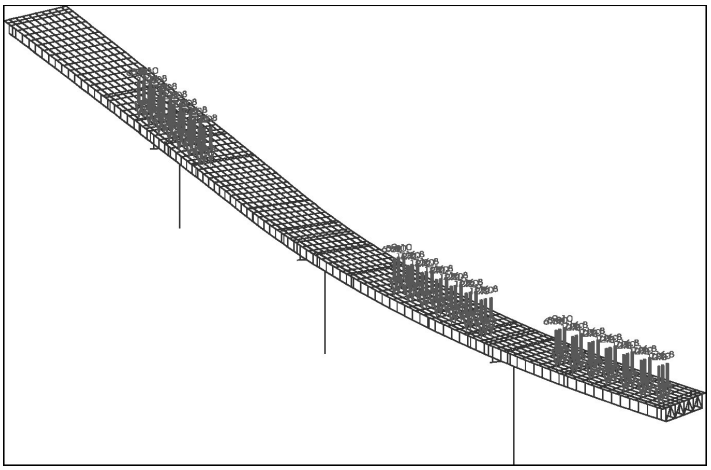

FIGURE 12.22 Truck load application example.

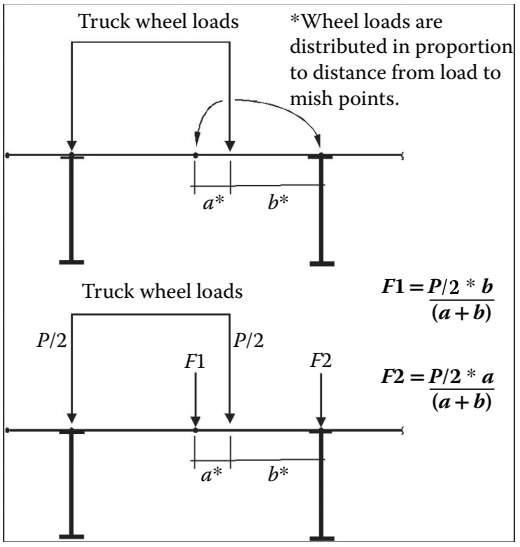

FIGURE 12.23 Equivalent truck load calculation example.

governs the behavior of structural systems subjected to these dynamic loads. In the high seismic zones, a multi-mode response spectrum analysis is required to evaluate the dynamic response of the bridge structures. In this case, the response spectrum loading is usually described by the relationship of the structural period versus ground acceleration, velocity, or displacement for a given structural damping. In some cases, usually for more complex bridge structures, a time history analysis is required. During these analytical investigations, a set of time history loads (normally displacement, or acceleration versus time) is applied to the boundary nodes of the structure. The most widely used theoretical reference (Clough and Penzien, 1993) presented the seismic analysis methodology for either response spectrum or time history analysis. Uang and Bertero (1998) discussed energy equation for the seismic response of structures. The fourth book of this series, *Seismic Design*, with 18 chapters, presents the latest in seismic bridge analysis and design.

12.4 Summary

In summary, the analysis effort should support the overall design effort by verifying the design and addressing any issues with respect to the efficiency and the viability of the design. Before modeling commences, the engineer must define the scope of the problem and ask himself what key results and types of data he is interested in obtaining from his analytical model. With these basic parameters in mind, the engineer can then apply technical knowledge to formulate the simplest, most elegant model to properly represent the structure and provide the range of solutions that are accurate and fundamentally sound. The engineer must bind the demands on the structure by looking at limiting load cases and modifying the structure parameters, such as boundary conditions or material properties. Rigorous testing of components, hand calculations, local modeling, and sound engineering judgment must be used to validate the analytical model at all levels. Through a rigorous analytical methodology and proper use of today's analytical tools, structural engineers can gain a better understanding of the behavior of the structure, evaluate the integrity of the structure, and validate and optimize the structural design.

References

Bathe, K. J. 1996. *Finite Element Procedures* (2nd Edition). Prentice Hall, Englewood Cliffs, NJ.

Chopra, A. K. 2007. *Dynamics of Structures, Theory and Applications to Earthquake Engineering* (3rd Edition). Prentice Hall, Englewood Cliffs, NJ.

Clough, R. W., and Penzien, J. 1993. *Dynamics of Structures* (2nd Edition). McGraw-Hill, Inc., NY.

Priestley, M. J. N., Seible, F., and Calvi, G. M. 1996. *Seismic Design and Retrofit of Bridges*. John Wiley & Sons, Inc., NY.

Uang, C. M., and Bertero, V. 1998. *Use of Energy as a Design Criterion in Earthquake-Resistant Design*. Technical Paper UCB/EERC-88/18. University of California, Berkeley, CA.

Wilson, E. L. 2009. *Static and Dynamic Analysis of Structures*. Computers and Structures Inc., Berkeley, CA.

Young, W. C., Budynas, R. G. and Sadegh, A. M. 2011. *Roark's Formulas for Stress and Strain* (8th Edition). McGraw-Hill, Inc., NY.

Zienkiewicz, O. C., Taylor, R. L., and Nithiarasu, P. 2005. *The Finite Element Method* (6th Edition). Elsevier, Oxford, UK.

13

Concrete Design

Monte Smith
Sargent Engineers, Inc.

13.1 Introduction

Concrete is one of the most common materials used in the construction of bridges. At the very least, concrete is used in the substructure even though it may not be used in the superstructure. Concrete responds very well under compression but it does not respond well in tension. The tensile resistance is usually only a small fraction of the compressive strength. Because of this, concrete used in bridges usually also contains other materials to resist the tensile forces that are created in a bridge member. This chapter discusses concrete design theory and practical design procedures used in highway structures.

13.2 Material Properties

Concrete used in bridges is usually composed of hydraulic cement concrete combined with some sort of element used to resist tensile stresses. The added elements are usually made from steel, although other reinforcing elements have been tested and tried in concrete. The focus of this discussion will be on properties that affect the design of concrete. It will not be on the properties that affect the service life of concrete. Recent developments in concrete have been focused on the improvement of the strength characteristics of concrete as well as the service characteristics of concrete.

13.2.1 Concrete

Concrete is a mixture of hydraulic cement (cement that chemically reacts with water) and aggregates. The aggregates consist of a gradation of sand and gravel so that there are no voids in the concrete. This provides a better strength concrete. Other additives are also added to increase the workability of the concrete or improve the properties of concrete.

Every different type of cement and aggregate behaves differently with each other. So it is imperative that trial mixes be made to determine the properties of the concrete. Enough samples of the trial mixes need to be made to determine a statistical average of the properties of the concrete. In particular, the properties need to be selected so that the final strength of the concrete meets the needs of the design. Usually, a 95% confidence limit is selected to meet the design strength requirements.

Concrete typically continues to gain strength over time as it ages or cures. The rate of strength gain is totally dependent on the ingredients that are in the concrete. In specifying the required strength of the concrete, it is usually specified at various ages. Typically, the strength of concrete is specified at an age of 28 days. However, as higher performance concretes are specified, it is not uncommon to specify a 56-day concrete strength.

Concrete properties that are important to the design of bridges include the following:

- Strength is important for obvious reasons. This will control the size of members especially for shear and compression. The AASHTO *LRFD Bridge Design Specifications* (AASHTO, 2012) require that the minimum specified compressive strength not be less than 2.4 kips/sq in (ksi) for structures, and that the minimum compressive strength for prestressed concrete and decks not be less than 4.0 ksi.
- Creep is important because it affects the final deflected shape of the member and it also can affect how forces in the reinforcing elements will change over time. For example, in a column as the concrete creeps, it transfers some of the load carried by the concrete to the reinforcing steel. In structures where the continuity changes over time, creep can redistribute the forces in the structure. As an example, if there are two simple spans and then they are made continuous, then the simple span dead load moments creep toward the continuous dead load moment. For most permanent loads the creep deflections will vary between two and four times the instantaneous deflections.
- Shrinkage affects the design of bridges in two ways. Shrinkage is the shortening of the member over time as excess water leaves the concrete. As the concrete shortens it can impart loads to the reinforcing members and it also can cause the concrete to crack to relieve tension stresses in the concrete. The ultimate shrinkage strain in concrete can vary between 0.0003 and 0.0006 for well-cured sections.
- Modulus of elasticity affects the relative distribution of forces between concrete and the reinforcing steel. It also affects the deformation properties of the concrete under load. It is not only important to make sure that bridge members can resist the load imparted to them, but they also have to provide a shape that can carry moving vehicles. So it is important to know how a bridge deck, beam, and so on will deflect over time. In the AASHTO *LRFD Bridge Design Specifications* (AASHTO, 2012) the modulus of elasticity is given by

$$E_c = 33{,}000\, K_1 \; w_c^{1.5} \sqrt{f_c'} \tag{13.1}$$

where k_1 is the correction factor for source aggregate to be taken as 1.0 unless determined by physical test; w_c is the unit weight of concrete (kips per cubic foot, kcf); and f_c' is the specified compressive strength of concrete (ksi). For normal weight concrete with w_c equal to 0.145 kcf

$$E_c = 1{,}820\sqrt{f_c'} \tag{13.2}$$

13.2.1.1 Unconfined Concrete Strength

Every concrete has its own stress–strain curve. It depends on all of the constituents in the concrete mix. So the stress–strain curves vary widely. A typical stress–strain curve of a concrete cylinder tested in uniaxial loading is shown in Figure 13.1.

The plot is shown with the sign convention that tensile stresses and strains are negative and compressive stresses and strains are positive. There is very little tensile strength in concrete; therefore, it is usually assumed that the concrete has no tensile strength, except for resisting shear. At the level of service loads it is usually assumed that the concrete is behaving linearly, which may or may not be actually true. The compression failure of concrete is very brittle and does not have any ductility. At the ultimate strength of the concrete some models use an assumed shape for the concrete stress–strain curve and some models replace the stress–strain curve with an assumed compression block with a uniform stress. The actual ultimate strain for unconfined concrete in compression is usually in the range of 0.003–0.005.

13.2.1.2 Confined Concrete Strength

If the concrete is confined transversely to the stress applied to the concrete, its properties improve dramatically. A typical stress–strain curve for confined concrete is shown in Figure 13.2.

These curves demonstrate the change in performance for the same concrete where one test specimen has confinement and the other specimen does not have confinement. The maximum stress can be increased to over two times the unconfined strength. Typically, if the code required amount of

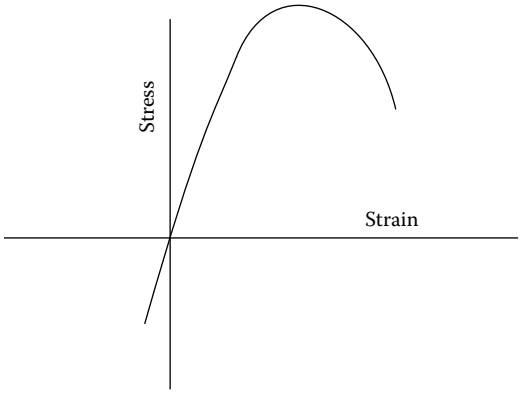

FIGURE 13.1 Typical stress–strain curve for unconfined concrete.

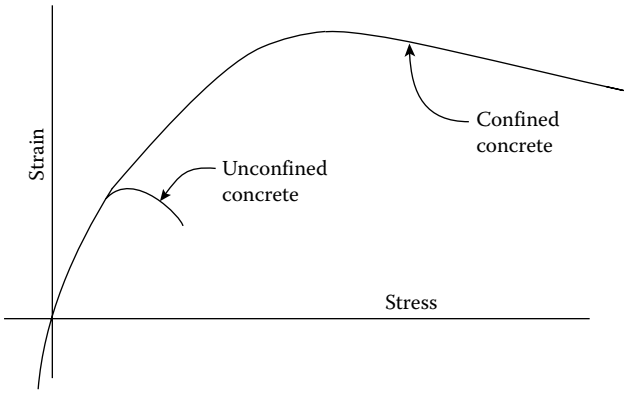

FIGURE 13.2 Typical stress–strain curve for confined concrete.

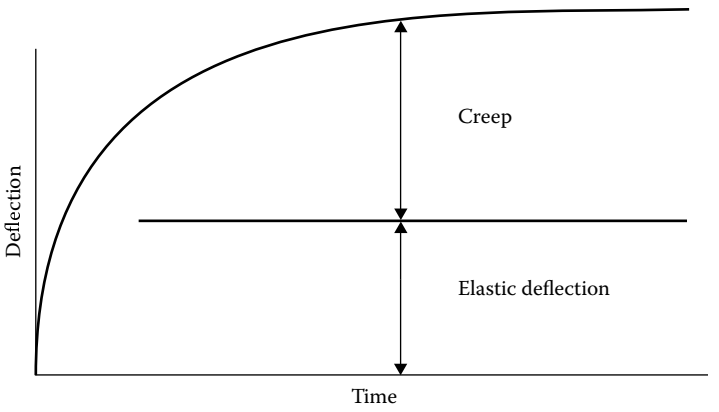

FIGURE 13.3 Typical curve for deflection of concrete.

confinement is provided at plastic hinges, the strength will increase by about 30%. The maximum strain is approximately six times that for unconfined concrete. Confinement can be provided by reinforcing steel, steel jacketing, or fiber reinforced plastic (FRP) composite wraps.

13.2.1.3 Creep

Creep is the phenomenon where once a load is applied to a material, the material initially deflects and then keeps deflecting over time. A plot of the phenomenon looks something like Figure 13.3.

The amount of creep that will occur can be as much as two to four times the initial deflection of the concrete. Creep is influenced by the concrete mix, humidity, age of the concrete at loading, shape of the member, and strength of the concrete at the time of loading. Historically two publications have been used to model creep in concrete, the recommendations of ACI Committee 209 and the CEB-FIP model code. Both of these approaches have been used to model the deflection of concrete structures. Both approaches are an approximation to what will really happen. Creep will vary with each concrete mix and environmental condition. Because of this it is recommended that the design of structures be done in such a way that creep is not a critical part of the design of the structure. But for some structures this cannot be avoided. So if it is critical then it is recommended that tests be performed on the mix of concrete that will be used in the structure.

13.2.1.4 Shrinkage

Shrinkage is a phenomenon where over time concrete will contract. This is due to three processes: drying shrinkage because of the loss of free water in the concrete, autogenous shrinkage because of the hydration of cement, and carbonation shrinkage because of the various cement hydration products carbonated in the presence of carbon dioxide. Shrinkage is influenced by the constituents of the concrete mix, humidity, water to cement ratio, type of cure, shape of the member, and length of cure. Typical values of shrinkage strain are in the order of 0.0005.

13.2.1.5 Fatigue

Concrete can fatigue just like any other material. If the strength requirements and service load requirements in the codes are met, then generally this requirement is satisfied.

13.2.2 Reinforcing Steel

Historically, concrete has been reinforced by uncoated mild steel. This steel has taken various forms over the years, but basically it is some sort of steel reinforcement oriented to resist the tensile forces in the concrete member. Currently, the reinforcing steel is in the form of round steel bars with deformations

on them to improve the bond characteristics with the concrete that it is imbedded in. Steel wire is also used that may or may not be deformed. In addition steel wire is sometimes made into welded wire fabric where the wire is placed perpendicular to each other and welded at all of the intersections of the wires. Predominantly individual bars are used most in concrete members.

Corrosion of the reinforcing steel is prevented by the acidity of the cement that coats the reinforcing steel. Therefore, it is important to have an adequate cover and limit crack sizes in the cover concrete to limit the corrosion potential of the reinforcing steel.

13.2.2.1 Strength Relationships

Reinforcing steel made according to ASTM A615 (AASHTO M31) does not have much control over the elements combined into the steel. It only has to meet strength requirements. If welding of the steel is important or the steel needs to meet certain ductility requirements, then the steel should be specified to be ASTM A706. The typical stress–strain curve for reinforcing steel is shown in Figure 13.4. The typical yield strength specified for reinforcing steel is 60 ksi. The typical modulus of elasticity for reinforcing steel is 29,000 ksi.

The properties for reinforcing steel are approximately the same in compression as they are in tension. The steel has an initial linear response until the steel hits its yield strength. This is followed by a relatively constant stress plateau until the steel starts to strain harden, where it gains strength again until it fractures. The amount of strain until fracture from first yield is a measure of the ductility of the steel. Lower strengths (or grades) of steel have more ductility than higher grades of steel.

13.2.2.2 Fatigue

Fatigue in steel has caused many failures in structures. This is also true in reinforcing steel. Fatigue is influenced by the composition of the steel, the stress range applied to the steel, and the constant stress in the steel. Generally, the higher the stress range, the fewer number of cycles that the steel can sustain. Also, the higher constant stress decreases the number of cycles that the steel can sustain.

13.2.3 Prestressing Steel

In the mid 1950s, the concrete industry started to impart permanent compression into concrete members so that they might perform better than concrete with only reinforcing steel. The original method of doing this was with wires that were pulled through holes in the concrete formed with tubes of ducts. The wires were then stressed and anchored to the ends of the concrete member. Over time this has evolved to include a number of different methods of prestressing a member with different types of prestressing steel.

Pretensioning a member usually occurs at a prestressed concrete plant where concrete members are constructed in a production facility. The method of applying the compression to the member is by the

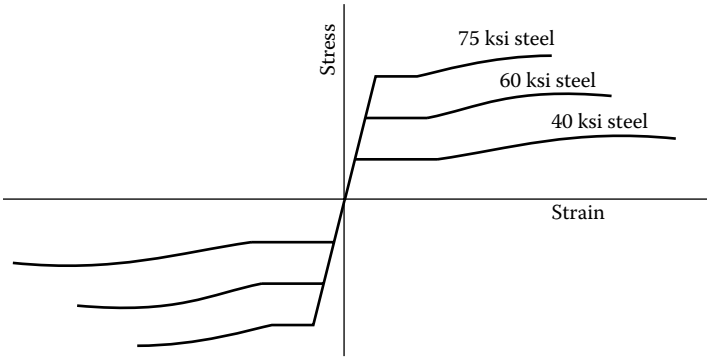

FIGURE 13.4 Typical stress–strain curves for reinforcing steel.

pulling of prestressing strand between jacks that are anchored to the floor of the facility. Then concrete is placed around the stressed strands. Once the concrete has cured and gained strength, the strands are released that then imparts a compressive stress to the concrete.

Posttensioning a member occurs after the concrete in the member is placed. The member is cast with voids in it formed by prestressing ducts or tubes. Prestressing strand or bars are then pulled through the ducts or tubes. Then prestressing jacks push on the concrete member and pull on the prestressing steel. The steel is then anchored to the end of the member through anchor plates. This then transfers the force in the steel to the concrete member that puts the member in compression. After the stressing is complete, the ducts are typically filled with grout to protect the steel from corrosion.

13.2.3.1 Prestressing Strand

Prestressing strand is made by wrapping six wires around a central wire. The individual wires have higher strength steel than normal reinforcing steel. The steel is cold drawn to increase the strength of the wire. Typical stress strain curves look something like Figure 13.5.

Prestressing strand is typically not very ductile compared to mild reinforcing steel. It also does not have a well-defined yield point or yield plateau. These characteristics need to be taken into account when investigating the ultimate strength of concrete members reinforced with prestressing steel.

13.2.3.2 Prestressing Bars

Prestressing bars are made out of alloy steel to give the steel a higher strength. The typical ultimate strength of a prestressing bar is 160 ksi as compared to 270 ksi for a prestressing strand. The advantage to prestressing bars is they are made with threads that a nut fits on to anchor the bar. This can be snugged up during the prestressing operation and essentially not lose any stress, while the bar is locked off. Prestressing strand, however, will lose some stress during the anchor operation because the anchoring is usually done with wedges that seat into an anchor. The typical stress stain curve is shown in Figure 13.5 for prestressing bars.

13.2.3.3 Relaxation

Generally steel does not lose any stress if you pull on it and then hold it at a specified strain. This is true for most structural steels. However, this is not true for prestressing steels. Prestressing steels will lose stress over time if it is held at a constant strain (relaxation). This is especially true for strands that were initially developed for use in the construction of prestressed members. More recently, low-relaxation

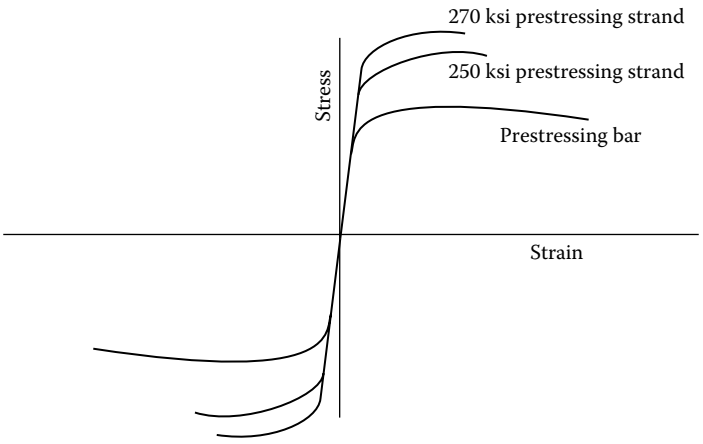

FIGURE 13.5 Typical stress–strain curves for prestressing steel.

strands have been developed for use in concrete. These strands do not lose as much stress over time. Low-relaxation strand is typically used for prestressed concrete.

13.2.3.4 Fatigue

Prestressing steel fatigues just like any other steel. Most of the time prestressing steel is bonded to the concrete around it. So the fatigue of the anchorage is usually not an issue. Fatigue is usually controlled in an indirect way. By limiting the concrete tensile stresses in concrete, the fatigue stresses in the prestressing steel are limited. So many times the limiting tensile stresses also limit the fatigue in the prestressing steel.

13.2.4 New Materials

Although steel and concrete are a good composite material, there have been research and test structures with other types of composites with concrete. Steel and concrete have similar coefficients of thermal expansion and under ideal conditions the concrete protects the steel from corrosion. However, as salts are used on roads, these salts change the pH of the concrete such that it no longer protects the reinforcing steel. This causes the steel to corrode, break the concrete cover, and then accelerate the corrosion process. Bridge decks are particularly susceptible to this type of deterioration. Because of this, other types of reinforcement are being developed.

13.2.4.1 Carbon Fiber

Carbon fiber is a high-strength material that when combined with concrete can improve the strength of concrete. Both carbon fiber bars and carbon fibers have been developed. The carbon fiber bars are used to replace reinforcing steel. Carbon fibers are mixed into the concrete mix to improve the tensile strength of the concrete.

Recently, carbon fiber fabric has been used to wrap columns and attached to beams to either repair the member or to improve the strength of the member. This works well in retrofit situations to provide confinement to columns.

Carbon fiber does not have the same coefficient of thermal expansion of concrete, so there can be some incompatibilities between these two materials.

13.2.4.2 Glass Fiber

Glass fiber performs the same functions as carbon fiber. Glass fibers and fabrics have been used for years in the construction of cars, boats, fishing rods, and other household items. It is just gaining momentum as a structural material. Glass fiber has the disadvantage that it creeps over time. This has to be taken into account when designing a structural member with concrete in it.

13.3 Design Limit States

With the development of the AASHTO *LRFD Bridge Design Specification* (AASHTO, 2012), different design requirements were translated into what are called Limit States. The four different limit states are the Service Limit State, the Strength Limit State, the Extreme Limit State, and Fatigue Limit State.

1. Service Limit State

   The Service Limit State is supposed to relate to serviceability concerns in the design of concrete members. This includes cracking (which relates to corrosion), excessive deflection, and fatigue. All of these effects are checked at the Service Limit State by applying loads with load factors of typically 1.0 and then checking to make sure that the stresses in the steel and concrete are low enough so that crack widths are kept below levels that would promote corrosion of the steel, the member does not sag excessively, or that the prestressed concrete member does not fatigue.

2. Strength Limit State

   The Strength Limit State is to ensure the member has adequate strength and stability for the loads that are being applied to it. The applied loads will frequently occur on the member including dead load, earth pressure loads, and vehicular live loads. The loads are typically modified by load factors and the nominal resistance is modified by resistance factors to meet target reliability for the member.

For conventional construction, the resistance factor, φ, specified in AASHTO *LRFD Specifications* (AASHTO, 2012) is listed as follows:

For tension controlled members where the strain in the reinforcing steel is > 0.005	0.90
For tension controlled members where the strain in the prestressing steel is > 0.005	1.00
For shear and torsion with normal weight concrete	0.90
For shear and torsion with lightweight concrete	0.70
For compression controlled sections where the strain in the tensile steel is < 0.002 with spirals or ties	0.75
For bearing on concrete	0.70
For compression in strut and tie models	0.70
For compression in anchorage zones with normal weight concrete	0.80
For compression in anchorage zones with lightweight concrete	0.65
For tension in steel in anchorage zones	1.00
For resistance during pile driving	1.00
For nonprestressed members that vary between the compression controlled and tension controlled limits (AASHTO, 2012)	

$$0.75 \le 0.65 + 0.15\left(\frac{d_t}{c} - 1\right) \le 0.9 \tag{13.3}$$

For prestressed members that vary between the compression controlled and tension controlled limits

$$0.75 \le 0.583 + 0.25\left(\frac{d_t}{c} - 1\right) \le 1.0 \tag{13.4}$$

where d_t is the distance from the extreme compression fiber to the centroid of the extreme tension steel element and c is the distance from the extreme compression fiber to the neutral axis.

3. Extreme Limit State

   The Extreme Limit State checks the member to see if it has adequate strength and ductility to survive events that will not occur very often in the life of the member. These loads include earthquakes and vessel impact. Again the loads are modified by load factors and the ideal strength of the member is modified by strength reduction factors. Both of these factors are typically one.

4. Fatigue Limit State

   The Fatigue Limit State checks the member for adequate fatigue strength to resist repetitive loads. Fatigue need not be checked for fully prestressed members satisfying the requirements for concrete stresses at the service limit state. Fatigue does not need to be checked for concrete deck slabs on multigirder bridges. For further fatigue requirements, see Section 5.5.3 of the AASHTO *LRFD Bridge Design Specifications* (AASHTO, 2012).

13.4 Plane Section Modeling

In designing structures, mathematical models are created to simulate what actually happens in the individual members. Some of these models work well in some situations and some of the models work well in other situations. The two models that are used most commonly in the design of concrete structures are the plane section model and the disturbed section model (strut and tie model).

For a typical beam under a point load, the stresses within the beam are well represented by a plane section model between the load and the reaction. But for the locations near the load or the reaction, for deep beam component such as deep beams, corbels, and brackets, the plane section model does not represent how the loads flow in the component. Figures 13.6 through 13.8 show the beam modeled with plane strain finite elements and the principal stresses in the beam.

13.4.1 Assumptions

In the plane section model the following assumption is made:

> A section perpendicular to the member will remain plane as the loads are applied to the member. In other words, the normal strains on the section are proportional to the distance from the neutral axis of the section.

Based on this assumption, the stresses in the section are determined based on the material properties. For instance, the stresses in the concrete on the tension side of the member resist tension up until the modulus of rupture. In nonprestressed concrete, no tension resistance is typically assumed.

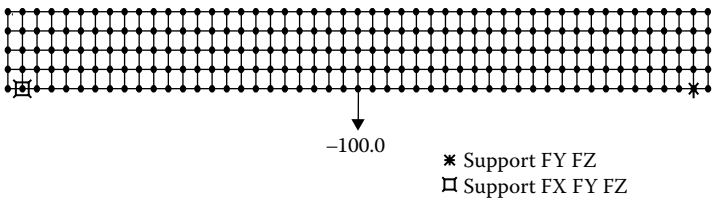

FIGURE 13.6 Example model of a beam.

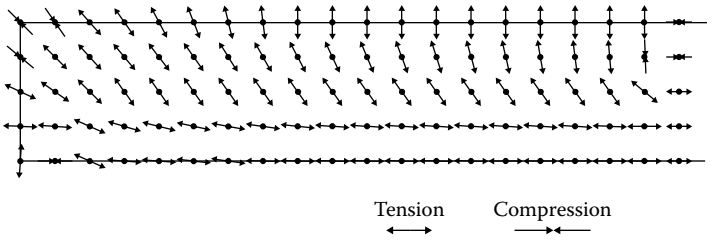

FIGURE 13.7 First-half of beam showing maximum principal stress direction.

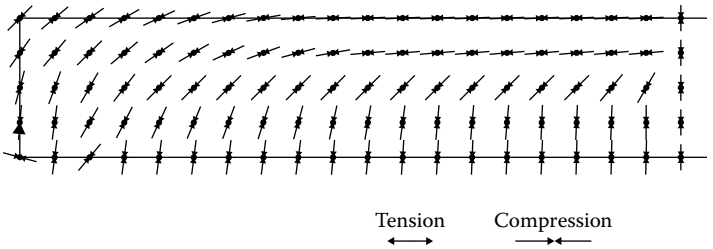

FIGURE 13.8 First-half of beam showing minimum principal stress direction.

In the AASHTO *LRFD Bridge Design Specifications* (AASHTO, 2012) a unified concrete plane section model has been developed for both prestressed and nonprestressed concrete. It also incorporates all of the forces that can be imposed on the section including moment, shear, axial load, and torsion. The following development follows this same approach showing that all of these forces interact with each other on the concrete section. In previous design codes, moment and shear were treated separately during design.

13.4.2 Service Limit State

Service considerations that need to be checked are cracking and fatigue of the concrete, and the fatigue of the reinforcing steel in the concrete. Traditionally, the fatigue of the longitudinal reinforcing steel is only checked. However, this may change after fatigue was found to cause distress in the shear steel in many bridges.

The AASHTO *LRFD Bridge Design Specifications* (AASHTO, 2012) adopts a unified approach to the design of concrete sections. However, there are differences depending on whether there is an initial prestress applied to the section with prestressing steel. The basic model that is used to check the stresses in a beam at the service level assumes the following for reinforced (sections without an initial prestress) and prestressed sections.

13.4.2.1 Reinforced Sections

Basic assumptions are as follows:

- The section remains plane, so stresses are proportional to the distance from the neutral axis.
- Tensile stresses in the concrete are ignored.

The internal forces in a reinforced beam are shown in Figure 13.9.

For a rectangular section without axial load, the following expressions can be derived.

The compression in the compression block is equal to

$$C = \frac{1}{2} f_c kdb \tag{13.5}$$

where b is the width of the section and f_c is the maximum stress in the concrete.

The tension in the reinforcing steel is equal to

$$T = f_s A_s \tag{13.6}$$

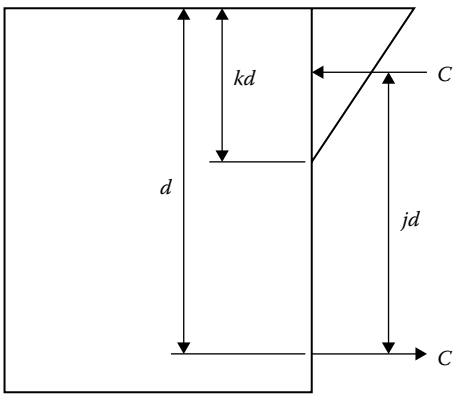

FIGURE 13.9 Beam stresses at service limit state for reinforced concrete section.

where A_s is the area of reinforcing steel on the tension side of the member and f_s is the stress in the reinforcing steel.

Since there is no axial load applied on the section, the tension and compressive forces must have the same magnitude.

$$\frac{1}{2} f_c kdb = f_s A_s \tag{13.7}$$

Since the section remains plane, the strains are proportional to their distance from the neutral axis. So the following ratio can be set up:

$$\frac{f_c/E_c}{kd} = \frac{f_s/E_s}{d-kd} \tag{13.8}$$

Rearranging this equation can be expressed as

$$0 = f_c(d-kd)\frac{E_s}{E_c} - f_s kd \tag{13.9}$$

Substituting Equation 13.7 into Equation 13.8 and substituting the modular ratio n for the ratio of the modulus of elasticities

$$0 = f_c(d-kd)n - \frac{\frac{1}{2} f_c kdb}{A_s} kd \tag{13.10}$$

$$n = \frac{E_s}{E_c} \tag{13.11}$$

The following quadratic for the variable kd is obtained:

$$0 = f_c dn - f_c nkd - \frac{f_c b}{2A_s}(kd)^2 \tag{13.12}$$

It is obvious that the concrete stress is not zero, so the quadratic solution of the remaining equation is

$$kd = \frac{n - \sqrt{n^2 - 4\left(-\frac{b}{2A_s}\right)dn}}{2\left(-\frac{b}{2A_s}\right)} \tag{13.13}$$

Now solving for k

$$k = -\frac{nA_s}{bd} + \sqrt{n^2 \frac{A_s^2}{(bd)^2} + 2n\frac{A_s}{bd}} \tag{13.14}$$

Substitute the reinforcing ratio ρ for the ratio $\frac{A_s}{bd}$:

$$k = -n\rho + \sqrt{(n\rho)^2 + 2n\rho} \tag{13.15}$$

j can be solved for by the following equation, knowing that the concrete stress block is triangular:

$$j = 1 - \frac{k}{3} \tag{13.16}$$

The moment on the section can be found by taking moments about the compressive resultant.

$$M = f_s A_s jd \tag{13.17}$$

So the stress in the steel now can be solved for by rearranging this equation:

$$f_s = \frac{M}{jdA_s} \tag{13.18}$$

Equations for k, j, and f_s can be used to solve for the stress in the steel to check both on the fatigue in the steel and the crack width requirements.

A similar approach can be used for flanged sections and for sections with axial load. Most of the time, these equations can be used to check almost all sections, since the compression block is usually within the flange of the section.

13.4.2.2 Prestressed Sections

The basic assumptions are as follows:

- The section remains plane, so stresses are proportional to the distance from the neutral axis.
- Tension stresses are not ignored in the concrete.
- The prestressing force precompresses the section so that stresses in the prestressing steel are usually ignored.

The internal forces in a section with prestressing are shown in Figure 13.10.

The section has an area of A, a moment of inertia of I, and section modulus of S_{top} and S_{bot}. The prestressing imparts a force on the section of P and a moment of Pe. So the stresses on the section can be determined as

$$\sigma_{top} = -\left(\frac{P}{A} + \frac{Pe}{S_{top}}\right) \tag{13.19}$$

$$\sigma_{bot} = -\left(\frac{P}{A} + \frac{Pe}{S_{bot}}\right) \tag{13.20}$$

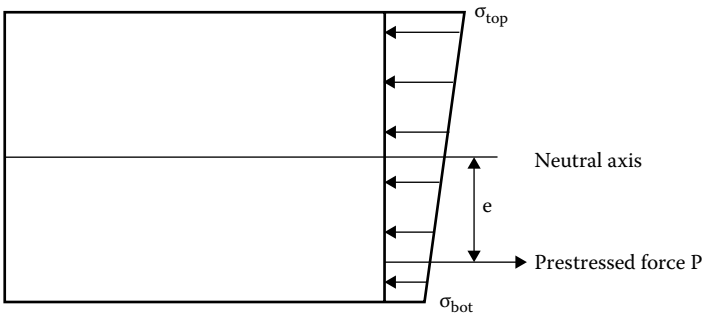

FIGURE 13.10 Beam stresses at service limit state for prestressed concrete section.

The signs in these equations are as follows:

- Tensile forces are positive
- Compressive stresses are positive
- e is positive if it is above the neutral axis up
- S_{top} is positive
- S_{bot} is negative

The stress range in the prestressing steel is usually not checked since fatigue is checked indirectly by the maximum allowable tensile stress in the concrete. Crack widths are also not checked since the maximum tensile stress in the concrete is limited.

13.4.2.3 Cracking

There have been many different expressions derived that check how wide the cracks are in concrete. The problem is that the cracks do not occur at a fixed spacing. So the strain in the concrete builds up and then relieves itself. The distribution of the cracks also depends on how many bars and the spacing of the bars that resist the cracking strain. The cracks decrease with the more bars and decreased spacing of the bars. So that is why most expressions relate the cracking to spacing of bars and the distance from the center of the bars to the surface of the concrete. In fully prestressed sections, cracking is not checked since at service load levels the concrete stresses are below the modulus of rupture for the concrete.

13.4.2.4 Fatigue

Steel fatigue is checked in the longitudinal reinforcing steel by looking at the stress range in the steel due to live loads. This is just like any other steel. The range is then checked against some criteria to make sure that fatigue will not be a problem for the steel. In prestressed concrete structures, the fatigue in the prestressing steel is checked indirectly. The tensile stress in the concrete is limited. By doing this, the fatigue in the steel is limited. This is an indirect way of doing this, but by keeping the concrete from cracking at service loads, the range of stresses in the prestressing steel is kept to an acceptable level.

13.4.3 Strength Limit State

13.4.3.1 General Concepts

The strength limit state checks the member to see if it can carry the loads that will be imposed on the member. Generally this is done by assuming an ultimate strain that the concrete can resist, the location of the neutral axis, and a crack angle for the middle of the section. Once this is done, then the strength of the section can be determined. The crack angle is important in determining the shear strength of the section.

Figure 13.11 shows the general strain, stress distribution, and crack angle for a beam section at the nominal resistance. The ultimate strain (maximum usable strain) is assumed to be 0.003 for the concrete. The neutral axis is then assumed. The stress strain properties of each material are used to determine the force in each material. It is not uncommon to replace the stress–strain relationship of the concrete with an equivalent stress block with a stress of $0.85\,f'_c$. The block makes it easier to calculate the forces on the section. The block is assumed to be β_1 times the distance from the neutral axis to the extreme compression fiber. β_1 can be found with the following equation:

$$0.85 \geq \beta_1 = 0.85 - (f'_c - 4)0.05 \geq 0.65 \tag{13.21}$$

Figure 13.12 shows a free body diagram of the forces along a cracked section of concrete. If the forces and moments are added up on a section, the following is obtained.

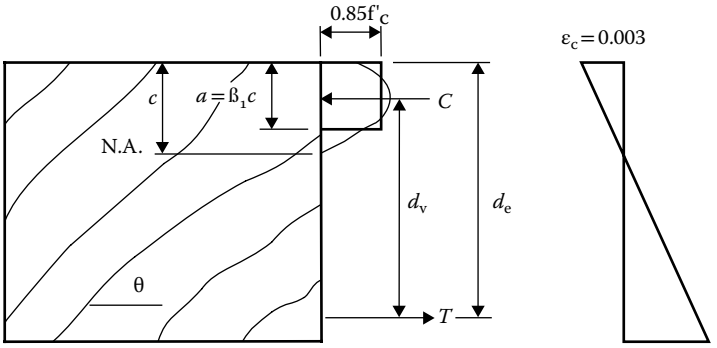

FIGURE 13.11 Beam stresses and forces at nominal (ultimate) strength.

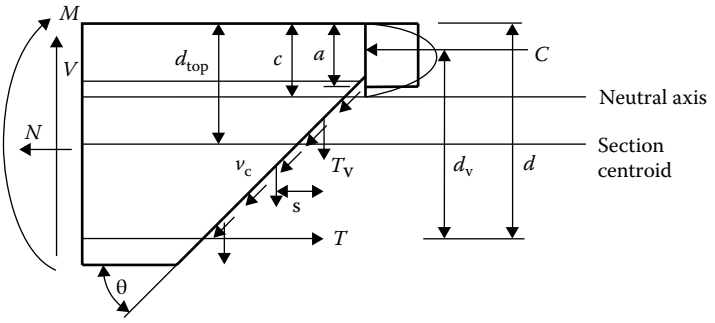

FIGURE 13.12 Stresses and forces along a cracked section of concrete.

Forces in the vertical direction

$$V = -v_c b_v d_v \sin(\theta) - \frac{T_v d_v}{\tan(\theta) s} \tag{13.22}$$

The sum of these must equal the shear applied to the section. The first component is the contribution from the strength of the concrete along a crack. This is the interlock between the rough surfaces that will form. The second term is the force due to the vertical reinforcing steel. Here it is assumed that the shear steel is perpendicular to the member. If the steel is not perpendicular to the member then this must be taken into account.

Forces in the horizontal direction

$$N = C + T - v_c b_v d_v \cos(\theta) \tag{13.23}$$

This sum equals the axial force on the section. Note that the concrete stress on the shear crack will increase tension in the tensile reinforcement. Therefore, additional reinforcement is necessary over that needed for moment and axial force.

Taking moments on the section about the centroid axis

$$M = C\left(\frac{a}{2} - d_{top}\right) + T(d - d_{top}) - v_c b_v d_v \sin(\theta)\frac{1}{2}\frac{d_v}{\tan(\theta)} - \frac{T_v d_v}{s\tan(\theta)}\frac{1}{2}\frac{d_v}{\tan(\theta)} \tag{13.24}$$

simplifying

$$M = C\left(\frac{a}{2} - d_{\text{top}}\right) + T(d - d_{\text{top}}) - v_c b_v d_v^2 \cos(\theta)\frac{1}{2} - \frac{T_v d_v^2}{s\tan^2(\theta)}\frac{1}{2} \tag{13.25}$$

The first two terms are the terms for the compression block and the reinforcing steel. The second two terms are for the shear on the crack and shear steel. The vertical components of the concrete shear stress and shear steel are assumed to act at approximately half the depth of the beam. So this generally means that the horizontal components do not create any moment.

The above equations have been modified for the AASHTO *LRFD Bridge Design Specifications* (AASHTO, 2012) to fit the modified compression field theory. The modified equations are shown below.

13.4.3.2 Nominal Flexural Resistance

For a member with a flanged section, the nominal flexural resistance without any shear or axial load may be taken approximately by

$$M_n = A_{\text{ps}} f_{\text{ps}}\left(d_p - \frac{a}{2}\right) + A_s f_s\left(d_s - \frac{a}{2}\right) - A_s' f_s'\left(d_s' - \frac{a}{2}\right) + 0.85 f_c'(b - b_w)h_f\left(\frac{a}{2} - \frac{h_f}{2}\right) \tag{13.26}$$

$$a = \beta_1 c \tag{13.27}$$

where A_{ps} is the area of prestressing steel; f_{ps} is the stress in the prestressing steel that can be achieved at the full nominal resistance of the member; d_p is the depth from the extreme compression fiber to the centroid of the prestressing steel; A_s is the area of mild steel on the tension side of the member; f_s is the stress in the mild steel on the tension side of the member at nominal resistance; d_s is the distance from the extreme compression fiber to the centroid of the mild steel on the tension side of the member; A_s' is the area of mild steel on the compressive side of the member; f_s' is the stress in the mild steel on the compressive side of the member at nominal resistance; d_s' is the distance from the extreme compression fiber to the centroid of the mild steel on the compression side of the member; f_c' is the specified strength of the concrete; b is the width of the compression flange; b_w is the width of the web; and h_f is the compression flange depth. The above equations also can be used for a rectangular section in which $b_w = b$. Stresses in all steel should be calculated by strain compatibility or approximate equations.

It should be noted that there is no explicit limit on maximum reinforcement. Sections are allowed to be over reinforced but shall be compensated for reduced ductility in the form of a reduced resistance factor. The minimum reinforcement shall be provided so that the factored resistance M_r, is at least equal to the lesser of 1.2 M_{cr} and 1.33 M_u.

13.4.3.3 Nominal Shear Resistance

Based on the modified compression field theory, the nominal shear resistance is contributed by concrete, tensile stresses in the transverse reinforcement, and the vertical component of prestressing force. For a detailed derivation of this method, refer to the book by Collins and Mitchell (1991). This method has been adapted to the AASHTO *LRFD Bridge Design Specifications* (AASHTO, 2012). The modified compression theory can really only be applied in a computer environment since it has an iterative solution. Each version of the AASHTO specification has a new approximation of the method trying to make it easier to use. It shall be determined by the following formula (AASHTO, 2012):

$$V_n = \text{the lesser of} \begin{cases} V_c + V_s + V_p \\ 0.25 f'_c b_v d_v + V_p \end{cases} \tag{13.28}$$

where

$$V_s = \frac{A_v f_y d_v (\cos\theta + \cot\alpha)\sin\alpha}{s} \tag{13.29}$$

$$V_c = 0.0316\beta\sqrt{f'_c}\, b_v\, d_v \tag{13.30}$$

or

$$V_c = \text{lesser of } V_{ci} \text{ and } V_{cw} \tag{13.31}$$

where b_v is the effective web width determined by subtracting the diameters of ungrouted ducts or one-half the diameters of grouted ducts; d_v is effective depth between the resultants of the tensile and compressive forces because of flexure, but not to be taken less than the greater of 0.9 d_e or 0.72h; A_v is area of transverse reinforcement within distance s; s is spacing of stirrups; α is angle of inclination of transverse reinforcement to the longitudinal axis of the member; V_p is component of the effective prestressing force in direction of the applied shear; V_c is nominal shear resistance provided by concrete; V_{ci} is nominal shear resistance provided by concrete when inclined cracking results from combined shear and moment; V_{cw} is nominal shear resistance provided by concrete when inclined cracking results from excessive principal tensions in web; β is a factor indicating ability of diagonally cracked concrete to transmit shear; and θ is angle of inclination of diagonal compressive stresses. The values of β and θ for sections can be determined by

$$\theta = 29 + 3500\varepsilon_s \tag{13.32}$$

$$\beta = \begin{cases} \dfrac{4.8}{(1+750\varepsilon_s)} & \text{when the minimum amount of transverse reinforcement is present} \\ \dfrac{4.8}{(1+750\varepsilon_s)}\dfrac{51}{(39+s_{xe})} & \text{when the minimum transverse reinforcement is not present} \end{cases} \tag{13.33}$$

$$\varepsilon_s = \frac{\dfrac{|M_u|}{d_v} + 0.5N_u + |V_u - V_p| - A_{ps}f_{po}}{E_s A_s + E_p A_{ps}} \tag{13.34}$$

where M_u and N_u are factored moment and axial force (taken as positive if tensile) associated with V_u; f_{po} is stress in prestressing steel when the stress in the surrounding concrete is zero and can be taken as

$0.7f_{pu}$; E_s, E_p, and E_c are modulus of elasticity for mild steel reinforcement, prestressing steel, and concrete, respectively.

$$s_{xe} = s_x \frac{1.38}{a_g + 0.63} \tag{13.35}$$

$$12\,\text{in.} \le s_{xe} \le 80.0\,\text{in.}$$

where a_g is maximum aggregate size (in.); s_x is the lesser of either d_v or the maximum distance between layers of longitudinal crack control reinforcement.

$$V_{ci} = 0.02\sqrt{f_c'}\,b_v d_v + V_d + \frac{V_i M_{cre}}{M_{max}} \ge 0.06\sqrt{f_c'}\,b_v d_v \tag{13.36}$$

where V_d is shear because of unfactored dead load including DC and DW; V_i is factored shear at the section associated with M_{max}; M_{cre} is externally applied moment causing flexural cracking; and M_{max} is maximum applied factored moment at section.

$$M_{cre} = S_c\left(f_r + f_{cpe} - \frac{M_{dnc}}{S_{nc}}\right) \tag{13.37}$$

where f_{cpe} is compressive stress in concrete because of effective prestress force only at extreme fiber where tensile stress is induced by applied load; M_{dnc} is total unfactored dead load moment acting on monolithic or noncomposite section; S_c is section modulus of the extreme fiber of the composite section where tensile stress is induced by applied load; and S_{nc} is section modulus of the extreme fiber of monolithic or noncomposite section where tensile stress is induced by applied load.

$$V_{cw} = \left(0.06\sqrt{f_c'} + 0.30 f_{pc}\right) b_v d_v + V_p \tag{13.38}$$

where f_{pc} is compressive stress in concrete (after all prestress losses) at centroid of cross-section resisting applied loads or at junction of web and flange when the centroid lies within the flange.

Longitudinal reinforcement requirement:

$$A_{ps} f_{ps} + A_s f_y \ge \frac{|M_u|}{d_v \phi_f} + 0.5\frac{N_u}{\phi_c} + \left(\left|\frac{V_u}{\phi_v} - V_p\right| - 0.5V_s\right)\cot\theta \tag{13.39}$$

where V_s is shear resistance provided by transverse reinforcement at the section, but shall not be taken as greater than V_u/ϕ_v; ϕ_f, ϕ_v, and ϕ_c are resistance factors for flexural, shear, and axial resistance, respectively.

Minimum transverse reinforcement:

$$A_{vmin} = 0.0316\sqrt{f_c'}\frac{b_v s}{f_y} \tag{13.40}$$

Maximum spacing of transverse reinforcement:

$$\text{For } V_u < 0.125\varphi f_c' b_v d_v s_{max} = \text{the smaller of } \begin{cases} 0.8d_v \\ 24\,\text{in.} \end{cases} \tag{13.41}$$

$$\text{For } V_u \geq 0.125\varphi f_c' b_v d_v \; s_{max} = \text{the smaller of } \begin{cases} 0.4d_v \\ 12\,\text{in.} \end{cases} \tag{13.42}$$

13.4.3.4 Nominal Axial Resistance

The nominal strength of a member in compression without moment or shear can be expressed by one of the following equations. For members with spiral reinforcement:

$$P_n = 0.85\left[0.85 f_c'\left(A_g - A_{st} - A_{ps}\right) + f_y A_{st} - A_{ps}\left(f_{pe} - E_p \varepsilon_{cu}\right)\right] \tag{13.43}$$

For members with tie reinforcement:

$$P_n = 0.80\left[0.85 f_c'\left(A_g - A_{st} - A_{ps}\right) + f_y A_{st} - A_{ps}\left(f_{pe} - E_p \varepsilon_{cu}\right)\right] \tag{13.44}$$

where A_g is the gross area of the section; A_{st} is the total area of longitudinal reinforcement; A_{ps} is the total area of prestressing steel; f_y is the yield stress of the longitudinal reinforcement; f_c' is the specified 28-day compressive strength of the concrete; f_{pe} is the effective stress in the prestressing steel after losses; E_p is the modulus of elasticity of the prestressing steel; and ε_{cu} is the failure of strain of concrete in compression.

13.4.4 Extreme Limit State

Under extreme conditions, the section should have enough strength to resist the forces that are applied to the section in addition to having enough ductility to not totally fracture once the load is removed. Extreme events are those that are normally not expected to occur more than once in the life of the structure. In concrete structures, two things can happen that will lead to collapse and decrease ductility. Either the concrete can crush and fall out of the member or the steel can fracture. To make sure that the concrete will not crush and fall out of the member, enough confining steel is provided to keep the concrete in place. The anticipated ductility of the section is compared to the predicted ductility demand. This is one area where deformations on the section are compared to the deformation demand. This can be done by generating a curve that shows the forces applied

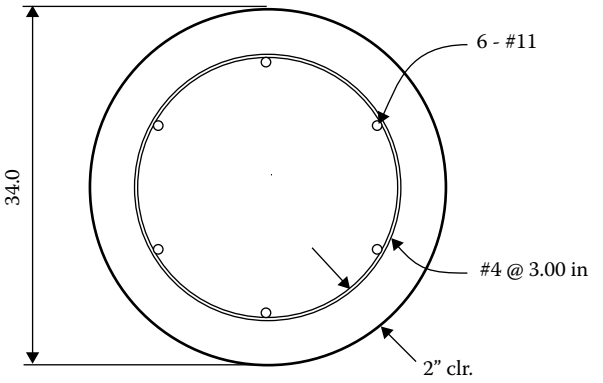

FIGURE 13.13 Example column.

to the section versus the curvature required on the section. This again is done assuming that plane sections remain plane.

13.4.5 Design Examples

13.4.5.1 Circular Column

Given: A circular column with 6 #11 bars is shown in Figure 13.13. The diameter of the column is 34 in. The column has a #4 spiral spaced at 3 in. on center. The 28-day compressive strength of the concrete is 4 ksi and the yield strength of the reinforcing steel is 60 ksi. Assume a neutral axis from the extreme fiber of 8 in. and a crack angle θ of 35°.

To Find: Determine the nominal flexural, axial and shear resistance at the strength limit state in accordance with the AASHTO *LRFD Bridge Design Specifications* (AASHTO, 2012).

Solution:

$$a = 0.85c$$
$$a = 0.85(8\,\text{in}) = 6.8\,\text{in}$$

The compressive force is then:

$$C = -0.85 f_c' \left(r^2 \operatorname{acos}\left(\frac{r-a}{r} \right) - r(r-a) \sin\left(\operatorname{acos}\left(\frac{r-a}{r} \right) \right) \right)$$

$$C = -0.85(4\,\text{ksi}) \left((17\,\text{in})^2 \operatorname{acos}\left(\frac{17\,\text{in} - 6.8\,\text{in}}{17\,\text{in}} \right) - 17\,\text{in}(17\,\text{in} - 6.8\,\text{in}) \sin\left(\operatorname{acos}\left(\frac{17\,\text{in} - 6.8\,\text{in}}{17\,\text{in}} \right) \right) \right) = -440\,\text{kips}$$

The centroid of the compressive force about the centroid of the column can be found by

$$C_{\text{centroid}} = \frac{2r\sin\left(\operatorname{acos}\left(\frac{r-a}{r}\right)\right)\left(1-\frac{1}{3}\left(\frac{(r-a)^2}{r^2}+2\right)\right)}{\operatorname{acos}\left(\frac{r-a}{r}\right)-\frac{r-a}{r}\sin\left(\operatorname{acos}\left(\frac{r-a}{r}\right)\right)}$$

$$C_{\text{centroid}} = \frac{2(17\,\text{in})\sin\left(\operatorname{acos}\left(\frac{17\,\text{in}-6.8\,\text{in}}{17\,\text{in}}\right)\right)\left(1-\frac{1}{3}\left(\frac{(17\,\text{in}-6.8\,\text{in})^2}{(17\,\text{in})^2}+2\right)\right)}{\operatorname{acos}\left(\frac{17\,\text{in}-6.8\,\text{in}}{17\,\text{in}}\right)-\frac{17\,\text{in}-6.8\,\text{in}}{17\,\text{in}}\sin\left(\operatorname{acos}\left(\frac{17\,\text{in}-6.8\,\text{in}}{17\,\text{in}}\right)\right)} = 13\,\text{in}$$

The tensile force in the steel is dependent on the strain on the section. The concrete is assumed to have an ultimate tensile strain of 0.003, so the strains on each of the steel bars are

$$\varepsilon = \frac{\text{concrete ultimate strain}}{c}(\text{distance from neutral axis to steel bar})$$

$$\varepsilon_1 = \frac{-0.003}{8\,\text{in}}(8\,\text{in}-3.25\,\text{in}) = -0.00178$$

$$\varepsilon_2 = \frac{-0.003}{8\,\text{in}}(8\,\text{in}-10.125\,\text{in}) = 0.000797$$

$$\varepsilon_3 = \frac{-0.003}{8\,\text{in}}(8\,\text{in}-23.875\,\text{in}) = 0.00595$$

$$\varepsilon_4 = \frac{-0.003}{8\,\text{in}}(8\,\text{in}-30.75\,\text{in}) = 0.00853$$

For a #11 longitudinal bar: $A_s = 1.56\ \text{in}^2$, $f_y = 60$ ksi, and the yield strain is

$$\varepsilon_y = \frac{60\,\text{ksi}}{29{,}000\,\text{ksi}} = 0.00207$$

So the top and second rows of steel will not have yielded yet. The force in each bar is then:

$$T = (\varepsilon E \text{ or } F_y)A_s$$

$$T_1 = -0.00178(29000\,\text{ksi})1.56\,\text{in}^2 = -80.53\,\text{kip}$$

$$T_2 = .000797(29{,}000\,\text{ksi})2(1.56\,\text{in}^2) = 72.11\,\text{kip}$$

$$T_3 = 60\,\text{ksi}2(1.56\,\text{in}^2) = 187.2\,\text{kip}$$

$$T_4 = 60\,\text{ksi}(1.56\,\text{in}^2) = 93.6\,\text{kip}$$

Nominal shear resistance is determined by the following:

$$V = v_c b_v d_v \sin\theta + \frac{T_v d_v}{s\tan\theta}$$

$$\theta = 35\,\text{deg}$$

$$d_{\text{centroid}} = \frac{10.125\,\text{in}(72.11\,\text{kip}) + 23.875\,\text{in}(187.2\,\text{kip}) + 30.75\,\text{in}(93.6\,\text{kip})}{72.11\,\text{kip} + 187.2\,\text{kip} + 93.6\,\text{kip}} = 22.89\,\text{in}$$

$$\varepsilon_s = \frac{-0.003}{8\,\text{in}}(8\,\text{in} - 22.89\,\text{in}) = 0.00558$$

$$\beta = \frac{4.8}{1 + 750\varepsilon_s}$$

$$\beta = \frac{4.8}{1 + 750(0.00558)} = 0.926$$

$$v_c \sin\theta = \beta 0.0316\sqrt{f'_c}$$

$$v_c \sin\theta = 0.926(0.0316)\sqrt{4\,\text{ksi}} = 0.0585\,\text{ksi}$$

$$d_v = 22.89\,\text{in} - (17 - 13)\,\text{in} = 18.89\,\text{in}$$

$$V = 0.0585(34\,\text{in})(18.89\,\text{in}) + \frac{60\,\text{ksi}(2)(0.2\,\text{in}^2)18.39\,\text{in}}{(3\,\text{in})\tan(35°)} = 248\,\text{kip}$$

The nominal axial resistance is determined as follows:

$$N = C + T - v_c b_v d_v \cos(\theta)$$

$$N = -440\,\text{kips} + (-80.53\,\text{kip} + 72.11\,\text{kip} + 187.2\,\text{kip} + 93.6\,\text{kip}) - \frac{0.0585\,\text{ksi}}{\sin(35°)}34\,\text{in}18.89\,\text{in}\cos(35°)$$

$$N = -114\,\text{kip}$$

The nominal flexural resistance is determined by the following:

$$M = C\left(\frac{a}{2} - d_{\text{top}}\right) + T(d - d_{\text{top}}) - v_c b_v d_v^2 \cos(\theta)\frac{1}{2} - \frac{T_v d_v^2}{s\tan^2(\theta)}\frac{1}{2}$$

$$M = -440\,\text{kip}(-13\,\text{in}) + -80.53\,\text{kip}(3.25 - 17)\,\text{in} + 72.11\,\text{kip}(10.125 - 17)\,\text{in}$$
$$+ 187.2\,\text{kip}(23.875 - 17)\,\text{in} + 93.6\,\text{kip}(30.75 - 17)\,\text{ink} - \frac{0.0585\,\text{ksi}}{\sin(35°)}34\,\text{in}(18.89\,\text{in})^2\cos(35°)\frac{1}{2}$$
$$- \frac{60\,\text{ksi}2(0.2\,\text{in}^2)(18.89\,\text{in})^2}{3\,\text{in}\tan^2(35°)}\frac{1}{2}$$

$$M = 5,490\,\text{in kips}$$

The nominal resistance shall be modified by the appropriate resistance factors for material uncertainties and construction tolerances. In the current AASHTO *LRFD Bridge Design Specifications*, the resistance factor depends on the strain in the reinforcing steel. A bigger reduction is taken for sections that have small steel tensile strains compared to sections that have large steel tensile strains. In order to check all loading conditions, the depth of the compression block and the crack angle are varied to generate nominal resistance surfaces.

13.4.5.2 Reinforced Concrete Beam

Given: A tee beam section with a flange depth of 8 in is shown in Figure 13.14. The 28-day compressive strength of the concrete is 4 ksi and the yield strength of the reinforcing steel is 60 ksi. At the service limit state the moment is 200 foot kips.

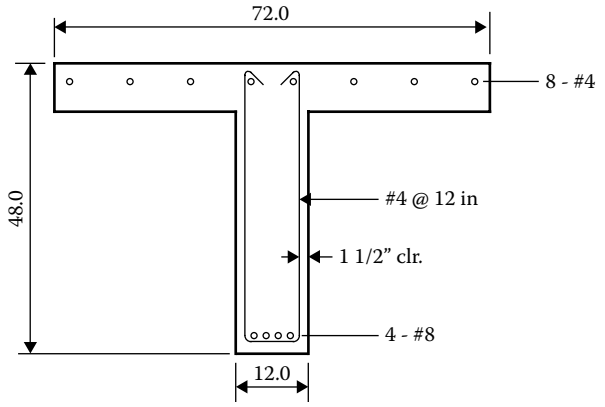

FIGURE 13.14 Example tee beam.

To Find: The stress in the bottom longitudinal steel at the service limit state and the nominal bending and shear resistance at the strength limit state according to the AASHTO *LRFD Bridge Design Specifications* (AASHTO, 2012). Do not include, in the evaluation, the steel that is in the flange of the beam and assume a crack angle of 35°.

Solution:

Service Limit State

The area of steel in positive bending is

$$A_s = 4(0.79\,\text{in}^2) = 3.16\,\text{in}^2$$

The depth to the reinforcing steel is

$$d = 48\,\text{in} - 1.5\,\text{in} - 0.5\,\text{in} - 0.5\,\text{in} = 45.5\,\text{in}$$

This is the total depth minus the clear cover, minus the diameter of the stirrup, minus half the bar diameter. Assuming the neutral axis is in the flange, the reinforcement ratio is

$$\rho = \frac{A_s}{bd}$$

$$\rho = \frac{3.16\,\text{in}^2}{72\,\text{in}(45.5\,\text{in})} = 0.000965$$

The modular ratio is

$$n = \frac{E_s}{E_c}$$

$$n = \frac{29{,}000\,\text{ksi}}{33{,}000K_1 w_c^{1.5}\sqrt{f_c'}}$$

$$n = \frac{29{,}000\,\text{ksi}}{33{,}000(1)(0.145\,\text{kcf})^{1.5}\sqrt{4\,\text{ksi}}} = 7.95$$

It is customary to round this to the nearest whole number. So in this case it would be 8.

The distance to the neutral axis can be found with the following equation:

$$k = -n\rho + \sqrt{(n\rho)^2 + 2n\rho}$$
$$k = -(8)0.000965 + \sqrt{(8(0.000965))^2 + 2(8)(0.000965)} = 0.117$$
$$kd = 0.117(45.5\,\text{in}) = 5.31\,\text{in}$$

Since kd is less than the flange depth (8 in) the equations for a rectangular section can be used to find the steel stress. Solving for the coefficient j:

$$j = 1 - \frac{k}{3}$$
$$j = 1 - \frac{0.117}{3} = 0.961$$

So the stress in the reinforcing steel is

$$f_s = \frac{M}{jdA_s}$$
$$f_s = \frac{200\,\text{kip ft}}{0.961(45.5\,\text{in})3.16\,\text{in}^2}\frac{12\,\text{in}}{\text{ft}} = 17.4\,\text{ksi}$$

This stress can then be compared to the requirements for crack control. The same procedure can also be used to calculate the fatigue stress range in the reinforcing steel.

Strength Limit State

The various variables are as follows:

$$b = 72\,\text{in}$$
$$d = 45.5\,\text{in}$$
$$d_{\text{top}} = 14.9\,\text{in}$$
$$b_v = 12\,\text{in}$$
$$A_s = 3.16\,\text{in}^2$$
$$s = 12\,\text{in}$$
$$f_c' = 4\,\text{ksi}$$

Given an initial guess of 0.901 in for c, the depth to the neutral axis, the following solution is obtained:

$$a = 0.85c$$
$$a = 0.85(0.901\,\text{in}) = 0.766\,\text{in}$$
$$C = -0.85f_c'ba$$
$$C = -0.85(4\,\text{ksi})72\,\text{in}(0.766\,\text{in}) = -188\,\text{kip}$$
$$\varepsilon_s = \frac{-0.003}{c}(c - d)$$
$$\varepsilon_s = \frac{-0.003}{0.901\,\text{in}}(0.901\,\text{in} - 45.5\,\text{in}) = 0.148$$

This is larger than the yield strain of the steel.

$$T = f_y A_s$$
$$T = 60\,\text{ksi}(3.16\,\text{in}^2) = 190\,\text{kip}$$

$$\beta = \frac{4.8}{1 + 750\varepsilon_s}$$
$$\beta = \frac{4.8}{1 + 750(0.148)} = 0.0429$$
$$v_c \sin(\theta) = \beta 0.0316\sqrt{f_c'}$$
$$v_c \sin(\theta) = 0.0429(0.0316)\sqrt{4\,\text{ksi}} = 0.00271\,\text{ksi}$$
$$d_v = d - \frac{a}{2}$$
$$d_v = 45.5\,\text{in} - \frac{0.766\,\text{in}}{2} = 45.1\,\text{in}$$

Nominal shear resistance is obtained as

$$V = v_c \sin(\theta) b_v d_v + \frac{T_v d_v}{s \tan(\theta)}$$
$$V = 0.00271\,\text{ksi}(12\,\text{in})45.1\,\text{in} + \frac{60\,\text{ksi}2(0.2\,\text{in}^2)45.1\,\text{in}}{12\,\text{in}\tan(35°)} = 130\,\text{kip}$$

The nominal axial resistance is found by

$$N = C + T - v_c b_v d_v \cos(\theta)$$
$$N = -188\,\text{kip} + 190\,\text{kip} - \frac{0.00271\,\text{ksi}}{\sin(35\,\text{deg})}12\,\text{in}(45.1\,\text{in})\cos(35°) = 0\,\text{kip}$$

This determined that the axial load on the section is zero, which is what is desired for this section. The depth to the neutral axis can be quickly found by assuming that the compression force C is equal to the tension force T and assuming that the longitudinal reinforcing steel has yielded.

Nominal moment resistance is obtained by

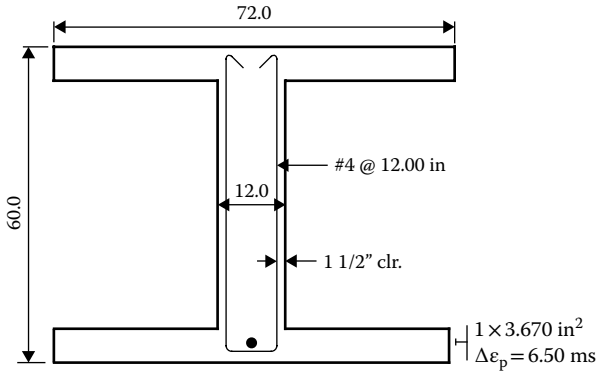

FIGURE 13.15 Example box girder.

$$M = C\left(\frac{a}{2} - d_{\text{top}}\right) + T(d - d_{\text{top}}) - v_c b_v d_v^2 \cos(\theta)\frac{1}{2} - \frac{T_v d_v^2}{s\tan^2(\theta)}\frac{1}{2}$$

$$M = -188\,\text{kip}\left(\frac{.766\,\text{in}}{2} - 14.9\,\text{in}\right) + 190\,\text{kip}(45.5 - 14.9)\,\text{in} +$$

$$-\frac{0.00271\,\text{ksi}}{\sin(35°)}12\,\text{in}(45.1\,\text{in})^2\cos(35°)\frac{1}{2} - \frac{60\,\text{ksi}\,2(0.2\,\text{in}^2)(45.1\,\text{in})^2}{12\,\text{in}\tan^2(35°)}\frac{1}{2}$$

$$M = 4347\,\text{in kips}$$

13.4.5.3 Prestressed Concrete Beam

Given: A section of a cast-in-place posttensioned box girder with webs spaced at 6 feet on center is shown in Figure 13.15. The centroid of the prestressing steel is located at 5 in from the bottom of the girder. The strength of the concrete is 5 ksi at 28 days, the yield strength of the mild reinforcing steel is 60 ksi, the area of prestressing steel is 3.67 in^2, the gross cross sectional area is 1,560 in^2, the moment of inertia is 802,000 in^4, the distance from the neutral axis to the top of the section is 28.2 in, the distance from the neutral axis to the bottom of the section is –31.8 in, the top section modulus is 28,400 in^3, and the bottom section modulus is –25,200 in^3. The prestrssing force after all losses because of friction, creep, shrinkage, and relaxation is 587 kips with an eccentricity of –26.8 in from the neutral axis. At this section, the prestressing has no slope with respect to the girder.

To Find: Calculate the stresses on the section under a service load moment of 1450 foot kips. Calculate the nominal flexural and shear resistance at the strength limit state.

Solution:

Service Level

$$A = 1{,}560\,\text{in}^2$$
$$I = 802{,}000\,\text{in}^4$$
$$y_{\text{top}} = 28.2\,\text{in}$$
$$y_{\text{bot}} = -31.8\,\text{in}$$
$$S_{\text{top}} = 28{,}400\,\text{in}^3$$
$$S_{\text{bot}} = -25{,}200\,\text{in}^3$$

The stresses on the top and bottom extreme fibers of the section can be calculated as follows:

$$\sigma_{\text{top}} = -\left(\frac{P}{A} + \frac{Pe}{S_{\text{top}}}\right)$$

$$\sigma_{\text{top}} = -\left(\frac{587\,\text{kip}}{1{,}560\,\text{in}^2} + \frac{587\,\text{kip}(-26.8\,\text{in})}{28{,}400\,\text{in}^3}\right) - \frac{1{,}250\,\text{ft} - \text{kip}}{28{,}400\,\text{in}^3}\frac{12\,\text{in}}{\text{ft}} = -0.350\,\text{ksi}$$

$$\sigma_{\text{bot}} = -\left(\frac{P}{A} + \frac{Pe}{S_{\text{bot}}}\right)$$

$$\sigma_{\text{bot}} = -\left(\frac{587\,\text{kip}}{1{,}560\,\text{in}^2} + \frac{587\,\text{kip}(-26.8\,\text{in})}{-25{,}200\,\text{in}^3}\right) - \frac{1{,}250\,\text{ft} - \text{kip}}{-25{,}200\,\text{in}^3}\frac{12\,\text{in}}{\text{ft}} = -0.405\,\text{ksi}$$

It is seen that the whole section remains in compression at the service level, so there is no fatigue or cracking issues.

Strength Limit State

The stress in the prestressing steel is determined through strain compatibility or some other method as specified in the AASHTO *LRFD Bridge Design Specifications*. For this example a crack angle of 35° is assumed. The distance to the neutral axis is chosen to be 3.92 in. This was selected by initially equating the ultimate prestressing force to the concrete compression block.

$$c = 3.92\,\text{in}$$
$$a = 0.8c$$
$$a = 0.8(3.92\,\text{in}) = 3.14\,\text{in}$$
$$C = -0.85 f_c' ba$$
$$C = -0.85(5\,\text{ksi})72\,\text{in}(3.14\,\text{in}) = -961\,\text{kip}$$
$$\varepsilon_s = \frac{-0.003}{c}(c-d) - 0.0065$$
$$\varepsilon_s = \frac{-0.003}{3.92\,\text{in}}(3.92\,\text{in} - 55\,\text{in}) - 0.0065 = 0.0326$$

For prestressing steel, this is equated to the steel stress. For most cases this should be close to the ultimate strength of the steel. In this example it is assumed that it is approximately 265 ksi.

$$T = f_{ps} A_s$$
$$T = 265\,\text{ksi}(3.67\,\text{in}^2) = 973\,\text{kip}$$
$$\beta = \frac{4.8}{1 + 750\varepsilon_s}$$
$$\beta = \frac{4.8}{1 + 750(0.0326)} = 0.189$$
$$v_c \sin(\theta) = \beta 0.0316\sqrt{f_c'}$$
$$v_c \sin(\theta) = 0.189(0.0316)\sqrt{5\,\text{ksi}} = 0.0134\,\text{ksi}$$
$$d_v = d - \frac{a}{2}$$
$$d_v = 55\,\text{in} - \frac{3.14\,\text{in}}{2} = 53.4\,\text{in}$$

Nominal shear, axial force, and moment are obtained with the following:

$$V = v_c \sin(\theta) b_v d_v + \frac{T_v d_v}{s \tan(\theta)}$$

$$V = 0.0134\,\text{ksi}(12\,\text{in})53.4\,\text{in} + \frac{60\,\text{ksi}2(0.2\,\text{in}^2)53.4\,\text{in}}{12\,\text{in}\tan(35°)} = 161\,\text{kip}$$

$$N = C + T - v_c b_v d_v \cos(\theta)$$

$$N = -961\,\text{kip} + 973\,\text{kip} - \frac{0.0134\,\text{ksi}}{\sin(35°)}12\,\text{in}(53.4\,\text{in})\cos(35°) = 0\,\text{kip}$$

$$M = C\left(\frac{a}{2} - d_{\text{top}}\right) + T(d - d_{\text{top}}) - v_c b_v d_v^2 \cos(\theta)\frac{1}{2} - \frac{T_v d_v^2}{s\tan^2(\theta)}\frac{1}{2}$$

$$M = -961\,\text{kip}\left(\frac{3.14\,\text{in}}{2} - 28.2\,\text{in}\right) + 971\,\text{kip}(55 - 28.2)\,\text{in} +$$

$$-\frac{0.0134\,\text{ksi}}{\sin(35°)}12\,\text{in}(53.4\,\text{in})^2\cos(35°)\frac{1}{2} - \frac{60\,\text{ksi}2(0.2\,\text{in}^2)(53.4\,\text{in})^2}{12\,\text{in}\tan^2(35°)}\frac{1}{2}$$

$$M = 45{,}500\,\text{in kips}$$

In the above solution the strain in the prestressing steel is modified by including the difference in strain between the steel and the concrete at initial stressing. Usually this is approximately 0.0065. This can be determined by the following:

Strain in the steel after elastic losses:

$$\varepsilon_{ps} = \frac{\sigma_{ps}}{E_{ps}}$$

$$\varepsilon_{ps} = \frac{180\,\text{ksi}}{28{,}000\,\text{ksi}} = 0.00643$$

Strain in the concrete at the level of the steel due to prestressing:

$$\sigma_c = -\left(\frac{P}{A} + \frac{Pe^2}{I}\right)$$

$$\sigma_c = -\left(\frac{587\,\text{kip}}{1{,}560\,\text{in}^2} + \frac{587\,\text{kip}(-26.8\,\text{in})^2}{802{,}000\,\text{in}^4}\right) = -0.902\,\text{ksi}$$

$$E_c = 33{,}000 K_1 w_c^{1.5}\sqrt{f_c'}$$

$$E_c = 33{,}000(1)(0.145\text{kcf})^{1.5}\sqrt{5\,\text{ksi}} = 4{,}070\,\text{ksi}$$

$$\varepsilon_c = \frac{\sigma_c}{E_c}$$

$$\varepsilon_c = \frac{-0.902\,\text{ksi}}{4{,}070\,\text{ksi}} = -0.00022$$

So the difference in strain is

$$\varepsilon = \varepsilon_{ps} - \varepsilon_c$$

$$\varepsilon = 0.00643 - (-0.00022) = 0.00665$$

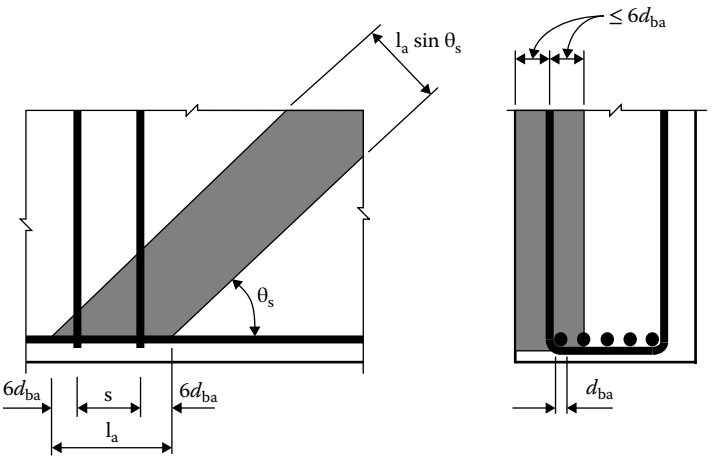

FIGURE 13.16 Strut anchored by reinforcement. (From AASHTO, *AASHTO LRFD Bridge Design Specifications,* American Association of State Highway and Transportation Officials, Washington, DC, 2012. With permission.)

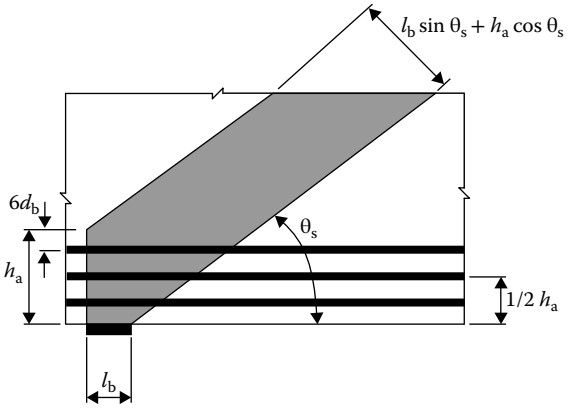

FIGURE 13.17 Strut anchored by bearing and reinforcement. (From AASHTO, *AASHTO LRFD Bridge Design Specifications*, American Association of State Highway and Transportation Officials, Washington, DC, 2012. With permission.)

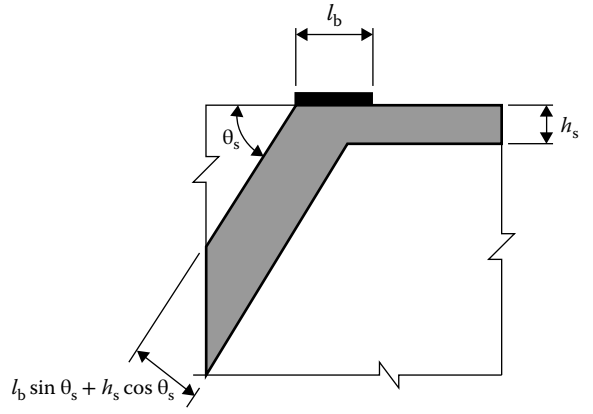

FIGURE 13.18 Strut anchored by bearing and strut. (From AASHTO, *AASHTO LRFD Bridge Design Specifications,* American Association of State Highway and Transportation Officials, Washington, DC, 2012. With permission.)

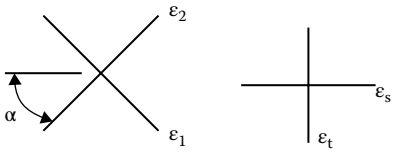

FIGURE 13.19 Strains on a strut. (From AASHTO, *AASHTO LRFD Bridge Design Specifications,* American Association of State Highway and Transportation Officials, Washington, DC, 2012. With permission.)

13.5 Strut and Tie Modeling

As was shown above for a beam, there are always sections of any member where the member does not follow the assumptions for plane sections. The way that the forces are transferred in the member can be very complex. Therefore, a simplified method (truss model with struts and ties) of predicting internal forces effects was developed. The truss model is composed of struts (compression members), ties (tension members), and nodal regions where these truss members join. It is possible to change how these forces flow depending on how the reinforcing steel is installed in the member. It is preferable to install the reinforcing steel in the same direction as the tension forces if the member is isotropic and homogenous. So all ties should be oriented in the same direction as the reinforcing steel in a model. More detailed information can be found in Collins and Mitchell (1991).

13.5.1 Assumptions

There are different formulations of the strut and tie model that lead to different requirements for different codes. The basic assumptions are that struts are stressed to the limiting compressive stress f_{cu} (AASHTO, 2012), ties are stressed to the yield strength of the reinforcing steel, and the nodes must not crush. It is also assumed that if reinforcing steel intersects a node, that it is adequately developed at the node. This is very important so that the forces from the struts can be developed in the member.

The width of a strut is determined by not only the forces carried by the strut but also by the reinforcing steel distribution. An example of this is shown in the following diagram per the AASHTO *LRFD Bridge Design Specifications* (Figure 13.16). The idea here is to distribute the reinforcing so that the nodes can distribute the forces to the struts and ties.

The size of the struts are also dependent on the size of the bearing plates as shown by Figures 13.17 and 13.18 from the AASHTO *LRFD Bridge Design Specifications*.

13.5.2 Struts

The nominal resistance of a compressive strut (AASHTO, 2012) is

$$P_n = f_{cu}A_{cs} + f_y A_{ss} \tag{13.45}$$

$$f_{cu} = \frac{f_c'}{0.8 + 170\varepsilon_1} \le 0.85 f_c' \tag{13.46}$$

The strut principal strains are ε_1 and ε_2, whereas the strain in the steel is ε_s. Figure 13.19 shows how these strains might be related in a strut. The strains can be related by the following equation that is derived from Mohr's circle:

$$\varepsilon_1 = \varepsilon_s + (\varepsilon_s - \varepsilon_2)\cot^2\alpha \tag{13.47}$$

In the AASHTO *LRFD Bridge Design Specification* (AASHTO, 2012) the principal compressive strain is assumed to be −0.002 and the equation is simplified to

$$\varepsilon_1 = \varepsilon_s + \left(\varepsilon_s + 0.002\right)\cot^2 \alpha_s \tag{13.48}$$

where f_{cu} is limiting compressive stress in strut; A_{cs} is effective cross-sectional area of strut as shown in Figures 13.16 through 13.18; A_{ss} is area of reinforcement parallel to strut; ε_s is tensile strain in concrete in the direction of tension tie; and α_s is the smallest angle between the compressive strut and adjoining tension tie.

13.5.3 Ties

The nominal resistance of a tension tie (AASHTO, 2012) is

$$P_n = f_y A_{st} + A_{ps}\left(f_{pe} + f_y\right) \tag{13.49}$$

where A_{st} is the total area of longitudinal mild steel in the tie; A_{ps} is area of prestressing steel; and f_{pe} is stress in the prestressing steel after losses.

13.5.4 Node Regions

Per the AASHTO *LRFD Bridge Design Specification* (AASHTO, 2012) compressive stress in concrete at a node region shall not exceed: $0.85\varphi f_c'$ for the regions bounded by struts and bearing areas; $0.75\varphi f_c'$ for the regions anchoring a tie in one direction; and $0.65\varphi f_c'$ for the regions anchoring ties in more than one direction.

13.5.5 Service Considerations

Typically, the strut and tie analysis is used to determine internal forces at the strength limit state. In order to address the service conditions of cracking and fatigue, extra reinforcing is usually placed in the member.

13.5.6 Deep Beam Example

Given: A single column bent cap is shown in Figure 13.20. The 28-day strength of the concrete is 4 ksi, the yield strength of the steel reinforcing steel is 60 ksi. The cap is 5 feet thick. The concentrated forces applied to the bent cap are 500 kips each.

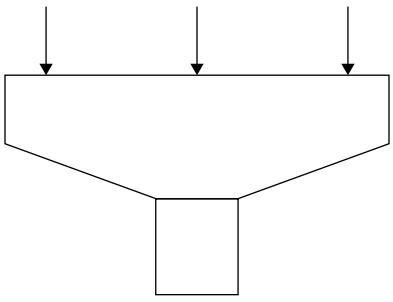

FIGURE 13.20 Example bent cap.

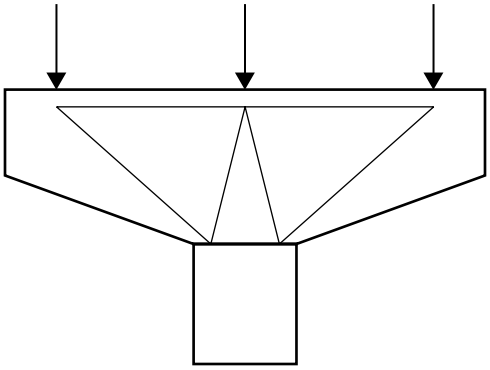

FIGURE 13.21 Example bent cap with simple truss.

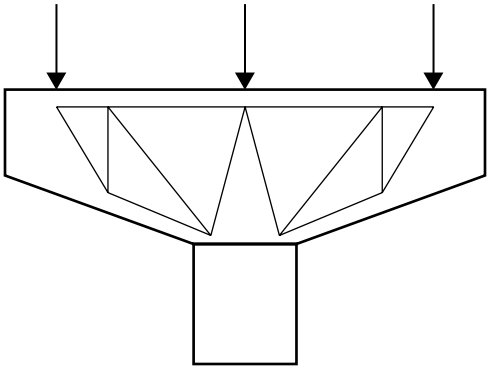

FIGURE 13.22 Example bent cap with more complex truss.

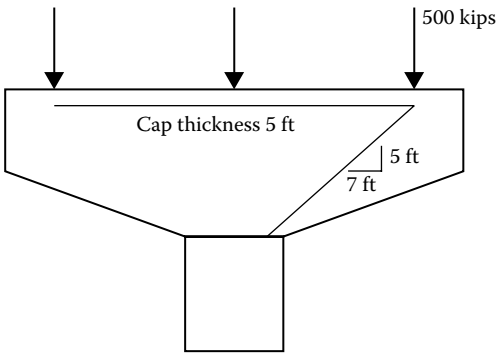

FIGURE 13.23 Forces and geometry of example bent cap.

To Find: Use the strut and tie method to design the bent cap.

Solution:

A simple strut and tie truss is shown in Figure 13.21. The top will be a tie and the diagonals will be struts. Two things can be learned from this model. First, in order to anchor the node under an exterior girder, the tie needs to be anchored. So there must be enough distance past the node to develop the tie. Second, the angle of the diagonal strut under each exterior girder also determines the force in the tie. Another strut and tie truss is shown in Figure 13.22.

This decreases the force in the top tie near the exterior girder, but forces are still added to the ties near the center of the pier. In this example, the first model will be used to design the bent cap. The details of the model are shown in Figure 13.23.

The compression force in the strut is

$$C = \frac{\sqrt{7^2 + 5^2}}{5} 500\,\text{kip} = 860\,\text{kip}$$

The tension force in the tie is

$$T = \frac{7}{5} 500\,\text{kip} = 700\,\text{kip}$$

The required steel is determined by taking the force in the tie and dividing it by the yield strength of the steel combined with the resistance factor.

$$A_s = \frac{T}{f_y \phi}$$

$$A_s = \frac{700\,\text{kip}}{60\,\text{ksi}(0.9)} = 12.96\,\text{in}^2$$

Now let us determine the compression in the strut. The strut compression is limited by any tensile stresses from adjoining ties.

Assuming the steel has reached yield strain:

$$\varepsilon_s = \frac{60\,\text{ksi}}{29000\,\text{ksi}} = 0.00207$$

$$\alpha = \text{atan}\frac{5\text{ft}}{7\text{ft}} = 35.5°$$

$$\varepsilon_1 = \varepsilon_s + (\varepsilon_s - \varepsilon_2)\cot^2\alpha$$

$$\varepsilon_1 = 0.00207 + (0.00207 - (-0.002))\cot^2(35.5°) = 0.0101$$

This is the principal tensile strain perpendicular to the compression strut. If there are ties in two directions, then use the tie and angle that produces the larger principal tensile stress. The maximum compressive stress a strut can resist is limited by this principal tensile strain in the strut. The limiting compressive stress in the strut is given by

$$f_{cu} = \frac{f_c'}{0.8 + 170\varepsilon_1} < 0.85 f_c'$$

$$f_{cu} = \frac{4\,\text{ksi}}{0.8 + 170(0.0101)} < 0.85(4\,\text{ksi})$$

$$f_{cu} = 1.59\,\text{ksi} < 3.4\,\text{ksi}$$

Using a resistance factor of 0.7 for a strut, the required size of the strut is then:

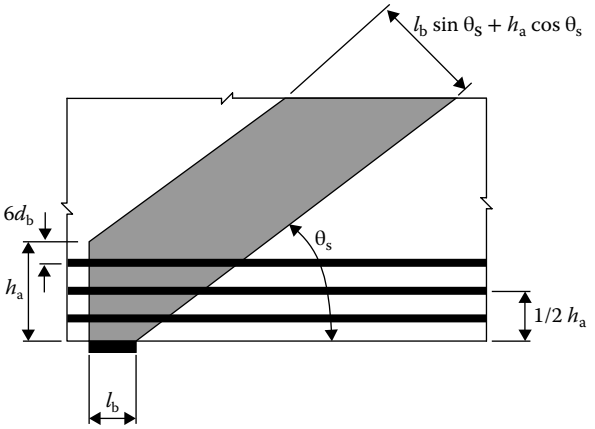

FIGURE 13.24 Strut anchored by bearing and reinforcement.

$$A_{strut} = \frac{C}{\varphi f_{cu}}$$

$$A_{strut} = \frac{860\ \text{kip}}{0.7(1.59\,\text{ksi})} = 773\,\text{in}^2$$

$$\text{width}_{strut} = \frac{773\,\text{in}^2}{60\,\text{in}} = 12.9\,\text{in}$$

Now the nodes of the truss are checked. The nodes are usually limited to the compressive stresses in them to take into account ties that may disrupt the node. If a node is totally in compression, then the node will have no reduction, whereas a node with tension on it will have a reduction. According to the AASHTO *LRFD Bridge Design Specifications* (AASHTO, 2012), the compressive stresses in a node with a tie in one direction is limited to $0.75\varphi f'_c$. For this problem this equates to

$$0.75\varphi f'_c$$

$$0.75(0.7)4\,\text{ksi} = 2.1\,\text{ksi}$$

This is more than what the other criterion for the compression strut gave us, so this will not control. Now let us size the node. The geometry of the problem is shown in Figure 13.24, which is the same as Figure 13.17.

The reinforcing has to total 12.96 in^2, so provide 13 #9 bars in one layer. If the length of the bearing is 24 in, then the reinforcing has to be distributed over the following height:

$$12.9\,\text{in} = l_b \sin\alpha + h_a \cos\alpha$$

$$12.9\,\text{in} = 24\,\text{in}\sin(35.5°) + h_a \cos(35.5°) = -1.27\,\text{in}$$

In other words, the reinforcing steel is not critical to the node size and one layer will be adequate. The #9 bars need to be anchored at the node, so they should extend their development length from the inside

face of the node. Hooks will be used to develop the bars. The hook development length is approximately 21 in. So the cap only needs to be made a nominal distance longer than the edge of the bearing.

To satisfy cracking requirements an orthogonal steel mesh needs to be installed on each face of the cap.

13.6 Summary

Reinforced and prestressed concrete is a composite material that has been used for years in the design of structures. The designer needs to think of it as concrete with added materials to improve the performance of the concrete. Usually the added material is some sort of steel, whether the steel has been stressed initially or not. Then if the steel is properly anchored to the concrete, the two will act as one and the steel will improve the poor tension properties of the concrete. So as long as the designer uses the concept of maintaining strain compatibility, then they can adequately design and detail the concrete.

Bibliography

AASHTO. 2012. *AASHTO LRFD Bridge Design Specifications*, 6th Edition. American Association of State Highway and Transportation Officials, Washington DC.

Bazant, Z. P., and Wittman, F. H. 1982. *Creep and Shrinkage in Concrete Structures*. John Wiley & Sons, Inc., New York, NY.

A definitive work on the subject of creep and shrinkage of concrete. Bazant has spent years researching creep and shrinkage in concrete and his prediction methods are as good as any (if you have all the necessary data and lots of time for calculation).

Collins, M. P., and D. Mitchell. 1991. *Prestressed Concrete Structures*. Prentice-Hall, Engelwood Cliffs, NJ.

This is one of the best modern references on prestressed (and reinforced concrete) analysis and design. It contains excellent treatment of the modified compression field theory (Colllins and Mitchell developed it). There is a good treatment of the strut and tie application. The 1st edition of the book contained a simple strain compatibility analysis called Response that has been recently updated and is available for down-loading on the web. This is a most useful tool for analysis of all concrete members.

Ghali, A., and Favre, R. 1986. *Concrete Structures: Stresses and Deformations*. Chapman & Hall, New York, NY.

Good material on creep and shrinkage along with one of the most theoretically consistent treatments of deflections including time dependent changes. A method for calculation is presented that handles everything (if you know what numbers to put in) but it would require computerization to be practical.

MacGregor, J.G. 1997. *Reinforced Concrete, Mechanics and Design* (3rd Edition). Prentice Hall, Englewood Cliffs, NJ.

An excellent general reference on reinforced concrete with a thorough chapter on strut and tie model application.

Park, R., and Paulay, T. 1975. *Reinforced Concrete Structures*. John Wiley & Sons, Inc., New York, NY.

Priestley, M. J. N., Seible, F., and Calvi, G.M. 1996. *Seismic Design & Retrofit of Bridges*. John Wiley & Sons, Inc. New York, NY.

This is the best reference on seismic design of bridges available. It has a thorough treatment of the philosophy and application of capacity protected seismic design. It covers joint shear, tie requirements for plastic hinge zones, shear design of columns, rocking footings, and a host of details for new design as well as retrofit of existing bridges. The treatment of retrofit includes methods to estimate the capacity of sections that do not meet current code detailing requirements.

14

Steel Design

James A. Swanson
University of Cincinnati

14.1 Introduction

Steel with its higher strength, ductility and toughness makes a vital material for bridge structures. In this chapter, basic steel design concepts and requirements for I-sections specified in the AASHTO-LRFD (AASHTO, 2012) for flexure, shear, compression, tension, and serviceability are presented. Bolted and welded connections are also addressed. For more detailed discussion, references may be made to Salmon et al. (2009) and Ziemian (2010). Design considerations, procedures and examples for steel plate girders and box girders will be presented in Chapters 4 and 5 of the second book in this series, *Superstructure Design*.

14.2 Material Properties

14.2.1 Structural Steels

Steel is a strong, ductile, and resilient material that is very well suited for many engineering applications. Four types of structural steels of ASTM A709 (structural carbon, high-strength low-alloy, heat-treated low-alloy, and high-strength heat-treated alloy steel) are commonly used for bridge structures.

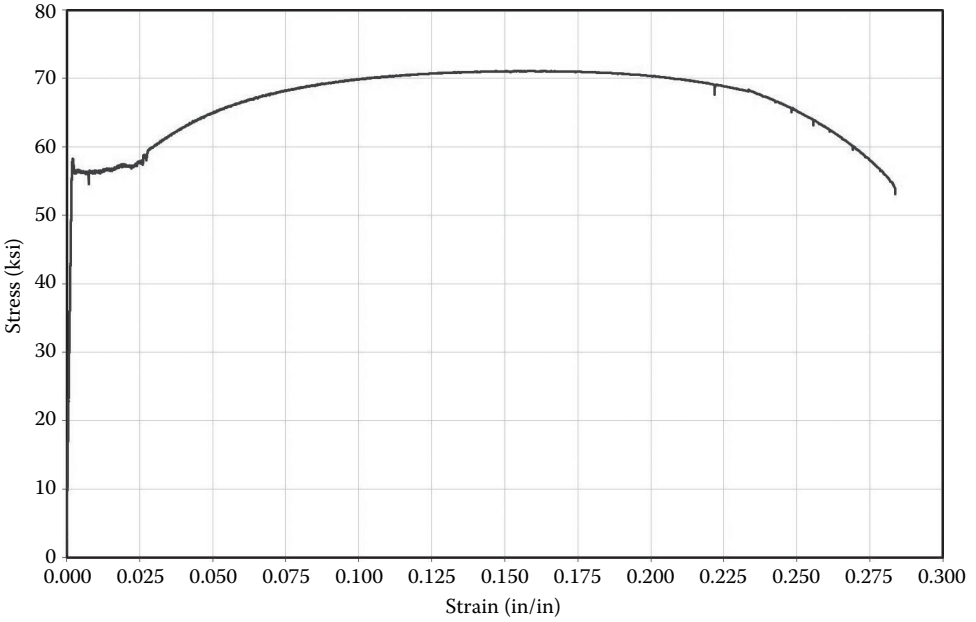

FIGURE 14.1 Stress–strain curve for A572-50 steel.

Mechanical properties that are important in the behavior of steel include strength, stiffness, ductility, toughness, hardness, and weldability. Tensile testing is the premier way of establishing the mechanical properties of steel that are most directly used in the design of steel structures. ASTM Specifications E8 (Cit ASTM E8) and A370 (Cit ASTM A370) govern the tensile testing of steel. Coupons are typically cut from the webs of rolled members in the direction of rolling and are tested to obtain a stress–strain curve like that shown in Figure 14.1 for A572-50 steel. Steel generally exhibits a linear elastic response up to a yield point, followed by a yield plateau that varies depending on the grade of steel, a strain hardening region, a period of necking after achieving the maximum stress or tensile stress, and then fracture. From these tests, the yield stress, F_y, tensile stress, F_u, and modulus of elasticity, E, and the percent elongation at fracture are determined.

A242 and A588 are common grades of weathering steel. High-performance steels (A709 HPS-50W, A709 HPS-70W, and A709 HPS-100W) have recently been introduced to bridge engineering that exhibit even better corrosion resistance. The weathering index is an empirical evaluation used to quantify corrosion resistance and is based on the chemical composition of the material benchmarked by observation of actual samples over a long period of time in several locations.

$$CI = 26.01(\%Cu) + 3.88(\%Ni) + 1.20(\%Cr) + 1.49(\%Si) + 17.28(\%P) - 7.29(\%Cu)(\%Ni) - 9.10(\%Ni)(\%P) - 33.39(\%Cu)^2 \tag{14.1}$$

A higher corrosion index indicates a better resistance to corrosion. A242 and A588 are in the range of $CI = 5.8$, A709 HPS-50W has an index of $CI \geq 6.0$, and A709 HPS-70W has an index of $CI \geq 6.5$.

Structural steel is available in several different grades with options currently available with yield stresses ranging from 36 to 100 ksi. In all cases, the modulus of elasticity is taken at 29,000 ksi for design and analysis purposes. Table 14.1 shows a summary of the types of structural steel used in practice today. ASTM material property standards differ from AASHTO in notch toughness and weldability requirements. Steel meeting the AASHTO-M requirements is prequalified for use in welded bridges.

TABLE 14.1 Structural Steel Grades

Designation	Grade	Carbon (%)	F_y (ksi)	F_u (ksi)	Comments
A36	36	0.26	36	58–80	Mild steel
A572	42	0.21	42	60	HSLA steel
	50	0.23	50	65	
	60	0.26	60	75	
	65	0.26	65	80	
A529	42	0.27	42	60–85	
A441			(Discontinued as of 1989; replaced by A572)		
A242	42–50	0.15	42–50	63–70	HSLA weathering steel
A588	50	0.17–0.19	50	70	HSLA weathering steel
A514	90–100	0.12–0.21	90–110	100–130	HS Q&T, plates only
A709	HPS-50W		50	65	HPS, Q&T or TMCP, plates only
	HPS-70W		70	85–110	
	HPS-100W		100	110	
A992	50		50	65	W-shapes only

14.2.2 Bolts, Nuts, and Washers

High-strength bolts are made of steel that is significantly stronger and harder than structural steel. Bolts typically start out as a medium carbon steel wire rod that is preprocessed to clean it and add formability. The wire is then cut to length and a head is formed by a process called cold forging. Next threads are rolled or cut onto the fastener to create final product. Finally, the fasteners are then quenched and tempered to obtain the mechanical properties that are required. A325 and the equivalent grades have a tensile strength* of 120 ksi, whereas A490 and the equivalent grades have a tensile strength of 150 ksi. Tension control bolts available in grades F1852 and F2280, which are mechanically equivalent to A325 and A490 bolts, respectively, are available for use having an alternate installation method. AASHTO designates A325 and A490 fasteners as AASHTO M164 and AASHTO M253, respectively (Kulak et al., 2001).

Nuts are typically manufactured using a process called hot forging. The threads of a nut are cut using a tap. Nuts for use with structural bolts are manufactured to ASTM A563 specification and carry an AASHTO designation of M291. Hardened washers conforming to ASTM F436 or AASHTO M293 specifications are installed in bolt assemblies to help distribute bolt forces over a larger area of the base metals, to aid in tensioning, and to cover oversized or slotted holes.

14.2.3 Weld Metal

Welding, discussed in Section 14.8, is a means of joining two pieces of steel together in an apparently seamless fashion. It consists of using an electric current to melt a weld electrode and a small amount of weld metal immediately adjacent to the joint. Several welding processes exist that have benefits and in different circumstances. The electrodes consumed in each of these processes to form the weld are specific to the process used. AWS D1.1 and D1.5 (AWS, 2010a and b) cover the specifications for consumables including the details of which types of flux to use, which electrodes are appropriate for which welding positions, hydrogen content, and other specifics. In all processes, though, the engineer specifies the grade of the electrode where F_{EXX} is the tensile strength of the weld metal. The tensile strength varies between 60 ksi and 110 ksi. When the tensile strength of the weld metal, F_{EXX}, is greater than or equal to

* A325 fasteners that are larger than 1 in in diameter technically have a minimum tensile strength of 105 ksi, but the design documents generally ignore this difference and base the design strength of all diameters of A325 bolts on a tensile strength of 120 ksi.

the tensile strength of the base metal, F_u, then the weld metal is said to be "matching" weld metal. When the tensile strength of the weld metal, F_{EXX}, is less than the tensile strength of the base metal, F_u, then the weld metal is said to be "under matched."

A good measure of the weldability of base metal is the carbon equivalent, or C_{EQ}, which is based on the content of carbon and other critical alloys in the base metal (Equation 14.2). A "lower" CE indicates that a steel will be "easier" to weld (i.e., minimal preheat requirements, high rate of weld deposition, minimal postweld cooling requirements, etc.) A "higher" CE indicates that a steel will be "more difficult" to weld and may be susceptible to cracking if precautions are not taken (Pollack, 1988; Somayaji, 2001).

$$C_{EQ} = C + \frac{(Mn + Si)}{6} + \frac{(Cr + Mo + V)}{5} + \frac{(Ni + Cu)}{15} \tag{14.2}$$

In general, when the carbon equivalent is <0.40%, no preheating or postheating is required. When the carbon equivalent falls between 0.40 and 0.60%, some preheating is required. When the carbon equivalent is >0.60%, both preheating and postheating are required to reduce the possibility of weld defects and cracking of the welds because of rapid cooling and heat-sink effects.

14.3 Section Classification

There are four fundamental failure modes for steel members; yielding, rupture, buckling, and fatigue. Buckling failures can be characterized by an instability of a member as a whole (global buckling) or as an instability of one or more of the elements of a cross section (local buckling). In this context, the word "element" is meant to describe a plate component that makes up part of a cross section. For instance, the web of an I-shaped girder or the flange of a channel are cross-sectional "elements." With respect to local buckling, classification of the cross-sectional elements as slender, nonslender, compact, or noncompact aids greatly in determining which of the four fundamental failure modes may govern and how they are addressed. This section provides the background needed to understand the classification of the sections for local buckling.

Two of the most critical conditions that affect the local stability of a cross sectional element are 1. whether the element is stiffened or unstiffened, and 2. whether the element is subjected to a uniform compressive stress or a flexural compressive stress. In the former case, a stiffened element is one that is connected along both longitudinal edges to another cross-sectional element, such as the web of an I-shaped section, or the wall of a square or rectangular hollow structural section. An unstiffened element, however, is one that is connected along only one edge to another cross-sectional element, such as the flange of a channel or angle, or the half-width of the flange of an I-shaped section.

The basis of local buckling can be found in the plate buckling formulations shown as Equation 14.3. In this relationship, the stress required to cause buckling of a plate is presented as a function of the modulus of elasticity, E, Poisson's ratio, ν, a constant k, and the width-to-thickness ratio, b/t. This formulation is based on the assumption that the plate is loaded along two transverse edges that are treated as pinned. The type of loading on the transverse edges and the support conditions of the two remaining longitudinal edges are reflected in the constant, k (Salmon et al., 2009).

$$F_{cr,local} = \frac{\pi^2 kE}{12\left(1-\nu^2\right)\left(b/t\right)^2} \tag{14.3}$$

Solving for b/t for a plate under uniform compression (as would be the case in a compression member, or in the compression flange of a flexural member) and taking $\nu = 0.30$

$$\frac{b}{t} = \sqrt{\frac{\pi^2 kE}{12\left(1-\nu^2\right)F_{cr,\,local}}} = 0.951\sqrt{\frac{kE}{F_{cr,\,local}}} \tag{14.4}$$

For the half-width of a compression flange of an I-shaped section, one longitudinal edge of the element is obviously unsupported, but the other edge can be treated as either fixed at the web intersection, or as pinned. If the former condition is chosen and the half-width is treated as fixed-free, the constant k can be found to be 1.277. However, if the latter boundary condition is assumed and the half-width is treated as pinned-free, then k can be found to be 0.425. Using engineering judgment and taking k as one-third of the way between pinned-free and fixed-free, k can be taken as 0.709.

$$\frac{b}{t} \leq 0.951\sqrt{\frac{(0.709)E}{F_{\text{cr, local}}}} = 0.801\sqrt{\frac{E}{F_{\text{cr, local}}}} \tag{14.5}$$

In most cases, the objective in examining this relationship to ensure that local buckling does not occur until after a different, more favorable limit state governs. In the case of a compression member, that would be to say that it is desirable for the local buckling strength of the member to be greater than the global buckling strength, or $F_{\text{cr,global}} \leq F_{\text{cr,local.}}$ With that objective in mind, $F_{\text{cr,local}}$ in Equation 14.5 could be replaced with the stress that would cause global buckling, $F_{\text{cr,global}}$. Although this is permissible, a simpler and more conservative approach is to simply say that it is desirable for the local buckling strength of the member to be greater than the yield strength of the member, or $F_y \leq F_{\text{cr,local}}$. Thus $F_{\text{cr,local}}$ in Equation 14.5 would be replaced by F_y. In doing so, however, care must be taken to account for residual stresses and imperfections in the member. A factor, λ_c, the discussion of which is beyond the scope of this text, is introduced to account for those phenomena and is taken as $\lambda_c = 0.70$ for the consideration of compression members. With that, Equation 14.5 can be rewritten as (Salmon et al., 2009)

$$\frac{b}{t} \leq 0.561\sqrt{\frac{E}{F_y}} \tag{14.6}$$

Compare this to $\lambda_r = 0.56\sqrt{E/F_y}$ found in AASHTO Table 6.9.4.2.1-1 (AASHTO, 2012) for the case of the flange of a rolled I-shaped section in a compression member.

When flexural members are considered, the discussion is a bit more complex. In some cases it is sufficient for a flexural member to be able to reach its yield moment, M_y, whereas in other cases it is desirable for the member to reach its full plastic moment, M_p. In the latter case, it is not sufficient to require that the flange be able to reach F_y before buckling local. Instead the flange must be able to sustain significant inelastic strain before buckling locally. To achieve this, a different value of $\lambda_c = 0.46$ is employed and Equation 14.3 becomes

$$\frac{b}{t} \leq 0.801\lambda_c\sqrt{\frac{E}{F_y}} = 0.368\sqrt{\frac{E}{F_y}} \tag{14.7}$$

Compare this to $\lambda_p = 0.38\sqrt{E/F_y}$ found in AASHTO Section A6.3.2 for the case of the compression flange of an I-shaped member in flexure.

This discussion could be expanded to include stiffened elements and elements under additional boundary conditions and loading situations. Suffice it to say here, however, that for all cross-section elements in compression, there are limits λ_r and λ_p that represent the upper bounds on element slenderness, that are needed to reach yield prior to local buckling and sustain significant inelastic strain before local buckling, respectively.

When an element has a slenderness greater than λ_r, then that element is classified as slender. However, when an element has a slenderness less than λ_r then that element is classified as nonslender. More specifically in the case of nonslender elements, when an element has a slenderness between λ_r and λ_p, that

TABLE 14.2 General Slenderness Limits for Classification of Cross-Sectional Elements

	$\frac{b}{t}$	λ_p	λ_r
Flange of an I-shaped member in flexure	$\frac{b_f}{2t_f}$	$0.38\sqrt{\frac{E}{F_y}}$	$0.83\sqrt{\frac{E}{F_y}}$
Web of an I-shaped member in flexure	$\frac{h}{t_w}$	$3.76\sqrt{\frac{E}{F_y}}$	$5.70\sqrt{\frac{E}{F_y}}$
Flange of an I-shaped member in compression	$\frac{b_f}{2t_f}$	—	$0.56\sqrt{\frac{E}{F_y}}$
Web of an I-shaped member in compression	$\frac{h}{t_w}$	—	$1.49\sqrt{\frac{E}{F_y}}$

element is classified as noncompact, and when an element has a slenderness less than λ_p, then that element is classified as compact. Classification of an element as slender or nonslender is needed in the context of compression members, whereas classification of an element as slender, noncompact, or compact is needed in the context of flexural members. Table 14.2 shows a summary of general slenderness limits used in the classification of I-shapes for compression and flexure.

14.4 Tension Members

Tension members are governed by the strength limit states of yielding and fracture. Yielding, as the word implies, means loading a tension member to a point where the yield stress of the steel is exceeded whereas, fracture, in this context, means loading the member beyond yielding to the point of rupture.

The limit state of yielding in tension members is checked on the gross section of a member and a uniform distribution of stress is assumed. The gross section of a member is defined as is the total cross section of the member, usually at some distance away from a connection on the member. The limit state of fracture in tension members is checked on the net section of a member. The net section of a member is defined as a section, typically at or near the end of the member, through bolt holes, welds, and so on. Figure 14.2 illustrates the gross and net sections for a channel tension member bolted to a gusset plate.

14.4.1 Gross Section Yielding

The gross area of a member is calculated by adding product of the width and thickness for each element in a cross section. The design strength of a member considering the limit state of gross section yielding is computed as

$$\phi P_{ny} = \phi_y F_y A \tag{14.8}$$

where

F_y = yield strength of the steel (ksi)
A_g = gross area of the member (in^2)
ϕ_y = resistance factor for yielding, 0.95

Yielding of the member in the gross section is considered a limit state because it could lead to excessive elongation of the member that could compromise the stability or safety of the structure. Yielding of the net section is not considered a limit state because this yielding would be isolated and would not lead to the same excessive elongation that yielding on the gross section would result in. Localized yielding in a member at or near a connection is acceptable and expected.

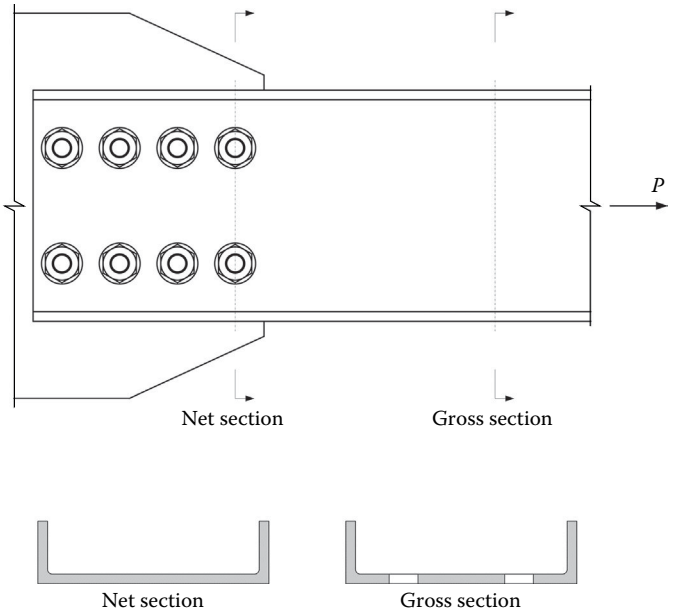

FIGURE 14.2 Illustration of gross and net cross sections for a bolted tension member.

14.4.2 Net Section Fracture

The net area of a member is computed by subtracting the cross-sectional area of material removed during fabrication of holes for a connection from the gross area of a member. In cases where bolted connections are used, the net area at a section will always be less than the gross area at that section. In cases where welded connections are used, however, the net area and gross area at a section may be equal.

At low to moderate load levels, a nonuniform distribution of stress exists at net sections in most tension members. After the yield stress of the material is exceeded at the net section, though, the stresses redistribute themselves to the point where a uniform distribution of stress can be assumed before rupture of the member. It is the inherent ductility of the steel that allows for this stress redistribution and permits the design strength of a member considering the limit state of gross section yielding to be computed as

$$\phi P_{nu} = \phi_u F_u A_n U \tag{14.9}$$

where

F_u = tensile strength of the steel (ksi)
A_n = net area of the member (in^2)
U = shear lag reduction coefficient
ϕ_y = resistance factor for yielding, 0.80

Rupture of a tension member at the net section is considered a limit state because the member would no longer be able to carry load.

The net area of a section is taken as the sum of the net areas of the elements making up the section. The net area of an element is computed as the product of the element thickness and the smallest net width. The width of each hole is taken as the nominal diameter of the hole, which is in contrast to the design of buildings where the width of each hole is taken as the nominal hole diameter plus some addition width, typically 1/16 in, to account for potential damage around the perimeter of the hole sustained

during fabrication. Note that some state DOTs require that holes in primary member be drilled or subpunched and reamed and prohibit punching holes to their final diameter. When a staggered bolt pattern is considered, the quantity $s^2/4g$ is added to the net width for each zigzag segment along the net width, where s is the pitch of any two consecutive holes measured parallel to the axis of the member and g is the gage of the same two holes measured perpendicular to the axis of the member.

When a tension member is loaded through all of its cross-sectional elements, the net section is considered to be fully effective. When a tension member is connected such that it is loaded through some, but not all, cross-sectional elements (such as the web in Figure 14.2, but not the flanges), then the efficiency of the net section is reduced. The mechanism by which stress in unconnected elements of the cross section makes its way through connected elements and then into the connected member is referred to as shear lag, and the associated loss in efficiency is accounted for by using the shear lag reduction coefficient, U. The amount of reduction is a function of (1) how much of the cross sectional area is unconnected, and (2) the length of the connection. In the former case, the eccentricity $\overline{x}$ of the connection is used as a measure of the unconnected material and is taken as the distance from the faying surface of the connection (the contact surface) to the center of gravity of the tension member. With respect to the latter, the longer a connection is, the less severe the reduction in efficiency. There are several equations provided in AASHTO (2012) Table 6.8.2.2-1 for determining U based on the specific case that is being considered, but one of the more general forms shown as Case 2 in the table is given as

$$U = 1 - \frac{\overline{x}}{L} \tag{14.10}$$

where

$\overline{x}$ = connection eccentricity (in)
L = length of connection (in)

14.4.3 Serviceability Considerations

The primary serviceability consideration with respect to the performance of tension members is with respect to the control of vibrations. To control vibrations, limits are imposed on the slenderness of members, L/r, where L is the unbraced length of the member and r is least radius of gyration of the member. For primary members that are subject to stress reversals the slenderness should not exceed 140, for primary members in tension only the slenderness should not exceed 200, and for secondary members the slenderness should not exceed 240.

14.5 Compression Members

In contrast to the behavior of a tension member, whose behavior is dominated by yielding and fracture, the behavior of a compression member is most often governed by buckling. Buckling of compression members is most often distinguished along the line of global and local buckling. Global buckling refers to a failure mechanism characterized by flexural buckling, torsional buckling, or a combination of flexural and torsional buckling, over the length of the member, with little local distortion to the cross-sectional geometry. Local buckling, however, is most often characterized by localized distortions of the cross-sectional elements without larger scale flexural or torsional displacements.

The load-deformation behavior of a compression member can be characterized as is shown in Figure 14.3, where δ represents the axial shortening of the member, P is the applied axial load (compression positive in this case), and P_{cr} is the buckling load of the member. A hypothetical member that is not subject to a buckling failure mode will follow Path A, whereas a realistic member subject to buckling failures will follow Path B. The departure of Path B from the linear elastic response shown as Path A is referred to as a bifurcation. In theory, the compressive capacity of an axially loaded member is bounded

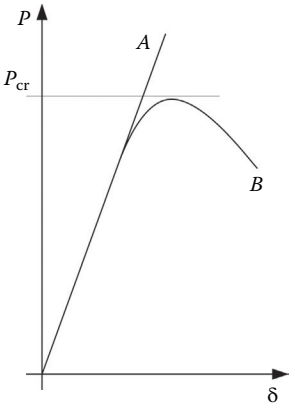

FIGURE 14.3 Load-deformation behavior of compression members.

by either yielding for short members (often referred to as "crushing" in the context of compression members), or global buckling for longer members, as shown in Figure 14.4. The crushing load is often given as $P_y = F_y A_g$ or is presented in AASHTO Section 6.9 as $P_o = QF_y A_g$, where Q is a reduction parameter to account for local buckling, which is taken as 1.00 for sections with nonslender elements. Euler is credited with being one of the first to derive the equation for elastic buckling; his formula is presented as

$$P_e = \frac{\pi^2 E A_g}{(KL/r)^2} \tag{14.11}$$

where

P_e = elastic buckling load of the compression member (ksi)
E = modulus of elasticity of steel (ksi)
A_g = gross area of the compression member (in^2)
K = effective length factor
L = length of member (in)
r = radius of gyration (in)

Achieving the theoretical capacities depicted in Figure 14.4 is impractical, however, because of a number of limitations, most noteworthy of which are residual stresses in the material and initial imperfections in the geometry of the members. Uneven cooling of the sections after they are rolled or fabricated into their final shapes leads to locked in thermal stresses that are referred to as residual stresses. Because of the mechanics of the cooling, the tips of the flanges and the center of the web of an I-shaped section tend to cool faster and have compressive residual stresses, whereas the intersection of the flanges and web tend to cool slower and have tensile residual stresses. The portions of the cross section with compressive residual stresses reach their yield point under an externally applied compressive load before the average stress on the cross section reaches F_y, and since the compressive residual stresses are found in the tips of the flanges, which provide the greatest contribution to the section's stability, this mechanism creates a destabilizing effect on the column that is illustrated in Figure 14.5. Similar situations are found in cross sections of different geometry. Since this buckling mode involves part of the cross section exceeding its elastic limit, it is often referred to as inelastic buckling.

The second limitation greatly affecting the capacity of compression members is initial out-of-straightness. ASTM provides tolerances for the sweep and camber of members. That is to say that perfectly acceptable rolled members coming from a steel mill are not perfectly straight. Even with externally applied loads that are purely axially compressive, this out-of-straightness leads to internal bending moments that compromise the stability of the member and reduce its compressive strength, as is illustrated in Figure 14.6.

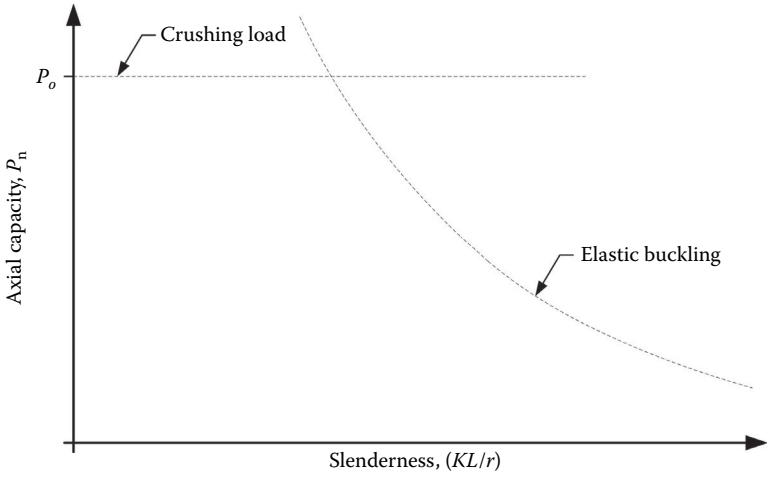

FIGURE 14.4 Fundamental failure modes for compression members.

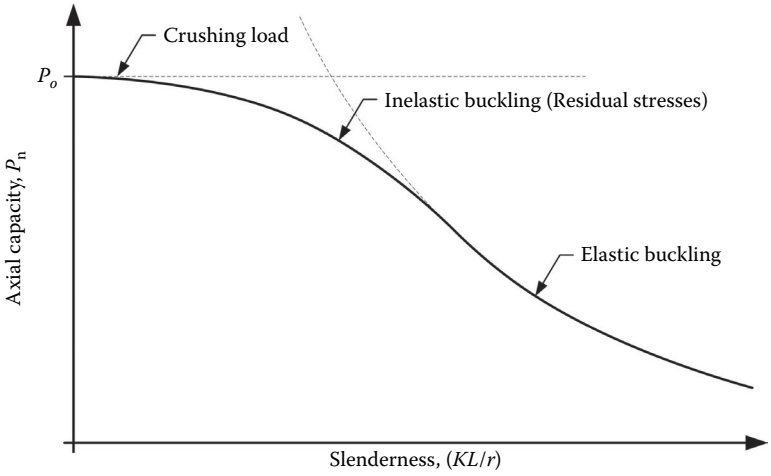

FIGURE 14.5 Impact of residual stresses on compression member strength.

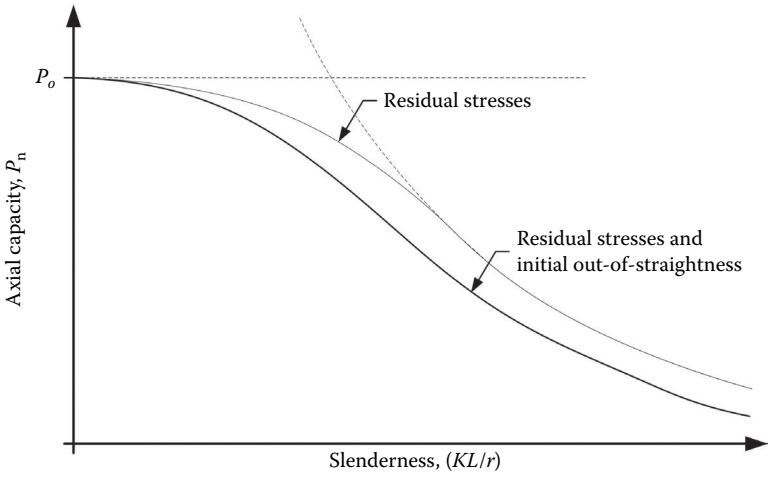

FIGURE 14.6 Impact of initial out-of-straightness on compression member strength.

Many different theories and models have been introduced to characterize the behavior of compression members, including Euler in 1744, Engesser in 1889 and 1895, and Shanley in 1946 (Salmon et al., 2009). In 1972, Bjorhovde assembled a database of 112 columns strength curves like that shown in Figure 14.6 (Ziemian, 2010). Based on that work, a strength model was adopted consisting of one equation characterizing the inelastic buckling capacity of columns with low to moderate slenderness, and a second equation charactering the elastic buckling capacity of columns with higher slenderness. The Guide to Stability Design Criteria (Ziemian, 2010) is an excellent source of information regarding seminal research on the topic of stability of the steel structures.

The global buckling provisions of the AASHTO Specifications (AASHTO, 2012) are found in Section 6.9.4 of AASHTO and are presented as

If $P_e/P_o \geq 0.44$,

$$P_n = \left(0.658^{\frac{P_o}{P_e}}\right) P_o \tag{14.12}$$

If $P_e/P_o < 0.44$,

$$P_n = 0.877 P_e \tag{14.13}$$

The first equation characterizes inelastic buckling, whereas the second characterizes elastic buckling.

14.5.1 Flexural Buckling

Equations 14.12 and 14.13 are applied to flexural buckling when the P_e is taken as

$$P_e = \frac{\pi^2 E A_g}{\left(KL/r_s\right)^2} \tag{14.14}$$

When considering flexural buckling, r_s is the radius of gyration about the cross-sectional axis perpendicular to the plane of buckling.

14.5.2 Effective Length

End conditions of compression members have a profound effect on their strength. The effective length factor, K, is intended to account for differing end conditions and effects of connecting members. The effective length factor for the baseline case, a pinned–pinned column, is unity. When more restraint is provided at the column ends, K is less than unity and when less restraint is provided, K is greater than unity. Chapter 18 provides a comprehensive discussion on effective length for compression members.

14.5.3 Local Buckling

The general approach taken by most design authorities is to proportion compression members with adequate global buckling capacity to resist applied loads, and then ensure that the cross section are proportioned such that the local buckling capacity of the member will be greater than the global buckling capacity, or greater even than the crushing capacity of the member. In those cases, the slender element reduction factor, Q, is taken as 1.00. Occasionally, however, members with slender elements must be used in compression. In those cases, the slender element reduction factor, Q, is determined based on the provisions in AASHTO Section 6.9.4.2.2, the details of which are beyond the scope of this work. Briefly, however, Q is taken as the product Q_a and Q_s, where Q_a is the governing factor for stiffened elements and Q_s is the governing factor for unstiffened elements.

14.5.4 Built-Up Compression Members

Compression members built-up from smaller rolled sections are encountered more often in bridge structures than in other structures. Characterizing the strength of built-up compression members is similar to the procedures presented earlier with two exceptions. First, care must be taken to ensure that the individual elements of a built-up member are adequately connected, typically by battens or lacing, so that the elements act together as a whole section instead of buckling individually. This is accomplished by requiring that the slenderness ratio of the individual elements between connectors is at most 75% of the governing slenderness of the member. Second, the means of connecting the individual elements of the built-up sections comes at some cost in terms of stiffness that acts to reduce, slightly, the compressive capacity of the built-up member with discretely connected elements relative to one that is rolled or continuously connected. As such, a modified effective slenderness ratio is used in Equations 14.15 and 14.16 to compute the capacity. This slenderness ratio is a function of distance between connectors and of the radii of gyration of the elements making up the built-up section.

For members built-up using welded or fully tension connectors,

$$\left(\frac{KL}{r}\right)_m = \sqrt{\left(\frac{KL}{r}\right)_o^2 + 0.82\left(\frac{\alpha^2}{1+\alpha^2}\right)\left(\frac{a}{r_{ib}}\right)^2} \tag{14.15}$$

For members built-up using snug-tight connectors,

$$\left(\frac{KL}{r}\right)_m = \sqrt{\left(\frac{KL}{r}\right)_o^2 + \left(\frac{a}{r_i}\right)^2} \tag{14.16}$$

where

$\left(\frac{KL}{r}\right)_m$ = modified effective slenderness
$\left(\frac{KL}{r}\right)_o$ = original effective slenderness
r_i = minimum radius of gyration of an individual element
r_{ib} = element radius of gyration parallel to member axis of buckling (in)
a = spacing of intermediate connectors (in)
α = separation ratio ($h/2r_{ib}$)

14.5.5 Members under Combined Compression and Flexural

When bending moment and axial forces are applied simultaneously, the resulting stresses must be considered together. One of the most fundamental approaches is to superimpose the resulting stresses, as is indicated in Equation 14.17 where the superimposed stresses are required to be less than or equal to some allowable stress. Although this approach is straightforward and easily implemented, is inappropriate in an LRFD context where a plastic moment, and not the yield moment, is defined as the ultimate limit state in flexure. Within the context of LRFD, the design basis is determined by examining the plastic capacity of a member under both flexure and axial force, as shown in Figure 14.7 for the case of major axis bending and axial compression. Based on longitudinal equilibrium of the stresses shown, the location of the plastic neutral axis (PNA) can be determined, and then M_{pc}, the plastic moment in the presence of axial compression, can be determined. The result is typically expressed as the ratio of M_{pc} to M_p and is a function of the ratio of axial compression to the axial crushing strength of the member, P to P_y. After accounting for the potential of the PNA to be in either the web or flange of the section, the interaction curve can be shown to be like those shown in Figure 14.8, where the outermost

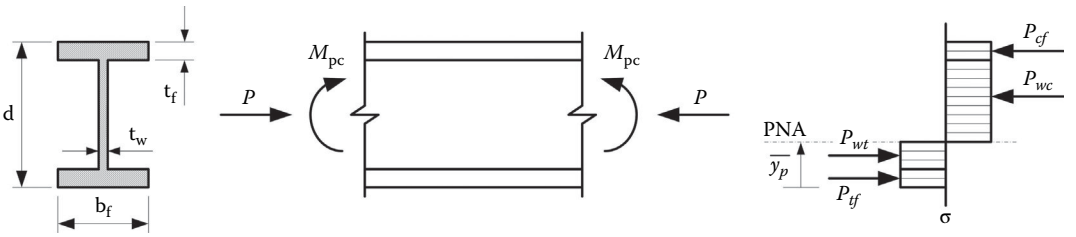

FIGURE 14.7 Plastic moment in the presence of axial compression.

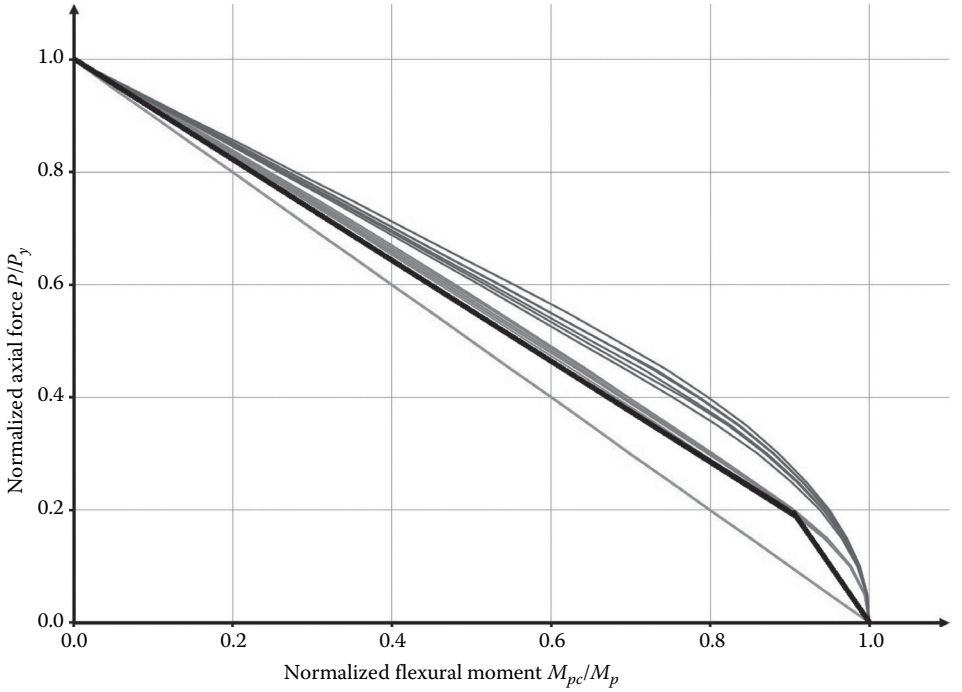

FIGURE 14.8 Interaction curve for flexure and axial compression.

curves are representative of deeper beam-type sections (W21s, W24s, W30s, etc.) and the inner curves are representative of shallower column-type sections (W10s, W12s, W14s). The straight line shown in Figure 14.8 represents the interaction curve for a rectangular cross section, whereas the bold bilinear line represents what is used for design. The general shape of the curve is similar for all I-shaped sections, but the exact shape and location varies somewhat depending on the specific section. A bilinear design curve is typically used as a lower bound representation of actual interaction for the purposes of design. The design curve is represented as Equations 14.18 and 14.19, which is written in terms of P_r and M_r, the design strengths in compression and flexure, respectively, instead of P_y and M_p.

$$\pm\frac{P}{A}\pm\frac{M_x}{S_x}\pm\frac{M_y}{S_y}\le F_a \tag{14.17}$$

If $P_u/P_r < 0.2$,

$$\frac{P_u}{2.0P_r}+\left(\frac{M_{ux}}{M_{rx}}+\frac{M_{uy}}{M_{ry}}\right)\le 1.0 \tag{14.18}$$

If $P_u/P_r \geq 0.2$,

$$\frac{P_u}{P_r}+\frac{8.0}{9.0}\left(\frac{M_{ux}}{M_{rx}}+\frac{M_{uy}}{M_{ry}}\right)\leq 1.0 \tag{14.19}$$

An additional consideration when axial compression and flexure are applied simultaneously is the effect that member deflections and joint displacements can have on the actual forces and moments felt by the members. In the former case, typically referred to as *P*-δ behavior, deflections of the member along its length resulting from flexure cause the axial force to be felt eccentrically, which imposes additional flexure, which in turn results in additional deflection, and so on. In the latter case, typically referred to as *P*-Δ behavior, joint displacements at either end of the member cause the axial force to be applied eccentrically, which results in additional flexure in the member, which in turn results in additional displacements at the joints, as so on. Both of these cases are second order in nature. That is to say that the conventional first-order assumption that deflections and displacements in the analysis are small enough that they do not affect the resulting member forces is not valid. In this case, a second-order analysis must be performed on the structure, which most computer software nowadays is readily capable of performing, or a method of approximating the second-order actions from a first-order analysis, such as the moment magnification approach outlined in Chapter 4 of the AASHTO-LRFD Specification, must be employed.

14.6 Flexural Members

The treatment of flexural members fundamentally depends on whether the member is considered to be a "beam" or "plate girder" since the failure modes and equations used to characterize their behavior are different in many cases. In general "beams" are members that are composed of elements (flanges, webs, etc.) that are stocky enough that moment capacity can reach or approach the yielding moment, M_y, or possibly the plastic moment, M_p, before local buckling occurs. "Beams" can be rolled sections or sections that are built-up by welding plates together. On the other hand, "plate girders" are members that are composed of elements that are slender enough that buckling of one or more of the elements occurs before the yield moment, M_y, can be reached. "Plate girders" are almost always built-up sections.

The most commonly accepted delineation is the web slenderness, h/t_w; when, $\frac{h}{t_w}\leq 5.70\sqrt{\frac{E}{F_{yw}}}$ the section is classified as a "beam" and when $\frac{h}{t_w}>5.70\sqrt{\frac{E}{F_{yw}}}$, the section is classified as a "plate girder."

14.6.1 Yield Moment and Plastic Moment

Two commonly accepted limits to a members flexural capacity are the yield moment, M_y, and the plastic moment, M_p. The yield moment is most often defined as the bending moment that causes first yielding in a cross section. Occasionally, the yield moment is defined as the bending moment that causes first yielding in the flanges of a cross section, neglecting yielding that may occur first in the webs of hybrid sections. In either case, reaching the yield moment of the cross section is rarely considered to be the limit of the usefulness of the section as additional bending moment can often be resisted. Typically, the plastic moment of a cross section, the moment associated with a section that has completely yielded in flexure, is considered to be the ultimate limit to moment capacity for beam-type sections.

The yield moment and plastic moment of a rectangular section is illustrated in Figure 14.9 and are taken as the resultant moment from the force couple created by either F_c or F_t with the moment arm *a*. In the case of an I-shaped section as shown in Figure 14.10, it is often more convenient to break the compressive and tensile forces into components in the compression flange, compression portion of the

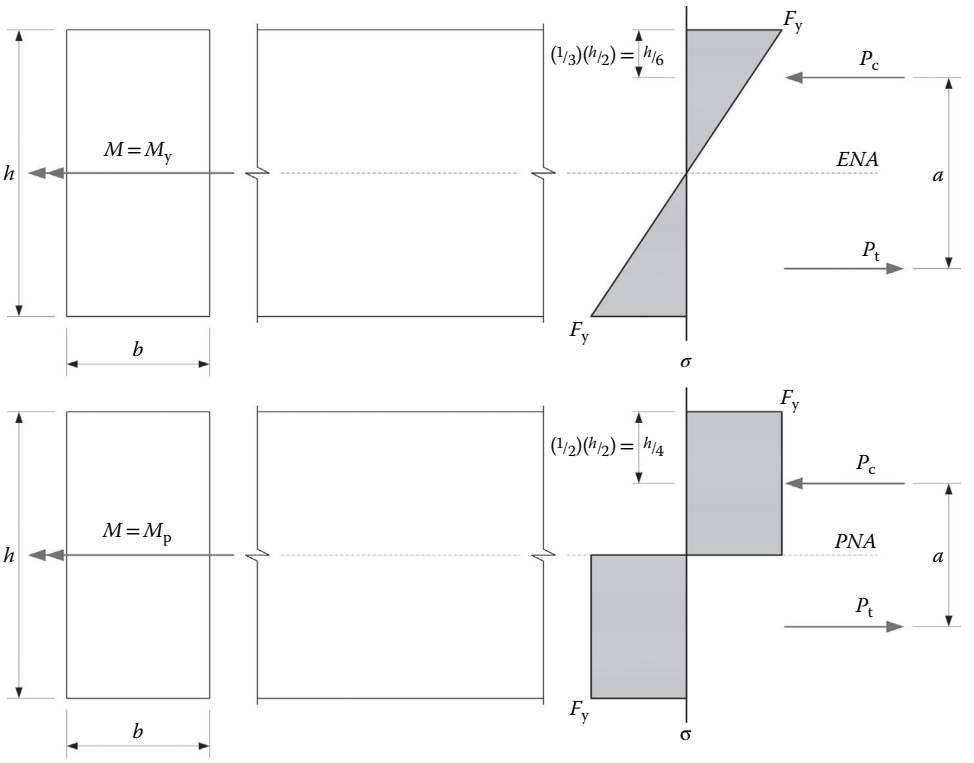

FIGURE 14.9 Illustration of yield moment and plastic moment.

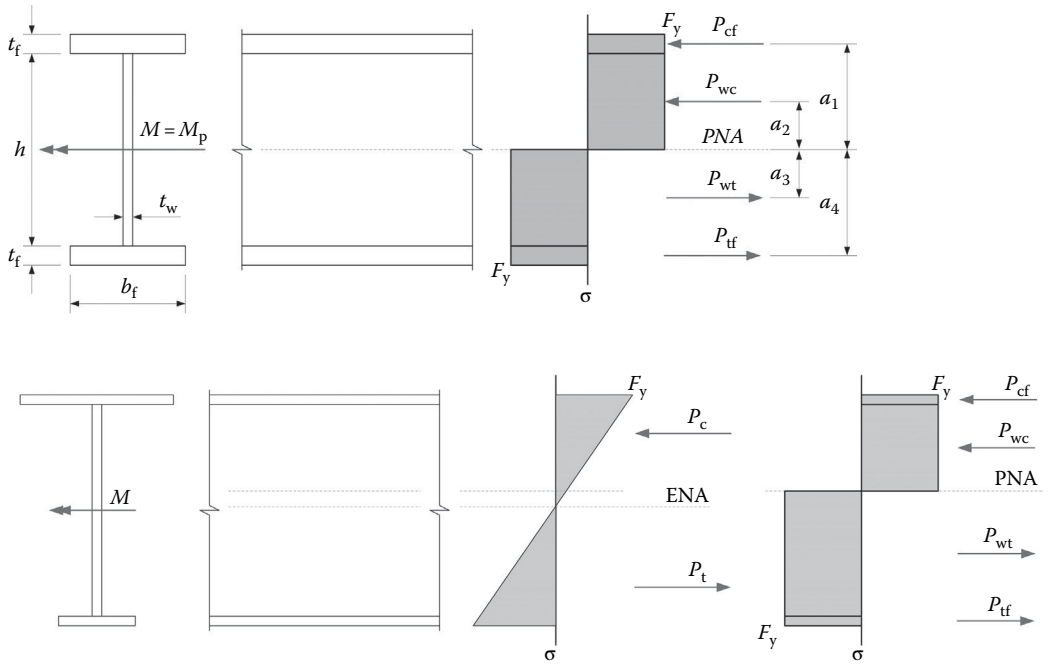

FIGURE 14.10 Illustration of plastic moment in I-shaped sections.

web, tensile portion of the web, and tension flange. The plastic moment is then taken as the sum of the moments created by each of these components about some point, often the PNA of the section. Note that in the case of a singly symmetric section (illustrated in Figure 14.10b), or in a hybrid section, the PNA may be at a different location in the section than the elastic neutral axis (ENA). In all cases, the PNA can be found as the axis that achieves the condition of the plastic force above the axis is equal to the plastic force below the axis.

Yield moment	Plastic moment
$M_y = F_c a = F_t a$	$M_p = F_c a = F_t a$
$F_c = F_t = \left(\frac{1}{2}\right)\left(F_y\right)\left(\frac{h}{2}\right)(b) = \frac{bh}{4}F_y$	$F_c = F_t = \left(F_y\right)\left(\frac{h}{2}\right)(b) = \frac{bh}{2}F_y$
$a = h - (2)\left(\frac{h}{6}\right) = \frac{2}{3}h$	$a = h - (2)\left(\frac{h}{4}\right) = \frac{h}{2}$
$M_y = Fa = \left(\frac{bh}{4}F_y\right)\left(\frac{2}{3}h\right) = \frac{bh^2}{6}F_y = S_x F_y$	$M_p = Fa = \left(\frac{bh}{2}F_y\right)\left(\frac{h}{2}\right) = \frac{bh^2}{4}F_y = Z_x F_y$

14.6.1.1 Shape Factor

The shape factor is defined as the ratio of the plastic moment, M_p, to the yield moment, M_y, and is often used as a measure of a cross-sections efficiency as a bending member. The shape factor will always be greater than 1.00 and a cross section with a smaller shape factor is more efficient in bending than a section with a larger shape factor. For a rectangular cross section, the shape factor is defined as is shown in Equation 14.20. Based on this and the strain demands near the neutral axis of the member, the plastic moment of a cross section is limited to a value no greater than 150% of the section's yield moment in many steel design specifications. The shape factor for most I-shaped sections ranges between 1.10 and 1.20, making them more efficient than a rectangular section for bending.

$$SF = \frac{M_p}{M_y} = \frac{\left(\frac{bh^2}{4}\right)F_y}{\left(\frac{bh^2}{6}\right)F_y} = 1.50 \tag{14.20}$$

Up to this point, we have considered doubly symmetric sections. In that case, the ENA and PNA are at the mid-height of the section. When the section is only singly symmetric (or nonsymmetric) the ENA and PNA will be at different locations. If the section is homogenous, find the PNA by setting the area above the PNA to the area below the PNA. Otherwise, set the force above the PNA to the force below the PNA.

14.6.2 Local Buckling

When a cross section contains a component (a flange or web, for example) that are either compact or slender as defined in Section 14.3, then the possibility that that component can buckling independently before the section reaching its yield moment, plastic moment, or a different failure mode must be investigated. Flange local buckling in a finite element model of a shallow beam section is illustrated in Figure 14.11 and the solution space for moment capacity of a section governed by flange and/or web local buckling is shown in Figure 14.12. The way that local buckling in flexure is handled in most design specifications (AASHTO, 2012, AISC, 2010b) depends on whether it is the flange, the web, or both components that susceptible.

Equations 14.21 through 14.23 show commonly used formulations for nominal moment capacity of sections susceptible to flange or web local buckling. Assuming that the section has a compact web, the strength of the beam-type section with a compact flange ($\lambda_{flange} \leq \lambda_p$) is governed by the plastic moment

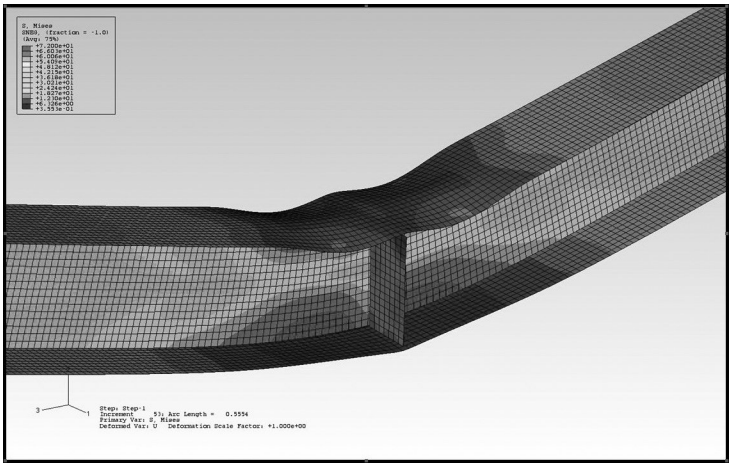

FIGURE 14.11 Flange local buckling of a shallow beam section.

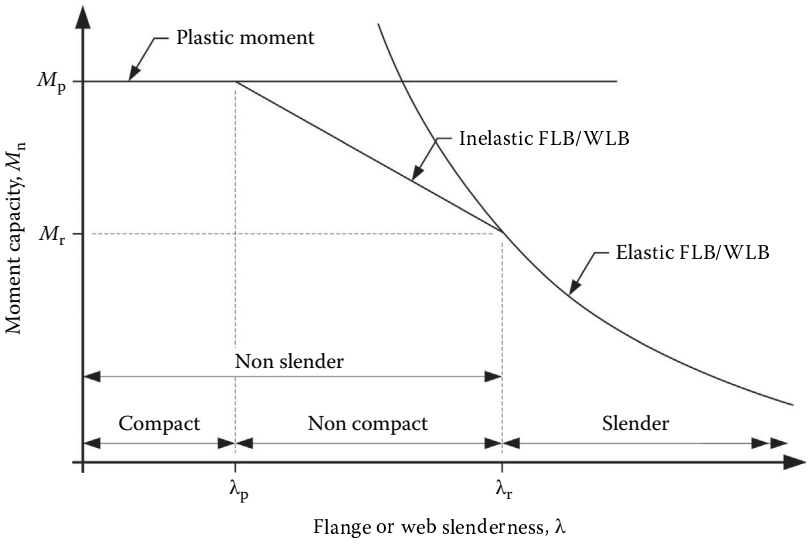

FIGURE 14.12 Solution space for flange local and web local buckling.

of the section. When the flange is classified as slender ($\lambda_{flange} \geq \lambda_r$), then elastic flange local buckling governs. The moment capacity at the slenderness equal to λ_r is often referred to as M_r, which is the product of the elastic section modulus for the compression flange, S_{xc}, and the yield stress for the flange accounting for residual stresses, F_{yr}. The moment capacity of a section with a noncompact flange ($\lambda_p < \lambda_{flange} < \lambda_r$) is taken as a linear interpolation between the anchor points of M_p with λ_p at the upper end and M_r with λ_r at the lower end.

To accommodate the effects of web local buckling, most specifications employ the use of web plastification factors, R_{pc} and R_{pt}, for the web adjacent to the compression flange and tension flange, respectively. Equations 14.24 and 14.25 show the plastification factors for the web adjacent to the compression flange. In the case of a compact web, the web plastification factor is equal to the shape factor of the section and when used in Equation 14.21 for a section with a compact flange results the plastic moment for the nominal moment capacity. In the case of a noncompact web, the web plastification factor is taken

as the linear interpolation between the plastic moment capacity of the web and the yielding moment of the web assuming that the flanges are compact, similar to the approach taken for noncompact flanges. Recall that a section with a slender web ($\lambda_{web} \geq \lambda_r$) is classified as a plate girder by most specifications and a different approach to bending capacity is generally taken.
For compact flanges ($\lambda_{flange} \leq \lambda_p$)

$$M_{nc} = R_{pc} M_{yc} \tag{14.21}$$

For noncompact flanges ($\lambda_p < \lambda_{flange} < \lambda_r$)

$$M_{nc} = \left[1 - \left(1 - \frac{F_{yr} S_{xc}}{R_{pc} M_{yc}}\right)\left(\frac{\lambda_f - \lambda_{pf}}{\lambda_{rf} - \lambda_{pf}}\right)\right] R_{pc} M_{yc} \tag{14.22}$$

For slender flanges ($\lambda_{flange} \geq \lambda_r$)

$$M_{nc} = R_{pc} M_{cr} \tag{14.23}$$

For compact webs ($\lambda_{web} \leq \lambda_p$)

$$R_{pc} = \frac{M_p}{M_{yc}} \tag{14.24}$$

For noncompact webs ($\lambda_p < \lambda_{web} < \lambda_r$)

$$R_{pc} = \left[1 - \left(1 - \frac{M_{yc}}{M_p}\right)\left(\frac{\lambda_w - \lambda_p}{\lambda_{rw} - \lambda_p}\right)\right] \frac{M_p}{M_{yc}} \leq \frac{M_p}{M_{yc}} \tag{14.25}$$

14.6.3 Lateral-Torsional Buckling

When a beam is laterally braced at discrete points along its length and is loaded such that it is bent about its strong axis, the possibility that the beam will buckle laterally and torsionally before reaching its plastic moment or local buckling moment must be investigated. Figure 14.13 shows moment resistance versus unbraced length of a flexural member. A fundamental form of the equation predicting the elastic lateral-torsional buckling capacity of a beam with an unbraced length, L_b, is shown in Equation 14.26 (Ziemian, 2010). The term under the second radical in Equation 14.26 is defined in Equation 14.27 and addresses warping in the section that occurs when a noncircular section is twisted.

$$M_{cr} = \frac{\pi}{L_b} \sqrt{EI_y GJ} \sqrt{1 + W^2} \tag{14.26}$$

$$W = \frac{\pi}{L_b} \sqrt{\frac{EC_w}{GJ}} \tag{14.27}$$

Equation 14.26 is presented in the AASHTO specification for beam-type sections in the form of

$$M_{cr} = S_{xc} F_{cr} \tag{14.28}$$

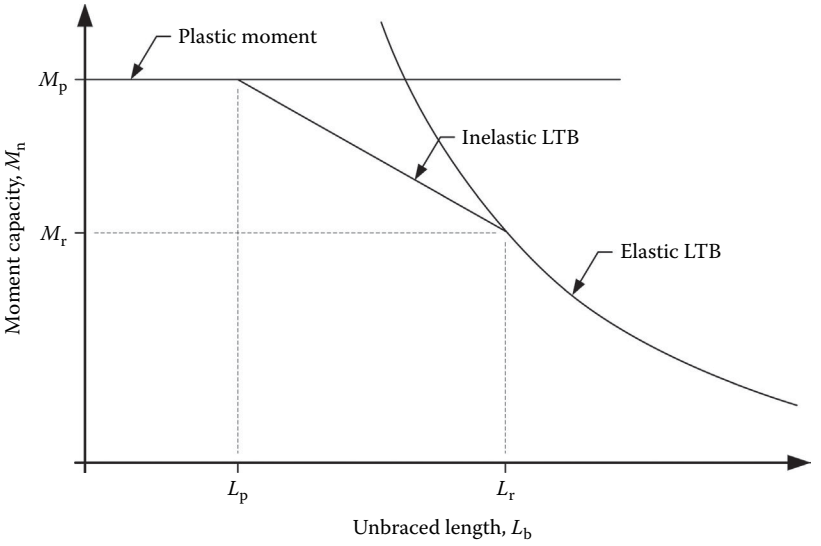

FIGURE 14.13 Lateral-torsional buckling solution space.

where

$$F_{cr} = \frac{C_b \pi^2 E}{\left(L_b / r_t\right)^2} \sqrt{1 + 0.078 \frac{J}{S_{xc} h} \left(\frac{L_b}{r_t}\right)^2} \tag{14.29}$$

$$r_t = \frac{b_{fc}}{\sqrt{12\left(1 + \frac{1}{3}\frac{D_c t_w}{b_{fc} t_{fc}}\right)}} \tag{14.30}$$

Equation 14.30 describes the radius of gyration of a hypothetical tee section composed of the compression flange of the beam section along with one-third of the portion of the web that is in compression. Beams with an unbraced length less than L_p as defined in Equation 14.31 need not be checked for lateral-torsional buckling. Instead their flexural strength will be governed by plastic moment, yield moment, or local buckling. The length at which M_{cr} is equal to M_r (the yield moment accounting for residual stresses in the section) is defined as the limiting length L_r and is shown in Equation 14.32. Beams with an unbraced length greater than L_r must be checked for elastic lateral-torsional buckling. A beam with an unbraced length L_b between L_p and L_r must be checked for inelastic lateral-torsional buckling as defined as a linear interpolation between the anchor points of M_p with L_p on the upper end and M_r with L_r on the lower end, as shown in Equation 14.33.

$$L_p = 1.0 r_t \sqrt{\frac{E}{F_{yc}}} \tag{14.31}$$

$$L_r = 1.95 r_t \frac{E}{F_{yr}} \sqrt{\frac{J}{S_{xc} h}} \sqrt{1 + \sqrt{1 + 6.76\left(\frac{F_{yr}}{E}\frac{S_{xc} h}{J}\right)^2}} \tag{14.32}$$

$$M_n = C_b \left[1 - \left(1 - \frac{F_{yr} S_{xc}}{R_{pc} M_{yc}}\right)\left(\frac{L_b - L_p}{L_r - L_p}\right)\right] R_{pc} M_{yc} \le R_{pc} M_{yc} \tag{14.33}$$

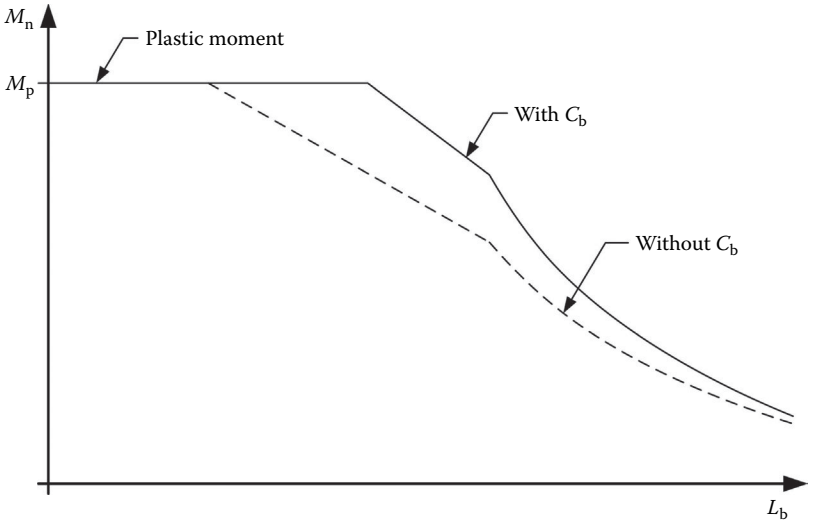

FIGURE 14.14 Influence of C_b on moment capacity of discretely braced beams.

Equations 14.26 and 14.29 are both formulated based on the assumption that a constant moment is present on the beam section over the entire unbraced length, L_b. If this is not the case, then these two equations will provide a conservative value for the strength of the section. To provide more accurate predictions of strength, the moment gradient factor, C_b, is used as shown in Equation 14.29 and as illustrated in Figure 14.14. One form of the moment gradient factor is shown in Equation 14.34, where M_1 and M_2 are the bending moments at the ends of the unbraced length. A second form of the moment gradient factor is shown in Equation 14.35, where M_A, M_B, and M_C are the bending moments at the one-quarter point, midpoint, and three-quarter point of the unbraced length. The second of the two formulations is currently used in the AISC Specification (2010b) because it captures the shape of the moment diagram between brace points but the first formulation is adopted by the AASHTO Specification (2012) with some modifications. Since bending moments in bridge design problems are often taken from moment envelopes as opposed to moment diagrams, the two moments M_1 and M_2 may come from nonconcurrent moment diagrams. That is to say that M_1 and M_2 may come from different truck positions and may not ever actually occur in the bending member simultaneously. As a result, definitions of M_1 and M_2 in the AASHTO Specifications (AASHTO, 2012) are significantly different than what appears above.

$$C_b = 1.75 + 1.05\left(\frac{M_1}{M_2}\right) + 0.3\left(\frac{M_1}{M_2}\right)^2 \leq 2.3 \tag{14.34}$$

$$C_b = \frac{12.5M_{max}}{2.5M_{max} + 3M_A + 4M_B + 3M_C} \leq 3.0 \tag{14.35}$$

14.6.4 Shear Behavior of Flexural Members

In a manner similar to the previous topics covered in this section, the shear strength of bending members is governed by yielding for webs that are sufficiently stocky. As the slenderness ratio of the web increases, so does the possibility that it will buckle before achieving its plastic strength. This buckling, often referred to as shear buckling, is actually buckling due to a compressive state of stress that exists in the web as a result of the shear forces present, as illustrated in Figures 14.15 and 14.16.

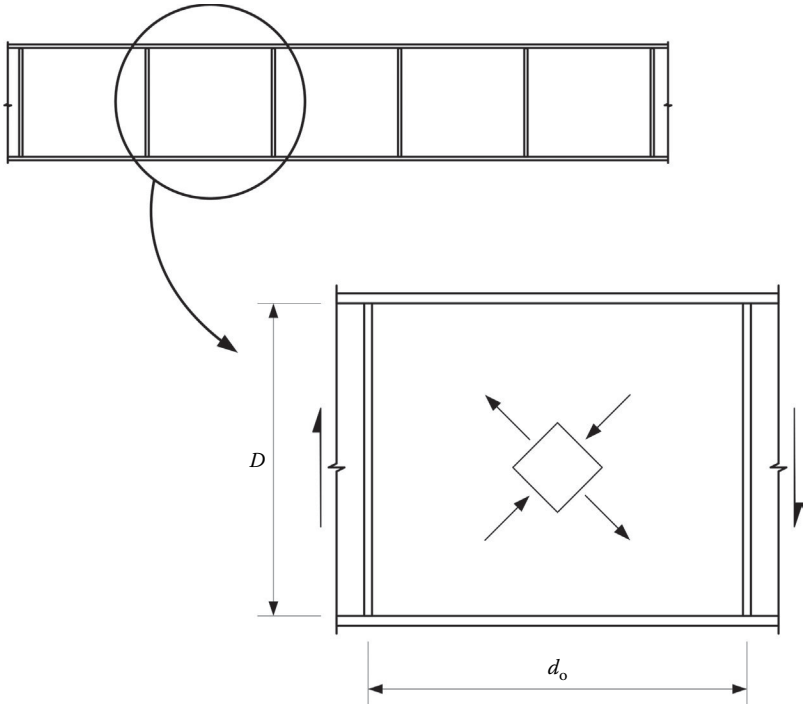

FIGURE 14.15 State of stress in the web of a beam.

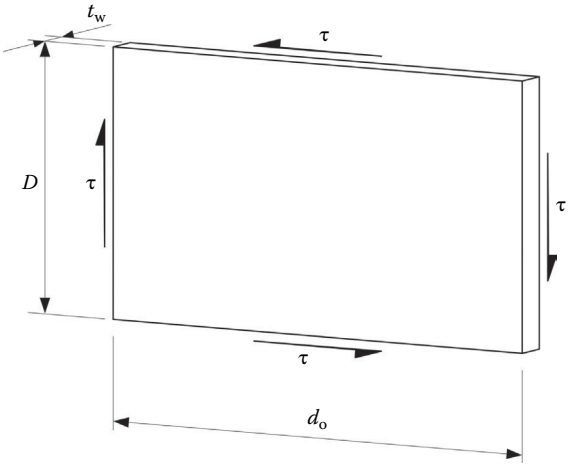

FIGURE 14.16 Shear buckling.

Timoshenko's (Salmon et al., 2008) formulation for plate buckling can be applied to this case as it was in the case of an edge compression. Buckling is presented in terms of the shear stress, τ, as

$$\tau_{cr} = \frac{\pi^2 k_v E}{12\left(1-\nu^2\right)\left(D/t_w\right)^2} \tag{14.36}$$

When intermediate transverse stiffeners are provided, k_v is taken as shown in Equation 14.37. When intermediate transverse stiffeners are not present, k_v is taken as the lower bound of 5.0:

$$k_v = 5 + \frac{5}{\left(d_o/D\right)^2} \tag{14.37}$$

The AISC and AASHTO specifications present the fundamental form of the shear strength equation as

$$V_n = V_{cr} = CV_p \tag{14.38}$$

where V_p is the plastic strength of the web taken as $0.58F_{yw}Dt_w$ and C is the ratio of the shear buckling strength to the plastic strength of the web. That ratio, in the context of elastic shear buckling, can be expressed as

$$\begin{aligned} C &= \frac{V_{cr}}{V_p} = \frac{\tau_{cr}}{0.58F_{yw}} \\ &= \frac{\pi^2 k_v E}{12\left(1-\nu^2\right)\left(D/t_w\right)^2\left(0.58F_{yw}\right)} = \frac{1.57k_v E}{\left(D/t_w\right)^2 F_{yw}} \end{aligned} \tag{14.39}$$

This elastic buckling strength is valid for webs slenderer than $D/t_w > 1.40\sqrt{Ek/F_{yw}}$. When D/t_w is between $1.12\sqrt{Ek/F_{yw}}$ and $1.40\sqrt{Ek/F_{yw}}$, inelastic shear buckling governs and C is taken as

$$C = \frac{1.12}{\left(\frac{D}{t_w}\right)}\sqrt{\frac{Ek}{F_{yw}}} \tag{14.40}$$

when the web slenderness is less than $D/t_w < 1.12\sqrt{Ek/F_{yw}}$, shear buckling will not occur, C is taken as 1.00, and the plastic shear strength of the web governs. The solution space for web shear strength is shown in Figure 14.17.

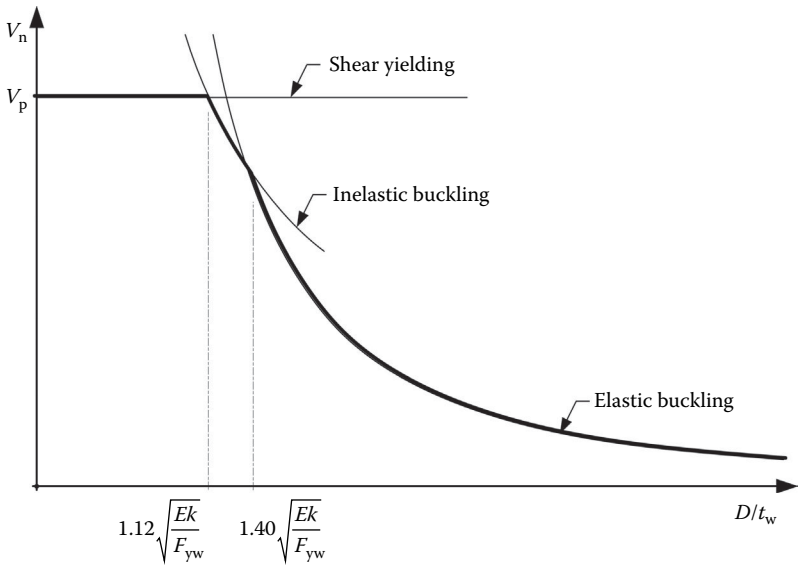

FIGURE 14.17 Solution space for shear strength of an I-shaped beam section.

14.6.5 Serviceability Considerations

Deflection and vibration issues are primary serviceability criteria for most flexural members. Excessive deflections can lead to unacceptable structural performance, whereas excessive vibrations can make a structure uninhabitable for occupants or unacceptable for sensitive equipment. The solution to both of these issues is typically to increase the stiffness of the beams. In bridge structures, deflections are not often an issue unless the bridge is used by pedestrians, in which case limits on deflection may be imposed to provide increased stiffness so as to indirectly limit vibrations. Most states require dead-load deflections to be accommodated through cambering. Some states impose live-load deflection limits as well. Deflection limits on bridges are addressed later in this work in Chapter 4 of the second book in this series, *Bridge Engineering Handbook, Second Edition: Superstructure Design*.

An additional issue that is specific to AASHTO design is the idea of limiting yielding in beams under service load levels. AASHTO permits beams and girders to be designed at the plastic moment in many cases, and in some cases permits limited buckling of webs, but only under strength-level loads. Strength-level loading is expected to occur relatively few times during the life of a bridge. Exceeding the yield stress of a beam or girder or experiencing limited web buckling is acceptable under this pretense, but would not be acceptable for an unlimited number of loading cycles. As a result, AASHTO restricts yielding and bend buckling in beams and girders at the service load level.

14.7 Plate Girder Issues

14.7.1 Local Buckling

Local buckling of sections under flexure was treated earlier in this chapter. A plate girder is basically defined as a section that has a slender web; that is a web where

$$\frac{h}{t_w} > 5.70\sqrt{\frac{E}{F_y}} \tag{14.41}$$

Going back to the fundamental plate buckling formula presenting F_{cr} as a function of k, and using D instead of h (Salmon et al., 2009),

$$F_{cr} = \frac{k \cdot \pi^2 \cdot E}{12(1-0.3^2)(D/t_w)^2} = \frac{0.9038 \cdot k \cdot E}{(D/t_w)^2} \tag{14.42}$$

where k can be defined as

$$k = \frac{9}{(D_c/D)^2} \tag{14.43}$$

For the case of the doubly symmetric shape, $D = 2D_c$, $k = 36.0$, and

$$F_{cr} = \frac{32.5E}{(D/t_w)^2} \tag{14.44}$$

This represents a practical upper bound on the stress that a slender web can carry without buckling locally. This equation is found in the AASHTO specification (AASHTO, 2012) but is a limit state only for service load combinations. For strength load combinations a different approach is employed.

14.7.2 Web Bend Buckling and Load Shedding

Since plate-girder webs usually have high h/t_w ratios, bucking may occur as a result of the bending about the strong axis of the girder. Generally, webs with $h/t_w > \lambda_r$ are susceptible to buckling. Since the web carries only a small portion of the bending moment on the section, however, this buckling does not generally represent the end of the usefulness of the girder. When a girder is designed properly, flexural local buckling of the web (sometimes referred to as bend buckling) does not represent an ultimate limit state for the girder.

To consider the postbuckling strength of the girder, the portion of the web that has buckled is disregarded. Considering the remaining, effective portions of the cross sections, it can be shown for a girder with $h/t_w = 320$, which is quite slender, that the ratio M_n to M_y can be adequately approximately linearly as (Salmon et al., 2009)

$$\frac{M_n}{M_y} = 1.0 - 0.09\frac{A_w}{A_f} \tag{14.45}$$

The value of $h/t_w = 320$ was selected as it is the limit above which the web becomes susceptible to vertical flange buckling, a failure mode where the compression flange buckles vertically into the web in a manner similar to but different from flange local buckling. Considering web slendernesses other than $h/t_w = 320$ results in the relationship shown as Equation 14.46.

$$\frac{M_n}{M_y} = 1.0 - 0.0005\left(\frac{A_w}{A_f}\right)\left(\frac{h}{t_w} - 5.70\sqrt{\frac{E}{F_{yw}}}\right) \tag{14.46}$$

The coefficient of 0.0005 in Equation 14.46 was originally developed by Basler (Basler, 1961; Salmon et al., 2009) and is valid for the ratio of $a_{wc} = A_w/A_f$ up to 3.0. An updated version of the above equation is valid for the ratio of a_{wc} up to 10.0.

$$\frac{M_n}{M_y} = 1.0 - \left(\frac{a_{wc}}{1200 + 300a_{wc}}\right)\left(\frac{h}{t_w} - 5.70\sqrt{\frac{E}{F_{yw}}}\right) \tag{14.47}$$

When M_y is replaced by the critical moment, $M_{cr} = S_{xc} F_{cr}$, which may be less than M_y, the form shown as in Equation 14.48 results:

$$M_n = S_{xc}F_{cr}\left[1.0 - \left(\frac{a_{wc}}{1200 + 300a_{wc}}\right)\left(\frac{h}{t_w} - 5.70\sqrt{\frac{E}{F_{yw}}}\right)\right] \tag{14.48}$$

$$M_n = S_{xc}F_{cr}R_b$$

Thus the load shedding factor (or plate girder factor) can be written as is shown in Equation 14.49, which is presented in the AASHTO Specification as Equation (6.10.1.10.2-3).

$$R_b = 1 - \left(\frac{a_{wc}}{1200 + 300a_{wc}}\right)\left(\frac{2D_c}{t_w} - 5.70\sqrt{\frac{E}{F_{yc}}}\right) \le 1.0 \tag{14.49}$$

In this form, R_b is limited to a value not greater than 1.00, h is replaced with $2D_c$ for the case where the neutral axis is not at mid-height, and F_{yw} is replaced with F_{yc}.

14.7.3 Hybrid Girders

It is often economical to proportion a built-up girder with a web that has a lower strength than the one or both flanges. In this case the girder is referred to as a hybrid girder. In general the strength of a girder is defined by yielding of the flanges and not yielding of the web but this results in an overestimation of the moment in the section when yielding occurs. One approach to determine the moment capacity of a hybrid girder is to use moment equilibrium of the stress distribution present at first yield or at the plastic moment, as is shown in Figure 14.18. This approach, while fundamentally sound, is rather tedious. Instead, a reduction factor, the hybrid girder factor, is typically employed to account for yielding of the web before first yielding of a flange or the flanges.

$$R_h = \frac{12 + a_{wc}(3m - m^3)}{12 + 2a_{wc}} \tag{14.50}$$

$$m = \frac{F_{yw}}{F_{yf}} \text{ and } a_{wc} = \frac{A_w}{A_f} \tag{14.51}$$

Compare this form of the hybrid factor to the form in the AASHTO Specifications (AASHTO, 2012), where m is replaced by ρ and a_{wc} is replaced by β, wherein the web area is taken as $2D_n t_w$ instead of h/t_w.

$$R_h = \frac{12 + \beta(3\rho - \rho^3)}{12 + 2\beta} \tag{14.52}$$

$$\rho = \frac{F_{yw}}{f_n} \le 1.0 \text{ and } \beta = \frac{2D_n t_w}{A_{fn}} \tag{14.53}$$

where

D_n = larger of the distances from the ENA to the inside face of either flange
f_n = yield stress of the flange corresponding the D_n
A_{fn} = area of the flange corresponding to D_n

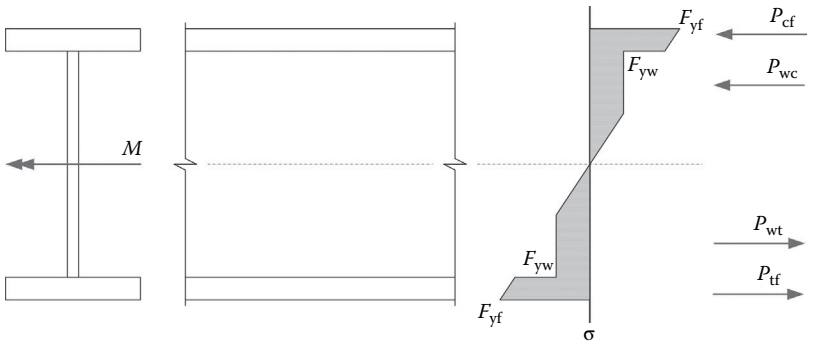

FIGURE 14.18 State of stress in a hybrid girder at the yield moment.

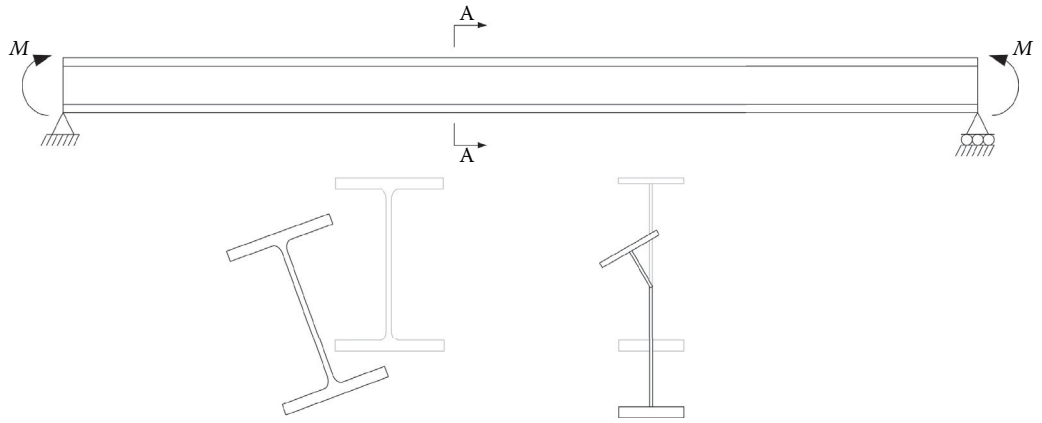

FIGURE 14.19 Lateral-torsional buckling versus compression flange lateral buckling.

14.7.4 Compression Flange Lateral Buckling

In the context of a plate girder, the beam failure mode known as "lateral-torsional buckling" is renamed "compression flange lateral buckling." Conceptually, the two failure modes are quite similar. One way of visualizing the difference, however, is to consider that a beam section reaching a lateral instability point is likely to retain its sectional shape, while displacing laterally and twisting, whereas a deeper plate girder with a slender web may experience the same failure with only its compression flange displacing laterally resulting in bending of the web. This difference is illustrated in Figure 14.19 where the deformed shapes of a beam 1 and plate girder 2 subjected to a positive moment are shown.

14.8 Connection Fundamentals

Connections in steel structures are typically made by means of either bolting or welding. Each of the two methods has advantages and shortcomings, and the selection of one or the other is generally made on a case by case basis and is often swayed by preferences of the engineer, fabricator, or erector. One rule of thumb that persists, however, is to favor welding in a shop where the climate can be controlled, and to favor bolting in the field.

Issues specific to bolting are discussed first in Section 14.8.1, issues specific to welding are then discussed in Section 14.8.2, and then issues common to both bolting and welding are discussed in Section 14.8.3.

14.8.1 Bolts and Bolted Connections

14.8.1.1 Failure Modes

Figure 14.20 shows a typical bolt used in structural steel connections. The failure modes associated with bolts and bolted connections are tension failure, shear failure, combined tension and shear interaction, bearing failure, and connection slip.

14.8.1.1.1 Tension Failure

When a bolt is subjected to tension the potential failure develops as a fracture through the threaded portion of the fastener. The cross-sectional area that carries the tensile stress in the bolt is referred to as the effective area of the fastener and is smaller than nominal area, which is based on the diameter of the shank, but is larger than the root area, which is based on the minimum diameter of the threads. The effective area is a function of the thread pitch and can be computed as shown in Equation 14.54 for imperial sizes (AISC, 2010a).

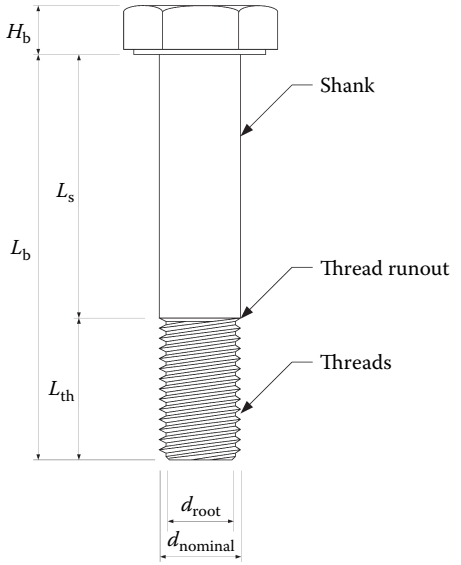

FIGURE 14.20 Bolt dimensions.

$$A_{eff} = \left(\frac{\pi}{4}\right)\left(d - \frac{0.9743}{n}\right)^2 \tag{14.54}$$

Use of this equation to compute the tensile strength of a fastener is felt by many engineers to be overly cumbersome since the engineer would need to know the pitch of the fastener, which changes for different bolt sizes. For commonly used bolt sizes, the ratio of the effective area to the nominal area is approximately 0.76. Thus as a simpler, though slightly less accurate, means of computing tensile strength, Equation 14.55 is used, which incorporates the nominal bolt area and the ratio of 0.76. Note that yielding is not considered a failure mode for bolts; only fracture needs to be considered. The resistance factor for bolts in tension is taken as $\phi = 0.80$.

$$T_n = 0.76 A_b F_{ub} \tag{14.55}$$

$$A_b = \left(\frac{\pi}{4}\right) d^2 \tag{14.56}$$

14.8.1.1.2 Shear Failure

The failure mode of bolts loaded in shear is fracture of the fastener on the plane of loading, which may exclude the threads or not exclude the threads depending on the thickness of the plies that are joined, the length of the fastener used, and the number and location of washers used, as illustrated in Figure 14.21. Generally, the shear strength of a single fastener loaded through its shank is approximately equal to 0.60 A_b F_{ub}. When the load is shared by a group of fasteners, however, the load is not shared equally and a reduction of 20% in required. Furthermore, a second reduction of 20% is required when the threads of the fasteners are not excluded from the shear plane.

$$R_n = 0.48 A_b F_{ub} N_s \tag{14.57}$$

$$R_n = 0.38 A_b F_{ub} N_s \tag{14.58}$$

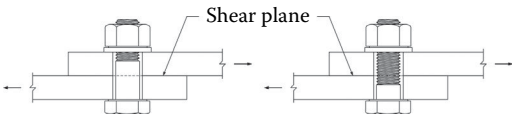

FIGURE 14.21 Illustration of threads excluded and not excluded from the shear plane.

14.8.1.1.3 Tension and Shear Interaction

When a bolt is loaded in tension and shear simultaneously, an interaction equation may be required to compute the fastener strength under the combined loading. When the shear force that the fastener is subjected to is less than 33% of the applied tensile force, the interaction is neglected. When the shear force is greater than 33% of the tensile force, however, Equation 14.59 is used to compute the strength under the combined loading. This formulation is based on an elliptical relationship between shear and tension on the failure envelope of the fastener, as described in Kulak et al., 2001.

$$T_n = 0.76 A_b F_{ub} \sqrt{1 - \left(\frac{P_u}{\phi_s R_n} \right)^2} \tag{14.59}$$

14.8.1.1.4 Connection Slip

When bolted connections area loaded in shear, the mechanism of load transfer from one member to the other is by means of either friction between the connection plies or by means of bearing between the bolts and inside of the bolt holes. In some cases, the frictional resistance of the connection is used to transfer the loads and the connection is designed as slip critical. In other cases, the frictional resistance is not relied upon for load transfer, is considered only to be a byproduct of the bolt pretension, and the joint is designed as a bearing connection. Even when a joint is considered to be slip critical, it must also be able to transfer all loads through bearing to accommodate the potential of connection slip and the bolt shear strength and bearing strength must be sufficient to carry the loads in the absence of friction.

The slip resistance of a connection is computed, as shown in Equation 14.60, and is dependent on the normal force imparted on the connection by the bolt pretension, P_t, the coefficient of friction, K_s, on the faying surfaces (the surfaces that are in contact within the connection), the number of faying surfaces or slip planes present in the connection, N_s, and to a lesser extent, the type of hole used in the connection, K_h. Pretension is prescribed in both AISC (2010b) and AASHTO (2012), and the number of slip planes is self-evident.

$$R_n = K_h K_s N_s P_t \tag{14.60}$$

The coefficient of friction is taken as a function of the surface condition. Class A surfaces include unpainted clean mill scale and blast-cleaned surfaces with Class A coatings and are assigned a condition factor of $K_s = 0.33$. Class B surfaces include unpainted blast-cleaned surfaces and blast-cleaned surfaces with Class B coatings, and are assigned a condition factor of $K_s = 0.50$. Class C surfaces include hot-dip galvanized surfaces roughened by wire brushing after galvanizing, and area assigned a condition factor of $K_s = 0.33$.

The effect of hole size and type is more on of the consequences of slip than it is on the actual slip resistance of a connection. Slippage of a joint with standard holes results in a displacement of up to roughly 1/8 in, whereas slippage of a joint with long slots loaded parallel to the slot may result in a displacement of up to ¾ in depending on the size of bolt used. This is reflected in the hole size factor, which is taken as $K_h = 1.00$ for connections with standard holes, $K_h = 0.85$ for connections with oversize holes or short slots, $K_h = 0.70$ for connections with long slots loaded perpendicular to the slot, and $K_h = 0.60$ for connections with long slots that are loaded parallel to slot.

14.8.1.1.5 Bolt Bearing

When a connection slips and the bolts bear against the inside of their holes, inelastic deformation occurs at relatively low loads. Excessive deformations of the plies being joined because of bearing stresses constitute a failure mode that must be investigated. (It is interesting to note that this failure mode is often referred to as a bolt-bearing failure, but the failure is in fact in the metal being joined and not in the bolts themselves.) Equation 14.61 gives the bearing strength of a single fastener, corresponds to a bearing deformation of approximately 1/4 in, where d is the diameter of the fastener, t is the thickness of a ply being considered, and F_u is the tensile strength of the ply being considered.

$$R_n = 2.4dtF_u \tag{14.61}$$

A second failure mode that is often considered at the same time as bolt bearing is bolt tearout. In this case material between the bolt hole and the end of the connected member, or material between adjacent bolt holes tears out in shear. The capacity of a bolt failing in this mode is given by Equation 14.62, where L_c is the clear distance between a hole and edge of a ply or the clear distance between adjacent bolts holes, t is the thickness of a ply being considered, and F_u is the tensile strength of the ply being considered.

$$R_n = 1.2L_ctF_u \tag{14.62}$$

14.8.2 Welds and Welded Connections

Welding of steel is governed AWS D1.1 in the case of buildings and general structures and AWS D1.5 for bridges. The following discussion of welding will focus on joint types, weld types, welding processes, and weld strength. Joint types include tee, butt, corner, lap, and corner joints, as illustrated in Figure 14.22. Weld types are limited to fillet welds, groove welds, plug welds, and slot welds as shown in Figures 14.23 through 14.26.

Welding process refers to the specific manner in which the weld metal is deposited making the finished welded joint. In all cases, an electric current is passed through an electrode to the base metal that creates heat that melts the weld metal and the base metal in the immediate area of the joint. Mixing of the weld and base metal occurs under the protection of a small gaseous cloud created by a flux and the two metals cool creating a continuous joint. In the case of shielded metal arc welding (SMAW often referred to as "stick welding"), the electrode is a rod approximately 12–16 in in length with the fluxing agent applied to the exterior of the electrode as a clay-like substance that burns during the welding process to form the gaseous cloud. In the case of flux core arc welding (FCAW), the electrode is a hollow wire with the cavity filled with a fluxing agent that burns during the process forming the gaseous shield. In the case of gas metal arc welding (GMAW), the electrode is a solid wire and the gaseous shield is

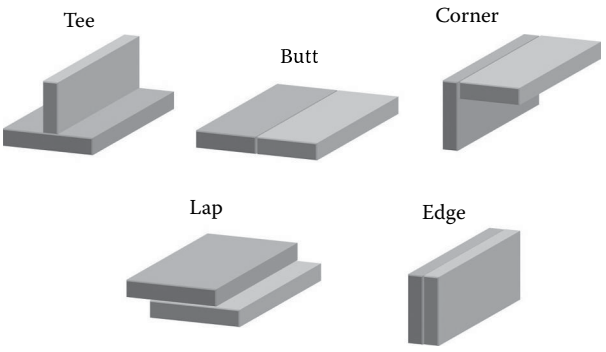

FIGURE 14.22 Joint types for welded joints.

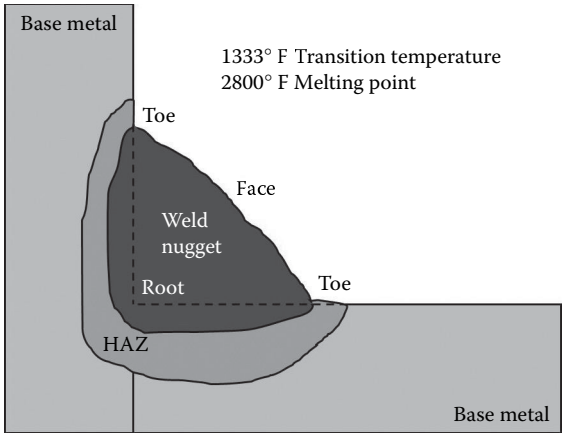

FIGURE 14.23 Profile for a fillet weld on a corner joint.

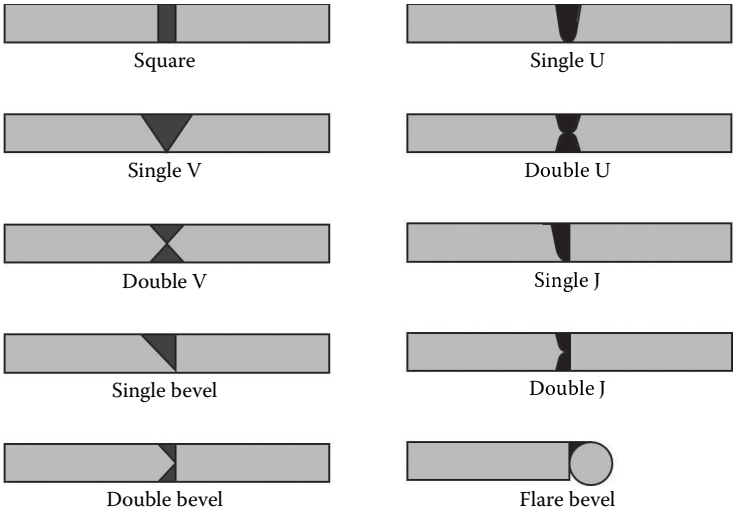

FIGURE 14.24 Types of groove welds for a butt joint.

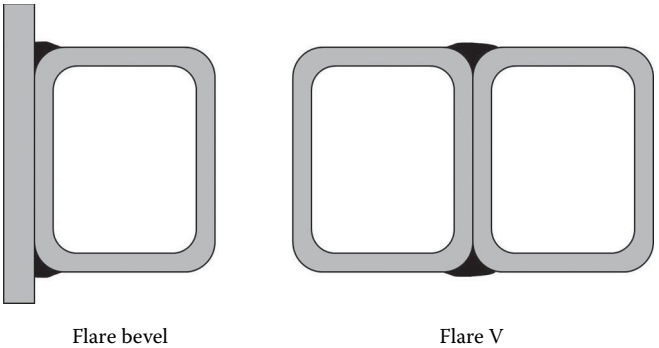

FIGURE 14.25 Flare bevel and flare versus groove welds.

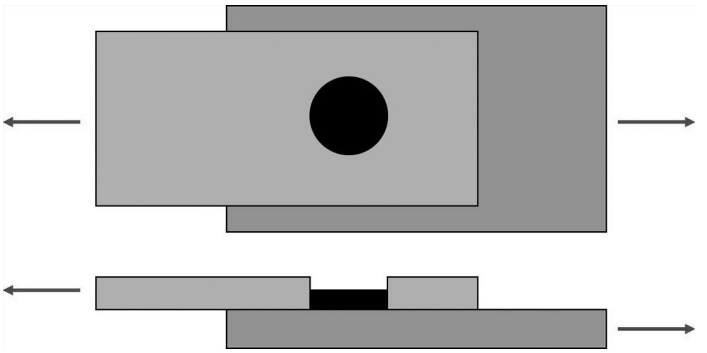

FIGURE 14.26 Plug or slot welds.

provided directly by means of an inert gas that is part of the welding equipment. Submerged arc welding (SAW) is an automated process where the electrode is again a solid wire and a flux, which is burned during the process forming the gaseous shield, is applied ahead of the weld such that the weld arc is submerged in the flux. Electroslag welding (ESW) is another automated process wherein the parts to be joined are oriented vertically and the gap between the parts is filled from the bottom up in a continuous pass to complete the joint.

14.8.2.1 Fillet Weld Strength

The strength of a fillet weld is based on a shear failure through the throat of the weld nugget. Regardless of how the joint is loaded, it is always assumed to fail in shear. Fillet welds are sized based on the leg dimension, w, and the face of the weld is taken as 45°, thus the throat thickness, t, is computed as $0.7071w$ as illustrated in Figure 14.27. Given that, the capacity of the weld is computed as shown in Equation 14.63, where F_{EXX} is the tensile strength of the weld metal and L is the length of the weld. Note that when submerged arc welding is used, improved penetration of the weld into the root of the joint is achieved and for fillet welds larger than 3/8 in an additional 0.11 in is permitted to be added to the throat. Also note that in addition to checking the strength of the weld metal, the strength of the base metal that is joined should also be checked. In checking the base metal strength, it is important to note that it is not the interface between the base metal and weld metal that is checked; instead it is the base metal adjacent to the weld that is checked as illustrated in Figure 14.27b.

$$R_n = 0.6F_{EXX}0.7071wL \tag{14.63}$$

14.8.2.2 Groove Weld Strength

The strength of a full penetration groove weld loaded in tension or compression perpendicular to the joint (Figure 14.28a) or in tension or compression parallel to the joint (Figure 14.28b), is taken as being greater than the strength of the base metal that is joined. As such, there is no strength check required for the weld metal of a full penetration groove weld. For a full penetration groove weld loaded in shear, the strength of the weld metal is taken as $0.6F_{EXX}A_w$, where A_w is the effective area of the weld, typically taken as the thickness of the base metal times the length of the joint. The strength of the base metal must also be checked.

Partial penetration groove welds are prohibited in almost all cases because of their poor fatigue resistance. Where permitted, the strength of a partial penetration groove weld loaded in compression perpendicular to the joint (Figure 14.29a) or tension or compression parallel to the joint (Figure 14.29b) is taken as the strength of the connected base metal. Where permitted, the strength of a partial penetration

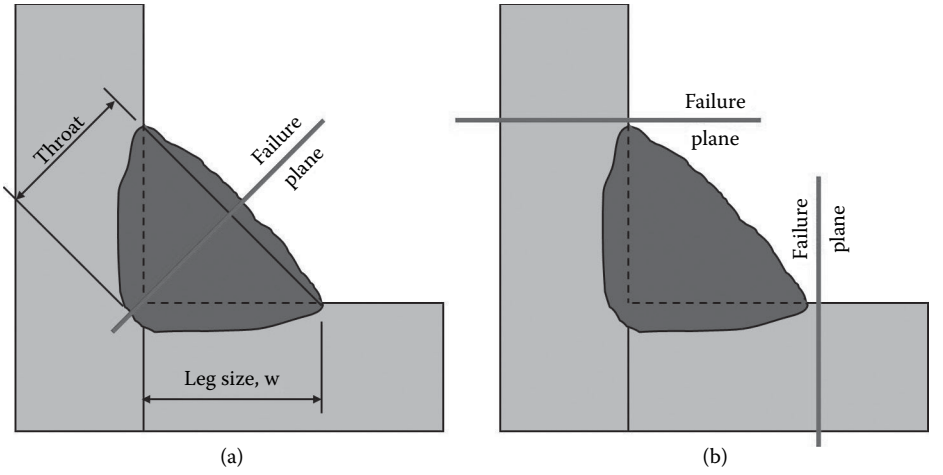

FIGURE 14.27 (a) Throat dimension and failure plane of a fillet weld and (b) failure plane of adjacent base metal.

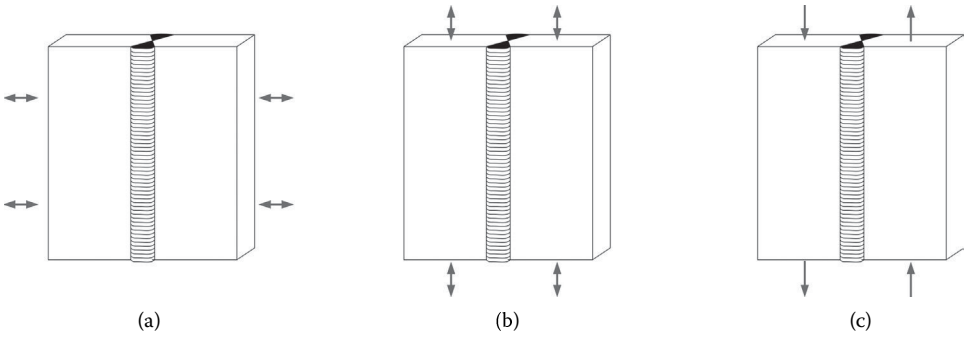

FIGURE 14.28 Loading conditions of full penetration groove welds.

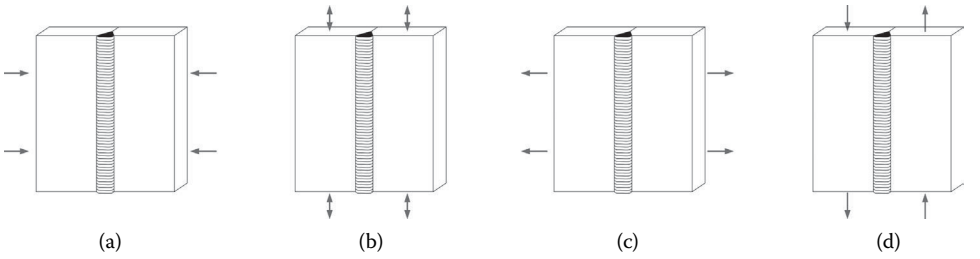

FIGURE 14.29 Loading conditions for partial penetration groove welds.

groove weld loaded in tension perpendicular to the joint (Figure 14.29c) or partial penetration groove welds loaded in shear (Figure 14.29d) is taken as $0.6F_{EXX}A_w$.

Defining Terms

A_{eff} Effective area in the threaded portion of a bolt (in^2)
A_b Nominal area of the unthreaded portion of a bolt (in^2)
A_f Area of a flange (in^2)
A_g Gross area (in^2)

A_n Net area (in^2)
A_w Area of a web (in^2)
B_f Breadth of a flange (in)
C Ratio of shear buckling capacity to plastic shear capacity
C_b Moment gradient factor
C_{EQ} Carbon equivalent of base metal
C_w Warping constant (in^6)
CI Corrosion index
D Depth of the web (in)
D_c Depth of the web in compression (in)
E Modulus of elasticity (ksi)
F_{cr} Critical buckling stress (ksi)
F_{EXX} Tensile strength of weld metal (ksi)
F_y Yield strength of base metal (ksi)
F_{yr} Yield strength of base metal less the residual stress (ksi)
F_{yw} Yield strength of the web (ksi)
F_u Tensile strength of base metal (ksi)
F_{ub} Tensile strength of bolt material (ksi)
G Shear modulus of elasticity (ksi)
J Torsional constant (in^4)
K Effective length factor
K_h Hole factor for bolt slip
K_s Condition factor for bolt slip
L Length of a member (in)
L Connection length (in)
L Length of a weld (in)
L_c Clear distance between bolt holes, or between a bolt hole and the end of a part (in)
L_b Unbraced length of the bending member (in)
L_p Unbraced length of a bending member corresponding to M_p (in)
L_r Unbraced length of a bending member corresponding to M_r (in)
M_{cr} Critical buckling moment (k-in)
M_p Plastic moment of a bending member (k-in)
M_r Yield moment of a bending member accounting for residual stresses (k-in)
M_y Yield moment of a bending member (k-in)
M_{yc} Yield moment of a bending member with respect to the compression flange (k-in)
N_s Number of shear planes
P_{cr} Critical load causing buckling in compression (kip)
P_c Force in compression
P_{cf} Force in the compression flange of a member
P_t Force in the tension
P_{tf} Force in the tension flange of a member
P_{wc} Force in the portion of the web of a member that is in compression
P_{wt} Force in the portion of the web of a member that is in tension
P_e Elastic buckling load of the compression member (ksi)
P_o Crushing load of the compression member (ksi)
P_t Pretension force in a bolt (kip)
Q Slender element reduction parameter
Q_a Slender element reduction parameter for stiffened elements
Q_s Slender element reduction parameter for unstiffened elements
R_b Load shedding factor

R_h Hybrid girder factor
R_{pc} Web plastification factor with respect to the compression flange
R_{pt} Web plastification factor with respect to the tension flange
S_x Elastic section modulus about the x axis (in^3)
S_{xc} Elastic section modulus about the x axis with respect to the compression flange (in^3)
SF Shape factor
U Shear lag reduction coefficient
V_{cr} Critical load causing buckling in shear (kip)
V_p Plastic shear force (kip)
a Spacing of intermediate connectors in a built-up column (in)
a_{wc} Ration of A_w to A_f
b Width of a plate or plate element of a cross section (in)
d Nominal diameter of a bolt (in)
h Height of the web of an I-shaped section (in)
h Distance between flange centroids (in)
k Boundary condition parameter for plate buckling
k_v Boundary condition parameter for plate buckling in shear
r Radius of gyration (in)
r_{ib} Element radius of gyration parallel to member axis of buckling (in)
r_i minimum radius of gyration of an individual element
r_t Radius of gyration of the compression flange and one-third of the depth of the web in compression (in)
r_s Radius of gyration about the cross-sectional axis perpendicular to the plane of buckling
t Thickness of a plate or plate element of a cross section (in)
t_f Thickness of a flange (in)
t_w Thickness of a web (in)
w Leg size of a weld (in)
$\overline{x}$ Connection eccentricity (in)
α Separation ratio for built-up columns
ϕ Resistance factor
λ_p Slenderness parameter needed to sustain significant plasticity
λ_r Slenderness parameter needed to achieve yielding
τ_{cr} Critical shear-buckling stress (ksi)
ν Poisson's ratio

References

AASHTO. 2012. *AASHTO LRFD Bridge Design Specifications*. US Customary Units, 2012. American Association of State Highway and Transportation Officials, Washington, DC.

AISC. 2010a. *Steel Construction Manual* (14th Edition). American Institute of Steel Construction, Chicago, IL.

AISC. 2010b. *Specification for Structural Steel Buildings*. ANSI/AISC 360-10. American Institute of Steel Construction, Chicago, IL.

ASTM A325 – 10e1. 2010. *Standard Specification for Structural Bolts, Steel, Heat Treated, 120/105 ksi Minimum Tensile Strength*, ASTM International, West Conshohocken, PA.

ASTM A370 – 12a. 2012. *Standard Test Methods and Definitions for Mechanical Testing of Steel Products*, ASTM International, West Conshohocken, PA.

ASTM A490 – 12. 2012. *Standard Specification for Structural Bolts, Alloy Steel, Heat Treated, 150 ksi Minimum Tensile Strength*, ASTM International, West Conshohocken, PA.

ASTM E8 /E8M – 11. 2011. *Standard Test Methods for Tension Testing of Metallic Materials,* ASTM International, West Conshohocken, PA.

ASTM F436 – 11. 2011. *Standard Specification for Hardened Steel Washers*, ASTM International, West Conshohocken, PA.

ASTM F1852 – 11. 2011. *Standard Specification for "Twist Off" Type Tension Control Structural Bolt/Nut/ Washer Assemblies, Steel, Heat Treated, 120/105 ksi Minimum Tensile Strength*, ASTM International, West Conshohocken, PA.

ASTM F2280 – 12. 2012. *Standard Specification for "Twist Off" Type Tension Control Structural Bolt/Nut/ Washer Assemblies, Steel, Heat Treated, 150 ksi Minimum Tensile Strength*, ASTM International, West Conshohocken, PA.

AWS. 2010a. *Structural Welding Code – Steel* (22nd Edition). ANSI/AWS D1.1/D1.1M: 2010. American Welding Society, Doral, FL.

AWS. 2010b. *Bridge Welding Code*. AASHTO/AWS D1.5M/D1.5:2010. American Welding Society, Doral, FL.

Basler, K. 1961. Strength of Plate Girders in Shear. *Journal of the Structural Division*, ASCE, 87(ST7), 151–180.

Kulak, G. L., Fisher, J. W., and Struik, J. H. 2001. *Guide to Design Criteria for Bolted and Riveted Joints* (2nd Edition). American Institute of Steel Construction, Chicago, IL.

Pollack, H. W. 1988. *Materials Science and Metallurgy* (4th Edition). Prentice-Hall, Englewood Cliffs, NJ.

Salmon, C. G., and Malhas, F. A. 2009. *Steel Structures—Design and Behavior* (5th Edition). Harper Collins, New York, NY.

Somayaji, S. 2001. *Civil Engineering Materials* (2nd Edition). Prentice-Hall, Englewood Cliffs, NJ.

Ziemian, R. D. 2010. *Guide to Stability Design Criteria for Metal Structures* (6th Edition). John Wiley & Sons, Hoboken, NJ.

15

Timber Design

Kenneth J. Fridley
University of Alabama

Lian Duan
California Department of Transportation

15.1 Introduction

Wood is one of the earliest building materials, and as such often its use has been based more on tradition than principles of engineering. However, the structural use of wood and wood-based materials has increased steadily in recent times, including a renewed interest in the use of timber as a bridge material. Supporting this renewed interest has been an evolution of our understanding of wood as a structural material and ability to analyze and design safe, durable, and functional timber bridge structures.

An accurate and complete understanding of any material is key to its proper use in structural applications, and structural timber and other wood-based materials are no exception to this requirement. This chapter focuses on introducing the fundamental mechanical and physical properties of wood that govern its structural use in bridges. Following this introduction of basic material properties, a presentation of common timber bridge types is made along with a discussion of fundamental considerations for the design of timber bridges.

15.1.1 Timber as a Bridge Material

Wood has been widely used for short- and medium-span bridges. Although wood has the reputation of being a material that provides only limited service life, wood can provide long-standing and serviceable bridge structures when properly protected from moisture. For example, many covered bridges from the

early nineteenth century still exist and are in use. Today, rather than protecting wood by a protective shelter as with the covered bridge of yesteryear, the use of wood preservatives that inhibit moisture and biological attack have been used to extend the life of modern timber bridges.

As with any structural material, the use of wood must be based on a balance between its inherent advantages and disadvantages, as well as consideration of the advantages and disadvantages of other construction materials. Some of the advantages of wood as a bridge material include the following:

- Strength
- Lightweight
- Constructability
- Energy absorption
- Economics
- Durability
- Aesthetics

These advantages must be considered against the three primary disadvantages:

- Decay
- Insect attack
- Combustibility

Wood can withstand short-duration overloading with little or no residual effects. Wood bridges require no special equipment for construction and can be constructed in virtually any weather conditions without any negative effects. It is competitive with other structural materials in terms of both first-costs and life-cycle costs. Wood is a naturally durable material resistant to freeze-thaw effects as well as deicing agents. Furthermore, large size timbers provide good fire resistance due to natural charring. However, if inadequately protected against moisture, wood is susceptible to decay and biological attack. With proper detailing and the use of preservative treatments, the threat of decay, and insects can be minimized. Finally, in many natural settings, wood bridges offer an aesthetically pleasing and unobtrusive option.

15.1.2 Past, Present, and Future of Timber Bridges

The first bridges built by humans were probably constructed with wood, and the use of wood in bridges continues today. As recent as a century ago, wood was still the dominant material used in bridge construction. Steel became an economical and popular choice for bridges in the early 1900s. Also during the early part of the twentieth century, reinforced concrete became the primary bridge deck material and another economical choice for the bridge superstructure. However, important advances were made in wood fastening systems and preservative treatments, which would allow for future developments for timber bridges. Then, in the mid-twentieth century, glued-laminated timber (or glulams) was introduced as a viable structural material for bridges. The use of glulams grew to become the primary material for timber bridges and has continued to grow in popularity. Today, there is a renewed interest in all types of timber bridges. Approximately 8% (37,000) of the bridges listed in the National Bridge Inventory in the United States having spans >20 ft (6.10 m) are constructed entirely of wood and 11% (51,000) use wood as one of the primary structural materials (Ritter and Ebeling, 1995). Table 15.1 lists the top 10 world's longest timber bridge spans. The future use of timber as a bridge material will not be restricted just to new construction. Owing to its high strength-to-weight ratio, timber is an ideal material for bridge rehabilitation of existing timber, steel, and concrete bridges.

15.2 Properties of Wood and Wood Products

It is important to understand the basic structure of wood in order to avoid many of the pitfalls relative to the misuse and/or misapplication of the material. Wood is a natural, cellular, anisotropic, hyrgothermal, and viscoelastic material, and by its natural origins contains a multitude of inclusions and other defects.

TABLE 15.1 Top 20 Longest Timber Bridge Spans

Rank	Bridge Name	Main Span Length m (ft)	Structure Features	Total Length m (ft)	Year Opened	Usage	Country	References
1	Remseck Neckar Bridge	80 (262.5)	Three Trusses	85 (278.9)	1990	Pedestrian	Germany	Remseck Neckar Bridge (2013)
2	Essing Bridge	73 (239.5)	Stress ribbon	192 (629.9)	1992	Pedestrian	Germany	Culling (2009).
3	Stuttgart – Bad Cannstatt Bridge	72 (239.5)	Stress ribbon	158 (518.4)	1977	Pedestrian	Germany	Baláž (2013) Stuttgart – Bad Cannstatt Bridge (2013)
4	Flisa Bridge	71 (232.9)	Truss, arch	181.5 (595.6)	2003	Hwy	Norway	Flisa Bridge (2013)
5	Tynset bridge,	70 (229.7)	Arch-truss	124 (406.8)	2001	Hwy	Norway	Nordic (2013)
6	Maribyrnong River Footbridge	68 (223.1)	Two-hinged arch	68 (223.1)	1995	Pedestrian	Australia	BSC (2013)
7	Sioux Narrows Bridge	64 (210.0)	Howe Truss	64 (210.0)	1936		Canada	Sioux Narrows Bridge (2013)
8	Bridgeport Covered Bridge	63.4 (208)	arch	71.0 (233)	1862	Hwy	USA	Bridgeport Covered Bridge (2013)
9	Jackson Covered Bridge	58.4 (191.5)	Covered	61.0 (200)	2000		USA	Jackson Covered Bridge (2013)
10	Hartland Bridge	55.86 (181.3)	Howe truss	391 (1282.8)	1901	Hwy	Canada	Hartland Bridge (2013)
11	Dragon's tail bridge	55 (180.4)	Stress ribbon	225 (738.2)	2007	Pedestrian	Germany	Dragon's tail bridge (2013)
12	Office Bridge	54.9 (180)	Howe Truss		1944	Hwy	USA	Oregon (2013)
13	Erdberger Steg Bridge	52.5 (172.2)	Rigid Frame	85.2 (279.5)	2003	Pedestrian	Austria	Baláž (2013) Erdberger Steg Bridge (2013)
14	Greensborough Footbridge	50 (164.0)	Three-hinged arch	50 (164.0)	1975	Pedestrian	Australia	BSC (2013)
15	Great Karikobozu Bridge	50 (164.0)	King-Post Truss	140 (459.3)	2002	Hwy	Japan	Nagai, et al. (2013)
16	Måsør Bridge	50		83	2005	Hwy	Norway	Aasheim (2011)
17	Vaires-sur-Marne Footbridge	49 (160.8)	Covered arch	75 (246.1)	2004	Pedestrian	France	Baláž (2013) Vaires-sur-Marne Footbridge (2013)
18	Dell' Accademia Bridgee	48 (157.5)	Arch	48 (157.5)	1933	Pedestrian	Italy	Pilot (2007)
19	Kicking Horse Bridge	46 (150.0)	Burr arch	46 (150.0)	2001	Pedestrian	Canada	Golden (2013)
20	Smolen–Gulf Bridge	45.7 (150)	truss	186.8 (613)	2008	Hwy	USA	Smolen–Gulf Bridge (2013)

The term "defect" may be misleading. Knots, grain characteristics (e.g., slope of grain, spiral grain, etc.), and other naturally occurring irregularities do reduce the effective strength of the member, but are accounted for in the grading process and in the assignment of design values. On the other hand, splits, checks, dimensional warping, etc., are the result of the drying process and, although they are accounted for in the grading process, may occur after grading and may be more accurately termed "defects." The reader is referred to basic texts that present a basic description of the fundamental structure and physical properties of wood as a material (e.g., USDA, 2010; Bodig and Jayne, 1982; Freas, 1995).

15.2.1 Physical Properties

One physical aspect of wood that deserves attention here is the effect of moisture on the physical and mechanical properties and performance of wood. Many problems encountered with wood structures, especially bridges, can be traced to moisture. The amount of moisture present in wood is described by the moisture content (MC), which is defined by the weight of the water contained in the wood as a percentage of the weight of the oven-dry wood. As wood is dried, water is first evaporated from the cell cavities then, as drying continues, water from the cell walls is drawn out. The point at which free water in the cell cavities is completely evaporated, but the cell walls are still saturated, is termed the fiber saturation point (FSP). The FSP is quite variable among and within species, but is on the order of 24–34%. The FSP is an important quantity since most physical and mechanical properties are dependent on changes in MC below the FSP, and the MC of wood in typical structural applications is below the FSP. Finally, wood releases and absorbs moisture to and from the surrounding environment. When the wood equilibrates with the environment and moisture is not transferring to or from the material, the wood is said to have reached its equilibrium moisture content (EMC). Table 15.2 provides the average EMC as a function of dry-bulb temperature and relative humidity. The *Wood Handbook* (USDA, 2010) provides other tables that are specific for given species or species groups and allow designers better estimates in-service MCs that are required for their design calculations.

Wood shrinks and swells as its MC changes below the FSP; above the FSP, shrinkage and swelling can be neglected. Wood machined to a specified size at a MC higher than that expected in service will therefore shrink to a smaller size in use. Conversely, if the wood is machined at an MC lower than that expected in service, it will swell. Either way, shrinkage and swelling due to changes in MC must be accounted for in design. In general, the shrinkage along the grain is significantly less than that across the grain. For example, as a rule of thumb, a 1% dimensional change across the grain can be assumed for each 4% change in MC, whereas a 0.02% dimensional change in the longitudinal direction may be assumed for each 4% change in MC. More accurate estimates of dimensional changes can be made with the use of published values of shrinkage coefficients for various species (*c.f.*, USDA, 2010).

In addition to simple linear dimensional changes in wood, drying of wood can cause warp of various types. Bow (distortion in the weak direction), crook (distortion in the strong direction), twist (rotational distortion), and cup (cross-sectional distortion similar to bow) are common forms of warp and, when excessive, can adversely affect the structural use of the member. Finally, drying stresses (internal stress resulting from differential shrinkage) can be quite significant and lead to checking (cracks formed along the growth rings) and splitting (cracks formed across the growth rings).

15.2.2 Mechanical Properties

The mechanical properties of wood are also functions of the MC. Above the FSP, most properties are invariant with changes in MC, but most properties are highly affected by changes in the MC below the FPS. For example, the modulus of rupture of wood increases by nearly 4% for a 1% decrease in MC below the FSP. The following equation is a general expression for relating any mechanical property to MC

TABLE 15.2 Moisture Content (%) of Wood in Equilibrium with Temperature and Relative Humidity

	Relative Humidity (%)																			
Temperature (°F)	5	10	15	20	25	30	35	40	45	50	55	60	65	70	75	80	85	90	95	98
32	1.4	2.6	3.7	4.6	5.5	6.3	7.1	7.9	8.7	9.5	10.4	11.3	12.4	13.5	14.9	16.5	18.5	21.0	24.3	26.9
41	1.4	2.6	3.7	4.6	5.5	6.3	7.1	7.9	8.7	9.5	10.4	11.3	12.3	13.5	14.9	16.5	18.5	21.0	24.3	26.9
50	1.4	2.6	3.6	4.6	5.5	6.3	7.1	7.9	8.7	‘9.5	10.3	11.2	12.3	13.4	14.8	16.4	18.4	20.9	24.3	26.9
59	1.3	2.5	3.6	4.6	5.4	6.2	7.0	7.8	8.6	9.4	10.2	11.1	12.1	13.3	14.6	16.2	18.2	20.7	24.1	26.8
68	1.3	2.5	3.5	4.5	5.4	6.2	6.9	7.7	8.5	9.2	10.1	11.0	12.0	13.1	14.4	16.0	17.9	20.5	23.9	26.6
77	1.3	2.4	3.5	4.4	5.3	6.1	6.8	7.6	8.3	9.1	9.9	10.8	11.7	12.9	14.2	15.7	17.7	20.2	23.6	26.3
86	1.2	2.3	3.4	4.3	5.1	5.9	6.7	7.4	8.1	8.9	9.7	10.5	11.5	12.6	13.9	15.4	17.3	20.8	23.3	26.0
95	1.2	2.3	3.3	4.2	5.0	5.8	6.5	7.2	7.9	8.7	9.5	10.3	11.2	12.3	13.6	15.1	17.0	20.5	22.9	25.6
104	1.1	2.2	3.2	4.1	5.0	5.7	6.4	7.1	7.8	8.6	9.3	10.1	11.1	12.2	13.4	14.9	16.8	20.3	22.7	25.4
113	1.1	2.2	3.2	4.0	4.9	5.6	6.3	7.0	7.7	8.4	9.2	10.0	11.0	12.0	13.2	14.7	16.6	20.1	22.4	25.2
122	1.1	2.1	3.0	3.9	4.7	5.4	6.1	6.8	7.5	8.2	8.9	9.7	10.6	11.7	12.9	14.4	16.2	18.6	22.0	24.7
131	1.0	2.0	2.9	3.7	4.5	5.2	5.9	6.6	7.2	7.9	8.7	9.4	10.3	11.3	12.5	14.0	15.8	18.2	21.5	24.2

$$P_{MC} = P_{12}\left(\frac{P_{12}}{P_g}\right)^{\left(\frac{12-MC}{FSP-MC}\right)} \tag{15.1}$$

where P_{MC} is property of interest at any MC below the FSP, P_{12} the property at 12% MC, and P_g property in the green condition (at FSP).

For structural design purposes, using an equation such as 15.1 would be cumbersome. Therefore, design values are typically provided for a specific maximum MC (e.g., 19%) and adjustments are made for "wet use."

Load history can also have a significant effect on the mechanical performance of wood members. The load that causes failure is a function of the rate and duration of the load applied to the member. That is, a member can resist higher magnitude loads for shorter durations or, stated differently, the longer a load is applied, the less able a wood member is able to resist that load. This response is termed load duration effects in wood design. Figure 15.1 illustrates this effect by plotting the time-to-failure as a function of the applied stress expressed in terms of the short term (static) ultimate strength. There are many theoretical models proposed to represent this response, but the line shown in Figure 15.1 was developed at the U.S. Forest Products Laboratory in the early 1950s (Wood, 1951) and is the basis for current design "load duration" adjustment factors.

The design factors derived from the relationship illustrated in Figure 15.1 are appropriate only for stresses and not for stiffness or, more precisely, the modulus of elasticity. Related to load duration effects, the deflection of a wood member under sustained load increases over time. This response, termed creep effects, must be considered in design when deformation or deflections are critical from either a safety or serviceability standpoint. The main parameters that significantly affect the creep response of wood are stress level, MC, and temperature. In broad terms, a 50% increase in deflection after a year or two is expected in most situations, but can easily be upward of 200% given certain conditions (Fridley, 1992). In fact, if a member is subjected to continuous moisture cycling, a 100%–150% increase in deflection could occur in a matter of a few weeks. Unfortunately, the creep response of wood, especially considering the effects of moisture cycling, is poorly understood and little guidance is available to the designer.

Wood, being a fibrous material, is naturally resistance to fatigue effects, particularly when stressed along the grain. However, the fatigue strength of wood is negatively affected by the natural presence of inclusions and other defects. Knots and slope of grain in particular reduce fatigue resistance. Regardless of this, wood performs well in comparison to structural steel and concrete. In fact, the fatigue strength of wood has been shown to be approximately double that of most metals when evaluated at comparable stress

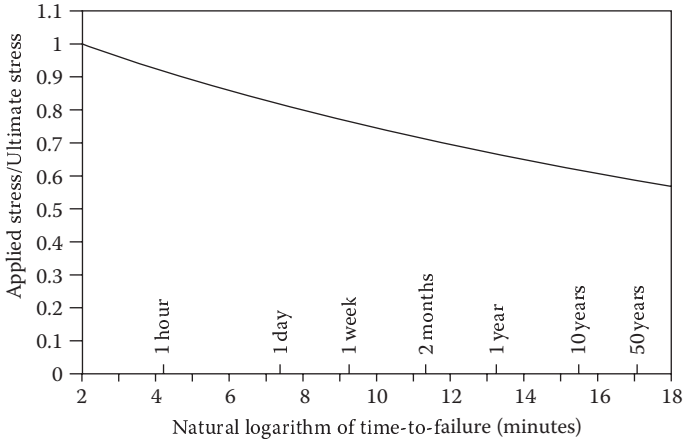

FIGURE 15.1 Load duration behavior of wood.

levels relative to the material's ultimate strength (USDA, 2010). The potential for fatigue-induced failure is considered to be rather low for wood, and thus fatigue is typically not considered in timber bridge design.

15.2.3 Wood and Wood-Based Materials for Bridge Construction

The natural form of timber is the log. In fact, many primitive and "rustic" timber bridges are nothing more than one or more logs tied together. For construction purposes, however, it is simpler to use rectangular elements in bridges and other structures rather than round logs. Solid sawn lumber is cut from logs and was the mainstay of timber bridge construction for years. Solid sawn lumber comes in a variety of sizes including boards (<1.5 in (38 mm) thick and from 1.5 to 15 in (38–387 mm) wide), dimension lumber 1.5–3.5 in (38–89 mm) thick and 1.5–15 in (38–387 mm) wide), and timbers (anything >3.5 in by 3.5 in [89–89 mm]). Based on size and species, solid sawn lumber is graded by various means, including visual grading, machine-evaluated lumber (MEL), and machine stress rated (MSR), and engineering design values are assigned.

In the mid-1900s glued-laminated timber began to receive significant use in bridges. Glulams are simply large sections formed by laminating dimension lumber together. Sections as large as 4 ft (1.5 m) deep are feasible with glulams. Today, while solid sawn lumber is still used extensively, the changing resource base and shift to plantation-grown trees has limited the size and quality of the raw material. Therefore, it is becoming increasingly difficult to obtain high quality, large dimension timbers for construction. This change in raw material, along with a demand for stronger and more cost-effective material, initiated the development of alternative products that can replace solid lumber such as glulams.

Other engineered products such as wood composite I-joists and structural composite lumber (SCL) also resulted from this evolution. SCL includes such products as laminated veneer lumber (LVL) and parallel strand lumber (PSL). These products have steadily gained popularity and now are receiving widespread use in building construction, and they are beginning to find their way into bridge construction as well. The future may see expanded use of these and other engineered wood composites.

15.2.4 Preservation and Protection

As mentioned previously, one of the major advances in the twentieth century allowing for continued and expanded use of timber as a bridge material is pressure treatment. Two basic types of wood preservatives are used: oil-type preservatives and waterborne preservatives. Oil-type preservatives include creosote, pentachlorophenol (or "penta"), and copper naphthenate. Creosote can be considered the first effective wood preservative and has a long history of satisfactory performance. Creosote also offers protection against checking and splitting caused by changes in MC. Although creosote is a natural byproduct from coal tar, penta is a synthetic pesticide. Penta is an effective preservative treatment; however, it is not effective against marine borers and is not used in marine environments. Penta is a "restricted-use" chemical, but wood treated with penta is not restricted. Copper naphthenate has received recent attention as a preservative treatment, primarily because of being considered an environmentally safe chemical, while still giving satisfactory protection against biological attack. Its primary drawback is its high cost relative to other treatments. All these treatments generally leave the surface of the treated member with an oily and unfinishable surface. Furthermore, the member may "bleed" or leach preservative unless appropriate measures are taken.

Most timber bridge applications utilize oil-type preservatives for structural elements such as beams, decks, piles, and so on. They offer excellent protection against decay and biological attack, are noncorrosive, and are relatively durable. Oil-type preservatives are not, however, recommended for bridge elements that may have frequent or repeated contact by humans or animals since they can cause skin irritations.

Waterborne preservatives have the advantage of leaving the surface of the treated material clean and, after drying, are able to be painted or stained. They also do not cause skin irritations and, therefore, can be used where repeated human and/or animal contact is expected. Waterborne preservatives use formulations of inorganic arsenic compounds in a water solution. They do, however, leave the material with a light green, gray, or brownish color. But again, the surface can be later painted or stained. A wide

variety of waterborne preservatives are available, but the most common include: chromated copper arsenate (CCA), ammoniacal copper arsenate (ACA), and ammoniacal copper zinc arsenate (ACZA). Leaching of these chemicals is not a problem with these formulations since they each are strongly bound to the wood. CCA is commonly used to treat southern pine, ponderosa pine, and red pine, all of which are relatively accepting of treatment. ACA and ACZA are used with species that are more difficult to treat, such as Douglas-fir and Larch. One potential drawback to CCA and ACA is a tendency to be corrosive to galvanized hardware. The extent to which this is a problem is a function of the wood species, the specific preservative formulation, and service conditions. However, such corrosion seems not to be an issue for hot-dipped galvanized hardware typical in bridge applications.

Waterborne preservatives are used for timber bridges in applications, where repeated or frequent contact with humans or animals is expected. Such examples include handrails and decks for pedestrian bridges. Additionally, waterborne preservatives are often used in marine applications where marine borer hazards are high.

Anytime a material is altered due to chemical treatment, its micro-level structure may be affected thus affecting its mechanical properties. Oil-type preservatives do not react with the cellular structure of the wood and, therefore, have little to no effect on the material's mechanical properties. Waterborne preservatives do react, however, with the cell material thus can affect properties. Although this is an area of ongoing research, indications are that the only apparent affect of waterborne preservatives is to increase load duration effects, especially when heavy treatment is used for salt-water applications. Currently, no adjustments are recommended for design values of preservative treated wood versus untreated materials.

In addition to preservative treatment, fire-retardant chemical treatment is also possible to inhibit combustion of the material. These chemicals react with the cellular structure in wood and can cause significant reductions in the material's mechanical properties, including strength. Generally, fire-retardants are not used in bridge applications. However, if fire-retardant treated material is used, the designer should consult with the material producer or treater to obtain appropriate design values.

15.3 Types of Timber Bridges

Timber bridges come in a variety of forms, many having evolved from tradition. Most timber bridges designed today, however, are the results of fairly recent developments and advances in the processing and treating of structural wood. The typical timber bridge is a single- or two-span structure. Single-span timber bridges are typically constructed with beams and a transverse deck or a slab-type longitudinal deck. Two-span timber bridges are often beams with transverse decks. These and other common timber bridge types are presented in this section.

15.3.1 Superstructures

As with any bridge, its structural makeup can be divided into three basic components: the superstructure, the deck, and the substructure. Timber bridge superstructures can be further classified into six basic types: beam superstructures, longitudinal deck (or slab) superstructures, trussed superstructures, trestles, suspension bridges, and glued-laminated arches.

15.3.1.1 Beam Superstructures

The most basic form of a timber beam bridge is a log bridge. It is simply a bridge wherein logs are laid alternately tip-to-butt and bound together. A transverse deck is then laid over the log beams. Obviously, spans of this type of bridge are limited to the size of logs available, but spans of 20–60 ft (6–18 m) are reasonable. The service life of a log bridge is typically 10–20 years.

The sawn lumber beam bridge is another simple form. Typically comprised of closely spaced 4–8 in (100–200 mm) wide by 12–18 in (300–450 mm) deep beams, sawn lumber beams are usually used for

clear spans up to 30 ft (9 m). With the appropriate use of preservative treatments, sawn lumber bridges have average service lives of approximately 40 years. A new alternative to sawn lumber is SCL bridges. Primarily, LVL has been used in replacement of solid sawn lumber in bridges. LVL can be effectively treated and can offer long service as well.

Glued-laminated timber beam bridges are perhaps the most prevalent forms of timber bridges today. A typical glulam bridge configuration is illustrated in Figure 15.2. This popularity is primarily because

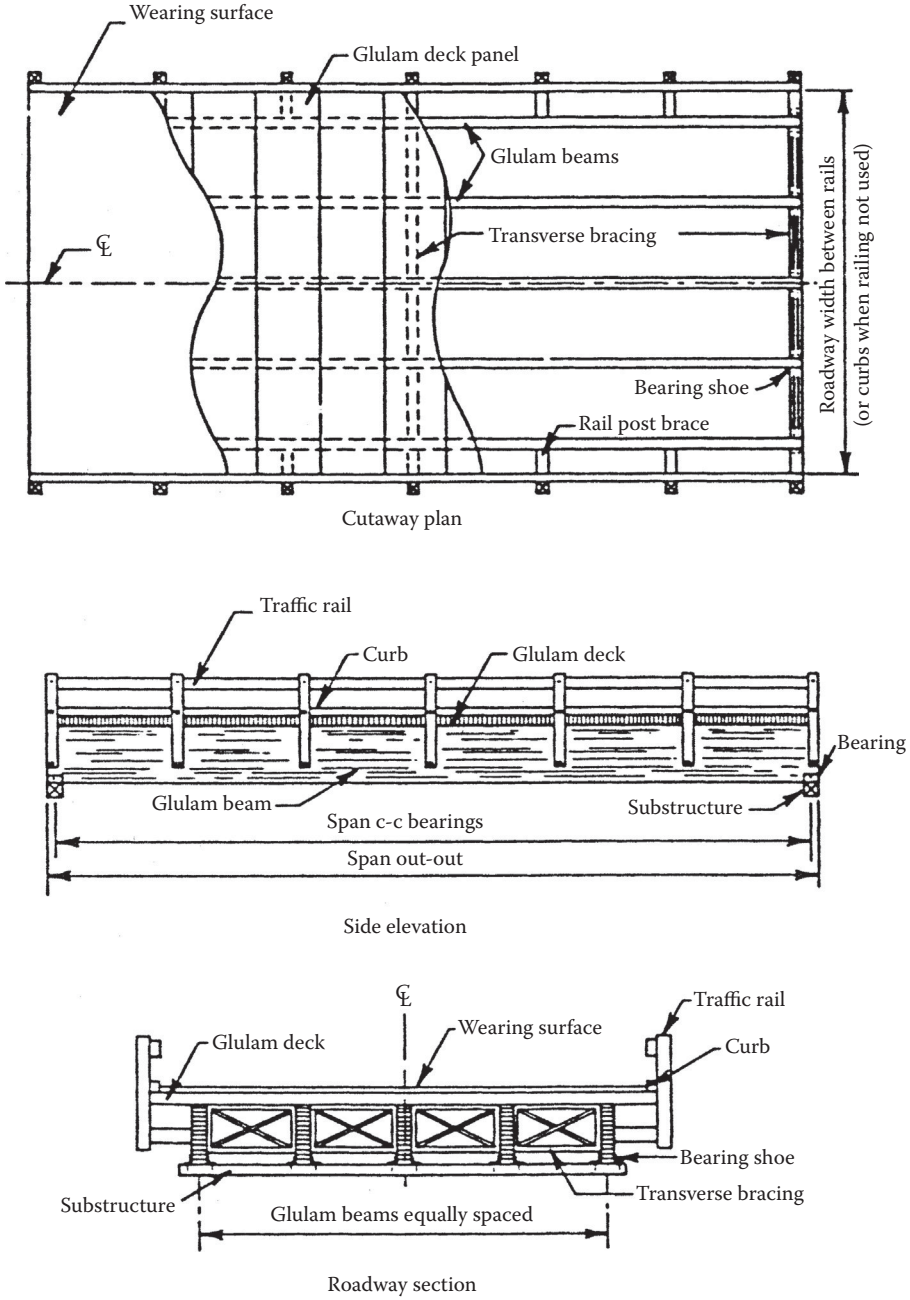

FIGURE 15.2 Glulam beam bridge with transverse deck. (From Ritter, M. A., *Timber Bridges: Design, Construction, Inspection, and Maintenance*, EM 7700-8. U.S.D.A., Forest Service, Washington, DC, 1990. With permission.)

of large variety of member sizes offered by glulams. Commonly used for clear spans ranging from 20 to 80 ft (6–24 m), glulam beam bridges have been used for clear spans up to 148 ft (45 m). Transportation restrictions rather than material limitations limit the length of beams, and therefore bridges. Since glued-laminated timber can be satisfactorily treated with preservatives, they offer a durable and long-lasting structural element. When designed such that field cutting, drilling, and boring are avoided, glulam bridges can provide a service life of at least 50 years.

15.3.1.2 Longitudinal Deck Superstructures

Longitudinal deck (or slab) superstructures are typically either glued-laminated or nail-laminated timber placed longitudinally to span between supports. A relatively new concept in the longitudinal deck systems is the stress-laminated timber bridge, which is similar to previous two forms but that continuity in the system is developed through the use of high-strength steel tension rods. In any case, the wide faces of the laminations are oriented vertically rather than horizontally as in a typical glulam beam. Figure 15.3 illustrates two types of glulam longitudinal decks: noninterconnected and interconnected. Since glulam timbers have depths typically less than the width of a bridge, two or more segments must be used. When continuity is needed, shear dowels must be used to provide interconnection between slabs. When continuity is not required, construction is simplified. Figure 15.4 illustrates a typical stress-laminated section.

Longitudinal deck systems are relatively simple, and offer a relatively low profile making them an excellent choice when vertical clearance is a consideration. Longitudinal decks are economical choices

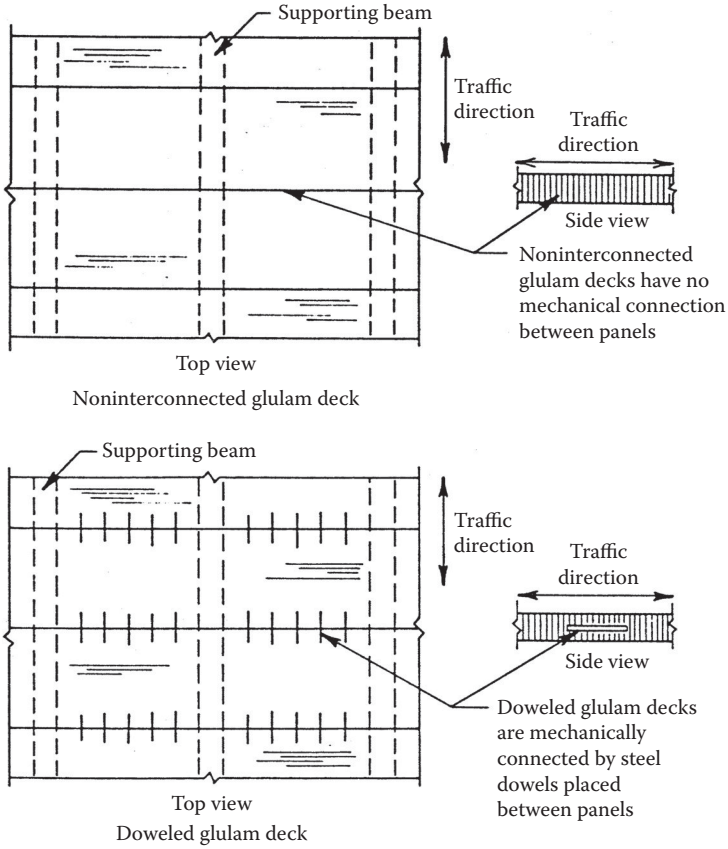

FIGURE 15.3 Glulam longitudinal decks. (From Ritter, M. A., *Timber Bridges: Design, Construction, Inspection, and Maintenance*, EM 7700-8. U.S.D.A., Forest Service, Washington, DC, 1990. With permission.)

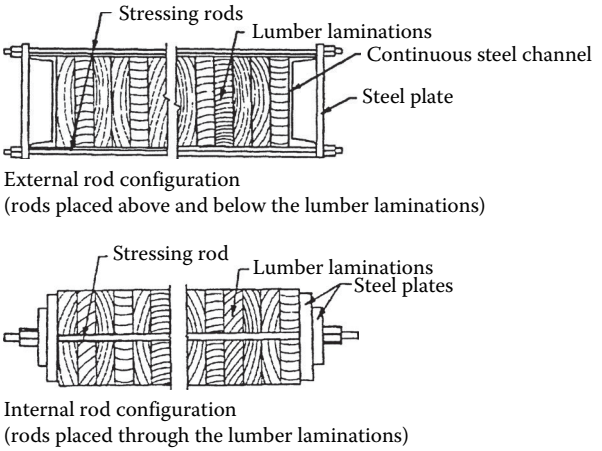

FIGURE 15.4 Stress-laminated bridge. (From Ritter, M. A., *Timber Bridges: Design, Construction, Inspection, and Maintenance*, EM 7700-8. U.S.D.A., Forest Service, Washington, DC, 1990. With permission.)

for clear spans up to approximately 33 ft (10 m). Since the material can be effectively treated, the average service life of a longitudinal timber deck superstructure is at least 50 years. However, proper maintenance is required to assure that an adequate level of prestress is maintained in stress-laminated systems.

15.3.1.3 Trussed Superstructures

Timber trusses were used extensively for bridges in the first half of the twentieth century. Many different truss configurations were used including king post, multiple king posts, Pratt, Howe, lattice, long, and bowstring trusses to name a few. Clear spans of up to 245 ft (75 m) were possible. However, their use has declined due primarily to high fabrication, erection, and maintenance costs. When timber trusses are used today, it is typically driven more by aesthetics than structural performance or economics.

15.3.1.4 Trestles

Another form of timber bridge that saw its peak usage in the first half of the twentieth century was the trestle. A trestle is a series of short-span timber superstructures supported on a series of closely spaced timber bents. During the railroad expansion in the early to mid 1900s, timber trestles were a popular choice. However, their use has all but ceased because of high fabrication, erection, and maintenance costs.

15.3.1.5 Suspension Bridges

A timber suspension bridge is simply a timber deck structure supported by steel cables. Timber towers in turn, support the steel suspension cables. Although there are examples of vehicular timber suspension bridges, the more common use of this form of timber bridge is as a pedestrian bridge. They are typically used for relatively long clear spans, upward of 500 ft (150 m). Since treated wood can be used throughout, 50 year service lives are expected.

15.3.1.6 Glued-Laminated Arches

One of the most picturesque forms of timber bridges is perhaps the glulam arch. Constructed from segmented circular or parabolic glulam arches, either two- or three-hinge arches are used. The glulam arch bridge can have clear spans in excess of 200 ft (60 m), and since glulam timber can be effectively treated, service lives of at least 50 years are well within reason. Although the relative first and life-cycle costs of arch bridges have become high, they are still a popular choice when aesthetics is an issue.

15.3.2 Timber Decks

The deck serves two primary purposes: (1) it is the part of the bridge structure that forms the roadway and (2) it distributes the vehicular loads to the supporting elements of the superstructure. Four basic types of timber decks are sawn lumber planks, nailed-laminated decks, glued-laminated decks, and composite timber-concrete decks. The selection of a deck type depends mainly on the level of load demand.

15.3.2.1 Lumber Planks

The lumber plank deck is perhaps the simplest deck type. It is basically sawn lumber, typically 3–6 in (75–150 mm) thick and 10–12 in (250–300 mm) wide, placed flatwise and attached to the supporting beams with large spikes. Generally, the planks are laid transverse to the beams and traffic flow, but can be placed longitudinally on cross-beams as well. Lumber planks are only used for low-volume bridges. They are also of little use when protection of the supporting members is desired since water freely travels between adjacent planks. Additionally, when a wearing surface such as asphalt is desired, lumber planks are not recommended since deflections between adjacent planks will results in cracking and deterioration of the wearing surface.

15.3.2.2 Nailed-Laminated and Glued-Laminated Decks

Nailed- and glued-laminated decks are essentially as described previously for longitudinal deck (or slab) superstructures. Nailed-laminated systems are typically 0.75 in (38 mm) thick by 3.5–11.25 in (89–285 mm) deep lumber placed side-by-side and nailed or spiked together along its length. The entire deck is nailed together to act as a composite section and oriented such that the lumber is laid transverse to the bridge span across the main supporting beams, which are spaced from 2 to 6 ft (0.6–1.8 m). Once a quite popular deck system, its use has declined considerable in favor of glued-laminated decks.

A glulam deck is a series of laminated panels, typically 5.125–8.125 in (130–220 mm) thick by 3–5 ft (0.9–1.5 m) wide. The laminations of the glulam panel are oriented with their wide face vertically. Glulam decks can be used with the panels in the transverse or longitudinal direction. They tend to be stronger and stiffer than nailed-laminated systems, and offer greater protection from moisture to the supporting members. Finally, although doweled glulam panels (see Figure 15.3) cost more to fabricate, they offer the greatest amount of continuity. With this continuity, thinner decks can be used and improved performance of the wearing surface is achieved due to reduced cracking and deterioration.

15.3.2.3 Composite Timber-Concrete Decks

The two basic types of composite timber-concrete deck systems are the T-section and the slab (see Figure 15.5). The T-section is simply a timber stem, typically a glulam, with a concrete flange that also serves as the bridge deck. Shear dowels are plates are driven into the top of the timber stem and develop the needed shear transfer. For a conventional single-span bridge, the concrete is proportioned such that it takes all the compression force, while the timber resists the tension. Composite T-sections have seen some use in recent years, however high fabrication costs has limited their use.

Composite timber-concrete slabs were used considerably during the second quarter of the twentieth century, but receive little use today. They are constructed with alternating depths of lumber typically nailed laminated and a concrete slab is poured directly on top of the timber slab. With a simple single span, the concrete again carries the compressive flexural stresses with the timber carries the flexural stresses. Shear dowels or plates are driven into the timber slab to provide the required shear transfer between the concrete and timber.

15.3.3 Substructures

The substructure supports the bridge superstructure. Loads transferred from the superstructures to the substructures are, in turn, transmitted to the supporting soil or rock. Specific types of substructures that can be used are dependent on a number of variables, including bridge loads, soil, and site

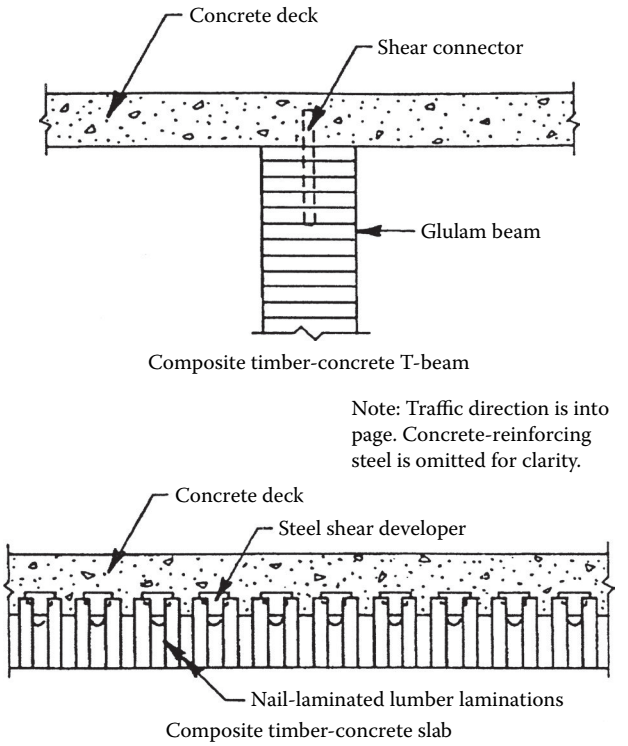

FIGURE 15.5 Composite timber-concrete decks. (From Ritter, M. A., *Timber Bridges: Design, Construction, Inspection, and Maintenance*, EM 7700-8. U.S.D.A., Forest Service, Washington, DC, 1990. With permission.)

conditions, and so on. Although a timber bridge superstructure can be adapted to virtually any type of substructure regardless of material, the following presentation is focused on timber substructures, specifically timber abutments and bents.

15.3.3.1 Abutments

Abutments serve the dual purpose of supporting the bridge superstructure and the embankment. The simplest form of a timber abutment is a log, sawn lumber, or glulam placed directly on the embankment as a spread footing. However, this form is not satisfactory for any structurally demanding situation. A more common timber abutment is the timber pile abutment. Timber piles are driven to provide the proper level of load carrying capacity through either end bearing or friction. A backwall and wingwalls are commonly added using solid sawn lumber to retain the embankment. A continuous cap beam is connected to the top of the piles on which the bridge superstructure is supported. A timber post abutment can be considered a hybrid between the spread footing and pile abutment. Timber posts are supported by a spread footing, and a backwall and wingwalls are added to retain the embankment. Pile abutments are required when soil conditions do not provide adequate support for a spread footing or when uplift is a design concern.

15.3.3.2 Bents

Bents are support systems used for multi-span bridges between the abutments. Essentially timber bents are formed from a set of timber piles with lumber cross-bracing. However, when the height of the bent exceeds that available for a pile, frame bents are used. Frame bents were quite common in the early days of the railroad, but because of high cost of fabrication and maintenance, they are not used often for new bridges.

15.4 Basic Design Concepts

In this section, the basic design considerations and concepts for timber bridges are presented. The discussion should be considered an overview of the design process for timber bridges, not a replacement for specifications or standards.

15.4.1 Specifications and Standards

The design of timber bridge systems has evolved over time from what was tradition and essentially a "master builder" approach. Design manuals and specifications are available for use by engineers involved with or interested in timber bridge design. These include *Timber Bridges: Design, Construction, Inspection, and Maintenance* (Ritter, 1990), AASHTO *LRFD Bridge Design Specifications* (AASHTO, 2012), and AASHTO *Standard Specifications for Highway Bridges* (AASHTO, 2002). The wood industry, through the American Wood Council (AWC), American Forest and Paper Association, published the *National Design Specification for Wood Construction* (AF&PA, 2005) to provide design values for solid sawn lumber and glued-laminated timber for both allowable stress design (ASD) and load and resistance factor design formats. Rather than presenting those aspects of bridge design common to all bridge types, the focus of the following presentation will be on those aspects specific to timber bridge design. Since highway bridge design is often governed by AASHTO, focus will be on AASHTO specifications. However, AF&PA is the association overseeing the engineering design of wood, much like ACI is for concrete and AISC is for steel, and AF&PA recommended design procedures will also be presented.

15.4.2 Design Values

Design values for wood are provided in a number of sources, including 2005 AF&PA specifications and AASHTO specifications (AASHTO, 2012). Although the design values published by these sources are based on the same procedures per ASTM standards, specific values differ because of assumptions made for end-use conditions. The designer must take care to use the appropriate design values with their intended design specification(s). For example, the design should not use AF&PA design values directly in AASHTO design procedures since AF&PA and AASHTO make different end-use assumptions.

15.4.2.1 AF&PA "Reference" Design Values

The *ASD/LRFD Manual* for Engineered Wood Construction (2005) provides nominal design values for visually and mechanically graded lumber, glued-laminated timber and connections. These values include reference bending strength, F_b; reference tensile strength parallel to the grain, F_t; reference shear strength parallel to the grain, F_v; reference compressive strength parallel and perpendicular to the grain, F_c and $F_{c\perp}$, respectively; reference bearing strength parallel to the grain, F_g; and reference modulus of elasticity, E; and are appropriate for use with the LRFD provisions.

Similarly, the *2005 NDS Supplement: Design Values for Wood Construction* (AF&PA, 2005) provides tables of design values for visually graded and MSR lumber, and glued-laminated timber for use in ASD. The basic quantities are the same as with the LRFD, but are in the form of allowable stresses and are appropriate for use with the ASD provisions of the NDS®. Additionally, the NDS® provides tabulated allowable design values for many types of mechanical connections.

One main difference between the ASD and LRFD design values, other than the ASD prescribing allowable stresses and the LRFD prescribing nominal strengths, is the treatment of duration of load effects. Allowable stresses (except compression perpendicular to the grain) are tabulated in the NDS® and elsewhere for an assumed 10-year load duration in recognition of the duration of load effect discussed previously. The allowable compressive stress perpendicular to the grain is not adjusted since a deformation definition of failure is used for this mode rather than fracture as in all other modes,

thus the adjustment has been assumed unnecessary. Similarly, the modulus of elasticity is not adjusted to a 10-year duration since the adjustment is defined for strength, not stiffness. For the LRFD, short-term (i.e., 20 minute) nominal strengths are tabulated for all strength values. In the LRFD, design strengths are reduced for longer duration design loads based on the load combination being considered. Conversely, in the NDS®, allowable stresses are increased for shorter load durations and decreased only for permanent (i.e., >10 years) loading.

15.4.2.2 AASHTO-LRFD "Base" Design Values

AASHTO-LRFD publishes its own design values that are different from those of the AF&PA *NDS*. AASHTO publishes base bending strength, F_{bo}; base tensile strength parallel to the grain, F_{to}; base shear strength parallel to the grain, F_{vo}; base compressive strength parallel and perpendicular to the grain, F_{co} and F_{cpo}, respectively; and base modulus of elasticity, E_0. Although the NDS publishes design values based on an assumed 10-year load duration and the AF&PA LRFD assumes a short-term (20-minute) load duration, AASHTO publishes design values based on an assumed 2 month duration.

Unfortunately, AASHTO's published design values are not as comprehensive (with respect to species, grades, sizes, as well as specific properties) as that of AF&PA. The AASHTO-LRFD does, however, provide for adjustments from AF&PA-published reference design values so they can be used in AASHTO specifications. For design values not provided in the AASHTO-LRFD, conversion factors are provided from NDS allowable stresses to AASHTO-LRFD base strengths. Table 15.3 provides these adjustments for solid sawn and glued-laminated timbers. The designer is cautioned that these conversion factors are from the NDS allowable stresses, not the AF&PA LRFD strength values.

15.4.3 Adjustment of Design Values

In addition to the providing reference or base design values, the AF&PA-NDS and the AASHTO-LRFD specifications provide adjustment factors to determine final adjusted design values. Factors to be considered include load duration (termed "time effect" in the LRFD), wet service, temperature, stability, size, volume, repetitive use, curvature, orientation (form), and bearing area. Each of these factors will be discussed further; however, it is important to note not all factors are applicable to all design values, nor are all factors included in all the design specifications. The designer must take care to properly apply the appropriate factors.

15.4.3.1 AF&PA Adjustment Factors

LRFD reference strengths and ASD allowable stresses are based on the following specified reference conditions: (1) dry use in which the maximum EMC does not exceed 19% for solid wood and 16% for glued wood products; (2) continuous temperatures up to 90°F (32°C), occasional temperatures up to 150°F (65°C) (or briefly exceeding 200°F (93°C) for structural-use panels); (3) untreated (except for poles and piles); (4) new material, not reused or recycled material; and (5) single members without load sharing

TABLE 15.3 Factors to Convert NDS-ASD Values to AASTHO-LRFD Values

	Property					
Material	F_{bo}	F_{vo}	F_{co}	F_{cpo}	F_{to}	E_o
Dimension lumber	2.35	3.05	1.90	1.75	2.95	0.90
Beams and Stringers posts and timbers	2.80	3.15	2.40	1.75	2.95	1.00
Glued laminated	2.20	2.75	1.90	1.35	2.35	0.83

or composite action. To adjust the reference design value for other conditions, adjustment factors are provided that are applied to the published reference design value:

$$R' = R \cdot C_1 \cdot C_2 \cdot C_n \tag{15.2}$$

where R' = adjusted design value (resistance), R = reference design value, and C_1, C_2, … C_n = applicable adjustment factors. Adjustment factors, for the most part, are common between LRFD and ASD. Many factors are functions of the type, grade, and/or species of material, whereas other factors are common to all species and grades. For solid sawn lumber, glued-laminated timber, piles, and connections, adjustment factors are provided in the AF&PA ASD/LRFD manual (AWC, 2005) and the NDS (AF&PA, 2005). For both LRFD and ASD, numerous factors need to be considered, including wet service, temperature, preservative treatment, fire-retardant treatment, composite action, load sharing (repetitive-use), size, beam stability, column stability, bearing area, form (i.e., shape), time effect (load duration), and so on. Many of these factors will be discussed as they pertain to specific designs; however, some of the factors are unique for specific applications and will not be discussed further. The four factors that are applied to all design properties are the wet service factor, C_M; temperature factor, C_t; preservative treatment factor, C_{pt}; and fire-retardant treatment factor, C_{rt}. Individual treaters provide the two treatment factors, but the wet service and temperature factors are provided in the AF&PA ASD/LRFD Manual. For example, when considering the design of solid sawn lumber members, the adjustment values given in Table 15.4 for wet service, which is defined as the maximum EMC exceeding 19%, and Table 15.5 for temperature, which is applicable when continuous temperatures exceed 90°F (32°C), are applicable to all design values. Often with bridges, since they are essentially exposed structures, the MC will be expected to exceed 19%. Similarly, temperature may be a concern, but not as commonly as MC.

Since, as discussed, LRFD and ASD handle time (duration of load) effects so differently and since duration of load effects are somewhat unique to wood design, it is appropriate to elaborate on it here. Whether using ASD or LRFD, a wood structure is designed to resist all appropriate load combinations—unfactored combinations for ASD and factored combinations for LRFD. The time effects (LRFD) and load duration (ASD) factors are meant to recognize the fact that the failure of wood is governed by a creep-rupture mechanism; that is, a wood member may fail at a load less than its short-term strength if that load is held for an extended period of time. In the LRFD, the time effect factor, λ, is based on the load combination being considered. In ASD, the load duration factor, C_D, is given in terms of the assumed cumulative duration of the design load.

15.4.3.2 AASHTO-LRFD Adjustment Factors

AASHTO-LRFD base design values are based on the following specified reference conditions: (1) wet use in which the maximum EMC exceeds 19% for solid wood and 16% for glued wood products (this is opposite from the dry use assumed by AF&PA, since typical bridge use implies wet use); (2) continuous

TABLE 15.4 AASHTO-LRFD Wet Service Factors, C_M

		F_{bo}			F_c				
Material	Thickness	$F_{bo}C_F$ <1.15 ksi (8 MPa)	$F_{bo}C_F$ <1.15 ksi (8 MPa)	F_{to}	$F_{co}C_F$ <0.75 ksi (5.2 MPa)	$F_{co}C_F$ <0.75 ksi (5.2 MPa)	F_{vo}	F_{cpo}	E_o
Sawn lumber	≤ 4 in. (90 mm)	1.00	0.85	1.00	1.00	0.80	0.97	0.67	0.90
	>4 in. (90 mm)	1.00	1.00	1.00	0.91	0.91	1.00	0.67	1.00
Glulams		0.8		0.8	0.73		0.875	0.53	0.833

TABLE 15.5 AF&PA-LRFD Temperature Adjustment Factors, C_t

	Dry Use		Wet Use	
Sustained Temperature (°F)	F_t, E	All Other Properties	F_t, E	All Other Properties
$T < 100$	1.0	1.0	1.0	1.0
$100 < T < 125$	0.9	0.8	0.9	0.7
$125 < T < 150$	0.9	0.7	0.9	0.5

temperatures up to 90°F (32°C), occasional temperatures up to 150°F (65°C); (3) untreated (except for poles and piles); (4) new material, not reused or recycled material; and (5) single members without load sharing or composite action. AASHTO has fewer adjustments available for the designer to consider, primarily but not entirely because of the specific application. To adjust the base design value for other conditions, AASHTO-LRFD provides the following adjustment equations:

$$F_b = F_{bo}C_{KF}C_M\left(C_F \text{ or } C_v\right)C_{fu}C_iC_dC_\lambda \tag{15.3}$$

$$F_v = F_{vo}C_{KF}C_MC_iC_\lambda \tag{15.4}$$

$$F_t = F_{to}C_{KF}C_MC_FC_iC_\lambda \tag{15.5}$$

$$F_c = F_{co}C_{KF}C_MC_FC_iC_\lambda \tag{15.6}$$

$$F_{cp} = F_{cpo}C_{KF}C_MC_iC_\lambda \tag{15.7}$$

$$E = F_oC_MC_i \tag{15.8}$$

where F = adjusted design value (resistance), F_b, F_v, F_t, F_c, or F_{cp}; F_o = base design value, F_{bo}, F_{vo}, F_{to}, F_{co}, or F_{cpo}; E = adjusted modulus of elasticity; E_o = reference modulus of elasticity; C_{KF} = format conversion factor; C_M = wet service factor; C_F = size adjustment factor; C_v = volume factor; C_{fu} = flat-use factor; C_i = incising factor; C_d = deck adjustment factor, and C_λ = time effect factor.

1. Format conversion factor, C_{KF}
   The format conversion factor were derived so that the same size member will be obtained based on both AASHTO-LRFD (AASHTO, 2012) and the NDS–ASD. $C_{KF} = 2.5/\phi$ except for compression perpendicular to grain, $C_{KF} = 2.1/\phi$.
2. Wet service factor, C_M
   The wet service factor mainly considers moisture effects. It is embedded in the published base design values specified by AF&PA. Unless otherwise noted, C_M should be assumed as unity. The only exception is when glulams are used and the moisture content is expected to be less than 16%. An increase in the design values is then allowed per Table 15.6. A similar increase is not allowed for lumber used at moisture contents less than 19% per AASHTO. This is a conservative approach in comparison to that of AF&PA.
3. Size factor, C_F
   The size factor is applicable only to bending, F_{bo} and is essentially the same as that used by AF&PA for solid sawn lumber. For sawn lumber beams with load applied to the narrow face and vertically laminated lumber, the size factor is defined

$$C_F = \left(\frac{12}{d}\right)^{\frac{1}{9}} \le 1.0 \tag{15.9}$$

TABLE 15.6 AASHTO-LRFD Moisture Content Adjustment Factors, C_M, for Glulam

Property					
F_b	F_v	F_c	F_{cp}	F_t	E
0.8	0.875	0.73	0.53	0.8	0.833

where d = width (in). The equation implies if lumber ≤12 in width is used, no adjustment is made. If, however, a width >12 in is used, a reduction in the published base bending design value is required.

4. Volume factor, C_V
   For horizontally glued-laminated timber with its width, depth, and length exceeding 12.0 in (300 mm), 5.125 in (130 mm), and 21.0 ft (6.4 m), respectively, when the load applied perpendicular to the wide face, the volume factor for glulam is given as

$$C_v = \left[\left(\frac{12}{d}\right)\left(\frac{5.125}{b}\right)\left(\frac{21}{L}\right)\right]^a \leq 1.0 \tag{15.10}$$

   where d = depth (in), b = width (in), L = span (ft), and a = 0.05 for southern pine and 0.10 for all other species glulam. C_V shall not be used simultaneously with the beam stability factor C_L. The lesser of two factors shall apply.
5. Flat-use factor, C_{fu}
   The flat-use factor is used when load applied to the wide face, but shall not apply to dimension lumber graded as Decking.
6. Incising factor, C_i
   When members are incised parallel to grain a maximum depth of 0.4 in, a maximum length of 0.375 in and a density of incisions up to 1100/ft^2, incising factor, $\boldsymbol{C_i}$ = 1.0 for F_{cpo}; 0.95 for E_o, 0.8 for F_{bo}, F_{to}, F_{co}, and F_{vo}, respectively.
7. Deck factor, C_d
   Deck adjustment factor, C_d, is again specific for the bending resistance, F_{bo}, of 2–4 in (–100 mm) wide lumber used in stress laminated and mechanically (nail or spike) laminated deck systems. For stress-laminated decks, the bending strength can be increased by a factor of C_d = 1.30 for select structural grade lumber, and C_d = 1.5 for no. 1 and no. 2 grade. For mechanically laminated decks, the bending strength of all grades can be increased by a factor of C_d = 1.15.
8. Time effects factor, C_λ
   Since, as discussed, AF&PA LRFD and ASD handle time (duration of load) effects so differently and since duration of load effects are somewhat unique to wood design, it is appropriate to elaborate on it here and understand how time effects are accounted for by AASHTO-LRFD. Implicit in the AASHTO-LRFD specification, C_λ = 1.0 is applied to Strength II, III, and Extreme Event I because of shorter duration of live load; C_λ = 0.8 is assumed for Strength I—vehicle live loads. The base design values are reduced by a factor of 0.80 for account for time effects. For Strength IV, however, a reduction of 0.6 is required. This load combination is for permanent loads consisting of dead load and earth pressure. The rationale behind this reduction is found in the AF&PA-LRFD time effects factors. For live load governed load combinations, AF&PA requires time effect factor = 0.8; and for dead load only, time effect factor of 0.6 is used. C_λ = 1.0.

15.4.3.3 Design Limit States

Timber bridge components are designed to satisfy the requirements of service, strength, and extreme event limit states for load combinations specified in AASHTO LRFD Table 3.4.1-1.

Service limit state for wood structure mainly controls deflection to prevent fasteners from loosening and brittle materials such as asphalt pavement, from cracking and breaking. Vehicular and pedestrian load deflection may be limited to Span/425, and the extreme relative deflection between adjacent edges due to vehicular load in wood planks and panels may be limited to 0.1 in. (AASHTO, 2012).

Strength limit states mainly consider axial, flexural, shear strength, stability, and wood components and connections due to vehicular related load combination. Resistance factors for strength limit states are discussed in Section 15.5. Extreme event limit state deals earthquake and appropriate collision forces by using the resistance factor of 1.0.

15.5 Components Design

The focus of the remaining discussion will be on the design provisions specified in the AASHTO-LRFD (AASHTO, 2012) for wood members. The design of wood beams follows traditional beam theory.

15.5.1 Flexural Members

The flexural strength of a beam is generally the primary concern in a beam design, but consideration of other factors such as horizontal shear, bearing, and deflection are also crucial for a successful design.

15.5.1.1 Moment Capacity

In terms of moment, the AASHTO-LRFD design factored resistance, M_r is given by

$$M_r = \phi M_n = \phi F_b S C_L \tag{15.11}$$

where ϕ = resistance factor for flexure = 0.85; M_n = nominal adjusted moment resistance; F_b = adjusted design value for flexure; S = section modulus; and C_L = beam stability factor.

The beam stability factor, C_L, is only used when considering strong axis bending since a beam oriented about its weak axis is not susceptible to lateral instability. Additionally, the beam stability factor need not exceed the value of the size effects factor. The beam stability factor is taken as 1.0 for members with continuous lateral bracing, otherwise C_L is calculated from

$$C_L = \frac{1+A}{1.9} - \sqrt{\frac{(1+A)^2}{3.61} - \frac{A}{0.95}} \tag{15.12}$$

where

$$C_L = \frac{1+A}{1.9} - \sqrt{\frac{(1+A)^2}{3.61} - \frac{A}{0.95}} \tag{15.13}$$

$$A = \frac{F_{bE}}{F_b} \tag{15.14}$$

$$F_{bE} = \frac{K_{bE} E}{R_b} \tag{15.15}$$

$$R_b = \sqrt{\frac{L_e d}{b^2}} \le 50 \tag{15.16}$$

$$K_{bE} = \begin{cases} 0.76 & \text{for visually graded lumber} \\ 0.98 & \text{for MEL lumber} \\ 1.06 & \text{for MSR lumber} \\ 1.10 & \text{for glulam and tension-reinforced glulam} \end{cases} \tag{15.17}$$

where E = modulus of elasticity; b = net width; d = net depth; L_e = effective length; and F_b = adjusted bending strength. The effective length, L_e, accounts for both the lateral motion and torsional phenomena and is given in the AASHTO-LRFD specifications for specific unbraced lengths, L_u, defined as the distance between points of lateral and rotations support.

$$L_E = \begin{cases} 2.06L_e & \text{for } L_u/d < 7 \\ 1.63L_u + 3d & \text{for } 7 \le L_u/d \le 14.3 \\ 1.84 & \text{for } L_u/d \le 14.3 \end{cases} \tag{15.18}$$

Although the basic adjustment factor for beam stability is quite similar between AASHTO and AF&PA, the consideration of beam stability and size effects combined differs significantly from the approach used by AF&PA. For solid sawn, AF&PA requires both the size factor and the beam stability factor apply. For glulams, AF&PA prescribes the lesser of the volume factor or the stability factor is to be used. AASHTO compared to AF&PA is potentially nonconservative with respect to lumber elements, conservative with respect to glulam elements.

15.5.1.2 Shear Capacity

Similar to bending, the basic design equation for the factored shear resistance of a rectangular cross-section, V_r, is given by

$$V_r = \phi V_n = \phi \frac{F_v bd}{1.5} \tag{15.19}$$

where ϕ = resistance factor for shear = 0.75; V_{an} = nominal adjusted shear resistance; F_v = adjusted shear strength. Since the last expression in (15.19) assumes a rectangular section, the nominal shear resistance could be determined from the relationship

$$V_n = \frac{F_v Ib}{Q} \tag{15.20}$$

where I = moment of inertia and Q = statical moment of an area about the neutral axis.

In timber bridges, notches are often made at the support to allow for vertical clearances and tolerances as illustrated in Figure 15.6; however, stress concentrations resulting from these notches significantly affect the shear resistance of the section. AASHTO-LRFD does not address this condition, but AF&PA does provide the designer with some guidance. At rectangular sections where the depth is reduced because of the presence of a notch in the tension face, the shear resistance of the notched section is determined from

$$V' = \left(\frac{2}{3} F_v' b d_n\right)\left(\frac{d_n}{d}\right)^2 \tag{15.21}$$

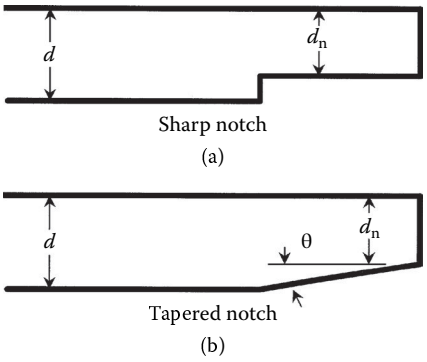

FIGURE 15.6 Notched beam: (a) sharp notch and (b) tapered notch.

where d = depth of the unnotched section and d_n = depth of the member after the notch. When the notch is made such that it is actually a gradual tapered cut at an angle θ from the longitudinal axis of the beam, the stress concentrations resulting from the notch are reduced and the above equation becomes

$$V' = \left(\frac{2}{3}F_v' b d_n\right)\left(1 - \frac{(d - d_n)\sin\theta}{d}\right)^2 \tag{15.22}$$

Similar to notches, connections too can produce significant stress concentrations resulting in reduced shear capacity. Where a connection produces at least one-half the member shear force on either side of the connection, the shear resistance is determined by

$$V' = \left(\frac{2}{3}F_v' b d_e\right)\left(\frac{d_e}{d}\right)^2 \tag{15.23}$$

where d_e = effective depth of the section at the connection that is defined as the depth of the member less the distance from the unloaded edge (or nearest unloaded edge if both edges are unloaded) to the center of the nearest fastener for dowel-type fasteners (e.g., bolts).

15.5.1.3 Bearing Capacity

The last aspect of beam design to be covered in this section is bearing at the supports. The governing design equation for factored bearing capacity perpendicular to the grain, P_{rp}, is

$$P_r = \phi P_n = \phi F_{cp} A_b C_b \tag{15.24}$$

where ϕ = resistance factor for compression = 0.90; P_n = nominal adjusted compression resistance perpendicular to the grain; F_{cp} = adjusted compression strength perpendicular to the grain, A_b = bearing area; and C_b = bearing factor.

The bearing area factor, C_b, allows an increase in the compression strength when the bearing length along the grain, l_b, is no more than 6 in (150 mm) along the length of the member, is at least 3 in (75 mm) from the end of the member, and is not in a region of high flexural stress. The bearing factor C_b is given by AF&PA as

$$C_b = \frac{l_b + 0.375}{l_b} \tag{15.25}$$

where l_b is in inch. This equation is the basis for the adjustment factors presented in the AASHTO-LRFD. For example, if a bearing length of 2 in is used, the bearing strength can be increased by a factor of (2 + 0.375)/2 = 1.19.

15.5.2 Axially Loaded Members

The design of axially loaded members is quite similar to that of beams. Tension, compression, and combined axial and flexural are addressed in AASHTO-LRFD (2012).

15.5.2.1 Tension Capacity

The governing design equation for factored tension capacity parallel to the grain, P_r, is

$$P_r = \phi P_n = \phi F_t A_n \tag{15.26}$$

where ϕ = resistance factor for tension = 0.80; P_n = nominal adjusted tension resistance parallel to the grain; F_t = adjusted tension strength; and A_n = smallest net area of the component.

15.5.2.2 Compression Capacity

In terms of compression parallel to the grain, the AASHTO-LRFD design factored resistance, P_r is given by

$$P_r = \phi P_n = \phi F_c A_g C_p \tag{15.27}$$

where ϕ = resistance factor for bending = 0.85; and P_n = nominal adjusted compression resistance; F_c = adjusted compression strength; A_g = gross cross-sectional area; and C_p = column stability factor.

The column stability factor, C_p, accounts for the tendency of a column to buckle. The factor is taken as 1.0 for members with continuous lateral bracing, otherwise C_p is calculated by

$$C_p = \frac{1+B}{2c} - \sqrt{\left(\frac{1+B}{2c}\right)^2 - \frac{B}{c}} \le 1.0 \tag{15.28}$$

$$B = \frac{F_{cE}}{F_c} \le 1.0 \tag{15.29}$$

$$F_{cE} = \frac{K_{cE} E d^2}{L_e^2} \tag{15.30}$$

$$c = \begin{cases} 0.85 & \text{for sawn lumber} \\ 0.85 & \text{for round timber piles} \\ 0.9 & \text{for glulam} \end{cases} \tag{15.31}$$

$$K_{cE} = \begin{cases} 0.52 & \text{for visually graded lumber} \\ 0.67 & \text{for MEL lumber} \\ 0.73 & \text{for MSR lumber} \\ 0.76 & \text{for glulam, tension-reinforced glulam and round piles} \end{cases} \tag{15.32}$$

where E = modulus of elasticity, d = net depth (about which buckling may occur), L_e = effective length = effective length factor times the unsupported length = KL_u.

15.5.3 Combined Axial and Flexural Members

15.5.3.1 Combined Tension and Flexure

AASHTO uses a linear interaction for tension and flexure to ensure that stress in tension face does not cause rupture (Equation 15.32) and member does not fail because of lateral torsional buckling of the compression face (Equation 15.33).

$$\frac{P_u}{P_r} + \frac{M_u}{M_r^*} \le 1.0 \tag{15.33}$$

$$\frac{M_u - \frac{d}{6} P_u}{M_r^{**}} \le 1.0 \tag{15.34}$$

where P_u and M_u = factored tension and moment loads on the member, respectively; P_r is factored tensile resistance; $M_r^* = \phi F_b S$; M_r^{**} = factored adjusted flexural resistance except C_v.

15.5.3.2 Combined Compression and Flexure

AASHTO uses a slightly different interaction for compression and bending than tension and bending:

$$\left(\frac{P_u}{P_r}\right)^2 + \frac{M_u}{M_r\left(1-\dfrac{P_u}{F_{cE}A_g}\right)} \le 1.0 \tag{15.35}$$

where P_u and M_u = factored compression and moment loads on the member, respectively, and P_r and M_r are the factored resistances as defined previously. The squared term on the compression term was developed from experimental observations and is also used in the 2005 NDS (AF&PA, 2005). However, AF&PA includes secondary moments in the determination of M_u, which AASHTO neglects. 2005 AF&PA NDS also includes biaxial bending in its interaction equations.

15.6 Connections

15.6.1 General

AASHTO-LRFD (2012) does not specifically address connections, so the designer is referred to the AF&PA NDS (2005). Decks must be attached to the supporting beams and beams to abutments such that vertical, longitudinal, and transverse loads are resisted. Additionally, the connections must be easily installed in the field. The typical timber bridge connection is a dowel-type connection directly between two wood components, or with a steel bracket.

The design of fasteners and connections for wood has undergone significant changes in recent years. Typical fastener and connection details for wood include nails, staples, screws, lag screws, dowels, and bolts. Additionally, split rings, shear plates, truss plate connectors, joist hangers, and many other types of connectors are available to the designer. The general LRFD design checking equation for connections is given as follows:

$$Z_u \le \lambda\phi Z' \tag{15.36}$$

where Z_u = connection force due to factored loads, λ = applicable time effect factor, ϕ = resistance factor for connections = 0.65, and Z' = connection resistance adjusted by the appropriate adjustment factors.

It should be noted that, for connections, the moisture adjustment is based on both in service condition and on conditions at the time of fabrication; that is, if a connection is fabricated in the wet condition but is to be used in service under a dry condition, the wet condition should be used for design purposes because of potential drying stresses that may occur. It should be noted that C_M does not account for corrosion of metal components in a connection. Other adjustments specific to connection type (e.g., end grain factor, C_{eg}; group action factor, C_g; geometry factor, C_Δ; toe-nail factor, C_{tn}; etc.) will be discussed with their specific use. It should also be noted that when failure of a connection is controlled by a nonwood element (e.g., fracture of a bolt), then the time-effects factor is taken as unity since time effects are specific to wood and not applicable to nonwood components.

In both LRFD and ASD, tables of reference resistances (LRFD) and allowable loads (ASD) are available that significantly reduce the tedious calculations required for a simple connection design. In this

section, the basic design equations and calculation procedures are presented, but design tables are not provided herein.

The design of general dowel-type connections (i.e., nails, spikes, screws, bolts, etc.) for lateral loading are currently based on possible yield modes. Based on these possible yield modes, lateral resistances are determined for the various dowel-type connections. Specific equations are presented in the following sections for nails and spikes, screws, bolts, and lag screws. In general, though, the dowel bearing strength, F_e, is required to determine the lateral resistance of a dowel-type connection. Obviously, this property is a function of the orientation of the applied load to the grain, and values of F_e are available for parallel to the grain, $F_{e||}$, and perpendicular to the grain, $F_{e\perp}$. The dowel bearing strength or other angles to the grain, $F_{e\theta}$, is determined by

$$F_{e\theta} = \frac{F_{e||} F_{e\perp}}{F_{e||} \sin^2 \theta + F_{e\perp} \cos^2 \theta} \tag{15.37}$$

where θ = angle between direction of load and direction of grain (longitudinal axis of member).

Nails, spikes, and screws are perhaps the most commonly used fastener in wood construction. Nails are generally used when loads are light such as in the construction of diaphragms and shear walls; however, they are susceptible to working loose under vibration or withdrawal loads. Common wire nails and spikes are quite similar, except that spikes have larger diameters than nails. Both a 12*d* (i.e., 12-penny) nail and spike are 3.5 in (88.9 mm) in length; however, a 12*d* nail has a diameter of 0.15 in (3.76 mm), whereas a spike has a diameter of 0.192 in (4.88 mm). Many types of nails have been developed to provide better withdrawal resistance, such as deformed shank and coated nails. Nonetheless, nails and spikes should be designed to carry laterally applied load and not withdrawal. Screws behavior in a similar manner to nails and spikes, but also provide some withdrawal resistance.

Bolts, lag screws and dowels are commonly used to connect larger dimension members where larger connection capacities are required. The provisions specified in NDS (AF&PA, 2005) are valid for bolts, lag screws, and dowels with diameters in the range of 0.25 in (6.3 mm) $\leq D \leq$ 1.0 in (25.4 mm).

15.6.2 Axial Resistance

For connections loaded axially, tension is of primary concern and is governed by either fastener capacity (e.g., yielding of the nail) or fastener withdrawal. The tensile resistance (withdraw design value) of the fastener (i.e., nail, spike, or screw) is determined using accepted metal design procedure. The reference withdrawal resistance (in lbs/in of penetration), for a single fastener, inserted in side grain, with its axis perpendicular to the wood fibers is given by

$$W = \begin{cases} 1800 G^{1.5} D^{0.75} & \text{for lag screws} \\ 2850 G^2 D & \text{for wood screws} \\ 1380 G^{2.5} D & \text{for nails and spikes} \\ \text{engineering machanics,} & \text{for drif bolts and pins} \end{cases} \tag{15.38}$$

where G is specific gravity of the wood; D is fastener diameter (in).

A minimum wood screw depth of penetration of at least 1.0 in (25 mm) or one-half the nominal length of the screw is required for Equation (15.38) to be applicable. No withdrawal resistance is assumed for nails, spikes, or wood screws used in end grain applications. For lag screwed, the end grain adjustment factor, C_{eg}, = 0.75 is applicable to the withdrawal resistance, and minimum edge and end distances, spacing are 1.5*D*, 4*D*, and 4*D*, respectively.

15.6.3 Lateral Resistance

The lateral shear resistance of single shear connections using dowel-type fasteners is taken as the least values determined by the following six yield limit equations.

$$\mathbf{I_m}: \qquad Z = \frac{Dl_m F_{em}}{R_d} \tag{15.39}$$

$$\mathbf{I_s}: \qquad Z = \frac{Dl_s F_{es}}{R_d} \tag{15.40}$$

$$\mathbf{II}: \qquad Z = \frac{k_1 Dl_s F_{es}}{R_d} \tag{15.41}$$

$$\mathbf{III_m}: \qquad Z = \frac{k_2 Dl_m F_{em}}{\left(1+2R_e\right)R_d} \tag{15.42}$$

$$\mathbf{II_s}: \qquad Z = \frac{k_3 Dl_s F_{em}}{\left(1+2R_e\right)R_d} \tag{15.43}$$

$$\mathbf{IV}: \qquad Z = \frac{D^2}{R_d}\sqrt{\frac{2F_{em}F_{yb}}{3\left(1+R_e\right)}} \tag{15.44}$$

$$k_1 = \frac{\sqrt{R_e + 2R_e^2\left(1+R_t+R_t^2\right)+R_t^2R_e^3} - R_e\left(1+R_t\right)}{\left(1+R_e\right)} \tag{15.45}$$

$$k_2 = -1+\sqrt{2\left(1+R_e\right)+\frac{2F_{yb}\left(1+2R_e\right)D^2}{3F_{em}l_m^2}} \tag{15.46}$$

$$k_3 = -1+\sqrt{\frac{2\left(1+R_e\right)}{R_e}+\frac{2F_{yb}\left(1+2R_e\right)D^2}{3F_{em}l_s^2}} \tag{15.47}$$

where D = diameter (in); t_s = thickness of the side member; F_{es} = dowel bearing strength of the side member, (psi); F_{em}, F_{es} = dowel bearing strength of the main member, (psi); R_e = ratio of dowel bearing strength of the main member to that of the side member = F_{em}/F_{es}; F_{yb} = bending yield strength of the dowel fastener; l_m = main member dowel bearing length (in); l_s = side member dowel bearing length (in); R_t = ratio of dowel bearing strength of the main member to that of the side member = l_m/l_s.

For fastener size $0.25'' \le D \le 1''$

$$R_d = \begin{cases} 4K_\theta & \text{for } \mathrm{I}_{m,}\,\mathrm{I}_s \\ 3.6K_\theta & \text{for II} \\ 3.2K_\theta & \text{for } \mathrm{III}_m,\,\mathrm{III}_s,\,\mathrm{IV} \end{cases} \tag{15.48}$$

For fastener size $D > 0.25$" with root diameter < 0.25"

$$R_d = (10D + 0.5)K_\theta \qquad \text{for all six yield modes} \tag{15.49}$$

For fastener size $0.17" < D < 0.25"$

$$R_d = 10D + 0.5 \qquad \text{for all six yield modes} \tag{15.50}$$

For fastener size $D < 0.17"$

$$R_d = 2.2 \qquad \text{for all six yield modes} \tag{15.51}$$

For multi-bolt, lag screw, and dowel connections, the least resistance is simply multiplied by the number of fasteners, n_f, in the connection detail. When multiple fasteners are used, the minimum spacing, edge distance, and end distance are dependent of the direction of loading.

The minimum spacing between fasteners in a row is $3D$ for reduced design values and $4D$ for $C_\Delta = 1.0$ in case of loading parallel to grain; $3D$ for reduced design values and required spacing for attached members for $C_\Delta = 1.0$ in case of loading perpendicular to grain. The minimum spacing between rows is dependent on smaller ratio (l/D) of the length of the fastener in the main member to the diameter of the fastener, l_m/D, and the length of the fastener in the side member to the diameter of the fastener, l_s/D. In case of loading parallel to grain, the minimum spacing between rows is $1.5D$. In case of loading perpendicular to grain, when $l/D \leq 2$, the minimum spacing is $2.5D$; when $2 < l/D < 6$, the minimum spacing is $(5l + 10D)/8$; when $(l/D > 6)$, the minimum spacing is $5D$. The spacing between outer rows parallel to the member is limited to 5 in.

In case of loading parallel to grain, when $l/D \leq 6$, the minimum edge distance is $1.5D$; when $l/D > 6$, the minimum edge distance is larger of $1.5D$ and 1/2 spacing between rows. In case of loading perpendicular to grain, the minimum edge distance is $4D$ for loaded edges and $1.5D$ for unloaded edges.

In case of loading parallel to grain for $C_\Delta = 1.0$, the minimum end distance is $4D$ for compression; and $7D$ (softwood) and $5D$ (hardwood) for tension. In case of loading perpendicular to grain for $C_\Delta = 1.0$, the minimum end distance is $4D$. When $C_\Delta = 0.5$, the minimum end distance is 50% of the values for $C_\Delta = 1.0$.

For lag screws loaded in withdrawal only, the minimum end distance and spacing is $4D$, and the minimum edge distance is $1.5D$.

15.6.4 Combined Load Resistance

The nail, spike, and wood screw under combined axial tension and lateral loading, allowable design value shall be determined as

$$Z'_\alpha = \begin{cases} \dfrac{(W'p)Z'}{(W'p)\cos^2\alpha + Z'\sin^2\alpha} & \text{for a lag screw and wood screw} \\ \dfrac{(W'p)Z'}{(W'p)\cos\alpha + Z'\sin\alpha} & \text{for a nail and spike} \end{cases} \tag{15.52}$$

where α = angle between the applied load and the wood surface (i.e., 0° = lateral load and 90° = withdrawal/tension); p = length of thread penetration in main member (in) as shown in Figure 15.7.

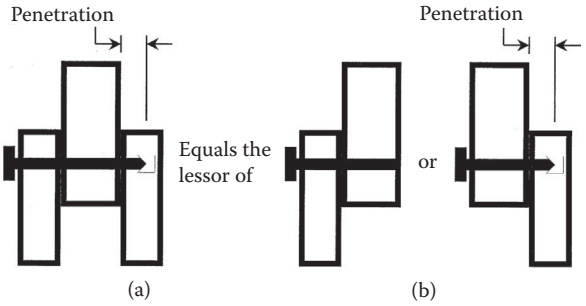

FIGURE 15.7 Double shear connection: (a) complete connection and (b) left and right shear planes.

15.6.5 Adjustment Factors

The reference resistance must be multiplied by all the appropriate adjustment factors. In determining the lateral resistance, it is necessary to consider group action, C_g, and geometry, C_Δ for bolts, lag screws and dowels, and end grain, C_{eg}, for nails, spikes, and wood screws.

15.6.5.1 Group Action Factor, C_g

The group action factor accounts for load distribution between bolts, lag screw, or dowels when one or more rows of fasteners are used and is defined by

$$C_g = \frac{1}{n_f}\sum_{i=1}^{n_r} a_i \tag{15.53}$$

where n_f = number of fasteners in the connection, n_r = number of rows in the connection, and a_i = effective number of fasteners in row i because of load distribution in a row and is defined by

$$a_i = \left(\frac{1+R_{EA}}{1-m}\right)\left[\frac{m\left(1-m^{2n_i}\right)}{\left(1+R_{EA}m^{n_i}\right)(1+m)-1+m^{2n_i}}\right] \tag{15.54}$$

$$m = u - \sqrt{u^2-1} \tag{15.55}$$

$$u = 1+\gamma\frac{s}{2}\left(\frac{1}{(EA)_m}+\frac{1}{(EA)_s}\right) \tag{15.56}$$

and where γ = load/slip modulus for a single fastener; s = spacing of fasteners within a row; $(EA)_m$ and $(EA)_s$ = axial stiffness of the main and side member, respectively; R_{EA} = smaller ratio of $(EA)_m/(EA)_s$ or $(EA)_s/(EA)_m$. The load/slip modulus, γ, is either determined from testing or assumed by

$$\gamma = \begin{cases} 500{,}000 & \text{lbs/in for 4" split ring or shear plate connector} \\ 400{,}000 & \text{lbs/in for 2.5" split ring or 2.635" shear plate connector} \\ 180{,}000D^{1.5} & \text{lbs/in for dowel-type wood-to-wood connector} \\ 270{,}000D^{1.5} & \text{lbs/in for dowel-type wood-to-metal connector} \end{cases} \tag{15.57}$$

15.6.5.2 Geometry Factor, C_Δ

The geometry factor, C_Δ, is used to adjust for connections in which either end distance and/or spacing within a row does not meet the limitations outlined previously. Defining a = actual minimum end distance, a_{min} = minimum end distance as specified previously, s = actual spacing of fasteners within a row, and s_{min} = minimum spacing as specified previously, the lesser of the following geometry factors are used to reduce the connection's adjusted resistance

$$\text{End distance}: C_\Delta = \begin{cases} 1.0 & \text{for } a \geq a_{min} \\ a/a_{min} & \text{for } a_{min}/2 \leq a \leq a_{min} \end{cases}$$

$$\text{Spacing}: C_\Delta = \begin{cases} 1.0 & \text{for } s \geq s_{min} \\ s/s_{min} & \text{for } 3D \leq s \leq s_{min} \end{cases}$$

15.6.5.3 End Grain Factor, C_{eg}

The end grain factor, C_{eg}, of 0.75 is applied when a lag screw is loaded in withdraw from end grain. C_{eg} of 0.67 is applicable to lateral resistance of a dowel-type fastener with its axis parallel to the wood fiber.

15.6.5.4 Toe-Nail Factor, C_{tn}

The toe-nail factor, C_{eg}, of 0.67 is applied when a nail or spike is loaded in withdraw. C_{eg} of 0.83 is applicable to lateral resistance of a toe-nail connection.

15.6.5.5 Diaphragm Factor, C_{di}

The diaphragm factor C_{di} of 1.1 is applied when nails and spikes are used in diaphragm connections.

References

Aasheim, E. 2011. Timber in Construction: Move Forward. *Keynote Address*, Nov. 17, Kuala Lumpur, Malaysia.

AASHTO. 2002. *Standard Specifications for Highway Bridges* (17th Edition). American Association of State Highway and Transportation Officials, Washington, DC.

AASHTO. 2012. *AASHTO LRFD Bridge Design Specifications*. US Customary Units, American Association of State Highway and Transportation Officials, Washington, DC.

AF&PA. 2005. *ASD/LRFD National Design Specification for Wood Construction with Supplement: Design Values for Wood Construction*, ANSI/AF&PA NDS-2005, American Forest and Paper Association, Washington, DC.

AWC. 2005. *ASD/LRFD Manual for Engineered Wood Construction*, American Wood Council, Leesburg, VA.

Baláž, I. 2013. Timber Bridges with Record Spans. *Eurostav*, No. 5, pp. 62-63. (in Slovak).

Bodig, J., and Jayne, B. 1982. *Mechanics of Wood and Wood Composites*. Van Nostrand Reinhold, New York, NY.

Bridgeport Covered Bridge. 2013. http://en.wikipedia.org/wiki/Bridgeport_Covered_Bridge.

BSC. 2013. http://www.bscconsulting.com.au/municipal_engineering.php.

Culling, D. 2009. Critical Analysis of the Essing Timber Bridge, Germany. *Proceedings of Bridge Engineering 2 Conference,* April 2009, University of Bath, Bath, UK. http://www.bath.ac.uk/ace/uploads/StudentProjects/Bridgeconference2009/Papers/CULLING.pdf.

Dragon's Tail Bridge. 2013. http://www.koeppl-ingenieure.de/cms/index.php?option=com_content&view=article&id=151&Itemid=174 (In Germany).

Erdberger Steg Bridge. 2013. http://en.structurae.de/structures/data/index.cfm?id=s0019561.
Flisa Bridge. 2013. http://en.structurae.de/structures/data/index.cfm?id=s0009160.
Freas, A. D. 1995. Wood Properties. In *Wood Engineering and Construction Handbook* (2nd Edition). K. F. Faherty, and T. G. Williamson (Eds.), McGraw-Hill, New York, NY.
Fridley, K. J. 1992. Designing for Creep in Wood Structures. *Forest Products Journal*, 42(3), 23–28.
Golden. 2013. http://en.wikipedia.org/wiki/Golden,_British_Columbia.
Hartland Bridge. 2013. http://en.wikipedia.org/wiki/Hartland_Bridge.
Jackson Covered Bridge. 2013. http://bridgehunter.com/il/cumberland/jackson/.
Nagai, M. et al. 2013. Chapter 22 Bridge Engineering in Japan. *Handbook of International Bridge Engineering*, Ed. Chen, W.F. and Duan, L., CRC Press, Roca Baton, FL.
Nordic. 2013. http://www.nordicroads.com/website/index.asp?pageID=64.
Oregon. 2013. http://www.oregon.gov/ODOT/HWY/GEOENVIRONMENTAL/historic_bridges_covered1.shtml.
Pilot G. 2007. *Bridges in Europe*, Presented at ECCE Athens meeting, October, Athens, Greece.
Remseck Neckar Bridge. 2013. http://www.karl-gotsch.de/Album/Neckar4.htm (in Germany).
Ritter, M. A. 1990. *Timber Bridges: Design, Construction, Inspection, and Maintenance*, EM 7700-8. U.S.D.A., Forest Service, Washington, DC.
Ritter, M. A., and Ebeling, D. W. 1995. Miscellaneous Wood Structures. In: *Wood Engineering and Construction Handbook* (2nd Edition). K. F. Faherty, and T. G. Williamson (Eds.). McGraw-Hill, New York, NY.
Smolen–Gulf Bridge. 2013. http://en.wikipedia.org/wiki/Smolen-Gulf_Bridge.
Sioux Narrows Bridge. 2013. http://en.wikipedia.org/wiki/Sioux_Narrows_Bridge.
Stuttgart–Bad Cannstatt Bridge. 2013. http://www.waymarking.com/waymarks/WM9AGY_Bad_Cannstatt_Holzsteg.
USDA. 2010. *Wood Handbook: Wood as an Engineering Material*, Forest Products Laboratory, United States Department of Agriculture, Madison, WI.
Vaires-sur-Marne Footbridge. 2013. http://en.structurae.de/structures/data/index.cfm?id=s0016522.
Wood, L.W. 1951. Relation of Strength of Wood to Duration of Load. *USDA Forest Service Report No. 1916*, Forest Products Laboratory, Madison, WI.

Further Reading

AITC. 1988. *Glulam Bridge Systems*. American Institute of Timber Construction, Englewood, CO.
AITC. 2010. *Design Standard Specifications for Structural Glued Laminated Timber of Softwood Species. AITC 117-2010*. American Institute of Timber Construction, Englewood, CO.
AITC. 2012. *Timber Construction Manual* (6th Edition). American Institute of Timber Construction, Wiley Inter-Science, New York, NY.
Wipf, T. J., Klaiber, F. W., and Sanders, W. W. 1986. Load Distribution Criteria for Glued Laminated Longitudinal Timber Deck Highway Bridges. *Transportation Research Record 1053*, Transportation Research Board, Washington DC.
WWPA. 1996. *Western Wood Use Book* (4th Edition). Western Wood Products Association, Portland, OR.

16

Application of Fiber Reinforced Polymers in Bridges

Dagmar Svecova
University of Manitoba

Aftab Mufti
University of Manitoba

Baidar Bakht
University of Manitoba

16.1 Introduction

Arguably, steel has been one of the best construction materials for a long time. It is with the help of this material that engineers have been able to span larger distances than would have been possible with other conventional building materials, namely concrete, wood, and masonry. Notwithstanding its admirable qualities, steel has one very significant shortcoming: its tendency to revert to its natural oxide state. Because of steel's tendency to corrode readily, engineers have often wished for an ideal building material, which is at least as strong as steel but is also far more durable than steel. Fiber reinforced polymers (FRPs) come close to such an ideal material.

FRPs have been used for decades for structures in the aeronautical, aerospace, automotive, and other fields; their use in civil engineering works dates back to the 1950s when glass FRP (GFRP) bars were first investigated for structural use in civil structures. However, it was not until the 1970s that the

superior performance of FRPs over epoxy-coated steel was recognized, and these materials were finally considered suitable for civil structural engineering applications. The first applications of GFRP were not successful because of its poor performance within thermosetting resins cured at high molding pressures (Parkyn, 1970).

In Canada, research on the use of FRPs in civil applications began in the late 1980s, leading to the formation of centers of excellence (e.g., Intelligent Sensing for Innovative Structures (ISIS) Canada: www.isiscanada .com) and several international conferences with voluminous proceedings. An attempt is made in this chapter to synthesize the recent research and development in the use of FRPs in civil applications.

16.2 Fiber Reinforced Polymers

Since their early application, many FRPs with different types of high-strength fibers have been developed. The fibers include aramid, carbon, improved glass, and basaltic fibers. FRPs are manufactured in many different forms such as bars, fabric, 2D grids, 3D grids, or standard structural shapes, some of which are shown in Figure 16.1. In this section, the two major components of FRPs, being the fibers and matrices (or resins), are discussed along with their individual properties and those of their composites.

16.2.1 Fiber Reinforced Polymer Constituents

FRPs are composite materials consisting of a matrix (resin) and reinforcing fibers. As shown in Figure 16.2, the fibers are stronger than the matrix. In order to provide the reinforcing function, the fiber-volume fraction should be more than 55% for FRP bars and rods and 35% for FRP grids (ISIS, 2006). The mechanical properties of the final FRP product depend on the fiber quality, orientation, shape, volumetric ratio, adhesion to the matrix, and on the manufacturing process. The manufacturing process is an important consideration because simply mixing superior fibers and matrix together does not guarantee a quality product. Accordingly, FRPs with nominally the same fibers, matrix, and fiber-volume ratio can differ significantly in their final properties. Additives and fillers appropriate for the fiber and resin systems are added for curing or other reasons. Diluents, such as styrene, and low-profile (shrink) additives should not exceed 10% and 20% by weight of the specified base resin, respectively. Inorganic fillers may be used but should not exceed 20% by weight of the specified base resin. Other additives, such as coupling agents, release agents, initiators, hardeners, promoters, catalysts, UV agents, fire retardants, wetting agents, foaming agents, and pigments may be added (ISIS, 2006).

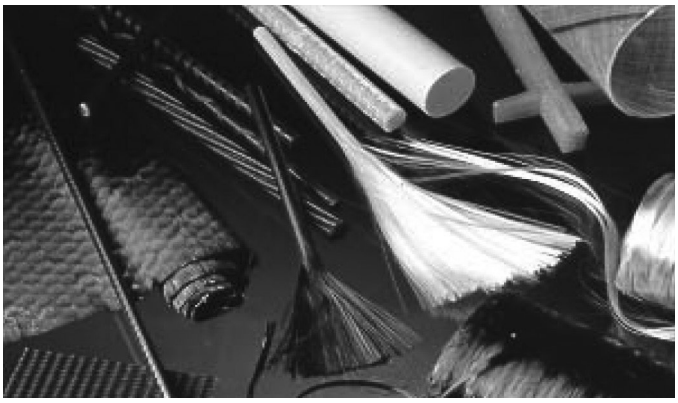

FIGURE 16.1 Available shapes of FRP products. (From ISIS, *Design Manual 3: Reinforcing Concrete Structures with Fibre Reinforced Polymers.* ISIS Canada, Intelligent Sensing for Innovative Structures, A Canadian Network of Centres of Excellence, University of Manitoba, Winnipeg, Manitoba, Canada, 2007a. With permission.)

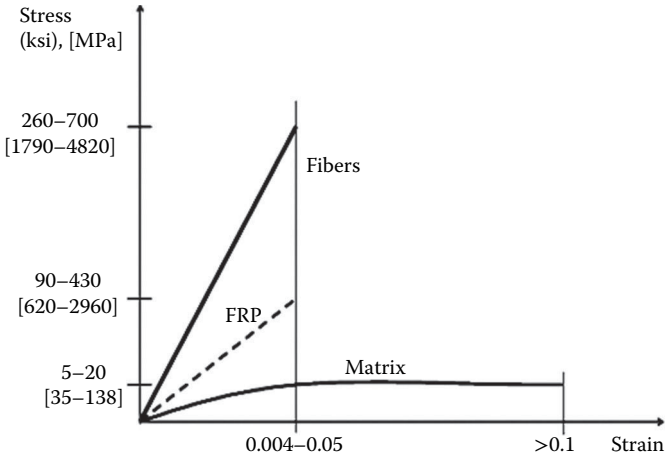

FIGURE 16.2 Stress–strain relationships for fibers, matrix, and FRP. (From ISIS, *Design Manual 3: Reinforcing Concrete Structures with Fibre Reinforced Polymers.* ISIS Canada, Intelligent Sensing for Innovative Structures, A Canadian Network of Centres of Excellence, University of Manitoba, Winnipeg, Manitoba, Canada, 2007a. With permission.)

16.2.1.1 Fibers

The role of the fibers is to provide the strength and stiffness of the composite material, because of which the fibers must have high strength, and axial stiffness, toughness, durability, and preferably low cost. The performance of fibers is affected by their length, cross-sectional shape, and chemical composition. Fibers are available in different cross-sectional shapes and sizes. The most commonly used fibers for FRPs are carbon, glass, and aramid, each category having various subcategories. Typical mechanical properties of the various fibers are given in Table 16.1. The coefficients of thermal expansion of fibers in the longitudinal and radial directions are denoted as α_{frpl} and α_{frpt}, respectively. Fibers must be treated with coupling agents to promote the bonding with the resin matrix.

TABLE 16.1 Typical Mechanical Properties of Fibers

Fiber Type		Tensile Strength (ksi) (MPa)	Modulus of Elasticity (ksi) (GPa)	Elongation (%)	Coefficient of Thermal Expansion ($x10^{-6}$)	Poisson's Ratio
			Carbon			
PAN	High strength	507 (3493)	29,007–34,809 (200–240)	1.4–1.7	(−1.2) to (−0.1) (α_{frpl}) 7 to 12 (α_{frpt})	–0.2
	High modulus	362–580 (2494-3996)	50,763–94,274 (350–650)	0.4–0.7		
Pitch	Ordinary	113–145 (779–999)	5511–5801 (38–40)	2.0–2.5	(−1.6) to (−0.9) (α_{frpl})	N/A
	High modulus	435–507 (2997–3493)	58,015–116,030 (400–800)	0.4–0.7		
			Aramid			
Kevlar 29		525 (3617)	11,994 (82,639)	4.4	N/A	0.35
Kevlar 49		406 (2797)	18,855 (129,911)	2.1	−2.0 (α_{frpl}), 59 (α_{frpt})	
Kevlar 129		610 (est.) (4203)	15,954 (est.) (109,923)	—	N/A	

(*Continued*)

TABLE 16.1 (*Continued*) Typical Mechanical Properties of Fibers

Fiber Type	Tensile Strength (ksi) (MPa)	Modulus of Elasticity (ksi) (GPa)	Elongation (%)	Coefficient of Thermal Expansion (x10^{-6})	Poisson's Ratio
		Aramid			
Kevlar 149	500 (3445)	24,946–25,961 (171,878–178,871)	1.9	N/A	
Twaron	406 (2797)	18,855 (129,911)	2.1	(−2.0) (α_{frpl}), 59 (α_{frpt})	
Technora	507 (3493)	10,732 (73,944)	4.7	N/A	
		Glass			
E-glass	507–522 (3493–3597)	10,732–10,877 (73,944–74,943)	4.8	5.0	0.2
S-glass	710 (4892)	12,618 (86,938)	5.6	2.9	0.22
Alkali resistant glass	261–507 (1798–3493)	10,152–11,022 (69,947–75,942)	2.0–4.0	N/A	N/A

TABLE 16.2 Chemical Resistance of Fibers

Fiber Type		Acid Resistance	Alkali Resistance	Organic Solvent Resistance
		Carbon		
PAN	High strength	Good	Excellent	Excellent
	High modulus	Excellent	Excellent	Excellent
Pitch	Ordinary	Excellent	Excellent	Excellent
	High modulus	Excellent	Excellent	Excellent
		Aramid		
Kevlar 49	Poor	Good	Excellent	
Technora	Good	Good	Good	
		Glass		
E-glass	Poor	Fair	Excellent	
S-glass	Good	Poor	N/A	
Alkali resistant glass	Good	Good	N/A	
		Others		
EC-polyethylene	Excellent	Excellent	Excellent	
Polyvinyl alcohol fiber	Good	Good	Good	
Steel fiber	Poor	Excellent to sodium Poor to brine	Excellent	

Source: ISIS, *Design Manual 3: Reinforcing Concrete Structures with Fibre Reinforced Polymers*. ISIS Canada, Intelligent Sensing for Innovative Structures, A Canadian Network of Centres of Excellence, University of Manitoba, Winnipeg, Manitoba, Canada, 2007a. With permission.

Table 16.2, based on the work of Japan Society of Civil engineers (JSCE, 1993) and Banthia and MacDonald (1996), provides information about the chemical resistance of various fibers in damaging environments, such as acids and alkalis, the former including hydrochloric acid, sulfuric acid, and nitric acid, and the latter sodium hydroxide and brine. The table also lists the resistance of various fibers against organic solutions, which include acetone, benzene, and gasoline. It can be seen in the table that carbon fibers have the highest resistance against the various deleterious agents.

16.2.1.2 Resins

A very important issue in the manufacture of FRPs is the selection of the proper matrix because the physical and thermal properties of the matrix significantly affect the final mechanical properties of the composites. In order to be able to exploit the full strength of the fibers, the matrix should be able to develop an ultimate strain that is higher than that of the fibers (Phillips, 1989). The matrix not only coats the fibers and protects them from mechanical abrasion, but also transfers stresses between the fibers. Other very important roles of the matrix are transfer of inter-laminar and in-plane shear in the FRPs, and provision of lateral support to fibers against buckling when subjected to compressive loads (ACI, 1995). Two types of polymeric matrices, being thermosetting and thermoplastic, are used widely for FRPs.

Thermosetting polymers are used more often than thermoplastic polymers. The former are low molecular-weight liquids with very low viscosity (ACI, 1995), and their molecules are joined together by chemical cross-links, because of which they form a rigid three-dimensional structure that after setting cannot be reshaped by heat or pressure. Thermosetting polymers are processed in a liquid state to obtain good wet-out of fibers. Some commonly used thermosetting polymers are polyesters, vinyl esters, and epoxies. These materials have good thermal stability, chemical resistance and undergo low creep and stress relaxation. The FRP reinforcing bars should be produced and properly cured with a degree of curing above 95% (ISIS, 2006). However, these polymers fail at relatively low strains, resulting in low impact strength. Their two major disadvantages are short shelf life and long manufacturing time. Mechanical properties of some thermosetting resins are provided in Table 16.3.

Thermoplastic polymers, having molecules in a linear structural form held in place by weak secondary bonds, can be destroyed by heat or pressure. After cooling, these matrices attain a solid shape, which can be altered by heating. It is noted reshaping by heating can degrade their mechanical properties.

16.2.2 Material Properties of Fiber Reinforced Polymers

FRPs are manufactured from continuous fibers embedded in matrices. Similar to steel reinforcement, FRP bars are produced in different diameters, depending on the manufacturing process. The surface of the rods can be spiral, straight, sanded-straight, sanded-braided, or deformed. The bond of these bars

TABLE 16.3 Typical Properties of Thermosetting Resins

Resin	Specific Gravity	Tensile Strength (ksi) (MPa)	Tensile Modulus (ksi) (MPa)	Cure Shrinkage (%)
Epoxy	1.20–1.30	8–19 (55–131)	400–595 (2756–4100)	1.00–5.00
Polyester	1.10–1.40	5–15 (35–103)	304–500 (2095–3445)	5.00–12.00
Vinyl ester	1.12–1.32	10–12 (69–83)	435–486 (2997–3349)	5.40–10.30

TABLE 16.4 Typical Mechanical Properties of FRP Reinforcing Bars

Trade Name	Tensile Strength (ksi) (MPa)	Modulus of Elasticity (ksi) (GPa)	Ultimate Tensile Strain
	Carbon FRPs		
V-ROD	220 (1516)	18,405 (126)	0.012
Aslan	300 (2067)	18,000 (124)	0.017
Leadline	328 (2260)	21,320 (146)	0.015
	Glass FRPs		
V-ROD	127 (875)	6680 (46)	0.019
Aslan	120 (827)	5920 (40)	0.020
SchöckComBAR	145 (999)	8702 (60)	0.007

with concrete is similar to, or better than, the bond of steel bars with concrete. The mechanical properties of some commercially available FRP reinforcing bars are given in Table 16.4.

16.2.3 Constitutive Relationship for Fiber Reinforced Polymers

16.2.3.1 Tensile Strength and Modulus of Elasticity

The stress–strain relationship for FRP in tension is linear up to failure. The ultimate tensile strength of FRP, f_{frpu}, used in design calculations may be obtained from the manufacturer or from tests in accordance with ACI (2002), Canadian Highway Bridge Design Code CHBDC (2006), or CSA (2010).

Owing to shear lag, fibers near the outer surface are stressed more than those near the center of the bar (Faza, 1991), because of which the tensile strengths of FRP bars are dependent on bar diameter. Smaller diameter bars are more efficient.

The values of tensile strength vary with fiber type, fiber-volume ratio, manufacturing process, and so on. Generally, GFRPs have the lowest strength, and CFRPs and AFRPs the highest. Figure 16.3 shows the stress–strain relationship of various commercially available FRPs.

Modulus of elasticity of FRP, depending on the type of fiber, can vary from 5,920 for GFRPs to 21,320 ksi for CFRPs. Modulus of elasticity of FRP can be obtained directly from tensile tests. Most manufacturers provide this information in their specifications.

16.2.3.2 Compressive Strength and Modulus of Elasticity

The compressive strength of FRPs is low compared to its tensile strength, and is dependent on the fiber type, the fiber-volume ratio, manufacturing process and so on. It has been reported that aramid bars do not behave well in compression (Bedard, 1992; Chaallal and Benmokrane, 1993). Higher compressive strengths are expected for bars with higher tensile strength (ACI, 1995).

The compressive modulus of elasticity of FRPs depends on length-to-diameter ratio, bar size and type, as well as other factors, such as boundary conditions. In the reported results from compression tests, it is generally agreed that the compressive stiffness ranges from 77% to 97% of the tensile stiffness (Bedard, 1992; Chaallal and Benmokrane, 1993).

According to Kobayashi and Fujisaki (1995), the compressive strength of AFRP bars is approximately 10% of their tensile strength, for CFRP bars it is in the range of 30%–50% of their tensile strength, and

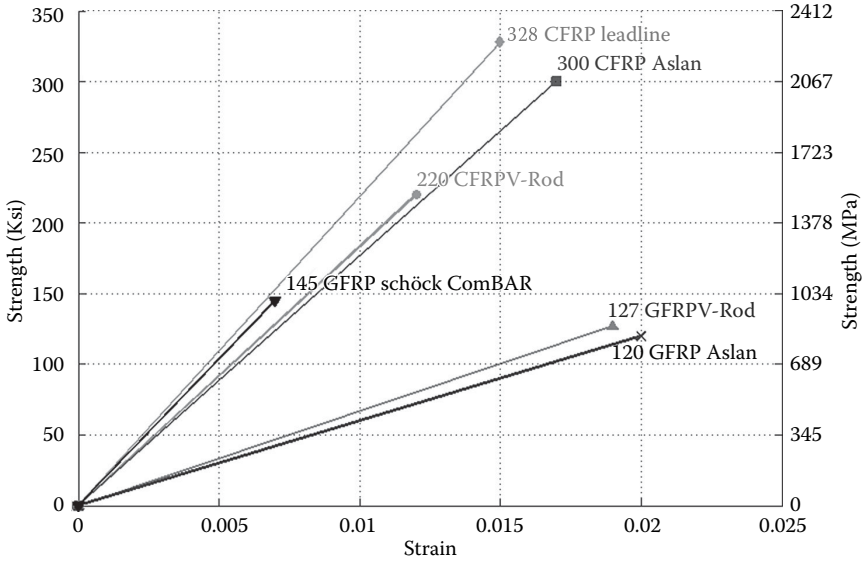

FIGURE 16.3 Stress–strain relationship of various commercially available FRPs.

for GFRP bars it is in the range of 30%–40% of their tensile strength. Chaallal and Benmokrane's (1993) tests on GFRP bar with 73%–78% E-glass fiber showed the compressive strength of GFRP bars to be approximately 80% of their tensile strength. This appears to be rather high and is not consistent with previous findings. However, it should be noted that this type of disparity is quite usual for FRP because there are many types of products differing in volumetric ratio of fibers, matrix type, and manufacturing process. A testing method for FRP materials is given in CSA (2010).

16.2.4 Behavior of Concrete Reinforced with Fiber Reinforced Polymer

Failure of an FRP-reinforced concrete section in flexure can be caused by rupture of the FRP or by crushing of the concrete. Research has established that the ultimate flexural strength for both types of failure can be calculated using the same approach irrespective of the type of reinforcement. Relevant equations for steel, given in several textbooks, are revised here and used in this chapter.

Assumptions used in designing FRP-reinforced sections* are summarized as follows:

- Maximum strain at the concrete compression fiber is equal to the ultimate concrete strain.
- Tensile strength of concrete is ignored for cracked sections.
- The strain in concrete and FRP at any level is proportional to the distance from the neutral axis.
- The stress–strain relationship for FRP is linear up to failure.
- Perfect bond exists between the concrete and the FRP reinforcement.

16.2.4.1 Strain Compatibility

The design philosophy is based on the assumption that a plane cross-section before deformation remains plane after deformation, leading to linear strain distribution over the cross-section.

Strain compatibility analysis is used for the analysis of FRP-reinforced concrete members. If it is shown by material testing that the maximum compressive strain in concrete is higher than the code recommended value, the higher value should be used for analysis. The value of maximum compressive strain is important when calculating the balanced failure reinforcement ratio, ρ_{frpb}, and assessing the failure mode of the member.

16.2.4.2 Modes of Failure

There are three possible modes of flexural failure of a concrete section reinforced with FRP bars:

- Balanced failure—simultaneous rupture of FRP and crushing of concrete
- Compression failure—concrete crushing, while FRP remains in the elastic range with a strain level smaller than the ultimate strain
- Tension failure—rupture of FRP before crushing of concrete

Compression failure is less violent and more desirable than tension failure and is similar to that of an over-reinforced concrete beam with steel reinforcing bars.

Tension failure, due to rupture of FRP while the strain in the extreme fibers of the compression zone is less than the ultimate compressive strain of the concrete, is sudden and brittle. It will occur when the reinforcement ratio is smaller than the balanced failure reinforcement ratio.

16.2.4.2.1 Balanced Failure Reinforcement Ratio

The balanced failure strain condition occurs when the concrete strain reaches its ultimate value ε_{cu}, while the outer layer of FRP reaches its ultimate strain ε_{frpu}, as shown in Figure 16.4. No lumping of FRP reinforcement is allowed. The term "balanced failure strain" has a very different meaning for

* Throughout this section, the term FRP reinforcement refers to a single layer of tensile FRP reinforcement, unless stated otherwise.

FRP-reinforced concrete than that for steel-reinforced concrete. Since the FRP does not yield at the balanced failure strain condition, an FRP-reinforced member will fail suddenly, without warning. This phenomenon will subsequently be referred to as "balanced failure". At this condition, the strain in concrete reaches its ultimate value in compression ε_{cu}, while the FRP reinforcement simultaneously reaches its ultimate strain ε_{frpu}. From the strain compatibility in the cross-section (Figure 16.4), the ratio of the neutral axis to the effective depth is

$$\frac{c_b}{d} = \frac{\varepsilon_{cu}}{\varepsilon_{cu} + \varepsilon_{frpu}} \tag{16.1}$$

where

c_b depth of neutral axis at balanced failure condition
d effective depth
ε_{cu} ultimate strain in concrete in compression
ε_{frpu} ultimate strain in FRP in tension

The stress distribution in the compressive zone of concrete is nonlinear, as shown in Figure 16.4.

The force equilibrium in the cross-section, without including the material resistance factors, is given as follows:

$$C_n = T_n \tag{16.2}$$

The stress resultants are calculated as follows:

$$C_n = 0.85 f_c' \beta_1 c_b b \tag{16.3}$$

$$T_n = \varepsilon_{frpu} E_{frp} A_{frpb} = f_{frpu} A_{frpb}$$

where

f_c' compressive strength of concrete
β_1 ratio of depth of rectangular compression block to the depth of the neutral axis
b width of compression face of a member
A_{frpb} area of FRP reinforcement for balanced conditions
E_{frp} modulus of elasticity of FRP
f_{frpu} ultimate tensile strength of FRP
ε_{frpu} ultimate tensile strain of FRP

Thus,

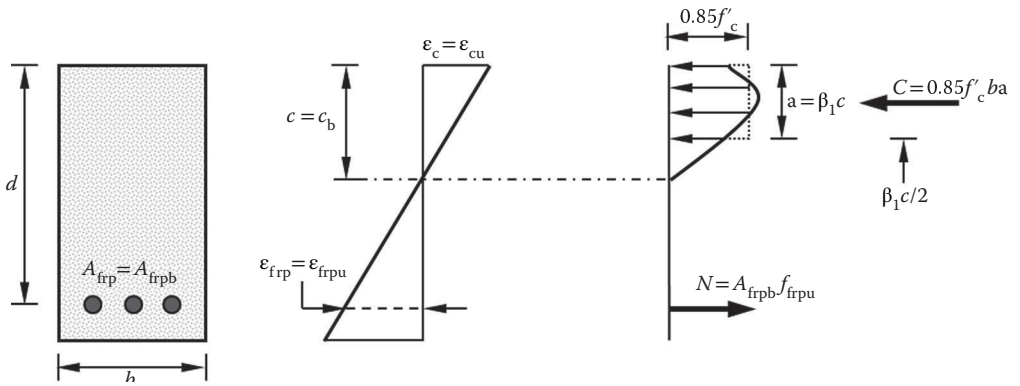

FIGURE 16.4 Strain and stress distributions at ultimate in the balanced condition.

$$0.85 f_c' \beta_1 c_b b = f_{frpu} A_{frpb}$$

Substituting Equations 16.1 into 16.2 and solving for the balanced failure, the reinforcement ratio ρ_{frpb} is obtained as follows:

$$\rho_{frpb} = A_{frpb} \Big/ (bd) \tag{16.5}$$

$$\rho_{frpb} = 0.85\beta_1 \frac{f_c'}{f_{frpu}} \left(\frac{\varepsilon_{cu}}{\varepsilon_{cu} + \varepsilon_{frpu}} \right) \tag{16.6}$$

Table 16.5 gives the balanced reinforcement ratios for several FRP-reinforced concrete cases. For some products, the value of f_{frpu} varies with the size of the cross-section. Owing to shear lag between the individual fibers at the core of the bars and those on the outer diameter, larger diameter bars can have lower values of f_{frpu} thus affecting the value of ρ_{frpb}. The values provided in Table 16.5 should be considered nominal for reference purposes only. The engineer should calculate the value of ρ_{frpb} for the actual product and bar size being used in design.

16.2.4.2.2 Failure Due to Crushing of Concrete

When flexural failure is induced by the crushing of concrete without rupture of the FRP reinforcement, the section is said to be over-reinforced. An over-reinforced T-section must have a large amount of reinforcement, which is considered to be impractical. Thus, only rectangular cross-sections are considered in the following.

The strain profile with the top fiber strain, equal to the ultimate compressive strain of concrete in compression, is shown in Figure 16.5. Under this strain distribution, the cross-section fails due to concrete crushing. The nonlinear distribution of concrete stresses in the compression zone is replaced by an equivalent uniform stress over a part of the compression zone, as shown in Figure 16.5, according to CSA (2004).

The ultimate moment resistance for such an over-reinforced section can be calculated as follows:

$$0.85 f_c' \beta_1 cb = A_{frp}\ \varepsilon_{frp}\ E_{frp} \tag{16.7}$$

where

TABLE 16.5 Balanced Reinforcement Ratio for FRP Reinforced Concrete

Fiber Type (f_{rpu} (ksi), E_{frp}(ksi))	Concrete Strength (psi) (MPa)			
	4000 (27.56)	6000 (41.34)	7000 (48.23)	9000 (62.00)
	GFRP			
ASLAN (120; 5,920)	0.00355	0.00469	0.00511	0.00610
V-Rod (127; 6,680)	0.00354	0.00468	0.00510	0.00609
SchÖckComBAR (145; 8,702)	0.00346	0.00519	0.00605	0.00778
	CFRP			
LEADLINE (328; 21,320)	0.00163	0.00216	0.00235	0.00281
ASLAN (300; 18,000)	0.00167	0.00221	0.00241	0.00288
V-Rod (220.15; 18,405.5)	0.00297	0.00393	0.00428	0.00511

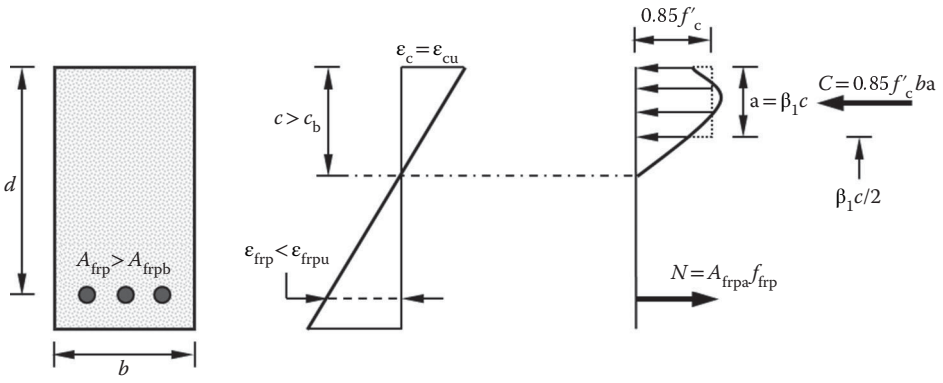

FIGURE 16.5 Strain and stress distributions at ultimate in the case of concrete crushing.

c is depth of neutral axis.

The tensile force in reinforcement is calculated as

$$T = A_{frp} f_{frp} \tag{16.8}$$

where

A_{frp} area of FRP reinforcement

f_{frp} stress in the FRP reinforcement at failure, which is smaller than the tensile strength

hence

$$f_{frp} = \left(\sqrt{\frac{\left(E_{frp}\varepsilon_{cu}\right)^2}{4} + \frac{0.85\beta_1 f_c^{'}}{\rho_{frp}} E_{frp}\varepsilon_{cu}} - 0.5E_f\varepsilon_{cu} \right) \leq f_{frpu} \tag{16.9}$$

where reinforcement ratio $\rho_{frp} = \dfrac{A_{frp}}{bd}$

Alternatively, an iteration process may be used. For each iteration, for an assumed depth of neutral axis, the forces in the concrete and in the reinforcement are calculated and their equilibrium is checked as follows:

$$0.85 f_c' \beta_1 cb = A_{frp}\ \varepsilon_{frp}\ E_{frp} \tag{16.10}$$

If this equilibrium is not satisfied, a new value of depth of neutral axis, c, is chosen and C and T are recalculated using the new values of c and ε_{frp}.

When the equilibrium between Equations 16.7 and 16.8 is satisfied, as a means of verifying the assumed value of c, the moment of resistance of the section is given by

$$M_r = C\left(d - \frac{\beta_1 c}{2}\right) \tag{16.11}$$

The curvature at ultimate is

$$\psi_u = \frac{\varepsilon_{cu} + f_{frp}/E_{frp}}{d} \tag{16.12}$$

16.2.4.2.3 Tension Failure

The theory for under-reinforced sections with steel bars is well-documented in textbooks. Before failure, the steel yields and the curvature increases rapidly until the strain in concrete at the extreme compressive surface reaches an ultimate value of 3000×10^{-6}, when failure occurs. The rectangular stress block typically idealizes the stress in concrete. However, when a section is under-reinforced with FRP, no yield occurs. Rather, the failure is caused by rupture of the FRP. The strain in the reinforcement is calculated as

$$\varepsilon_{frpu} = \frac{f_{frpu}}{E_{frp}} \tag{16.13}$$

The corresponding strain ε_c at the extreme compressive fiber is less than ε_{cu} as shown in Figure 16.6. Since the traditional rectangular block cannot idealize the distribution of compressive stress in the concrete zone, the stress block parameters α and β need to be developed for values of ε_c varying up to 3000×10^{-6} because the coefficients α_1 and β_1, are valid only for $\varepsilon_c = \varepsilon_{cu}$.

The process starts by specifying the strain in the reinforcement equal to the ultimate tensile strain, ε_{frpu}. An iterative approach is used and an assumed value of the depth of neutral axis, c, is used for every iteration. The strain in the top fibers, ε_c, is calculated using strain compatibility, and must be less than the ultimate strain of concrete in compression, ε_{cu}. The stress-block parameters α and β depend on the strain in concrete; when this strain reaches 3500×10^{-6} they are identical to parameters $\alpha_1$and β_1 of CSA (2004). The resultant of the compressive stresses in concrete, C, is then calculated as

$$C = \alpha\ \varphi_c f_c' \beta\ cb \tag{16.14}$$

where

α stress-block factor for concrete

β stress-block factor for concrete

Using the factors α_1 and β_1 specified by CSA (2004) for given material values provides moment resistance values within 5%–10% of the actual value.

The tensile force in the reinforcement is calculated as

$$T = A_{frp}\varphi_{frp}\varepsilon_{frpu}E_{frp} \tag{16.15}$$

Equilibrium in a cross-section is found by equating Equations 16.14 and 16.15.

$$\alpha\ \varphi_c f_c' \beta\ cb = A_{frp}\varphi_{frp}\varepsilon_{frpu}E_{frp} \tag{16.16}$$

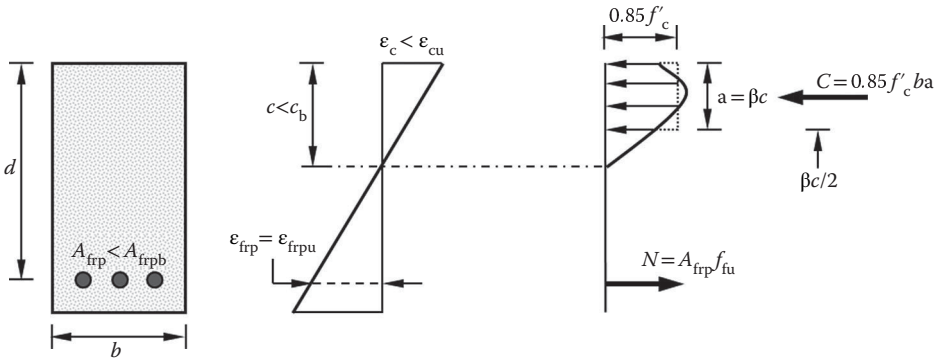

FIGURE 16.6 Strain and stress distributions at ultimate in the case of the rupture of FRP.

If these two forces are not in equilibrium, another iteration is required using a different value of the depth of neutral axis, c, whereas the strain in FRP remains equal to ε_{frpu}, until force equilibrium is satisfied.

The moment of resistance of the member can be found using the following equation:

$$M_r = T\left(d - \frac{\beta c}{2}\right) \tag{16.17}$$

For this type of failure, serviceability requirements typically control the design.

The curvature in this case can be determined as

$$\psi_u = \frac{\varepsilon_c + \varepsilon_{frpu}}{d} \tag{16.18}$$

16.3 Durability of Fiber Reinforced Polymers

One of the main reasons for considering FRP bars for concrete reinforcement is that steel bars corrode in concrete subjected to harsh environments, resulting in a loss of strength and structural integrity. Concrete exposed to chlorides in a marine environment or through de-icing salts is particularly prone to corrosion of reinforcing steel. Concrete is highly alkaline, having a pH of approximately 12.5–13.5, and the alkalinity decreases with carbonation (Coomarasamy and Goodman, 1997). Durability tests are conducted to determine the strength and stiffness reduction due to natural aging of FRP bars under service environments during 50–100 years of service life. Many researchers are establishing these reduction factors. Additional work is being conducted to establish calibration factors based on field results.

Simple extrapolation of results from weathering exposure programs, although extremely valuable, is not sufficient to support the rapid increase in the use of FRP reinforcement. Some form of an accelerated aging test procedure and predictive method is needed in order to provide appropriate long-term strength estimates. The designer is referred to existing literature for information on the conditioning environment for accelerated testing (Coomarasamy and Goodman, 1997; Porter et al., 1997; Porter and Barnes, 1998).

Research on the effects of temperature on the durability of FRP bars in a concrete alkaline environment indicates that an acceleration factor for each temperature difference can be defined by using Arrhenius laws. These factors differ for each product, depending on the type of fiber, type of resin, and bar size. In addition, the factors are affected by the environmental condition, such as surrounding solution media, temperature, pH, moisture, and freeze-thaw conditions (Gerritse, 1992; Coomarasamy and Goodman, 1997; Porter et al., 1997; and Porter and Barnes, 1998).

In another set of tests (Coomarasamy and Goodman, 1997), the mass uptake results and morphological studies on samples indicated a similar pattern qualitatively and, therefore, the simple test method could be used as a screening procedure to eliminate poor quality products without conducting extensive testing on them. The results of the mass uptake show an average increase of 0.6% after seven weeks for samples that retained 75% of their structural integrity versus up to 2.4% for samples that lost their structural integrity.

In another set of tests, an increase in average moisture uptake of the GFRP samples made of low-viscosity, urethane-modified vinyl ester was measured for a year under tap water, salt solutions, and alkaline solutions. Maximum moisture uptake was observed to be under 0.6% at room temperature. For tap and salt water immersion, moisture uptake was under 0.3%. Alkaline conditioning produced about twice the moisture absorption rate in GFRP as compared to tap water and salt solution conditioning. This is an indication of the rate and magnitude of strength and stiffness degradation in GFRP bars caused by an alkaline environment compared to plain water and salt solution (Vijay et al., 1998).

With regard to the durability characteristics of FRP bars, one is referred to the provisional standard test methods (CSA, 2010). The designer should always consult with the bar manufacturer before finalizing the design.

It is noted that the results from these accelerated test methods should be interpreted cautiously. The conditioning environments to promote accelerated deterioration are often unrealistic when compared with the actual environment in the field (Debaiky et al., 2006). Most accelerated tests lack correlation with actual field results over many years. To address this gap, ISIS recently undertook a field evaluation of existing structures with GFRP reinforcement (Mufti et al. 2005). Experienced contractors were employed to extract cores from five structures in service under the supervision of senior engineers. The extracted core samples were found to be in excellent condition. The specimens with GFRP were sent for analysis to three independent research teams comprised of expert material scientists at the University of Manitoba, the Université de Sherbrooke, and the University of British Columbia in collaboration with the University of Saskatchewan.

Five field demonstration projects were chosen in this study:

- Hall's Harbor Wharf
- Joffre Bridge
- Chatham Bridge
- Crowchild Trail Bridge
- Waterloo Creek Bridge

These structures are located across Canada from Atlantic to Pacific coasts. The demonstration structures perform in a wide range of environmental conditions, and were designed for normal use (i.e., heavy truck traffic) (Newhook et al., 2000; Benmokrane et al., 2002; Tadros et al., 1998; Aly et al., 1997).

The GFRP reinforcement rods or grids in all of the selected demonstration structures were made of E-glass and vinyl ester matrix. The structure type from which the core samples were taken, the age, GFRP type and general environmental conditions for each demonstration structure included in this study are shown in Table 16.6.

TABLE 16.6 Field Demonstration Structures' Age and Environmental Conditions

Demonstration Project (Year of Construction)	Structure (Type)	Age at Testing (Year)	GFRP (Type)	Environmental Conditions
Hall's Harbor, Nova Scotia (1999)	Wharf	5	GFRP V-ROD™	Thermal range +35°C and –35°C; wet-dry cycles (splash and tidal; salt water); Freeze-thaw cycles
Joffre Bridge, Quebec (1997)	Sidewalk Barrier Walls	7	GFRP C-BAR™	Thermal range +35°C and –35°C; Wet-dry and Freeze-thaw cycles; De-icing salt
Chatham Bridge, Ontario (1996)	Barrier Walls	8	GFRP NEFMAC™	Thermal range +35°C and –35°C; Wet-dry and Freeze-thaw cycles; De-icing salt
Crowchild Trail Bridge, Alberta (1996)	Barrier Walls and Bridge Deck	8	GFRP C-BAR™	Thermal range +35°C and –35°C; Freeze-thaw cycles; De-icing salt
Waterloo Creek Bridge, British Columbia (1998)	Barrier Walls	6	GFRP NEFMAC™	Thermal range +35°C and –35°C; Wet-dry and Freeze-thaw cycles

From each field demonstration structure, at least 10 specimens of GFRP reinforced concrete were removed from various areas of each structure. The cores were cylinders with 75 mm diameter and 140 to 180 mm length. A set of analytical methods was used to evaluate the state of degradation of the GFRP materials. This included Optical Microscopy (OM), Scanning Electron Microscopy (SEM), Energy Dispersive X-ray (EDX), Differential Scanning Calorimetry (DSC), and Fourier Transformed Infrared Spectroscopy (FTIS).

Based on the results of the analyses described above, the study stated that there was no visible degradation of the GFRP reinforcement (rods and grids) in the concrete environment in real-life engineering structures exposed to natural environmental conditions for duration of five to eight years. GFRP reinforcement is durable and highly compatible with the concrete material and should be allowed as the primary reinforcement in the concrete structures. Readers of this chapter are encouraged to obtain the detailed report of this study available through ISIS Canada for more details on the procedures and specific conclusions.

In its first edition, the CHBDC (2000) permitted GFRP only as secondary reinforcement. As a result of the ISIS durability study noted above, the second edition of the CHBDC (2006) permits the use of GFRP as primary reinforcement and prestressing tendons in concrete components. The maximum stress in GFRP, however, is not permitted to exceed 25% of its ultimate strength.

16.4 Bridge Decks

16.4.1 Fiber Reinforced Polymer Bridge Decks

With a very large number of structurally deficient or functionally obsolete bridges in the United States (Nystrom et al., 2003), emphasis is being placed on designing and building bridges that will last longer, while requiring minimal maintenance. Steel reinforcement and structural steel members are known to be susceptible to corrosion, whereas concrete could also crack and spall due to sulfate attack, freeze-thaw cycles and other detrimental processes. The combination of material degradation and substandard load ratings has led many bridge structures to be classified as structurally deficient or functionally obsolete. It is estimated that the cost of repair or replacement of these bridges can be as high as 75%–90% of the total annual maintenance cost of the structure (Karbhari et al., 2001). When repair or replacement is imminent, there is not only the associated cost of materials and labor, but also the cost of losses because of delays and detours. FRP bridge decks offer a durable, light-weight, and easy-to-install alternative to current deck slabs. Recently, the Federal Highway Administration (FHWA) has supported the Transportation Equity Act of the 21st Century that established the Innovative Bridge Research and Construction Program (IBRCP) and that employed 44 projects utilizing FRP bridge deck systems throughout the United States (Tang, 2003). As many as 83 FRP bridge decks have been installed in the United States between 1996 and 2004 (Telang et al., 2006). Detailed list of these decks can be found in Table 16.7. However, the current lack of design specifications, and testing procedures prevents more widespread use of these types of bridge decks (Hong and Hastak, 2006). Initiatives such as the one by IBRCP will help in the long run to promote the use of the decks and provide sufficient evidence of their long-term performance.

Numerous types of FRP bridge decks exist on the U.S. market that can be categorized in three groups: honeycomb sandwich, solid core sandwich, and hollow core sandwich. Figure 16.7 shows an example of honeycomb sandwich configuration, whereas Figure 16.8 shows a pultruded hollow core sandwich configuration.

Most FRP decks require validation by testing before being implemented in the field, and they are perfect candidates for deck replacement on low volume roads (Hong, and Hastak, 2006). The safety factor against failure of GFRP decks is usually between 3 and 8 (Alagusundaramoorthy et al. 2006); however the governing design feature for these decks is their stiffness that affects the maximum service load deflection.

TABLE 16.7 FRP Deck Construction in the United States

Manufacturer	Number of Decks Installed in Each Year									
	1996*	1997	1998	1999	2000	2001	2002	2003	2004	Total
Kansas Structural Composite, Inc.	1			2	5	3		1		12
Infrastructure Composites, Inc.				1						1
Martin Marietta Composites, Inc.	1	2		1	2	8	4	6	3	27
Hardcore Composites, Inc.		2	3	4	7	9	1			26
Creative Pultrusions, Inc.		3	2	2	1		1			9
Strongwell, Inc.	1	2						1		4
Others							2	2		4
Total each year	3	9	5	10	15	20	8	10	3	83

* Bridge decks before and including 1996.

Source: Telang, N. M. et al., NCHRP Report 564, Filed Inspection of In-Service FRP Bridge Decks, Transportation Research Board, Washington, DC, 2006.

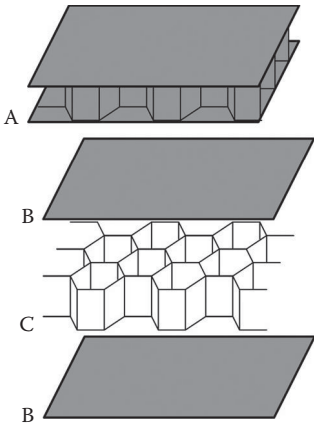

FIGURE 16.7 Honey comb sandwich configuration of FRP bridge panel.

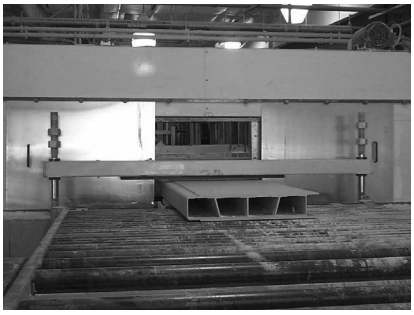

FIGURE 16.8 Pultruded hollow core FRP bridge deck. (From Godwin, G. et al., *Proceeding of 3rd International Conference on Composites in Infrastructure (ICCI'02)*, Omipress (CD-ROM), Paper 036, p. 12, 2002. With permission.)

16.4.2 Bridge Deck Slabs with Fiber Reinforced Polymer

Since FRPs are generally more expensive than protected steel reinforcement, it is prudent to utilize the arching action in the design of concrete bridge deck slabs, especially if they are exposed to corrosive environments. It is noted that both CHBDC (S6-06) and AASHTO LRFD design specifications permit the use of the arching action in the design of concrete deck slabs of girder bridges, the latter, however, does not deal with FRP reinforcement. The CHBDC in permitting the use of FRPs in bridge deck slabs divides these slabs into two categories: (1) internally restrained deck slabs, and (2) externally restrained deck slabs.

16.4.2.1 Internally Restrained Deck Slabs

An internally restrained deck slab is a concrete slab with embedded bottom transverse reinforcement that is designed according to Clause 16.8.8 of the CHBDC; the design provisions of this clause are summarized in the following, it being noted that as demonstrated by Khanna et al. (2000), the axial stiffness of the bottom transverse reinforcement governs the degree of arching in a deck slab.

General. The design method described herein is applicable to composite deck slabs supported on parallel girders, the center-to-center spacing of which does not exceed 3.7 m, or about 12 ft. When this method is used, the deck slab need not be analyzed, except for the effect of loads on the cantilever overlays and for negative longitudinal moment in continuous span bridges, and shall be deemed to have met all the requirements of the relevant design code.

Deck Slab Thickness. Unless a greater thickness is required to provide thicker cover to the reinforcement from considerations of durability, the minimum deck slab thickness should be the greater of 175 mm, or 7 in, and $S/15$, where S is the center-to-center spacing of girders. An additional thickness of 10 mm, or 0.4 in, at the top surface of exposed deck slabs should be provided to allow for wear.

Concrete Strength. The concrete used in the deck slab should have a minimum strength of 30 MPa, or 4.4 ksi.

Reinforcement. The deck slab with FRP bars should contain two orthogonal assemblies of FRP bars with the clear distance between the top and bottom transverse bars being a minimum of 55 mm, or 2.2 in.

For the transverse FRP bars in the bottom assembly, the area of cross-section in mm^2/mm should not be less than $500\, d_s/E_{FRP}$, where d_s is the distance from the top of the deck slab to the centroid of the bottom transverse bars in mm, and E_{FRP} is the modulus of elasticity of the FRP bars in MPa; for U.S.-customary units the area of cross-section of the FRP bars in square inches should not be $< 75 d_s/E_{FRP}$, where d_s is the distance from the top of the deck slab to the centroid of the bottom transverse bars in inches, and E_{FRP} is the modulus of elasticity of the FRP bars in ksi.

Longitudinal bars in the bottom assembly and both the longitudinal and transverse bars in the top assembly should be of GFRP with the minimum reinforcement ratio ρ being 0.0035. ρ should be calculated as the ratio of the area of cross-section of the bars and the area of the relevant section of the slab above the centroid of the bottom transverse bars.

The minimum cover to the FRP bars should be 35 mm with a construction tolerance of $\pm$10 mm or 1.4 in with a construction tolerance of $\pm$0.4 in.

Deck slabs of all continuous-span bridges should have cross-frames or diaphragms extending through the cross-section at all support lines or girders. Steel I-girders supporting deck slabs designed in accordance with the empirical design method should have intermediate cross-frames or diaphragms at a spacing of not > 8.0 m, or 26 ft, center-to-center.

Except as required in the following, deck slabs on box girders should have intermediate diaphragms, or cross-frames, at a spacing not exceeding 8.0 m, or 26 ft, center-to-center between the boxes. In lieu of the intermediate cross-frames or diaphragms between the boxes, the deck slab should contain reinforcement over the internal webbing, in addition to that required by the empirical method, to provide for the global transverse bending due to eccentric loads.

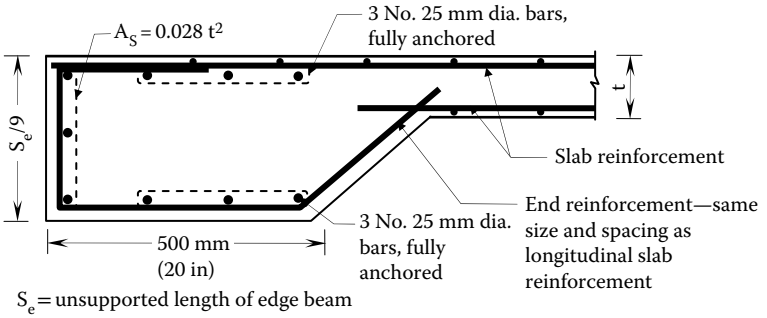

FIGURE 16.9 Edge stiffening at transverse free edges (in metric units). (From CHBDC, *CAN-CSA S6-06 Canadian Highway Bridge Design Code*. Canadian Standards Association, Mississauga, ON, Canada, 2006. With permission.)

Edge Stiffening. Free transverse edges of the deck slab at the bridge ends and other discontinuities should be supported by composite diaphragms either having the details as shown in Figure 16.9 or with details adopted from Clause 16.7 of the CHBDC (2006).

Overhangs. The transverse length of the deck slab overhangs beyond the outermost girders should be equal to or greater than the development length of the transverse reinforcement in the bottom layer.

16.4.2.2 Externally Restrained Deck Slabs

An externally restrained deck slab is a composite concrete slab with external straps or other confining systems designed in accordance with Clause 16.7 of the CHBDC (2006). The design provisions of this clause are summarized in the following.

General. An externally restrained deck slab supported on girders or stringers, being the supporting beams, and satisfying the following conditions need not be analyzed except for negative transverse moments because of loads on the overhangs and barrier walls, and for negative longitudinal moments in continuous span bridges.

Composite Action. The deck slab is composite with parallel supporting beams in the positive moment regions of the beams.

Beam Spacing. The spacing of the supporting beams, S, does not exceed 3000 mm, or 9.8 ft.

Slab Thickness. The total thickness, t, of the deck slab including that of the stay-in-place formwork if present is at least 175 mm, or 7 in, and not $< S/15$.

Diaphragms. The supporting beams are connected with transverse diaphragms, or cross-frames, at a spacing of not more than 8000 mm, or 26 ft.

Straps. The deck slab is confined transversely by means of straps, and the distance between the top of the straps and the bottom of the slab is between 25 and 125 mm, or 1 and 5 in.

The spacing of straps, S_l, is not more than 1250 mm, or 50 in, and each strap has a minimum cross-sectional area, A, in mm^2, given by

$$A = \frac{F_s S^2 S_l}{Et} \tag{16.19}$$

where F_s is 6.0 MPa for outer panels and 5.0 MPa for inner panels, S is the girder spacing in mm, S_l is strap spacing in mm, and E is the modulus of elasticity of the material of the strap in MPa. For U.S.-customary units, A is in in^2, S, S_l, and t are in inches, E is in ksi, and F_s is 0.87 ksi for outer panels and 0.72 ksi for inner panels. The direct or indirect connection of a strap to the supporting beams is designed to have a shear strength in Newtons of at least $200A$, or in kips of at least $29A$, where A is in in^2.

Shear Connectors. Either the projection of the shear connectors in the deck slab, t_s, is a minimum of 75 mm or 3 in, or additional reinforcement with a minimum t_s of 75 mm or 3 in is provided having at least the same shear capacity as that of the shear connectors.

Cover to Shear Connectors. The cover distance between the top of the shear connecting devices and the top surface of the deck slab shall be at least 75 mm, or 3 in, when the slab is not exposed to moisture containing chlorides; otherwise, either this cover distance is at least 100 mm or 4 in, or the shear connecting devices are provided with a coating approved by the authority having jurisdiction on the bridge.

Crack-Control Grid. The deck slab is provided with a crack control orthogonal grid of GFRP bars, placed near the bottom of the slab, with the area of cross-section of GFRP bars being at least $0.0015t^2$ mm^2/mm, where t is in mm; in U.S.-customary units, the area of cross-section of GFRP bars being at least $0.038t^2$ in^2/in, where t is in inches. In addition, the spacing of transverse and longitudinal crack control bars is not more than 300 mm, or 12 in.

Fiber Volume Fraction. For deck slabs with only one crack control grid, the fiber volume fraction shall be at least 0.002, but shall not exceed 0.005. For deck slabs with two reinforcement grids, no fiber need be added to the concrete.

Edge Stiffening. The transverse edges of the deck slab are stiffened by composite edge beams having the details of the edge beam as shown in Figure 16.10a, b, c, or d.

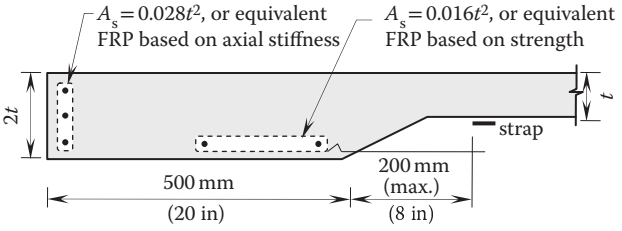

(a) Edge beam with thickened slab

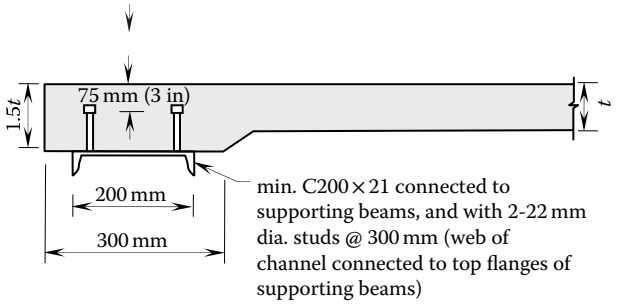

(b) Edge beam with composite steel channel

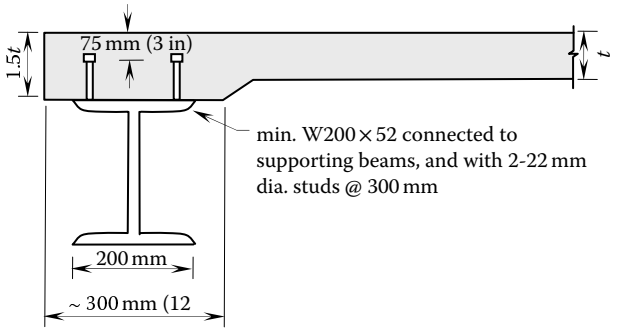

(c) Edge beam with composite steel I-beam

FIGURE 16.10 Details of permitted edge stiffening for steel-free deck slabs (in metric units). (From CHBDC, *CAN-CSA S6-06 Canadian Highway Bridge Design Code*. Canadian Standards Association, Mississauga, ON, Canada, 2006. With permission.)

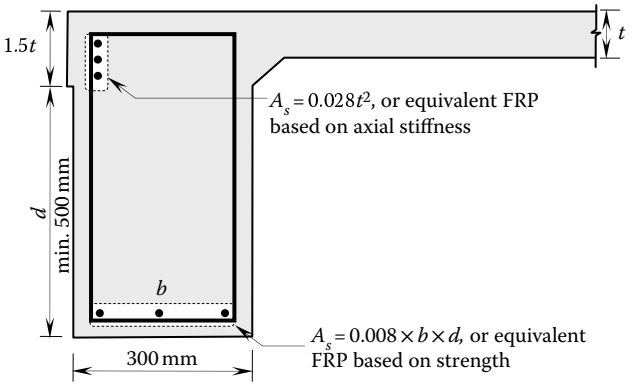

(d) Edge beam with reinforced concrete beam

FIGURE 16.10 (*Continued*) Details of permitted edge stiffening for steel-free deck slabs (in metric units). (From CHBDC, *CAN-CSA S6-06 Canadian Highway Bridge Design Code*. Canadian Standards Association, Mississauga, ON, Canada, 2006. With permission.)

Longitudinal Transverse Negative Moment. For continuous span bridges, the deck slab contains longitudinal negative moment reinforcement in at least those segments in which the flexural tensile stresses in concrete because of service loads are larger than $0.6f_{cr}$, where f_{cr} is calculated as follows in metric units:

$$f_{cr} = 0.4\sqrt{f_c'} \tag{16.20}$$

In U.S.-customary units, f_{cr} is calculated as follows:

$$f_{cr} = 0.25\sqrt{f_c'} \tag{16.21}$$

16.5 Rehabilitation of Concrete Bridges

16.5.1 General

The CHBDC (2006) specifies design provisions for the rehabilitation of concrete structures with FRP; these provisions, which are largely based on the works of Täljsten (1994; 2004a and 2004b), are applicable to existing concrete structures having the specified concrete strength $f_c' \leq 50$ MPa or 7 ksi, and strengthened with FRP comprising externally bonded systems or near surface mounted reinforcement (NSMR). If the concrete cover is < 20 mm or 0.8 in, NSMR is not permitted to be used. Rehabilitation of concrete structures having f_c' more than 50 MPa, or 7ksi, requires approval by authority having jurisdiction over the structure.

The behavior of concrete elements strengthened with FRP is highly dependent on the quality of the concrete substrate. Corrosion-initiated cracks are more detrimental for bond-critical applications than for contact-critical applications. The code defines bond-critical applications as those applications of FRP that rely on bond to the substrate for load transfer; an example of this application is an FRP strip bonded to the underside of a beam to improve its flexural capacity. Similarly, the contact-critical applications of FRP rely on continuous intimate contact between the substrate and the FRP system. An example of a contact-critical application is an FRP wrap around a circular column, which depends upon the radial pressure that it exerts on the column to improve its compressive strength.

Before developing a rehabilitation strategy, an assessment of the existing structure or elements is required to be conducted following the requirements of the evaluation section of the CHBDC (2006), ACI (2007), or ISIS (2007 b). Only those structures are permitted to be strengthened that have a live load

capacity factor F of 0.5 or greater. It is recalled that the evaluation section of the code defines F as follows for a structural component for the ultimate limit state (ULS):

$$F = \frac{U\phi R - \sum \alpha_D D - \sum \alpha_A A}{\alpha_L L(1+I)} \tag{16.22}$$

where

U = the resistance adjustment factor, depending upon the category of resistance; for example, its value for axial compression of reinforced concrete components is 1.11
φ = the resistance factor specified in the concrete section of the code with a value of 0.75 for concrete
R = nominal unfactored resistance of the component
α_D = load factor for effects because of dead loads
D = nominal load effect because of unfactored dead load
α_A = load factor for force effects because of additional loads including wind, creep, shrinkage, etc.
A = force effects because of the additional loads
α_L = load factor force effects because of live loads
L = force effects because of nominal, i.e. unfactored live loads
I = dynamic load allowance

16.5.2 Strengthening of Flexural Components

FRP rehabilitation systems of the externally bonded and NSMR types may be exposed to impact or fire. To provide safety against collapse in the event that the FRP reinforcement is damaged, the structures that are to be strengthened with FRP require a live load capacity factor, F, defined above, > 0.5. With $F > 0.5$, the structure without rehabilitation will thus be able to carry all the dead loads and a portion of the live loads. Similar stipulations can be found in CSA (2002) and ACI (2002). The requirement that $F > 0.5$ also provides some benefits under normal service conditions; the stresses and strains in all materials including, concrete, steel, and FRP, are limited and the risk of creep or yielding is avoided.

In addition to the conditions of equilibrium and compatibility of strains, the calculation for ULS is to be based on the material resistance factors for the materials of the parent component and those of the FRP, the assumptions implicit in the design of the parent component, and the following additional assumptions: (1) strain changes in the FRP strengthening systems are equal to the strain changes in the adjacent concrete; and (2) the contribution of the FRP in compression is ignored.

For an externally bonded flexural strengthening system, the maximum value of the strain in the FRP is not to exceed 0.006; this conservative requirement has been formulated to avoid a possible failure by the delamination of the FRP initiating at cracks in externally bonded flexural strengthening systems (Täljsten, 2002; Teng et al., 2002).

In the FRP strengthening of concrete components, the failure modes required to be considered are: (1) crushing of the concrete in compression before rupture of the FRP or yielding of the reinforcing steel; (2) yielding of the steel followed by rupture of the FRP in tension; (3) in the case of members with internal prestressing, additional failure modes controlled by the rupture of the prestressing tendons; (4) anchorage failure; (5) peeling failure or anchorage failure of the FRP system at the cut-off point; and (6) yielding of the steel followed by concrete crushing, before rupture of the FRP in tension.

For externally bonded FRP strengthening systems, the anchorage length beyond the point where no strengthening is required is not to be less than l_a given by

$$l_a = 0.5\sqrt{E_{FRP} t_{FRP}} \tag{16.23}$$

where t_{FRP} is the total thickness of externally bonded FRP plates or sheets in mm and E_{FRP} is the modulus of elasticity of the FRP, in MPa. For U.S.-customary units, l_a is given by the following equation in which t is in inches and E_{FRP} is in ksi.

$$l_a = 0.26\sqrt{E_{FRP}t_{FRP}} \tag{16.24}$$

In addition to the above requirement, the anchorage length should be at least 300 mm, or 12 in; otherwise the FRP needs to be suitably anchored.

The anchorage length is of central importance if an effective strengthening design is to be achieved. A good design will always lead to concrete failure.

16.5.3 Strengthening of Compression Components

When a column is strengthened with FRP, the compressive strength of the confined concrete, f'_{cc}, is determined from the following equation:

$$f'_{cc} = f'_c + 2f_{lFRP} \tag{16.25}$$

The confinement pressure because of FRP strengthening at the ULS, $f_{\ell FRP}$, is determined from the following equation:

$$f_{lFRP} = \frac{2\phi_{FRP} f_{FRPu} t_{FRP}}{D_g} \tag{16.26}$$

For columns with circular cross-sections, D_g is the diameter of the column; for columns with rectangular cross-sections having aspect ratios $\leq$1.5 and a smaller cross-sectional dimension not > 800 mm, or 32 in, D_g is equal to the diagonal of the cross-section.

Various formulae for determining the compressive strength of FRP-confined concrete have been assessed by Teng et al. (2002), Thériault and Neale (2000), and Bisby et al. (2005).

The confinement pressure at the ULS is required to be designed to lie between 0.1 and 0.33f'_c. The minimum confinement pressure is specified in order to ensure the ductile behavior of the confined section, and the maximum confinement pressure is specified in order to avoid excessive axial deformations and creep under sustained loads. The limit provided is such that the factored resistance of the FRP-confined concrete does not exceed the equivalent nominal strength of the unconfined concrete; that is, $0.8\varphi_c f'_{cc} \leq f'_c$.

16.5.4 Strengthening for Shear

The shear-strengthening scheme is to be of the type in which the fibers are oriented perpendicular or at an angle θ to the member axis. The shear reinforcement is to be anchored by suitable means in the compression zone by one of the following schemes:

- The shear-strengthening scheme is to be of the type in which the fibers are orientated perpendicular, or at an angle β, to the member axis. The shear reinforcement is to be anchored by suitable means in the compression zone by one of the following schemes: the shear reinforcement is fully wrapped around the section, as shown in Figure 16.11a.
- The anchorage to the shear reinforcement near the compression flange is provided by additional horizontal strips, as shown in Figure 16.11b.

FIGURE 16.11 Anchorage of externally bonded FRP shear reinforcement (a) fully wrapped section, (b) anchorage with horizontal strips, and (c) anchorage in compression zone.

- The anchorage is provided in the compression zone, as shown in Figure 16.11c. If none of these schemes can be provided, special provisions must be made.

For reinforced concrete members with rectangular or T-sections and having the FRP shear reinforcement anchored in the compression zone of the member, the factored shear resistance, V_r, is calculated from

$$V_r = V_c + V_s + V_{FRP} \tag{16.27}$$

where V_c and V_s are calculated as for steel-reinforced sections, and V_{FRP} is obtained from the following:

$$V_{FRP} = \frac{\phi_{FRP} E_{FRP} \varepsilon_{FRPe} A_{FRP} d_{FRP} (\cot\theta + \cot\beta)\sin\beta}{s_{FRP}} \tag{16.28}$$

where

$$A_{FRP} = 2t_{FRP} w_{FRP} \tag{16.29}$$

For completely wrapped sections

$$\varepsilon_{FRPe} = 0.004 \le 0.75\varepsilon_{FRPu} \tag{16.30}$$

For other configurations, ε_{FRPe} is calculated from

$$\varepsilon_{FRPe} = \kappa_V \varepsilon_{FRPu} \le 0.004 \tag{16.31}$$

where for continuous U-shape configurations of the FRP reinforcement, the bond-reduction coefficient, κ_V, is as follows:

$$\kappa_V = \frac{k_1 k_2 L_e}{11900\varepsilon_{FRPu}} \le 0.75 \tag{16.32}$$

and

$$k_1 = \left(\frac{f_c'}{27}\right)^{2/3} \tag{16.33}$$

$$k_2 = \frac{d_{FRP} - L_e}{d_{FRP}} \tag{16.34}$$

$$L_e = \frac{23,300}{\left(t_{FRP} E_{FRP}\right)^{0.58}} \tag{16.35}$$

It is noted that the value of ε_{FRP_e} is limited to 0.004 in order to maintain aggregate interlock in the evaluation of V_c.

For prestressed concrete components, V_r is the sum of V_c, V_s, V_p, and V_{FRP}, where the general theory for steel reinforced concrete is used to calculate V_c, V_s, and V_p, and the equations given above to calculate V_{FRP}.

16.5.5 Case Histories of Rehabilitation using Fiber Reinforced Polymers

Sheikh and Homam (2007) have described two severely deteriorated concrete columns, which were rehabilitated with GFRP. Several deteriorated columns, which are under a bridge in Toronto, Canada, can be seen in Figure 16.12.

In 1995, using a steel formwork, one of the deteriorated columns was encased in grout of expansive cement, developed by Timusk and Sheikh (1977). A part of the formwork can be seen in Figure 16.13.

It is important to note that no effort was made to remove either the corroded steel or concrete contaminated with chlorides from de-icing salts. Approximately 20 hours after casting the grout, the formwork was removed and the grout layer was first wrapped in a polyethylene sheet and then with two layers of a GFRP sheet, in which most of the fibers were aligned in the circumferential direction of the column. Three days after grouting, the GFRP wrapping was instrumented with strain gauges measuring circumferential strains. The rehabilitated column can be seen in Figure 16.13b. Sheikh and Homam

FIGURE 16.12 Deteriorated concrete columns.

(a) (b)

FIGURE 16.13 Rehabilitation of a concrete column. (a) Partial formwork for grout with expansive cement. (b) Rehabilitated column.

FIGURE 16.14 Rehabilitated columns of the Portage Creek Bridge in British Columbia, Canada.

(2007) report that within about 7 days after the pouring of the grout, the tensile circumferential strains in the GFRP wrapping grew to about 1500 με, thus effectively applying a radial prestressing pressure to the column. As noted by Erki and Agarwal (1995), the concept of using expansive grout to prestress the rehabilitated column radially was introduced by Baidar Bakht.

The strains in the rehabilitated column are being monitored periodically. It has been found that over the past 12 years, the circumferential strains in the GFRP wrapping have dropped only slightly, thus confirming that the radial pressures generated by the expansive grout exist on a long-term basis.

Several half-cells were installed in the rehabilitated column to monitor the corrosion activity of the steel reinforcement. Data collected in these half-cells, by the Ministry of Transportation of Ontario, has shown that the corrosion activity in the steel reinforcement of the rehabilitated column has decreased over 12 years of monitoring. The reduction of the corrosion activity is likely to be the result of preventing the ingress of the main elements necessary for steel corrosion, namely oxygen and water.

The case history described above confirms the effectiveness of repairing deteriorated columns by wrapping them with FRP. It is also important to note that the seismic resistance of columns, especially those with circular cross-sections, can be improved considerably by wrapping them with FRPs. One example of enhancing the seismic resistance of bridge columns is the Portage Creek Bridge in British Columbia, Canada. Wrapping the columns with GFRP sheets is described by Mufti et al. (2003); the rehabilitated columns can be seen in Figure 16.14.

16.6 Rehabilitation of Timber Bridges

Many U.S. and Canadian jurisdictions have a large number of timber bridges that have been in service for more than five decades. These structures need to be either rehabilitated or replaced to satisfy current load rating requirements. FRPs have high strength and low weight and therefore, they are perfect material for strengthening timber structures. This rehabilitation technique can provide a cost-effective way of increasing the life span of some of these structures. Research has found that FRP reinforcement acts to cross any defects that may be present in the timber (Gentile et al., 2002) and increases its strength. Both shear and flexural strengthening systems have been developed. To increase a beam's shear capacity, FRP bars, inserted perpendicular to the beam axis, are used as shear dowels, or beams can be wrapped in the shear zone using straps of FRP sheets shown in Figure 16.18f later in the chapter. Flexural strengthening can be similarly achieved by using either FRP bars, or FRP sheets. The first system using bars is referred to as near surface mounted reinforcement. As a rule, both flexural and shear strengthening needs to be provided at the same time. The Canadian Bridge Design Code CSA (2006) provisions for the strengthening of timber beams are briefly described in the following.

Bars that may be used for flexural strengthening need to have a fiber-volume fraction of at least 60%. At least two bars per beam are recommended, that are embedded in grooves with rounded inside edges,

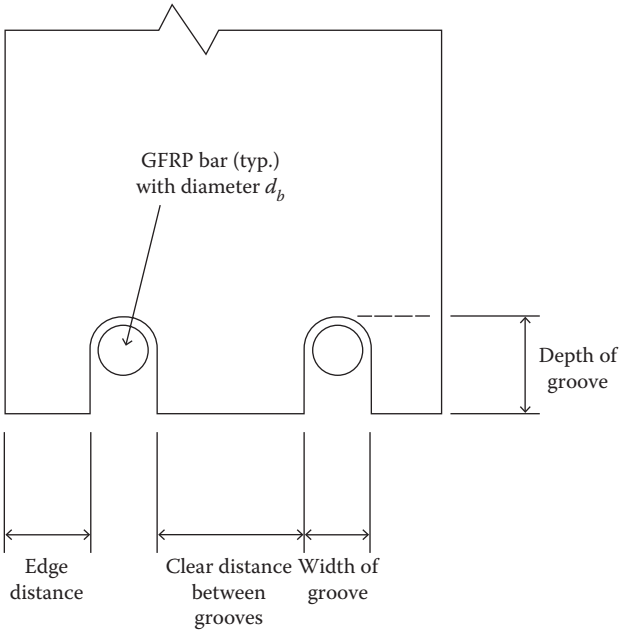

FIGURE 16.15 Cross-section of timber beam with NSM reinforcement. (From CHBDC, *CAN-CSA S6-06 Canadian Highway Bridge Design Code*. Canadian Standards Association, Mississauga, Ontario, Canada, 2006. With permission.)

FIGURE 16.16 Tour and Creek Bridge, Manitoba, Canada after strengthening for flexure.

and depth of 1.6–2d_b and width equal to d_b plus 5 mm (1/5 in). The distance between the grooves should be 25 mm (1 in) for best performance. Figure 16.15 illustrates the strengthening scheme.

The epoxy that is used for strengthening has to be compatible with the treatment of the timber, and the grooves need to be cleaned by pressurized air before application of epoxy, to provide adequate bond between the two materials. The photograph in Figure 16.16 shows a bridge after completion of the strengthening for flexure.

Strengthening for shear can be provided either by dowels or sheets. The dowels are inserted either perpendicular to the axis of the beam, or at a 45° angle, as shown in Figure 16.17. Any splits need to be mechanically closed before the application of strengthening scheme. The diameter of the dowels should be at least 15 mm (5/8 in) and they should be spaced a distance h equal to the depth of the section on the center.

Shear strengthening using FRP sheets is a popular method of increasing shear capacity of reinforced and prestressed concrete structures; however, it does not have known in-situ applications to date on timber structures. Timber is usually treated with protective coating that may interfere with the bond between

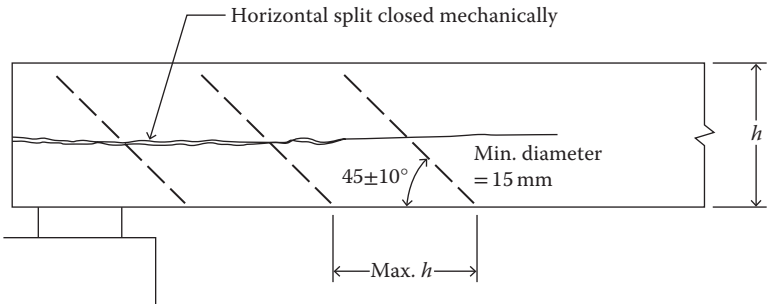

FIGURE 16.17 Part elevation of timber beam with FRP dowels for shear strengthening. (From CHBDC, *CAN-CSA S6-06 Canadian Highway Bridge Design Code*. Canadian Standards Association, Mississauga, Ontario, Canada, 2006. With permission.)

(a)

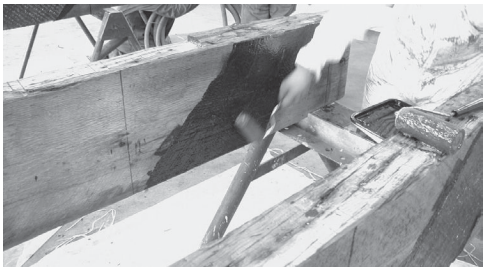

(b)

(c)

FIGURE 16.18 Stages of specimen strengthening using GFRP sheet. (a) Application of primer. (b) Application of saturant. (c) Placing of GFRP sheet.

(d)

(e)

(f)

FIGURE 16.18 (*Continued*) Stages of specimen strengthening using GFRP sheet. (d) Embedding sheet into saturant using steel roller. (e) Applying final coat of saturant. (f) Timber beam after strengthening.

the substrate and the epoxy used to glue the FRP sheet. The Canadian Bridge Design Code CSA S6-06 allows the use of this technique if the splits were mechanically closed, and the width of the sheets is at least the width of the beam. The sheets need to be inclined at 45° angle along the beam length, beginning as close to the center of the support as possible. The sheets wrap around the side of the beam and therefore

edges of the beam have to be rounded to 12 mm (1/2 in) radius to avoid any stress concentrations. The photographs in Figure 16.18 show the various stages of the strengthening process using GFRP sheets.

The CHBDC method of strengthening timber beams is very simple to apply. If a timber beam is strengthened for flexure according to the specified procedure then the specified bending strength of its species can be increased by 20% and 50% for Grades 1 and 2, respectively. If the grade of the beam is determined to be Select Structural, then the increase in the specified bending strength is 5% if the beam is strengthened for only flexure; however, if the beam is also strengthened for shear then the permitted increase in the specified bending strength is 10%.

For beams strengthened for shear by GFRP sheets according to the CHBDC specifications, the specified shear strength is permitted to be increased by 100%, and if the shear strengthening by GFRP embedded bars, the permissible increase in the specified shear strength is 120%.

16.7 Case Histories

16.7.1 Crowchild Trail Bridge, Alberta

Many of Canada's bridges require upgrading because they were not built to handle the weight of today's increased traffic loads. Calgary's Crowchild Bridge shown in Figure 16.19 is one such case. The 90 m (295 ft) long, 11 m (36 ft) wide, rehabilitated bridge carries two lanes of traffic over its three continuous spans. The deck slab, free of reinforcing steel, is supported by five steel girders and is restrained transversely by external steel straps. GFRP C-bars were used to provide the continuity and to minimize the transverse cracks of the steel-free deck over the intermediate bridge piers.

FIGURE 16.19 Crowchild Trail Bridge, Alberta.

FIGURE 16.20 Hall's Harbor Wharf, Nova Scotia.

Based on the results of a full-scale model test at the University of Manitoba, GFRP C-bars were also used to reinforce the cantilever slabs of the bridge. On a tendered basis, it proved to be the least costly option.

The deck slab has cantilevers on either side, reinforced with GFRP rods. In order to reduce surface cracks, the bridge deck concrete contains short random polypropylene fibers. The completed bridge is stronger, more resistant to corrosion, and less expensive to maintain than if it had been constructed using traditional methods and materials.

The bridge is also outfitted with remote monitoring technology: 81 strain gauges, 19 embedded gauges, 5 thermisters, 3 smart glass rebars, and 2 fiber-optic gauges.

16.7.2 Hall's Harbor Wharf, Nova Scotia

Figure 16.20 Hall's Harbor Wharf is Canada's first wharf utilizing lightweight, noncorroding GFRP V-Rod bars and a steel-free deck slab.

Following the failure of a 40 m (131 ft) section of wharf timber piles, the need to rehabilitate the 1904 structure took on an even higher level of urgency than had already been allotted. Like many East Coast communities, Hall's Harbor had assumed the responsibility for its marine infrastructure from the federal government.

In preliminary design work with Vaughan Engineering, the ISIS Canada's team of engineers in Halifax showed that the cost of using innovative materials and technologies was only slightly more than the cost associated with conventional materials. The additional cost of the GFRP reinforcements and steel-free deck over conventional steel reinforced concrete was $20,000 or 4.5% of the total cost of the rehabilitated structure.

The long-term benefits, however, were substantially more attractive because the absence of steel reinforcements extends the life of the wharf from approximately 30 years to between 60 and 80 years with minimal maintenance. This is a critical factor given that communities like Hall's Harbor are solely responsible for maintaining their wharfs. The inclusion of fiber-optic monitoring technology embedded in GFRP rods provides solid data to support the application of FRPs in other marine environment structures.

The wharf incorporates several innovative technologies. It is constructed with concrete deck panels on deep concrete beams or pile caps spaced at approximately 4 m (13 ft). The transverse beams are supported on steel piles at both the front face and back. The pile caps contain a unique design where an outer layer of GFRP V-Rod reinforcement under low stress protects an inner layer of minimum steel reinforcement. The deck panels contain synthetic fiber-reinforced concrete and utilize an internal

FIGURE 16.21 Aerial view of Joffre Bridge during construction. (From ISIS, *Design Manual 3: Reinforcing Concrete Structures with Fibre Reinforced Polymers*. ISIS Canada, Intelligent Sensing for Innovative Structures, A Canadian Network of Centres of Excellence, University of Manitoba, Winnipeg, Manitoba, Canada, 2007a. With permission.)

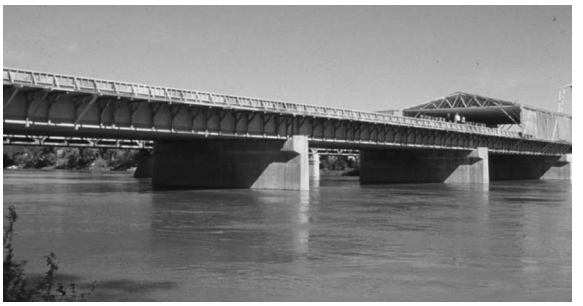

FIGURE 16.22 The Taylor Bridge, in Headingley, Manitoba, during construction.(From ISIS, *Design Manual 3: Reinforcing Concrete Structures with Fibre Reinforced Polymers*. ISIS Canada, Intelligent Sensing for Innovative Structures, A Canadian Network of Centres of Excellence, University of Manitoba, Winnipeg, Manitoba, Canada, 2007a. With permission.)

compressive arching technology. The panels also contain GFRP rods to reinforce against uplift force created by wave action during severe storms.

16.7.3 Joffre Bridge, Québec

Early in August of 1997, the province of Québec decided to construct a bridge using CFRPs. The Joffre Bridge, spanning the Saint Francois River, was another contribution to the increasing number of FRP-reinforced bridges in Canada. A portion of the Joffre Bridge concrete deck slab is reinforced with CFRP, as are portions of the traffic barrier wall and the sidewalk.

The bridge, shown in Figure 16.21, is outfitted extensively with various kinds of monitoring instruments including fiber-optic sensors embedded within the FRP reinforcement. Over 180 monitoring instruments are installed at critical locations in the concrete deck slab and on the steel girders, to monitor the behavior of the FRP reinforcement under service conditions. The instrumentation is also providing valuable information on long-term performance of the concrete deck slab reinforced with FRP materials.

16.7.4 Taylor Bridge, Manitoba

A significant research milestone was achieved on October 8, 1998, when Manitoba's Department of Infrastructure and Transportation opened the Taylor Bridge in Headingley, Manitoba, Canada. The two-lane, 165.1 m (541 ft) long structure has four out of 40 precast concrete girders reinforced with CFRP stirrups. These girders are also prestressed with CFRP cables and bars. GFRP reinforcement has been used in portions of the barrier walls. The bridge during construction can be seen in Figure 16.22.

As a demonstration project, it was vital the materials be tested under the same conditions as conventional steel reinforcement. Thus, only a portion of the bridge was designed using FRPs.

Two types of CFRPs were used in the Taylor Bridge. CFRP cables produced by Tokyo Rope, Japan, were used to pretension two girders, whereas the other two girders were pretensioned using Leadline bars produced by Mitsubishi Chemical Corporation, Japan. Two of the four FRP-reinforced girders were reinforced for shear using carbon FRP stirrups and Leadline bars in a rectangular cross-section. The other two beams were reinforced for shear using epoxy-coated steel reinforcement.

The deck slab was reinforced by indented Leadline bars similar to the reinforcement used for prestressing. GFRP bars produced by Marshall Industries Composites Inc. were used to reinforce a portion of the New Jersey-type barrier wall. Double-headed, stainless steel tension bars were used for the connection between the barrier wall and the deck slab.

FIGURE 16.23 Lower Deck of Centre Street Bridge, Calgary, Alberta.(From ISIS, *Design Manual 3: Reinforcing Concrete Structures with Fibre Reinforced Polymers*. ISIS Canada, Intelligent Sensing for Innovative Structures, A Canadian Network of Centres of Excellence, University of Manitoba, Winnipeg, Manitoba, Canada, 2007a. With permission.)

16.7.5 Centre Street Bridge, Alberta

In 2000, the Centre Street Bridge in Calgary underwent a major rehabilitation to remove deteriorated concrete and upgrade the structure, originally built in 1903, to modern design standards. Beneath the main arches, the old deck structure was removed and a new reinforced concrete deck constructed (Figure 16.23). The design of this deck incorporated a hybrid reinforcement design concept that is expected to be more durable deck slabs.

It has been shown that top reinforcement does not contribute significantly to the strength of a concrete slab on girder bridge deck and that it can be removed entirely from the deck (Khanna et al., 2000). The current orthotropic steel reinforcement approach has two major drawbacks. Nonessential reinforcement is responsible for most of the costly maintenance deterioration problems and the protection of this same reinforcement leads to higher initial construction costs.

Although this top layer may not be essential for strength, it is desirable for reasons of serviceability and continuity to have secondary reinforcement in the upper portion of a deck slab. The Centre Street Bridge lower deck utilizes a hybrid design concept with GFRP reinforcement for the top layer and steel reinforcement for the bottom layer. Based on an improved understanding of concrete bridge deck slab behavior, the bottom layer of steel reinforcement is designed for stiffness based on arching principles and the top layer of noncorrodible FRP reinforcement is provided as secondary reinforcement.

The lower deck is constructed with a 200 mm (8 in) thick reinforced concrete deck slab supported by four steel stringers at a spacing of 1870 mm (6.1 ft) across the width of the deck. Steel transverse floor beams support the deck and stringers at 4510 mm (14.8 ft) intervals. The floor beams are suspended from hanger rods that are attached to the heavy concrete arches forming the main support system for the entire structure. The bottom reinforcement is 15 M steel bars (with a diameter of 0.63 in) at 300 mm, or 12 in, in both directions, satisfying the 0.3% reinforcement criteria of the empirical design method of the CHBDC. The top layer was a GFRP grid made from 10 × 13 mm, or 0.39 × 0.51 in, grid element at 250 mm (10 in) in the transverse direction and 10 × 10 mm, or 0.39 × 0.39 in, element in the longitudinal direction. The properties of the grid are an ultimate strength of 600 MPa, or 86 ksi, and a modulus of elasticity of 30 GPa, or 4350 ksi. As required by CHBDC provisions, this amount of GFRP provides the equivalent strength to the steel layer it replaces.

16.7.6 Université de Sherbrooke Pedestrian Bridge, Québec

A student design competition for a pedestrian bridge enabled the use of new-generation structural technologies. Set up by ISIS, the aim of this competition was to design a pedestrian bridge with a covered

FIGURE 16.24 Université de Sherbrooke Pedestrian Bridge. (From ISIS, *Design Manual 3: Reinforcing Concrete Structures with Fibre Reinforced Polymers*. ISIS Canada, Intelligent Sensing for Innovative Structures, A Canadian Network of Centres of Excellence, University of Manitoba, Winnipeg, Manitoba, Canada, 2007a. With permission.)

FIGURE 16.25 Tourand Creek Bridge in Manitoba, Canada.

span of 6 m, or 19.7 ft, providing access to a new entrance to the Faculty of Engineering at the Université de Sherbrooke. The objective of this project was to provide the opportunity for ISIS Canada students to participate in the design of a construction project incorporating composite materials with the integration of new fiber-optic monitoring technologies. For this project, V-ROD GFRP and CFRP bars have been used as reinforcement for the deck slab and the beams, respectively.

The composite materials for the structures and the monitoring of fiber optics were two main research goals of ISIS Canada. The winning team from Queen's University was invited to participate in the final design of the project with the engineering firm responsible for the project (Figure 16.24).

16.7.7 Tourand Creek Bridge, Manitoba, Canada

The Tourand Creek timber bridge south of Winnipeg on Highway 59, Manitoba, Canada was selected as the first of its kind to undergo an innovative strengthening technique developed by ISIS Canada, whereby GFRP bars are embedded in the timber stringers and adhered to the wood beams with an epoxy resin. The structure shown in Figure 16.25, which is over 40 years old, is now at least 30% stronger and can carry normal traffic loads. Manitoba has 575 timber bridges, all built before 1980 and requiring strengthening in order to accommodate the increased traffic load weights permitted by the Transportation Association of Canada. Manitoba transportation has estimated that replacing the province's aging structures would require an investment of approximately $260 million. Using the ISIS

FIGURE 16.26 Reinforcement of the bridge deck slab and barrier walls, Val-Alain Bridge.(From ISIS, *Design Manual 3: Reinforcing Concrete Structures with Fibre Reinforced Polymers*. ISIS Canada, Intelligent Sensing for Innovative Structures, A Canadian Network of Centres of Excellence, University of Manitoba, Winnipeg, Manitoba, Canada, 2007a. With permission.)

technique, bridges like Tourand Creek can achieve the same strength as a new structure for < 15% of the cost estimated to completely replace the bridge.

16.7.8 Val-Alain Bridge on Highway 20 East (Québec)

The Val-Alain Bridge is located in the Municipality of Val-Alain on Highway 20 East, and crosses over Henri River in Québec, Canada. The bridge is a slab-on-girder type with a skew angle of 20° over a single span of 49.89 m, or 163 ft, and a total width of 12.57 m, or 41 ft. The bridge has four simply supported steel girders spaced at 3145 mm, or 10.3 ft. The deck slab is a 225 mm, or 9 in thick, with semi-integral abutments, continuous over the steel girders with an overhang of 1570 mm, 5.15 ft, on each side. The concrete deck slab and the bridge barriers were reinforced with sand-coated V-Rod GFRP composite bars utilizing high-performance concrete.

The deck slab was designed based on serviceability criteria. The crack width and allowable stress limits were the controlling design factors. The Ministry of Transportation Quebec has selected to limit the maximum allowable crack width to 0.5 mm, or 0.02 in, and the stresses in the GFRP bars between 30% and 15% of the ultimate strength of the material under service and sustained loads, respectively. Based on this design approach, the bridge deck slab was entirely reinforced with two identical reinforcement mats using No. 19 GFRP bars. For each reinforcement mat, No. 19 GFRP bars spaced at 125 and 185 mm, or 5 and 7.25 in, in the transverse and longitudinal directions, respectively, were used. A 40 and 35 mm, or 1.4 in, top and bottom clear concrete cover, respectively, was used. Additional No.19 GFRP bars

FIGURE 16.27 Deck rehabilitation of Glendale Avenue Bridge.(From ISIS, *Design Manual 3: Reinforcing Concrete Structures with Fibre Reinforced Polymers*. ISIS Canada, Intelligent Sensing for Innovative Structures, A Canadian Network of Centres of Excellence, University of Manitoba, Winnipeg, Manitoba, Canada, 2007a. With permission.)

spaced at 250 mm, or 10 in, were placed in the top transverse layer at the two cantilevers, as well as in the top longitudinal layer at the ends of the deck slab.

The bridge was constructed in 2004 and was well-instrumented at critical locations to record internal temperature and strain data. The bridge was tested for service performance as specified by the CHBDC using two four-axle calibrated trucks (Benmokrane et al., 2005). The Val-Alain bridge, shown during construction in Figure 16.26, is Canada's first concrete bridge deck totally reinforced with GFRP bars with an expected service life of more than 75 years.

16.7.9 Deck Rehabilitation of Glendale Avenue Bridge (Region of Niagara, Ontario)

A new parapet wall was constructed on the existing bridge deck using GFRP V-Rod reinforcement. The design was completed following current codes and design standards outlined in the ACI 318, ACI 440, and CSA S6. The design was supported by lab and field pull-out tests. It was determined that the use of GFRP provided the region with the best reinforcement solution considering long-term sustainable benefits and noncorrosive properties of GFRP. The durability of GFRP was the driving factor in using GFRP reinforcement. The actual costing also proved to be very favorable in comparison with conventional epoxy-coated reinforcement. The region of Niagara has accepted the design and use of GFRP in certain components of bridge structures (Figure 16.27), with consideration for future use in other bridge structures.

References

ACI. 1995. *State-of-the-Art Report on Fiber Reinforced Plastic (FRP) Reinforcement for Concrete Structures.* American Concrete Institute, Farmington Hills, MI.

ACI. 2002. 440.2R-02 *Guide for the Design and Construction of Externally Bonded FRP Systems for Strengthening Concrete Structures.* American Concrete Institute, Farmington Hills, MI.

ACI. 2007. *Guide for Evaluation of Concrete Structures Prior to Rehabilitation*, American Concrete Institute, Farmington Hills, MI (ACI364.1R–07).

Alagusundaramoorthy, A., Harik, I. E., & Choo, C. C. 2006. Structural Behaviour of FRP Composite Bridge Deck Panels. *ASCE Journal of Bridge Engineering*, 11(4), 384–393.

Aly, A., Bakht, B., & Schaeffer, J. 1997. Design and Construction of Steel-fee Deck Slab in Ontario. *Annual Conference of Canadian Society for Civil Engineering*, Montreal, Que., 6, 81–90.

Banthia, N., & MacDonald, R. 1996. Durability of Fiber-Reinforced Plastics and Concretes, Part 1: Durability of Components. Submitted to ACMBS Network of Canada, p. 25.

Bedard, C. 1992. Composite Reinforcing Bars: Assessing their Use in Construction. *Concrete International*, Volume 14 Issue 1 pp. 55–59.

Benmokrane, B., Wang, P., Ton-That, T. M., Rahman, H., & Robert, J-F. 2002. Durability of GFRP reinforcing bars in concrete. *ASCE Journal of Composites for Construction*, 6(3), 143–155.

Benmokrane, B., El-Salakawy, E., Goulet, S., & Nadeau, D. 2005. Design, Construction, and Testing of Innovative Concrete Bridge Decks Using Glass FRP Composite Bars, *Proceedings of the 3rd International Conference on Composites in Construction (CCC-2005).* Vol. 2, pp. 873–880, Lyon, France.

Bisby, L. A., Dent, A. J. S., & Green, M. 2005. Comparison of Confinement Models For Fibre-Reinforced Polymer-Wrapped Concrete. *ACI Structural Journal*, 102(1), 62–72.

Chaallal, O., & Benmokrane, B. 1993. Physical and Mechanical Performance of an Innovative Glass-Fibre-Reinforced Plastic Rod. *Canadian Journal of Civil Engineering*, 20(2), 254–268.

CHBDC. 2000. *CAN-CSA S6-00 Canadian Highway Bridge Design Code.* Canadian Standards Association, 5060 Spectrum Way, Suite 100, Mississauga, ON, Canada L4W 5N6.

CHBDC. 2006. *CAN-CSA S6-06 Canadian Highway Bridge Design Code.* Canadian Standards Association, 5060 Spectrum Way, Suite 100, Mississauga, ON, Canada L4W 5N6.

Coomarasamy, A., & Goodman, S. 1997. *Investigation of the Durability Characteristics of Fiber Reinforced Polymer (FRP) Materials in Concrete Environment*, American Society for Composites-Twelfth Technical Conference, Dearborn, Michigan.

CSA. 2002. *CAN-CSA S806-02 Design and construction of building structures with fibre-reinforced polymers.* Canadian Standards Association, 5060 Spectrum Way, Suite 100, Mississauga, ON, Canada L4W 5N6.

CSA. 2004. *CAN-CSA A23.3-04 Design of Concrete Structures.* Canadian Standards Association, 5060 Spectrum Way, Suite 100, Mississauga, ON, Canada L4W 5N6.

CSA. 2010. *CAN-CSA S807-10 Specifications for fibre-reinforced polymers.* Canadian Standards Association, 5060 Spectrum Way, Suite 100, Mississauga, ON, Canada L4W 5N6.

Debaiky, A. S., Nkurunziza, G., Benmokrane, B., & Cousins, P. 2006. Residual Tensile Properties of GFRP Reinforcing Bars after Loading in Severe Environments. *ASCE Journal of Composites for Construction*, 10(5), 1–11.

Erki, M.-A, & Agarwal, A. C. 1995. Strengthening of reinforced concrete axial members using fibre composite materials: a survey. *Proceedings, Annual Conference of Canadian Society for Civil Engineering*, Ottawa, Vol. II, p. 565–574.

Faza, S. S. 1991. Bending and Bond Behavior and Design of Concrete Beams Reinforced with Fiber Reinforced Plastic Rebars. Ph.D. Dissertation, West Virginia University, Morgantown, West Virginia.

Gentile, C., Svecova, D., & Rizkalla, S. H. 2002. Timber Beams Strengthened with GFRP Bars – Development and Application. *ASCE Journal of Composites for Construction*, 6(1), 11–20.

Gerritse, A. 1992. Durability Criteria for Non-Metallic Tendons in an Alkaline Environment. *Proceedings of the First International Conference on Advance Composite Materials in Bridges and Structures (ACMBS-I).* Canadian Society of Civil Engineers, Sherbrooke, Québec, pp. 129–137.

Godwin, G., Toddie, J., & Steggall, P. 2002. Lewis County, New York, Bridge Using a Low Profile, 5" Deep Fiber-Reinforced Polymer Composite Deck, *Proceeding of 3rd International Conference on Composites in Infrastructure (ICCI'02)*, Omipress (CD-ROM), Paper 036, p. 12.

Hong, T., and Hastak, M. 2006. Construction, Inspection and Maintenance of FRP Bridge Deck Panels. *ASCE Journal of Composites for Construction*, 10(6), pp. 561–572.

ISIS. 2006. *Specifications for Product Certification of Fibre Reinforced Polymers (FRPs) as Internal Reinforcement in Concrete Structures.* ISIS Canada, Intelligent Sensing for Innovative Structures, A Canadian Network of Centres of Excellence, A250 Agriculture Engineering Building, University of Manitoba, Winnipeg, Manitoba, R3T 2N2, Canada.

ISIS. 2007a. *Design Manual 3: Reinforcing Concrete Structures with Fibre Reinforced Polymers.* ISIS Canada, Intelligent Sensing for Innovative Structures, A Canadian Network of Centres of Excellence, A250 Agriculture Engineering Building, University of Manitoba, Winnipeg, Manitoba, R3T 2N2, Canada.

ISIS. 2007b. *Design Manual 4: Strengthening Reinforced Concrete Structures with Externally-Bonded Fibre Reinforced Polymers.* ISIS Canada, Intelligent Sensing for Innovative Structures, A Canadian Network of Centres of Excellence, A250 Agriculture Engineering Building, University of Manitoba, Winnipeg, Manitoba, R3T 2N2, Canada.

JSCE. 1993. *State-of-the-Art Report on Continuous Fiber Reinforcing Materials.* Research Committee on Continuous Fiber Reinforcing Materials, Japan Society of Civil Engineers, Tokyo, Japan.

Karbhari, V., Wang, D., & Gao, Y. 2001. Processing and Performance of Bridge Deck Subcomponents Using Two Schemes of Resin Infusion. *Composite Structures*, 51(3), 257–271.

Khanna, O. S., Mufti, A. A., and Bakht, B. 2000. Reinforced concrete bridge deck slabs. Canadian *Journal of Civil Engineering*, 27(3), 475–480.

Kobayashi, K., and Fujisaki, T. 1995. Compressive Behaviour of FRP Reinforcement in Non-prestressed Concrete Members. *Proceedings of the Second International Symposium on Non-metallic (FRP) Reinforcement for Concrete Structures (FRPRCS-2).* Taerwe (Ed.), RILEM proceedings 29, Ghent, Belgium, pp. 267–274

Mufti, A. A., Neale, K. W., Rahman, S., and Huffman, S. 2003. GFRP seismic strengthening and structural health monitoring of Portage Creek Bridge concrete columns. *Proceedings, fib2003 Symposium—Concrete Structures in Seismic Regions*, Athens, Greece.

Mufti, A., Onofrei, M., Benmokrane B., Banthia, N., Boulfiza, M., Newhook, J., Bakht, B., Tadros, G., & Brett, P. 2005. Durability of GFRP Reinforced Concrete in Field Structures. *Proceedings of 7th International Symposium on Fiber Reinforced Polymer Reinforcement for Concrete Structures*, FRPRCS-7, pp.1361–1377.

Newhook, J. P., Bakht, B., & Mufti, A. A. 2000. Design and Construction of a Concrete Marine Structure Using Innovative Technology. *Proceedings of the 3rd International Conference on Advanced Composite Materials in Bridges and Structures.* Canadian Society for Civil Engineering, pp. 777–784.

Nystrom, H. E., Watkins, S. E., Nanni, A., & Murray, S. 2003. Financial Viability of Fiber-Reinforced Polymer (FRP) Bridges. *ASCE Journal of Management in Engineering*, 19(1), 2–8.

Parkyn, B. 1970. *Glass Reinforced Plastics*, Iliffe Books, London.

Phillips, L. N. 1989. *Design with Advanced Composite Materials*, Springer-Verlag, Berlin.

Porter, M. L., Mehus, J., Young, K. A., O'Neil, E. F., & Barnes, B. A. 1997. Aging of Fiber Reinforcement in Concrete. *Proceedings of the Third International Symposium on Non-Metallic (FRP) Reinforcement for Concrete Structures (FRPRCS-3).* Japan Concrete Institute, Sapporo, Japan, Vol. 2, pp. 59–66.

Porter, M. L., & Barnes, B. A. 1998. Accelerated Durability of FRP Reinforcement for Concrete Structures. *Proceedings of the First International Conference on Composites for Construction (CDCC 1998).* Sherbrooke, Québec, pp. 191–198.

Sheikh, S. A., & Homam, S. M. 2007. *Long-Term Performance of Gfrp Repaired Bridge Columns.* Third International Conference on Structural Health Monitoring of Intelligent Infrastructure, Vancouver, British Columbia, Canada (proceedings on CD).

Tadros, G., Tromposch, E., & Mufti, A. A. 1998. *Superstructure Replacement of Crowchild Trail Bridge.* 5th International Conference on Short and Medium Span Bridges, L. Dunaszegi (Ed.), Canadian Society for Civil Engineering, Montreal, Que., pp. 499–506.

Täljsten, B. 1994. Plate Bonding, Strengthening of Existing Concrete Structures with Epoxy Bonded Plates of Steel of Fibre Reinforced Plastics. Ph.D. Thesis. Department of Structural Engineering, Luleå University of Technology.Luleå, Sweden.

Täljsten, B. 2002. *FRP Strengthening of Existing Concrete Structures: Design Guidelines.* Luleå University of Technology. Luleå, Sweden.

Täljsten B. 2004a. Design Guideline for CFRP Strengthening of Concrete Structures. IABMAS. Kyoto, Japan.

Täljsten, B. 2004b. *FRP Strengthening of Existing Concrete Structures—Design Guidelines.* (Third Edition) ISBN 91-89580-03-6: 230. Luleå University of Technology, Division of Structural Engineering, Luleå, Sweden.

Tang, B. M. 2003. *FRP Composites Technology Brings Advantage to the American Bridge Building Industry.* 2nd International workshop on Structural Composites for Infrastructure Applications, Cairo, Egypt, December 16–18.

Telang, N. M., Dumlao, C., Mehrabi A., B., Ciolko, A. T., & Guttierez, J. 2006. *Filed Inspection of In-Service FRP Bridge Decks.* NCHRP Report 564. Transportation Research Board, Washington, DC.

Telang, N. M., Dumalo, C., Mehrabi, A. B., Ciolko, A. T., & Gutierrez, J. 2006. *NCHRP Report 564, Filed Inspection of In-Service FRP Bridge Decks.* Transportation Research Board, Washington, DC.

Teng, J. G., Chen, J. F., Smith, S. T. & Lam, L. 2002. *FRP-Strengthened RC Structures.* John Wiley & Sons, Ltd. West Sussex, UK.

Thériault, M., & Neale, K. W. 2000. Design Equations for Axially Loaded Reinforced Concrete Columns Strengthened with Fibre Reinforced Polymer Wraps. *Canadian Journal of Civil Engineering*, 27(6) 1011–1020.

Timusk, J., & Sheikh, S. A. 1977. Expansive Cement Jacks. *Journal of ACI*, 74(2), 80–85.

17

High Performance Steel

Eiki Yamaguchi
Kyushu Institute of Technology

17.1 Introduction

High-performance steels (HPS) are now available in many parts of the world such as the United States, Europe, Korea, and Japan. HPS for bridges were initiated in the United States as a cooperative research program in 1994. The participants were the Federal Highway Administration (FHWA), the U.S. Navy and the American Iron and Steel Institute (AISI). A steering committee was formed, which consisted of experts from FHWA, Navy, AISI, plate producing member companies, steel fabricators, and American Welding Society (AWS).

The specific target of the project was the development of steels that possessed high strength, improved weldability, good ductility, and weathering property. HPS70W, the HPS version of the 70W grade steel, which had those features was developed first and registered in ASTM in 1997. HPS70W is produced by quenching and tempering (Q&T) or Thermal-Mechanical Controlled Processing (TMCP). The Q&T processing limits plate lengths to 50 ft (15.2 m) in the United States. For producing larger plates, the TMCP version was developed. A plate up to 2 in (51 mm) thick and up to 125 ft (38 m) long can be produced by TMCP.

Experiencing the characteristics of HPS70W, bridge engineers requested the development of HPS50W, the HPS version of the 50W grade steel. HPS50W is now available, which is produced using conventional hot-rolling or controlled rolling up to 4 in (102 mm) thick. HPS100W was also developed and registered in ASTM in 2004.

Research continues under a cooperative agreement between FHWA, Navy, and AISI. An HPS steering committee and a welding advisory group oversee research and development of HPS. They also monitor the use of HPS for bridges.

The first bridge utilizing HPS was constructed by the Nebraska DOT in 1997. In four years, more than 30 bridges with HPS components (HPS bridges) were opened to traffic, and as of 2007, over 250 HPS bridges were in service in the United States. Most of the states have constructed HPS bridges already, and the number of HPS bridges continues to increase. HPS bridges have also been constructed in Europe, Korea, and Japan.

17.2 Material Properties

Some material properties of HPS are presented in Table 17.1. Obviously, each has mechanical properties and toughness much superior to conventional grade steels. For further details, relevant standards should be referred to.

TABLE 17.1 Material Properties

Standard	Steel Grade		Minimum Yield Strength (MPa)	Minimum/Range of Tensile Strength (MPa)	Minimum Impact Energy (J)[a]
ASTMA709/A709M	HPS50W		345	485	27@−12°C[b,d] 41@−12°C[c,d]
	HPS70W		485	585–760	34@−23°C[b,e] 48@−23°C[c,e]
	HPS100W	$t^f \leq 2.5$ in (65 mm)	690	760–895	34@−34°C[b] 48@−34°C[c]
		2.5 in $< t \leq 4$ in (100 mm)	620	690–895	48@−34°C[b] Not permitted[c]
KS D 3868	HSB500(L, W)		380	500	47@−5°C 47@−20°C (L)
	HSB600(L, W)		450	600	47@−5°C 47@−20°C (L)
	HSB800(L, W)		690	800	47@−20°C 47@−40°C (L)
JIS G 3140	SBHS400(W)		400	490–640	100@−0°C[g]
	SBHS500(W)		500	570–720	100@−5°C[g]
	SBHS700(W)		700	780–930	100@−40°C[g]
EN10025 Part4	S420M(L)		420[h]	520–680[i]	40@−20°C (M)
	S460M(L)		460[h]	540–720[i]	27@−50°C (ML)
EN10025 Part6	S460Q(L, L1)		460[j]	550–720[k]	27@−20°C (Q) 27@−40°C (QL) 27@−60°C(QL1)
	S500Q(L, L1)		500[j]	590–770[k]	
	S550Q(L, L1)		550[j]	640–820[k]	
	S620Q(L, L1)		620[j]	700–890[k]	
	S690Q(L, L1)		690[j]	770–940[i]	
	S890Q(L, L1)		890[j]	940–1100[l]	
	S960Q(L, L1)		960[j]	980–1150[l]	

[a] Charpy V-notch (CVN) value.

[b,c] For use as tension components of nonFCM and of FCM, respectively.

[d] If the yield strength exceeds 450 MPa, the testing temperature shall be reduced by 8°C for each increment of 70 MPa above 450 MPa.

[e] If the yield strength exceeds 585 MPa, the testing temperature shall be reduced by 8°C for each increment of 70 MPa above 585 MPa.

[f] Plate thickness.

[g] Based on impact test on transverse test pieces; the other values listed in this Table are on longitudinal test pieces.

[h] For $t \leq 16$ mm; the value is smaller for larger thickness.

[i] For $t \leq 40$ mm; the range is different for larger thickness.

[j] For 3 mm$\leq t \leq$50 mm; the value is smaller for larger thickness.

[k] For 3 mm$\leq t \leq$100 mm; the range is different for larger thickness.

[l] For 3 mm$\leq t \leq$50 mm; the range is different for larger thickness: note that S890Q(L, L1) and S960Q(L, L1) are not available beyond $t = 100$ mm and 50 mm, respectively.

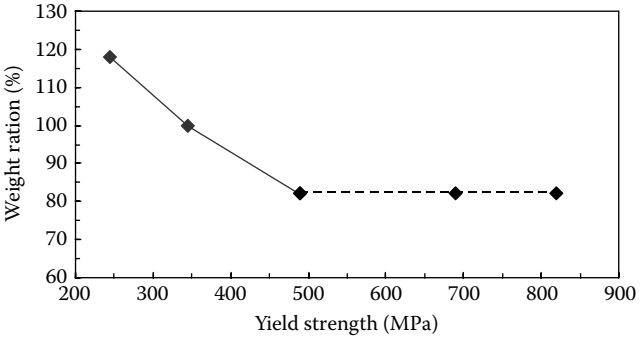

FIGURE 17.1 Weight change with yield strength.

17.3 Fatigue and Fracture Properties

Fatigue resistance of a steel bridge is controlled mostly by the welded details of the connections. Hence, material strengths of steels do not have much to do with the fatigue resistance, implying HPS are not necessarily superior in this aspect.

The most popular type of steel bridge is a plate-girder bridge in Japan. The application of HPS to this type of bridge has been studied (JSCE, 2009). Since HPS are not advantageous in terms of the fatigue resistance, those studies have revealed that the fatigue limit state rather than the strength limit state would eventually control the bridge design as the yield strength became larger. To be specific, when the yield strength reaches approximately 500 MPa, the fatigue limit state would be governing and the weight of the bridge would be hardly reduced even if the steel with higher yield strength than 500 MPa is used. The point is illustrated schematically in Figure 17.1, where the design along the broken line is controlled by the fatigue limit state. It has been also shown that HPS with higher strength would be useful for some bridges such as suspension bridges and cable-stayed bridges, where dead load has a significant influence on construction costs.

On the other hand, as observed in Table 17.1, the impact energy (fracture toughness) of HPS is much better than that of conventional grade steels. The brittle-ductile transition of HPS occurs at a lower temperature. This is an important advantage of HPS, as HPS would then have higher crack tolerance, allowing more time for detection and repair of fatigue cracks before the bridge safety is threatened. The superior toughness of HPS enables the production of HPS structural members that meet the FCM specification in the United States.

17.4 Weldability

The cost of welding can be quite high, since good quality of weld requires stringent controls of preheating, heat input, postweld treatment, to name a few. Unsatisfactory quality welding can lead to problems that threaten bridge safety in the long run if not in the short run. The most common and serious problem encountered in steel weldments is hydrogen-induced cracking, which is also called delayed cracking or cold cracking.

In addition to the chemical composition and carbon equivalent of a steel, the following factors can influence the hydrogen-induced cracking (AISI, 2011):

- Joint restraint/base metal thickness
- Filler metal and base metal strength compatibility
- Diffusible hydrogen content of deposited weld metal
- Preheat and interpass temperatures

- Filler metal and base metal cleanliness
- Heat input
- Time delay between successive weld passes

Restraint can be controlled by design. High restraint is therefore unlikely in properly detailed bridges. The primary concern is for hydrogen control during the welding of steels.

The effective method of eliminating the hydrogen-induced cracking is to specify minimum preheat temperature for welding. However, preheating is time consuming and costly. Therefore, the reduction or elimination of the preheat was one of the crucial aspects in the development of HPS. And the preheat requirement has been indeed improved successfully: some of the achievements are shown in Table 17.2.

Guide Specification for Highway Bridge Fabrication with HPS (AISI, 2011) is a very good source of information on fabrication with HPS70W. Some of its remarks on the welding of HPS70W are as follows:

1. Only submerged arc welding (SAW) and shield metal arc welding (SMAW) processes were recommended for welding HPS initially. Consumables for the flux cored arc welding (FCAW) and gas metal arc welding (GMAW) are now available.
2. Possibility of the hydrogen-induced cracking is minimized when diffusible hydrogen Hd ("d" mL/l00g) is limited to a maximum of H8. Regardless of the welding process used, consumables or fabrication practices that produce weld deposits within excess of H8 should never be allowed.
3. The control of diffusible hydrogen to H4 or less can be achieved in fabrication shops without much difficulty. Controls must be therefore implemented to ensure a maximum H4 for all matching strength SAW of HPS70W when the reduced preheats are used, unless specific evidence is presented that satisfactory welds can be produced at higher levels up to H8.
4. Consumables for Grade 50W base metal are considered matching strength for hybrid designs, where HPS70W base metal is joined to 50W base metal. Consumables must conform to the requirements with diffusible hydrogen levels not to exceed H8.
5. The use of undermatched consumables is highly recommended for all fillet welds joining HPS70W to HPS70W plates to reduce the possibility of hydrogen-induced cracking.
6. For the SAW and SMAW processes, filler metals recommended for Grade 50W base metal should be specified to ensure the welds are undermatched but not significantly understrengthened: minimum ultimate tensile strength should be near 485 MPa. Weathering properties should be similar for unpainted applications.
7. The control of heat input is very important to ensure quality welds and to minimize the effects on the strength, toughness, and weldability of HPS70W.

TABLE 17.2 Minimum Preheat Temperature

Grade	$t^a \leq$ 3/4 in (19 mm)	3/4 in $< t \leq$ 1.5 in (38 mm)	1.5 in $< t \leq$ 2.5 in (64 mm)	2.5 in $< t$
HPS70W[b]	10°C	20°C	20°C	50°C
	$t \leq$ 80 mm		80 mm $< t \leq$ 100 mm	
HBS500(L, W)	Not requited		Not requited	
HBS600(L, W)	Not requited		Not requited	
HBS800(L, W)	50°C			
	6 mm $\leq t \leq$ 75 mm		75 mm $< t \leq$ 100 mm	
SBHS400(W)	Not requited		Not requited	
SBHS500(W)	Not requited		Not requited	
SBHS700(W)	50°C			

[a] Plate thickness.

[b] The minimum preheat temperature of HPS70W is for the case of H4 (4 mL/100g of diffusible hydrogen in the weld metal) by SAW and SMAW processes. FCAW and GMAW require higher temperature for thicker plate with $t >$ 1.5 in (64 mm).

In any case, it should be noted that even though HPS have improved weldability, good workmanship that includes proper hydrogen control practices and weldment procedures is still absolutely essential to successful welding HPS70W.

17.5 Weathering Property

The control of corrosion is very important for the steel bridge, as corrosion could be a governing factor of determining the working life of the steel bridge. The effective method of protecting the steel bridge from corrosion is painting. However, painting is costly, and yet the paint does not last forever: repainting is required. Environmental protection is getting more and more strictly imposed in recent years so that the repainting of the steel bridge becomes more difficult and more expensive. The weathering property is therefore even more important these days.

The weathering property expected is the formation of a layer of densely-formed fine rust on the steel surface, suppressing corrosion rate by itself. In an effort to reduce a life-cycle cost, weathering steel accounts for more than 40% of steel used for the construction of steel bridges in the United States and 20% or so in Japan.

HPS in the United States have been therefore developed to possess the weathering property. HPS with the weathering property are also available in Korea and Japan. The minimum Corrosion Index suggests that HPS70W has better corrosion resistance than 50W and former 70W steel grades (Hamby et al., 2002). But it has not been substantiated by tests yet.

The weathering property however is not effective in all the atmospheric conditions. The weathering steel may not be able to develop an expected rust layer, if the atmospheric condition is not appropriate. For the successful use of HPS without painting, the same guidelines for conventional weathering grade steels can be utilized (Hamby et al., 2002).

For instance, the region near a coast, in a continuously wet atmosphere and/or exposed to high sulfur dioxide does not suit weathering-steel application. The following criteria are used for the judgment of applicability in the U.S. practices:

- Air borne salt deposition rate $\leq$ 0.5 mg/100cm^2/day (mdd)
- Yearly average wetness time rate $\leq$ 60%
- Sulfur dioxide rate $\leq$ 2.1 mdd

Japan has stricter applicability criterion for the air born salt deposition rate for highway bridges (Japan Road Association, 2012):

Air borne salt deposition rate $\leq$ 0.05 mdd

However, the wetness time and the sulfur dioxide are not taken into consideration for the applicability judgment explicitly.

Even when the atmospheric conditions are satisfied, structural details need be carefully taken care of so as not to keep the weathering steel constantly wet. To this end, practices for conventional weathering grade steels in the United Staes are of great use, which can be found in FHWA Technical Advisory T 5140.22 (Willett, 1989).

Technological advancement of weathering steel bridges in recent years is described separately in Section 17.7.

17.6 Studies and Experiences of Bridge Design with HPS

In 1997, the first HPS bridge, the Snyder South Bridge, was built in Nebraska. The original design with Grade 50W was changed to the one with HPS70W to gain experience in the HPS fabrication process. The second HPS bridge was opened to traffic in Tennessee in 1998. Since then, many more HPS bridges have been constructed and are now in service. Along with the construction of these bridges, many

studies have been conducted and many experiences have been gained in the United States. Similarly, the effective use of the Japanese version of HPS, SBHS grade steels, has been explored in Japan. Some of those studies and experiences are reviewed briefly in this section.

17.6.1 United States (Hamby et al., 2002)

17.6.1.1 Cost Study of Girder Design

A study to compare cost differences between bridge designs using HPS70W and conventional Grade 50W was conducted. A total of 42 different girders were designed using the AASHTO LRFD Bridge Design Specifications (AASHTO, 2012) with HL-93 Live Load. The girders were two-span continuous, covering a span range of 150 ft (45.7 m), 200 ft (61.0 m), and 250 ft (76.2 m) with variable girder spacing of 9 ft (2.7 m) and 12 ft (3.7 m). Grade 50W, HPS70W and various hybrid combinations of the two grade steels were tried out.

The following conclusions were obtained:

1. HPS70W saves weight and depth for all the span lengths and the girder spacing.
2. Hybrid designs are more economical for all the cases considered. The most economical hybrid combination is Grade 50W for all the webs and positive-moment top-flanges and HPS70W for negative-moment top-flanges and all the bottom flanges.
3. Deflection limit is optional in the AASHTO LRFD Bridge Design Specifications (AASHTO, 2012). If a deflection limit of 1/800 of the span is imposed, it may control designs with HPS70W for shallow web depth.

17.6.1.2 Tennessee Experience

In 1996, Tennessee Department of Transportation (TNDOT) was completing the design of the steel bridge, SR53 Bridge, over the Martin Creek using Grade 50W. The bridge consisted of two 235.5 ft (71.8 m) spans, carrying a 28 ft (8.5 m) roadway on three continuous welded plate girders spaced at 10.5 ft (3.2 m).

When HPS70W steel became available, TNDOT offered to test the application of HPS70W in SR53 Bridge with support from FHWA. TNDOT optimized the design using HPS70W for the girders and Grade 50W shapes for the cross frames. The HPS redesign resulted in a 24.2% reduction in steel weight and 10.6% savings in cost. With some other successful HPS bridges, the use of HPS has become a routine practice in Tennessee.

Some of Tennessee's optimization techniques are as follows:

1. The usage of uncoated HPS steels
2. The application of HPS70W to flanges and webs over interior supports, where moments and shears are high
3. The use of hybrid girder sections for composite sections in positive bending, where moments are high, but shears are low
4. The use of undermatching fillet welds with HPS70W to reduce the cost of consumables
5. The use of constant width plates except at field splices wherever practical
6. Waiving live load deflection limits for lane loads
7. The use of TMCP plates to greatest extent possible
8. The use of the new AASHTO Guide for highway bridge fabrication with HPS70W steel (AASHTO, 2003), following its recommendations with no more stringent requirements added

17.6.1.3 Pennsylvania Experience

The Pennsylvania Department of Transportation (PennDOT) has used HPS70W in the Ford City Bridge, for which full-scale tension and fatigue testing, extensive material testing and weld testing were performed.

The Ford City Bridge is a three-span continuous welded steel plate girder bridge with spans of 320 ft (97.5 m)-416 ft (126.8 m)-320 ft (97.5 m). The first span is curved horizontally with a radius of 508 ft (154.8 m). The other two spans are on tangent. The bridge has four main girders spaced at 13.5 ft (4.1 m).

HPS70W was used in the negative moment regions and grade 50W elsewhere. The hybrid combination of the two steels resulted in a 20% reduction in steel weight, and the depths of the girder cross sections were made constant. The constant depth led to the elimination of a costly longitudinal bolted web splice.

17.6.2 Japan

17.6.2.1 Plate-Girder Bridge (JSCE, 2009)

The design of a two-plate-girder bridge consisting of three spans of 60 m-60 m-60 m was studied in three ways: one with the conventional grade steel SM570, another with SBHS500 and the other with SBHS700. This was a three-span continuous composite girder bridge.

In comparison with the SM570 bridge, the study has yielded the following conclusions:

1. The use of SBHS500 leads to a 7% reduction in steel weight, whereas that of SBHS700 results in a 15% reduction.
2. The flange thickness can be 19% smaller by the application of SBHS500, considerably reducing the fabrication cost.

The conclusions as to reductions in steel weight and construction cost are tabulated in Table 17.3.

Although the study showed the advantages of SBHS grade steels in the application to the bridge, it also pointed out four issues that need attention in the design with SBHS grade steels:

1. Live-load deflection
2. Fatigue
3. Buckling
4. Instability induced by wind

The issues here are associated with the fact that the fatigue strength and Young's modulus of SBHS grade steels are the same as those of the conventional steels. When one of the four phenomena listed above is critical to the design, SBHS grade steels are not necessarily advantageous, and lower strength steels may be dictated.

17.6.2.2 Longer Plate-Girder Bridge (JSCE, 2009)

A three-span continuous composite plate-girder bridge was studied. The bridge had two girders. A typical span of this type of bridge in Japan is 50–60 m. Explored herein was the extension of the span by the use of SBHS grade steels. Three bridges B1–B3 were designed. The differences between them lay in the spans: B1 consists of 65 m-80 m-65 m; B2 consists of 80 m-100 m-80 m; B3 consists of 90 m-120 m-90 m. For comparison, the three bridges were designed also by the conventional grade steel SM570.

The following are the conclusions of this study:

1. B1: The use of SBHS500 reduces steel weight by 12%.
2. B2: The use of either SBHS500 or SBH700 leads to a 19% reduction in steel weight.
3. B3: The use of SM570 results in an unrealistically wide flange near the intermediate supports.
4. The use of SBH700 yields a reasonable section and reduces the steel weight by 20%.

TABLE 17.3 Relative Steel Weight and Construction Cost

	SM570 Bridge	SBHS500 Bridge	SBHS700 Bridge
Steel weight	1.00	0.93	0.85
Construction cost	1.00	0.90	0.99

Some other observations made in the study are as follows:

1. Live-load deflection is not critical even though the use of SBHS grade steels reduces the cross section.
2. The fatigue limit state does not control the design. A more detailed study made separately has revealed that some welded connections may reach the fatigue limit state, which requires a careful design of the welding details, but not the change of the cross section.
3. The buckling controls the design in some cases. Since the buckling strength is determined by the member stiffness, SBHS grade steels become less advantageous in those cases, requiring the method of increasing the buckling strength for the effective use of SBHS grade steels.

17.6.2.3 Two-Span Continuous Composite Plate-Girder Bridge (JSCE, 2009)

Two different steel plate-girder bridges were designed: one had four girders spaced at 3 m and the other two girders spaced at 6 m. The former bridge had a RC deck, whereas the latter a steel plate-concrete composite deck. Either bridge consists of two spans of 70 m and 70 m. The transportation of the girder was assumed to restrict the girder height to 2.95 m, as is often the case with Japanese practices. For each bridge, two designs were carried out by using one of two grade steels, SM570 and SBHS500, for the flange plate whose thickness exceeded 40 mm.

The study revealed the following:

1. In the four-girder bridge, an approximately 2% reduction in steel weight is estimated by using SBHS500 instead of SM570.
2. In the two-girder bridge, the usage of SBHS500 leads to a saving of approximately 10% on steel weight.

The two-girder bridge consists of thicker plates inevitably, which explains why the usage of SBHS500 is more effective in the two-girder bridge.

17.6.2.4 Steel Truss Bridge (JSCE, 2009)

The usage of HPS in truss bridges was studied. To this end, a 120 m simple truss bridge and a continuous truss bridge with two spans of 120 m–120 m were considered.

In this study, the conventional grade steel SM400 was used for the plate with thickness $t \leq 25$ mm, and the conventional grade steel SM490Y for the plate with $t \leq 40$ mm, whereas either SM570 or SBHS500 was used for the plate with $t > 40$ mm.

The following conclusions were obtained:

1. In the simple truss bridge, 155 ton SM570 can be replaced by 135 ton SBHS500, which is a 13% reduction in weight. The reduction in total steel weight is 3%. The small reduction in total steel weight results from that many members consist of plates with $t \leq 40$ mm. Yet the usage of HPS further saves fabrication cost: an approximately 5% reduction in the construction cost can be expected.
2. In the two-span continuous truss bridge, merely a 0.5% reduction is achieved in total steel weight. Most of the thick plates are needed near the intermediate support where the buckling tends to control the design. Under the circumstances, HPS are not very advantageous.

17.6.2.5 Steel Girder with Compact Section (Yamaguchi et al., 2011)

Three girders G1–G3 were designed: G1 used SM490 and G2 SBHS500, whereas G3 was a hybrid girder consisting of a SM490 web and SBHS500 flanges. Their cross sections were made compact for all the girders. Under a certain bending moment, the cross section of each of the three girders was optimized. The results are presented in Table 17.4.

The table shows that the cross-sectional areas of G2 and G3 are 19% and 15% smaller than that of G1, respectively. However, SBHS500 is more expensive than SM490, G2 is not necessarily the least expensive

TABLE 17.4 Optimum Compact Sections

	Flange	Web
G1 (SM490)	540 mm × 52 mm	2566 mm × 39 mm
G2 (SBHS500)	461 × 50	2237 × 36
G3 (SBHS500 + SM490)	450 × 52	2527 × 34

FIGURE 17.2 Tokyo Gate Bridge.

TABLE 17.5 Criteria for Steel Selection

Steel	Maximum Plate Thickness
SS400, SM400	22 mm
SM490Y, SM520	22 mm
SBHS500	50 mm

while it is the lightest. Assuming that the market price of SBHS500 is 33% higher than that of SM490, the most economical girder has been found G3, which is 7% and 14% less expensive than G1 and G2, respectively.

17.6.2.6 Tokyo Gate Bridge (JSCE, 2009)

Tokyo Gate Bridge was opened to traffic in 2012. This is a three-span continuous truss bridge (Figure 17.2). Depending on the plate thickness, different steels have been utilized. The criteria for the steel-grade selection are presented in Table 17.5.

Tokyo Gate Bridge made use of 10,250 ton SBHS500, just about a half of the total amount of steel used for the bridge. The usage of SBHS500 has reduced the construction cost by approximately 10%.

The orthotropic bridges connected to the truss bridge also employed SBHS500. Altogether, in this project, the use of SBHS500 came to 13,250 tons, whereas the total amount of steel used, including the conventional grade steels, was 36,470 tons.

17.7 Weathering Steel Bridges

Protection against corrosion is one of the key issues for steel bridges to have a long life. To this end, steel bridges are painted usually. Painting is effective but quite costly, amounting to an estimated 10% of the initial construction cost of a superstructure. Besides, repainting is required every 10 years or so

during the service period of a bridge. Conventional steel bridges therefore may not be very competitive economically, especially when a life-cycle cost is considered.

One way to reduce a life-cycle cost is to apply weathering steel to a bridge. This steel possesses a unique property of suppressing the development of corrosion by a layer of densely formed fine rust on its own steel surface: the corrosion rate gradually decreases to the level that causes virtually no damage from an engineering viewpoint, as the layer of fine rust grows. Thus the painting is not required in the weathering steel bridge, the life-cycle cost of which can be much lower than that of the painted steel bridge. This is the driving force behind the popularity of weathering steel bridges in Japan in recent years. The data of the Japan Iron and Steel Federation (JISF and JBA, 2003) is plotted in Figure 17.3: in fiscal 2008, weathering steel bridges accounted for over 30% of steel used for the construction of steel bridges. In a local government, some 80% of recent steel bridges are weathering steel bridges. In the United States, even more weathering steel bridges are built: over 40% of steel is the weathering steel, and the recent steel bridges of New Jersey Turnpike Authority (NJTP) are all weathering steel bridges. Figure 17.4 shows how the appearance of a weathering steel bridge changes until a layer of densely formed fine rust is formed in an actual bridge.

However, it should be noted that the weathering steel is not a panacea. It has to be used in the right place in the right way. Otherwise, the performance of the weathering steel bridge would be against expectations and not be satisfactory. For example, if weathering steel is in a wet state constantly, a problem takes place. Water leakage may create such a condition.

Water leakage often occurs from joints at girder ends. Then a layer of densely formed fine rust may not be formed, leading to an unfavorable corrosion state. Figure 17.5 is an example of such a case. To be interesting, in this particular bridge, since the transverse stiffness prevents the water flow, the corrosion state on the left side is very different than on the other side that is closer to the girder end, and it is in a good corrosion state (Figure 17.5b).

The color of the weathering steel bridge is usually dark brown and inevitably rusty. Because of that, there are some people who criticize the weathering steel bridge from an aesthetic point of view.

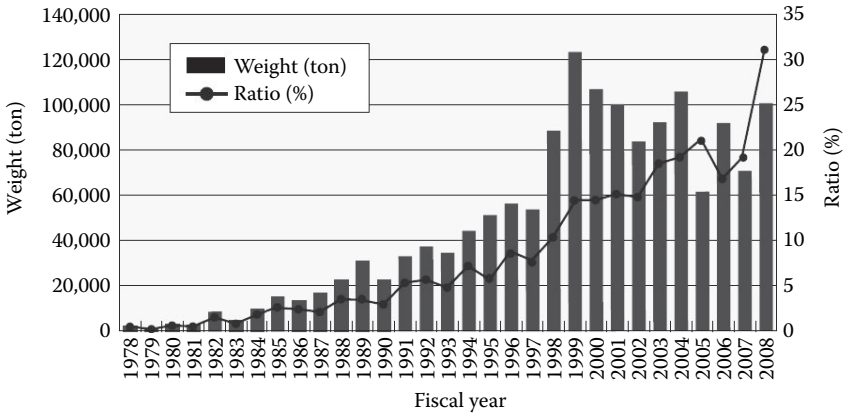

FIGURE 17.3 Weathering steel used for bridges in Japan.

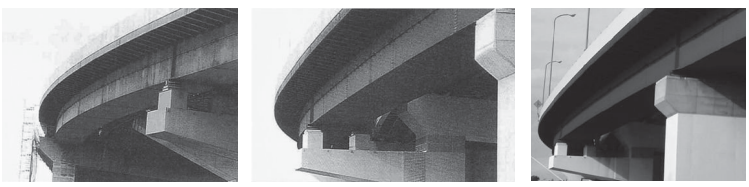

(a) (b) (c)

FIGURE 17.4 Change of appearance of weathering steel bridge with time: (a) two months old, (b) one year old, (c) 28 years old. (Courtesy of The Japan Iron and Steel Federation, and The Japan Bridge Association.)

(a) (b)

FIGURE 17.5 Unfavorable corrosion state: (a) view from girder end, (b) side view.

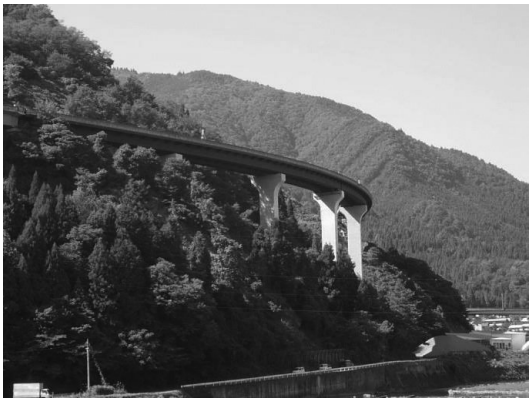

FIGURE 17.6 Scenery with weathering steel bridge.

FIGURE 17.7 Artwork made of weathering steel.

On the contrary, the weathering steel bridge often contributes to the creation of a splendid view, as may be realized in Figure 17.6. In fact, many architects are fond of using weathering steel for their artwork. Figure 17.7 shows such an art work in the award-winning project of Kaze-no-Oka Crematorium in Japan.

This section deals with the weathering steel bridge. To be specific, recent studies in Japan are reviewed.

17.7.1 Performance of Weathering Steel Bridges

Several reports have documented the unexpected type of rust, flaky, or laminar corrosion, in some weathering steel bridges. Herein the study that has inspected a large number of weathering steel bridges is reviewed to give some idea about the performance of weathering steel bridges in Japan (Yamaguchi et al., 2006).

This study covers 337 weathering steel bridges constructed in Kyushu-Yamaguchi region, Japan, all the weathering steel bridges constructed by the member companies of the Japan Bridge Association (JBA) in the region by the time of the inspection. The general information on these bridges was provided by JBA. The field investigation was conducted during the two-year period of 2001–2003.

The study consisted of general investigation and corrosion inspection. The former recorded a bridge type, environment, bridge details, and so on. The latter evaluated overall and local corrosion states in a bridge. Since a bridge is a large structure, a state of corrosion is not uniform in general. Especially, corrosion near the end of a bridge tends to differ from that in the other part. The corrosion inspection was therefore made up of two kinds: the overall and local evaluations.

A state of corrosion is judged by conducting the so-called Scotch-tape test, when the bridge can be approached. In this test, the Scotch tape is pressed against the weathering steel to capture rust. Then the rust density and the sizes of rust particles are examined. More details of the Scotch-tape test are described in Section 17.7.3.3.

Based on the appearance of rust, the Japan Iron and Steel Federation, and the Japan Bridge Association (2003) have classified corrosion states into 5 levels. The criteria are presented in Table 17.6. While Levels 3–5 are satisfactory corrosion states, Levels 1–2 require attention; more information on this aspect is given in Section 17.7.3.4.

The main finings in this study are as follows:

1. Many weathering steel bridges have been constructed in the areas that do not satisfy the distance criteria of specifications for Highway Bridges Part 2 Steel Bridges (JRA, 2012).*
2. The number of weathering steel bridges is increasing rapidly in the region. In early years, quite a few weathering steel bridges with supplemental rust controlling surface treatment† were constructed. But in the past 15 years more than 80% of the weathering steel bridges are without the surface treatment.
3. The distance criteria were established in 1993 (PWRI, 1993). Even after that, the weathering steel bridges that do not satisfy the criteria have been constructed, whereas the ratio of those bridges has reduced from 15.2% to 9%. The number of weathering steel bridges without the surface treatment increases remarkably after 1993.
4. More than 80% of weathering steel bridges without the surface treatment are located in mountains and rural areas. 45.5% of weathering steel bridges with the surface treatment are in urban areas.
5. 1.6% of weathering steel bridges without the surface treatment have the overall corrosion state of Level 1 or 2. 28.8% of weathering steel bridges without the surface treatment have the local corrosion state of Level 1 or Level 2. Although most of the weathering steel bridges in the region are in good shape, more than a quarter of the bridges locally developed the corrosion state of Level 1 or 2 that requires attention.
6. The main cause for over 70% of Level 1 or 2 corrosion states is water leakage. In many of those cases, the water leakage is caused by an inappropriate expansion joint.

---

* The distance criteria has not been changed since its establishment in 1993 by Public Work Research Institute (1993). Thecriteria are explained in Section 17.7.2.

† The supplemental rust controlling surface treatment is to control stains due to corrosion at the initial stage by delaying the formation of a layer of densely formed fine rust on its own steel surface so as to alleviate staining of neighboring objects such as bridge piers and abutments. This is a sort of coating, but different from regular painting. It is done only once at the time of construction. Therefore, the bridge with the surface treatment is still classified as an uncoated bridge.

TABLE 17.6 Classification of Corrosion States

Level	Description of Rust	Rust Thickness
5	Few in quantity; relatively bright	less than approximately 200 μm
4	Less than 1 mm in size; fine and uniform	less than approximately 400 μm
3	1–5 mm in size	less than approximately 400 μm
2	5–25 mm in size; flaky	less than approximately 800 μm
1	Formation of laminar layer	more than approximately 800 μm

The investigation suggests that while the performance of most of the weathering steel bridges in the region is satisfactory, the durability design is not always practiced well. There seems to be a lack of understanding of the durability design as well.

17.7.2 Assessment of Atmospheric Corrosiveness (JSSC, 2006, 2009; Yamaguchi, 2007)

Most of the weathering steel bridges in Japan have utilized JIS-SMA weathering steel (Japan Industrial Standard G 3114 SMA), equivalent to the weathering steel commercialized by U.S. Steel Corporation in 1930s. Based on the exposure test data on JIS-SMA weathering steel in 41 bridges in Japan, the construction of a JIS-SMA weathering steel highway bridge without painting is permitted under the atmospheric environment where the corrosion loss of 0.3 mm or less per side is expected in 50-year exposure (JWRI, 1993). This atmospheric environment has been found equivalent to that of the corrosion loss of 0.5 mm or less per side in 100-year exposure. It is noted that bridges in Japan are designed for the service life of 100 years in general.

Such an atmospheric environment in Japan has been further identified as the region where the value of air born salt deposition rate is less than 0.05 mdd when measured by the method described in JIS Z2381 (PWRI, 1993).

For the sake of convenience, Specifications for Highway Bridges Part 2 Steel Bridges (JRA, 2012) defines the region in the atmospheric environment that satisfies the above requirement by the distance from the coast. To that end, Japan is divided into 5 zones: for each zone, the distance from the coast is specified (Figure 17.8), beyond which an unpainted JIS-SMA weathering steel highway bridge can be built without the investigation of air born salt deposition rate.

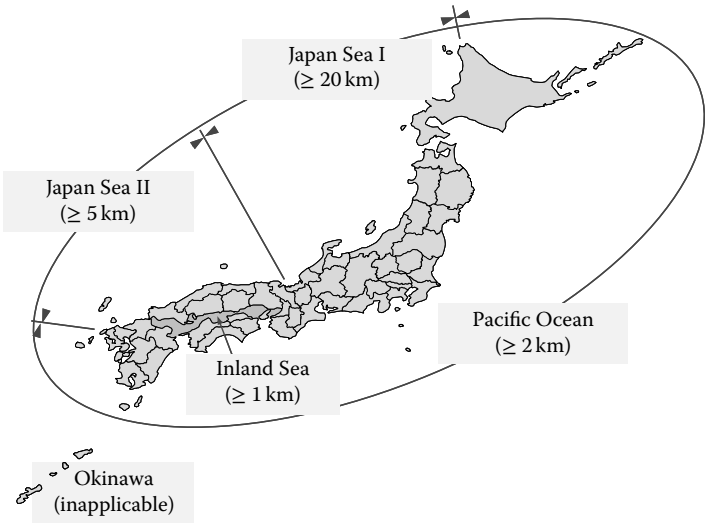

FIGURE 17.8 Schematic of distance criteria.

The distance criteria are very convenient for the assessment of atmospheric corrosiveness and help promote the weathering steel bridge. However, weathering steel bridges located outside such a region are not necessarily in a state of unexpected corrosion, whereas some bridges inside the region are (Yamaguchi et al., 2006). The distance criteria are surely simple and convenient, but the simplicity appears to inevitably impose limitations on the validity.

A problem of the distance criteria is that the specification has been solely based on the air born salt. The air born salt is not the only factor that influences the way corrosion develops. There are many other influential factors such as wetness time and temperature.

It is known that the corrosion loss of weathering steel can be expressed generally by a function in the following form:

$$Y = AX^B \tag{17.1}$$

where X is time (year), Y is the penetration (mm), A is the first-year corrosion loss (mm) and B is the index of corrosion loss rate diminution. The penetration is the corrosion loss and herein it is defined as the amount of decrease in the thickness of a weathering steel plate per side of the plate. As this equation implies, A indicates the severity of the environment, whereas $1/B$ shows the rust-layer effect on the reduction of the corrosion rate.

Using the exposure test data on JIS-SMA weathering steel in 41 bridges in Japan (Public Work Research Institute, 1993), A_{SMA} (A for JIS-SMA weathering steel) and B_{SMA} (B for JIS-SMA weathering steel) were obtained for those bridges, and the relationship between A_{SMA} and B_{SMA} was examined. As may be expected, they were not independent. Then formulas have been proposed for estimating B_{SMA} (Japanese Society of Steel Construction, 2006).

For different weathering steels such as the nickel-type weathering steel, A_{SMA} and B_{SMA} are replaced with A_S and B_S, respectively. Formulas for the evaluation of A_S/A_{SMA} and B_S/B_{SMA} have been proposed: the evaluation formulas depend on the weathering alloy index V, which in turn is a function of the mass percentage of alloying elements. The penetration Y for any type of weathering steel can thus be evaluated by Equation 17.1. Then the relationship between A_{SMA}, V, and Y_{100} (the penetration at the end of 100-year working life) can be obtained. Figure 17.9 shows a schematic relationship between A_{SMA} and V, when $Y_{100} = p$ is required. In general, Y_{100} is 0.5 mm, but a different value can be specified. The line for a smaller value of p would be located above the line for $Y_{100} = p$ and the line for a larger value of p would be located below the line for $Y_{100} = p$, respectively, since the steel with larger value of V is required as the demand is higher, that is, Y_{100} decreases, and vice versa. This kind of figure helps select an appropriate weathering steel grade that satisfies the performance requirement in terms of Y_{100} in design for the atmospheric corrosiveness at the construction site described by A_{SMA}. It is therefore essential to evaluate A_{SMA} for the assessment of atmospheric corrosiveness and a good durability design.

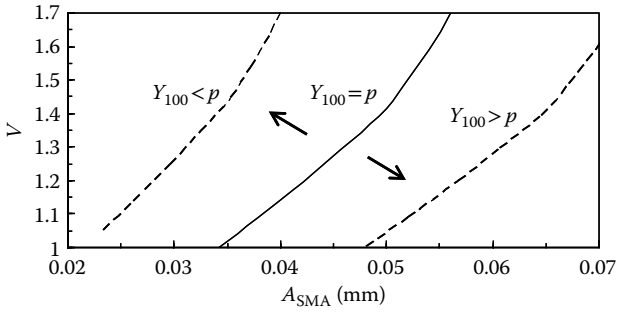

FIGURE 17.9 Schematic relationship between A_{SMA}, V and Y_{100}

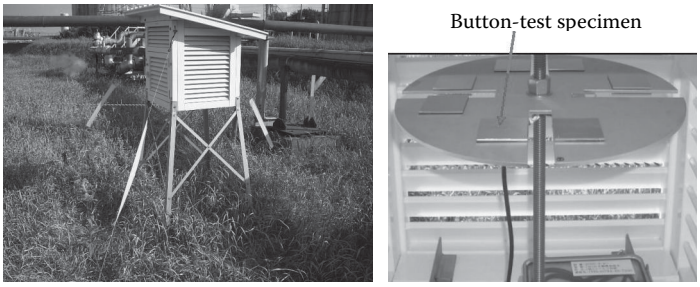

FIGURE 17.10 Button test: (a) Stevenson screen, (b) Button-test specimen.

An economical and simple means of assessing A_{SMA} has been proposed. The method has been named the "button test."

The button test is essentially an exposure test, using button-shaped weathering steel test specimens. In this method, if a steel bridge exists in the neighborhood of the construction site of a new bridge, the exposure test will be conducted by attaching the test specimens to the existing bridge. Otherwise, the test will be done by installing a Stevenson screen (Figure 17.10). After one-year exposure, the weight losses of the test specimens are measured to yield the site-specific first-year corrosion loss A_{SMA}.

As mentioned earlier, the supplemental rust controlling surface treatment is often applied to the weathering steel bridge in Japan. Its basic function is to control stains so as to alleviate staining of neighboring objects such as bridge piers and abutments. This is a technology closely related to the serviceability of the weathering steel bridge. Some of the surface treatment products are said to possess a corrosion control function as well. The use of that function in the durability design however requires the establishment of the method of evaluating corrosion loss when the surface treatment is applied.

17.7.3 Maintenance of Weathering Steel Bridges (JSSC, 2006, 2009; Yamaguchi, 2008)

17.7.3.1 Basics

The penetration can vary as depicted schematically in Figure 17.11: the curve "a" corresponds to the expected behavior of weathering steel as the corrosion rate decreases with time, whereas the curve "b" is the case when the behavior of weathering steel deviates from what is expected.

As is described earlier, if the two coefficients, A and B in Equation 17.1, are given, the corrosion loss can be estimated at any time during the working life. For the maintenance of a weathering steel bridge, it is possible and important at the stage of design to predict the variation of corrosion loss. It is then essential to inspect the actual corrosion loss and compare it with the predicted value in order to monitor the performance of weathering steel during the working life of the bridge.

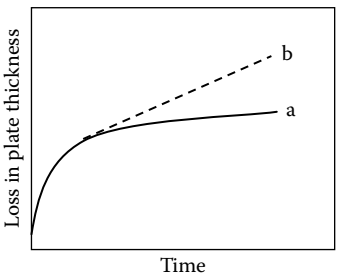

FIGURE 17.11 Schematic of corrosion-loss variation with time.

Two classes of corrosion-oriented inspection of a weathering steel bridge are to be performed: the initial inspection and the periodic inspection. All the bridges, regardless of the type, need be subjected to general inspections periodically. For example, all the bridges on national highways in Japan are inspected every five years. Therefore, it is convenient and economical to conduct the corrosion-oriented inspections on those occasions of the periodic general inspections.

17.7.3.2 Inspections

The initial inspection of a weathering steel bridge is conducted at an early stage of its working life. It is intended to detect initial defects. The standard method is a visual inspection, which should be carried out in the place very close to the bridge. If the bridge is not approachable, tools such as a pair of binoculars must be used. Specifically, the occurrence of water leakage and the wetness of the weathering steel must be carefully checked.

If unexpected corrosion development such as a state of flaky or laminar corrosion is observed all over the bridge, the misjudgment of atmospheric corrosiveness is doubted: the maintenance scheme needs to be reviewed and revised if necessary. If the unexpected corrosion development is observed only locally, there is a chance of water leakage in the neighborhood; if so, the cause must be identified and a measure needs to be taken to remove it as soon as possible.

The main purpose of the periodic inspection is to estimate corrosion loss. To this end, this class of inspection is conducted after corrosion development is stabilized. It is therefore generally recommended that the corrosion-oriented inspection of this class be started after approximately 10 years since the erection of a bridge.

The mainstay of corrosion-loss estimate is external corrosion appearance by a visual inspection from very near the steel surface. Close-up pictures of the corrosion should be taken for the record as well. The Scotch tape test and the rust-thickness measurement are also conducted to obtain further information for the estimation of the corrosion loss. General remarks about how to conduct these inspection items will be given in the next section.

The frequency of the corrosion-oriented periodic inspection should be determined based on the condition of corrosion. If it is in good shape, a 10-year interval can be recommended since the corrosion rate does not change much in general. Even in such a case, however, if the bridge is located in the region where a large quantity of de-icing salt is used, the inspection interval had better be made shorter, since abnormal corrosion could develop very fast once it is initiated under that environment (Yamaguchi et al., 2005).

If the actual corrosion loss is significantly different from the predicted value, further investigation is required, which will be described in Section 17.7.3.4.

Even in periodic general inspections in which no corrosion-oriented inspection is conducted, corrosion environment must be checked: even after corrosion development becomes stable, the corrosion rate can pick up if corrosion environment changes. To this end, close attention has to be paid so as not to overlook the events such as the breakage of drainage pipes, the clogging of ditches, water leakage from concrete slabs/expansion joints, and water/sand deposit around bearings, since those events could possibly deteriorate the corrosion environment. A corrosion state must also be inspected. If laminar rust layers are found, they must be taken care of immediately. If the corrosion state in some portion is different from that in the other part, closer inspection is required and photos are taken for the record.

17.7.3.3 Inspection Methods

Three inspection items are mentioned above. Remarks about them are given in this section. In addition, the method of measuring plate thickness is described at the end.

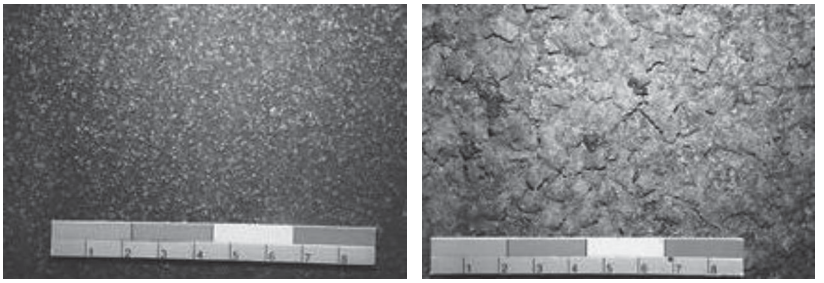

(a) (b)

FIGURE 17.12 Close-up picture with scale and color sample: (a) level 4, (b) level 2.

17.7.3.3.1 Evaluation of External Appearance

1. The corrosion appearance reflects environmental condition. The colors and the sizes of rust particles provide information on corrosion rate.
2. The visual inspection is the mainstay for this evaluation. When the bridge is not approachable, tools such as a pair of binoculars must be used.
3. Close-up pictures of corrosion are taken for the record. A scale and a color sample are attached to the bridge and included in the pictures of the rust (Figure 17.12).
4. The corrosion states are classified by the criteria given in Table 17.6. It is noted that the classification is prepared for 9-year-old or older rusts and is not applicable to younger rusts.

17.7.3.3.2 Scotch-Tape Test

1. Scotch tape is pressed against weathering steel to capture rust. Then the rust density and the sizes of rust particles are examined.
2. The test should be conducted at the same points as those of the close-up pictures.
3. Dust must be removed before the Scotch tape is pressed. It is conducted only once at each point.
4. Scotch tape 50 mm wide is recommended. Alternatively, Scotch tape 24 mm wide may be used. The tape is pressed against weathering steel lightly and uniformly by a rubber roller or a finger.
5. After removal, the tape is attached to a sheet such as transparency and is kept for the record. It would be useful to take a photocopy of the sheet.

17.7.3.3.3 Measurement of Rust Thickness

1. An electromagnetic coating-thickness tester is used.
2. Measurement by the electromagnetic coating-thickness tester is influenced by the roughness of surface. Sensitivity depends on sensor shape. It is recommended that the sensor be placed at the convex portion of rust surface.
3. Rust thickness is measured without cleaning rust surface, unless materials such as dust appear to influence the measurement greatly. In case of an abnormal corrosion state such as a state of flaky or laminar corrosion, the cleaning should not be done.
4. Rust thickness is measured at 9 points in a square region 10 cm on a side. The average of them is treated as the representative thickness. Alternatively, it is measured at 10 points, and the average of 8 thicknesses excluding the largest and smallest values may be used as the representative thickness.

17.7.3.3.4 Measurement of Plate Thickness

Although not mentioned in the above, plate thickness may be measured as an inspection item on a regular basis, which directly provides information on corrosion loss. When an unfavorable corrosion

state is found, the plate-thickness measurement may also be conducted to judge the necessity of further actions for the safety of the bridge.

1. An ultrasonic thickness gauge with the precision down to 0.01 mm is used.
2. For a regular measurement, monitoring points are set in a square region 10 cm on one side. The surface on the other side of this plate region is painted right after the initial abrasive blast cleaning to prevent corrosion. When the thickness is measured, the coating must be removed, and it is painted again after the measurement.
3. To see the variation of plate thickness with time, measurement interval is approximately 10 years in general. However, the interval should be made shorter when abnormal corrosion development is observed.
4. For the thickness measurement of a badly corroded plate, the probe is placed on the plate surface with a better corrosion state condition. The rust around the contact point must be removed until steel surface comes out. If an electric tool is used for the removal, caution must be used so as not to damage the steel surface.
5. The number of measurements is decided considering the remaining plate thickness and its variation, since larger scatter tends to be observed as corrosion progresses. The measurements at 10 points are preferable: at least 5 measurements are needed. The average of the plate thicknesses is then computed and is treated as the representative thickness.
6. Accuracy of the measurement is low where the steel surface is rough. Careful treatment of the data and judgment are needed when the measurement is done under such a condition.

17.7.3.4 Performance Verification

From the evaluation result of the external appearance, the penetration at the end of the 100-year working life can be estimated, as indicated in Table 17.7. The corrosion states of Levels 3–5 are satisfactory performance and no further actions are needed.

The corrosion states of Levels 1–2 may not be satisfactory performance. In the case of Level 2, if the cause for this corrosion state is indentified and removed successfully, no further actions are needed. Otherwise, the plate thickness is measured. The following three cases are conceivable:

1. If the corrosion loss turns out to be smaller than the predicted value at this time of the working life, no further actions are needed.
2. If the penetration is bigger than the predicted value at this time of the working life, yet the penetration at the end of the 100-year working life predicted based on the measured plate thickness is smaller than the value required in design, no further actions are needed at this stage. However, it is recommended that the next inspection be conducted earlier and with great care.
3. If the penetration at this stage already exceeds the value expected at the end of the 100-year working life in design, further investigation needs be conducted to estimate the corrosion condition of this bridge at the end of the 100-year working life. The investigation includes the distribution of corrosion loss over the bridge, and then the safety of the bridge at the end of the 100-year working life is examined. If the safety requirement is found satisfied, no further actions are needed at this stage. However, it is recommended that the next inspection be conducted earlier and with great

TABLE 17.7 Penetration at End of 100-Year Working Life

Level	Penetration
5	less than approximately 0.5 mm
4	approximately 0.5 mm
3	approximately 0.5 mm
2	1.0–2.0 mm

TABLE 17.8 Material Cost of HPS Relative to Grade 50W

Grade	Relative Material Cost
HPS50W	1.2
HPS70W (Q&T)	1.4
HPS70W (TMCP)	1.3

care. On the other hand, if the examination concludes the violation of the safety, a measure must be taken immediately to improve the situation and ensure the safety of the bridge over its remaining service period.

17.8 Availability and Cost

The availability and the cost of HPS are significant and of great interest for building HPS bridges. They could be even crucial for the use of HPS. However, they are varying as market demand changes. Nothing definite can be said. Herein, just for a reference, the description in HPS Designers' Guide (Hamby et al., 2002) is quoted: the delivery time of HPS in the United States is approximately 6–10 weeks and the approximate material cost relative to Grade 50W is shown in Table 17.8.

17.9 Concluding Remarks

HPS have been developed so as to possess characteristics superior to conventional grade steels for bridge construction. The advantageous properties are well-recognized in strength, weldability, and ductility.

Those properties make it possible to reduce the weight and cost of a bridge by allowing fewer lines of girders, shallower girders, longer spans, fewer piers, and so on. Improvement of weldment quality, reduction in fabrication cost, longer allowable time for detection and repair preparation of fatigue cracks can be also expected.

To take full advantage of HPS, experiences are needed and important, not to mention studies on the effective use of HPS. Some of the experiences gained and studies conducted so far are summarized in this chapter. Recent advancement of the weathering steel bridge is also presented, the achievement of which can be utilized for HPS bridges as well. More experiences and study results are being accumulated and become available. Bridge engineers are advised to keep an eye on the latest information on HPS: as is always the case with new technology, advancements would be fast.

References

AASHTO. 2003. *Guide Specifications for Highway Bridge Fabrication with HPS 70W (HPS 485W) Steel*, 2nd Edition, American Association of State Highway and Transportation Officials, Washington, DC.

AASHTO. 2012. *AASHTO LRFD Bridge Design Specifications*. Customary US Units. American Association of State Highway and Transportation Officials, Washington, DC.

AISI. 2011. *Guide Specification for Highway Bridge Fabrication with High Performance Steel.* 2011 (3rd Edition). Steel Market Development Institute, American Iron and Steel Institute, Washington, DC.

Hamby, G., Clinton, G., Nimis, R., and Lwi, M. M. 2002. *High Performance Steel Designers' Guide* (2nd Edition). Federal Highway Administration, U.S. Department of Transportation.

JISF and JBA. 2003. *Application of Weathering Steel to Bridges.* The Japan Iron and Steel Federation, and the Japan Bridge Association, Tokyo, Japan.

JRA. 2012. *Specifications for Highway Bridges Part 2 Steel Bridges.* Japan Road Association, Tokyo, Japan.

JSSC. 2006. *Potentials and New Technologies of Weathering Steel Bridges*, JSSC Technical Report No. 73. Japanese Society of Steel Construction. Tokyo, Japan.

JSSC. 2009. *Applicability Evaluation and Preventive Anticorrosion Scheme for Weathering Steel Bridges*, JSSC Technical Report No. 86. Japanese Society of Steel Construction, Tokyo, Japan.

JSCE. 2009. *Research Report on New Technology to Use High Performance Steel*, Committee on Steel Structures, Japan Society of Civil Engineers, Tokyo, Japan.

PWRI, Kozai Club and JASBC. 1993. *Report on Application of Weathering Steel to Highway Bridges (XX),* Public Work Research Institute of Ministry of Construction, The Kozai Club (Iron and Steel Mill Products Association) and Japan Association of Steel Bridge Construction. Public Work Research Institute, Tsukuba, Japan.

Willett, T. O. 1989. *Uncoated Weathering Steel in Structures.* Technical Advisory T 5140.22, Office of Engineering, Federal Highway Administration. Washington, DC.

Yamaguchi, E., Miyoshi, T., Sakaguchi, T., Kano, I., and Fujii, Y. 2005. Influence of Deicing Salt on Performance of Weathering Steel Bridge, *Proceedings of JSCE Annual Conference I,* JSCE, Tokyo, Japan, Vol. 60, pp. 35–36.

Yamaguchi, E., Nakamura, S., Hirokado, K., Morita, C., Sonoda, Y., Aso, T., Watanabe, H., Yamaguhci, K., and Iwatusbo, K. 2006. Performance of Weathering Steel in Bridges in Kyushu-Yamaguchi Region, *Doboku Gakkai Ronbunshuu A*, JSCE, Tokyo, Japan, Vol. 62(2) 243–254.

Yamaguchi, E. 2007. Assessment Method for Atmospheric Corrosiveness and Durability Design of Weathering Steel Bridges, *Proceedings of the 23rd US-Japan Bridge Engineering Workshop*, Public Work Research Institute, Tsukuba, Japan, pp. 386–394.

Yamaguchi, E. 2008. A Proposal for Maintenance Manual of Weathering Steel Bridges, *Proceedings of the 24th US-Japan Bridge Engineering Workshop*, Public Work Research Institute, Tsukuba, Japan, pp.125–132.

Yamaguchi, E. 2011. Effective Use of SBHS for Gider, *Technical Report to JISF,* Japan Iron and Steel Federation, Tokyo, Japan.

18

Effective Length of Compression Members

Lian Duan
California Department of Transportation

Honggang Lei
Taiyuan University of Technology

Wai-Fah Chen
University of Hawaii

18.1 Introduction

The concept of *effective length factor* or *K-factor* plays an important role in compression member design. Although much effort has been made in recent years to eliminate the *K-factor* in column design, the *K-factors* are still popularly used in practice for routine design (AASHTO, 2012; ACI, 2011; AISC, 2010; ECS, 2004 and 2005).

Mathematically, the *effective length factor* or the *elastic K-factor* is defined as

$$K = \sqrt{\frac{P_e}{P_{cr}}} = \sqrt{\frac{\pi^2 EI}{L^2 P_{cr}}} \tag{18.1}$$

where P_e is Euler load, elastic buckling load of a pin-ended column, P_{cr} is elastic buckling load of an end-restrained framed column, E is modulus of elasticity, I is moment of inertia in the flexural buckling plane, and L is unsupported length of column in the flexural buckling plane.

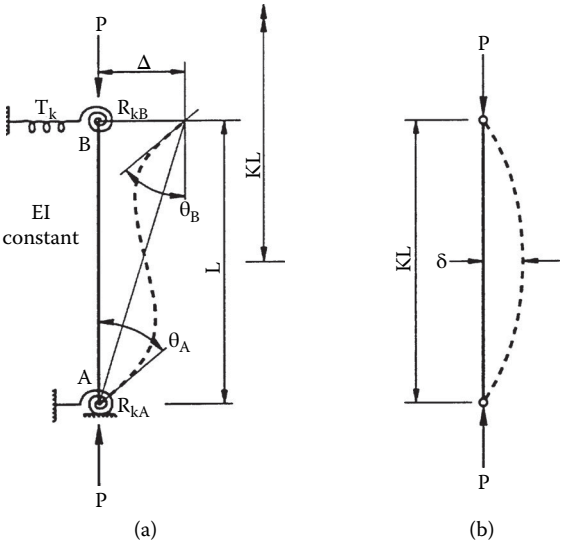

FIGURE 18.1 Isolated columns.

Physically, the *K-factor* is a factor that when multiplied by actual length of the end-restrained column (Figure 18.1a) gives the length of an equivalent pin-ended column (Figure 18.1b), whose buckling load is the same as that of the end-restrained column. It follows that the effective length *KL* of an end-restrained column is the length between adjacent inflection points of its pure flexural buckling shape.

Practically, design specifications provide the resistance equations for pin-ended columns, whereas the resistance of farmed columns can be estimated through the *K-factor* to the pin-ended column strength equations. Theoretical *K-factor* is determined from an elastic eigenvalue analysis of the entire structural system, whereas practical methods for the *K-factor* are based on an elastic eigenvalue analysis of selected subassemblages. This chapter presents a state-of-the-art engineering practice of the *effective length factor* for the design of columns in bridge structures.

18.2 Isolated Columns

From an eigenvalue analysis, the general *K-factor* equation of an end-restrained column, as shown in Figure 18.1, is obtained as

$$\det\begin{vmatrix} C+\dfrac{R_{kA}L}{EI} & S & -(C+S) \\ S & C+\dfrac{R_{kB}L}{EI} & -(C+S) \\ -(C+S) & -(C+S) & 2(C+S)-\left(\dfrac{\pi}{K}\right)^2+\dfrac{T_kL^3}{EI} \end{vmatrix} = 0 \tag{18.2}$$

where the stability function *C* and *S* are defined as

$$C=\frac{(\pi/K)\sin(\pi/K)-(\pi/K)^2\cos(\pi/K)}{2-2\cos(\pi/K)-(\pi/K)\sin(\pi/K)} \tag{18.3}$$

Buckled shape of column is shown by dashed line	(a)	(b)	(c)	(d)	(e)	(f)
Theoretical K value	0.5	0.7	1.0	1.0	2.0	2.0
Recommended design value when ideal conditions are approximated	0.65	0.80	1.2	1.0	2.10	2.0
End condition code		Rotation fixed and translation fixed Rotation free and translation fixed Rotation fixed and translation free Rotation free and translation free				

FIGURE 18.2 Theoretical and recommended *K-factors* for isolated columns with idealized end conditions. (From AISC, *Design Specification for Structural Steel Buildings, (ANSI/AISC 360-10)*, American Institute of Steel Construction, Chicago, IL, 2010. With permission.)

$$S = \frac{(\pi/K)^2 - (\pi/K)\sin(\pi/K)}{2 - 2\cos(\pi/K) - (\pi/K)\sin(\pi/K)} \tag{18.4}$$

The largest value of K satisfying Equation 18.2 gives the elastic buckling load of an end-retrained column.

Figure 18.2 summarizes the theoretical *K-factors* for columns with some idealized end conditions (AASHTO, 2012; AISC, 2010). The recommended *K-factors* are also shown in Figure 18.2 for practical design applications. Since actual column conditions seldom comply fully with idealized conditions used in buckling analysis, the recommended *K-factors* are always equal or greater than their theoretical counterparts.

18.3 Framed Columns: Alignment Chart Method

In theory, the *effective length factor K* for any columns in a framed structure can be determined from a stability analysis of the entire structural analysis—eigenvalue analysis. Methods available for stability analysis include slope-deflection method (Chen and Lui, 1991), three-moment equation method (Bleich, 1952), and energy methods (Johnson, 1960). In practice, however, such analysis is not practical, and simple models are often used to determine the *effective length factors* for farmed columns (Lu, 1962; Kavanagh, 1962; Gurfinkel and Robinson, 1965; Wood, 1974). One such practical procedure that provides an approximate value of the elastic *K-factor* is the alignment chart method (Julian and Lawrence, 1959). This procedure has been adopted by the AISC and AASHTO Specifications (AISC, 2010; AASHTO, 2012) and ACI-318-11 Code (ACI, 2011), among others. At present, most engineers use the alignment chart method in lieu of an actual stability analysis.

18.3.1 Alignment Chart Method

The structural models employed for determination of *K-factor* for framed columns in the alignment chart method are shown in Figure 18.3. The assumptions (Chen and Lui, 1991; AISC, 2010) used in these models are

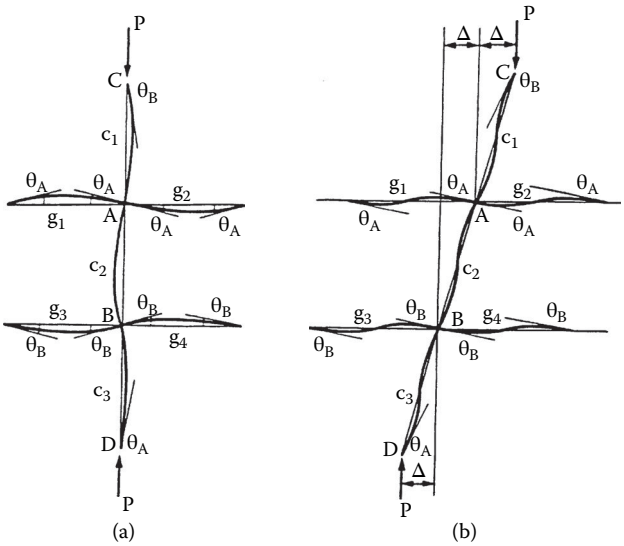

FIGURE 18.3 Subassemblage models for K-factors of framed columns.

1. All members have constant cross section and behave elastically.
2. Axial forces in the girders are negligible.
3. All joints are rigid.
4. For braced frames, the rotations at near and far ends of the girders are equal in magnitude and opposite in direction (i.e., girders are bent in single curvature).
5. For unbraced frames, the rotations at near and far ends of the girders are equal in magnitude and direction (i.e., girders are bent in double curvature).
6. The stiffness parameters $L\sqrt{P/EI}$, of all columns are equal.
7. All columns buckle simultaneously.

Using the slope-deflection equation method and stability functions, the *effective length factor* equations of framed columns are obtained as

for columns in braced frames:

$$\frac{G_A G_B}{4}(\pi/K)^2 + \left(\frac{G_A + G_B}{2}\right)\left(1 - \frac{\pi/K}{\tan(\pi/K)}\right) + \frac{2\tan(\pi/2K)}{\pi/K} - 1 = 0 \tag{18.5}$$

for columns in unbraced frames

$$\frac{G_A G_B(\pi/K)^2 - 36^2}{6(G_A + G_B)} - \frac{\pi/K}{\tan(\pi/K)} = 0 \tag{18.6}$$

where G is stiffness ratios of columns and girders, subscripts A and B refer to joints at the two ends of the column section being considered. G is defined as

$$G = \frac{\sum(E_c I_c/L_c)}{\sum(E_g I_g/L_g)} \tag{18.7}$$

where Σ indicates a summation of all members rigidly connected to the joint and lying in the plane in which buckling of column is being considered; subscripts c and g represent columns and girders, respectively.

Equations 18.5 and 18.6 can be expressed in form of alignment charts as shown in Figure 18.4. It is noted that for columns in braced frames, the range of K is $0.5 \le K \le 1.0$; for columns in unbraced frames,

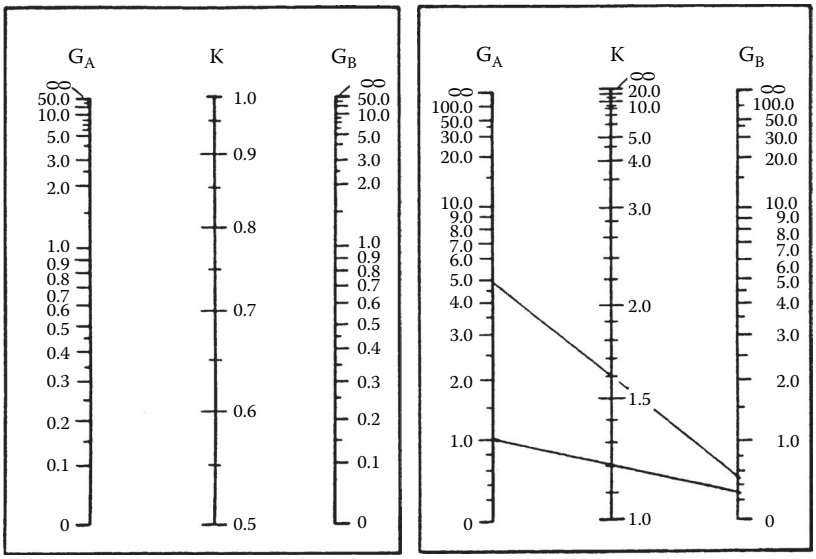

FIGURE 18.4 Alignment charts for effective length factors of framed columns. (a) Braced Frames, (b) Unbraced Frames. (From AISC, *Design Specification for Structural Steel Buildings, (ANSI/AISC 360-10)*, American Institute of Steel Construction, Chicago, IL, 2010. With permission.)

the range is $1.0 \leq K \leq \infty$. For column ends supported by but not rigidly connected to a footing or foundations, G is theoretically infinity, but, unless actually designed as a true friction free pin, may be taken as 10 for practical design. If column end is rigidly attached to a properly designed footing, G may be taken as 1.0.

Example 18.1

Given: A four-span reinforced concrete bridge is shown in Figure 18.5. Using the alignment chart, determine the *K-factor* for the Column DC. $E = 25{,}000$ MPa (3,626 ksi).

Section properties are

Superstructure: $I = 3.14(10^{12})$ mm^4 $A = 5.86(10^6)$ mm^2
Columns: $I = 3.22(10^{11})$ mm^4 $A = 2.01(10^6)$ mm^2

SOLUTION:

(1) Calculate G-factor for Column DC.

$$G_D = \frac{\sum_D (E_c I_c / L_c)}{\sum_D (E_g I_g / L_g)} = \frac{3.22(10^{12})/12{,}000}{2(3.14)(10^{12})/55{,}000} = 0.235$$

$GD = 1.0$

(2) From the alignment chart in Figure 18.4b, $K = 1.21$ is obtained.

18.3.2 Requirements for Braced Frames

In stability design, one of the major decisions engineers have to make is the determination of whether a frame is braced or unbraced. The AISC (2010) states that a frame is braced when "lateral stability is

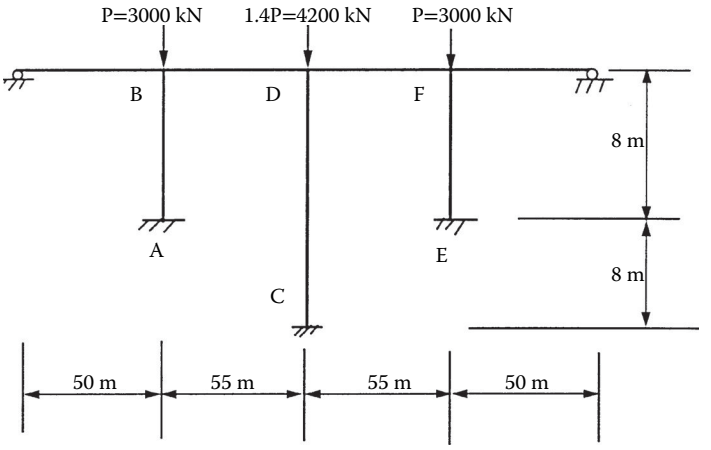

FIGURE 18.5 A four-span reinforced concrete bridge.

provided by diagonal bracing, shear walls, or equivalent means." However, there is no specific provision for the "amount of stiffness required to prevent sidesway buckling" in the AISC, AASHTO, and other specifications. In actual structures, a completely braced frame seldom exists. But in practice, some structures can be analyzed as braced frames as long as the lateral stiffness provided by bracing system is large enough. The following brief discussion may provide engineers with the tools to make engineering decisions regarding the basic requirements for a braced frame.

1. Lateral Stiffness Requirement

   Galambos (1964) presented a simple conservative procedure to estimate the minimum lateral stiffness provided by a bracing system so that the frame is considered braced.

$$\text{Required Lateral Stiffness } T_k = \frac{\sum P_n}{L_c} \tag{18.8}$$

   where Σ represents summation of all columns in one story, P_n is nominal axial compression strength of column using the *effective length factor* $K = 1$, and L_c is unsupported length of column.

2. Bracing Size Requirement

   Galambos (1964) employed Equation 18.8 to a diagonal bracing (Figure 18.6) and obtained minimum requirements of diagonal bracing for a braced frame as

$$A_b = \frac{\left[1+(L_b/L_c)^2\right]^{3/2} \sum P_n}{(L_b/L_c)^2 E} \tag{18.9}$$

   where A_b is cross-sectional area of diagonal bracing and L_b is span length of beam.

A recent study by Aristizabal-Ochoa (1994) indicates that the size of diagonal bracing required for a totally braced frame is about 4.9% and 5.1% of the column cross section for "rigid frame" and "simple farming," respectively, and increases with the moment inertia of the column, the beam span and with beam to column span ratio L_b/L_c.

18.3.3 Requirements for Column Bracings

AISC (2010) permits to brace an individual column at end and intermediate points along the column length using either relative or nodal bracing, and to design columns based on the unbraced length, L_b,

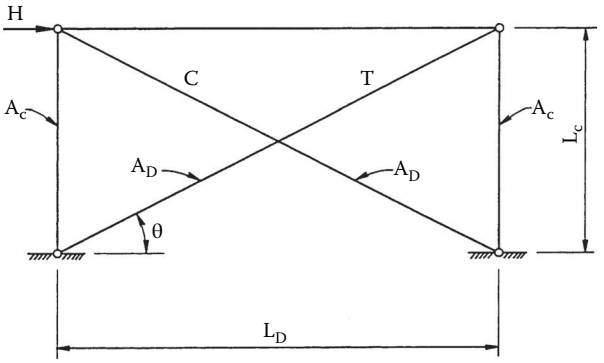

FIGURE 18.6 Diagonal cross-bracing system.

between the braced points with an effective length factor, $K = 1.0$. A relative brace controls the movement of the braced point with respect to adjacent braced points. A nodal brace controls the movement at the braced point without direct interaction with adjacent braced points. Bracing requirements are as follows:

1. Relative Bracing
   The required bracing force is

$$P_{rb} = 0.004P_r \tag{18.10}$$

   The required stiffness is

$$\beta_{rb} = \frac{1}{\varphi}\left(\frac{2P_r}{L_b}\right) \tag{18.11}$$

2. Nodal Bracing
   The required bracing force is

$$P_{rb} = 0.01P_r \tag{18.12}$$

   The required stiffness is

$$\beta_{rb} = \frac{1}{\varphi}\left(\frac{8P_r}{L_b}\right) \tag{18.13}$$

18.3.4 Simplified Equations to Alignment Charts

1. AASHTO Equations
   A graphical alignment chart determination of the *K-factor* is easy to perform, whereas solving the chart Equations 18.5 and 18.6 always involves iteration. To achieve both accuracy and simplicity for design purpose, the following alternative *K-factor* equations proposed by Duan et. al. (1993) are adapted by AASHTO Specifications (2012).

$$\text{For braced frames: } K = 1 - \frac{1}{5+9G_A} - \frac{1}{5+9G_B} - \frac{1}{10+G_AG_B} \tag{18.14}$$

   For unbraced frames:
   For $K < 2$

$$K = 4 - \frac{1}{1+0.2G_A} - \frac{1}{1+0.2G_B} - \frac{1}{1+0.01G_AG_B} \tag{18.15}$$

For $K \geq 2$

$$K = \frac{2\pi a}{0.9 + \sqrt{0.81 + 4ab}} \tag{18.16}$$

where

$$a = \frac{G_A G_B}{G_A + G_B} + 3 \tag{18.17}$$

$$b = \frac{36}{G_A + G_B} + 6 \tag{18.18}$$

2. French Equations

$$\text{For braced frames: } K = \frac{3G_A G_B + 1.4(G_A + G_B) + 0.64}{3G_A G_B + 2.0(G_A + G_B) + 1.28} \tag{18.19}$$

$$\text{For unbraced frames: } K = \sqrt{\frac{1.6G_A G_B + 4.0(G_A + G_B) + 7.5}{G_A + G_B + 7.5}} \tag{18.20}$$

Equations 18.19 and 18.20 were first appeared in the *French Design Rules for Steel Structure* (France, 1975) since 1966, and were later incorporated into the *European Recommendation for Steel Construction* (ECCS, 1978). They provide a good approximation to the alignment charts (Dumonteil, 1992).

18.4 Modifications to Alignment Charts

In using the alignment charts in Figure 18.4 and Equations 18.5 and 18.6, engineers must always be aware of the assumptions used in the development of these charts. When actual structural conditions differ from these assumptions, unrealistic design may result (AISC, 2010; Johnston, 1976; Liew et. al., 1991). The SSRC Guide (Johnston, 1976) provides methods enabling engineers to make simple modifications of the charts for some special conditions, such as, for example, unsymmetrical frames, column base conditions, girder far end conditions, and flexible conditions. A procedure that can be used to account for far ends of restraining columns being hinged or fixed was proposed by Duan and Chen (1988, 1989, and 1996) and Essa (1997). Consideration of effects of material inelasticity on the *K-factor* for steel members was developed originally by Yura (1971) and expanded by Disque (1973). LeMessurier (1977) presented an overview of unbraced frames with or without leaning columns. An approximate procedure is also suggested by AISC (2010). Several commonly used modifications for bridge columns are summarized in this section.

18.4.1 Different Restraining Girder End Conditions

When the end conditions of restraining girders are not rigidly jointed to columns, the girder stiffness (I_g/L_g) used in the calculation of *G-factor* in Equation 18.7 should be multiplied by a modification factor α_k given below.

$$\text{For a braced frame: } \alpha_k = \begin{Bmatrix} 1.0 & \text{rigid far end} \\ 2.0 & \text{fixed far end} \\ 1.5 & \text{hinged far end} \end{Bmatrix} \tag{18.21}$$

$$\text{For an unbraced frame: } \alpha_k = \begin{Bmatrix} 1.0 & \text{rigid far end} \\ 2/3 & \text{fixed far end} \\ 0.5 & \text{hinged far end} \end{Bmatrix} \tag{18.22}$$

18.4.2 Consideration of Partial Column Base Fixity

In computing the *K-factor* for monolithic connections, it is important to properly evaluate the degree of fixity in foundation. The following two approaches can be used to account for foundation fixity.

1. Fictitious Restraining Beam Approach

   Galambos (1960) proposed that the effect of partial base fixity can be model as a fictitious beam. The approximate expression for the stiffness of the fictitious beam accounting for rotation of foundation in the soil has the form

$$\frac{I_s}{L_B} = \frac{qBH^3}{72E_{steel}} \tag{18.23}$$

   where q is modulus of subgrade reaction (varies from 50–400 lb/in^3, 0.014–0.109 N/mm^3); B and H are width and length (in bending plane) of foundation, and E_{steel} is modulus of elasticity of steel.

   Based on Salmon et. al. (1957) studies, the approximate expression for the stiffness of the fictitious beam accounting for the rotations between column ends and footing because of deformation of base plate, anchor bolts, and concrete can be written as

$$\frac{I_s}{L_B} = \frac{bd^2}{72E_{steel}/E_{concrete}} \tag{18.24}$$

   where b and d are width and length of the base plate, subscripts concrete and steel represent concrete and steel, respectively. Galambos (1960) suggested that the smaller of the stiffness calculated by Equations 18.23 and 18.24 be used in determining *K-factors*.

2. AASHTO-LRFD Approach

   The following values are suggested by AASHTO-LRFD (2012)

   $G = 1.5$ footing anchored on rock
   $G = 3.0$ footing not anchored on rock
   $G = 5.0$ footing on soil
   $G = 1.0$ footing on multiple rows of end bearing piles

Example 18.2

Given: Determine *K-factor* for the Column AB as shown in Figure 18.5 by using the alignment chart with the necessary modifications. Section and material properties are given in Example 18.1 and spread footings are on soil.

SOLUTION:

(1) Calculate G-factor with modification for Column AB

Since the far end of restraining girders are hinged, girder stiffness should be multiplied by 0.5.

Using section properties in Example 18.1 we obtain:

$$G_B = \frac{\sum_B (E_c I_c / L_c)}{\sum_B \alpha_k (E_g I_g / L_g)}$$

$$= \frac{3.22(10^{12})/8{,}000}{(3.14)(10^{12})/55{,}000 + 0.5(3.14)(10^{12})/50{,}000} = 0.454$$

$G_A = 5.0$ (AASHTO, 2012)

(2) From the alignment chart in Figure 18.4b, $K = 1.60$ obtained.

18.4.3 Column Restrained by Tapered Rectangular Girders

A modification factor α_T was developed by King et. al. (1993) for those framed columns restrained by tapered rectangular girders with different far end conditions. The following modified *G-factor* is introduced in connection with the use of alignment charts:

$$G = \frac{\sum (E_c I_c / L_c)}{\sum \alpha_T (E_g I_g / L_g)} \tag{18.25}$$

where I_g is moment of inertia of the girder at near end. Both closed-from and approximate solutions for modification factor α_T were derived. It is found that the following two-parameter power-function can describe the closed-from solutions very well.

$$\alpha_T = \alpha_k (1-r)^{\beta} \tag{18.26}$$

in which the parameter α_k is a constant (Equations 18.21 and 18.22) depending on the far end conditions, and β is a function of far end conditions and tapering factor *a* and *r* as defined in Figure 18.7.

1. For a linearly tapered rectangular girder (Figure 18.7a)

$$\text{For a braced frame: } \beta = \left\{ \begin{array}{ll} 0.02 + 0.4r & \text{rigid far end} \\ 0.75 - 0.1r & \text{fixed far end} \\ 0.75 - 0.1r & \text{hinged far end} \end{array} \right\} \tag{18.27}$$

$$\text{For an unbraced frame: } \beta = \left\{ \begin{array}{ll} 0.95 & \text{rigid far end} \\ 0.70 & \text{fixed far end} \\ 0.70 & \text{hinged far end} \end{array} \right\} \tag{18.28}$$

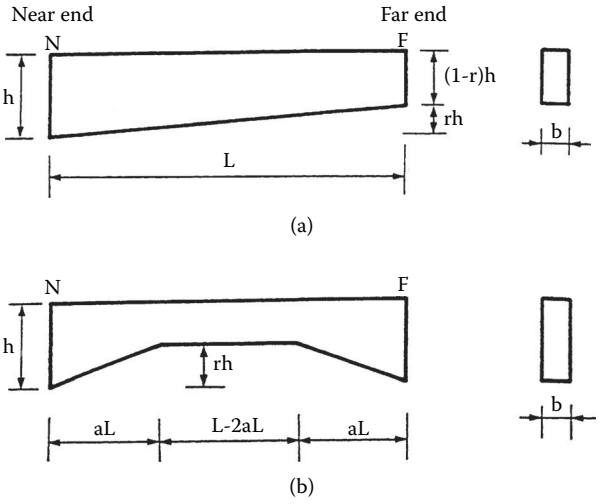

FIGURE 18.7 Tapered rectangular girders.

2. For a symmetrically tapered rectangular girder (Figure 18.7b)

$$\text{For a braced frame: } \beta = \left\{ \begin{array}{ll} 3 - 1.7a^2 - 2a & \text{rigid far end} \\ 3 + 2.5a^2 - 5.55a & \text{fixed far end} \\ 3 - a^2 - 2.7a & \text{hinged far end} \end{array} \right\} \tag{18.29}$$

$$\text{For an unbraced frame: } \beta = \left\{ \begin{array}{ll} 3 + 3.8a^2 - 6.5\,a & \text{rigid far end} \\ 3 + 2.3a^2 - 5.45a & \text{fixed far end} \\ 3 - 0.3\,a & \text{hinged far end} \end{array} \right\} \tag{18.30}$$

Example 18.3

Given: A one-story frame with a symmetrically tapered rectangular girder is shown in Figure 18.8. Assuming $r = 0.5$, $a = 0.2$, and $I_g = 2$, $I_c = 2\,I$, determine *K-factor* for column AB.

SOLUTION:

1. Using the alignment chart with modification
   For joint A, since the far end of girder is rigid, use Equations 18.30 and 18.26.

$$\beta = 3 + 3.8(0.2)^2 - 6.5(0.2) = 1.852$$

$$\alpha_T = (1 - 0.5)^{1.852} = 0.277$$

$$G_A = \frac{\sum E_c I_c / L_c}{\sum \alpha_T E_g I_g / L_g} = \frac{EI/L}{0.277\,E(2I)/2L} = 3.61$$

$$G_B = 1.0 \quad \text{(AISC, 2010)}$$

   From the alignment chart in Figure 18.4b, $K = 1.59$ is obtained
2. Using the alignment chart without modification
   A direct use of Equation 18.7 with an average section (0.75 h) result in

$$I_g = 0.75^3\,(2I) = 0.844I$$

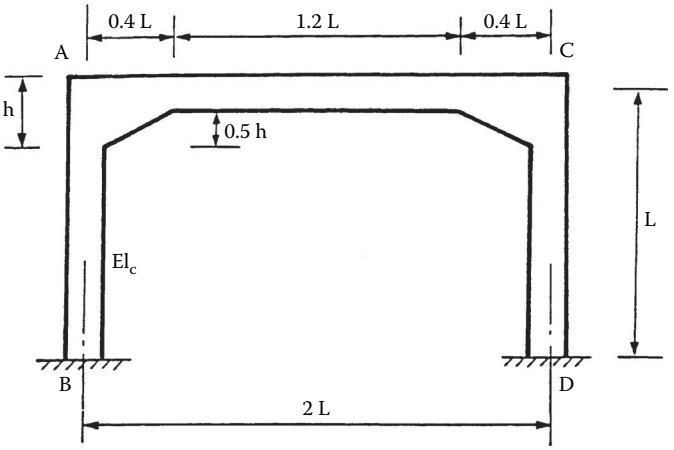

FIGURE 18.8 A simple frame with rectangular sections.

$$G_A = \frac{EI/L}{0.844\,EI/2L} = 2.37 \quad G_B = 1.0$$

From the alignment chart in Figure 18.4b, $K = 1.50$, or (1.50–1.59)/1.59 = 6% in error on the less conservative side.

18.5 Framed Columns: Alternative Methods

18.5.1 LeMessurier Method

Considering that all columns in a story buckles simultaneously and strong columns will brace weak columns (Figure 18.9), a more accurate approach to calculate *K-factors* for columns in a sidesway frame was developed by LeMessurier (1977). The K_i value for the *i*-th column in a story can be obtained by the following expression:

$$K_i = \sqrt{\frac{\pi^2 EI_i}{L_i^2 P_i}\left(\frac{\sum P + \sum C_L P}{\sum P_L}\right)} \tag{18.31}$$

where P_i is axial compressive force for member i, and subscript i represents the *i*-th column and ΣP is sum of axial force of all columns in a story.

$$P_L = \frac{\beta EI}{L^2} \tag{18.32}$$

$$\beta = \frac{6(G_A + G_B) + 36}{2(G_A + G_B) + G_A G_B + 3} \tag{18.33}$$

$$C_L = \left(\beta \frac{K_o^2}{\pi^2} - 1\right) \tag{18.34}$$

in which K_o is the *effective length factor* obtained by the alignment chart for unbraced frames, and P_L is only for those columns that provide sidesway stiffness.

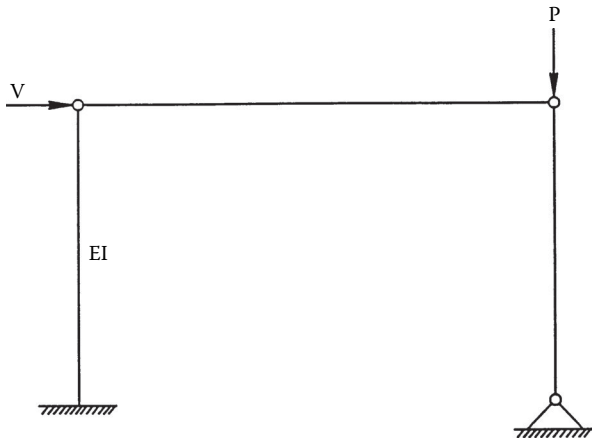

FIGURE 18.9 Subassemblage of LeMessurier method.

TABLE 18.1 Example 18.4: Detailed Calculations by LeMessurier Method

Members	AB and EF	CD	Sum	Notes
I (mm$^4 \times 10^{11}$)	3.217	3.217	-	
L (mm)	8,000	12,000	-	
G_{top}	0.454	0.235	-	Equation 18.7
G_{bottom}	0.0	0.0	-	Equation 18.7
β	9.91	10.78	-	Equation 18.33
K_{io}	1.082	1.045	-	Alignment chart
C_L	0.176	0.193	-	Equation 18.34
P_L	50,813E	24,083E	123,709E	Equation 18.32
P	P	1.4P	3.4P	P = 3,000 kN
$C_L P$	0.176P	0.270P	0.622P	P = 3,000 kN

Example 18.4

Given: Determine *K-factors* for bridge columns shown in Figure 18.5 by using LeMessurier method. Section and material properties are given in Example 18.1.

SOLUTIONS:

The detailed calculations are listed in Table 18.1.

By using Equation 18.36, we obtain:

$$K_{AB} = \sqrt{\frac{\pi^2 EI_{AB}}{L_{AB}^2 P_{AB}}\left(\frac{\sum P + \sum C_L P}{\sum P_L}\right)}$$

$$= \sqrt{\frac{\pi^2 E(3.217)(10^{11})}{(8.000)^2 (P)}\left(\frac{3.4P + 0.622P}{123{,}709E}\right)} = 1.270$$

$$K_{CD} = \sqrt{\frac{\pi^2 EI_{CD}}{L_{CD}^2 P_{CD}}\left(\frac{\sum P + \sum C_L P}{\sum P_L}\right)}$$

$$= \sqrt{\frac{\pi^2 E(3.217)(10^{11})}{(12{,}000)^2 (1.4P)}\left(\frac{3.4P + 0.622P}{123{,}709E}\right)} = 0.715$$

18.5.2 Lui Method

A simple and straightforward approach for determining the *effective length factors* for framed columns without the use of alignment charts and other charts was proposed by Lui (1992). The formulas take into account both the member instability and frame instability effects explicitly. The *K-factor* for the *i*-th column in a story was obtained in a simple form:

$$K_i = \sqrt{\left(\frac{\pi^2 EI_i}{P_i L_i^2}\right)\left[\left(\sum \frac{P}{L}\right)\left(\frac{1}{5\sum \eta} + \frac{\Delta_1}{\sum H}\right)\right]} \tag{18.35}$$

where $\Sigma(P/L)$ represents the sum of axial force to length ratio of all members in a story, ΣH is the story lateral load producing Δ_1, Δ_1 is the first-order inter-story deflection, η is member stiffness index and can be calculated by

$$\eta = \frac{(3 + 4.8m + 4.2m^2)EI}{L^3} \tag{18.36}$$

in which m is ratio of the smaller to larger end moments of the member; it is taken as positive if the member bents in reverse curvature, and negative for single curvature.

It is important to note that the term ΣH used in Equation 18.35 is not the actual applied lateral load. Rather, it is a small disturbing or fictitious force (taken as a fraction of the story gravity loads) to be applied to each story of the frame. This fictitious force is applied in a direction such that the deformed configuration of the frame will resemble its buckled shape.

Example 18.5

Given: Determine the *K-factors* for bridge columns shown in Figure 18.5 by using Lui method. Section and material properties are given in Example 18.1.

SOLUTIONS:

Apply fictitious lateral forces at B, D, and F (Figure 18.10b) and perform a first-order analysis. Detailed calculation is shown in Table 18.2.

By using Equation 18.35, we obtain

$$K_{AB} = \sqrt{\left(\frac{\pi^2 EI_{AB}}{P_{AB}L_{AB}^2}\right)\left[\left(\sum\frac{P}{L}\right)\left(\frac{1}{5\sum\eta}+\frac{\Delta_1}{\sum H}\right)\right]}$$

$$= \sqrt{\left(\frac{\pi^2(25{,}000)(3.217)(10^{11})}{P(8{,}000)^2}\right)\left[\left(\frac{1.1P}{3{,}000}\right)\left(\frac{1}{5(417{,}789)}+2.843(10^{-6})\right)\right]}$$

$$= 1.229$$

$$K_{CD} = \sqrt{\left(\frac{\pi^2 EI_{CD}}{P_{CD}L_{CD}^2}\right)\left[\left(\sum\frac{P}{L}\right)\left(\frac{1}{5\sum\eta}+\frac{\Delta_1}{\sum H}\right)\right]}$$

$$= \sqrt{\left(\frac{\pi^2(25{,}000)(3.217)(10^{11})}{1.4P(12{,}000)^2}\right)\left[\left(\frac{1.1P}{3{,}000}\right)\left(\frac{1}{5(417{,}789)}+2.843(10^{-6})\right)\right]}$$

$$= 0.693$$

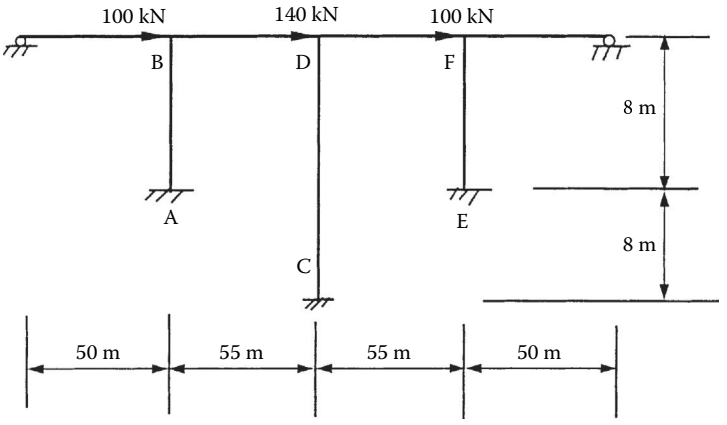

FIGURE 18.10 A bridge structure subjected to fictitious lateral loads.

TABLE 18.2 Example 18.5: Detailed Calculations by Lui Method

Members	AB and EF	CD	Sum	Notes
I (mm^4 $\times 10^{11}$)	3.217	3.217	-	
L (mm)	8,000	12,000	-	
H (kN)	150	210	510	
Δ_1 (mm)	0.00144	0.00146	-	
$\Delta_1/\Sigma H$ (mm/kN)	-	-	2.843(10^{-6})	Average
M_{top} (kN-m)	−476.9	−785.5	-	
M_{bottom} (kN-m)	−483.3	−934.4	-	
M	0.986	0.841	-	
η (kN/mm)	185,606	46,577	417,789	Equation 18.36
P/L (kN/mm)	P/8,000	1.4 P/12,000	1.1P/3,000	P = 3,000 kN

TABLE 18.3 Comparison of *K-factors* for Frame in Figure 18.5

Columns	Theoretical	Alignment Chart	Lui Equation 18.35	LeMessurier Equation 18.31
AB	1.232	1.082	1.229	1.270
CD	0.694	1.045	0.693	0.715

18.5.3 Remarks

For a comparison, Table 18.3 summarizes the *K-factors* for the bridge columns shown in Figure 18.5 obtained from the alignment chart, LeMessurier and Lui Methods as well as an eigenvalue analysis. It is seen that errors of alignment chart results are rather significant in this case. Although the *K-factors* predicted by Lui's and LeMessurier's formulas are almost the same in most cases, the simplicity and independence of any chart in the case of Lui's formula make it more desirable for design office use (Shanmugam and Chen, 1995).

18.6 Framed Columns: Eurocode Methods

18.6.1 Eurocode 2: Concrete Structures

The Eurocode 2 (ECS, 2004) proposes the following approximate expressions for *K-factors* in concrete structures:

$$\text{For braced frames: } K = 0.5\sqrt{\left(1+\frac{k_A}{0.45+k_A}\right)\left(1+\frac{k_B}{0.45+k_B}\right)} \tag{18.37}$$

$$\text{For unbraced frames: } K = \max\left\{\sqrt{1+10\frac{k_A k_B}{k_A+k_B}};\left(1+\frac{k_A}{1+k_A}\right)\left(1+\frac{k_B}{1+k_B}\right)\right\} \tag{18.38}$$

$$k = \frac{\sum\left(\frac{EI}{L}\right)_c}{\sum\left(\beta\frac{EI}{L}\right)_g} \tag{18.39}$$

where β is parameter dependent of the end restraints of girder, equal to 4 for far end is fixed and 3 if it is pinned, and so on.

18.6.2 Eurcode 3: Steel Structures

The Eurocode 3 (ECS, 2005) proposes the following approximate expressions for *K-factors* in steel structures:

$$\text{For braced frames: } K = 0.5 + 0.14(\eta_A + \eta_B) + 0.055(\eta_A + \eta_B)^2 \tag{18.40}$$

$$\text{For unbraced frames: } K = \sqrt{\frac{1 - 0.2(\eta_A + \eta_B) - 0.12\eta_A\eta_B}{1 - 0.8(\eta_A + \eta_B) + 0.6\eta_A\eta_B}} \tag{18.41}$$

$$\eta_i = \frac{\sum\left(\frac{4EI}{L}\right)_c}{\sum\left(\frac{4EI}{L}\right)_c + \sum_i\left(\beta\frac{EI}{L}\right)_g} \tag{18.42}$$

where β is parameter dependent of the end restraints of girder, equal to 4 for far end is fixed and 3 if it is pinned, and so on; subscript i corresponds to *A* and *B* joints at the two ends of the column being considered.

18.6.3 Remarks

It is noted that the Eurocode expressions for *K-factors* have no physical interpretation, but are merely numerical approximation to the exact solution of Westerberg (2004). Comparisons between above Eurocodes equations and the alignment chart method shows that both of them are essentially the same (Sousa and Barros, 2009).

18.7 Crossing Bracing Systems

18.7.1 Angle Diagonal Members

Picard and Beaulieu (1987 and 1988) reported theoretical and experimental studies on double diagonal cross bracings (Figure 18.6) and found that

- A general *effective length factor* equation is given as

$$K = \sqrt{0.523 - \frac{0.428}{C/T}} \geq 0.50 \tag{18.43}$$

- where *C* and *T* represent compression and tension forces obtained from an elastic analysis, respectively.
- When the double diagonals are continuous and attached at intersection point, the *effective length* of the compression diagonal is 0.5 times the diagonal length, that is, $K = 0.5$, because C/T ratio is usually smaller than 1.6.
- EL-Tayem and Goel (1986) reported a theoretical and experimental study about the X-bracing system made from single equal-leg angles. They concluded that
  - Design of X-bracing system should be based on an exclusive consideration of one half diagonal only.
  - For X-bracing systems made from single equal-leg angles, an *effective length* of 0.85 times the half diagonal length is reasonable, that is, $K = 0.425$.

18.7.2 Rectangular Hollow Diagonal Members

Tremblay et. al. (2003) reported an experimental study on the seismic performance of concentrically braced steel frames made with cold-formed rectangular tubular bracing members and found that

- For the single brace specimens, the rotational stiffness of the gusset plates resulted in *KL* ranged between 0.88 and 0.96 times total diagonal length.
- For the X-bracing configuration, *KL* ranged between 0.83 and 0.9 times half diagonal length.
- For simplicity, however, *KL* in design can be set equal to the total diagonal length for single diagonal bracing and to the half of diagonal length for X bracing.

18.8 Latticed and Built-Up Members

It is a common practice that when buckling model involves relative deformation produced by shear forces in the connectors, such as lacing bars and batten plates, between individual components, a modified *effective length factor* K_m or effective slenderness ratio $(KL/r)_m$ is used in determining the compressive strength. K_m is defined as

$$K_m = \alpha_v K \tag{18.44}$$

in which K is the usual *effective length factor* of a latticed member acting as a unit obtained from a structural analysis; and α_v is the shear factor to account for the effect of shear deformation on the buckling strength. Details of the development of the shear factor α_v can be found in textbooks by Bleich (1952) and Timoshenko and Gere (1961). The following section briefly summarizes α_v formulas for various latticed members.

18.8.1 Latticed Members

By considering the effect of shear deformation in the latticed panel on buckling load, shear factor α_v of the following form has been introduced:

Laced Compression Members (Figures 18.11a and b)

$$\alpha_v = \sqrt{1 + \frac{\pi^2 EI}{(KL)^2} \frac{d^3}{A_d E_d a b^2}} \tag{18.45}$$

Compression Members with Battens (Figure 18.11c)

$$\alpha_v = \sqrt{1 + \frac{\pi^2 EI}{(KL)^2} \left(\frac{ab}{12 E_b I_b} + \frac{a^2}{24 E I_f} \right)} \tag{18.46}$$

Laced-Battened Compression Members (Figure 18.11d)

$$\alpha_v = \sqrt{1 + \frac{\pi^2 E I}{(KL)^2} \left(\frac{d^3}{A_d E_d a b^2} + \frac{b}{a A_b E_b} \right)} \tag{18.47}$$

Compression Members with Perforated Cover Plates (Figure 18.11e)

$$\alpha_v = \sqrt{1 + \frac{\pi^2 EI}{(KL)^2} \left(\frac{9c^3}{64 a E I_f} \right)} \tag{18.48}$$

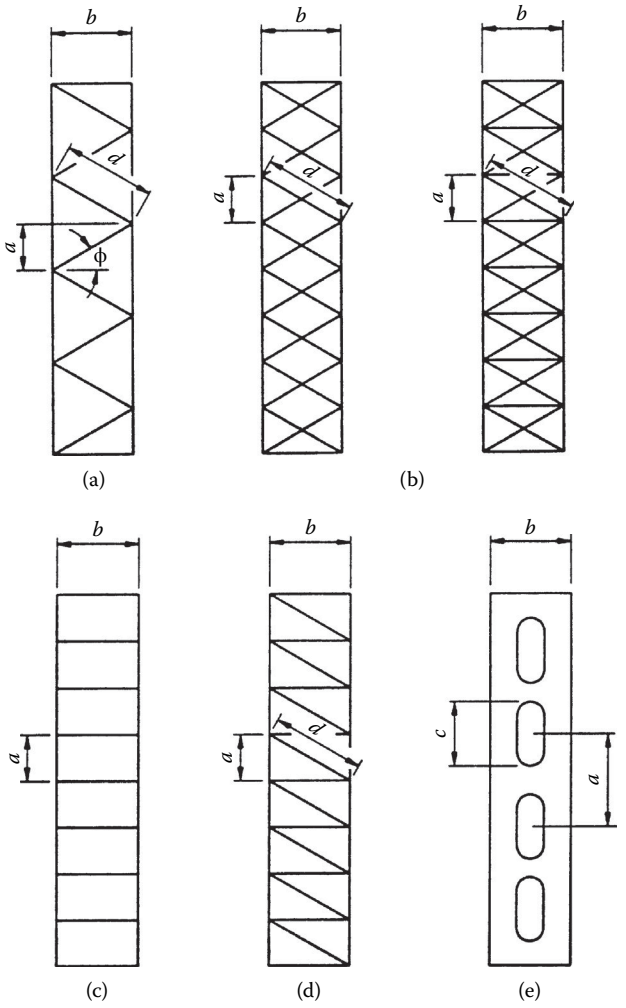

FIGURE 18.11 Typical configurations of latticed members.

where E_d is modulus of elasticity of materials for lacing bars, E_b is modulus of elasticity of materials for batten plates, A_d is cross-sectional area of all diagonals in one panel, I_b is moment inertia of all battens in one panel in the buckling plane, and I_f is moment inertia of one side of main components taken about the centroid axis of the flange in the buckling plane, *a, b, d* are height of panel, depth of member and length of diagonal, respectively, *c* is the length of a perforation.

The Structural Stability Research Council (Galambos, 1988) suggested that a conservative estimating of the influence of 60° or 45° lacing, as generally specified in bridge design practice, can be made by modifying the overall *effective length factor K* by multiplying a factor α_v, originally developed by Bleich (1952) as follows:

$$\text{For } \frac{KL}{r} > 40,\ \alpha_v = \sqrt{1 + 300/(KL/r)^2} \tag{18.49}$$

$$\text{For } \frac{KL}{r} \le 40,\ \alpha_v = 1.1 \tag{18.50}$$

It should be pointed out that the usual *K-factor* based on a solid member analysis is included in Equations 18.45 through 18.48. However, since the latticed members studied previously have pin-ended conditions, the *K-factor* of the member in the frame was not included in the second terms of the square root of the above equations in their original derivations (Bleich, 1952; Timoshenko and Gere, 1961).

18.8.2 Built-Up Members

AISC (2010) and AASHTO (2012) Specifications specify that if the buckling of a built-up member produces shear forces in the connectors between individual component members, the usual slenderness ratio KL/r for compression members must be replaced by the modified slenderness ratio $(KL/r)_m$ in determining the compressive strength.

1. For snug-tight bolted connectors

$$\left(\frac{KL}{r}\right)_m = \sqrt{\left(\frac{KL}{r}\right)_o^2 + \left(\frac{a}{r_i}\right)^2} \tag{18.51}$$

2. For welded connectors and for fully tightened bolted connectors

$$\left(\frac{KL}{r}\right)_m = \sqrt{\left(\frac{KL}{r}\right)_o^2 + 0.82\frac{\alpha^2}{(1+\alpha^2)}\left(\frac{a}{r_{ib}}\right)^2} \tag{18.52}$$

where $(KL/r)_o$ is the slenderness ratio of built-up member acting as a unit, $(KL/r)_m$ is modified slenderness ratio of built-up member, a/r_i is the largest slenderness ratio of the individual components, a/r_{ib} is the slenderness ratio of the individual components relative to its centroidal axis parallel to axis of buckling, a is the distance between connectors, r_i is the minimum radius of gyration of individual components, r_{ib} is the radius of gyration of individual components relative to its centroidal axis parallel to member axis of buckling, α is the separation ratio $= h/2r_{ib}$, and h is the distance between centroids of individual components perpendicular to the member axis of buckling.

Equation 18.51 is the same as that used in the current Italian code as well as other European specifications, based on test results (Zandonini, 1985). In this equation, the bending effect is considered in the first term in square root, and shear force effect is taken into account in the second term. Equation 18.52 was derived from elastic stability theory and verified by test data (Aslani and Goel, 1991). In both cases the end connectors must be welded or slip-critical bolted.

18.9 Tapered Columns

The state-of-the-art design for tapered structural members was provided in the SSRC guide (Galambos, 1988). The charts as shown in Figure 18.12 can be used to evaluate the *effective length factors* for tapered column restrained by prismatic beams (Galambos, 1988). In these figures, I_T and I_B are the moment of inertia of top and bottom beam, respectively; b and L are length of beam and column, respectively; and γ is tapering factor as defined by

$$\gamma = \frac{d_1 - d_o}{d_o} \tag{18.53}$$

where d_o and d_1 are the section depth of column at the smaller and larger end, respectively.

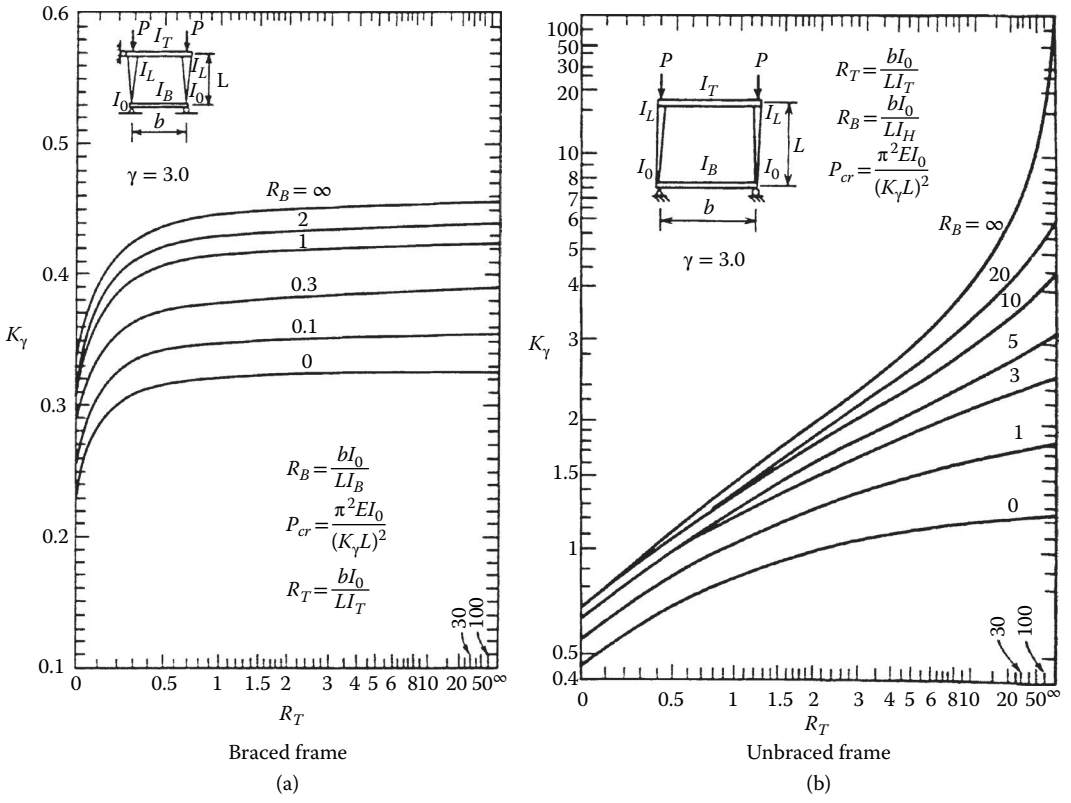

FIGURE 18.12 Effective length factor for tapered columns. (From Galambos, T. V. [Ed.], *Structural Stability Research Council, Guide to Stability Design Criteria for Metal Structures* (4th edition), John Wiley & Sons, New York, NY, 1988. With permission.)

18.10 Half-Through Truss

Holt (1952, 1956) developed a procedure to determine effective length factor for compression chord of a half-through truss (pony truss). *K-factor* listed in Table 18.4 is a function of n (numbers of panels) and CL/P_c. The bridge should be proportioned to lead to values of $K < 2.0$.

Symbols in Table 18.5 are defined as follows:

C = lateral stiffness of the U-frame (Figure 18.13) made of the truss verticals and the floor-beam (kip/in)
L = length of the chord between panel points (in)
P_c = desired critical buckling load (kip) of the truss chord member, which shall be taken as 1.33 times the factored compressive load
n = number of panels in the truss in one vertical plan

18.11 Friction Pile Shafts

Ye et. al. (2009) performed buckling analysis to determine the effective length of friction pile shafts and the influence of the resistance of surrounding soil based on m-method. The *K-factors* for friction pile shafts as listed in Table 18.5 were proposed for practical use (Ye et. al., 2009).

TABLE 18.4 Approximate *K-factors* for Friction Pile Shafts

Pile Shaft Diameter ft (m)	Pier Height ft (m)									
	32.8 (10)	65.6 (20)	98.4 (30)	131.2 (40)	164.0 (50)	196.9 (60)	229.7 (70)	262.5 (80)	295.3 (90)	328.1 (100)
3.28 (1.0)	0.85	1.15	1.25	1.35	1.45	1.50	1.55	1.65	1.65	1.65
4.92(1.5)	0.95	1.20	1.30	1.40	1.50	1.55	1.60	1.65	1.65	1.70
6.56 (2.0)	1.05	1.25	1.40	1.50	1.55	1.60	1.65	1.65	1.70	1.70
8.20 (2.5)	1.15	1.30	1.45	1.50	1.60	1.65	1.65	1.70	1.70	1.75
9.84 (3.0)	1.20	1.40	1.50	1.55	1.60	1.65	1.70	1.70	1.75	1.75
11.48 (3.5)	1.30	1.45	1.50	1.60	1.65	1.70	1.70	1.75	1.75	1.80

TABLE 18.5 Values of *1/K* for Various Values of CL/P_c and *n*

	$n = 4$	$n = 6$	$n = 8$	$n = 10$	$n = 12$	$n = 14$	$n = 16$
1/K				CL/P_c			
1.000	3.686	3.616	3.660	3.714	3.754	3.785	3.809
0.980		3.284	2.944	2.806	2.787	2.771	2.774
0.960		3.000	2.665	2.542	2.456	2.454	2.479
0.950			2.595				
0.940		2.754		2.303	2.252	2.254	2.282
0.920		2.643		2.146	2.094	2.101	2.121
0.900	3.352	2.593	2.263	2.045	1.951	1.968	1.981
0.850		2.460	2.013	1.794	1.709	1.681	1.694
0.800	2.961	2.313	1.889	1.629	1.480	1.456	1.465
0.750		2.147	1.750	1.501	1.344	1.273	1.262
0.700	2.448	1.955	1.595	1.359	1.200	1.111	1.088
0.650		1.739	1.442	1.236	1.087	0.988	0.940
0.600	2.035	1.639	1.338	1.133	0.985	0.878	0.808
0.550		1.517	1.211	1.007	0.860	0.768	0.708
0.500	1.750	1.362	1.047	0.847	0.750	0.668	0.600

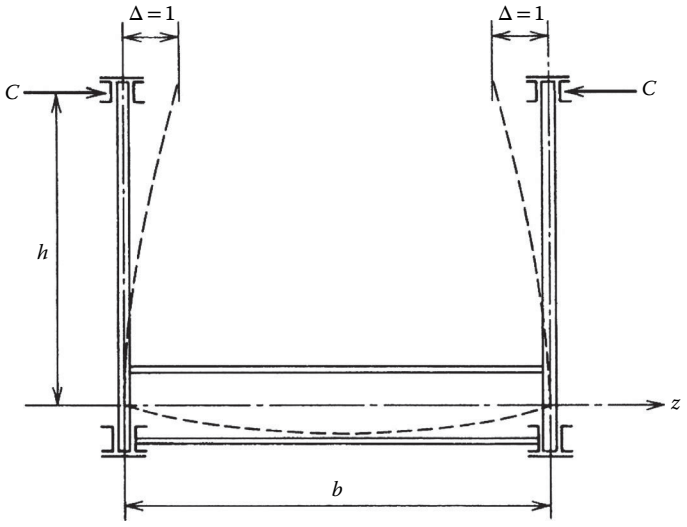

FIGURE 18.13 U-frame.

18.12 Summary

This chapter summarizes the state-of-the-art practice of the *effective length factors* for isolated columns, framed columns, diagonal bracing systems, latticed and built-up members, tapered columns, half-through trusses, and friction piles. Design implementation with formulas, charts, tables, various modification factors adopted in current codes and specifications, as well as those used in bridge structures are described. Several examples are given to illustrate the steps of practical applications of these methods.

References

AASHTO. 2012. *AASHTO LRFD Bridge Design Specifications*, Customary US Units (2012 Edition). American Association of State Highway and Transportation Officials, Washington, DC.

ACI. 2011. *Building Code Requirements for Structural Concrete and Commentary (ACI 318-11)*, American Concrete Institute, Farmington Hills, MI.

AISC. 2010. *Design Specification for Structural Steel Buildings, (ANSI/AISC 360-10)*, American Institute of Steel Construction, Chicago, IL.

Aristizabal-Ochoa, J. D. 1994. K-Factors for columns in any type of construction: nonparadoxical approach. *J. Struct. Eng., ASCE*, 120(4), 1272–1290.

Aslani, F., and Goel, S. C. 1991. An analytical criteria for buckling strength of built-up compression members. *AISC Eng. J.*, 28(4), 159–168.

Bleich, F. 1952. *Buckling Strength of Metal Structures*. McGraw-Hill, New York, NY.

Chen, W. F., and Lui, E. M. 1991. *Stability Design of Steel Frames*, CRC Press, Boca Raton, FL.

Disque, R. O. 1973. Inelastic K-factor in design. *AISC Eng. J.*, 10(2), 33–35.

Duan, L., and Chen, W. F. 1988. Effective length factor for columns in braced frames. *J. Struct. Engrg., ASCE*, 114(10), 2357–2370.

Duan, L., and Chen, W. F. 1989. Effective length factor for columns in unbraced frames. *J. Struct. Eng., ASCE*, 115(1), 150–165.

Duan, L., and Chen, W. F. 1996. Errata of Paper: Effective length factor for columns in unbraced frames. *J. Struct. Eng., ASCE*, 122(1), 224–225.

Duan, L., King, W. S., and Chen, W. F. 1993. K-factor equation to alignment charts for column design. *ACI Struct. J.*, 90(3), 242–248.

Dumonteil, P. 1992. Simple equations for effective length factors. *AISC Eng. J.*, 29(3), 111–115.

ECCS. 1978. *European Recommendations for Steel Construction*, European Convention for Construction Steelworks, Brussels, Belgium.

ECS. 2004 European Committee for Standardization, *Eurocode 2: Design of concrete structures Part 1-1 General rules and rules for buildings*. European Committee for Standardization, CEN, Brussels.

ECS. 2005. European Committee for Standardization, *Eurocode 3: Design of steel structures Part 1-1 General rules and rules for buildings*. European Committee for Standardization, CEN, Brussels.

El-Tayem, A. A., and Goel, S. C. 1986. Effective length factor for the design of X-bracing systems. *AISC Eng. J.*, 21(1), 41–45.

Essa, H. S. 1997. Stability of columns in unbraced frames, *J. Struct. Engrg., ASCE*, 123(7), 952–957.

France. 1975. *Regles de Cacul des Constructions en acier* CM66, Eyrolles, Paris, France.

Galambos, T. V. (Ed.). 1988. *Structural Stability Research Council, Guide to Stability Design Criteria for Metal Structures* (4th edition). John Wiley & Sons, New York, NY.

Galambos, T. V. 1960. Influence of partial base fixity on frame instability. *J. Struct. Div., ASCE*, 86(ST5), 85–108.

Galambos, T. V. 1964. Lateral support for tier building frames. *AISC Eng. J.*, 1(1), 16–19.

Gurfinkel, G., and Robinson, A. R. 1965. Buckling of elasticity restrained column. *J. Struct. Div., ASCE*, 91(ST6), 159–183.

Holt, E.C. 1952. Buckling of a Pony Truss Bridge. In: *Stability of Bridge Chords without Lateral Bracing, Column Research Council*, Report. No.2. Pennsylvania State College, University Park, PA.

Holt, E.C. 1956. The Analysis and Design of Single Span Pony Truss Bridge. In: *Stability of Bridge Chords without Lateral Bracing, Column Research Council*, Report. No.3. Pennsylvania State College, University Park, PA.

Johnson, D. E. 1960. Lateral Stability of Frames by Energy Method. *J. Eng. Mech., ASCE*, 95(4), 23–41.

Johnston, B. G. (Ed.). 1976. *Structural Stability Research Council, Guide to Stability Design Criteria for Metal Structures* (3rd Edition). John Wiley & Sons, New York, NY.

Julian, O. G., and Lawrence, L. S. 1959. *Notes on J and L Nomograms for Determination of Effective Lengths*, Unpublished Report.

Kavanagh, T. C. 1962. Effective length of framed column. *Trans., ASCE*, 127(II), 81–101.

King, W. S., Duan, L., Zhou, R. G., Hu, Y. X., and Chen, W. F. 1993. K-factors of framed columns restrained by tapered girders in US codes. *Eng. Struct.*, 15(5), 369–378.

LeMessurier, W. J. 1997. A practical method of second order analysis part 2- rigid frames. *AISC Eng. J.*, 14(2), 49–67.

Liew, J. Y. R., White, D. W., and Chen, W. F. 1991. Beam-column design in steel frameworks-insight on current methods and trends. *J. Const. Steel. Res.*, 18, 269–308.

Lu, L. W. 1962. A Survey of Literature on the Stability of Frames. *Weld. res. Conc. Bull.*, 81, New York, NY.

Lui, E. M. 1992. A novel approach for k-factor determination. *AISC Eng. J.*, 29(4), 150–159.

Picard, A., and Beaulieu, D. 1987. Deign of diagonal cross bracings part 1: Theoretical study. *AISC Eng. J.*, 24(3), 122–126.

Picard, A., and Beaulieu, D. 1988. Deign of diagonal cross bracings part 2: Experimental study. *AISC Eng. J.*, 25(4), 156–160.

Salmon, C. G., Schenker, L., and Johnston, B. G. 1957. Moment-rotation characteristics of column anchorage. *Trans., ASCE*, 122, 132–154.

Shanmugam, N. E., and Chen, W. F. 1995. An assessment of K factor formulas, *AISC Eng. J.*, 32(1), 3–11

Sousa, A. C., and Barros, R. C. 2009. *Harmonizing Effective Length K-Factors between European and American Codes of Practice*, Paper Ref: S2603_P0580, The 3rd International Conference on Integrity, Reliability and Failure, Porto, Portugal, 20–24 July.

Timoshenko, S. P., and Gere, J. M. 1961. *Theory of Elastic Stability*, (2nd Edition). McGraw-Hill Book Co., New York, NY.

Tremblay, R, Archambault, M. H., and Filiatrault, A. 2003. Seismic Response of Concentrically Braced Steel Frames Made with Rectangular Hollow Bracing Members. *J. Struct. Eng.*, 129(12), 1626–1636.

Westerberg, B. 2004. *Second Order Effects in Slender Concrete Structures, in Background to the rules in EC2*. KTH Civil and Architectural Engineering, Stockholm.

Wood, R. H. 1974. Effective lengths of columns in multi-storey buildings. *Struct. Engr.*, 50(7,8,9), 235–244; 295–302; 341–346.

Ye, Y., Zhang, Z., Li, W. W., Guo, F. and Fu, H. 2009. Effective length of friction piles in bridge bonstruction, *Int. Geotech. Eng. Mag.*, 14, 1–8. http://www.ejge.com/2009/Ppr0957/Ppr0957r9.pdf.

Yura, J. A. 1971. The effective length of columns in unbraced frames. *AISC Eng. J.*, 8(2), 37–42.

Zandonini, R. 1985. Stability of compact built-up Struts: Experimental investigation and numerical simulation, (in Italian), *Construzioni Metalliche*, 4.

19

Fatigue and Fracture

Robert J. Dexter
University of Minnesota

John W. Fisher
Lehigh University

Sougata Roy
Lehigh University

19.1 Introduction

Bridges do not usually fail because of inadequate load capacity, except when an overweight truck is illegally driven onto an old bridge with very low load rating. When bridge superstructures "fail," it is usually because of excessive deterioration by corrosion and/or fatigue cracking rather than inadequate load capacity. Although most deterioration can be attributed to lack of proper maintenance, there are choices made in design that also can have an impact on service life. Yet the design process for bridges is focused primarily on load capacity rather than durability.

This chapter of the handbook will inform the reader about a particular aspect of durability, that is, the fatigue and fracture failure mode, and about detailing for improved resistance to fatigue and fracture. Only aspects of fatigue and fracture that are relevant to design or assessment of bridge deck and superstructure components are discussed. Concrete and aluminum structural components are discussed briefly, but the emphasis of this section is on steel structural components.

The fatigue and fracture design and assessment procedures outlined in this chapter are included in the American Association of State Highway and Transportation Officials (AASHTO) Specifications for highway bridges (AASHTO, 2012). Some of the bridges built before the mid 1970s (when the present fatigue-design specifications were adopted) may be susceptible to fatigue cracking. There are valuable lessons that can be learned from the problems that these bridges experienced, and several examples will be used in this chapter to illustrate various points. These lessons (Fisher, 1984; Fisher, 1997) have been incorporated into the present AASHTO specifications. As a result, steel bridges that have been built in the last few decades did not and will not have any significant problems with fatigue and fracture (Fisher, 1997).

These case histories of fatigue cracking should not create the false impression that there is an inherent fatigue problem with steel bridges. The problems that occur are confined to older bridges. These problems are, for the most part, relatively minor and can be corrected with inexpensive retrofits. The

problems are even easier to avoid in new designs. Therefore, because there are some fatigue problems with older bridges, one should not get the impression that there are ongoing fatigue problems with modern bridges designed by the present fatigue-design specifications.

Detailing rules are perhaps the most important part of the fatigue and fracture design and assessment procedures. The detailing rules are intended to avoid notches and other stress concentrations. These detailing rules are useful for the avoidance of brittle fracture as well as fatigue. Because of the detailing rules, modern steel bridges are detailed in a way that appears much cleaner than those built before the 1970s. There are fewer connections and attachments in modern bridges, and the connections use more fatigue-resistant details such as high-strength bolted joints.

For example, AWS D1.5 Bridge Welding Code (AASHTO, 2010) does not permit backing bars to be left in place on welds. This rule is a result of experience such as that shown in Figure 19.1. Figure 19.1 shows lateral gusset plates on the Lafayette St. Bridge in Minneapolis that cracked and led to a fracture of a primary girder in 1976 (Fisher, 1984; Fisher et al., 1997). In this detail, backing bars were left in place under the groove welds joining the lateral gusset plate to the transverse stiffener and to the girder web. The backing bars create a crack-like notch, often accompanied by a lack-of-fusion defect. Fatigue cracks initiate from this crack-like notch and lack of fusion in the weld to the transverse stiffener because in this case, the plane of the notch is perpendicular to the primary fluctuating stress.

The Bridge Welding Code presently requires that backing bars be removed from all bridge welds to avoid these notches. Before 1994, this detailing rule was not considered applicable to seismic moment-resisting building frames. Consequently, many of these frames fractured when the 1994 Northridge Earthquake loaded them. Backing bars left on the beam flange to column welds of these frames created a built-in crack-like notch. This notch contributed to the Northridge fractures, along with lack-of-fusion defects and low-toughness welds (Fisher et al., 1997; Kaufmann et al., 1996; Kaufmann et al., 1997).

Figure 19.2 shows a detail where a primary girder flange penetrates and is continuous through the web of a cross girder of the Dan Ryan Elevated structures in Chicago (ENR, 1979). In this case, the short

FIGURE 19.1 View of cracked girder of Lafayette Street Bridge in Minneapolis showing fatigue crack originating from backing bars and lack of fusion on the weld attaching the lateral bracing attachment plate to the web and to the transverse stiffener.

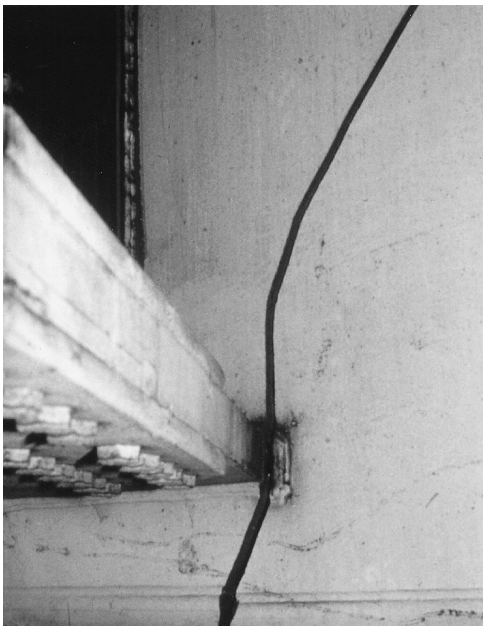

FIGURE 19.2 View of cracked cross girder of Dan Ryan elevated structure in Chicago showing cracking originating from short vertical welds that are impossible to make without lack of fusion defects.

vertical welds at the sides of the flange were defective. Fatigue cracks initiated at these welds that led to fracture of the cross girder. It is unlikely that good welds could have been made for this detail. A better alternative would have been to have cope holes at the ends of the flange. Note that in Figures 19.1 and 19.2, the fractures did not lead to structural collapse. The reason for this reserve tolerance to large cracks will be discussed in Section 19.2.

In bridges, there are usually a large number of cycles of significant live load, and fatigue will almost always precede fracture. Therefore, controlling fatigue is practically more important than controlling fracture. The civil engineering approach for fatigue is explained in Section 19.3. The fatigue life (N) of particular details is determined by the nominal stress range (S_r) from S_r-N curves. The nominal stress S_r-N curves are the lower bound curves to a large number of full-scale fatigue test data. The full-scale tests empirically take into account a number of variables with great uncertainty; for example, residual stress, weld profile, environment, and discontinuities in the material from manufacturing. Consequently, the variability of fatigue life data at a particular stress range is typically about a factor of ten.

Usually, the only measures taken in design that are primarily intended to assure fracture resistance are to specify materials with minimum specified toughness values (such as a Charpy V-Notch [CVN] test requirement). As explained in Section 19.4, toughness is specified so that the structure is resistant to brittle fracture despite manufacturing defects, fatigue cracks, and/or unanticipated loading. These material specifications are less important for bridges than the S_r-N curves and detailing rules, however.

Steel structures have exhibited unmatched ductility and integrity when subjected to seismic loading. Modern steel bridges in the United States that are designed to resist fatigue and fracture from truck loading have not exhibited fractures in earthquakes. It would appear that the modern bridge design procedures that consider fatigue and fracture from truck loading are also adequate to assure resistance to brittle fracture under seismic loading. Although rare, fractures of bridge structural elements have occurred during earthquakes outside the United States. For example, brittle fractures occurred on several types of steel bridge piers during the 1995 Hyogo-Ken Nanbu Earthquake in Japan (Miki, 1997).

These fatigue and fracture design and assessment procedures for bridges are also applicable to many other types of cyclically loaded structures that use similar welded and bolted details; for example,

cranes, buildings, chimneys, transmission towers, sign, signal, and luminaire support structures. In fact these procedures are similar to those in the American Welding Society AWS D1.1, "Structural Welding Code—Steel" (AWS, 2010), which is applicable to a broad range of welded structures.

This "civil engineering" approach to fatigue and fracture could also be applied to large welded and bolted details in structures outside the traditional domain of civil engineering, including: ships, offshore structures, mobile cranes, and heavy vehicle frames. However, the civil-engineering approach to fatigue presented herein is different than traditional mechanical-engineering approaches. The mechanical-engineering approaches are well suited to smooth machined parts and other applications where a major portion of the fatigue life of a part is consumed in forming an initial crack. In the mechanical-engineering approaches, the fatigue strength is proportional to the ultimate tensile strength of the steel. The experimental data show this is not true for welded details, as discussed in Section 19.2.

19.2 Redundancy, Ductility, and Structural Collapse

Fatigue is considered a serviceability limit state for bridges because the fatigue cracks and fractures that have occurred have mostly not been significant from the standpoint of structural integrity. Redundancy and ductility of steel bridges have prevented catastrophic collapse. Only in certain truly nonredundant structural systems can fatigue cracking lead to structural collapse.

The I-79 Bridge at Neville Island in Pittsburgh is an example of the robustness of even so-called fracture critical or nonredundant two-girder bridges. In 1977, one of the girders developed a fatigue crack in the tension flange at the location of a fabrication repair of an electroslag weld splice at midspan of the center span (Fisher, 1984). As shown in Figure 19.3, the crack completely fractured the bottom flange and propagated up the web of this critical girder. A tugboat captain happened to look up and notice the crack extending as he passed under the bridge.

Although two-girder bridges are considered nonredundant, other elements of the bridge, particularly the deck and continuity of the girders, are usually able to carry the loads and prevent collapse as in the case of the I-79 bridge. Today, because of the penalties in design and fabrication for nonredundant or fracture critical members, and concern for traffic maintenance during redecking, the simple and low-cost two-girder bridges are seldom built. Note that the large cracks shown in the bridges in Figures 19.1 and 19.2 also did not lead to structural collapse. Unfortunately, this built-in redundancy shown by these structures is sometimes difficult to predict and is not explicitly recognized in design.

The beneficial effects of redundancy on fatigue and fracture are best explained in terms of the boundary conditions on the structural members. The truck loads and wind loads on bridges are essentially

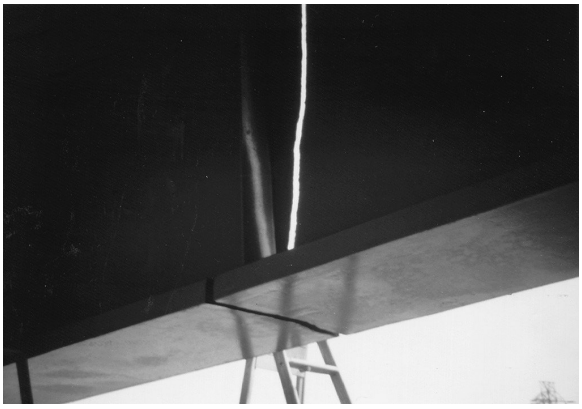

FIGURE 19.3 View of cracked girder of I-79 Bridge at Neville Island in Pittsburgh as an example of a bridge that is sufficiently redundant to avoid collapse despite a fracture of the tension flange and the web.

"fixed-load" or "load-control" boundary conditions. On a local scale, however, most individual members and connections in redundant structures are essentially under "displacement-control" boundary conditions. In other words, because of the stiffness of the surrounding structure, the ends of the member have to deform in a way that is compatible with nearby members. A cracked member in parallel with other similar but uncracked members will experience a decreasing load range and nominal stress range as the stiffness of the cracked member decreases. This behavior under displacement control is referred to as load shedding and it can slow down the rate of fatigue crack propagation.

If a fatigue crack forms in one element of a bolted or riveted built-up structural member, the crack cannot propagate directly into neighboring elements. Usually, a riveted member will not fail until additional cracks form in one or more additional elements. Therefore, riveted built-up structural members are inherently redundant. Once a fatigue crack forms, it can propagate directly into all elements of a continuous welded member and cause failure at service loads. Welded structures are not inferior to bolted or riveted structures, they require more attention to design, detailing, and quality.

Ductility is required in order for redundancy to be completely effective. As the net section of a cracking bridge member decreases, the plastic moment capacity of the member decreases. If a member is sufficiently ductile, it can tolerate a crack so large that the applied moment exceeds the plastic moment capacity for the net section and a mechanism will form in the member (Dexter, 1995; Dexter and Gentilcore, 1997 and 1998). If the member can then deform to several times the yield rotation, the load will be shed to the deck and other members.

Minimum levels of fracture toughness are necessary to achieve ductility, but are not sufficient. The fracture toughness assures that brittle fracture does not occur before general yielding of the net cross section. However, net-section yielding is not very ductile unless the yielding can spread to the gross section, which requires strain hardening in the stress–strain relationship of the steel, or a reasonably low yield-to-tensile ratio (Dexter and Gentilcore, 1997; Dexter and Gentilcore, 1998; Dexter, 1997).

19.3 Fatigue Resistance

Low-cycle fatigue is a possible failure mode for structural members or connections that are cycled into the inelastic region for a small number of cycles (usually < 1000) (Castiglioni, 1995; Krawinkler and Zohrei, 1983). For example, bridge pier structures may be subjected to low-cycle fatigue in an earthquake (Miki, 1997). Brittle fractures occurred in Japan in steel piers that underwent large plastic strain cycles during the 1995 Hyogo-Ken Nanbu Earthquake in Japan (Miki ,1997). However, in order to focus on the more common phenomenon of high-cycle fatigue, low-cycle fatigue is not discussed further in this section.

Truck traffic is the primary cause of high-cycle fatigue of bridges. Wind loads may also be a fatigue design consideration in bridges. Wind-induced vibration has caused numerous fatigue problems in sign, signal, and luminaire support structures (Kaczinski et al., 1988; Roy et al., 2012).

Although cracks can form in structures cycled in compression, they arrest and are not structurally significant. Therefore, only members or connections for which the stress cycle is at least partially in tension need to be assessed.

In most bridges, the ratio of the strength-design load to the fatigue-design-truck load is large enough that fatigue may control the design of much of the structure. In long-span bridges, the load on much of the primary supporting members is dominated by the dead load, with the fluctuating live load part relatively small. These members will not be sensitive to fatigue. However, the deck, stringers, and floorbeams of bridges are primarily subjected to localized effects of live load and therefore will be controlled by fatigue. Fortunately, the deck, stringers, and floorbeams are secondary members that, if cracked, would not lead to structural collapse.

When information about a specific crack is available, a fracture mechanics crack growth rate analysis should be used to calculate remaining life (Barsom and Rolfe, 1987; Broek, 1987; Kober et al., 1994). However, in the design stage, without specific initial crack size data, the fracture mechanics approach

is not any more accurate than the S_r-N curve approach (Kober et al., 1994). Therefore, the fracture mechanics crack growth analysis will not be discussed further.

Welded and bolted details for bridges and buildings are usually designed based on the nominal stress range rather than the local "concentrated" stress at the weld detail. The nominal stress is usually obtained from standard design equations for bending and axial stress and does not include the effect of stress concentrations of welds and attachments. Since fatigue is typically only a serviceability problem, fatigue design is carried out using service loads as discussed in Section 19.3.4. Usually, the nominal stress in the members can be easily calculated without excessive error. However, the proper definition of the nominal stresses may become a problem in regions of high stress gradients as occur in poles and luminaires and in some orthotropic deck details (Connor and Fisher, 2005; Dexter et al., 1994; Roy et al., 2012; Yagi et al., 1991).

It is a standard practice in fatigue design of welded structures to separate the weld details into categories having similar fatigue resistance in terms of the nominal stress. Each category of weld details has an associated S_r-N curve. The S_r-N curves for steel in the AASHTO (2012), AISC (2010), AWS (2010), and AREMA (2012) American Railway Engineers Association (AREA) provisions are shown in Figure 19.4. S_r-N curves are presented for seven categories of weld details; A through E', in order of decreasing fatigue strength. These S-N curves are based on a lower bound to a large number of full-scale fatigue test data with a 97.5% survival limit as illustrated in Figure 19.5 for Category E.

The slope of the log–log regression line fit to the test data for welded details is typically in the range 2.9–3.1 (Dexter, Fisher and Beach, 1993; Keating and Fisher, 1986). Therefore, in the AISC (2010) and AASHTO codes (AASHTO, 2012) as well as in Eurocode 3 (CEN, 2005), the slopes have been standardized at 3.0 for the exponential relationship between stress range and life $N = C_f S_r^{-n}$. The effect of the welds and other stress concentrations are reflected in the ordinate of the S_r-N curves for the various detail categories.

Figure 19.4 shows the fatigue threshold or constant amplitude fatigue limit (CAFL) for each category as a horizontal dashed line. When constant amplitude tests are performed at stress ranges below the CAFL, detectable cracking does not occur. The number of cycles associated with the CAFL is whatever number of cycles corresponds to that stress range on the S_r-N curve for that category or class of detail. The CAFL occurs at an increasing number of cycles for lower fatigue categories or classes. Sometimes, different details, which share a common S_r-N curve (or category) in the finite-life regime, have different CAFL.

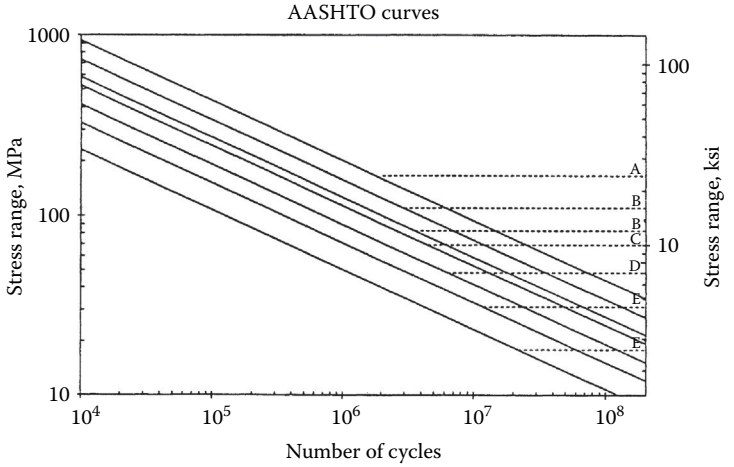

FIGURE 19.4 The lower-bound S-N curves for the seven primary fatigue categories from the AASHTO, AREMA, AWS, and AISC specifications. The dotted lines are the Constant Amplitude Fatigue Limits (CAFL) and indicate the detail category.

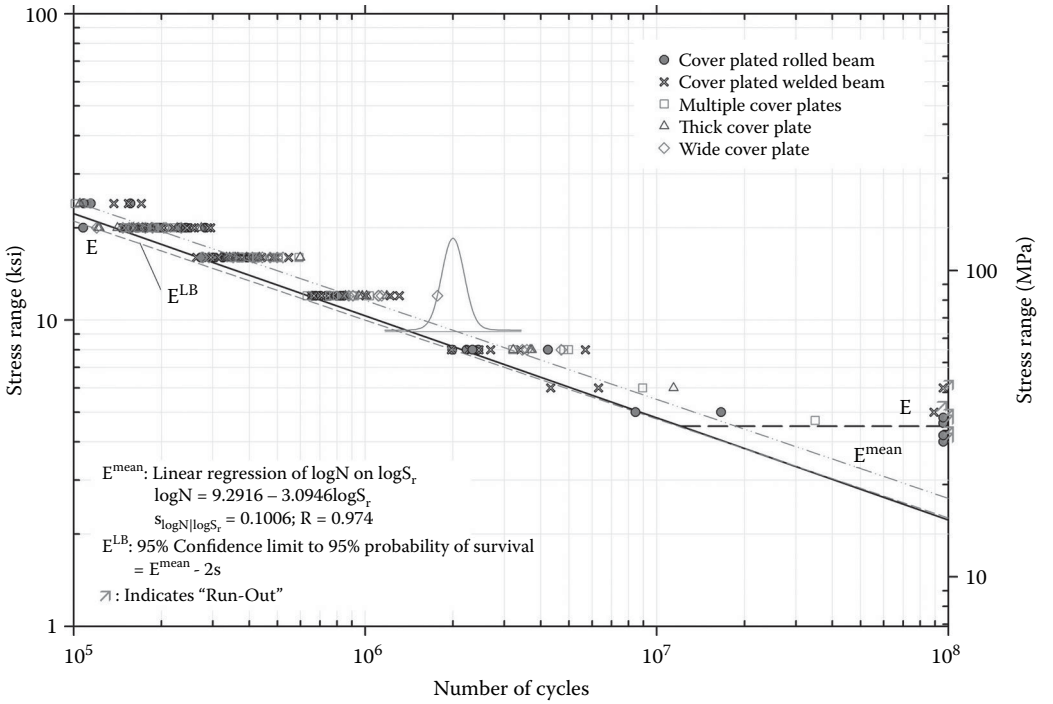

FIGURE 19.5 Stress range test data for Category E details showing log normal distribution of fatigue life for all stress range levels.

Typically, small-scale specimen tests will result in longer apparent fatigue lives. Therefore, the S_r-N curve must be based on tests of full size structural components such as girders. Testing on full-scale welded members has indicated that the primary effect of constant amplitude loading can be accounted for in the live-load stress range, that is, the mean stress is not significant (Dexter et al., 1993; Fisher et al., 1970; Fisher et al., 1974; Keating and Fisher, 1986). The reason that the dead load has little effect on the lower bound of the results is that, locally, there are very high residual stresses from welding. Mean stress may be important for some details that are not welded, such as anchor bolts (Kaczinski et al., 1988; VanDien et al., 1996). In order to be conservative for nonwelded details, in which there may be a significant effect of the mean stress, the fatigue test data should be generated under loading with a high tensile mean stress and conservatively applied to lower mean stress levels.

The strength and type of steel have only a negligible effect on the fatigue resistance expected for a particular detail (Dexter et al., 1993; Fisher et al., 1970, 1974; Keating and Fisher 1986). The welding process also does not typically have an effect on the fatigue resistance (Dexter et al., 1993; Fisher et al., 1970; Fisher et al., 1974; Keating and Fisher, 1986). The independence of the fatigue resistance from the type of steel greatly simplifies the development of design rules for fatigue since it eliminates the need to generate data for every type of steel.

Full-scale fatigue experiments have been carried out in moist air and therefore reflect some degree of environmental effect or corrosion fatigue. Full-scale fatigue experiments in seawater do not show significantly lower fatigue lives (Roberts et al., 1986), provided that corrosion is not so severe that it causes pitting. The fatigue lives seem to be more significantly influenced by the stress concentration at the toe of welds and the initial discontinuities. Therefore, these lower-bound S_r-N curves can be used for design of bridges in any natural environmental exposure, even near salt spray. However, pitting from severe corrosion may become a fatigue critical condition and should not be allowed (Albrecht and Shabshab, 1994; Out et al., 1984).

TABLE 19.1 Constant Amplitude Fatigue Limits for AASHTO and Aluminum Association S-N Curves

Detail Category	CAFL for Steel (MPa)	CAFL for Aluminum (MPa)
A	165	70
B	110	41
B'	83	32
C	69	28
D	48	17
E	31	13
E'	18	7

Similar S_r-N curves have been proposed by the Aluminum Association (Menzemer and Fisher, 1995) for welded aluminum structures. Table 19.1 summarizes the CAFL for steel and aluminum for categories A through E'. The design procedures are based on associating weld details with specific categories. For both steel and aluminum, the separation of details into categories is approximately the same.

The categories in Figure 19.4 range from A to E' in order of decreasing fatigue strength. There is an eighth Category F in the specifications (not shown in Figure 19.4) that applies to fillet and plug welds loaded in shear. However, there have been very few if any failures related to shear, and the stress ranges are typically very low such that fatigue rarely would control the design. Therefore, the shear stress Category F will not be discussed further. In fact there have been very few if any failures that have been attributed to details that have fatigue strengths greater than Category C.

19.3.1 Classification of Details in Metal Structural Components

Details must be associated with one of the drawings in the specification (AASHTO, 2012) to determine the fatigue category. The following is a brief simplified overview of the categorization of fatigue details. In some cases, this overview has left out some details so the specification should always be checked for the appropriate detail categorization. The AISC specification (2010) has a similar presentation of the sketches and explanation of the detail categorization as the current AASHTO specifications (AASHTO, 2012). Also, several reports have been published that show a large number of illustrations of details and their categories (Demers and Fisher, 1990; Yen et al., 1990). The Eurocode 3 CEN 2005 and the British Standard 7608 (BSI 1994) provide illustrations for their categorization that are similar to the current AISC and AASHTO specifications. A book by Maddox (1991) discusses categorization of many details in accordance with BS 7608, from which equivalent AISC and AASHTO categories can be inferred.

Small holes are considered Category D details. Therefore, riveted and mechanically fastened joints (other than preloaded high-strength bolted joints) loaded in shear are evaluated as Category D in terms of the net-section nominal stress. Properly tensioned high-strength bolted joints loaded in shear may be classified as Category B for the connected material and the bolts are not fatigue critical in shear. Pin plates and eyebars are designed as Category E details in terms of the stress on the net section.

Welded joints are considered longitudinal if the axis of the weld is parallel to the primary stress range. Continuous longitudinal welds are Category B or B' details. However, the terminations of longitudinal fillet welds are more severe (Category E). (The termination of full-penetration groove longitudinal welds requires a ground transition radius but gives greater fatigue strength, depending on the radius.) If longitudinal welds must be terminated, it is better to terminate at a location where the stress ranges are less severe.

Attachments normal to flanges or plates that do not carry significant load are rated Category C if < 51 mm long in the direction of the primary stress range, D if between 51 and 101 mm long, and E if > 101 mm long. (The 101 mm limit may be smaller for plate thinner than 9 mm). If there is not at least 10 mm edge distance, then Category E applies for an attachment of any length. The Category E', slightly worse than Category E, applies if the attachment plates or the flanges exceed 25 mm in thickness.

Transverse stiffeners are treated as short attachments (Category C). Transverse stiffeners that are used for cross bracing or diaphragms are also treated as Category C details with respect to the stress in the main member. In most cases, the stress range in the stiffener from the diaphragm loads is not considered, because these loads are typically unpredictable. However, the detailing of attachment plates is critical to avoid distortion-induced fatigue, as discussed in Section 19.3.2.

In most other types of load-carrying attachments, there is interaction between the stress range in the transverse load-carrying attachment and the stress range in the main member. In practice, each of these stress ranges is checked separately. The attachment is evaluated with respect to the stress range in the main member and then it is separately evaluated with respect to the transverse stress range. The combined multiaxial effect of the two stress ranges is taken into account by a decrease in the fatigue strength; that is, most load-carrying attachments are considered Category E details.

The fatigue strength of longitudinal attachments can be increased if the ends are given a radius and the fillet or groove weld ends are ground smooth. For example, a longitudinal attachment (load bearing or not) with a transition radius > 50 mm can be considered Category D. If the transition radius of a groove-welded longitudinal attachment is increased to > 152 mm (with the groove-weld ends ground smooth), the detail (load bearing or not) can be considered Category C.

19.3.2 Detailing to Avoid Distortion-Induced Fatigue

It is clear from the type of cracks that occur in bridges that a significant proportion of the cracking is due to distortion that results from such secondary loading (Fisher, 1984; Fisher et al., 1990). The solution to the problem of fatigue cracking because of secondary loading usually relies on the qualitative art of good detailing (Fisher and Keating 1989). Often, the best solution to distortion cracking problems may be to stiffen the structure. Typically, the better connections are more rigid.

One of the most overlooked secondary loading problems occurs at the interface of structures with different flexural rigidities and curvatures (Fisher, Kaufmann et al., 1995; Fisher, Yen et al., 1995). Figure 19.6 shows a typical crack at the floorbeam flange cope in the Throg's neck bridge in New York. One of the closed trapezoidal ribs of an orthotropic steel deck is visible in Figure 19.6 bolted to the transverse diaphragm flange. The orthotropic deck was added to the structure to replace a deteriorating deck by bolting onto the transverse diaphragms and floorbeams. However, the superstructure has curvature that is incompatible with the stiff deck. The difference in curvature manifests as out-of-plane rotation of the flange of the transverse diaphragm shown in Figure 19.6. The crack is caused by out-of-plane bending of the diaphragm web at the location of the cope, which had many built in discontinuities due to the flame cutting.

FIGURE 19.6 View of floorbeam of Throg's Neck Bridge in New York showing crack in the cope that has been repaired by drilling a stop hole. The crack is caused by incompatibility between the curvature of the superstructure and the orthotropic steel deck that is bolted onto the floorbeams.

Another example of secondary loading from out-of-plane distortion may occur at connection plates for a transverse bracing or for a floorbeam. These connection plates, which may have out-of-plane loads, should be welded directly to both flanges as well as the web. In older bridges, it was common practice to not weld transverse stiffeners and connection plates to the tension flange of welded I girders and box girders. The practice of not allowing transverse fillet welds on the tension flange is not necessary because of unwarranted concern about brittle fracture of the tension flange (Fisher et al., 1990; Fisher and Keating, 1989). Unfortunately, this practice is not harmless, because numerous fatigue cracks have occurred because of distortion in the "web gap," that is the narrow gap between the termination of the connection plate fillet welds and the flange (Fisher et al., 1990; Fisher and Keating, 1989). Figure 19.7 shows an example of a crack that formed along the fillet weld that attaches a diaphragm connection plate to the web of a box girder.

In most cases, these web-gap cracking problems can be solved by rigidly attaching the attachment plate to the tension flange. To retrofit existing bridges, a very thick tee or angle may be used with high-strength bolts to join the attachment plate to the tension flange (Fisher and Keating, 1989). The cracked detail shown in Figure 19.7 was retrofitted this way. In other cases a better solution is to make the detail more flexible. This flexibility can be accomplished by increasing the size of the gap, allowing the distortion to take place over a greater length so that lower stresses are created.

The flexibility approach is used to prevent cracking at the terminations of transverse stiffeners that are not welded to the bottom flange. If there is a narrow web gap between the ends of a transverse stiffener and the bottom flange, cracking can occur because of distortion of the web gap from inertia loading during handling and shipping. To prevent this type of cracking, the gap between the flange and the bottom end of the stiffener should be between 4 and 6 times the thickness of the web (Fisher and Keating, 1989).

Another example, where the best details are more flexible, is the connection angle for "simply-supported" beams. Despite our assumptions, such simple connections transmit up to 40% of the theoretical fixed-end moment, even though they are designed to transmit only shear forces. This unintentional end moment may crack the connection angle and/or the beam web cope. The cracked connection angle shown in Figure 19.8 was from the stringer to floorbeam connection on a bridge that was formerly on I-94 over the St. Croix River (now replaced).

For a given load, the moment in the connection decreases significantly as the rotational stiffness of the connection decreases. The increased flexibility of connection angles allows the limited amount of end

FIGURE 19.7 View of crack in the fillet weld joining the diaphragm connection plate to the web of a box section in the Washington Metro elevated structures. The crack is caused by distortion in the small gap between the bottom of the attachment plate and the box girder flange.

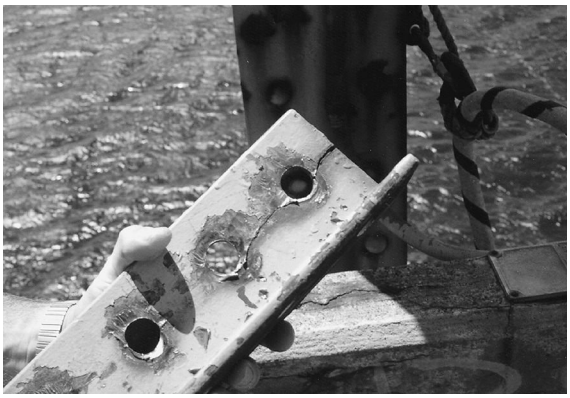

FIGURE 19.8 Connection angle from stringer to floorbeam connection of a bridge that was over the St. Croix River on I-94 that cracked because it was too stiff.

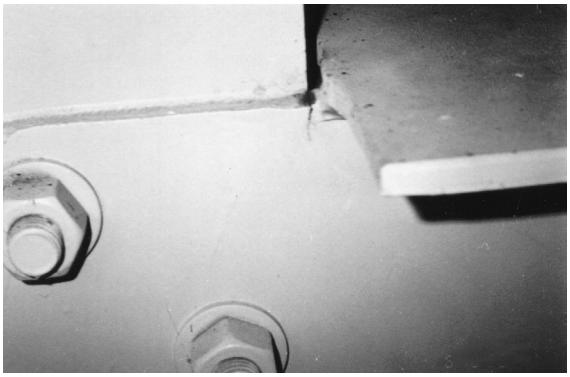

FIGURE 19.9 Close-up view of a crack originating at the termination of a flange on a floorbeam with a "simple" connection to an attachment plate in the Dresbach Bridge in Minnesota. The crack is an indication of an end moment in the simple connection that is not predicted in design.

rotation to take place with reduced angle bending stresses. A criterion was developed for the design of these angles to provide sufficient flexibility (Yen et al., 1991). The criterion states that the angle thickness (t) must be

$$t < \frac{12g^2}{L} \tag{19.1}$$

where (g) is the gage and L is the span length. For example, using S.I. units, for connection angles with a gage of 76 mm and a beam span of 7000 mm, the angle thickness should be just < 10 mm. To solve a connection-angle-cracking problem in service, the topmost rivet or bolt may be removed and replaced with a loose bolt to ensure the shear capacity. For loose bolts, steps are required to ensure that the nuts do not back off.

Another result of unintended end moment on a floorbeam end connection is shown in Figure 19.9 from the Dresbach Bridge in Minnesota. In this bridge, the web of the welded built-up floorbeam extends beyond the flanges in order to bolt to the floorbeam connection plate on the girder. The unintended moment at the end of the floorbeam is enough to cause cracking in the web plate at the termination of the flange fillet welds as the web plate alone has significantly reduced bending capacity. There is a large stress concentration and higher bending stresses at this location caused by the abrupt change in section at the end of the flange; that is, this is also a Category E' detail. An improved condition is the use of a blocked flange with a curved radius transition so the bending resistance is increased, which will reduce the stress range and improve the detail category.

Significant stresses from secondary loading are often in a different direction than the primary stresses. Fortunately, experience with multiaxial loading experiments on large-scale welded structural details indicate the loading perpendicular to the local notch or the weld toe dominates the fatigue life. The cyclic stress in the other direction has no effect if the stress range is below 83 MPa and only a small influence above 83 MPa (Dexter et al., 1994; Fisher et al., 1990). The recommended approach for multiaxial loads (Dexter et al., 1994) is as follows:

1. Decide which loading (primary or secondary) dominates the fatigue cracking problem (typically the loading perpendicular to the weld axis or perpendicular to where cracks have previously occurred in similar details).
2. Perform the fatigue analysis using the stress range in this direction (i.e., ignore the stresses in the orthogonal directions).

19.3.3 Classification of Details in Concrete Structural Components

Concrete structures are typically less sensitive to fatigue than welded steel and aluminum structures. However, fatigue may govern the design when impact loading is involved, such as pavement, bridge decks, and rail ties. Also, as the age of concrete girders in service increases, and as the applied stress ranges increase with increasing strength of concrete, the concern for fatigue in concrete structural members has also increased.

According to ACI Committee Report 215R-74 in the Manual of Standard Practice (ACI Committee 215, 1996), the fatigue strength of plain concrete at 10 million cycles is approximately 55% of the ultimate strength. However, even if failure does not occur, repeated loading may contribute to premature cracking of the concrete, such as inclined cracking in prestressed beams. This cracking can then lead to localized corrosion and fatigue of the reinforcement (Hahin, 1994).

The fatigue strength of straight, unwelded reinforcing bars and prestressing strand can be described (in terms of the categories for steel details described in Section 19.3.1.) with the Category B S_r-N curve. ACI Committee 215 suggests that members be designed to limit the stress range in the reinforcing bar to 138 MPa for high levels of minimum stress (possibly increasing to 161 MPa for less minimum stress). Fatigue tests show that previously bent bars had only about half the fatigue strength of straight bars, and failures have occurred down to 113 MPa (Pfister and Hognestad, 1964). Committee 215 recommends that half of the stress range for straight bars be used, that is 69 MPa for the worst case minimum stress. Equating this recommendation to the S_r-N curves for steel details, bent reinforcement may be treated as a Category D detail.

Provided the quality is good, butt welds in straight reinforcing bars do not significantly lower the fatigue strength. However, tack welds reduce the fatigue strength of straight bars approximately 33%, with failures occurring at a stress range as low as 138 MPa. Fatigue failures have been reported in welded wire fabric and bar mats (Sternberg, 1969).

If prestressed members are designed with sufficient precompression that the section remains uncracked, there is not likely to be any problem with fatigue. This is because the entire section is resisting the load ranges and the stress range in the prestressing strand is minimal. Similarly, for unbonded prestressed members, the stress ranges will be very small. However, there is a reason to be concerned for bonded prestressing at cracked sections because the stress range increases locally. The concern for cracked sections is even greater if corrosion is involved. The pitting from corrosive attack can dramatically lower the fatigue strength of reinforcement (Hahin, 1994). The loss of prestressing strands has even resulted in complete collapse of a prestressed box girder (Naito et al., 2006).

Although the fatigue strength of prestressing strand in air is about that of Category B, when the anchorages are tested as well the fatigue strength of the system is as low as half the fatigue strength of the wire alone (i.e., about Category E). When actual beams are tested, the situation is very complex but it is clear that much lower fatigue strength can be obtained (Rabbat et al., 1979; Overnman et al., 1984). Committee 215 has recommended the following for prestressed beams:

1. The stress range in prestressed reinforcement, determined from an analysis considering the section to be cracked, shall not exceed 6% of the tensile strength of the reinforcement. (This is approximately equivalent to the resistance of Category C details.)
2. Without specific experimental data, the fatigue strength of unbonded reinforcement and their anchorages shall be taken as half of the fatigue strength of the prestressing steel. (This is approximately equivalent to the resistance of Category E details.) Lesser values shall be used at anchorages with multiple elements.

19.3.4 Classification of Stay Cables

The Posttensioning Institute has issued "Recommendations for Stay Cable Design and Testing" (PTI, 1986). The PTI recommends that uncoupled bar stay cables are Category B details, whereas coupled (glued) bar stay cables are Category D. The fatigue strengths of stay cables are verified through fatigue testing. Two types of tests are performed: (1) fatigue testing of the strand; and (2) testing of relatively short lengths of the assembled cable with anchorages. The recommended test of the system is two-million cycles at a stress range of 158 MPa, which is 35 MPa greater than the allowable fatigue resistance of Category B details at two-million cycles. This test should pass with less than 2% wire breaks. A subsequent proof test must achieve 95% of the actual ultimate tensile strength of the tendons.

19.3.5 Characterization of Truck Loading for Fatigue

An actual service load history is likely to consist of cycles with a variety of different load ranges, that is variable-amplitude loading. However, the S_r-N curves that are the basis of the fatigue design provisions are based on constant amplitude loading. A procedure is shown below to convert variable stress ranges into an equivalent constant-amplitude stress range with the same number of cycles. This procedure is based on the damage summation rule jointly credited to Palmgren and Miner, commonly referred to as Miner's rule (Fisher et al., 1993; Gurney, 2006; Miner, 1945; Schilling et al., 1978). If the slope of the S-N curve is equal to 3, then the relative damage of stress ranges is proportional to the cube of the stress range. Therefore, the effective stress range (S_{Re}) is equal to the cube root of the mean cube (rmc) of the stress ranges, that is

$$S_{Re} = \left[\left(\frac{n_i}{N_{total}} \right) S_i^3 \right]^{1/3} \tag{19.2}$$

where n_i is the number of stress ranges of magnitude S_i, and N_{total} is the total number of stress ranges.

The fatigue design truck in the AASHTO LRFD bridge design specification is a three-axle HS20 truck. The front axle has a weight of 36 kN and the rear two axles each have a weight of 142 kN. It is very important to note that the single rear axles of the HS-20 fatigue truck are actually intended to represent pairs of tandem axles (Moses et al., 1987). This simplification eases design of main members by decreasing the number of axles (loads) that must be considered. Representation as a single axle is also reasonable for fatigue design of bridge main members, since the close spacing of tandem axles (approximately 1.2 m) effectively generates only one stress cycle.

This simplified three-axle truck is not appropriate for the design of deck elements such as orthotropic and grid decks and even some floorbeams. Each axle of a tandem axle group creates a unique stress cycle in a deck element. When the entire distribution of trucks is considered, this results in approximately 4.5 axles or cycles of loading on average for every truck. The 2012 AASHTO LRFD code clearly indicates that this should be taken into account in the fatigue design of these elements. If the HS20 tandem axle load is split when applied to orthotropic and grid decks, the effective axle load is 71 kN for each axle.

The HS20 truck is used in strength calculations with a load factor > 1.0. However, there is a load factor of 0.75 for fatigue in the LRFD specification, which indicates that the actual fatigue design truck is equivalent to HS15, that is, an axle load of 107 kN (really a pair of tandem of 53 kN axles). Thus, the

AASHTO LRFD Specifications use a 0.75×HS20 loading for finite life fatigue design or Fatigue I Limit State. Load factors for infinite life design or Fatigue II Limit State are different as discussed later. The load factor was developed so that an additional and possibly confusing design truck would not have to be defined.

The use of a fatigue truck as representative of the rmc of the variable series of trucks is based on extensive weigh in motion (WIM) data and was originally recommended in NCHRP Report 299 "Fatigue Evaluation Procedures for Steel Bridges" (Moses et al., 1987). A constant axle spacing of 30 ft was found to best approximate the axle spacing of typical 4 and 5 axle trucks responsible for most fatigue damage to bridges. The fatigue truck is supposed to represent the effective or rmc gross vehicle weight (GVW) for a distribution of future trucks.

In the AASHTO LRFD specification, the effective stress range is computed from this effective load, and the effective stress range is compared to an allowable stress range. The allowable stress range is obtained from the constant amplitude S_r-N curve, using the same number of cycles as the number of variable cycles used to compute the rmc stress range.

This concept is illustrated schematically in Figure 19.10. Figure 19.10 shows the lower part of an S_r-N curve with three different variable stress-range distributions superposed. The effective stress range, shown as S_{re} in Figure 19.10, is the root mean cube (rmc) of the stress ranges for a particular distribution, as defined in Equation 19.2. The effective variable-amplitude stress range is used with S_r-N curves the same way as a constant-amplitude stress range is used, as shown for Case 1 in Figure 19.10.

Full-scale variable-amplitude fatigue tests show that if more than 0.01% of the stress ranges in a distribution are above the CAFL (Case 2 in Figure 19.10), fatigue cracking will still occur (Fisher et al., 1993; Gurney, 2006). The few cycles that are above the CAFL seem to keep the process going, such that even the stress ranges that are below the CAFL apparently contribute to the fatigue crack growth. The effective stress range and number of cycles to failure data from these tests fell along a straight-line extrapolation of the constant amplitude curve. Therefore, the approach in the AASHTO LRFD specification is to use the straight-line extrapolation of the S_r-N curve below the CAFL to compute the allowable stress range.

The British fatigue design standard BS 7608 (BSI, 1994) uses this same approach for variable amplitude loading, that is a rmc stress range is used with an extrapolation of the S-N curve below the CAFL. Eurocode 3 (CEN, 2005) also uses the effective stress range concept, however they use a different slope of 5 for the extrapolation of the S_r-N curve below the CAFL (Gurney, 2006).

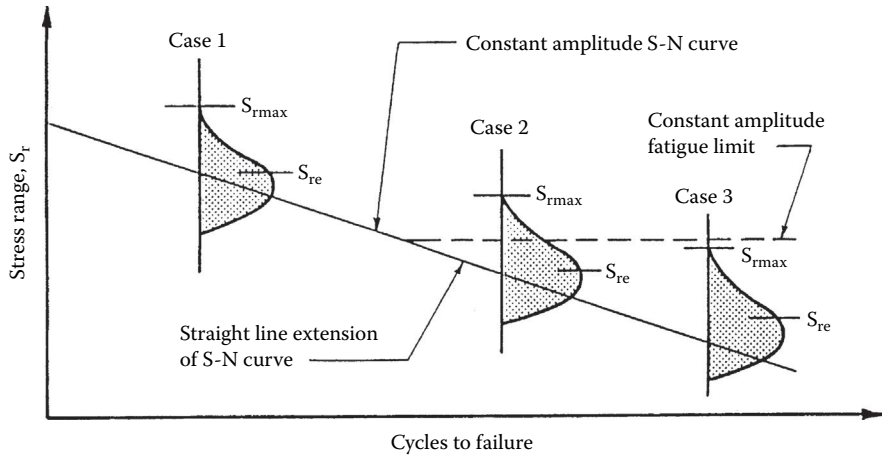

FIGURE 19.10 Schematic of three different cases of the relationship between the spectrum of applied stress ranges and the S-N curve. S_{re} is the effective or root-mean-cube stress range and S_{rmax} is the fatigue limit-state stress range with an exceedance of 1:10,000. Case 1 and 2 are in the finite-life regime, whereas case 3 illustrates the infinite-life regime.

Case 1 and 2 in Figure 19.10 are in what is called the finite-life regime because the calculations involve a specific number of cycles. Case 3 in Figure 19.10 represents what is referred to as the infinite-life regime. In the infinite-life regime, essentially all of the stress ranges in the variable spectrum are below the CAFL. The full-scale variable-amplitude fatigue tests referred to earlier (Fisher et al., 1993) show that as many as 0.01% of the stress ranges can exceed the CAFL without resulting in cracking. Consequently, the stress range associated with an exceedance probability of 0.01% is often referred to as the "fatigue-limit-state" stress range.

The cutoff of the straight-line extrapolation of the S-N curve in the AASHTO LRFD specification is related to this infinite-life phenomenon. Specifically, the AASHTO LRFD specification cuts off the extrapolation of the S-N curve at an estimated maximum stress range equal to the CAFL. The maximum stress range is taken as twice the effective stress range from the fatigue truck for bridge members other than decks. The intent of this limit is actually to assure that the fatigue-limit-state stress range is just below the CAFL. The AASHTO LRFD procedure assumes that there is a fixed relationship between the rmc or effective stress range and the limit-state stress range.

Depending on the type of details, the infinite-life regime begins at approximately 14.5 million cycles for Category A to 177.5 million cycles for Category E′ details corresponding to the effective stress range. When designing for a life greater than these limits, it is no longer important to quantify the precise number of cycles. Any design, other than orthotropic decks, where twice the rmc stress range is less than the CAFL, or where the fatigue-limit-state stress range is less than the CAFL, should theoretically result in essentially infinite life.

The ratio of the fatigue-limit-state stress range to the effective stress range is assumed to be the same as the ratio fatigue-limit-state load range to an adjusted effective load range, which considers actual measured stresses and their relationship to the measured loads. The fatigue-limit-state load range is defined as having a probability of exceedance over the lifetime of the structure of 0.01%. A structure with millions of cycles is likely to see load ranges exceeding this magnitude hundreds of times, therefore the fatigue-limit-state load range is not as large as the extreme loads used to check ultimate strength or permissible overloads. The fatigue limit-state load range is assumed to be about twice the effective rmc load range in the LRFD specification for main load carrying members. For deck elements it is taken as three times the effective rmc stress range.

Recall that the HS20 loading with a load factor of 0.75, that is equivalent to an HS15 loading, was defined as the effective load in the AASHTO LRFD Specification for Fatigue I limit state or finite life design. Therefore, the LRFD Specification implies that the fatigue limit-state truck would be equivalent to HS30 for main load carrying members other than decks, and equivalent to HS45 for deck elements. These are implemented in the AASHTO LRFD Specifications as load factors of 1.5 and 2.25 for main load carrying members and deck elements, respectively. The designer computes a stress range using the HS20 truck with a load factor of 1.5 or 2.25 as appropriate. By assuring that this computed stress range is less than the CAFL, the AASHTO LRFD specification assures that the stress ranges from random variable traffic will not exceed the CAFL more than 0.01% of the time.

The ratio of the effective GVW to the GVW of the fatigue-limit-state truck in the measured spectrum is often referred to in the literature as the "alpha factor" (Kober et al., 1994). This recognizes that the ratio of the actual measured stress ranges in bridges to computed stress ranges is always less than estimated directly from the vehicle measurements. The LRFD Specifications imply that alpha equals 0.5 for main load carrying members.

The alpha factor of 0.5 implied by the LRFD specifications is not consistent with NCHRP Report 299 (Moses et al., 1987) that indicated that the alpha factor should be closer to 0.33. This finding was based on a reliability analysis, comparison with the original AASHTO fatigue limit check, review of nationwide WIM data, but only limited examination of measured stress range histograms in hundreds of bridges.

According to the statistics of the GVW histograms (Moses et al., 1987), this HS45 fatigue-limit-state truck has only a 0.023% probability (approximately 1 in 5,000) of exceedance, which is almost consistent with the recommendation from NCHRP 354 (Fisher et al., 1993) that the fatigue-limit-state stress range

has an exceedance of less than 1:10,000. Recent measurements on orthotropic decks have shown that an alpha of 0.33 is correct, the stress range produced by the fatigue truck should be increased by three times when compared to the CAFL rather than twice as used for main members.

The exceedance level of the fatigue-limit-state truck weight was intentional and was a result of "calibrating" the LRFD bridge specifications to give fatigue design requirements that are similar to those of preceding specifications and the known response of members in hundreds of bridge structures. The theoretically low exceedance level of the fatigue-limit-state truck weight implied by the LRFD code was used because it was felt that other aspects of the design process are over conservative, such as the assumptions in the structural analysis (Dexter and Fisher, 1996). The Guide Specification for Fatigue Design of Steel Bridges (AASHTO, 1989) was withdrawn by AASHTO as it provided overly conservative estimates of fatigue life for main members when compared to observed field behavior. As a result, the LRFD Specification was "calibrated" to match existing field experience.

Measured axle load data (Nowak and Laman, 1995) show axle loads substantially exceed the 107 kN fatigue-limit-state axle load (half of the tandem axle load from the HS30 truck) implied by the AASHTO LRFD specifications. The shape of the axle-load spectra are essentially the same as the GVW spectra, that is the alpha factor is approximately 0.33. This alpha factor suggested the fatigue-limit-state axle load with an exceedance level of approximately 1:10,000 would be approximately 160 kN for deck elements for orthotropic or grid decks considering dual axles (Connor and Fisher, 2005; FHWA, 2012). In fact, measured axle load data (Nowak and Laman, 1995) show infrequent axle loads exceeding 160 kN in some overload cases.

Aside from the fatigue-limit-state axle load or maximum GVW, the rest of the loading spectrum does not matter when using the infinite-life approach. Also, the precise number of cycles does not have to be forecast. Rather, it is only necessary to establish that the total number of cycles exceeds the number of cycles associated with the CAFL. Therefore, it is not necessary to know precisely the expected life of the deck and future traffic volumes. Thus, despite the uncertainty in the appropriate value for the fatigue limit-state axle or GVW load, the infinite-life approach is considerably simpler than trying to account for the cumulative damage of the whole distribution of future axle or gross vehicle loads.

The infinite-life approach relies upon the CAFL as the parameter determining the fatigue resistance. The emphasis in fatigue testing of details should therefore be on defining the CAFL. Unfortunately, there is a need for additional testing to better define these CAFL. Many of the CAFL values in Table 19.1 were based on judgment rather than specific test data at stress ranges down near the CAFL. Additional research has been performed to investigate the validity of many of the CAFL for signal, sign, and luminaires details (Roy et al., 2012).

Clearly, most structures carry enough truck traffic to justify an infinite-life fatigue design approach, especially for the deck elements. For example, assuming 75 year life and a Category C detail it can be shown that the maximum permissible single lane ADTT is approximately 1290 trucks/day if number of cycles associated with the CAFL is considered. In most cases, designing for infinite fatigue life rather than designing for a finite number of cycles add little cost. This infinite-life approach as noted has been applied in developing AASHTO fatigue design specifications for wind-loaded sign, signal, and luminaire support structures (Roy et al., 2012), orthotropic deck elements (Connor and Fisher, 2005; FHWA, 2012) and modular bridge expansion joints (Dexter et al., 1997; Dexter et al. 1995; Kaczinski et al., 1996).

In the fatigue design of bridge deck elements according to the AASHTO LRFD specifications, the fatigue design stress range is obtained from a static analysis where the wheel loads (half the axle loads) are applied in patches. The patch has a fixed width of 508 mm and a length of 250mm. The LRFD specifications require that a load factor of two or three as appropriate be used in calculating the patch load.

19.3.6 Enhancement of Fatigue Resistance by Postweld Treatments

The fatigue problems with the older bridges can be avoided in new construction if good detailing practice is followed and each detail is designed such that the stress range because of applied live load is below the design allowable stress range. It is also possible to retrofit or upgrade the fatigue strength of existing steel bridges

with poor details. In addition, postweld enhancement of fatigue resistance of welded details such as cover-plates, gussets, and stiffeners that are known to experience crack growth from a weld toe is essential for an effective use of modern high performance steels such as HPS Grade 485W and HPS Grade 690W and non-magnetic stainless steels. Fatigue resistance of these steels is no different than other high strength steels in use during the last four decades (Fisher et al., 1970). Typical fatigue resistance improvement techniques for welded connections are grinding, shot peening, air hammer peening (AHP), and tungsten inert gas (TIG) gas tungsten arc (GTA) remelting with or without welding consumables. These techniques involve plastic deformation of the surface and/or improvement of weld toe geometric and microstructural characteristics.

Peening works primarily by inducing a state of compressive residual stress near the weld toe (Fisher et al., 1979). Because the benefit of peening is derived from lowering the effective tensile stress range, it has been found to be the most effective when conducted under dead load. In this case, the peening only needs to be effective against live load. AHP can be a successful repair as long as the crack depth does not exceed the zone of compressive stress. The depth of compressive stress is maximized by using air pressure lower than 290 kPa and up to six passes with a peening tool. Fatigue cracks up to 3 mm deep and 50 mm long at the cover-plate weld toe can be arrested by peening provided the stress ranges do not exceed 40 MPa. Peened beams with crack depths larger than 3 mm usually show no measurable increase in life and other repair procedures such as bolted splices may be required.

Fatigue cracks at the weld toe of the end-welded cover plate in the Yellow Mill Pond Bridge, Connecticut were retrofitted by AHP and GTA remelting in the 1970s. This prevented subsequent crack growth in this heavily used structure until it was replaced in 1997. Subsequently, several beams removed from the original structure were tested in the laboratory (Takamori and Fisher, 2000) at a stress range of 70 MPa, which exceeded the maximum stress range in the variable amplitude spectrum that the bridge was subjected to for over 20 years of service after treatment. The tests verified that no fatigue crack growth had occurred in the bridge details after more than 60 million cycles of truck loading, and the peened and gas tungsten arc remelted retrofitted details had successfully prevented further fatigue crack growth. At the higher test stress range, the laboratory tests were found to develop fatigue cracks in the weld throat and not at the treated weld toe.

Over the past decade, ultrasonic impact treatment (UIT) has proved to be a consistent and effective means of improving fatigue strength of welded connections. UIT involves postweld deformation treatment of the weld toe by impacts from single or multiple indenting needles excited at ultrasonic frequency, generating force impulses at the weld toe (Statnikov, 1997). The treatment introduces beneficial compressive residual stresses at the weld toe and also reduces the stress concentration by enhancing the profile of the weld toe. The UIT equipment consists of a handheld tool consisting of an ultrasonic transducer, a wave guide, and a holder with impact needles; an electronic control box and a water pump to cool the system. Compared with traditional impact treatment methods such as AHP, shot peening and needle peening, UIT appears to be more efficient and environmentally acceptable. It involves a complex effect of strain hardening, reduction in weld strain, relaxation in residual stress, and reduction in the stress concentration from profiling (Statnikov, 1997). Research at Lehigh University on large-scale specimens having stiffener and cover-plate welded details demonstrated that substantial increases in fatigue strength of high performance steel welded details can be achieved by UIT, in particular the elevation of their fatigue limit (Roy et al., 2003; Roy and Fisher, 2005; Roy and Fisher, 2006). The large scale beam tests showed that although the treated details suppressed crack growth from the weld toe, the failure mode changed to fatigue crack growth from the weld root when a usual end weld size of about half the cover plate thickness was used. This usually resulted in a longer life compared to an as-welded detail, but still led to cracking and failure (Roy et al., 2003; Roy and Fisher, 2005). For enhanced fatigue resistance it was desirable to prevent root cracking and this was achieved by increasing the size of the end weld at the cover-plate to the plate thickness, which reduced the stress concentration at the weld root (Takamori and Fisher, 2000). This concept was verified by the subsequent fatigue tests as can be seen from the experimental results plotted in Figure 19.11. These results showed that the enhancement in fatigue resistance was dependent on both the stress range S_r and the minimum stress S_{min}. A substantial improvement was realized at the lower level of minimum stress. This improvement was reduced when subjected to higher levels of minimum stress

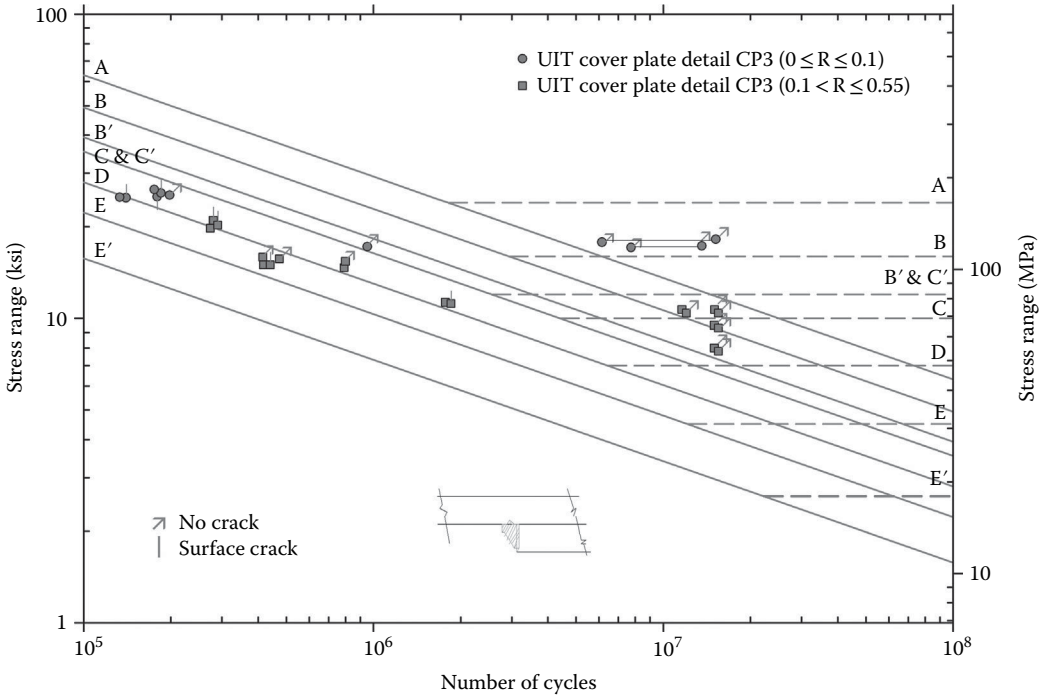

FIGURE 19.11 Fatigue performance of end welded cover-plate details having weld size the same as the plate thickness treated by ultrasonic impact treatment.

that was applied after the treatment. This characteristic is typical of other improvement techniques that introduce compression residual stress through plastic deformation (Fisher et al., 1979; Roy and Fisher, 2006, 2008). Under low levels of minimum stress, the residual compression stress at the treated weld toe is more effective in suppressing crack growth as the discontinuities are not opened until a higher stress range is applied. At higher minimum stress this condition is reached at a lower stress range causing a reduction in the level of enhancement and a lower fatigue limit. Substantial enhancement results when the treatment is applied under a high level of minimum stress. The treatment is then effective in reducing both the residual tensile stress from welding as well as the tension from the applied gravity load. This was also verified experimentally for weld toes treated by AHP (Fisher et al., 1979).

Cover-plate end welds on existing bridges are not likely to have end weld size the same as the plate thickness. More likely the weld size will be about half the plate thickness. There is a high probability that fatigue crack will initiate at the weld root of the treated connections as was demonstrated in the test girders removed from the Yellow Mill Pond bridge that were treated by AHP and GTA remelting (Takamori and Fisher, 2000). This would indicate that inspections should focus on the weld throat to ascertain if root cracking would subsequently develop. Fortunately, there is a significant increase in life for root cracking to occur and the cycles (time) necessary for the crack to propagate across the cover-plate end to the longitudinal welds, which is the only way the crack can enter into the girder flange. Normal periods of inspection should identify such throat cracking if it ever occurs.

19.3.7 Assessment of Fatigue Performance Based on Advanced Analyses

Assessment of fatigue performance for connections having complex geometry requires advanced analyses. These connections are subjected to complex local stress fields that cannot be described by a nominal stress determined from simple strength of material calculations. Stresses local to the potential fatigue

crack initiation sites, obtained by advanced Finite Element Analyses (FEA) are employed for fatigue assessment of these connections (Hobbacher, 2005; Radaj and Sonsino, 1998).

Fatigue cracking of welded connections mostly occurs at the weld toe notch, where the local stresses are theoretically infinite. A steep stress gradient exists approaching the weld toe that includes the effect of the connection discontinuity as well as the discontinuity because of the weld toe notch. The local stress at the weld toe (also called the "hot-spot") obtained from FEA is sensitive to the mesh density, and asymptotically approaches the theoretical stress with decreasing mesh size, but never converges. Therefore, the stress at the weld toe, extrapolated from converged stresses ahead of the weld toe, is used as a reference local stress for assessment of the connection fatigue performance. This stress is often referred in the literature as the "hot-spot stress." The extrapolation points are located beyond the influence of the weld toe discontinuity and thus the hot-spot stress captures the geometric effect of the connecting elements or the connection geometry. Hence the hot-spot stress is also referred as the "geometric stress."

Several recommendations for estimating the hot-spot stress exist in the offshore, ship building, and automobile industries (ABS, 2010; DNV, 2010; Hobbacher, 2005; Radaj and Sonsino, 1998) that differ in the FE modeling, the stresses to be considered, and the extrapolation approaches. Typically an FE model using shell or solid elements of acceptable formulation and having a mesh density of $t \times t$ is recommended, where t is the thickness of the stressed plate element. The hot-spot stress is estimated perpendicular to the weld toe and usually determined by linearly extrapolating principal or normal stresses at two reference points located on the surface of the FE model. This hot-spot stress is used in conjunction with a "master" S-N curve, which is usually the same as the AASHTO Category C design curve, for predicting the fatigue life of the connection. The reasoning is that the hot-spot stress captures the geometric effect of the connection, and any variability because of the weld toe notch or the weld toe micro discontinuities is included in the experimentally obtained S-N curve. Since the fatigue resistance of a short attachment because of crack growth at the weld toe normal to the stress in the primary plate is defined as Category C, this design curve essentially captures the effect of the weld toe discontinuities without any geometric effect of the connection.

A local stress-based approach, using the stress at a singular reference point on the surface ahead of the weld toe, was originally developed and successfully applied for fatigue cracking at the weld toe of tubular structures in the offshore industry (Marshall and Wardenier, 2005), where significant out-of-plane bending arises at the connections to maintain compatibility of deformation between the components. Research efforts of developing local stress based approaches for plated structures using the extrapolated stress at the weld toe from two reference points have produced mixed results, particularly where the out-of-plane bending effects are nominal and in-plane stress components are dominant (Marshall and Wardenier, 2005).

Assessment of fatigue performance of welded connections using the hot-spot stress was calibrated against fatigue cracking at the weld toes of small-scale cruciform and T-connections. As such, the hot-spot stress approach can only be used for predicting finite life. This method cannot be used for assessing fatigue cracking from weld root and specifically for infinite life design (i.e., no fatigue crack growth at all). For distortion-induced fatigue (see Section 19.3.2), where cracking of welded connections is precipitated by local secondary bending stresses at the weld toe, the hot-spot stress can be used to determine the finite life fatigue performance of the connection.

An alternative local stress based approach (DNV, 2010; Radaj and Sonsino, 1998; Roy et al., 2012; Roy and Fisher, 2005) can be used for assessing infinite life fatigue resistance of welded connections. This approach considers the fatigue effective local stress at the weld toe notch and compares it against the endurance limit of the material to suppress the possibility of cyclic crack initiation or propagation. A notch of 1 mm radius is introduced at the toe of the nominal weld geometry, and the converged maximum (tensile) surface stress at the center of the rounded notch is used as the local stress (also defined as the "notch stress") for assessment of infinite life fatigue resistance.

19.4 Fracture Resistance

As explained previously, it is considered more important to focus on the prevention of fatigue cracks in bridges than to focus on the resistance to fracture. However, for structural components that are not subjected to significant cyclic loading, fracture could still possibly occur without prior fatigue crack growth. The primary tension chords of long-span truss would be one example. Usually, this would occur as the loads are applied for the first time during construction.

Unlike fatigue, fracture behavior depends strongly on the type and strength level of the steel or filler metal. In general, fracture toughness has been found to decrease with increasing yield strength of a material suggesting an inverse relationship between the two properties. In practice, however, fracture toughness is more complex than implied by this simple relationship since steels with similar strength levels can have widely varying levels of fracture toughness.

Steel exhibits a transition from brittle to ductile fracture behavior as the temperature increases. For example, Figure 19.12 shows a plot of the energy required to fracture Charpy V-Notch (CVN) impact test specimens of A588 structural steel at various temperatures. These results are typical for ordinary hot-rolled structural steel. The transition phenomenon shown in Figure 19.12 is a result of changes in the underlying microstructural fracture mode.

There are three types of fracture with different behavior:

1. Brittle fracture is associated with cleavage of individual grains on select crystallographic planes. This type of fracture occurs at the lower end of the temperature range, although the brittle behavior can persist up to the boiling point of water in some low-toughness materials. This part of the temperature range is called the lower shelf because the minimum toughness is fairly constant up to the transition temperature. Brittle fracture may be analyzed with linear elastic fracture mechanics (Barsom and Rolfe, 1987; Broek, 1987; Fisher, 1997) because the plasticity that occurs is negligible.
2. Transition-range fracture occurs at temperatures between the lower shelf and the upper shelf and is associated with a mixture of cleavage and fibrous fracture on a microstructural scale. Because of the mixture of micromechanisms, transition-range fracture is characterized by extremely large variability.
3. Ductile fracture is associated with a process of void initiation, growth, and coalescence on a microstructural scale, a process requiring substantial energy. This higher end of the temperature range is referred to as the upper shelf because the toughness levels off and is essentially constant

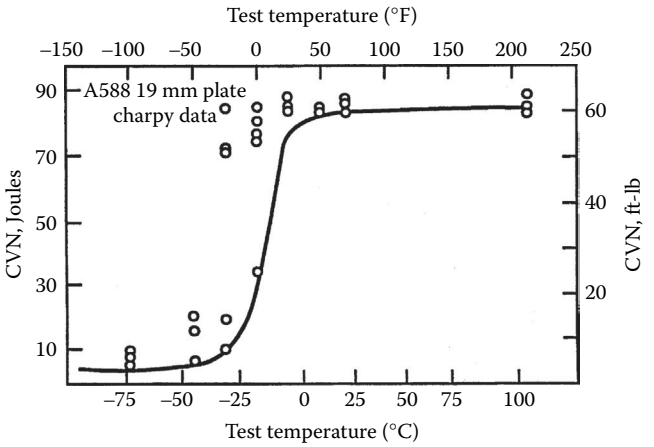

FIGURE 19.12 Charpy energy transition curve for A588 Grade 50 (350 MPa yield strength) structural steel.

for higher temperatures. Ductile fracture is also called fibrous fracture because of the fibrous appearance of the fracture surface, or shear fracture because of the usually large slanted shear lips on the fracture surface.

Ordinary structural steel such as A36 or A572 is typically only hot rolled, whereas to achieve very high-toughness steels must be controlled rolled, that is, rolled at lower temperatures, or must receive some auxiliary heat treatment such as normalization. In contrast to the weld metal, the cost of the steel is a major part of the total material costs. The expense of the high-toughness steels has not been found to be warranted for most bridges, whereas the cost of high-toughness filler metal is easily justifiable. Hot-rolled steels, which fracture in the transition region at the lowest service temperatures, have sufficient toughness for the required performance of most welded buildings and bridges.

ASTM specifications for bridge steel (A709) provide for minimum Charpy V-Notch (CVN) impact test energy levels. Structural steel specified by A36, A572, or A588, without supplemental specifications, does not require the Charpy test to be performed. The results of the CVN test, impact energies, are often referred to as "notch-toughness" values.

The CVN specification works by assuring that the transition from brittle to ductile fracture occurs at some temperature less than service temperature. This requirement ensures that brittle fracture will not occur as long as large cracks do not develop. Because the CVN test is relatively easy to perform, it will likely continue to be the measure of toughness used in steel specifications. Often 34 J (25 ft-lbs), 27 J (20 ft-lbs), or 20 J (15 ft-lbs) are specified at a particular temperature. The intent of specifying any of these numbers is the same, that is, to make sure that the transition starts below this temperature.

Some Charpy toughness requirements for steel and weld metal for bridges are compared in Table 19.2. This table is simplified and does not include all the requirements.

Note that the bridge steel specifications require a CVN at a temperature that is 38°C greater than the minimum service temperature. This "temperature shift" accounts for the effect of strain rates, which are lower in the service loading of bridges (on the order of 10^{-3}) than in the Charpy test ($> 10^{1}$) (Barsom and Rolfe, 1987). It is possible to measure the toughness using a Charpy specimen loaded at a strain rate characteristic of bridges, called an intermediate strain rate, although the test is more difficult and the results are more variable. When the CVN energies from an intermediate strain rate are plotted as a function of temperature, the transition occurs at a temperature approximately 38°C lower for materials with yield strength up to 450 MPa.

As shown in Table 19.2, the AWS D1.5 Bridge Welding Code specifications for weld metal toughness are more demanding than the specifications for base metal. The extra margin of fracture toughness in the weld metal is reasonable because the weld metal is always the location of discontinuities and high tensile residual stresses. Because the cost of filler metal is relatively small in comparison to the overall cost of materials, it is usually worth the cost to get high-toughness filler metal.

The minimum CVN requirements are usually sufficient to assure damage tolerance, that is, to allow cracks to grow quite long before fracture occurs. Fatigue cracks grow at an exponentially increasing rate,

TABLE 19.2 Minimum Charpy Impact Test Requirements for Bridges and Buildings

Material	Minimum Service Temperature		
	–17°C	–34°C	–51°C
	Joules@°C	Joules@°C	Joules@°C
Steel: nonfracture critical members[a,b]	20@21	20@4	20@-12
Steel: fracture critical members[a,b]	34@21	34@4	34@-12
Weld metal for nonfracture critical[a]	27@-18	27@-18	27@-29
Weld metal for fracture critical[a,b]	34@-29°C for all service temperatures		

[a] These requirements are for welded steel with minimum specified yield strength up to 350 MPa up to 38 mm thick. Fracture critical members are defined as those that, if fractured would result in collapse of the bridge.

[b] The requirements pertain only to members subjected to tension or tension because of bending.

therefore most of the fatigue life transpires while the crack is very small. Additional fracture toughness, greater than the minimum specified values, will allow the crack to grow to a larger size before sudden fracture occurs. However, the crack is growing so rapidly at the end of life that the additional toughness may increase the life only insignificantly. Modern high performance steels are low carbon and often manufactured by advanced processing. These steels have outstanding levels of toughness that ensure that cleavage fracture will not likely occur.

The fractures of steel connections that occurred in the Northridge earthquake of 1994 is an example of what can happen if there are no specifications for filler metal toughness. At that time, there were no requirements for weld metal toughness in AWS D1.1 for buildings, even for seismic welded steel moment frames (WSMF). This lack of requirements was rationalized because typically the weld deposits are higher toughness than the base metal. However, this is not always the case. For example, the self-shielded flux-cored arc welds (FCAW-S) used in many of the WSMF that fractured in the Northridge earthquake were reported to be of very low toughness (Fisher et al., 1997; Kaufmann et al., 1996; Kaufmann et al., 1997; Xue et al., 1996).

ASTM A673 has specifications for the frequency of Charpy testing. The H frequency requires a set of three CVN specimens to be tested from one location for each heat or approximately 50 tons. These tests can be taken from a plate with thickness up to 9 mm different from the product thickness if it is rolled from the same heat. The P frequency requires a set of three specimens to be tested from one end of every plate, or from one shape in every 15 tons of that shape. For bridge steel, the AASHTO specifications require CVN tests at the H frequency as a minimum. For fracture critical members, the guide specifications require CVN testing at the P frequency. In the AISC specifications, CVN tests are required at the P frequency for thick plates and jumbo sections. A special test location in the core of the jumbo section is specified, as well as requirement that the section tested be produced from the top of the ingot.

Even the P testing frequency may be insufficient for as-rolled structural steel. In a recent report for NCHRP (Frank et al., 1993), CVN data were obtained from various locations on bridge steel plates. The data show that because of extreme variability in CVN across as-rolled plates, it would be possible to miss potentially brittle areas of plates if only one location per plate is sampled. For plates that were given a normalizing heat treatment, the excessive variability was eliminated.

Quantitative means for predicting brittle fracture are available, that is, fracture mechanics (Barsom and Rolfe, 1987; Broek, 1987; BSI, 1991; Dexter, 1995; Dexter and Gentilcore, 1997 and 1998; Fisher, 1997; Fisher et al., 1997). These quantitative fracture calculations are typically not performed in design, but are often used in service to assess a particular defect. This is at best only about plus or minus 30% accuracy in these fracture predictions, however. Several factors contributing to this lack of accuracy include: (1) variability of material properties; (2) changes in apparent toughness values with changes in test specimen size and geometry; (3) differences in toughness and strength of the weld zone; (4) complex residual stresses; (5) high gradients of stress in the vicinity of the crack because of stress concentrations; and (6) the behavior of cracks in complex structures of welded intersecting plates.

19.5 Summary

1. Structural elements where the live-load is a large percentage of the total load are potentially susceptible to fatigue. Many factors in fabrication can increase the potential for fatigue including notches, misalignment and other geometrical discontinuities, thermal cutting, weld joint design (particularly backing bars), residual stress, nondestructive evaluation and weld defects, intersecting welds, and inadequate weld access holes. The fatigue design procedures in the AASHTO specifications are based on control of the stress range and knowledge of the fatigue strength of the various details. Using these specifications, it is possible to identify and avoid details that are expected to have low fatigue strength.
2. The simplified fatigue design method for infinite life is justified because of the uncertainty in predicting the future loading on a structure. The infinite-life fatigue design philosophy requires that

essentially all the stress ranges are less than the constant-amplitude fatigue limit (CAFL). One advantage of this approach for structures with complex stress histories is that it is not necessary to accurately predict the entire future stress range distribution. The fatigue design procedure simply requires a knowledge of the maximum stress range with an exceedance level of 1:10,000. The infinite-life approach relies upon the CAFL as the parameter determining the fatigue resistance. The emphasis in fatigue testing of details should therefore be on defining the CAFL. Additional research should be performed to investigate the validity of many of the CAFL in the present specification.

3. Welded connections and thermal-cut holes, copes, blocks, or cuts are potentially susceptible to brittle fracture. Many interrelated design variables can increase the potential for brittle fracture including lack of redundancy, large forces and moments with dynamic loading rates, thick members, geometrical discontinuities, and high constraint of the connections. Low temperature can be a factor for exposed structures. The factors mentioned above which influence the potential for fatigue have a similar effect on the potential for fracture. In addition, cold work, flame straightening, weld heat input, and weld sequence can also affect the potential for fracture. The AASHTO specifications require a minimum CVN "notch toughness" at a specified temperature for the base metal and the weld metal of members loaded in tension or tension because of bending. Almost two decades of experience with these bridge specifications have proved that they are successful in significantly reducing the number of brittle fractures.

References

AASHTO. 1989. *Guide Specifications for Fracture Critical Non-Redundant Steel Bridge Members* (with Interim).American Association of State Highway and Transportation Officials, AASHTO, Washington DC.

AASHTO 2010. *ASHTO/AWS D1.5M/D1.5:2010 Bridge Welding Code* (6th Edition). American Association of State Highway Transportation Officials, Washington, DC.

AASHTO. 2012. *AASHTO LRFD Bridge Design Specifications*. Customary U.S. Unit. American Association of State Highway Transportation Officials, Washington, DC.

ABS. 2010. *Guide for the Fatigue Assessment of Offshore Structures*, American Bureau of Shipping, Houston, TX.

ACI Committee 215. 1996. *Considerations for Design of Concrete Structures Subjected to Fatigue Loading*. ACI 215R-74 (Revised 1992). ACI Manual of Standard Practice, Vol. 1. Farmington Hills, MI.

AISC. 2010. *Specification for Structural Steel Buildings*, ANSI/AISC 360-10, American Institute of Steel Construction, Chicago, IL.

Albrecht, P., and Shabshab, C. 1994. Fatigue strength of weathered rolled beam made of A588 steel. *Journal of Materials in Civil Engineering, ASCE*, 6(3), 407–428.

AREMA. 2012. *Manual for Railway Engineering,* American Railway Engineering and Maintenance-of-Way Association, Lanham, MD.

AWS. 2010. *ANSI/AWS D1.1:Structural Welding Code - Steel*, American Welding Society, Miami, FL.

Barsom, J. M., and Rolfe, S. T. 1987. *Fracture and Fatigue Control in Structures* (2nd Edition). Prentice-Hall, Englewood Cliffs, NJ.

Broek, D. 1987. *Elementary Fracture Mechanics* (4th Edition). Martinis Nijhoff Publishers, Dordrecht, Netherlands.

BSI. 1991. PD 6493: *Guidance on the Methods for Assessing the Acceptability of Flaws in Fusion Welded Structures*, British Standards Institution, London, UK.

BSI. 1994. BS 7608, *Code of practice for fatigue design and assessment of steel structures*. British Standards Institute, London, UK.

Castiglioni, C. A. 1995. Cumulative Damage Assessment in Structural Steel Details. *IABSE Symposium San Francisco 1995, Extending the Lifespan of Structures,* IABSE Reports, 73/2. pp. 1061–1066.

CEN 2005. ENV 1993-1-1, Eurocode 3: Design of steel structures: Part 1.1: General rules and rules for buildings, European Committee for Standardization (CEN), Brussels.

Connor, R. J., and Fisher, J. W. 2005. Field Testing Orthotropic Bridge Decks. *International Journal of Steel Structures*, 5(3). pp. 225–231.

Demers, C., and Fisher, J. W. 1990. Fatigue Cracking of Steel Bridge Structures. Volume I: A Survey of Localized Cracking in Steel Bridges- 1981 to 1988. Report No. FHWA-RD-89-166, also, Volume II, A Commentary and Guide for Design, Evaluation, and Investigating Cracking, Report No. FHWA-RD-89-167, FHWA, McLean, VA.

Dexter, R. J. 1995. Load-Deformation Behavior of Cracked High-Toughness Steel Members. *Proceedings of the 14th International Conference on Offshore Mechanics and Arctic Engineering Conference* (OMAE), Salama et al. (Eds.). ASME, Vol. III, Materials Engineering, Copenhagen, Denmark, pp. 87–91.

Dexter, R. J. 1997. Significance of Strength Undermatching of Welds in Structural Behavior. *Mis-Matching of Interfaces and Welds*. K.-H. Schwalbe and Kocak, M. (Eds.). ISBN 3-00-001951-0, GKSS Research Center, Geesthacht, Germany, pp. 55–73.

Dexter, R. J., Connor, R. J., and Kaczinski, M. R. 1997. Fatigue Design of Modular Bridge Expansion Joints. *NCHRP Report 402*, Transportation Research Board, Washington, DC.

Dexter, R. J., and Fisher, J. W. 1996. The Effect of Unanticipated Structural Behavior on the Fatigue Reliability of Existing Bridge Structures, *Structural Reliability in Bridge Engineering.* D.M. Frangopol, and Hearn, G. (Eds.). *Proceedings of a Workshop*, University of Colorado at Boulder, McGraw-Hill, New York, NY, pp. 90–100.

Dexter, R. J., Fisher, J. W., and Beach, J. E. 1993. Fatigue behavior of welded HSLA-80 members. *Proceedings, 12th International Conference on Offshore Mechanics and Arctic Engineering*, Vol. III, Part A, Materials Engineering, ASME, New York, NY, pp. 493–502.

Dexter, R. J., and Gentilcore, M. L. 1997. Evaluation of Ductile Fracture Models for Ship Structural Details. *Report SSC-393*, Ship Structure Committee, Washington, DC.

Dexter, R. J., and Gentilcore, M. L. 1998. Predicting Extensive Stable Tearing in Structural Components. *Fatigue and Fracture Mechanics*, 29th Volume, ASTM STP 1321, T. L. Panontin and Sheppard, S. D. (Eds.). American Society for Testing and Materials, Washington, DC.

Dexter, R. J., Kaczinski, M. R, and Fisher, J. W. 1995. Fatigue Testing of Modular Expansion Joints for Bridges, *IABSE Symposium, Extending the Lifespan of Structures*, 73(2), 1091–1096, San Francisco, CA.

Dexter, R. J., Tarquinio, J. E., and Fisher, J. W. 1994. An Application of Hot-Spot Stress Fatigue Analysis to Attachments on Flexible Plate. *Proceedings of the 13th International Conference on Offshore Mechanics and Arctic Engineering*, ASME. New York, NY.

DNV. 2010. Recommended Practice DNV-RP-C203: Fatigue Design of Offshore Steel Structures, Det Norske Veritas, Høvik, Norway.

ENR. 1979. Engineers Investigate Cracked El. *Engineering News Record*, 200(3).

FHWA. 2012. Manual for Design, Construction, and Maintenance of Orthotropic Steel Deck Bridges, FHWA-IF-12-027, Federal Highway Administration, Washington, DC.

Fisher, J. W. 1984. *Fatigue and Fracture in Steel Bridges,* ISBNO-471-80469-X, John Wiley & Sons, New York, NY.

Fisher, J. W. 1997. The evolution of fatigue resistant steel bridges. *1997 Distinguished Lectureship*, Transportation Research Board, 76th Annual Meeting, Paper No. 971520, 1–22, Washington, DC.

Fisher, J. W., Albrecht, P. A., Yen, B. T., Klingerman, D. J., and McNamee, B. M. 1974. Fatigue Strength of Steel Beams with Welded Stiffeners and Attachments. *NCHRP Report 147*, Transportation Research Board, Washington, DC.

Fisher, J. W., Dexter, R. W., and Kaufmann, E. J. 1997. Fracture Mechanics of Welded Structural Steel Connections. *Background Reports: Metallurgy, Fracture Mechanics, Welding, Moment Connections, and Frame Systems Behavior*, Report No. SAC 95-09, FEMA-288, March.

Fisher, J. W., Frank, K. H., Hirt, M. A., and McNamee, B. M. 1970. Effect of Weldments on the Fatigue Strength of Steel Beams. *NCHRP Report 102*, Highway Research Board, Washington, DC.

Fisher, J. W., Hausammann, H., Sullivan, M. D., and Pense, A. W. 1979. Detection and Repair of Fatigue Damage in Welded Highway Bridges. *NCHRP Report 206*, Transportation Research Board, Washington, DC.

Fisher, J. W., Jian, J., Wagner, D. C., and Yen, B. T. 1990. Distortion-Induced Fatigue Cracking In Steel Bridges. *NCHRP Report 336*, Transportation Research Board, Washington, DC.

Fisher, J. W., Kaufmann, E. J., Koob, M. J., and White, G. 1995. Cracking, fracture assessment, and repairs of Green River bridge, I-26, *Proceedings of Fourth International Bridge Engineering Conference*, Vol 2. National Academy Press, Washington DC, pp. 3–14.

Fisher, J. W., and Keating, P. B. 1989. Distortion-induced fatigue cracking of bridge details with web gaps. *Journal of Constructional Steel Research.* 12, pp. 215–228.

Fisher, J. W., Nussbaumer, A., Keating, P. B., and Yen, B. T. 1993. Resistance of Welded Details under Variable Amplitude Long-Life Fatigue Loading. *NCHRP Report 354*, Transportation Research Board, Washington, DC.

Fisher, J. W., Pense, A. W., and Roberts, R. 1977. Evaluation of fracture of Lafayette Street bridge. *Journal of the Structural Division*, ASCE, 103(ST7).

Fisher, J. W., Yen, B. T., Kaufmann, E. J., Ma, Z. Z., and Fisher, T. A. 1995. Cracking evaluation and repair of cantilever bracket tie plates of Edison bridge. *Proceedings of Fourth International Bridge Engineering Conference.* Vol 2. National Academy Press, Washington, DC, pp. 15–25.

Frank, K. H., George, D. A., Schluter, C. A., Gealy, S., Horos, D. R. 1993. Notch Toughness Variability in Bridge Steel Plates. *NCHRP Report 355*, Transportation Research Board, Washington, DC.

Gurney, T. R. 2006. *Cumulative Damage of Welded Joints*, Woodhead Publishing, Cambridge, UK.

Hahin, C. 1994. Effects of Corrosion and Fatigue on the Load-Carrying Capacity of Structural Steel and Reinforcing Steel. *Illinois Physical Research Report No. 108*, Illinois Department of Transportation, Springfield, IL.

Hobbacher, A. 2005. Recommendations for fatigue design of welded joints and components. *Document XIII-1965-03/XV-1127-03*. International Institute of Welding, Paris.

Kaczinski, M. R., Dexter, R. J., and Connor, R. J. 1996. Fatigue Design and Testing of Modular Bridge Expansion Joints. *Proceedings of the Fourth World Congress on Joint Sealing and Bearing Systems for Concrete Structures*, Sacramento, CA.

Kaczinski, M. R., Dexter, R. J., and Van Dien, J. P. 1988. Fatigue-Resistant Design of Cantilevered Signal, Sign, and Light Supports. *NCHRP Report 412*, Transportation Research Board, Washington, DC.

Kaufmann, E. J., Fisher, J. W., Di Julio, R. M. Jr., and Gross, J. L. 1997. Failure Analysis of Welded Steel Moment Frames Damaged in the Northridge Earthquake. *NISTIR 5944*, National Institute of Standards and Technology, Gaithersburg, MD.

Kaufmann, E. J., Xue, M., Lu, L.-W., and Fisher, J. W. 1996. Achieving Ductile Behavior of Moment Connections. *Modern Steel Construction*, 36(1), 30–39. See also, Xue, M., Kaufmann, E. J., Lu, L.-W., and Fisher, J. W., 1996. Achieving Ductile Behavior of Moment Connections - Part II. *Modern Steel Construction*, 36(6), 38–42.

Keating, P. B., and Fisher, J. W. 1986. Evaluation of Fatigue Tests and Design Criteria on Welded Details. *NCHRP Report 286*, National Cooperative Highway Research Program, Washington, DC.

Kober, G. R., Dexter, R. J., Kaufmann, E. J., Yen, B. T., and Fisher, J. W. 1994. The Effect of Welding Discontinuities on the Variability of Fatigue Life. *Fracture Mechanics*, Twenty-Fifth Volume, ASTM STP 1220. F. Erdogan and R. J., Hartranft (Eds.), American Society for Testing and Materials, Philadelphia, PA.

Krawinkler, H., and Zohrei, M. 1983. Cumulative Damage in Steel Structures Subjected to Earthquake Ground Motion. *Computers and Structures*, 16(1–4), 531–541.

Maddox, S. J. 1991. *Fatigue Strength of Welded Structures* (2nd Edition). Abington Publishing, Cambridge, UK.

Marshall, P.W., and Wardenier, J. (2005). Tubular versus non-tubular hot spot stress methods. *Proceeding of the 15th International Offshore and Polar Engineering Conference*, ISOPE-2005, Seoul, Korea, June 19–24.

Menzemer, C. C., and Fisher, J. W. 1995. Revisions to the aluminum association fatigue design specifcations. *6th International Conference on Aluminum Weldments*, Cleveland, Available from AWS, Miami, FL, pp. 11–23.

Miki, C. 1997. Fractures in seismically loaded bridges. *Progress in Structural Engineering and Materials*, 1(1), 115–121.

Miner, M. A. 1945. Cumulative damage in fatigue. *Journal of Applied Mechanics*, 12, A-159.

Moses, F., Schilling, C. G., and Raju, K. S. 1987. Fatigue Evaluation Procedures for Steel Bridges. *NCHRP Report 299*, Transportation Research Board, Washington, DC.

Naito, C., Sause, R., Hodgson, I. C., Pessiki, S., and Desai, C. 2006. Forensic Evaluation of Prestressed Box Beam from Lake View Drive Bridge over I-70, *ATLSS Report 06-13*, Bethlehem, PA.

Nowak, A. S., and Laman, J. A. 1995. Monitoring Bridge Load Spectra. *IABSE Symposium, Extending the Lifespan of Structures*, San Francisco, CA.

Out, J. M. M., Fisher, J. W., and Yen, B. T. 1984. Fatigue strength of weathered and deteriorated riveted members. *Report DOT/OST/P-34/85/016*, Department of Transportation, Federal Highway Administration, Washington DC.

Overnman, T. R., Breen, J. E., and Frank, K. H. 1984. Fatigue Behavior of Pretensioned Concrete Girders, *Research Report 300-2F*, Center for Transportation Research, University of Texas, Austin, TX.

Pfister, J. F., and Hognestad, E. 1964. High Strength Bars as Concrete Reinforcement, Part 6, Fatigue Tests. *Journal PCA Research and Development Laboratories*, 6(1), 65–84.

PTI. 1986. *Recommendations for Stay Cable Design and Testing*, Ad-hoc Committee on Cable-Stayed Bridges, Post-Tensioning Institute, Phoenix, AZ.

Rabbat, B. G., Kaar, P. H., Russell, H. G., and Bruce, R. N., Jr. 1979. Fatigue Tests of Pretensioned Girders with Blanketed and Draped Strands. *Journal, Prestressed Concrete Institute,* 24(4), 88–115.

Radaj, D., and Sonsino, C. M. 1998. *Fatigue Assessment of Welded Joints by Local Approaches*, Abington Publishing, Cambridge, UK.

Roberts, R., Irwin, G. R., Fisher, J. W., Chen, G., Chakravarti, P., Ma, Z. A., and Yen, B. T. 1986. Corrosion Fatigue of Bridge Steels. *Reports FHWA/RD-86/165, 166, and 167*, Vol. 1–3, Federal Highway Administration, Washington, DC.

Roy, S., and Fisher, J. W. 2005. Enhancing fatigue strength by ultrasonic impact treatment. *International Journal of Steel Structures,* 5(3), 241–252.

Roy, S., and Fisher, J. W. 2006. Modified AASHTO design S-N curves for post-weld treated welded details. *Journal of Bridge Structures: Assessment, Design and Construction*, 2(4), 207–222.

Roy, S., and Fisher, J. W. 2008. Assessment of the Fatigue Threshold of Welded Details subjected to Post-Weld Ultrasonic Impact Treatment. *Proceedings of ASCE Structures Congress* 2008, Vancouver, Canada.

Roy, S., Fisher, J. W., and Yen, B. T. 2003. Fatigue resistance of welded details enhanced by ultrasonic impact treatment (UIT). *International Journal of Fatigue*, 25(9–11), 1239–1247.

Roy, S., Park, Y. C., Sause, R., Fisher, J. W., and Kaufmann, E. J. 2012. Cost-Effective Connection Details for Highway Sign, Luminaire, and Traffic Signal Structures, *Final Report, NCHRP web-only Document 176*, Transportation Research Board, Washington, DC, March 2011.

Schilling, C. G., Klippstein, K. H., Barsom, J. M., and Blake, G. T. 1978. Fatigue of welded Steel Bridge Members Under Variable-Amplitude Loadings. *NCHRP Report 188*, Transportation Research Board, Washington, DC.

Statnikov, E. S. 1997. Applications of operational ultrasonic impact treatment (UIT) technologies in production of welded joint. IIW Doc. No. XII-1667-97. International Institute of Welding, Paris.

Sternberg, F. 1969. Performance of Continuously Reinforced Concrete Pavement, I-84 Southington, Connecticut State Highway Department, >Newington, CT

Takamori, H., and Fisher, J. W. 2000. Tests of large girders treated to enhance fatigue strength. *Transportation Research Record*, 1696, 93–99.

VanDien, J. P., Kaczinski, M. R., and Dexter, R. J. 1996. Fatigue Testing of Anchor Bolts. *Building an International Community of Structural Engineers,* Vol.1, *Proceedings of Structures Congress XIV*, Chicago, pp. 337–344.

Yagi, J., Machida, S., Tomita, Y., Matoba, M., and Kawasaki, T. 1991. Definition of Hot-Spot Stress in Welded Plate Type Structure for Fatigue Assessment, *International Institute of Welding*, IIW-XIII-1414-91.

Yen, B. T., Huang, T., Lai, L.-Y., and Fisher, J. W. 1990. *Manual for Inspecting Bridges for Fatigue Damage Conditions, FHWA-PA-89-022 + 85-02*, Fritz Engineering Laboratory report number 511.1, Pennsylvania Department of Transportation, Harrisburg, PA.

Yen, B. T. Zhou, Y., Fisher, J. W. and Wang, D. 1991. Fatigue Behavior of Stringer-Floorbeam Connections. *Proceedings of the Eighth International Bridge Conference*, Paper IBC-91-19, Engineers' Society of Western, PA, pp. 149–155.

20

Weight Distributions of Highway Steel Bridges

Shouji Toma
Hokkai-Gakuen University

20.1 Introduction

In designing steel bridges, a precise estimation of the steel weight as a part of the dead loads is essential at the beginning. However, the steel weight depends on the sizes of girder section, which will be determined in the final design. The assumption of the steel weight at the beginning of design must be made as accurate as possible based on the data from actual constructions. If this assumption was not right, the design might lead to inadequate results and must be redesigned. Hence, the estimation of the steel weight is very important.

In order to estimate the steel weight accurately, the past data must be provided. In the first edition of *Bridge Engineering Handbook,* the data of the steel weight for various types of steel highway bridges constructed in Japan were provided (Toma, 2000). This chapter is an update to cover the new data for 24 years from 1978 to 2001 (completed year) and provides the new average regression equations and the standard deviations. Total number of the collected data is approximately 12,500.

The data are taken from "Annual Report of Bridges" published by Japan Bridge Association (JBA, 1978–2001). The steel weight here is expressed per unit road surface area (= effective road width times span length); that is, kN/m^2 (0.021 ksf). They are not distinguished by road width, number of girders, with or without pedestrian lanes, strength of steel, and others. This means that the data will scatter somewhat when the weights are plotted with respect to the span length. The structural features will be known by the degree of scattered position (deviation from the average) in the distribution figures.

It should be noted that data for bridges which have the concrete slab deck and the span length longer than 30 m.

In this chapter, a bridge design assessment method is also proposed using the Standard Gaussian technique. The deviation from the average weight is one of indices to show the characteristics of bridge. If the bridge is a quite standard type, the steel weight would be close to average. If the bridge has some irregularities, the deviation of the steel weight would be large.

20.2 Number of Bridge Constructions

Numbers of steel bridges constructed in Japan from 1978 to 2001 (completed year) are shown in Figure 20.1 for all bridges and different types of girder bridges. It can be seen in this figure that there is no big change in the total number of bridges in each year but more continuous supported bridges were constructed recently than simply supported bridges. The reason is because the continuous bridges have superior seismicity because of the structural redundancy and supply a comfortable car drive with no expansion joint between bridges.

It is interesting that the constructions of composite girder bridges have consistently decreased in Japan after 1975. The concrete deck slabs have been damaged seriously because of heavy traffic in Japan, and the slab of composite girders is not easy to replace comparing to noncomposite girders because of the shear connectors. Therefore, the Japanese government prefers to use noncomposite girders.

20.3 Steel Weight of Girder Bridges

20.3.1 Simply-Supported Noncomposite Plate Girder Bridges

As can be seen in Figure 20.1, more simply supported noncomposite plate girder bridges have been constructed in Japan than the composite girder bridges since 1996. Weight distributions for this type are shown in Figures 20.2 through 20.6, separated by a group of years in each figure. All bridges have concrete slab deck; that is, excluding the orthotropic steel deck. Although a large scatter is seen in those figures, the steel weight has a good corelation with the span length and the average weight can be approximated well by a linear equation.

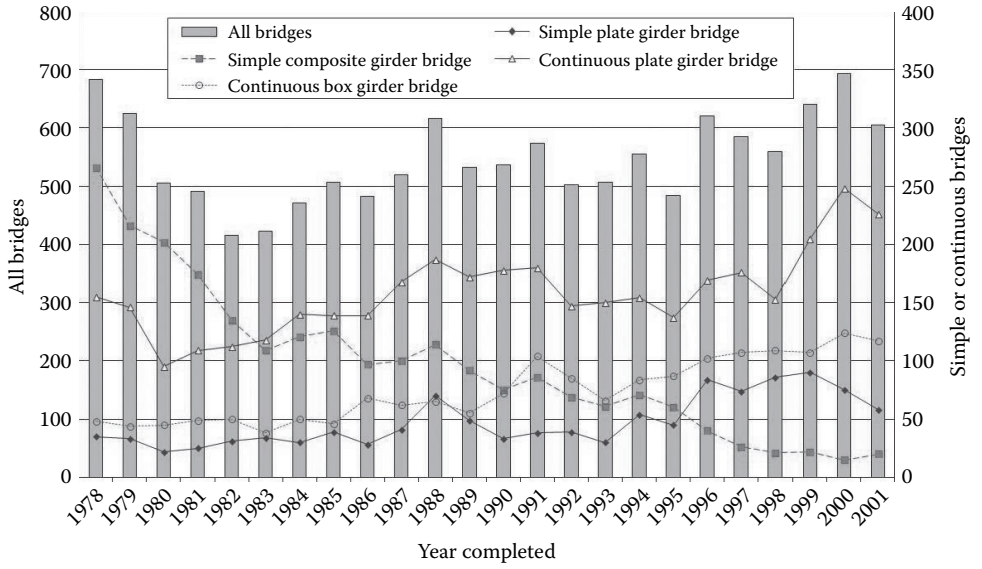

FIGURE 20.1 Number of steel bridge constructions.

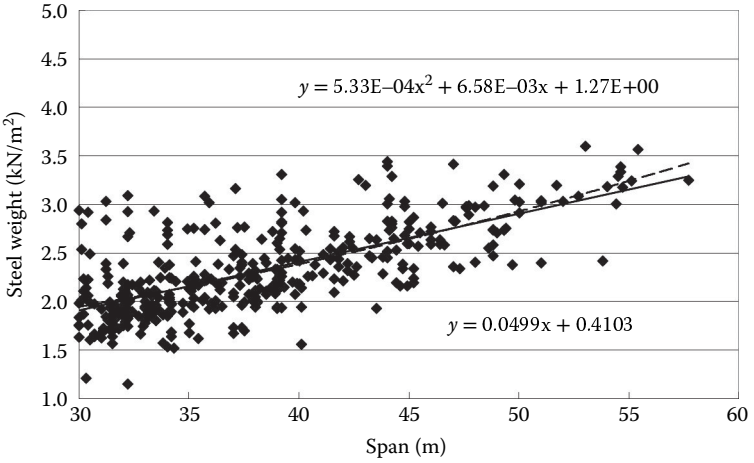

FIGURE 20.2 Simply supported noncomposite plate girder bridge (1978–1986, Data, 388).

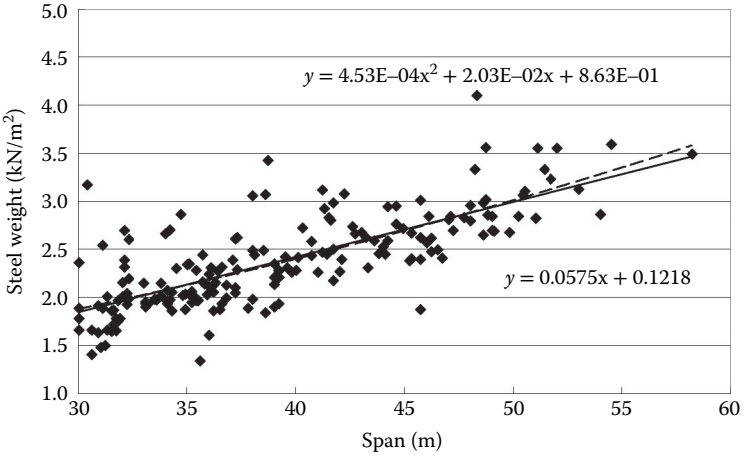

FIGURE 20.3 Simply supported noncomposite plate girder bridge (1989–1993, Data, 189).

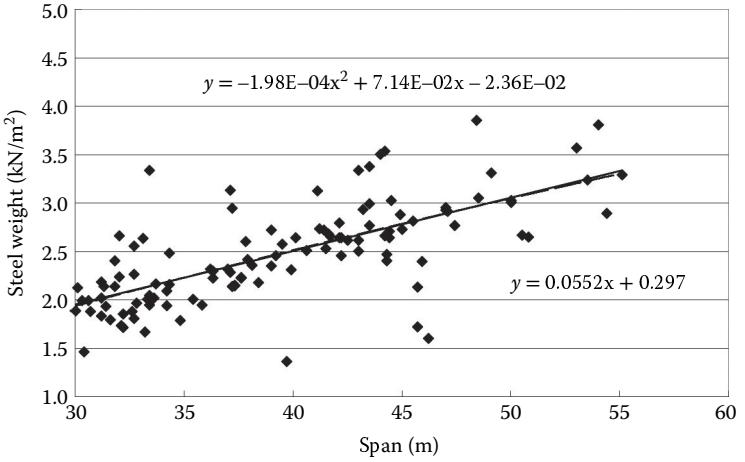

FIGURE 20.4 Simply supported noncomposite plate girder bridge (1994–1996, Data, 112).

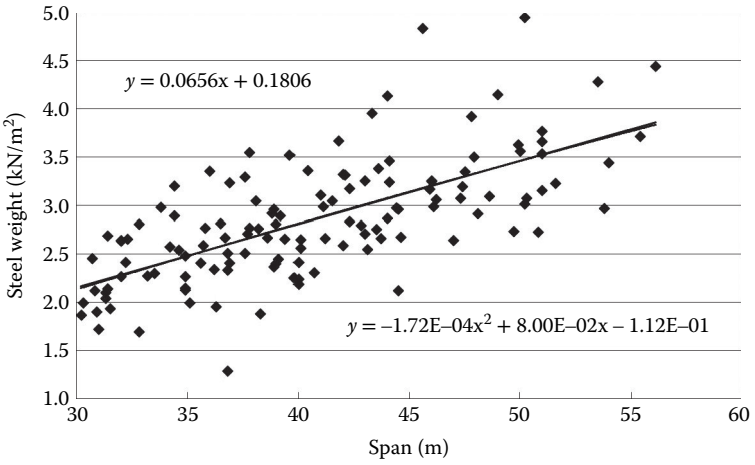

FIGURE 20.5 Simply supported noncomposite plate girder bridge (1997–1998, Data, 127).

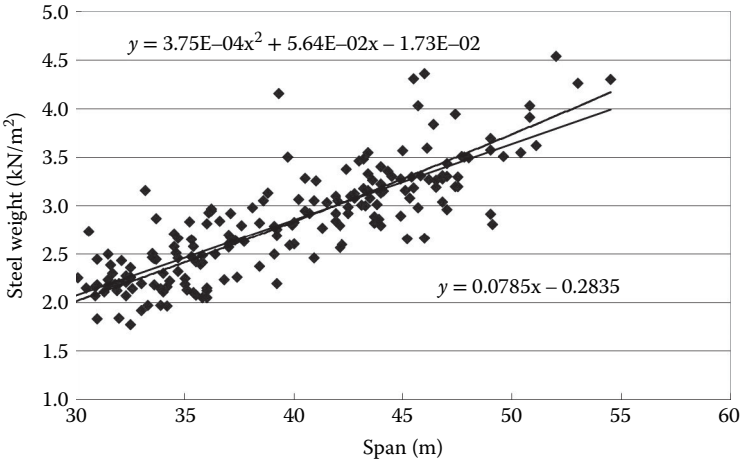

FIGURE 20.6 Simply supported noncomposite plate girder bridge (1999–2001, Data, 189).

The design live load was increased by 25% in Japan to avoid the damages of the concrete deck slab and fatigue problems because of increasing heavy traffic (JRA, 1996); the design truck weight was increased from 200kN (440kip) to 245kN (540kip). The average steel weights in Figures 20.2 and 20.3 are very similar. These data were the bridges built before the live load increase in 1993. Although the design live load was increased in 1993, the bridges in Figure 20.4 for 1994–1996 (completed year) seems to be still affected by the old live load. After 1997, shown in Figures 20.5 and 20.6, it is obvious that the new live load is applied in the design.

Figure 20.7 shows the weight distributions in 1994–2001 after increasing the live load, which is a sum of Figures 20.4 through 20.6. In order to obtain reliable estimation for the steel weight, it will be better to have more data. Therefore, the weight data after the increase of the live load are gathered in Figure 20.7. The standard deviation that gives a distance from the average linear line is $\sigma = 0.489$ in this case. The standard deviation can be calculated by Equation 20.2, which will be explained later. Knowing the average and the standard deviation, the steel weight can be estimated more accurately at the initial design in consideration of particular features of the bridge such as curved or skewed bridges, wide pedestrian lanes or no pedestrian lanes, two-girder bridge or small spacing with many girders, and so on, that affect the design. The corelation factor (ρ) is also shown in Figure 20.7.

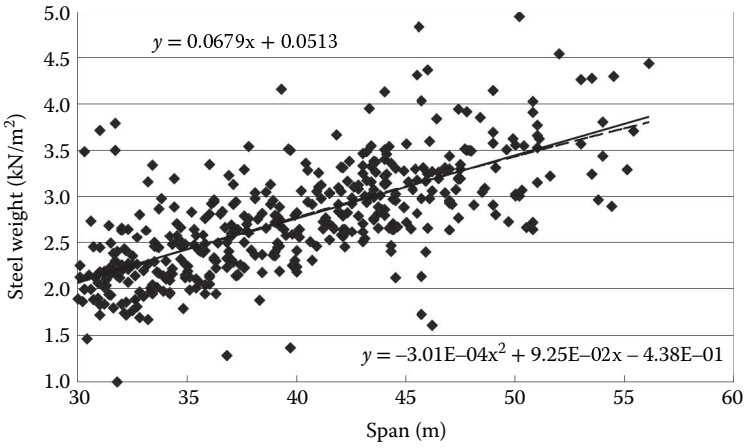

FIGURE 20.7 Simply supported noncomposite plate girder bridge (1994–2001, Data, 428, $\sigma = 0.489$, $\rho = 0.653$).

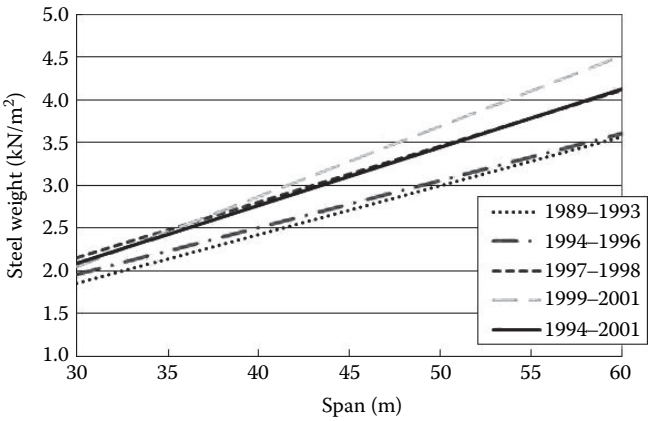

FIGURE 20.8 Comparisons by constructed years for simply supported noncomposite plate girder bridges.

Figure 20.8 is a comparison of the linear lines for groups of the average approximations in Figures 20.3 through 20.7. As seen in Figure 20.4 for 1994–1996 immediately after the new live loads were adopted, only slight weight increase is observed. However, after 1997 the steel weights were increased, that is, clearly affected by the live load increase.

As the years proceed from 1997–1998 to 1999–2001 in Figure 20.8, the steel weight increases further. Recently, since a cut of the labor cost reduces the total cost more than saving the steel material, the influence appears here. It was found that the difference in steel weight between the old and new live loads was approximately 10%.

20.3.2 Simply Supported Composite Plate Girder Bridges

The weight distributions of simply supported composite plate girder bridges are shown in Figures 20.9 through 20.13 for the years from 1978 to 2001. In early years, this type of bridge was constructed more than any others because of economical reason. In recent years, as mentioned before, the constructions of composite plate girder bridges are getting less than noncomposite girder bridges in Japan. However, there are a sufficient number of data to study statistically, and the linear and second order polynomial regression equations to give the average weight are shown in each figure.

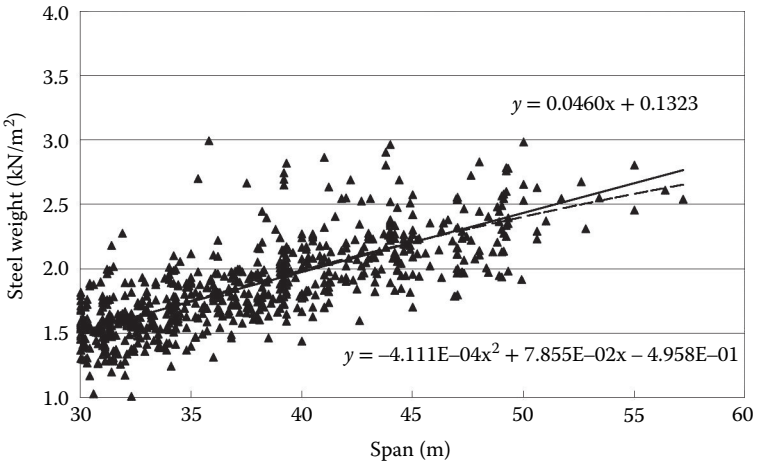

FIGURE 20.9 Simply supported composite plate girder bridge (1978–1980, Data, 684).

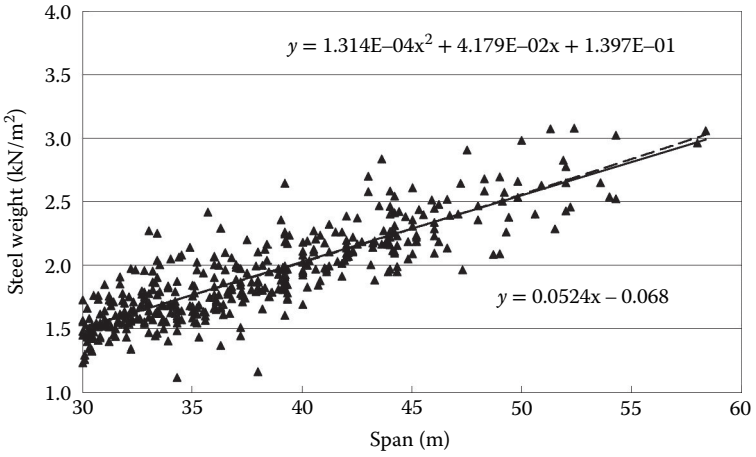

FIGURE 20.10 Simply supported composite plate girder bridge (1981–1983, Data, 418).

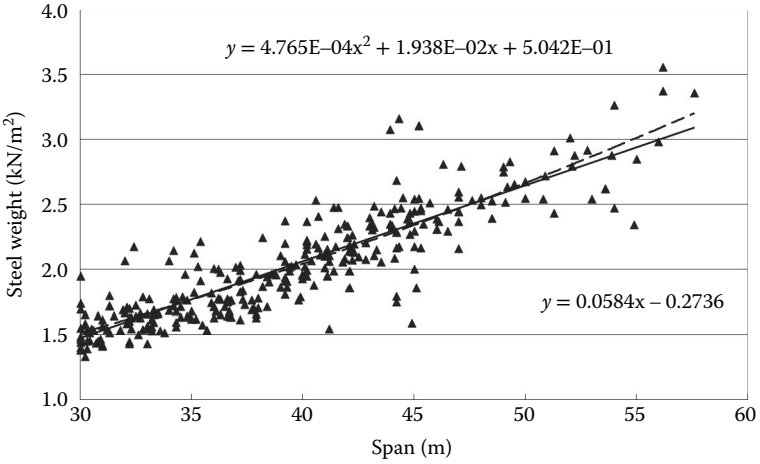

FIGURE 20.11 Simply supported composite plate girder bridge (1986–1988, Data, 311).

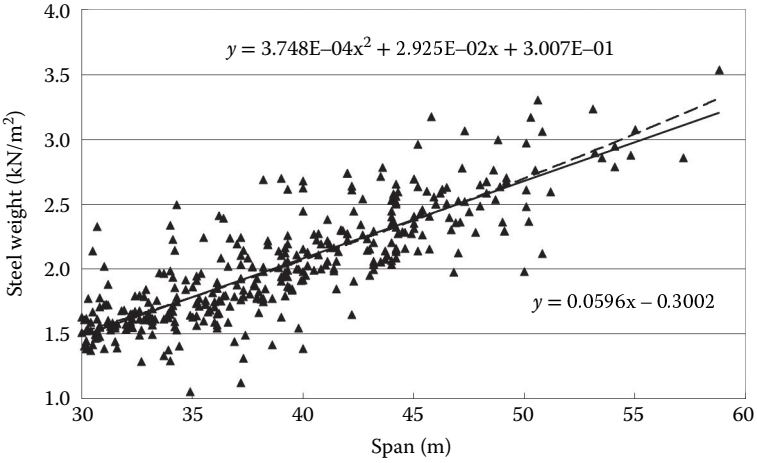

FIGURE 20.12 Simply supported composite plate girder bridge (1989–1993, Data, 383).

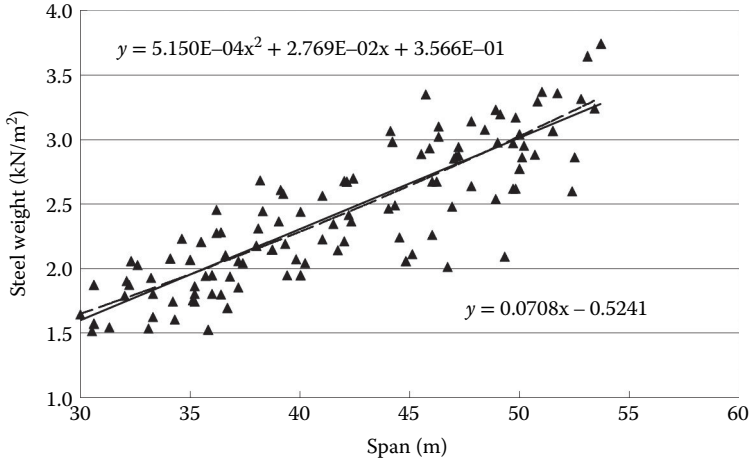

FIGURE 20.13 Simply supported composite plate girder bridge (1994–2001, Data, 132, $\sigma = 0.310$, $\rho = 0.831$).

The old live load was used before 1993 in Figures 20.9 through 20.12. The weight distribution in Figure 20.13, in which the new design live load is applied, can be used for weight estimation for this type of bridge. The standard deviation from the average linear line is calculated as $\sigma = 0.310$ in this case.

In Figure 20.14, a comparison of the linear lines for the year average approximations is shown. It can be seen that steel weight of the bridges designed by the old live loads before 1993 are gradually increasing. This is probably because the safety factor for concrete slab was increased by the Japanese government in 1978, which results in the dead load increase, to solve the damage problem occurred frequently in the concrete slab.

After the design live loads were increased by 25% in 1994, the steel weight is obviously increasing. It was found from Figure 20.14 that the difference of the steel weights between the old and new loads was approximately 10% as seen before.

20.3.3 Continuous Noncomposite Plate Girder Bridges

As seen in Figure 20.1, a continuously supported noncomposite plate girder bridge is the most constructed type of bridge recently in Japan. Specifically in Japan, the continuous bridges have a vital advantage to the earthquake resistance. The steel weights are shown in Figures 20.15 through 20.17, in which the concrete slab deck is used similarly to other bridges; the orthotropic steel deck is not included.

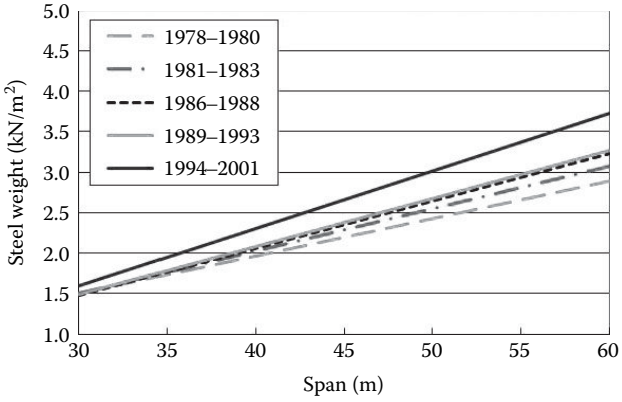

FIGURE 20.14 Comparisons by constructed years for simply supported composite plate girder bridges.

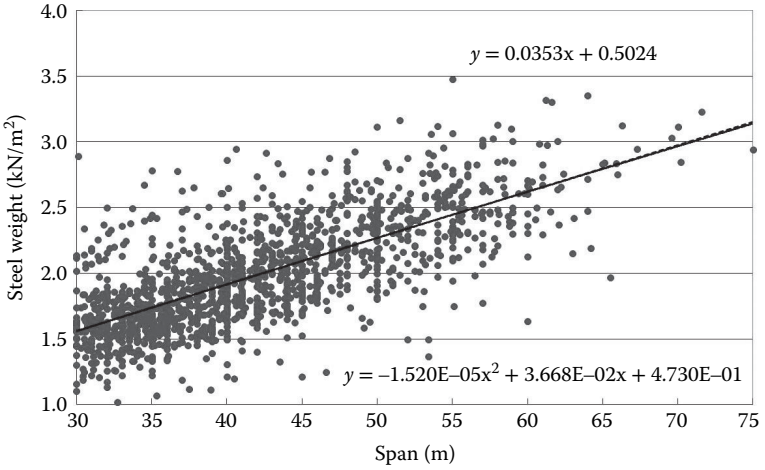

FIGURE 20.15 Continuous noncomposite plate girder bridge (1978–1988, Data, 1508).

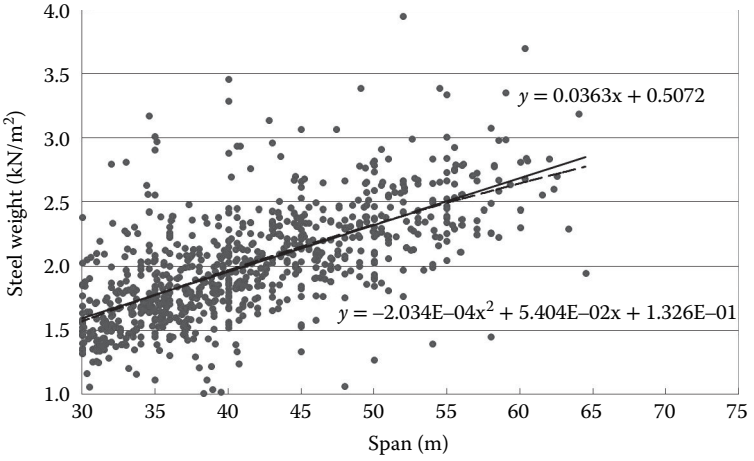

FIGURE 20.16 Continuous noncomposite plate girder bridge (1989–1993, Data, 827).

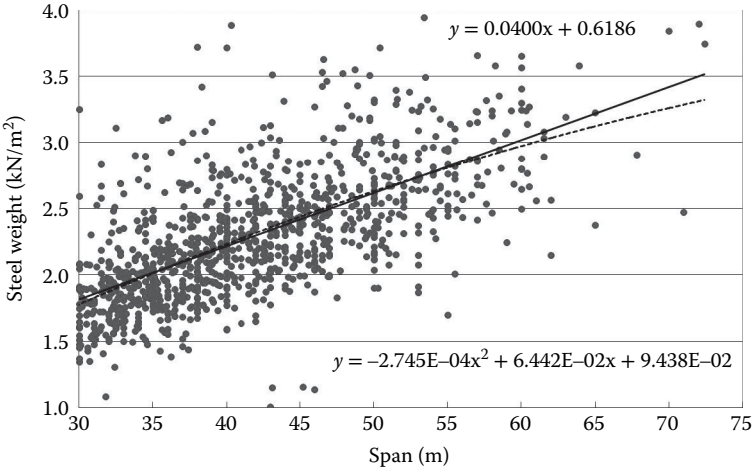

FIGURE 20.17 Continuous noncomposite plate girder bridge (1994–2001, Data, 1082, $\sigma = 0.398$, $\rho = 0.629$).

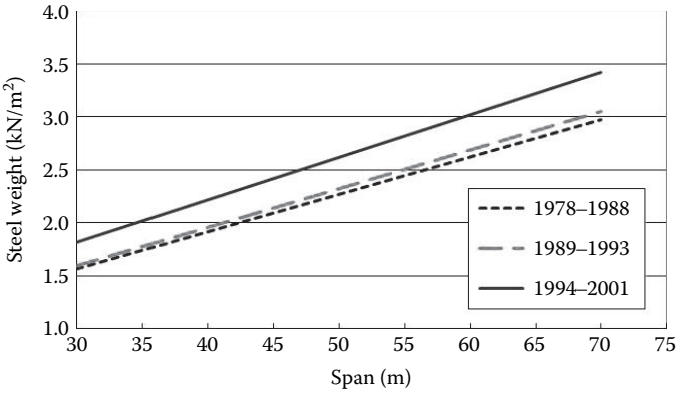

FIGURE 20.18 Comparisons by constructed years for continuous noncomposite plate girder bridges.

Steel weight of the continuously supported bridges is affected by number of spans, each span length, span ratio, and so on, but only the central span length is used as a representative parameter. Since the continuously supported bridges have more influential factors on the steel weight than simply supported bridges, the data scatter widely. Therefore, more data are put together in each figure for comparison.

The old live load was used before 1993 in Figures 20.15 and 20.16. Figure 20.17 is the data for the new live load, in which the average linear line and the standard deviation $\sigma = 0.398$ can be used to estimate for the continuously supported girder bridge.

According to the comparison of the linear average lines in Figure 20.18, the steel weights of the bridges designed and constructed by using the new live load after 1994 are obviously increasing. The increasing rate is approximately 10%, which is the same as seen before in other types of bridges.

20.3.4 Simply Supported Noncomposite Box Girder Bridges

The steel weights of simply supported noncomposite box girder bridges are shown in Figures 20.19 through 20.21 for a group of years, in which the concrete slab deck is used and the orthotropic steel deck is not included. The old live load was used before 1993 in Figures 20.19 and 20.20. Figure 20.21 is the data

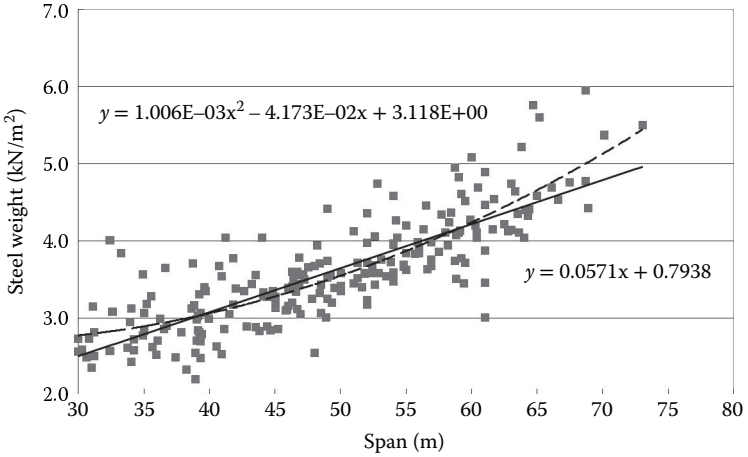

FIGURE 20.19 Simply supported noncomposite box girder bridge (1978–1988, Data, 221).

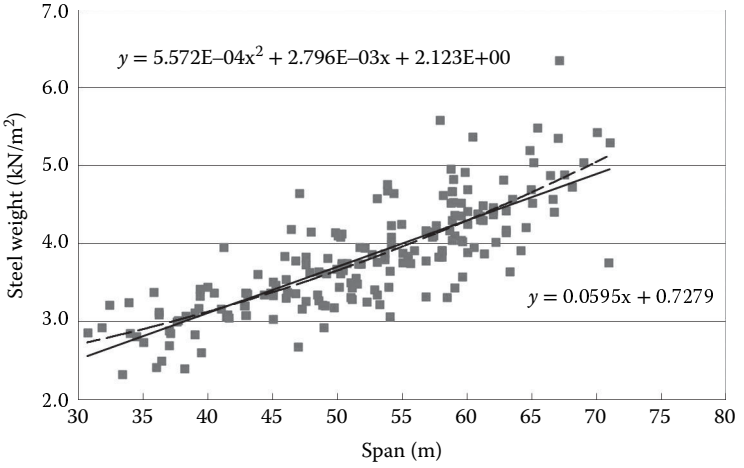

FIGURE 20.20 Simply supported noncomposite box girder bridge (1989–1993, Data, 187).

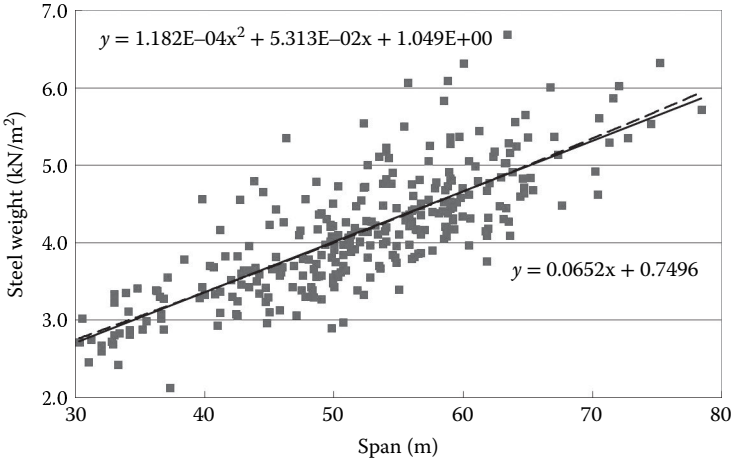

FIGURE 20.21 Simply supported noncomposite box girder bridge (1994–2001, Data, 292, $\sigma = 0.491$, $\rho = 0.779$).

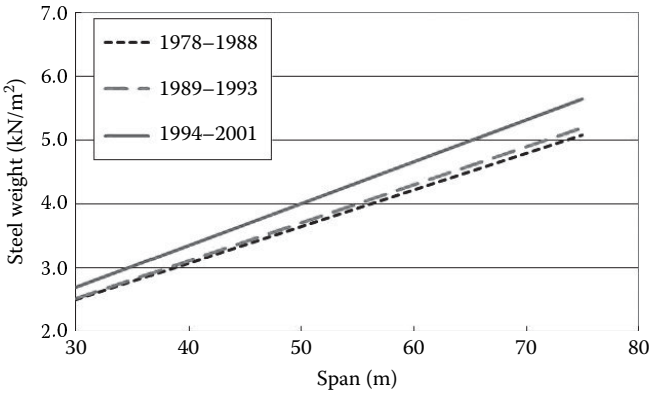

FIGURE 20.22 Comparisons by constructed years for simply supported noncomposite box girder bridges.

for the new live load, in which the average linear line and the standard deviation $\sigma = 0.491$ can be used to estimate for the continuously supported girder bridge. The corelation factor is fairly large ($\rho = 0.779$), but the linear approximation can express the average weight well.

Figure 20.22 is a comparison for the averages in Figures 20.19 through 20.21. It is obvious that the bridges designed by the old live loads before 1993 are lighter than the bridges designed by the new live loads after 1994. The difference here is a little less than 10%.

20.3.5 Continuous Noncomposite Box Girder Bridges

A number of the continuous noncomposite box girder bridges were constructed as can be seen in Figure 20.1. The steel weight distributions are shown in Figures 20.23 through 20.26. They can be distinguished before 1993 and after 1994 because the new live load was introduced in 1994. The old live load was used in Figures 20.23 and 20.24. Whole data after the new load was applied are plotted in Figure 20.27. The linear average line and the standard deviation in Figure 20.27 (or Figure 20.26) can be used for weight estimation of the continuously supported box girder bridges.

Figure 20.28 gives a comparison of the year averages. It can be seen that after the new live load is adopted, the rate of weight increase is quite different between the first period until 1997 and the

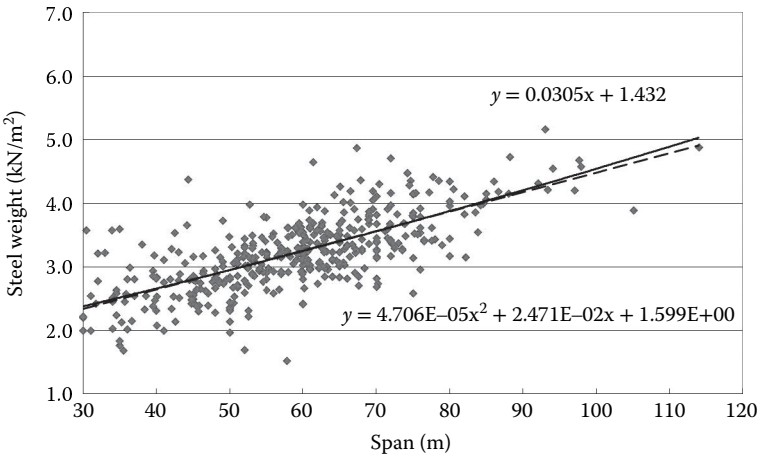

FIGURE 20.23 Continuous noncomposite box girder bridge (1981–1988, Data, 428).

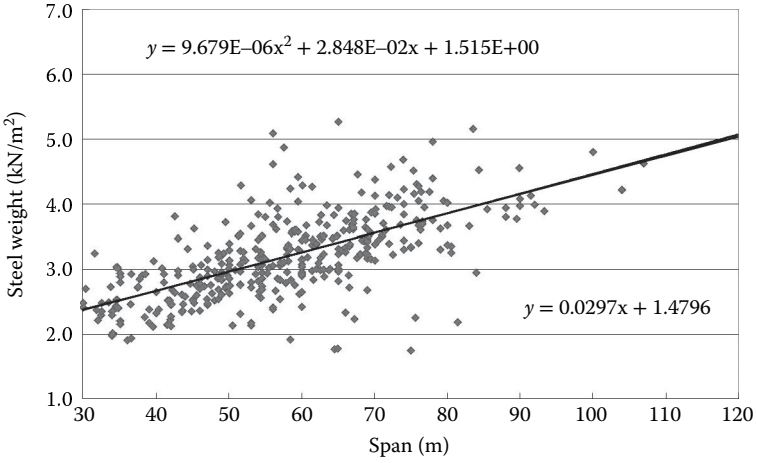

FIGURE 20.24 Continuous noncomposite box girder bridge (1989–1993, Data, 382).

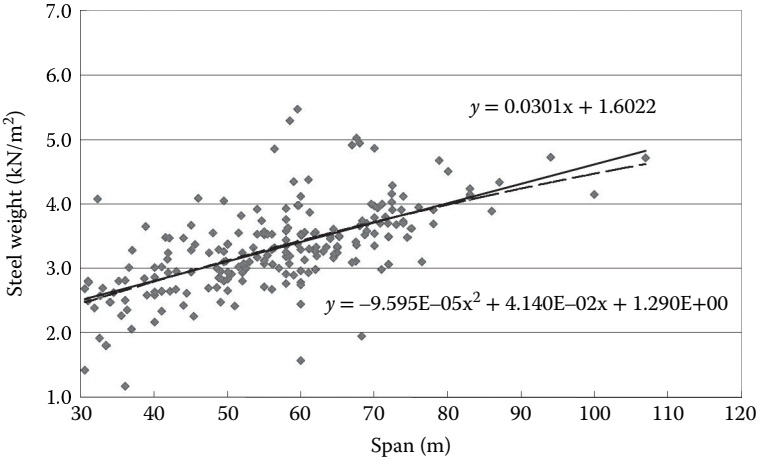

FIGURE 20.25 Continuous noncomposite box girder bridge (1994–1997, Data, 208).

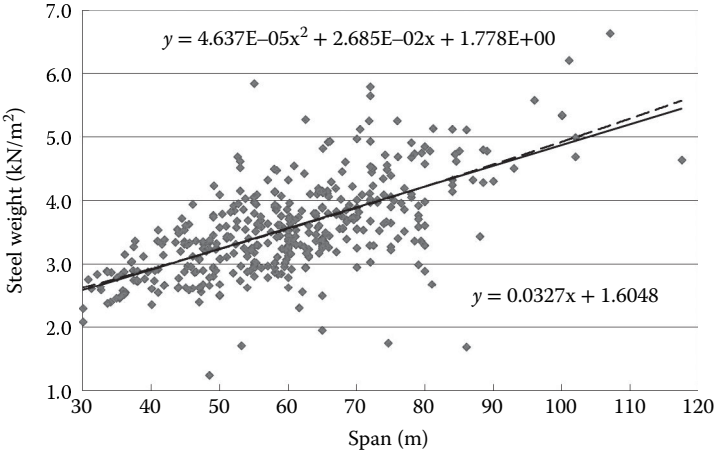

FIGURE 20.26 Continuous noncomposite box girder bridge (1998–2001, Data, 404, $\sigma = 0.576$, $\rho = 0.638$).

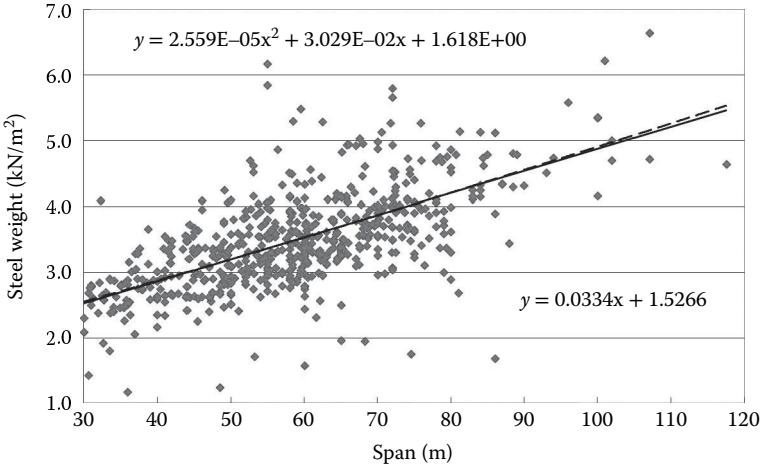

FIGURE 20.27 Continuous noncomposite box girder bridge (1994–2001, Data, 612, $\sigma = 0.614$, $\rho = 0.620$).

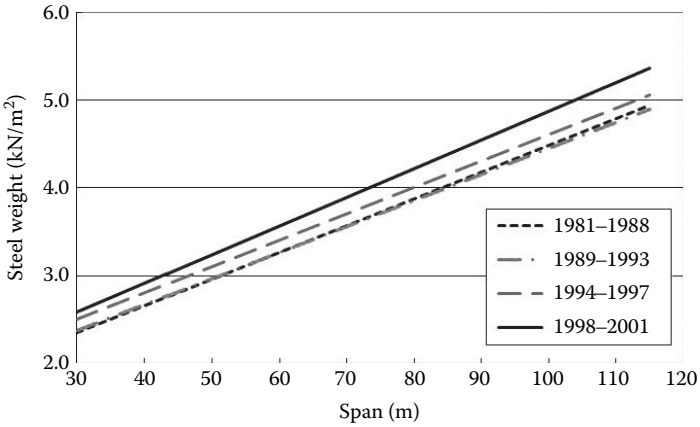

FIGURE 20.28 Comparisons by constructed years for continuous noncomposite box girder bridges.

following period after 1998. After 1998 the weight increase comparing to the old live loads is larger, and the rate is approximately 10%. This is probably because even the completed years are after 1994, some of the bridges are designed before 1993 still using the old live load.

20.3.6 Comparisons of Girder Bridges

Weights of various types of girder bridges described so far are compared by the linear average lines in Figure 20.29. The linear average weight lines are derived by using the data in 1994–2001 after the transition to the new live load. At the same time the figure shows the applicable span length of each type of girder bridges by the length of the linear lines in the horizontal axis.

In Figure 20.29, it can be seen that steel weight of the simply supported composite plate girder is significantly small comparing to the noncomposite. Also, the simply supported box girder is heavier than the plate girder bridges. It is interesting that the weights of those three types of simply supported bridges are parallel as the center span length increases.

However, the continuous noncomposite bridges have lighter weight than the same type of simply supported bridges, and wider applicable span length. Also, the average weights of the continuous plate and box girder bridges are almost parallel as span length varies.

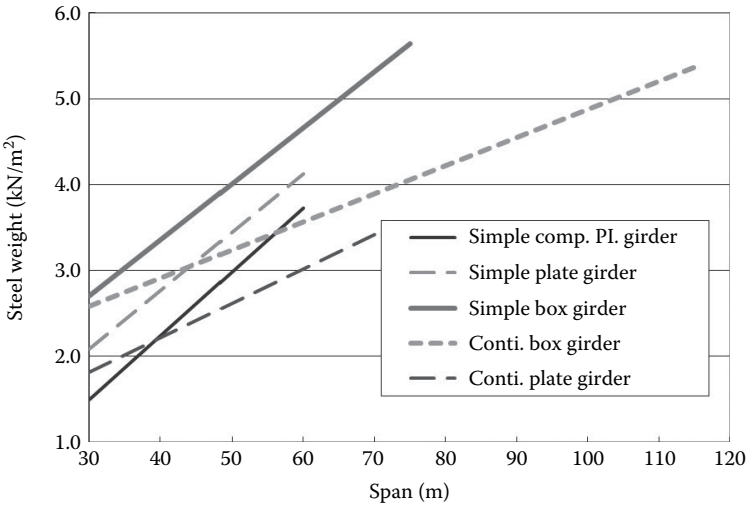

FIGURE 20.29 Comparisons of girder bridges.

20.4 Steel Weight of Truss Bridges

A weight comparison of truss bridges designed by the old live load is shown in Figure 20.30. Since there are not many truss bridges designed by the new live load, whole data including both the old and new live loads are shown in Figure 20.31. In the same way, whole data for continuous truss bridges are shown with respect to the center span in Figure 20.32.

Comparisons of those data for the simple and continuous truss bridges are shown in Figure 20.33. The weight average line of simply supported truss bridges that include for both the old and new live loads is higher than that before 1993, but the difference is smaller than 10%. The continuous truss bridge has fairly smaller weight than the simply supported.

20.5 Steel Weight of Framed Bridges

20.5.1 Arch Bridges

There are many types of framed bridges. As for the framed "arch" bridges, the steel weights of Langer bridge, trussed Langer bridge, Lohse bridge, and Nielsen bridge are shown in Figures 20.34 through 20.37, respectively. The so-called "arch" bridges generally consist of girders hanged from or supported by thick arch members. In order to see the schematic explanation for the types of arch bridges, readers are advised to refer to Chapter 54 of the first edition (Toma, 2000).

The Langer bridge in Figure 20.34 has thin arch members and vertical hangers, which are assumed in design to resist to axial force only. The trussed Langer bridge in Figure 20.35 has diagonals for web members instead of vertical hangers of the Langer bridge. However, the Lohse bridge in Figure 20.36 has thin hangers but thick arch members that resist both axial and bending moment. Tension rods are used for diagonal hanger members in the Nielsen bridge in Figure 20.37. Weight of the general arch bridge is given in Figure 20.38.

Since there are not many weight data for the framed bridges, the years collected the data are all from 1978 through 2001. Among those a good estimation equation is obtained for the Langer, the Lohse, and the Nielsen bridges, but the data of the trussed Langer and the general arch bridges are very few. Especially the general arch bridges should be careful to use for the steel weight estimation.

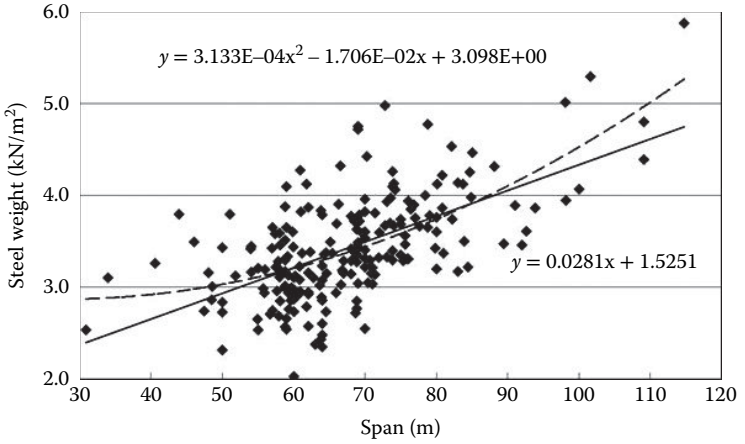

FIGURE 20.30 Simply supported truss bridge (1978–1993, Data, 211).

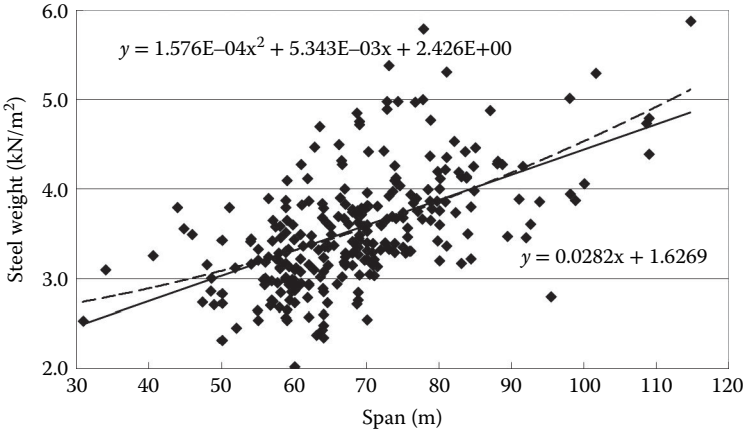

FIGURE 20.31 Simply supported truss bridge (1978–2001, Data, 274, $\sigma = 0.563$, $\rho = 0.527$).

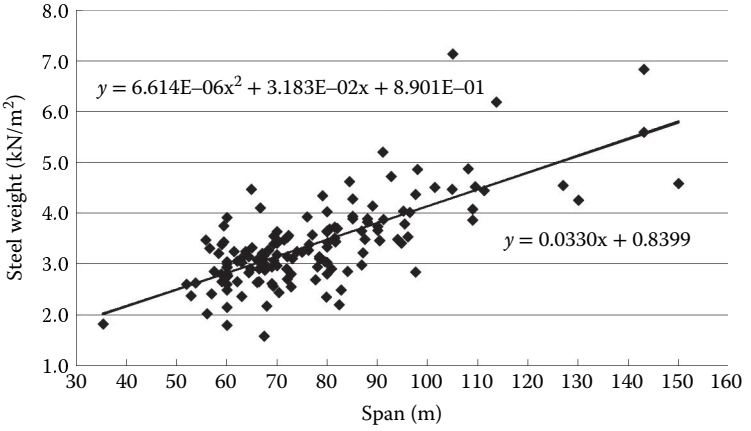

FIGURE 20.32 Continuous truss bridge (1978–2001, Data, 148, $\sigma = 0.583$, $\rho = 0.716$).

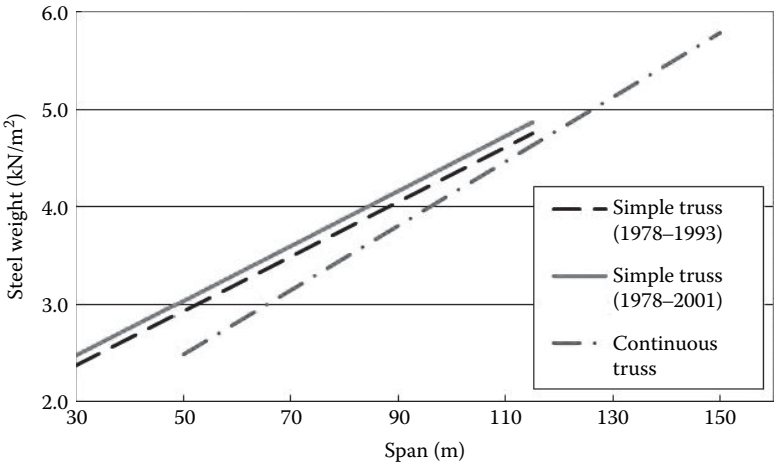

FIGURE 20.33 Comparisons by constructed years for truss bridges.

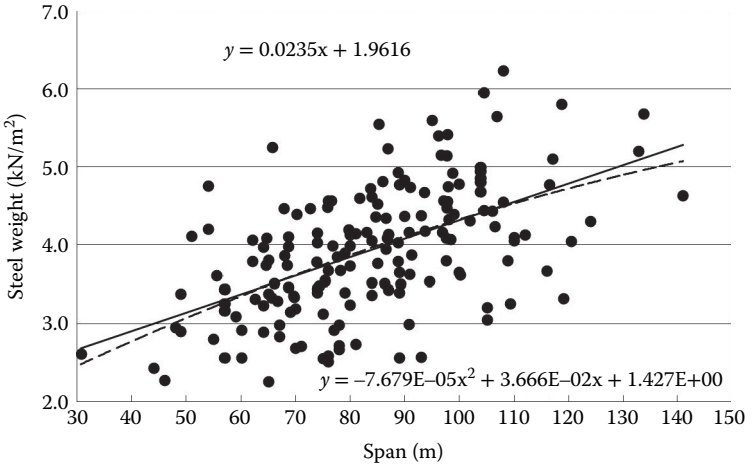

FIGURE 20.34 Langer arch bridge (1978–2001, Data, 170, $\sigma = 0.685$, $\rho = 0.544$).

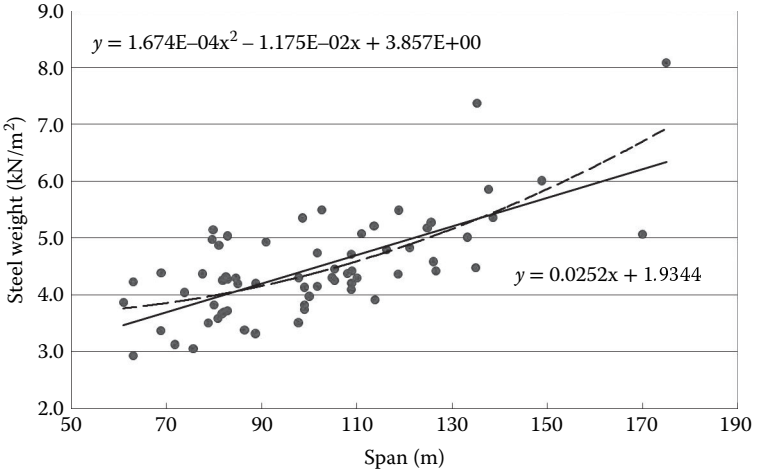

FIGURE 20.35 Trussed–Langer arch bridge (1978–2001, Data, 66, $\sigma = 0.646$, $\rho = 0.679$).

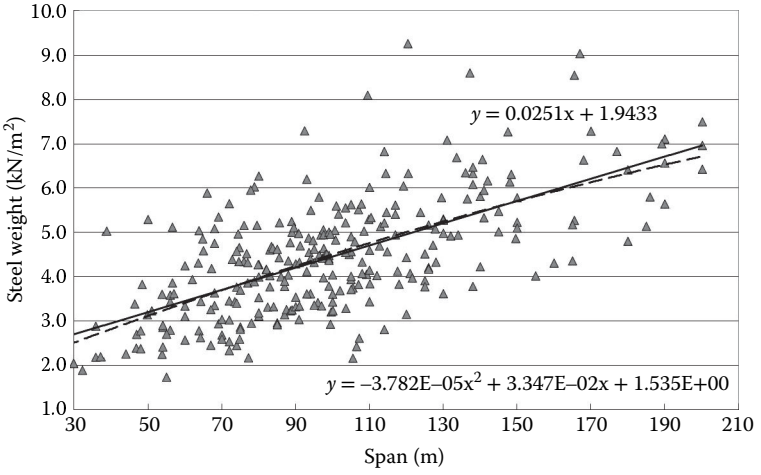

FIGURE 20.36 Lohse arch bridge (1978–2001, Data, 283, σ = 1.026, ρ = 0.648).

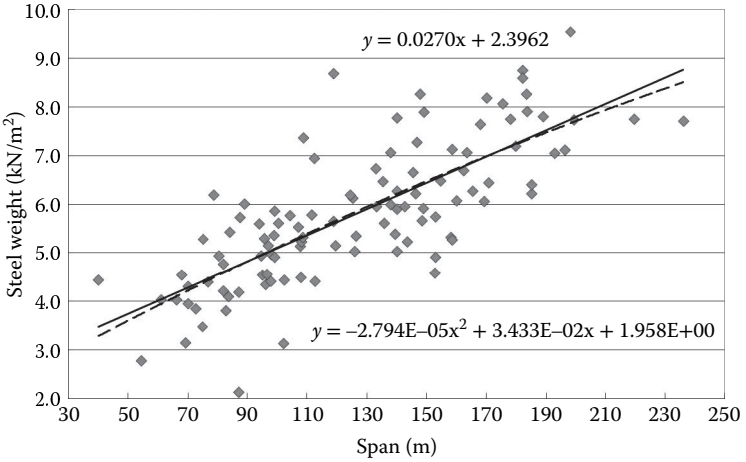

FIGURE 20.37 Nielsen arch bridge (1978–2001, Data, 106, σ = 0.926, ρ = 0.759).

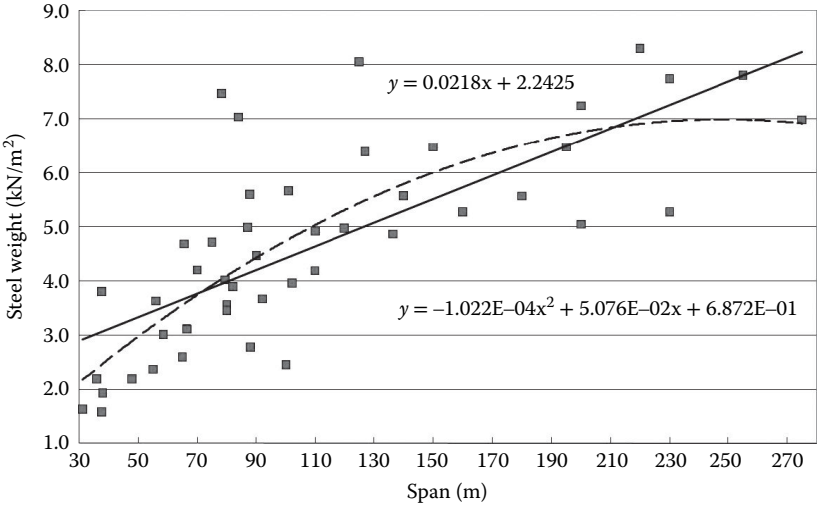

FIGURE 20.38 Arch bridge (1978–2001, Data, 47, σ = 1.223, ρ = 0.731).

20.5.2 Other Types of Framed Bridges

Weight distribution of the Rahmen (rigid frame) bridges is shown in Figure 20.39 in which the weights have a wide scatter because there are many structural variations in this type. The standard deviation is significantly large. However, the average estimation equations can be expressed linearly to the span length. Steel weights of the π-Rahmen (rigid frame) bridge, which is common structure in the rigidly framed bridges, are picked up from Figure 20.39 and separately shown in Figure 20.40. The average weight of the π-Rahmen (rigid frame) in Figure 20.40 is a little less than that of whole Rahmen (framed) bridges in Figure 20.39.

Figure 20.41 is steel weight of the cable stayed bridges that have the reinforced concrete slab. The weight data scatter and the standard deviation is large, but again the linear average approximation line expresses good corelation with the span length.

20.5.3 Comparisons of Framed Bridges

Comparisons of the average steel weights for various framed bridges are shown by linear lines in Figure 20.42, in which different characteristics can be seen for each type of bridge. The Nielsen bridge is

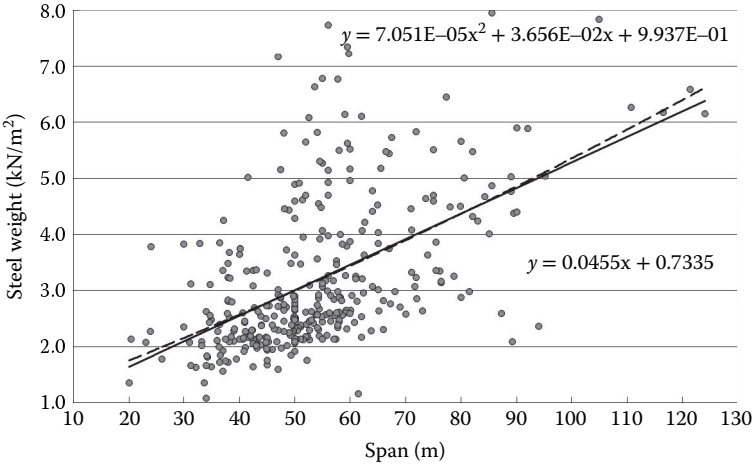

FIGURE 20.39 Rahmen (Frame) bridge (1978–2001, Data, 347, σ = 1.120, ρ = 0.538).

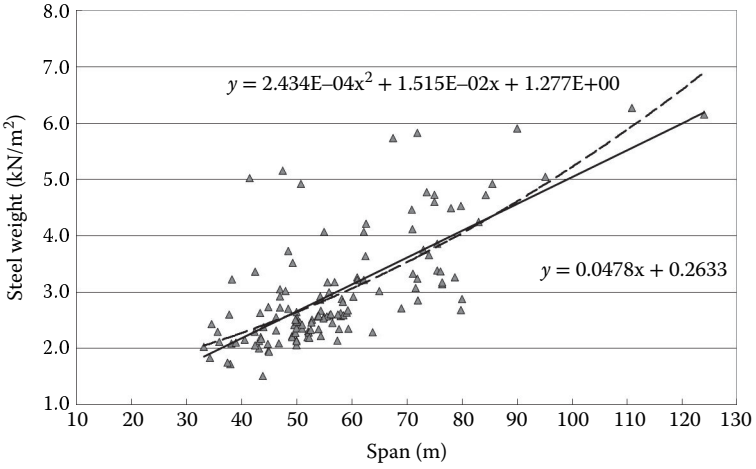

FIGURE 20.40 π-Rahmen bridge (1978–2001, Data, 129, σ = 0.708, ρ = 0.710).

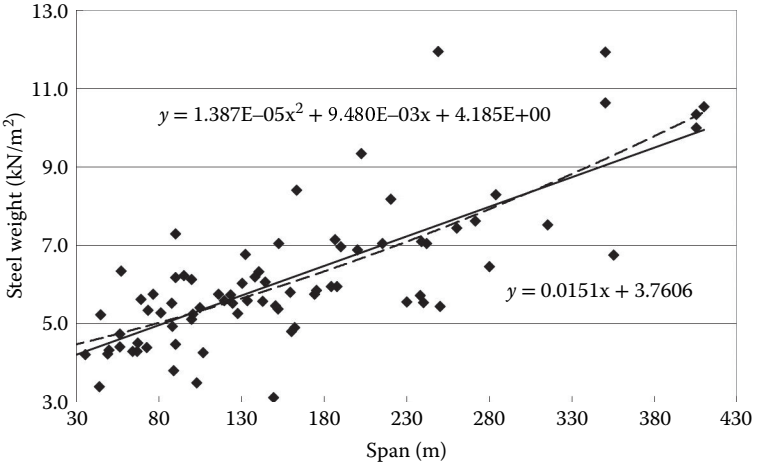

FIGURE 20.41 Cable-stayed bridge (1978–2001, Data, 78, $\sigma = 1.169$, $\rho = 0.761$).

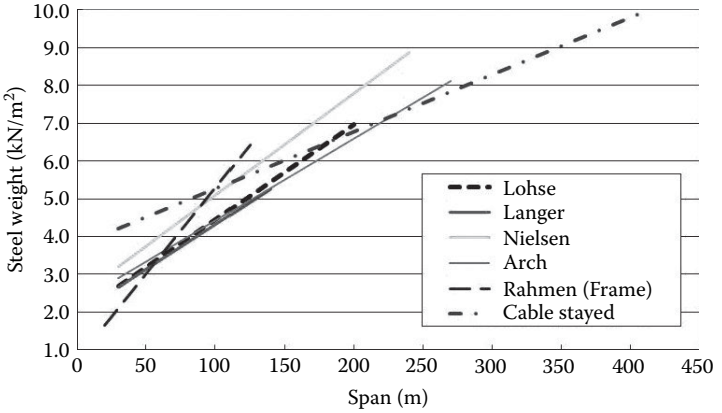

FIGURE 20.42 Comparisons of framed bridges.

heavier than the others. The cable stayed bridge has longer applicable span length, and has smaller steel weight for long spans but not true for short spans.

The Lohse and the Langer bridges have a similar average weight. Steel weight of the Rahmen (framed) bridges is increasing significantly as the span becomes long.

20.6 Assessment of Steel Weight by Standard Deviation

20.6.1 Deviation

One way in bridge design assessment is proposed from a view point of the steel weight in this section. Distribution of the weights can be expressed by the Standard Gaussian techniques, in which a mean value of 50 and a standard deviation of 10 are used, as shown in Figure 20.43. The mean value $X(L)$ is calculated by the regression equations given in the figures of the weight distributions for each type of bridges and is converted to 50 in this technique. The standard deviation (σ) are also given in the weight distribution figures for the bridges, and converted into 10 using the Standard Gaussian procedures. The characteristics of the bridge design can be known by a location of the weight in the Gaussian distribution chart in Figure 20.43.

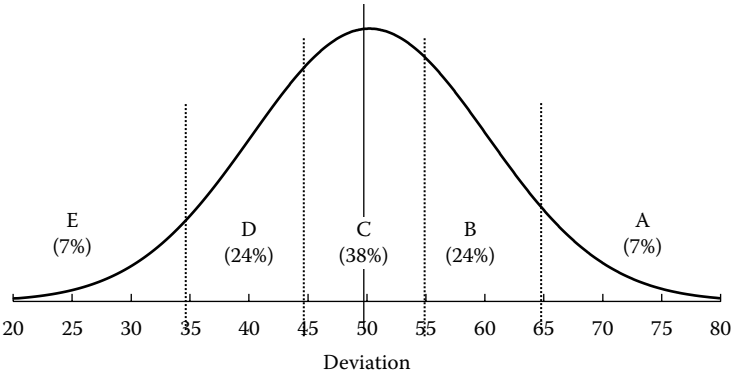

FIGURE 20.43 Gaussian distributions.

The deviation (H) of the steel weight is defined by the following equation:

$$H = \frac{X - X(L)}{\sigma} \times 10 + 50 \tag{20.1}$$

in which H = the deviation in the Standard Gaussian distribution, X = steel weight of the bridge, $X(L)$ = average steel weight, and L = span length.

The standard deviation (σ) are given in the weight distribution figures and can be obtained by the equation

$$\sigma = \sqrt{\frac{\Sigma\left\{X - \bar{X}(L)\right\}^2}{n-1}} \tag{20.2}$$

in which n = total number of data.

The deviation (H) can be used as an index to compare the designs statistically to others and to make a simple assessment of the designs. In Figure 20.43 an example of the classifications from A to E is shown. If the deviation of the design is located in the classification C, it is a standard design and categorized in the middle 38% of the distribution. If the deviation is located in the classification A, it is the heaviest in the top 7%. In this way the deviation indicates how much off from the average design, namely how far from the standard design.

20.6.2 Example of Assessment

An example assessment of the proposed method for the simply supported noncomposite plate girder bridges in Figure 20.7 is discussed in the following. Using Equation 20.1, the deviations for the weight distributions can be calculated. Then, the frequency distribution of the deviations becomes as shown in Figure 20.44. It can be seen that the frequency distribution is reasonably approximated by the Gaussian distribution curve.

Let us have an example of the average weight 2.77 kN/m^2 (0.058 ksf) for the span length 40 m and the standard deviation $\sigma = 0.489$ from Figure 20.7. Suppose that a designed steel weight is 3.05 kN/m^2 (0.064 ksf), which is approximately 10% heavier than the average, the deviation can be calculated as (H) = 55.7 by Equation 20.1, which is located at the boundary between the classifications B and C in Figure 20.43. This means that the weight is located at top 31% in whole same type of bridges. This result

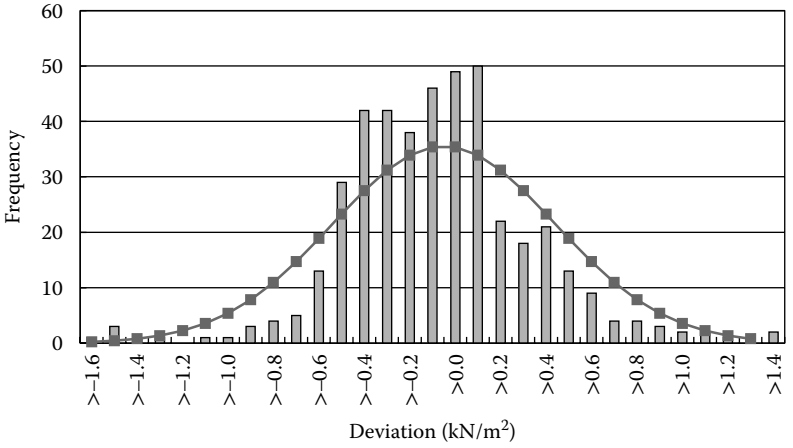

FIGURE 20.44 Distributions of deviation of simply supported plate girder bridge (noncomposite).

implies that the bridge has some reasons to increase the weight such as the bridge might be curved or skewed, has additional dead load for infrastructures, or other structural irregularities.

20.7 Summary

Steel weight of bridges might be a general indication that tells an overall feature of the design. It includes every influential design factor. In this chapter, a data base has been analyzed to enable an assessment of designs and an initial prediction of the steel weight for various types of highway bridges. The steel weight distributions are plotted for various types of bridges. From the weight distribution figures, the regression equations for mean weight and the standard deviations are derived, from which designers can estimate the steel weight for the initial design at the beginning of design work and can observe economical or structural features of the bridge comparing to others after the design.

A way of design assessment is proposed using the Standard Gaussian technique. From the regression equations and the standard deviations, the designed weight can be expressed by the deviation in the Standard Gaussian distribution. The deviation could be a measure of the design result. An example of this assessment is also given.

Acknowledgment

The data base in this statistical research has been made by the students of Hokkai-Gakuen University in their dissertation. The author would like to express his deep appreciation to them.

References

JBA. 1978–2001. *Annual Report of Steel Bridge Construction, 1978 to 2001*, Japan Bridge Association, Tokyo, Japan (in Japanese).

JRA. 1996. *Specifications for Highway Bridges, Part 1 Common*, Japan Road Association, Tokyo, Japan (in Japanese).

Toma, S. 2000. *Chapter 55 Statistics of Steel Weight of Highway Bridges, Bridge Engineering Handbook* (*1st edition*), W. F. Chen and L. Duan (eds.), CRC Press, Boca Raton, FL.

21

Design and Damage Evaluation Methods for Reinforced Concrete Beams under Impact Loading

Norimitsu Kishi
Kushiro National College of Technology

21.1 Introduction

In the design of bridge structures, usually only seismic and wind loads are considered as dynamic loads. But sometimes accidental loads may be surcharged, for example, to bridge deck slabs because of heavy objects falling from moving vehicles at a high speed or to a bridge railing because of an automobile crashing into it at a high speed. In the case of cross-channel bridges, the basement of bridge pylons should be designed to withstand an impact force because of collision of ferries, oil tankers, and container vessels. In these cases, up until now, dynamic response analyses of modeling the structure as a single or multidegree of freedom system are usually performed. A rational impact-resistant design procedure not only for bridge and other road infrastructures but also for reinforced concrete (RC) beams/slabs has not yet been established.

Nowadays, with the development of computer technology, 3D dynamic behavior of the structures under impact loading can be precisely analyzed from local failure to the global dynamic response. However, it is not easy to understand the dynamic response behavior of these structures under impact loading.

From this point of view, this chapter emphasizes impact response behavior and analyses of the RC beam/girder as the simplest structural member under falling-weight impact loading. In Section 21.2, the typical dynamic response behavior of small RC beams under falling-weight impact loading and the evaluation formulae for statically designing the beams under impact loading are described. In Section 21.3, the 3D elasto-plastic dynamic response analysis method to appropriately evaluate the damage of RC beams under single and/or consecutive impact loading is introduced. In Section 21.4, the analysis method of full-scale RC girders under impact loading using a coarse finite element (FE) mesh is discussed.

On the basis of this chapter, impact-resistant problems concerning bridge structures can be more readily treated.

21.2 Design Formula for Reinforced Concrete Beams under Falling-Weight Impact Loading

21.2.1 Introduction

Until now, impact-resistant RC and prestressed concrete (PC) structures except nuclear power plants have been designed by applying as a statical surcharge of the maximum impact force according to the allowable stress design concept (JRA, 2000; ASTRA, 2008). However, it is evident from experimental and numerical studies that these allowable stress design-based structures have a high safety margin for a design event. Therefore, these should be designed appropriately considering the characteristics of the impact-resistant capacity of these structures. In recent years, even though several impact tests and numerical analyses on small (Banthia et al., 1987; Ando et al., 1999; Kishi and Mikami et al., 2000 and 2002; May et al., 2005; Kaewunruen and Remennikov, 2009; Tachibana et al., 2010) and large size (Sugano et al., 1993; Kishi et al., 2002; Delhomme et al. 2005; Schellenberg et al., 2007; Zineddin and Krauthammer, 2007; Nishi et al., 2009; Kon-No et al., 2010) RC/PC members and structures have been conducted, an appropriate impact-resistant design procedure has not been specified in some design codes.

To develop impact-resistant design formulae for RC members under impact loading, falling-weight impact tests for a total 36 beams were conducted in the author's laboratory. Based on these results, new empirical formulae for designing RC beams for various limit states have been obtained (Kishi and Mikami, 2012). Applicability was confirmed comparing with the experimental results of Tachibana et al. (2010). Meanwhile, in these tests, the maximum concentrate load-carrying capacity of the beams considered in this section is 237.5 kN (53.4 kip). The input-impact energy varies from 2.4 to 14.7 kJ (1.77–10.85 kips·ft) by varying the mass of the weight (300–500 kg, 675–1125 lb) and the impact velocity (3.1–7.7 m/s, 10.17–25.26 ft/s).

In this section, these experimental results and empirical formulae for designing RC beams under impact loading will be briefly presented.

21.2.2 Experimental Investigations

21.2.2.1 Dimensions and Static Design Values of RC Beams

The dimensions and static flexural and shear capacities for all beams considered in this section are listed in Table 21.1. Beams belonging to the same test series are denoted by adding the letter "G" and the sequential number by a hyphen in ascending order of impact velocity of the falling weight. The second beam of Series G1 is identified by adding the letter "S" to the sequential number because of the same test conditions. Three beams of Series G2 were discriminated by adding "L" for the beam impacted by a larger mass of falling weight (400 kg, 900 lb). All beams were divided into 16 series with respect to beam dimensions and test duration.

TABLE 21.1 List of Specimens

Specimen	Cross section	Main rebar ϕ (mm)	Main rebar #	Clear span length L (m)	Main rebar ratio p_t (%)	Mass of weight M (kg)	Comp. strength of concrete f'_c (MPa)	Static flexural capacity P_{usc} (kN)	Static shear capacity V_{usc} (kN)	Shear-flexural capacity ratio α	Impact velocity V (m/s)
G1-1	200×300	19	2	3.0	1.10	300	33.7	69.6	195.4	2.81	7.0
G1-1S											
G2-1	150×250	13	2	2.0	0.80	300	32.2	38.1	139.7	3.67	4.0
G2-2											5.0
G2-3											6.0
G2L-1	150×250	13	2	2.0	0.80	400	32.2	38.1	139.7	3.67	4.0
G2L-2											5.0
G2L-3											6.0
G3-1	150×250	13	2	2.0	0.80	300	34.6	40.2	141.1	3.51	4.0
G3-2											5.0
G3-3											6.0
G4-1	150×250	13	2	2.0	0.80	300	32.3	39.7	139.8	3.52	4.0
G4-2											5.0
G5-1	200×300	19	2	3.0	1.10	400	39.2	70.4	200.4	2.85	6.0
G5-2											7.0
G6-1	250×250	19	2	2.0	1.09	300	34.7	87.4	191.4	2.19	5.0
G7-1	250×250	19	2	3.0	1.09	300	34.7	58.3	162.3	2.78	5.0
G7-2											6.0
G8-1	200×200	25	2	2.0	3.17	300	34.7	102.3	158.4	1.55	6.0
G9-1	200×200	25	2	3.0	3.17	300	34.7	68.2	136.3	2.00	5.0
G9-2											6.0

(*Continued*)

TABLE 21.1 (*Continued*) List of Specimens

Specimen	Cross section	Main rebar		Clear span length L (m)	Main rebar ratio p_t (%)	Mass of weight M (kg)	Comp. strength of concrete f'_c (MPa)	Static flexural capacity P_{usc} (kN)	Static shear capacity V_{usc} (kN)	Shear-flexural capacity ratio α	Impact velocity V (m/s)
		ϕ (mm)	#								
G10-1	200×250	19	2	3.0	1.36	300	23.5	56.6	289.3	5.11	4.0
G10-2											5.0
G10-3											6.0
G10-4											7.0
G11-1	200×300	22	2	2.7	1.55	500	23.6	99.2	164.8	1.66	3.13
G11-2											4.20
G11-3											5.05
G11-4											5.78
G11-5											6.42
G11-6											7.00
G12-1	200×300	19	3	2.7	1.72	500	23.6	110.8	168.1	1.52	7.67
G13-1	200×400	25	2		1.45			190.0	400.2	2.11	
G14-1	200×350				1.69			159.5	312.2	1.96	
G15-1	200×400	29			1.84			237.5	850.1	3.58	
G16-1	200×370	25			1.58			171.7	371.7	2.16	

1 mm = 0.04 in, 1 m = 3.3 ft, 1 kg = 2.25 lb, 1 MPa = 0.145 ksi, 1 kN = 0.225 kips

They have a rectangular cross section of 150–250 mm (6–10 in) width, 200–400 mm (8–16 in) depth, and 2–3 m (6.56–9.84 ft) clear span length. The main rebar ratios are in the range 0.8%–3.17%. Dimensions and layout of the reinforcement for each beam are shown in Figure 21.1. Each rebar was welded to steel plate of 9 mm (0.36 in) thickness at the ends of the beam to save the anchoring length. Stirrups were placed at corresponding intervals to obtain the desired shear capacity V_{usc}. The flexural concentrate load-carrying capacity P_{usc} for each beam under 3-point loading conditions was in the range 38.1–237.5 kN (8.6–53.4 kips), which was estimated by using material properties to be hereinafter described. Since the shear-flexural capacity ratios $\alpha = V_{usc}/P_{usc}$ for all beams are > 1, these would statically fail in flexure.

21.2.2.2 Experimental Method

Impact loading tests (JSCE, 2004) for RC beams were conducted by dropping the weight from a prescribed height onto the midspan of the beam using the falling-weight impact test apparatus as shown in Figure 21.2. The RC beams were placed on the supports equipped with load cells for measuring the reaction force and were clamped at their ends using cross beams to prevent lifting off. The supports were able to rotate freely, whereas restraining horizontal movements of the beam. Figure 21.3 shows a view of the test setup. The impact force was applied to the beam without considering any limit states.

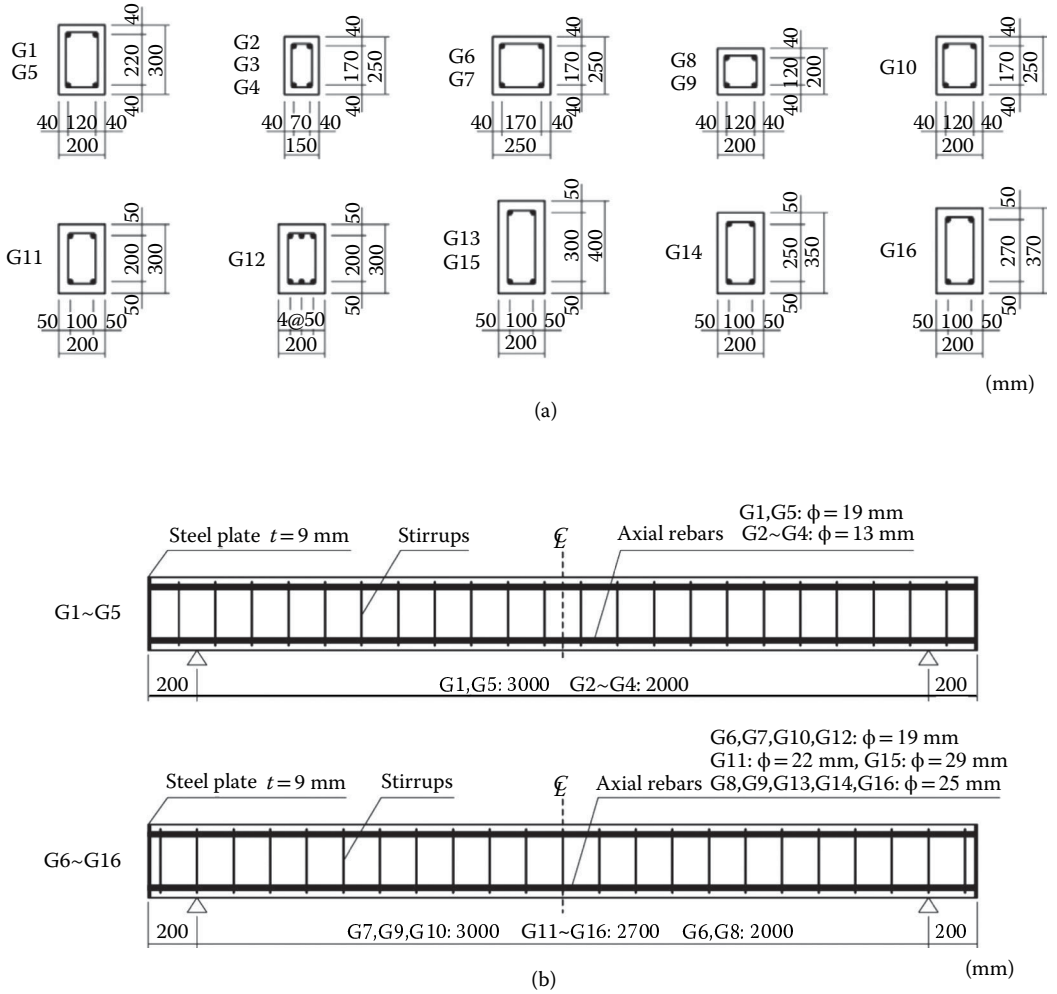

FIGURE 21.1 Details of RC beams of each series (1 mm = 0.04 in): (a) Cross section of beams; (b) layout of reinforcement for each beam.

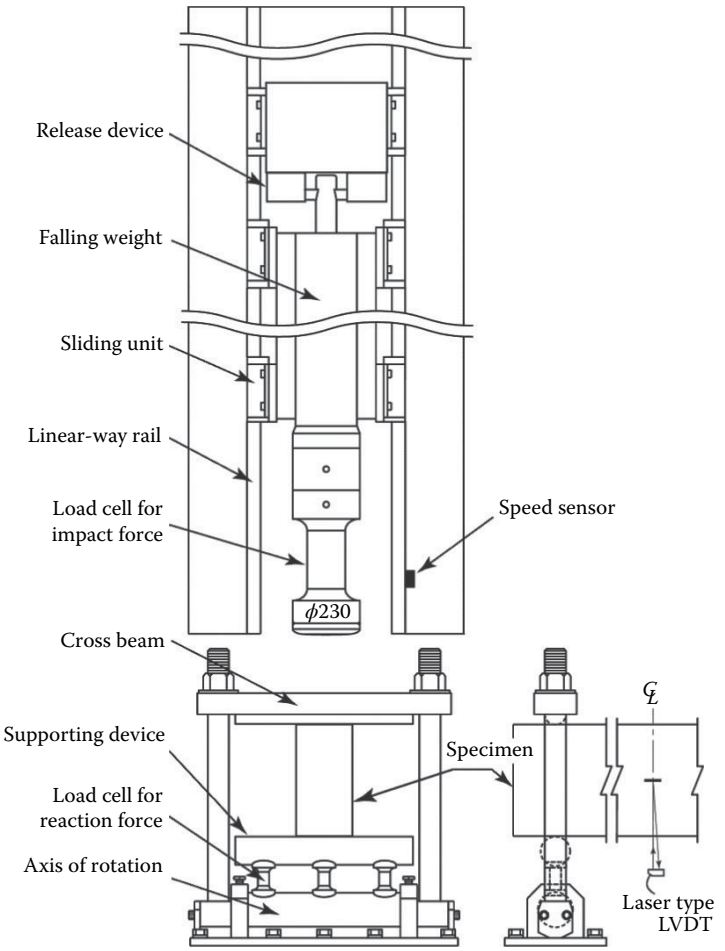

FIGURE 21.2 Falling-weight impact test apparatus.

The measured quantities were the time histories of the impact force *P*, the reaction force *R*, and the midspan deflection *D* (hereinafter, deflection). After each test, the residual deflection δ_{rs} was measured and the crack pattern observed on the side surface of the beam was sketched. The impact force *P* was measured using a load cell installed in the falling weight with a capacity of 1960; 2940; and 2940 kN (441.0, 661.5, 661.5 kips) for a 300, 400, and 500 kg (675, 900, and 1125 lb) falling weight, respectively, and a measuring frequency higher than 4 kHz for all kinds of weight used in this section. The reaction force *R* was measured using six load cells with a capacity of 294 kN (66.1 kips) and a measuring frequency of 2.4 kHz. The dynamic deflection *D* of the beam was measured by using a laser-type linear variable displacement transducer (LVDT) with a maximum stroke of 200 mm (8 in) and a measuring frequency of 915 Hz.

Analog signals from the sensors were amplified and recorded using 40 kHz wide-band data recorders. These analog data were converted into digital data at 0.1 ms time intervals. Subsequently, the time histories of the reaction force *R* and deflection *D* were smoothed numerically by means of the moving rectangular average method with a 0.5 ms window.

21.2.2.3 Material Properties

The compressive strength f_c' of concrete in each series ranged from 23.5 to 39.2 MPa (3.4–5.7 ksi). The yield strengths of the rebars were in the range 373–407 MPa (54–59 ksi). The aforementioned static

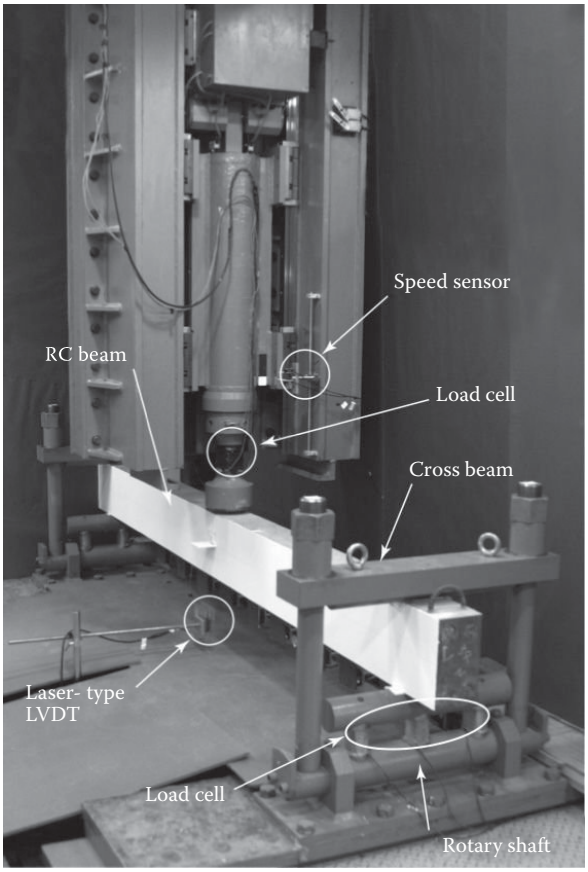

FIGURE 21.3 View of test setup.

flexural and shear capacities (P_{usc} and V_{usc}) of the beam were estimated according to the Japanese Concrete Standards (JSCE, 2005).

21.2.3 Experimental Results

21.2.3.1 Time Histories of Impact Force, Reaction Force, and Deflection

Figure 21.4 shows the time histories of the impact force *P*, reaction force *R*, and deflection *D* for the beams in Series G2L and G10. The dimensions of cross section, clear span length, and mass of falling height were different in these series. In these figures, the origin of the time axis is taken as the time when the weight impacts the beam. The reaction forces *R* in the upward direction were assumed to be positive as in the case of static loading.

Figure 21.4a shows the impact force time histories *P* during 20 ms time intervals from the beginning of impact. From these figures, it is observed that the responses of all the beams in the same series have a similar time history. At the beginning of impact, the time history exhibits a triangular shape with high amplitude and short time duration of a few milliseconds and after that high frequency components with low amplitude are excited for longer time durations than at the beginning of impact.

Figure 21.4b shows the reaction force time histories *R*. From these figures, at the beginning of impact, a negative reaction force was excited because the beam's ends tend to lift off because of rebound of the applied impact load. The main response is composed of half-sine wave or a triangular-shaped component and high-frequency components. After that, the time history exhibits damped sinusoidal shapes

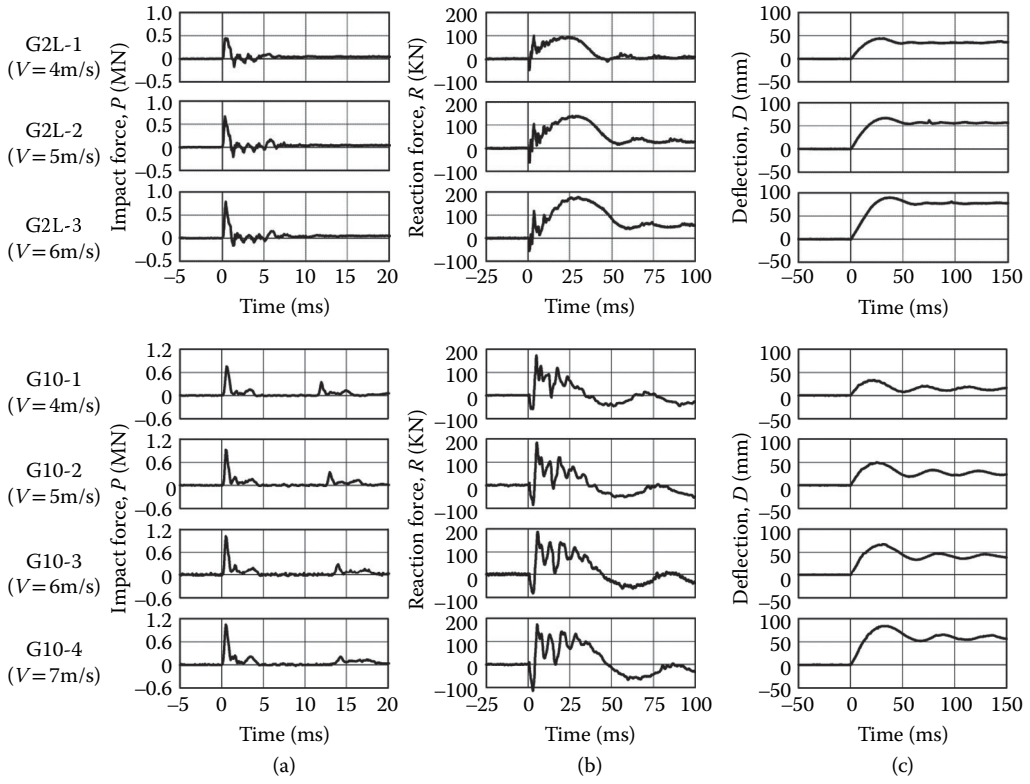

FIGURE 21.4 Time history of dynamic response of RC beams of Series G2L and G10 (1 MN = 225 kips, 1 mm = 0.04 in). (a) Impact force; (b) reaction force; (c) deflection.

corresponding to the vibration of the beam. Focusing on the maximum reaction force R_{max}, in the case of the Series G2L, R_{max} is excited not at the beginning of impact but when oscillating with a half-sine wave. However, in the case of Series G10, R_{max} is excited at the beginning of impact and the values are very similar for the beams in the same series irrespective of the magnitude of impact velocity V. Then, it is seen that the characteristics of the reaction force are influenced not only by the amount of impact velocity but also by the static concentrate load-carrying capacity P_{usc} of the beam.

Figure 21.4c shows the deflection time histories D. From these figures, the shapes of the time history curves were similar for all the beams. The main response consists of a half-sine wave, after which the deflection was restrained. In the case of beams in Series G2L, the time histories of deflection D after unloading indicate a constant value without any vibration because of the beams being severely damaged. However, in the case of Series G10, the time histories of the beams after unloading exhibit drift and vibrate with small amplitude, since the damage to these beams may be less than that to the beams in the Series G2L.

21.2.3.2 Crack Patterns

Figure 21.5 shows the crack patterns of the beams for Series G2L and G10. From these figures, it is observed that: (1) flexural cracks developed not only from the bottom fiber but also from the upper fiber over the whole span area; (2) diagonal shear cracks were also distributed around the midspan area; and (3) these cracks became more severe with increasing impact velocity V.

21.2.4 Characteristics of Relationships for Maximum Response Values

The maximum impact force P_{max}, maximum reaction force R_{max}, maximum deflection D_{max}, residual deflection δ_{rs}, the ratio of maximum reaction force R_{max} to static concentrate load-carrying capacity

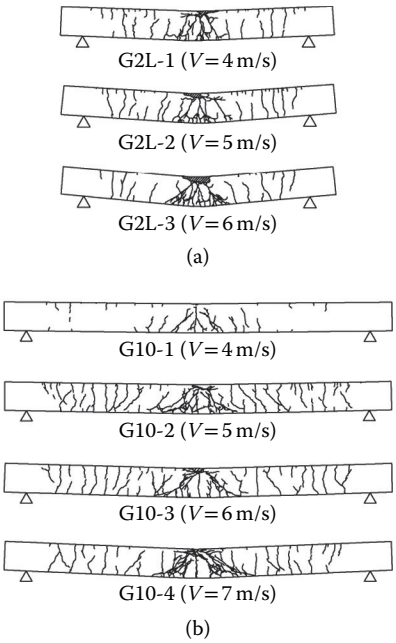

FIGURE 21.5 Crack patterns in beams of Series G2L and G10 (1 m/s = 3.3 ft/s). (a) Series G2L; (b) series G10.

P_{usc} (hereinafter, reaction capacity ratio) r_{rcap}, and the ratio of residual deflection δ_{rs} to the clear span length (hereinafter, residual deflection ratio) r_{rd} obtained from the experimental results are listed in Table 21.2. The characteristics of the relationships for maximum response values are briefly discussed in this section.

Figure 21.6a shows the relationship between maximum reaction force R_{max} and static concentrate load-carrying capacity P_{usc} for all beams. From this figure, it is observed that the maximum reaction force R_{max} depends not only a static concentrate load-carrying capacity P_{usc} but also on input impact energy E.

Figure 21.6b shows the relationship between maximum reaction force R_{max} and input impact energy E for all beams. From this figure, it is observed that the characteristics of the maximum reaction force R_{max} may be classified into two parts: (1) the series in which R_{max} increases linearly corresponding to increasing E; and (2) the series in which R_{max} has an almost constant value irrespective of the magnitude of E. Thus, the impact-resistant capacity for various types of beam cannot be better evaluated by using the maximum impact forces R_{max} without considering other parameters.

Figure 21.7 shows the relationships between maximum deflection D_{max} and input impact energy E and between residual deflection δ_{rs} and input impact energy E. From these figures, it is observed that the maximum and residual deflections of beams in the same series tend to linearly increase with increasing input impact energy E and the slope of the regression line decreases with an increase of the static concentrate load-carrying capacity P_{usc} of the beam.

From these results, the following hypotheses may be proposed: maximum and/or residual deflections of the beams are always proportional to the input impact energy; and the inclinations of the regression lines of the beams depend on the static concentrate load-carrying capacity.

21.2.5 Empirical Formulae for the Impact Resistant Design of RC Beams

Based on the abovementioned hypotheses, taking static concentrate load-carrying capacity P_{usc} as abscissa, the maximum and residual deflections per unit input impact energy E (hereinafter, coefficient

TABLE 21.2 List of Maximum Dynamic Response Values of Beams

Specimen	Impact velocity V (m/s)	Falling height h (m)	Input impact energy E (KJ)	Max. impact force P_{max} (kN)	Max. reaction force R_{max} (kN)	Max. deflection D_{max} (mm)	Residual deflection δ_{rs} (mm)	Reaction capacity ratio r_{rcap}	Residual deflection ratio r_{rd}
G1-1	7.00	2.50	7.35	1495.6	278.5	64.3	47.3	4.00	0.016
G1-1S			7.35	1600.6	287.6	58.0	41.6	4.13	0.014
G2-1	4.00	0.82	2.41	510.2	95.3	28.3	19.5	2.50	0.010
G2-2	5.00	1.28	3.77	779.3	92.9	44.0	34.5	2.44	0.017
G2-3	6.00	1.84	5.41	853.5	149.6	57.0	46.2	3.93	0.023
G2L-1	4.00	0.82	3.22	446.6	99.0	44.2	34.6	2.60	0.017
G2L-2	5.00	1.28	5.02	668.4	138.8	66.8	56.6	3.64	0.028
G2L-3	6.00	1.84	7.22	786.9	177.9	89.7	79.5	4.67	0.040
G3-1	4.00	0.82	2.41	1208.5	80.6	36.7	28.9	2.00	0.014
G3-2	5.00	1.28	3.77	1469.5	126.4	52.0	43.6	3.14	0.022
G3-3	6.00	1.84	5.41	1038.6	169.0	70.6	60.6	4.20	0.030
G4-1	4.00	0.82	2.41	800.3	122.5	39.7	30.9	3.09	0.015
G4-2	5.00	1.28	3.77	985.8	153.6	56.1	45.2	3.87	0.023
G5-1	6.00	1.84	7.22	1313.2	317.2	63.5	43.9	4.51	0.015
G5-2	7.00	2.5	9.81	1557.1	363.3	83.4	62.5	5.16	0.021
G6-1	5.00	1.28	3.77	1335.9	268.4	26.4	16.0	3.07	0.008
G7-1	5.00	1.28	3.77	1242.8	181.1	45.8	27.8	3.11	0.009
G7-2	6.00	1.84	5.41	1588.3	192.8	60.9	40.7	3.31	0.014
G8-1	6.00	1.84	5.41	1192.1	277.5	36.5	21.2	2.71	0.011
G9-1	5.00	1.28	3.77	931.2	208.6	43.2	20.8	3.06	0.007
G9-2	6.00	1.84	5.41	1102.7	248.2	57.9	31.3	3.64	0.010
G10-1	4.00	0.82	2.41	750.7	173.3	33.7	14.0	3.06	0.005
G10-2	5.00	1.28	3.77	922.3	183.6	49.5	26.5	3.24	0.009

G10-3	6.00	1.84	5.41	1016.9	188.3	67.8	39.5	3.33	0.013
G10-4	7.00	2.50	7.35	1042.3	172.7	83.9	58.0	3.05	0.019
G11-1	3.13	0.50	2.45	702.8	230.8	20.5	8.9	2.33	0.003
G11-2	4.20	0.90	4.41	971.0	380.0	33.2	19.2	3.83	0.007
G11-3	5.05	1.30	6.37	1461.5	372.4	43.1	28.1	3.75	0.010
G11-4	5.78	1.70	8.34	1877.8	379.0	55.5	39.1	3.82	0.014
G11-5	6.42	2.10	10.3	1764.8	379.3	67.2	49.4	3.82	0.018
G11-6	7.00	2.50	12.26	1906.6	408.1	83.4	58.8	4.11	0.022
G12-1	7.67	3.00	14.71	1675.0	397.5	85.4	63.7	3.59	0.024
G13-1				2150.0	598.7	60.6	31.0	3.15	0.011
G14-1				2258.1	539.6	63.7	35.0	3.38	0.013
G15-1				2062.9	630.4	40.5	26.5	2.65	0.010
G16-1				2022.6	567.7	52.9	35.8	3.31	0.013

1 m/s = 3.3 ft/s, 1 m = 3.3 ft, 1 kJ = 0.738 kips·ft, 1 kN = 0.225 kips, 1 mm = 0.04 in

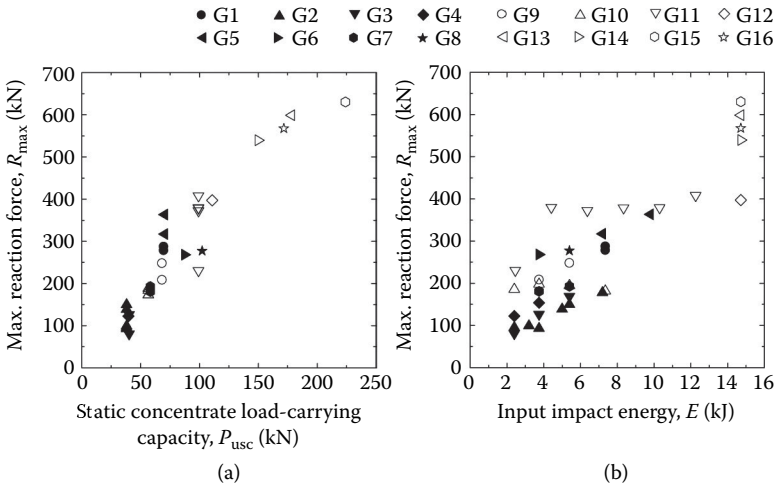

FIGURE 21.6 Experimental results: (a) Relationship between maximum reaction force R_{max} and static concentrate load-carrying capacity P_{usc}; and (b) relationship between max. reaction force R_{max} and input impact energy E (1 kN = 0.225 kips, 1 kJ = 0.74 kips·ft).

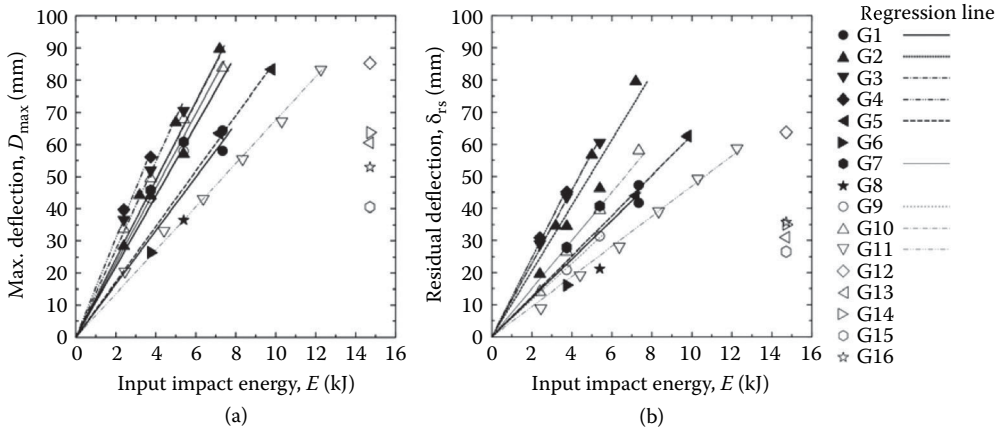

FIGURE 21.7 Experimental results: (a) Relationship between maximum deflection D_{max} and input impact energy E; and (b) relationship between residual deflection δ_{rs} and input impact energy E (1 mm = 0.04 in, 1 kJ = 0.74 kips·ft).

of maximum and residual deflections α_{def} and α_{rs}) can be plotted as shown in Figure 21.8. The empirical equations for α_{def} and α_{rs} can be obtained as

$$\alpha_{def} = \frac{0.63}{P_{usc}} \tag{21.1}$$

$$\alpha_{rs} = \frac{0.42}{P_{usc}} \tag{21.2}$$

in which the units of α_{def} and α_{rs} are 1/kN and that of P_{usc} is kN. With use of Equations 21.1 and 21.2, the following can be obtained as

$$P_{usc}(\text{kN}) = 0.63\frac{E(\text{kJ})}{D_{max}(\text{m})}, \left(P_{usc}(\text{kips}) = 0.142\frac{E(\text{kips}\cdot\text{ft})}{D_{max}(\text{ft})}\right) \tag{21.3}$$

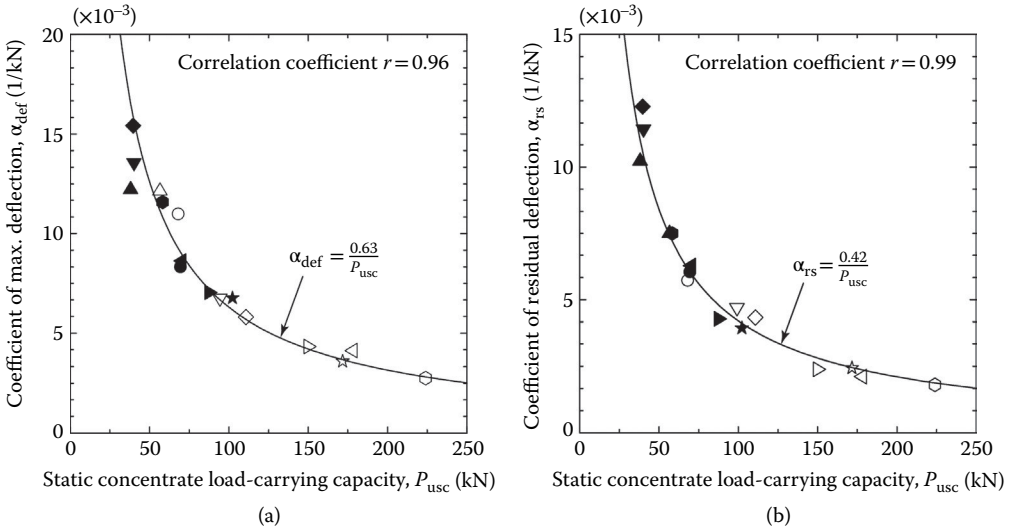

FIGURE 21.8 Regression curves: (a) Regression curve between coefficient of maximum deflection α_{def} and static concentrate load-carrying capacity P_{usc}; and (b) regression curve between coefficient of residual deflection α_{rs} and static concentrate load-carrying capacity P_{usc} (1 kN = 0.225 kips, 1 kJ = 0.74 kips·ft).

$$P_{usc}(\text{kN}) = 0.42\frac{E(\text{kJ})}{\delta_{rs}(\text{m})}, \left(P_{usc}(\text{kips}) = 0.0945\frac{E(\text{kips}\cdot\text{ft})}{\delta_{rs}(\text{ft})} \right) \tag{21.4}$$

Thus, specifying the maximum deflection D_{max} or residual deflection δ_{rs} for each limit state of the beam, the static concentrate load-carrying capacity P_{req} required for designing the RC beam can be determined from Equations 21.3 or 21.4 under a given maximum input impact energy E_{max}. It means that Equations 21.3 and 21.4 can be used as design formulae following the performance-based design concept for RC beams.

If the maximum input impact energy E_{max} and the static concentrate load-carrying capacity P_{usc} in both equations are the same, the ratio of maximum deflection D_{max} and residual deflection δ_{rs} becomes

$$\frac{D_{max}}{\delta_{rs}} = 1.5 \tag{21.5}$$

If one parameter of these is applied for designing RC beams, the other parameter can be applied by using the above equation for checking the adequacy of the design for a given limit state.

To discuss the applicability of the proposed empirical formulae, comparisons were made between experimental results including Tachibana et al.'s data (Tachibana et al., 2010) and the empirical formula for maximum deflection. In Tachibana et al.'s experimental results, the static concentrate load-carrying capacity of the beams was evaluated by using that for the static loading test. Figure 21.9 shows the comparisons. From this figure, it is confirmed that the proposed empirical formula for the maximum deflection will be applicable in practice with the limitations mentioned later.

At the present state of knowledge, for the condition of input impact energy of $E < 15$ kJ (11.1 kips·ft), Equations 21.3 through 21.5 are applicable for RC beams with a static concentrate load-carrying capacity of $P_{usc} < 240$ kN (54 kip) and a shear flexural capacity ratio of $\alpha > 1.5$. Extending the applicability of these equations would require further large-scale experiments and/or numerical simulations.

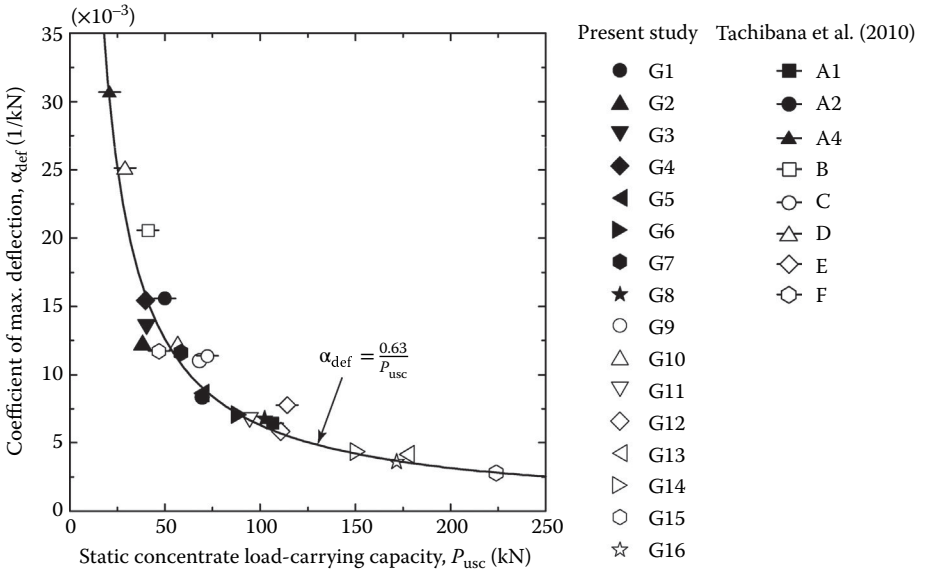

FIGURE 21.9 Comparisons of experimental results and regression curve for coefficient to maximum deflection α_{def} (1 kN = 0.225 kips, 1 kJ = 0.74 kips·ft).

21.3 FE Analysis of Reinforced Concrete Beams under Single and Consecutive Impact Loading

21.3.1 Introduction

In Section 21.2, the empirical formulae for designing RC beams under single impact loading following the performance-based design concept are derived based on the falling-weight impact test results. However, with regard to various real events such as rockfall and/or some falling objects from moving cars, the structures may be subjected not only to a single-impact loading but also a series of consecutive impacts. Damage to such structures will be then accumulated by consecutive impact loading and the cracks and residual deflection will also be increased. Therefore, the structures should be designed on the basis of damage evaluation for both single and consecutive loading. However, research on evaluation methods for the accumulated damage and residual load-carrying capacity of the structures under consecutive impact loading has not yet been paid much attention. Generally, the impact tests for RC structures require special techniques for applying impact forces, as well as measuring and processing the dynamic signals. Conducting this kind of test is not an easy task for not only researchers but also engineers. Rational impact-resistant design procedures for RC members should be established by considering the knowledge obtained from the experimental results and numerical simulations.

From this point of view, to adequately evaluate the dynamic response behavior of structural members under impact loading, Ghadimi Khasraghy et al. (2009) and Kishi et al. (2011) proposed the 3D elasto-plastic FE analysis method for RC slabs and beams under consecutive impact loading. The applicability of each analysis method was confirmed by comparing with falling-weight impact test results.

This section presents a numerical analysis method for RC beams under single and/or consecutive impact loading reported by Kishi et al. (2011). They confirmed the applicability of the method by using two types of experiments that is (1) consecutive impact loading with gradually increasing impact velocity for the beam to the ultimate state and (2) two consecutive loading cases close to the ultimate state of the beams. These numerical simulations were conducted using the LS-DYNA code—Version 971 (Hallquist, 2007).

21.3.2 Experimental Investigations

21.3.2.1 Dimensions and Static Design Values of RC Beams

RC beams used for the consecutive falling-weight impact loading have a rectangular cross section of 200 mm (8 in) width and 250 mm (10 in) depth. The clear span is 3000 mm (120 in). The dimensions and layout of the reinforcement of the beam are shown in Figure 21.10. Four deformed steel bars of diameter $\phi = 19$ mm (0.76 in) were welded to steel plates of 9 mm (0.36 in) thickness at the ends of the beam to save the anchoring length. Stirrups of diameter $\phi = 10$ mm (0.4 in) are placed at intervals of 100 mm (4 in) to the desired shear capacity V_{usc}.

The static material properties of concrete and reinforcement for the experiments are given by compressive strength and Poisson's ratio: $f'_c = 23.7$ MPa (3.4 ksi); and $\nu_c = 0.26$, respectively, and a yield stress $f_y = 404$ MPa (58.6 ksi) for both reinforcement and stirrups. The static flexural and shear resistances (P_{usc} and V_{usc}) are evaluated as 57.2 kN (12.9 kips) and 289.5 kN (65.1 kips), respectively, according to the Japanese Concrete Standards (JSCE, 2005). Therefore, the shear-bending capacity ratio $\alpha = V_{usc}/P_{usc}$ is > 1. This means that the beam will collapse in the flexural failure mode under static loading.

21.3.2.2 Experimental Method

Using the experimental apparatus explained in the previous section and shown in Figure 21.3, the RC beams were simply supported. A 300 kg (675 lb) weight was freely dropped from a prescribed height onto the midspan of the beam. The weight consists of a solid cylinder. Its impacting part has a spherical bottom with $r = 1{,}407$ mm (56.3 in) radius and a 2 mm (0.08 in) taper.

21.3.2.3 Experiments

Two types of experiments are conducted: (1) consecutive impact loading with an initial and incremental impact velocity of 1 m/s (3.3 ft/s) for the beam up to the ultimate state; and (2) two loading cases with the impact velocity close to the velocity leading to the ultimate state of the beams in the previous consecutive loading test. Here, the ultimate state of the beam was defined to be when the accumulated residual deflection of the beam δ_{ar} reaches 2% of the clear span length (Kishi and Mikami et al., 2000), that is 60 mm (2.4 in). The impact velocity V of the beam reaching the ultimate state was set to $V = 6$ m/s (19.7 ft/s) because the accumulated deflection of the beam reached $\delta_{ar} = 82.4$ mm (3.3 in) after the impact test with an impact velocity $V = 6$ m/s (19.7 ft/s).

All specimens used here are listed in Table 21.3. In this table, the specimen used for consecutive impact loading is denoted by Series CL16 and those for the two subsequent impact loading cases are denoted by Series TL*mn*, in which the digits "*m*" and "*n*" refer to the impact velocities (m/s) for the first and second impact loading, respectively. In these specimens, the impact velocity for the second loading is $V = 6$ m/s (19.7 ft/s) for all beams, which is the same as the final velocity of the consecutive loading case CL16.

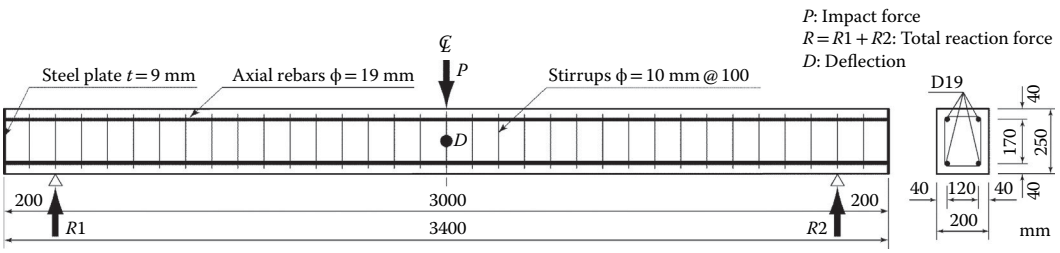

FIGURE 21.10 Dimensions and reinforcement layout of RC beam (1 mm = 0.04 in).

TABLE 21.3 List of Specimens

Specimen	Impact velocity V at 1st loading m/s (ft/s)	Impact velocity V at 2nd loading m/s (ft/s)	Impact velocities V at consecutive loading m/s (ft/s)
CL6	-	-	1.0, 2.0, 3.0, 4.0, 5.0, 6.0 (3.3, 6.6, 9.9, 13.1, 16.4, 19.7)
TL46	4.0 (13.1)	6.0 (19.7)	-
TL56	5.0 (16.4)	6.0 (19.7)	
TL66	6.0 (19.7)	6.0 (19.7)	

21.3.3 Numerical Analysis

21.3.3.1 Numerical Modeling

Figure 21.11 shows the FE model of the RC beam. Since the beam is symmetric about two axes, only one quarter of the beam including the falling weight and support was modeled in 3D for numerical simulation. The main rebars cast in the beam were modeled using a rectangular solid element and stirrups were modeled with a beam element. These elements are assumed to be perfectly bonded to the concrete elements. All other components are modeled using an eight-node solid element. The actual shape of falling weight and support were modeled. The nodal points along the middle of the base of the support are fixed so as to be able to rotate about the x-axis. The number of integration points for the solid element is 8 for the elements representing the main rebar and 1 for the other solid elements, whereas for the beam

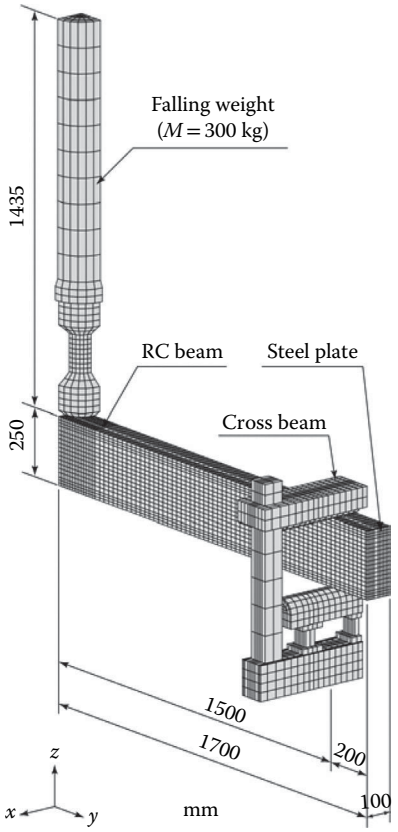

FIGURE 21.11 FE model (1 kg = 2.25 lb, 1 mm = 0.04 in).

element it is 4. In total, approximately 30,000 nodal points and 25,000 elements are used for modeling the whole structure.

The contact surface elements are introduced to take into account the interaction between the beam and the bottom of the falling weight as well as between the beam and the support elements. These elements can treat contact, detachment, and sliding of two adjacent elements.

The beam is analyzed by inputting a predetermined impact velocity for all elements of the falling weight. Before inputting the impact velocity, the weight was subjected only to gravity for analyzing the dynamic response of the beam because of the weight rebounding. The viscous damping factor is set to $h = 0.5\%$ for the first natural vibration frequency of the beam.

21.3.3.2 Procedure of Numerical Simulation for Consecutive Loading

In order to numerically and adequately reproduce the dynamic behavior of the RC beams under consecutive impact loading, the numerical simulations are performed using the following steps:

1. Set several falling weights initially at the same location for representing the falling weight during a specific impact. Therefore, the total number of impacting bodies modeled is equal to that of the consecutive loads.
2. Input the predetermined impact velocity for the first falling weight. During this step, $h = 0.5\%$ is set for the viscous damping factor, and the period of the numerical analysis is 200 ms from the beginning of impact up to the beam reaching a steady vibration state.
3. Continue the numerical analysis for a period of 200 ms from the previous termination point, inputting the critical viscous damping factor for the beam to be in a state of rest.
4. Remove the FE model of the previous impacting falling weight.
5. Perform the numerical analysis for a period of 200 ms by inputting the next predetermined impact velocity for another FE model of the falling weight, in which $h = 0.5\%$ is set for the viscous damping factor.
6. Repeat steps from 3 to 5 until reaching the prescribed final loading, in which the last falling weight model is subjected to its prescribed impact velocity.

The period of each numerical analysis and the viscous damping factor should be determined considering the dynamic characteristics and/or the dimensions of the structures.

21.3.3.3 Constitutive Models for the Materials

Figure 21.12 shows the stress–strain relationships for concrete and reinforcing steel. The constitutive model for each material is briefly explained below:

1. Concrete
   The stress–strain relationship for concrete is defined by using a bilinear model in compression and a linear cut-off model in tension as shown in Figure 21.12a. In this section, it is assumed that: (1) the concrete yields at 0.15% strain and its strength is equal to the compressive strength f_c'; (2) the tensile stress is lowered to zero when an applied negative pressure reaches the tensile strength of concrete; and (3) the tensile strength is one tenth of the compressive strength 0.1 f_c'. Here, the negative pressure is evaluated by averaging three normal stresses in the element. Yielding of the concrete is evaluated using Drucker-Prager's yield criterion (Chen, 1982).
2. Reinforcing steel
   The stress–strain relationship for reinforcing steel and stirrups is defined by using a bilinear isotropic hardening model as shown in Figure 21.12b. The plastic hardening modulus H' is assumed to be 1% of the elastic modulus E_s (E_s: Young's modulus). Yielding of the steel is estimated on the basis of the von Mises yield criterion.
3. Falling weight, supports, load cells, and anchor plates
   The falling weight, supports, and load cells for measuring the impact and reaction forces and the anchor plates for the main rebars were assumed to be elastic bodies based on the experimental

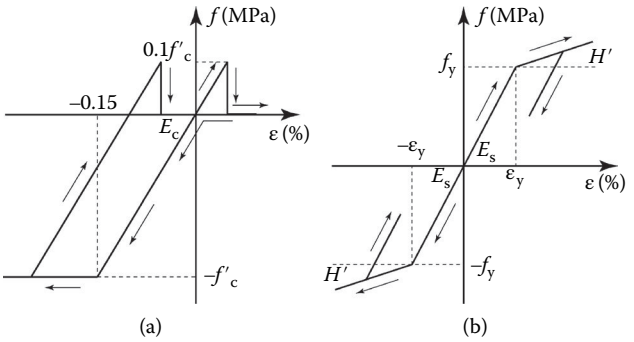

FIGURE 21.12 Stress–strain relationships for the materials: (a) Concrete; (b) steel.

observation that they exhibited no plastic deformation. The corresponding material properties are: Young's modulus $E_s = 206$ GPa (30,000 ksi); Poisson's ratio $\nu_s = 0.3$; and density $\rho_s = 7.85 \times 10^3$ kg/m^3 (490 lb/ft^3).

21.3.4 Comparisons between Numerical and Experimental Results

In order to confirm the applicability of the abovementioned numerical analysis method for RC beams under consecutive impact loading, numerical results for Series CL16 and TL*m*6 (*m* = 4, 5, and 6) are compared with the experimental results. In this section, the time histories of the impact force *P*, the reaction force *R*, and the deflection *D* at each loading step are compared.

21.3.4.1 Case of Series CL16

21.3.4.1.1 Time Histories of Dynamic Responses

Figure 21.13 shows the comparisons of time histories of the impact force *P*, the reaction force *R* and the deflection *D* obtained from numerical and experimental results for Series CL16. In Figure 21.13a, in which the impact forces up to 40 ms time intervals from the beginning of impact are displayed. It is observed that: (1) the temporal variations of the time histories obtained from numerical analysis and the impact test are similar for all cases of the impact velocity $V = 1$ m/s (3.3 ft/s) up to the final impact velocity $V = 6$ m/s (19.7 ft/s); but (2) the maximum impact forces from the numerical analysis are smaller than those from the experimental results.

Comparing the reaction forces *R* (Figure 21.13b), it may be seen that the low frequency components and time duration of the force time histories given by the numerical analysis are similar to those of the experimental results for all impact tests. However, the amplitudes of the high frequency components from the numerical analysis are higher than those from the experimental results.

The temporal variations of the deflection *D* are shown in Figure 21.13c. These time histories show the deflection response under each loading in the consecutive loading test. From this comparison, the numerical results of the maximum deflection, frequency characteristics during and after impacting, and the residual deflection, are in good agreement with the experimental ones.

From these comparisons, it is confirmed that: (1) the variations of time history of the impact force *P* and reaction force *R* can be approximately predicted by numerical analysis; but (2) the corresponding maximum values cannot be accurately predicted; and (3) the variations of the time history of the deflection *D* including the maximum deflection, the residual deflection and vibration frequency after unloading can be predicted satisfactorily for all cases of consecutive impact loading steps. For the evaluation of the accumulated damage under consecutive impact loading by means of the numerical analysis method, the maximum and residual deflections as well as the vibration characteristics after impacting are the most appropriate indicators.

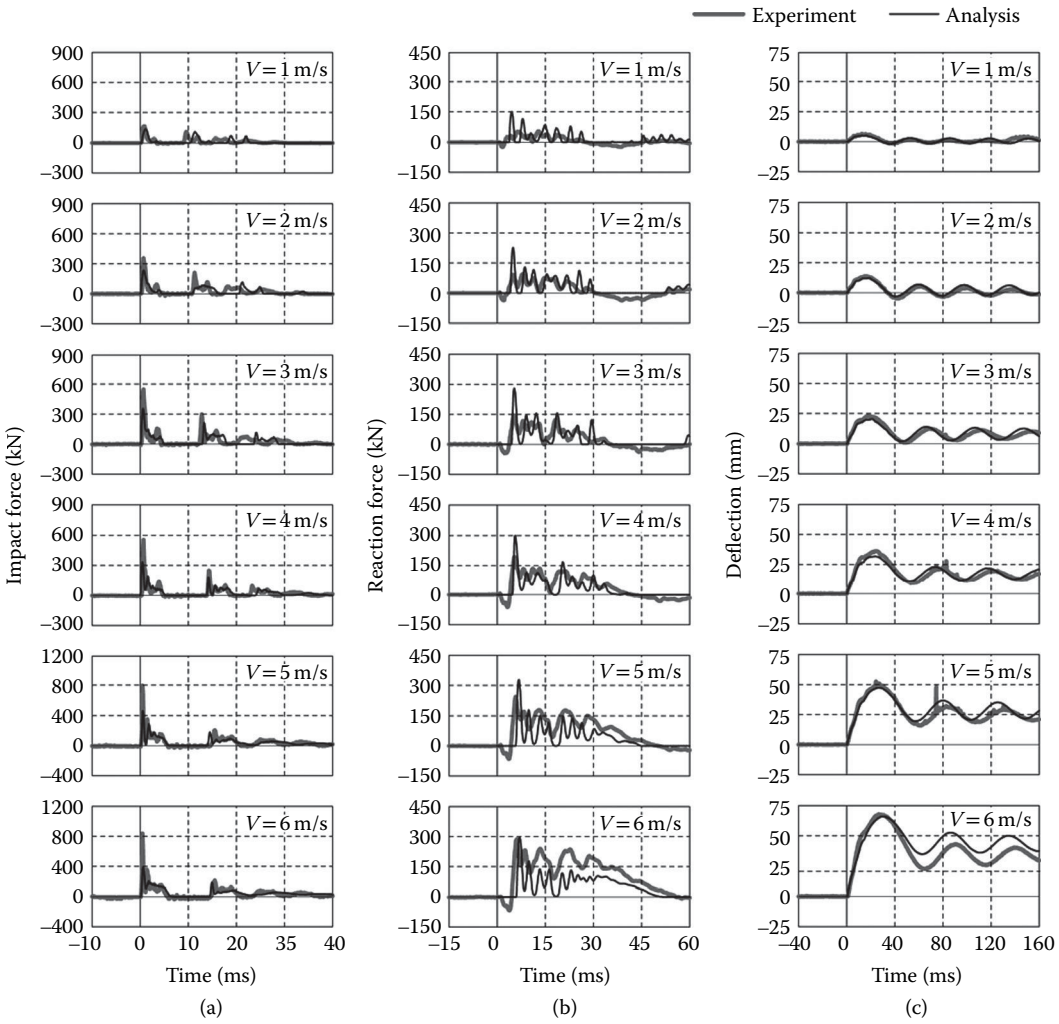

FIGURE 21.13 Comparison of results for Series CL16 (1 kN = 0.225 kips, 1 mm = 0.04 in, 1 m/s = 3.3 ft/s). (a) Impact force; (b) reaction force; (c) deflection.

21.3.4.1.2 Crack Patterns

When the tensile stress in the concrete element reached the cut-off value in the constitutive model shown in Figure 21.12a, the tensile stress was reduced to zero. Consequently, a maximum principal stress equal to zero was used to predict crack patterns.

Figure 21.14 shows comparisons between the crack patterns developed on the lateral surface of the beam after an experiment and the zero stress contours at the maximum deflection in a numerical analysis. The contour of zero stress is indicated in white with a range from –0.001 to 0.001 MPa (–0.0001 to 0.0001 ksi), in which cracks may occur in the element. Crack patterns observed in the experiment are indicated by black solid lines. From this figure, it is observed that: (1) a series of white elements develops vertically and toward the supports corresponding to an increase of the impact velocity V at $V = 1$ and 2 m/s (3.3 and 6.6 ft/s); (2) for the impact velocities of $V = 3$ and 4 m/s (9.9 and 13.1 ft/s), the white elements form not only vertical but also diagonal crack patterns; (3) the damage because of cracking evaluated by numerical analysis may be a little greater than that obtained experimentally under the first ($V = 1$ m/s, 3.3 ft/s) through to the fourth ($V = 4$ m/s, 13.1

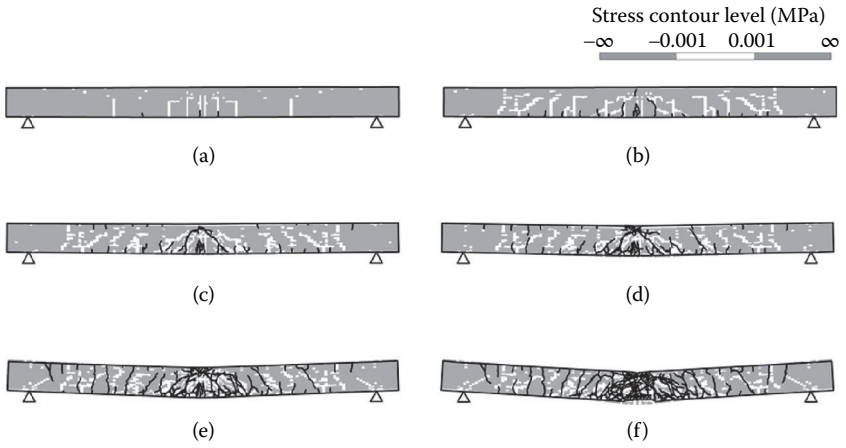

FIGURE 21.14 Crack patterns in Series CL16: (a) $V = 1$ m/s (3.3 ft/s); (b) $V = 2$ m/s (6.6 ft/s); (c) $V = 3$ m/s (9.9 ft/s); (d) $V = 4$ m/s (13.1 ft/s); (e) $V = 5$ m/s (16.4 ft/s); (f) $V = 6$ m/s (19.7 ft/s).

ft/s) impact loading; and (4) after the fourth impact loading, spalling of the upper and lower concrete cover cannot be simulated but the damage near the loading area can be better simulated by the proposed method.

21.3.4.2 Cases of Series TL*m*6

Here, the applicability of the method for analysis of the beam for the two loading cases near the ultimate impact velocity is discussed by comparing with the experimental results. The numerical analysis was conducted for three beams TL*m*6 ($m = 4$, 5, and 6).

21.3.4.2.1 Time Histories of Dynamic Responses

Figure 21.15 compares the time histories of the impact force P, the reaction force R and the deflection D for the three beams. The comparisons for the impact force P are shown in the figures in the left column of the figure. From this figure, it is observed that as in the results in the case of Series CL16, the development of the time histories obtained from numerical analysis are similar to those experimentally. However, the maximum amplitudes are underestimated by the analysis, irrespective of the magnitude of the impact velocity in the first loading.

Comparisons of the reaction force R are shown in the middle column of the figure. It is observed that in all cases, the amplitude of the low-frequency components and the time duration of the force can be better predicted but the maximum reaction force is overestimated in the numerical analysis.

However, regarding the comparison of deflections D shown in the right column of the figure, it is seen that the development of the time history, the maximum deflection, the residual deflection, and the vibration characteristics after impacting are in good agreement with the experimental results.

The maximum deflection, the residual deflection, and vibration characteristics after impacting may be the most appropriate indicators for evaluating the abovementioned damage. Thus accumulated damage and residual impact load-carrying capacity of the beams under consecutive impact loading would be accurately evaluated using the method outlined here.

21.3.4.2.2 Crack Patterns

Figure 21.16 shows the comparisons between crack patterns developed on the side surface of the beams and the maximum principal stress contours at the maximum deflection for each loading step in the three beams. In this figure, the elements with the zero stress contour indicated in white may be cracked

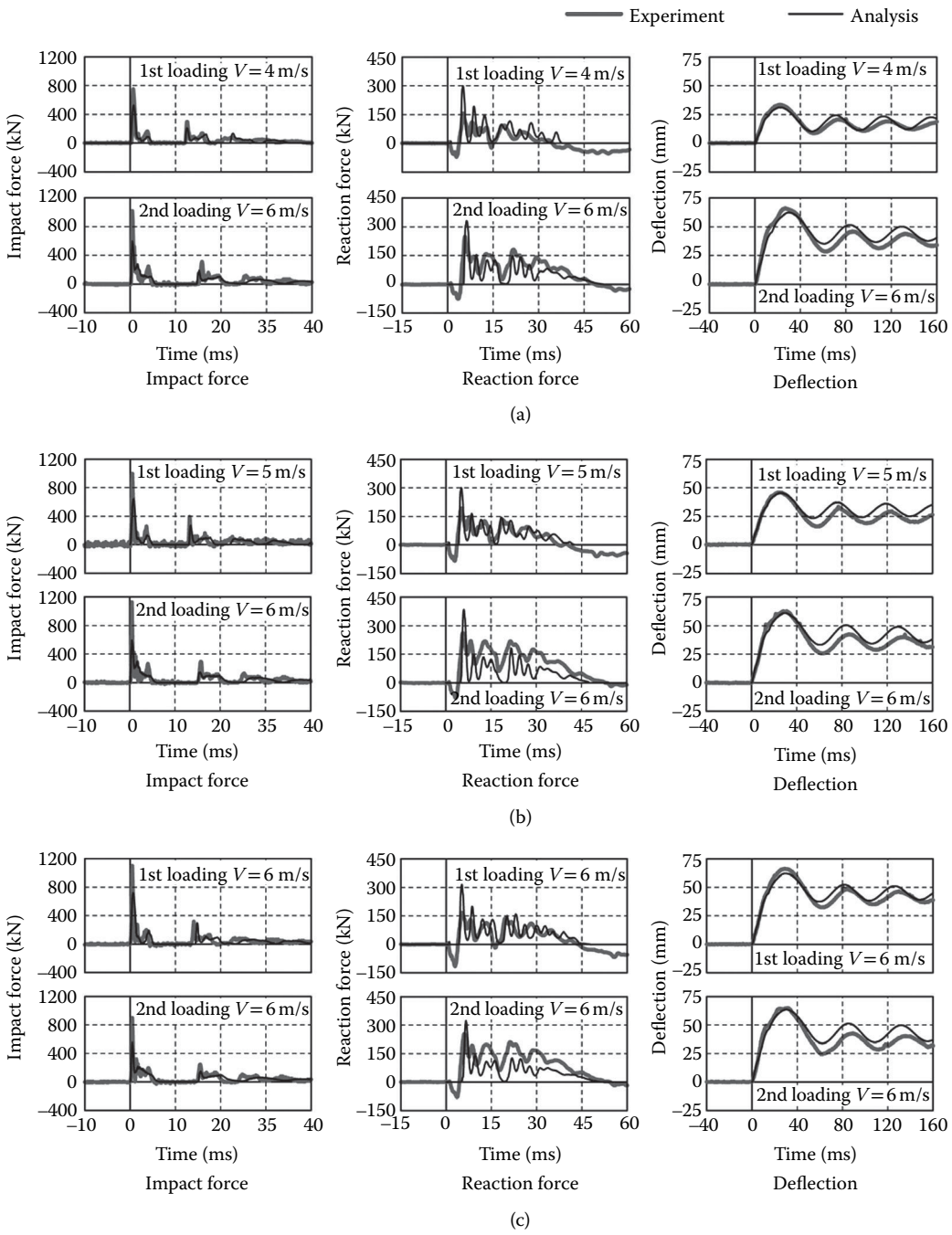

FIGURE 21.15 Comparison of results for Series TL*m*6 (m = 4, 5, and 6) (1 kN = 0.225 kips, 1 mm = 0.04 in, 1 m/s = 3.3 ft/s). (a) Beam TL46; (b) beam TL56; (c) beam TL66.

as with those shown in Figure 21.14. From this figure, it is observed that: (1) the flexural cracks are widely distributed and the diagonal cracks are formed near the loading area after the first impact loading; and (2) after the second impact loading, near the loading areas there is severe damage and some concrete blocks in the upper and/or lower concrete cover exhibited spalling. Numerically evaluated crack patterns are in good agreement with the experimental ones.

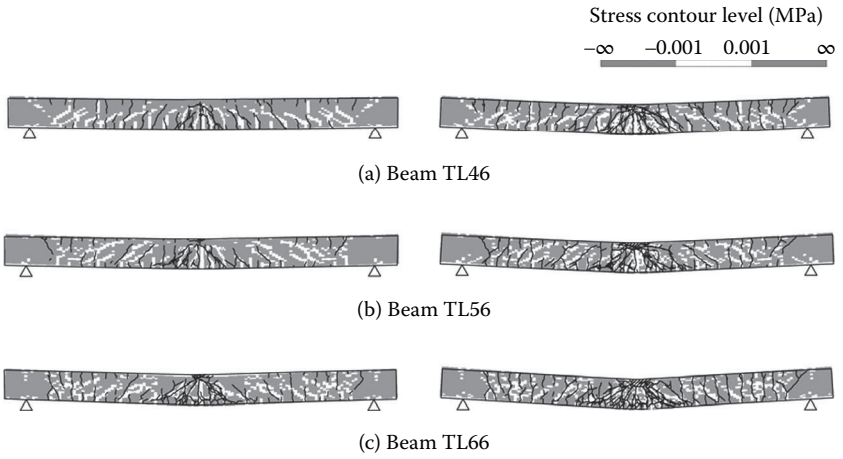

FIGURE 21.16 Crack patterns in Series TL*m*6 ($m = 4$, 5, and 6): (a) Beam TL46; (b) beam TL56; (c) beam TL66.

Thus, it can be confirmed that the crack patterns from these experimental results near the ultimate state can be approximately predicted using this method.

21.3.5 Remarks

The 3D elasto-plastic FE method of analysis presented in this section can be used to adequately evaluate the accumulated damage and residual load-carrying capacity of the RC beams under single and/or consecutive impact loading. The applicability of the method is confirmed by comparing with the results of two types of experiments: (1) consecutive falling-weight impact loading with gradually increasing impact velocity up to the beam reaching the ultimate state; and (2) two falling-weight impact loading cases around the beam reaching the ultimate state.

Then, when the RC beams are impacted singly and/or consecutively because of some objects, the damage level and residual load-carrying capacity can be easily evaluated by means of the numerical analysis method proposed in this section.

21.4 FE Analysis of Full-Scale Reinforced Concrete Girders under Impact Loading

21.4.1 Introduction

In Section 21.2, empirical formulae were derived for designing RC beams subjected to impact load, based on the falling-weight impact loading tests of RC beams. In Section 21.3, the numerical analysis method for the design and damage evaluation of RC beams under single and/or consecutive impact loading was described and the applicability of this analysis method was discussed by comparing with the experimental results. In these numerical analyses, the element size in the longitudinal direction of each element was kept close to 35 mm (1.4 in). However, it is not an easy task to numerically analyze full-scale RC girders using this elemental size, because very large matrices must be handled and the computation time for the numerical simulation rapidly increases.

One of the rational 3D FE analysis methods for accurately evaluating the dynamic response characteristics of the full-scale RC structures under impact loading is introduced by Kishi and Bhatti (2010). It is based on an equivalent tensile fracture energy concept, whose applicability is discussed numerically by comparing with the experimental results. The LS-DYNA code—Version 971 (Hallquist, 2007) was used for the numerical calculations.

21.4.2 Experimental Investigations

21.4.2.1 Dimensions and Static Design Values of Reinforced Concrete Girders

RC girders used for a full-scale falling-weight impact test have a rectangular cross section of 1 m (40 in) width and 0.85 m (34 in) depth. The clear span is 8 m (26.4 ft). The layout of the reinforcement and the measuring points are shown in Figure 21.17. Deformed steel bars of diameter of ϕ 29 mm (1.16 in) were used for axial reinforcement. The main reinforcement ratio is 0.64%. Axial reinforcement is welded to steel plates of 12 mm (0.48 in) thickness at the ends of the girder to reduce the anchoring length. Stirrups of diameter ϕ 13 mm (0.52 in) are placed every 250 mm (10 in), which is less than half of the effective depth of the girder following Japanese Concrete Standards (JSCE, 2005). The concrete cover is 150 mm (6 in).

To design the girder to reach the ultimate state in the flexural failure mode, the stirrups are arranged so as to increase the shear resistance. The static material properties of concrete and reinforcement during the experiment were given by a compressive strength of concrete $f_c' = 31.2$ MPa (4.5 ksi) and a yield stress $\sigma_y = 390$ MPa (56.6 ksi) and 401 MPa (58.1 ksi) for the stirrups and axial reinforcement, respectively.

The static flexural and shear resistances (P_{usc} and V_{usc}) for the girder are calculated according to the Japanese Concrete Standards (JSCE, 2005) as 621 kN (139.6 kip) and 1794 kN (403.3 kip), respectively. Therefore, the shear-bending capacity ratio α becomes 2.89 and the girder will be caused to collapse in the flexural failure mode statically.

21.4.2.2 Experimental Method

In the experiment, a 2000 kg (4.5 kip) weight was freely dropped from a prescribed height onto the midspan of the girder by using a release device. The weight is made of a steel outer shell of ϕ = 1 m (40 in) diameter, 97 cm (39 in) height, and a spherical base with $r = 80$ cm (32 in) radius as shown in Figure 21.18a. It was filled with steel balls and concrete to give a total mass of $M = 2000$ kg (4.5 kip). Figures 21.18b and c show the support with the load cells and a clamping device to prevent the ends of the girder from lifting off. The two supports are able to rotate freely, whereas they restrain horizontal movement. Figure 21.19 gives a pictorial view of the test setup. In this test, the impact force time history *P*, the reaction force time history *R*, and the deflection time histories *D*s were measured at six points along the girder from the midspan to the support. Each measuring point is shown in Figure 21.17.

Here, the residual deflection at the ultimate state of the girder was assumed to be 2% of the clear span length based on the test results of falling-weight impact tests for small-scale RC beams conducted by Kishi et al. (2000). Substituting the residual deflection (0.16 m, 6.4 in) and the static concentrate ultimate load-carrying capacity as $P_{usc} = 621$ kN (139.6 kips) estimated above into Equation 21.4 derived in Section 21.2, input impact energy was estimated as $E_{kd} = 237$ kJ (174.9 kips·ft) based on this result, the height of falling weight was chosen as 10 m (33 ft), which produces an estimated input impact energy of 196 kJ (144.6 kips·ft).

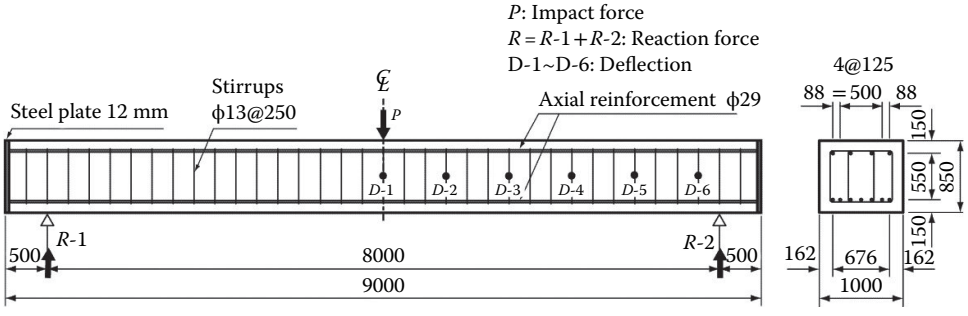

FIGURE 21.17 Dimensions of full-scale RC girder, layout of reinforcement, and measuring points (1 mm = 0.04 in).

(a) (b) (c)

FIGURE 21.18 Pictorial views of weight and supporting device: (a) View of weight; (b) supporting device; (c) device for preventing girder's end from lifting off.

FIGURE. 21.19 Pictorial view of falling-weight impact test of full-scale RC girder.

The impact force P was estimated by measuring the deceleration of the weight. Therefore, a strain gauge-type accelerometer is attached to its top surface, in which the capacity is 1000 times gravity and a range of measuring frequency up to 7 kHz. Each load cell for measuring the reaction force R has a capacity of 1500 kN (337.2 kips) and a measuring frequency of more than 1 kHz. Dynamic deflections Ds of the girder were measured using laser-type LVDTs, which have a maximum stroke of 200 mm (8 in) and a range of measuring frequency up to 915 Hz.

21.4.3 Summary of Test Results

Figure 21.20 shows the time histories of the experimental results of the impact force P, the reaction force R measured at one of the supports, and the deflections (D-1–D-6). In these figures, the origin of the time axis is taken as the time when the weight impacted with the girder. The positive responses are assumed to be the same as those in the case of static loading. Figures 21.20a and b show the impact force time history P, in which Figure 21.20a gives an expanded time history at 8 ms time interval focusing on the first dominant response at the beginning of impact, and Figure 21.20b shows the results at a 100 ms time interval considering an amplitude up to 1 MN (224.8 kips). From these figures, it is observed that the response exhibits the time history of a half-sine shape with approximately 3.5 ms time duration and 11.7 MN (2630 kips) maximum amplitude, and after that high frequency components

alternating in both positive and negative directions are excited for approximately 20 ms. However, since the impact force excited in the weight is because of the reaction against the impact force by the girder, negative components of the impact force may not actually occur under falling-weight impact. This suggests that the high frequency components of the force shown in Figure 21.20b may not be those of the true impact force, but may be because of the elastic wave traveling through the weight. After that, the response has the time history of two half-sine shapes of approximately 10 ms time duration, followed by a half-sine shape of 35 ms time duration and a damped sine shape with a period of approximately 8–10 ms. Finally, the time history of the impact force reaches zero amplitude after 80 ms from the beginning of impact.

Figure 21.20c shows the reaction force time histories *R* measured at a support. From this figure, it can be observed that a response with high amplitude is excited over approximately 80 ms from the beginning of impact. This implies that this response is excited by a falling-weight impacting against the girder because the duration is almost the same to that of the impact force. The reaction force time history *R* exhibits a half-sine shape of approximately 70 ms time duration and a damped sine shape of approximately 8–10 ms period as for the impact force time history *P* mentioned above, and after 80 ms elapsed time the girder changed to a state of the negative loading.

Figure 21.20d shows all deflection time histories *D*s measured here. Focusing on the configurations of the time histories during 100 ms from the beginning of impact, it is shown that the amplitude of the time histories decrease and become more damped with distance from the mid-span. Comparing with the configuration of the reaction force time history *R* (Figure 21.20c), it can be seen that the periods of the low-frequency component are very similar.

Figure 21.21 shows the crack pattern sketched after the experiment. Focusing on the damaged area near the lower concrete cover around the midspan, not only flexural but also shallow-angled diagonal cracks have clearly developed. Cracks developed vertically from the upper to the lower edge are also observed. This may be because of the following two reasons: (1) when the flexural vibration

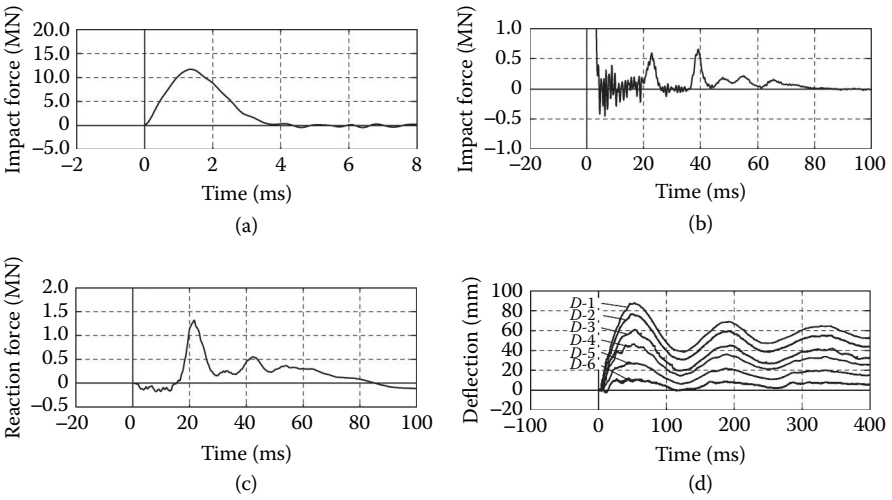

FIGURE 21.20 Time histories of responses obtained from experimental results (1 MN = 225 kips, 1 mm = 0.04 in). (a) Impact force (initial impact). (b) impact force (second waveform 100 ms); (c) reaction force for one support; (d) deflection.

FIGURE 21.21 Crack patterns on the side-surface of RC girder after experiment.

propagates toward the supports at the beginning of impact, the area near the supports behaves like a fixed end; and (2) horizontal tensile reaction forces may occur as soon as the girder deflects because the girder's supports are fixed not only vertically but also horizontally by the cross beams as shown in Figure 21.18c.

21.4.4 Numerical Analysis

21.4.4.1 Numerical Modeling

The RC girder is modeled in 3D for numerical analysis similar to that for small-scale RC beams mentioned in Section 21.3. Figure 21.22a shows a control analysis model of the RC girder. Here, because of the two axes of symmetry, only one quarter of the girder was modeled. Figure 21.22b shows the FE model for axial reinforcement and stirrups cast in the girder. These are modeled using beam elements of equivalent flexural stiffness, cross sectional area, and mass. These elements are assumed to be perfectly bonded to the concrete elements. All other components are modeled using an eight-node solid element.

A 2000 kg (4.5 kip) weight is modeled accurately following the real shape and assuming material properties of steel except its density. The density is evaluated by dividing the mass (2000 kg, 4.5 kip) by the volume of the weight. The supporting apparatus with the load cells and a clamping device for preventing the girder from lifting off are also accurately modeled. The number of integration points for solid and beam elements is one and four, respectively. In total, approximately 39,000 nodal points and 35,000 elements are used for modeling the whole structure.

Contact surface elements are defined in order to take into account the interaction between the girder and the bottom surface of the falling weight as well as between the girder and the support elements. These elements can treat contact, detachment, and sliding of two adjacent elements, in which the contact force can be estimated by applying the penalty method to the contact surfaces. Friction between the contact elements is ignored.

The girder is analyzed by inputting a predetermined impact velocity for whole elements of the weight and the gravity is considered for only the elements of the weight. The impact velocity is set to $V = 14$ m/s (45.9 ft/s), which is obtained by assuming a free fall from the height of 10 m (33 ft). The damping factor is set to $h = 1.5\%$ based on the preanalysis results. The numerical analysis is performed for a time period of 400 ms from the beginning of impact up to the girder reaching a steady vibration state.

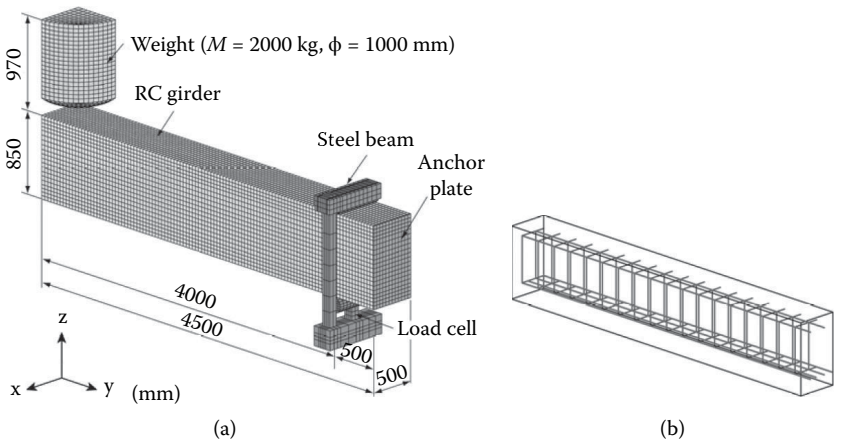

FIGURE 21.22 FE model for control analysis (1 mm = 0.04 in, 1 kg = 2.25 lb). (a) FE model; (b) layout of reinforcement.

21.4.4.2 Mesh Geometry for Control Analysis Model

The control analysis model was based on the numerical investigations for prototype RC girder conducted by Kishi et al. (2006). It suggests that a rectangular solid element should be used for concrete elements and its element size in the span direction should be 40–50 mm (1.6–2 in) long.

Describing the control analysis model in detail, the mesh geometry of the girder in the sectional direction is composed of (1) in the vertical direction, 12 elements for concrete between the upper and lower axial rebars (mesh size is 48.75 mm [2 in] for each element) and 4 elements (mesh size is 37.5 mm [1.5 in] for each element) for concrete cover so as to keep the element size between 40 and 50 mm [1.6–2 in]; and (2) in the horizontal direction, 4 elements for side concrete cover (mesh size is 48.75 mm [2 in] for each element) and 2–3 elements (mesh size is 40.5 mm [1.6 in] for each element) for concrete between two adjoining axial rebars for total 7 axial rebars.

In the span direction, in order to better simulate an interaction between RC girder and steel beams installed for preventing the ends of the girder from lifting up, an interval (250 mm [10 in] long) of stirrups for the inside and outside of the support was divided into 7 elements (mesh size in the span direction is 35.7 mm [1.4 in] long), respectively, irrespective of the magnitude of mesh size varied in the central area of the RC girder for investigating the applicability of the introduced method here. The central area of the RC girder except the supporting area was divided into 7 elements for each interval of stirrups for controlled mesh geometry, which is 35.7 mm (1.4 in) long.

21.4.4.3 Modeling of Materials

The stress–strain relationships for concrete and reinforcement are assumed to be similar to those defined in Section 21.3 (see Figure 21.12).

For concrete, a bilinear model on the compression side and a cut-off model on the tension side were applied. It is assumed that: (1) the yield stress is equal to the compressive strength f_c'; (2) the concrete yields at 0.15% strain; (3) the tensile stress vanishes when an applied negative pressure reaches the tensile strength f_t of concrete; and (4) the tensile strength f_{t0} is 10% of the compressive strength f_c' for the control analysis model. Yielding of concrete is according to Drucker-Prager's yield criterion (Chen, 1982).

For axial reinforcement and stirrups, a bilinear isotropic hardening model is applied. The plastic hardening modulus H' is assumed to be 1% of the elastic modulus E_s (E_s: Young's modulus of steel). Yielding of the reinforcement is based on the von Mises yield criterion.

Falling weight, supporting devices, load cells, and anchor plate are assumed to be elastic materials according to the experimental observations, because no plastic deformation was observed in them. Their material properties: Young's modulus E_s, Poisson's ratio ν_s, and density p_s are assumed as $E_s = 206$ GPa (30,000 ksi), $\nu_s = 0.3$, and $\rho_s = 7.85 \times 10^3$ kg/m^3, respectively.

21.4.5 Tensile Fracture Model of Concrete Element

21.4.5.1 Outline

In the case of FE numerical analysis for RC girders under impact loading, so far the influence of the element size of concrete on dynamic response characteristics of the girders has been investigated by varying the magnitude of the element size keeping the material properties constant. However, focusing on the tensile strength of concrete when applying the smeared crack model, it is assumed that for concrete elements of large size in the span direction: (1) the surcharged load at crack initiation may be increased corresponding to the magnitude of the element size because the tensile fracture energy of the element also increases; and (2) the total strain energy accumulated in the element tends to be underestimated as also the damage level compared to the true value because the stresses acting in the element tend to be smoothed out.

In order to improve on such drawbacks when using large size concrete elements, it is proposed to make the fracture strain energy for large size elements equivalent to that of the control concrete element. The concept of such a tensile fracture model for a concrete element is described in detail below.

21.4.5.2 Equivalent Tensile Fracture Energy Concept

Emphasizing the numerical impact response analysis of the prototype RC girders, it can be assumed that the cracks are almost uniformly developed across the width. Therefore, the problem is to be able to adequately evaluate crack distributions in the span direction.

A rectangular concrete block element of arbitrary size x, y, and z in the width, span, and depth directions, respectively, is considered as shown in Figure 21.23a. In this element, it is assumed that: (1) a continuous crack parallel to the zx plane occurs as shown in Figure 21.23b; (2) the crack is because of the same tensile fracture energy irrespective of the magnitude of the element size in the y direction; and (3) the tensile fracture energy is estimated by using the tensile strain energy accumulated in the concrete element. Since a discrete crack model was not applied here, when the strain energy accumulated in the concrete element reaches the value of the tensile fracture energy, it can be assumed that a smeared crack occurs in the whole of the element and the tensile stress cannot be transferred.

Here, this concept will be explained in detail by applying it to the rectangular concrete block elements in the 1D stress state. It is assumed that: (1) the control concrete element has the dimensions x_0, y_0, and z_0 in the x, y, and z directions, respectively, as shown in Figure 21.23c; and (2) an arbitrary element i has the arbitrary length of y_i in the y direction as shown in Figure 21.23d. Assuming that a continuous crack parallel to the zx plane occurs in the control element as shown in Figure 21.23c, the tensile fracture energy G_f of the element can be represented by considering a linear stress–strain relationship as follows:

$$G_f = \frac{f_{t0}\varepsilon_{t0}}{2} V_0 \tag{21.6}$$

where f_{t0}, ε_{t0}, and V_0 are the tensile strength of concrete, the ultimate tensile strain, and the volume of the control element, respectively.

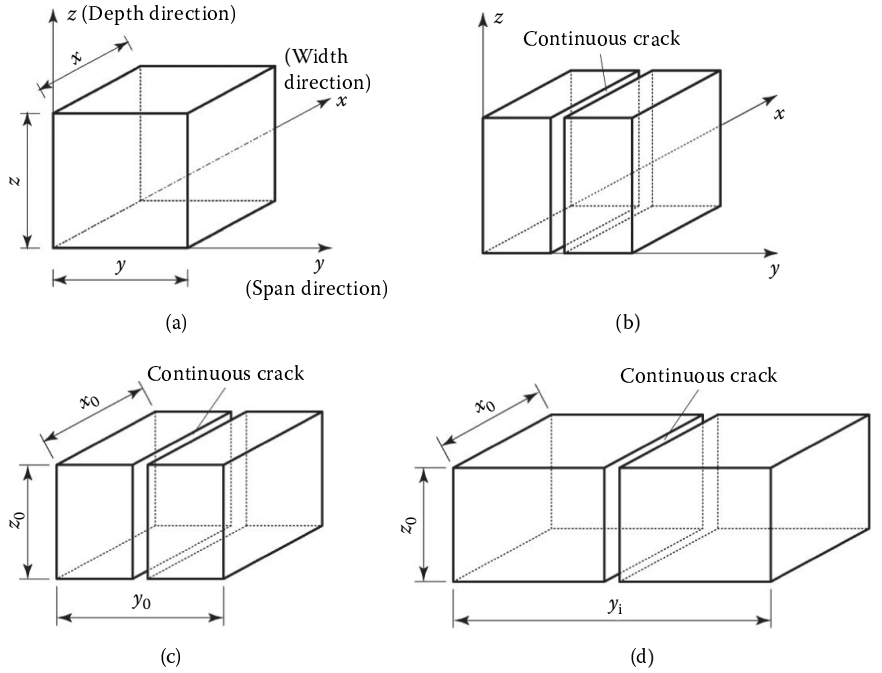

FIGURE 21.23 Continuous crack model in a concrete element. (a) Concrete model; (b) continuous crack model; (c) crack model of control element; (d) crack model of element i with arbitrary length y_i.

According to the relationship between equivalent stress and strain for the concrete element as shown in Figure 21.23a, the ultimate tensile strain ε_{t0} of the control element can be represented using the tensile strength f_{t0} and Young's modulus E_c of concrete as follows:

$$\varepsilon_{t0} = \frac{f_{t0}}{E_c} \tag{21.7}$$

The volume of the control element is given as

$$V_0 = x_0 y_0 z_0 \tag{21.8}$$

Substituting Equations 21.7 and 21.8 into Equation 21.6, the tension fracture energy G_f of the control element can be simplified as

$$G_f = \frac{f_{t0}^2}{2E_c} x_0 y_0 z_0 \tag{21.9}$$

Here, assuming that a single continuous crack parallel to the *zx* plane occurs in element *i* as well as in the control element, the tensile fracture energy of element *i* must be set to be equal to that of the control element. Therefore, setting a fictitious tensile strength of element *i* as f_{ti}, the following equation can be formulated

$$\frac{f_{t0}^2}{2E_c} x_0 y_0 z_0 = \frac{f_{ti}^2}{2E_c} x_0 y_i z_0 \tag{21.10}$$

Thus, the fictitious tensile strength f_{ti} of element *i* can be obtained as

$$f_{ti} = f_{t0} \sqrt{\frac{y_0}{y_i}} \tag{21.11}$$

Equation 21.11 shows that using element *i* instead of the control element, inputting the fictitious tensile strength of concrete f_{ti}, a crack occurs in element *i* as soon as the same tensile fracture energy is reached as in the control element.

21.4.6 Applicability of the Equivalent Tensile Fracture Energy Concept

21.4.6.1 Analytical Cases

Here, the applicability of the numerical analysis method using fictitious tensile strength for the concrete elements will be discussed by comparing with the experimental results for the full-scale RC girder mentioned above.

In the proposed method, the intervals of stirrups (250 mm, 10 in) are divided into 1, 3, 5, and 7 elements, respectively, which are listed in Table 21.4. In this table, the digit following the notation "MS" represents the approximate value (millimeter unit) of the element size in the span direction and the hyphenated notations "*N*" and "G_f" represent the cases using the normal and fictitious tensile strengths for the concrete elements, respectively.

From this table, it is shown that the total number of nodal points and/or elements in the case MS250 is less than one-third of that in the case MS35. In each case the fictitious tensile strength for the concrete element is listed in Table 21.5. From this table, it can be confirmed that the fictitious tensile strength of the concrete for the case MS250-G_f is 1.2 MPa (0.17 ksi) and is less than half that of MS35-G_f. The side-view of the mesh geometry for each analysis model is shown in Figure 21.24.

TABLE 21.4 List of Numerical Analysis Cases

Analysis case	Element size of concrete in span direction mm (in)	Total no. of elements	Total no. of nodal points
MS250-N/G_f	250.0 (10)	12,757	11,234
MS83-N/G_f	83.3 (3.3)	21,493	18,914
MS50-N/G_f	50.0 (2)	29,593	26,456
MS35-N/G_f	35.7 (1.4)	38,875	34,832

TABLE 21.5 Details of Tensile Strength for Concrete Element

Analysis case	Assumed tensile strength MPa (ksi)	Remarks
MS250-N	3.12 (0.45)	Without G_f concept
MS83-N		
MS50-N		
MS35-N		
MS250-G_f	1.18 (0.17)	With G_f concept
MS83-G_f	2.04 (0.30)	
MS50-G_f	2.64 (0.38)	
MS35-G_f	3.12 (0.45)	

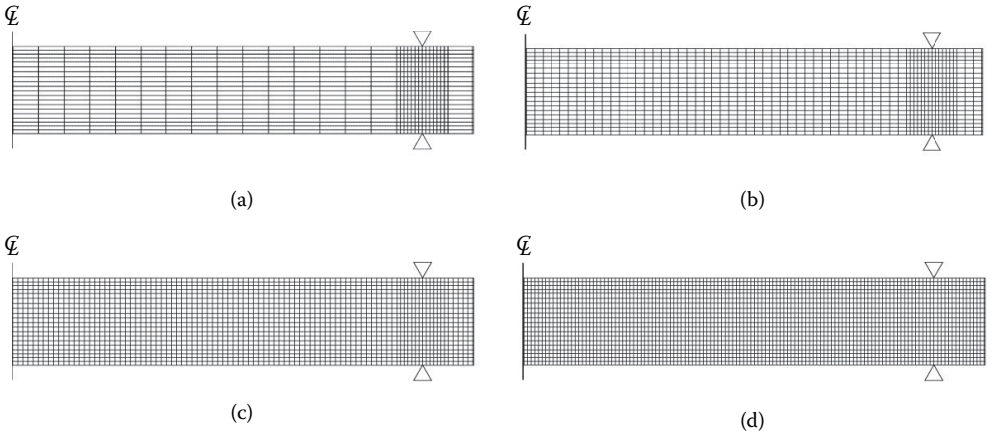

FIGURE 21.24 FE numerical analysis models: (a) MS250-N/G_f; (b) MS83-N/G_f; (c) MS50-N/G_f; (d) MS35-N/G_f.

21.4.6.2 Comparison of Numerical Results in Case MS250 with/without G_f Concept

In order to investigate the practical applicability of the equivalent tensile fracture energy concept (hereinafter, G_f concept), numerical results obtained using each element size in the span direction listed in Table 21.4 are compared with the experimental results. Figure 21.25 shows the comparisons of the time histories of the impact force P, reaction force R at one of the supports, and the deflections at D-1/2 in the case MS250, in which P, R, and Ds are compared for the durations of 10 ms, 100 ms, and 400 ms, respectively, from the beginning of impact. From these comparisons, the following results were obtained: (1) the influence of the tensile fracture energy accumulated in the concrete element on the impact force time history P may not be significant; (2) if the G_f concept is not applied, the reaction force R is excited having a half sine shape time history with large amplitude and short duration time at the beginning of impact, and the duration of the main response is almost half that of the test

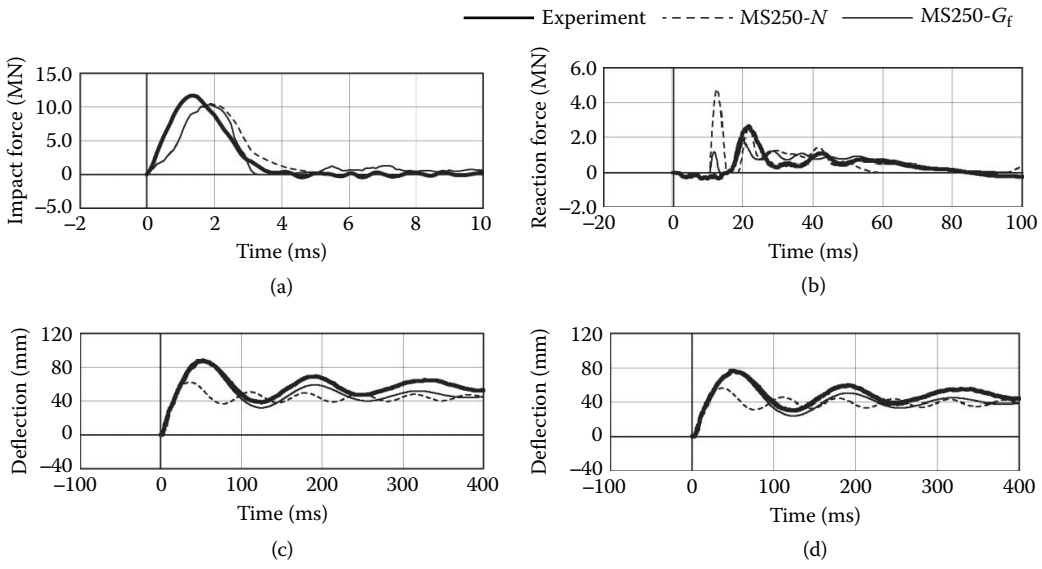

FIGURE 21.25 Comparisons between numerical and experimental results in case MS250 (1 MN = 225 kips, 1 mm = 0.04 in). (a) Impact force; (b) reaction force; (c) deflection at *D*-1; (d) deflection at *D*-2.

results; and (3) however, if the G_f concept is applied, the amplitude and duration of the main response of the force are similar to those of the experimental results. From the comparisons of deflection time histories *D*s (Figures 21.25c and d), it can be observed that if the G_f concept is not applied, the maximum amplitude of each time history is 25% less than that of the experimental results and the vibration period for the free vibration after unloading is almost half that of the test values. It suggests that the damage to the girder is underestimated. However, if the G_f concept is applied, it is shown that the maximum amplitude and the vibration period for the free vibration are in good agreement with the experimental results.

21.4.6.3 Comparison of Numerical Results in Cases Applying the G_f Concept

Figure 21.26 shows the comparisons between the numerical results for all cases applying the G_f concept and the experimental results. From Figure 21.26a, it can be observed that the variations of the impact force time history *P* are similar to those of the experimental results irrespective of the magnitude of the element size in the span direction. However, the slope of the curve at the beginning of impact is slightly smaller than that of the experimental results as mentioned above. The maximum amplitude of the impact force *P* in the case MS250-G_f is the closest to that of the experimental results for all the cases considered here.

From Figure 21.26b, it is shown that the variations of the reaction force time history *R* are similar for all four cases. Comparing with the experimental results, even though the incidence time of the positive reaction force is approximately 5 ms earlier than that of the experimental results, the amplitude and duration of the main response can be better simulated by applying the G_f concept.

From Figures 21.26c and d for the comparisons of the deflection time histories at *D*-1/2, it can be confirmed that: (1) the maximum deflection, the residual deflection, and the amplitude and period of free vibration after unloading in all the cases considered here are similar to those of the experimental results; and (2) since the numerical results in the case MS250-G_f give similar variations of the time histories to those obtained in the case MS35-G_f, the accuracy of the numerical results using the coarse mesh (250 mm, 10 in) can be ensured by inputting the fictitious tensile strength for the concrete elements based on the G_f concept.

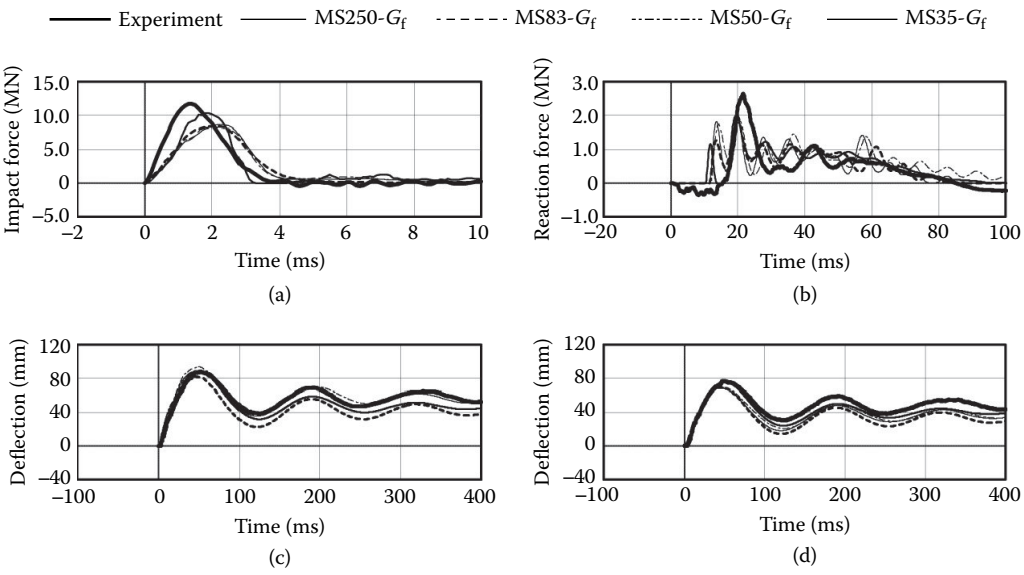

FIGURE 21.26 Comparisons between numerical results for all cases with G_f concept and experimental results (1 MN = 225 kips, 1 mm = 0.04 in). (a) Impact force; (b) reaction force; (c) deflection at *D*-1; (d) deflection at *D*-2.

21.4.7 Remarks

The modified method for the tensile strength of the concrete elements based on an equivalent tensile fracture energy concept (G_f concept) allowing the use of a coarse mesh presented in this section can be used to accurately estimate the dynamic response characteristics of the full-scale RC girders under impact loading. Its applicability is confirmed by comparing the numerical results with the experimental results for a full-scale RC girder under falling-weight impact loading. Applying the G_f concept, the total number of nodes can be decreased to less than one third of that for the control model.

References

Ando, T., Kishi, N., Mikami, H., Sato, M., and Matsuoka, K. G. 1999. Experimental study on impact resistance of bending failure type of RC beams, *Proceedings of the 7th East Asia-Pacific Conference on Structural Engineering & Construction*, Kochi, Japan, pp. 1075–1080.

ASTRA. 2008. *Einwirkungen infolge Steinschlags auf Schutzgalerien, Richtlinie, Bundesamt fur Strassen*, Baudirektion SBB, Eidgenossische Drucksachen- und Materialzentrale, Bern, Switzerland.

Banthia, N. P., Mindess, S., and Banter, A. 1987. Impact behavior of concrete beams, *Materials and Structures*, 20(4), 293–302.

Chen, W. F. 1982. *Plasticity in reinforced concrete*, McGraw-Hill, New York, NY.

Delhomme, F., Mommesin, M., Mougin, J. P., and Perrotin, P. 2005. Behavior of a structurally dissipating rock-shed: experimental analysis and study of punching effects, *International Journal of Solids and Structures*, 42, 4203–4219.

Ghadimi Khasraghy, S., Kishi, N., and Vogel, T. 2009. Numerical Simulation of Consecutive Impacts on Reinforced Concrete Slabs, *Sustainable Infrastructure*, *33rd IABSE Symposium*, Bangkok, Thailand, 218–219.

Hallquist, J. O. 2007. *LS-DYNA Version 971 User's Manual*, Livermore Software Technology Corporation, Livermore, CA.

JRA. 2000. *Design Guideline for Anti-Impact Structures Against Falling Rocks*, Japan Road Association, Tokyo, Japan (in Japanese).

JSCE. 2004. *Practical methods for impact tests and analysis, Structural Engineering Series* 15, Japan Society of Civil Engineers, Tokyo, Japan (In Japanese).

JSCE. 2005. *Structural Performance Verification, Standard Specification for Concrete Structures-2002,* Japan Society of Civil Engineers, Tokyo, Japan.

Kaewunruen, S., and Remennikov, A. M. 2009. Progressive failure of prestressed concrete sleepers under multiple high-intensity impact loads, *Journal of Engineering Structures*, 31, 2460–2473.

Kishi, N., and Bhatti, A. Q. 2010. An equivalent fracture energy concept for nonlinear dynamic response analysis of prototype RC girders subjected to falling-weight impact loading, *International Journal of Impact Engineering*, 37, 103–113.

Kishi, N., Ghadimi Khasraghy, S., and Kon-No, H. 2011. Numerical simulation of reinforced concrete beams under consecutive impact loading, *Structural Journal*, ACI, 108-S42, 444–452.

Kishi, N., Konno, H., Ikeda, K., and Matsuoka, K. G. 2002. Prototype impact tests on ultimate impact resistance of PC rock-sheds, *International Journal of Impact Engineering*, 27, 969–985.

Kishi, N., Mikami, H., Matsuoka, K. G., and Ando, T. 2000. An empirical impact resistant design formula of RC beans with statically bending failure mode, *Journal of JSCE*, 647/I-51, 177–190 (in Japanese).

Kishi, N., Mikami, H., Matsuoka, K. G., and Ando, T. 2002. Impact behavior of shear-failure-type RC beams without shear rebar, *International Journal of Impact Engineering*, 27, 955–968.

Kishi, N., Ohno, T., Konno, H., and Bhatti, A. Q. 2006. Dynamic response analysis for a large scale RC girder under a falling weight impact loading, *Proceedings of an International Conference on Advances in Engineering Structures, Mechanics & Construction*, University of Waterloo, Ontario, Canada, pp. 99–109.

Kishi, N. and Mikami, H. 2012. Empirical formulas for designing reinforced concrete beams under impact loading, *Structural Journal*, ACI, 109–4, 509–519.

Kon-No, H., Yamaguchi, S., Nishi, H., Kishi, N., and Kurihashi, Y. 2010. Falling-weight impact test for 2/5 scale model of rockfall protection gallery with/without sand cushion, *Proceedings of 3rd Euro-Mediterranean Symposium on Advances in Geomaterials and Structures*, Djerba, Tunisia, Vol. 2, pp. 355–360.

May, I. M., Chen, Y., Owen, D. R. J., Feng, Y. T., and Bere, A. T. 2005. Experimental testing and finite element simulation of the behavior of reinforced concrete beams under impact loading, *Proceedings of VIII International Conference on Computational Plasticity,* Barcelona.

Nishi, H., Kon-No, H., Ishikawa, H., Okada, S., and Kishi, N. 2009. Experimental study on impact resistant behavior of full-scale arch type RC structures without cushion materials, *Proceedings of 3rd International Workshop of Performance, Protection & Strengthening of Structures under Extreme Loading*, Hayama, Japan, CD-ROM.

Schellenberg, K., Volkwein, A., Roth, A., and Vogel, T. 2007. Large-scale impact tests on rock fall galleries, *Proceedings of 7th International Conference on Shock & Impact Loads on Structures,* Beijing, pp. 497–504.

Sugano, T., Tsubota, H., Kasai, Y., Koshika, N., Ohnuma, H., von Riesemann, W. A., Bickel, D. C., and Parks, M. B. 1993. Local damage to reinforced concrete structures caused by impact of aircraft engine missiles Part 1. Test program, *Nuclear Engineering and Design*, 140, 387–405.

Tachibana, S., Masuya, H., and Nakamura, S. 2010. Performance based design of reinforced concrete beams under impact, *Journal of Natural Hazards and Earth System Sciences,* 10(6), 1069–1078.

Zineddin., M., and Krauthammer, T. 2007. Dynamic response and behavior of reinforced concrete slabs under impact loading, *International Journal of Impact Engineering*, 34, 1517–1534.

22

Wind Effects on Long-Span Bridges

Steve C. S. Cai
Louisiana State University

Wei Zhang
University of Connecticut

Serge Montens
Jean Muller International

22.1 Introduction

The development of modern materials and construction techniques has resulted in a new generation of light weight flexible structures. Such structures are usually susceptible to the action of winds. Suspension bridges and cable-stayed bridges shown in Figure 22.1 are typical structures susceptible to wind-induced problems.

The most renowned bridge collapse because of winds is the Tacoma Narrows suspension bridge linking the Olympic Peninsula with the rest of the state of Washington. It was completed and opened to traffic on July 1, 1940. Its 853 m (2799 ft) main suspension span was the third longest in the world. This bridge became famous for its serious wind-induced problems that began to occur soon after it opened. "Even in winds of only 3 to 4 miles per hour, the center span would rise and fall as much as four feet..., and drivers would go out of their way either to avoid it or cross it for the roller coaster thrill of the trip. People said you saw the lights of cars ahead disappearing and reappearing as they bounced up and down. Engineers monitored the bridge closely but concluded that the motions were predictable and tolerable" (Berreby, 1992).

On November 7, 1940, four months and six days after the bridge was opened, the deck oscillated through large displacements in the vertical vibration modes at a wind velocity of about 68 km/h. The motion changed to a torsional mode about 45 minutes later. Finally, some key structural members became overstressed and the main span collapsed.

Some bridges were destroyed by wind action before the failure of the Tacoma Narrows Bridge. However, it was this failure that shocked and intrigued bridge engineers to conduct scientific investigations of bridge aerodynamics. Some existing bridges, such as the Golden Gate suspension bridge in California

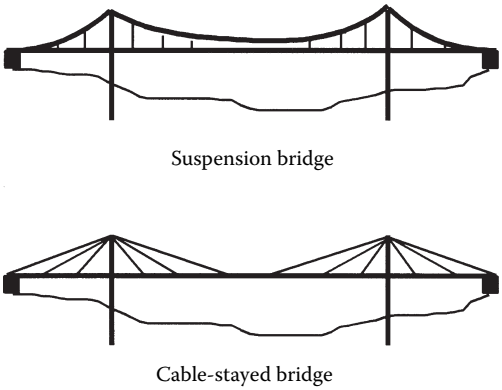

FIGURE 22.1 Typical wind-sensitive bridges.

with a main span of 1280 m (4200 ft), also experienced large wind-induced oscillations, though not to the point of collapse. In 1953, the Golden Gate Bridge was stiffened against aerodynamic action (Cai, 1993).

Following the earlier research work from Farquharson, Bleich, and Theodorsen on investigations on bridge aerodynamics after the collopas of Tacoma Narrows Bridge, Pugsley suggested a framework for the introduction of measured aerodynamic forces into the bridge flutter problem (Miyata, 2003). These research works led thereafter to the development of long-span bridge projects in Europe, for instance, the Forth Bridge in 1964 with the main span of 1006 m (3300 ft) and Severn Bridge in 1966 with the main span of 988 m (3240 ft). After the pioneering work of Davenport and Scanlan on bridge aerodynamics, it is possible to build bridges with larger main spans. Multiple long-span bridges were built in the Honshu-Shikoku Bridges project in Japan from 1980s, for instance, the Akashi Kaikyo Bridge in 1998 with the main suspension span of 1991 m (6532 ft) and the Tatara Bridge in 1999 with the main cable-stayed span of 890 m (2920 ft). More long-span bridges were built in China from 1990s, for instance, the Xihoumen Bridge in 2009 with the main suspension span of 1650 m (5414 ft), Runyang Bridge in 2005 with the main suspension span of 1490 m (4888 ft) and the Sutong Bridge in 2008 with the main cable-stayed span of 1018 m (3340 ft) (Hui and Yau, 2011, Xiang and Ge, 2009). In other countries, there was also some long-span bridges built within the past 20 years, for instance, the Pont de Normandie in 1995 with the main cable-stayed span of 856 m (2808 ft) in France and the Great Belt Bridge in 1998 with the main suspension span of 1624 m (5328 ft) in Denmark.

Wind-induced vibration is one of the main concerns in a long-span bridge design. With more long-span bridges being built with larger span lengths, more challenges have to be solved toward building more reliable infrastructures. This chapter will give a brief description of wind-induced bridge vibrations, experimental and theoretical solutions, and state-of-the-art applications.

22.2 Wind Field Modeling

22.2.1 Velocity Profiles

The atmospheric wind is caused by temperature differentials resulting from solar radiations. When the wind blows near the ground, it is retarded by obstructions making the mean velocity at the ground surface zero. This zero-velocity layer retards the layer above and this process continues until the wind velocity become constant. The distance between the ground surface and the height of constant wind velocity varies between 300 m and 1 km. This one kilometer layer is referred to as the boundary layer. Owing to the surface roughness and atmospheric stability, the wind profile of the atmospheric boundary layer usually follows a logarithmic or exponential law. The equations to estimate the wind speed (u) at height z (meters) above the ground for logarithmic and exponential law are listed as the following, respectively.

Logarithmic law:

$$u_z = \frac{u_*}{\kappa}\left[\ln\left(\frac{z - z_h}{z_0}\right)\right] \tag{22.1}$$

where u_z is the wind speed (m/s) at height z (m), u_* is the shear velocity (m/s), κ is von Karman's constant, z_h is the zero plane displacement, and z_0 is the roughness length.

Exponential law:

$$u_z = u_r\left(\frac{z}{z_r}\right)^{\alpha} \tag{22.2}$$

where u_r is the known wind speed at a reference height z_r and the exponent α is an empirically derived coefficient and will change with the terrain roughness.

22.2.2 Turbulence

The velocity of boundary wind is defined by three components: the along-wind component consisting of the mean wind velocity, $\overline{U}$, plus the turbulent component $u(t)$, the cross-wind turbulent component $v(t)$, and the vertical turbulent component $w(t)$. The turbulence is described in terms of turbulence intensity, integral length, and spectrum (Simiu and Scanlan, 1996).

The turbulence intensity I is defined as

$$I = \frac{\sigma}{\overline{U}} \tag{22.3}$$

where σ = the standard deviation of wind component $u(t)$, $v(t)$, or $w(t)$; and $\overline{U}$ = the mean wind velocity.

Integral length of turbulence is a measurement of the average size of turbulent eddies in the flow. There are a total of nine integral lengths (three for each turbulent component). For example, the integral length of $u(t)$ in the x direction is defined as

$$L_u^x = \frac{1}{\sigma_u^2}\int_0^{\infty} R_{u_1 u_2}(x)\,dx \tag{22.4}$$

where $R_{u_1 u_2}(x)$ = cross-covariance function of $u(t)$ for a spatial distance x.

The wind spectrum is a description of wind energy versus wind frequencies. As an example, the von Karman spectrum is given in dimensionless form as

$$\frac{nS(n)}{\sigma^2} = \frac{4\,\dfrac{nL}{\overline{U}}}{\left[1 + 70.8\left(\dfrac{nL}{\overline{U}}\right)^2\right]^{\frac{5}{6}}} \tag{22.5}$$

where n = frequency (Hz); S = auto spectrum; and L = integral length of turbulence. The integral length of turbulence is not easily obtained. It is usually estimated by curve fitting the spectrum model with the measured field data.

For a long-span bridge, appropriate modeling and inclusion of imperfect correlation of the random processes are needed to simulate the wind speeds at a very large number of points along the span, which requires simulating the wind speed from univariate to multivariate processes. In some

cases, non-Gaussian features observed in the pressure fluctuations under separated flow regions, nonstationarity in wind storms, and conditional simulations because of limited number of sensors bring more difficulties in computational stochastic modeling of wind load effects on long-span bridges (Kareem, 2008).

22.2.3 Design Wind Speeds

In order to ensure the bridge safety, the establishment of appropriate design wind speeds is a critical first step (Holmes, 2007). After Gumbel's promotion of the use of the Type I extreme value distribution for design wind speeds, several countries had applied extreme value analysis to predict design wind speeds. Jenkinson introduced the Generalized Extreme Value Distribution (G.E.V.) and combines the three extreme value distributions into a single mathematical form. The cumulative probability distribution function of the maximum wind speed in a defined period $F_U(U)$ is

$$F_U(U) = \exp\left\{-\left[1-k(U-u)/a\right]^{1/k}\right\} \tag{22.6}$$

where k is a shape factor and a is a scale factor. When $k<0$, the G.E.V. is the Type II Extreme Value distribution; when $k>0$, it is a Type III Extreme Value Distribution; whereas k tends to be 0, the limit of the equation will become Type I Extreme Value Distribution. The inverse of the complementary cumulative distribution of the extremes is defined as Return Period.

$$R = \frac{1}{1-F_U(U)} \tag{22.7}$$

Based on the Gumbel's methodology for fitting recorded annual maxima to the Type I Extreme Value distribution, the predicted extreme wind speed can be obtained as the following for large values of return periods:

$$U_R \cong u + a\ln R \tag{22.8}$$

22.3 Experimental Investigation

Wind tunnel testing is commonly used for "wind-sensitive" bridges such as cable-stayed bridges, suspension bridges, and other bridges with span lengths or structure types significantly outside of the common bridges. The objective of a wind tunnel test is to determine the susceptibility of the bridges to various aerodynamic phenomena.

The bridge aerodynamic behavior is controlled by two types of parameters, that is, structural and aerodynamical. The structural parameters are the bridge layout, boundary conditions, members' stiffness, natural modes, and frequencies, and so on. The aerodynamic parameters are mainly wind climate, and bridge section shape and details. The design engineers need to provide all the information to the wind specialist to conduct the testing and analysis.

22.3.1 Scaling Principle

In a typical structural test, a prototype structure is scaled down to a scale model according to mass, stiffness, damping, and other parameters. The wind in testing blows in different vertical angles (attack angles) or horizontal angles (skew angles) to cover the worst case at the bridge site. To obtain reliable information from a test, similarity must be maintained as much as possible between the specimen and the prototype structure. The geometric scale λ_L, a basic parameter that is controlled by the size of an

available wind tunnel, is denoted as the ratio of the dimensions of the model (B_m) to the dimensions of the prototype bridge (B_p) as (Scanlan, 1981)

$$\lambda_L = \frac{B_m}{B_p} \tag{22.9}$$

where subscripts m and p indicate model and prototype, respectively.

To maintain the same Froude number for both scale model and prototype bridge requires,

$$\left(\frac{U^2}{Bg}\right)_m = \left(\frac{U^2}{Bg}\right)_p \tag{22.10}$$

where g is the air gravity, which is the same for the model and prototype bridge. From Equations 22.9 and 22.10 we have the wind velocity scale λ_v as

$$\lambda_V = \frac{U_m}{U_p} = \sqrt{\lambda_L} \tag{22.11}$$

Reynolds number equivalence requires

$$\left(\frac{\rho U B}{\mu}\right)_m = \left(\frac{\rho U B}{\mu}\right)_p \tag{22.12}$$

where μ = viscosity and ρ = wind mass density. Equations 22.9 and 22.12 gives the wind velocity scale as

$$\lambda_V = \frac{1}{\lambda_L} \tag{22.13}$$

which contradicts with Equation 22.11. It is therefore impossible in model scaling to satisfy both the Froude number equivalence and Reynolds number equivalence simultaneously. For bluff bodies such as bridge decks, flow separation is caused by sharp edges and therefore, the Reynolds number is usually believed not to be important except it is too small. The too small Reynolds number can be avoided by a careful selection of λ_L. Therefore, the Reynolds number equivalence is usually sacrificed and Froude number equivalence is maintained. In the recent research based on the high Reynolds number wind tunnel experiments, it is found that slender bodies with sharp edged cross sections, such as bridge box girders, may suffer pronounced Reynolds number effects, and the conventional wind tunnel test results in low Reynolds number regions are conservative (Schewe and Larsen, 1998; Matsuda et al., 2001).

To apply the flutter derivative information to the prototype analysis, nondimensional reduced velocity must be the same, that is,

$$\left(\frac{U}{NB}\right)_m = \left(\frac{U}{NB}\right)_p \tag{22.14}$$

Solving Equations 22.9, 22.11, and 22.14 gives the natural frequency scale as

$$\lambda_N = \frac{N_m}{N_p} = \frac{1}{\sqrt{\lambda_L}} \tag{22.15}$$

The above equivalence of reduced velocity between the sectional model and the prototype bridge is the basis to use the sectional model information to prototype bridge analysis. Therefore, it should be strictly satisfied.

22.3.2 Sectional Model

A typical sectional model represents a unit length of a prototype deck with a scale from 1:25 to 1:100. It is usually constructed from materials such as steel, wood, or aluminum to simulate the scaled mass and moment of inertia about the center of gravity. The sectional model represents only the outside shape (aerodynamic shape) of the deck. The stiffness and the vibration characteristics are represented by the spring supports.

By rigidly mounding the section in the wind tunnel, the static wind forces, such as lift, drag, and pitch moment, can be measured. To measure the aerodynamic parameters such as the flutter derivatives, the sectional model is supported by a spring system and connected to a damping source as shown in Figure 22.2. The spring system can be adjusted to simulate the deck stiffness in the vertical and torsional directions, and therefore simulate the natural frequencies of the bridges. The damping characteristics are also adjustable to simulate different damping.

A sectional model is less expensive and easier to conduct than a full model. It is thus widely used in (1) the preliminary study to find the best shape of a bridge deck; (2) to identify the potential wind-induced problems such as vortex-shedding, flutter, and galloping and to guide a more sophisticated full model study; (3) to measure aerodynamic and aeroelastic data, such as flutter derivatives, static force coefficients for analytical prediction of actual bridge behavior; and (4) to observe bridge performance directly for some less important bridges that cannot be economically justified for a full model test.

22.3.3 Full Bridge Model

A full bridge model, representing the entire bridge or a few spans, is also called an aeroelastic model since the aeroelastic deformation is reflected in the full model test. The deck, towers, and cables are built according to the scaled stiffness of the prototype bridge. The scale of a full bridge model is usually from 1:100 to 1:300 to fit the model in the wind tunnel. The full model test is used for checking many kinds of aerodynamic phenomena and determining the wind loading on bridges.

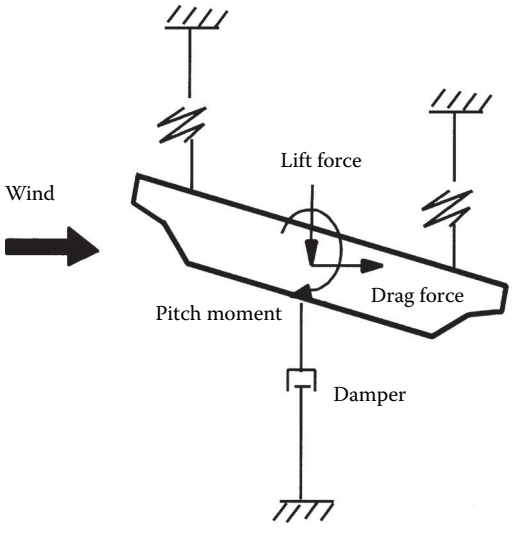

FIGURE 22.2 End view of sectional model.

A full bridge model is more expensive and difficult to build than a sectional model. It is used only for large bridges at the final design stage, particularly to check the aerodynamics of the construction phase. However, a full model test has many advantages over a sectional model: (1) it simulates the three-dimensional and local topographical effects; (2) it reflects the interaction between vibration modes; (3)≈wind effects can be directly visualized at the construction and service stages; and (4) it is more educational to the design engineers to improve the design.

22.3.4 Taut Strip Model

For this model, taut strings or tubes are used to simulate the bridge's stiffness and dynamic characteristics such as the natural frequencies and mode shapes for the vertical and torsional vibrations. A rigid model of the deck is mounted on the taut strings. This model allows, for example, the main span of a deck to be represented. The taut strip model falls between sectional model and full model with respect to cost and reliability. For less important bridges, the taut strip model is sufficient and an economical choice. The taut strip model is used to determine critical wind velocity for vortex shedding, flutter, and galloping and displacement and acceleration under smooth or turbulent winds.

22.3.5 Flow Visualization

Flow visualization is the process to make fluid flows visible and could make it possible to view various properties of flows, such as flow structures, turbulence, separations, and so on. Flows can be visualized by surface flow visualization, optical methods (e.g., laser-induced fluorescence) or particle tracer methods (e.g., particle image velocimetry or called PIV). In addition to the flow pattern, particle tracer methods can measure the velocity of the whole fluid field simultaneously. Based on the light scattering characteristics and the aerodynamic tracking capabilities, certain PIV seeding particles could be added into the fluid of interest. If the particles have almost the same speed as the fluid, the velocity of the particles can represent the velocity of the fluid. A high-energy laser illuminates the particles in the fluid, whereas charge-coupled device (CCD) captors and fast frame grabbers take pairs of images at the same time in a nanosecond time interval, and the images are transferred at a high speed to computers (Raffel et al., 1998). Suitable particle image pattern matching scheme and PIV algorithms are used to obtain the velocity of the fluid. After the development in the last three decades, PIV has become an accurate and quantitative measurement of fluid velocity vectors at a very large number of points simultaneously (Adrian, 2005).

22.4 Analytical Solutions

22.4.1 Long-Span Bridge Response to Wind

Wind may induce instability and excessive vibrations in long-span bridges. Instability is the onset of an infinite displacement granted by a linear solution technique. Actually, displacement is limited by structural nonlinearities. Vibration is a cyclic or random movement induced by dynamic effects. Since both instability and vibration failures in reality occur at finite displacement, it is often hard to judge whether a structure failed because of instability or excessive vibration-induced damage to some key elements.

Instability caused by the interaction between moving air and a structure is termed aeroelastic or aerodynamic instability. The term aeroelastic emphasizes the behavior of deformed bodies, and aerodynamic emphasizes the vibration of rigid bodies. Since many problems involve both deformation and vibration, these two terms are used interchangeably hereafter. Aerodynamic instabilities of bridges include divergence, galloping, and flutter. Typical wind-induced vibrations consist of vortex shedding and buffeting. These types of instabilities and vibrations may occur alone or in combination. For example, a structure must experience vibrations to some extent before flutter instability starts.

The interaction between the bridge vibration and wind results in two kinds of forces: motion-dependent and motion-independent. The former vanishes if the structures are rigidly fixed. The latter, being purely dependent on the wind characteristics and section geometry, exists whether or not the bridge is moving. The aerodynamic equation of motion is expressed in the following general form

$$[\mathbf{M}]\{\ddot{\mathbf{Y}}\} + [\mathbf{C}]\{\dot{\mathbf{Y}}\} + [\mathbf{K}]\{\mathbf{Y}\} = \{\mathbf{F(Y)}\}_{\mathbf{md}} + \{\mathbf{F}\}_{\mathbf{mi}} \tag{22.16}$$

where $[\mathbf{M}]$ = mass matrix; $[\mathbf{C}]$ = damping matrix; $[\mathbf{K}]$ = stiffness matrix; $\{\mathbf{Y}\}$ = *displacement* vector; $\{\mathbf{F(Y)}\}_{\mathbf{md}}$ = motion-dependent aerodynamic force vector; and $\{\mathbf{F}\}_{\mathbf{mi}}$ = motion-independent wind force vector.

The motion-dependent force causes aerodynamic instability, and the motion-independent part together with the motion-dependent part causes deformations or vibrations. The difference between a short- and a long-span bridge lies in the motion-dependent part. For a short-span bridge, the motion-dependent part is insignificant and there is no concern about its aerodynamic instability. For flexural structures like long-span bridges, however, both instability and vibrations need to be carefully examined.

22.4.2 Vortex Shedding

Vortex shedding is a wake-induced effect occurring on bluff bodies such as bridge decks and pylons. Wind flowing against a bluff body forms a stream of alternating vortices called a von Karman vortex street shown in Figure 22.3a. Alternating shedding of vortices creates an alternative force in a direction

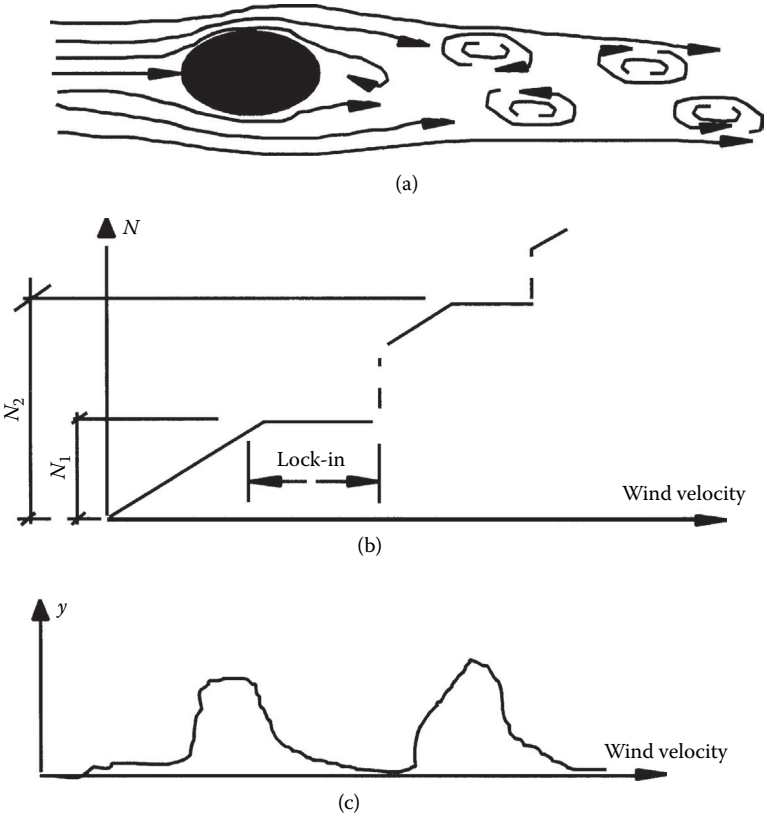

FIGURE 22.3 Explanation of vortex shedding. (a) Von Karman Street; (b) lock-in phenomenon; (c) bridge vibration.

normal to the wind flow. This alternative force induces vibrations. The shedding frequency of vortices from one surface, in either torsion or lift, can be described in terms of a nondimensional Strouhal number, *S*, as

$$S = \frac{N D}{\overline{U}} \tag{22.17}$$

where N = shedding frequency and D = characteristic dimension such as the diameter of a circular section or depth of a deck.

The Strouhal number (ranging from 0.05 to 0.2 for bridge decks) is constant for a given section geometry and details. Therefore, the shedding frequency (N) increases with the wind velocity to maintain a constant Strouhal value (S). The bridge vibrates strongly but self-limited when the frequency of vortex shedding is close to one of the natural frequencies of a bridge, say N_1 as shown in Figure 22.3. This phenomenon is called lock-in and the corresponding wind velocity is called critical velocity of vortex shedding.

The lock-in occurs over a small range of wind velocity within which the Strouhal relation is violated since the increasing wind velocity and a fixed shedding frequency results in a decreasing Strouhal number. The bridge natural frequency, not the wind velocity, controls the shedding frequency. As wind velocity increases, the lock-in phenomenon disappears and the vibration reduces to a small amplitude. The shedding frequency may lock-in with another higher natural frequency (N_2) at a higher wind velocity. Therefore, many wind velocities can cause vortex shedding.

To describe the above experimental observation, much effort has been made to find an expression for forces resulting from vortex shedding. Since the interaction between the wind and the structure is very complicated, no completely successful model has yet been developed for bridge sections. Most models deal with the interaction of wind with circular sections. A semiempirical model for the lock-in is given as (Simiu and Scanlan, 1996)

$$m\ddot{y} + c\dot{y} + ky = \frac{1}{2}\rho U^2(2D)\left[Y_1(K)\left(1 - \varepsilon\frac{y^2}{D^2}\right)\frac{\dot{y}}{D} + Y_2(K)\frac{y}{D} + \frac{1}{2}C_L(K)\sin(\omega t + \varphi)\right] \tag{22.18}$$

where $k = B\omega/\overline{u}$ = reduced frequency; Y_1, Y_2, ε and C_L = parameters to be determined from experimental observations. The first two terms of the right side account for the motion-dependent force. More particularly, the $\dot{y}$ term accounts for aerodynamic damping and y term for aerodynamic stiffness. The ε accounts for the nonlinear aerodynamic damping to ensure the self-limiting nature of vortex shedding. The last term represents the instantaneous force from vortex shedding alone that is sinusoidal with the natural frequency of bridge. Solving above equation gives the vibration y.

Vortex shedding occurs in both laminar and turbulent flow. According to some experimental observations, turbulence helps to break up vortices and therefore helps to suppress vortex shedding responses. A more complete analytical model must consider the interaction between modes, the span-wise correlation of aerodynamic forces and the effect of turbulence.

For a given section shape with a known Strouhal number and natural frequencies, the lock-in wind velocities can be calculated with Equation 22.18. The calculated lock-in wind velocities are usually lower than the maximum wind velocity at bridge sites. Therefore, vortex shedding is an inevitable aerodynamic phenomenon. However, vibration excited by vortex shedding is self-limited because of its nonlinear nature. A relatively small damping is often sufficient to eliminate, or at least reduce, the vibrations to acceptable limits.

Although there are no acceptance criteria for vortex shedding in the design specifications and codes in the United States, there is a common agreement that limiting acceleration is more appropriate than limiting deformation. It is usually suggested that the acceleration of vortex shedding is limited to 5%

of gravity acceleration when wind speed is < 50 km/h and 10% of gravity acceleration when wind speed is higher. The acceleration limitation is then transformed into the displacement limitation for a particular bridge.

22.4.3 Galloping

Consider that in Figure 22.4a a bridge deck is moving upward with a velocity $\dot{y}$ under a horizontal wind U. This is equivalent to the case of Figure 22.4b where the deck is motionless and the wind blows downward with an attack angle α (tan(α) = $\dot{y}/U$). If the measured static force coefficient of this case is negative (upward), then the deck section will be pushed upward further resulting in a divergent vibration or galloping. Otherwise, the vibration is stable. Galloping is caused by a change in the effective attack angle because of the vertical or torsional motion of the structure. A negative slope in the plot of either static lift or pitch moment coefficient versus the angle of attack, shown in Figure 22.4c, usually implies a tendency for galloping. Galloping depends mainly on the quasi-steady behavior of the structure.

The equation of motion describing this phenomenon is

$$\ddot{m}y + c\dot{y} + ky = -\frac{1}{2}\rho U^2 B\left(\frac{dC_L}{d\alpha} + C_D\right)_{\alpha=0}\frac{\dot{y}}{U} \tag{22.19}$$

The right side represents the aerodynamic damping and C_L and C_D are static force coefficients in the lift and drag directions, respectively. If the total damping is < 0, that is,

$$c + \frac{1}{2}\rho UB\left(\frac{dC_L}{d\alpha} + C_D\right)_{\alpha=0} \le 0 \tag{22.20}$$

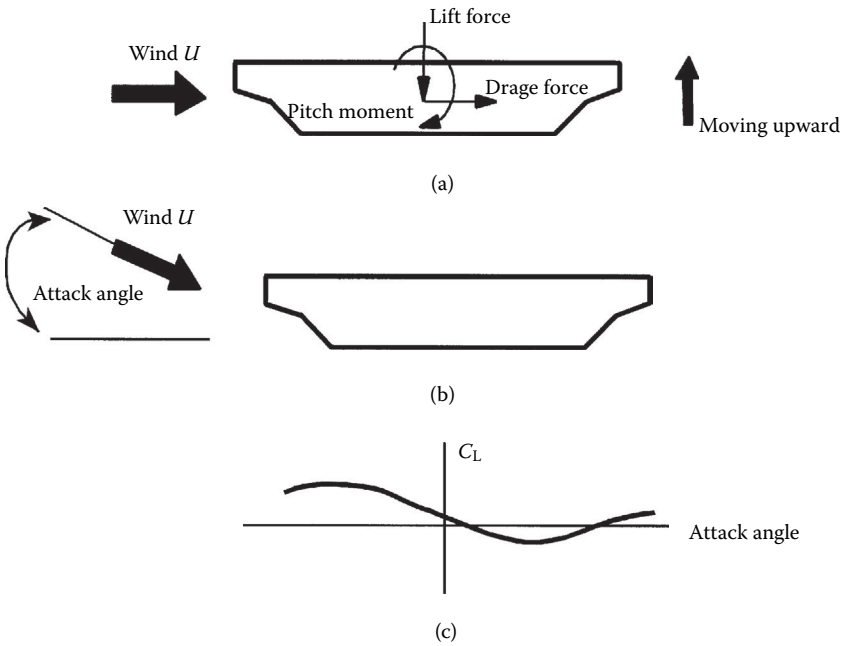

FIGURE 22.4 Explanation of galloping. (a) Section moving upward; (b) motionless section with a wind attack angle; (c) static force coefficient versus attack angle.

then the system tends toward instability. Solving the above equation gives the critical wind velocity for galloping. Since the mechanical damping c is positive, the above situation is possible only if the following Den Hartog criterion (Scruton, 1981) is satisfied, that is, $\left(\frac{dC_L}{d\alpha}+C_D\right)_{\alpha=0} \le 0$. Therefore, a wind tunnel test is usually conducted to check against Equation 22.20 and to make necessary improvement of the section to eliminate the negative tendency for the possible wind velocity at a bridge site.

Galloping rarely occurs in highway bridges, but noted examples are pedestrian bridges, pipe bridges, and ice-coated cables in power lines. There are two kinds of cable galloping: cross-wind galloping, which creates large-amplitude oscillations in a direction normal to the flow, and wake galloping caused by the wake shedding of upwind structures or components.

22.4.4 Flutter

Flutter is one of the earliest recognized and most dangerous aeroelastic phenomena in airfoils. It is created by self-excited forces that depend on motion. If a system immersed in wind flow is given a small disturbance, its motion will either decay or diverge depending on whether the energy extracted from the flow is smaller or larger than the energy dissipated by the mechanical damping. The theoretical line dividing decaying and diverging motions is called the critical condition. The corresponding wind velocity is called the critical wind velocity for flutter or simply the flutter velocity at which the motion of the bridge deck tends to grow exponentially as shown in Figure 22.5a.

When flutter occurs, the oscillatory motions of all degrees of freedom in the structure couple to create a single frequency called the flutter frequency. Flutter is an instability phenomenon; once it takes place, the displacement is infinite per the linear theory. Flutter may occur in both laminar and turbulent flows.

The self-excited forces acting on a unit deck length are usually expressed as a function of the flutter derivatives. The general format of the self-excited forces written in matrix form (Cai, 1993; Namini et al., 1992) for finite element analysis is

$$\begin{Bmatrix} L_{se} \\ D_{se} \\ M_{se} \end{Bmatrix} = \frac{1}{2}\rho U^2 (2B) \left(\begin{bmatrix} \frac{k^2 H_4^*}{B} & \frac{k^2 H_6^*}{B} & k^2 H_3^* \\ \frac{k^2 P_4^*}{B} & \frac{k^2 P_6^*}{B} & k^2 P_3^* \\ k^2 A_4^* & k^2 A_6^* & k^2 A_3^* B \end{bmatrix} \begin{Bmatrix} h \\ p \\ \alpha \end{Bmatrix} + \begin{bmatrix} \frac{kH_1^*}{\overline{U}} & \frac{kH_5^*}{\overline{U}} & \frac{kH_2^* B}{\overline{U}} \\ \frac{kP_1^*}{\overline{U}} & \frac{kP_5^*}{\overline{U}} & \frac{kP_2^* B}{\overline{U}} \\ \frac{kA_1^* B}{\overline{U}} & \frac{kA_5^* B}{\overline{U}} & \frac{kA_2^* B^2}{\overline{U}} \end{bmatrix} \begin{Bmatrix} \dot{h} \\ \dot{p} \\ \dot{\alpha} \end{Bmatrix} \right) \tag{22.21}$$

$$= U^2 [F_d] \{q\} + U^2 [F_v] \{\dot{q}\}$$

where L_{se}, D_{se}, and M_{se} = self-excited lift force, drag force, and torsional moment, respectively; h, p, and α = displacements at the center of a deck in the directions corresponding to L_{se}, D_{se}, and M_{se}, respectively; ρ = mass density of air; B = deck width; H_i^*, P_i^*, and A_i^* (i = 1 to 6) = generalized flutter derivatives; $k = B\omega/\overline{u}$ = reduced frequency; ω = oscillation circular frequency; $\overline{u}$ = mean wind velocity; and $[F_d]$ and $[F_v]$ = flutter derivative matrices corresponding to displacement and velocity, respectively.

Although the flutter derivatives H_i^* and A_i^* have been experimentally determined for i = 1 to 4, the term P_i^* is theoretically derived in state-of-the-art applications. The other flutter derivatives (for i = 5 and 6) have been neglected in most the state-of-the-art analysis.

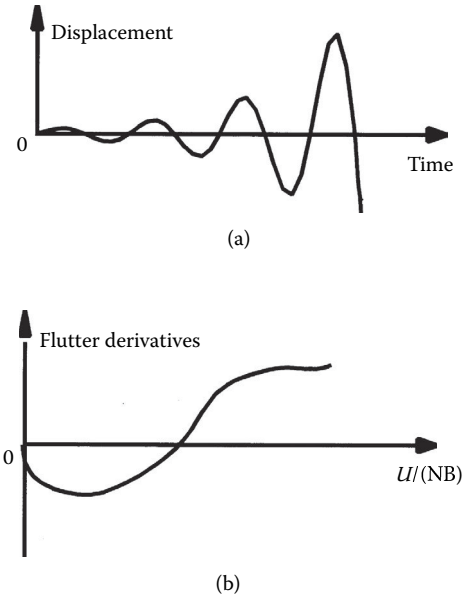

FIGURE 22.5 Explanation of flutter. (a) Bridge flutter vibration; (b) typical flutter derivations.

In linear analyses, the general aerodynamic motion equations of bridge systems are expressed in terms of the generalized mode shape coordinate {ξ}

$$[M^*]\{\ddot{\xi}\} + \left([D^*] - U^2[AD^*]\right)\{\dot{\xi}\} + \left([K^*] - U^2[AS^*]\right)\{\xi\} = 0 \tag{22.22}$$

where $[M^*]$, $[D^*]$, and $[K^*]$ = generalized mass, damping, and stiffness matrices, respectively; and $[AS^*]$ and $[AD^*]$ = generalized aerodynamic stiffness and aerodynamic damping matrices respectively. Matrices $[M^*]$, $[D^*]$, and $[K^*]$ are derived the same way as in the general dynamic analysis. Matrices $[AS^*]$ and $[AD^*]$, corresponding to $[F_d]$ and $[F_v]$ in Equation 22.21 respectively, are assembled from aerodynamic element forces. It is noted that even the structural and dynamic matrices $[K^*]$, $[M^*]$, and $[D^*]$ are uncoupled between modes, the motion equation is always coupled because of the coupling of aerodynamic matrices $[AS^*]$ and $[AD^*]$.

Flutter velocity, U, and flutter frequency, ω, are obtained from the nontrivial solution of Equation 22.22 as

$$\left| \left(\omega^2[M^*] + [K^*] - \overline{U}^2[AS^*] + \omega\left([D^*] - \overline{U}^2[AD^*]\right) i \right) \right| = 0 \tag{22.23}$$

For a simplified uncoupled single degree of freedom, the above equation reduces to

$$\omega^2 = \frac{[K^*] - \overline{U}^2[AS^*]}{[M^*]} \tag{22.24}$$

and

$$U_{cr}^2 = \frac{[D^*]}{[AD^*]} \tag{22.25}$$

Since the aerodynamic force $[AS^*]$ is relatively small, it can be seen that the flutter frequency in Equation 22.24 is close to the natural frequency $[K^*]/[M^*]$. Equation 22.25 can be also derived from Equation 22.22 as the zero-damping condition. Zero-damping cannot occur unless $[AD^*]$ is positive. The value of $[AD^*]$ depends on the flutter derivatives. An examination of the flutter derivatives gives a preliminary judgment of the flutter behavior of the section. Necessary section modifications should be made to eliminate the positive flutter derivatives as shown in Figure 22.5b, especially the A^*_2 and H^*_1. The A^*_2 controls the torsional flutter and the H^*_1 controls the vertical flutter. It can be seen from Equation 22.25 that an increase in the mechanical damping $[D^*]$ increases the flutter velocity. It should be noted that for a coupled flutter, zero-damping is a sufficient but not a necessary condition.

A coupled flutter is also called stiffness-driven or classical flutter. An uncoupled flutter is called damping-driven flutter since it is caused by zero-damping. Since flutter of a suspension bridge is usually controlled by its first torsional mode, the terminology "flutter" was historically used for a torsional aerodynamic instability. Vertical aerodynamic instability is traditionally treated in a quasi-static approach, that is, as is galloping. In the recent literature, flutter is any kind of aerodynamic instabilities because of self-excited forces, whether vertical, torsional, or coupled vibrations (Scanlan, 1988).

Turbulence is assumed beneficial for flutter stability and is usually ignored. A number of analytical studies were conducted to predict changes in the flutter instability because of turbulence in the approach flows (Lin and Li, 1993). Some studies include turbulence effect by treating along-wind velocity U as mean velocity, $\overline{u}$, plus a turbulent component, $u(t)$. The random nature of $u(t)$ results in an equation of random damping and stiffness. Complicated mathematics, such as stochastic differentiation, need to be involved to solve the equation (Lin and Ariaratnam 1980). The dynamic response of a long-span bridge under the effects of a turbulent wind field with uncertain span-wise correlation between two structural modes was investigated by simulating the response as an equivalent Markov-type multivariate process (Caracoglia, 2008). Although the stabilizing effects of span-wise coherence loss may be apparent for single-mode flutter scenarios, the turbulence-induced changes in the flutter instability of bridges cannot be explained entirely because of a decrease in the coherence of self-excited forces (Chen and Kareem, 2003).

Time history and nonlinear analyses can be conducted on Equation 22.22 to investigate postflutter behavior and to include the effects of both geometric and material nonlinearities. Diana et al. (1999) proposed a nonlinear aerodynamic force model, namely, quasi-static corrected theory. This model attempted to incorporate frequency-dependent characteristics by decomposing the total response into components with different frequencies. Chen and Kareem (2003) proposed the associated time domain analysis framework for the nonlinear aerodynamic force model for predicting the aeroelastic response of the bridges under turbulent winds. However, this is not necessary for most practical applications.

22.4.5 Buffeting

Buffeting is defined as the forced response of a structure to random wind and can only take place in turbulent flows. Turbulence resulting from topographical or structural obstructions is called oncoming turbulence. Turbulence induced by bridge itself is called signature turbulence. Since the frequencies of signature turbulence are generally several times higher than the important natural frequencies of the bridge, its effect on buffeting response is usually small.

Buffeting is a random vibration problem with limited displacement. The effects of buffeting and vortex shedding are similar, except that typically vibration is random in the former and periodic in the latter. Both buffeting and vortex shedding influence the bridge's serviceability behavior and may result in fatigue damage that could lead to an eventual collapse of bridges. Buffeting also influences ultimate strength behavior.

Similar to Equation 22.21, the buffeting forces are expressed in the matrix form (Cai, 1993) for finite element analysis as

$$\begin{Bmatrix} L_b \\ D_b \\ M_b \end{Bmatrix} = \frac{1}{2}\rho \overline{U}^{\,2} B \begin{bmatrix} 2C_L & \left(\frac{dC_L}{d\alpha} + C_D\right) \\ 2C_D & \frac{dC_D}{d\alpha} \\ 2C_M B & \frac{dC_M}{d\alpha} B \end{bmatrix} \begin{Bmatrix} \frac{u(t)}{\overline{U}} \\ \frac{w(t)}{\overline{U}} \end{Bmatrix} = \overline{U}^{\,2} [C_b]\{\eta\} \tag{22.26}$$

where C_D, C_L, and C_M = static aerodynamic coefficients for drag, lift, and pitch moment, respectively; α = angle of wind attack; $[C_b]$ = static coefficient matrix; and $\{\eta\}$ = vector of turbulent wind components normalized by mean wind velocity.

The equation of motion for buffeting is similar to Equation 22.22, but with one more random buffeting force as

$$[M^*]\{\ddot{\xi}\} + \left([D^*] - U^2[AD^*]\right)\{\dot{\xi}\} + \left([K^*] - U^2[AS^*]\right)\{\xi\} = \overline{U}^2[f^*]_b\{\eta\} \tag{22.27}$$

Fourier transform of Equation 22.27 yields

$$f(\{\xi\}) = \overline{U}^2[G_1]\{f^*\}_b * f(\{\eta\}) \tag{22.28}$$

where

$$[G_1] = \frac{1}{\left(\omega^2[M^*] + [K^*]\ \overline{U}^2[AS^*] + \omega\,([D^*]\ \overline{U}^2[AD^*])\,i\right)}$$

Similarly, taking the conjugate transform of Equation 22.28 yields

$$\overline{f(\{\xi\})^T} = \overline{U}^2\overline{f(\{\eta\})^T}\{f^*\}_b^T[G_2]^T \tag{22.29}$$

where

$$[G_2] = \frac{1}{\left(\omega^2[M^*] + [K]^*\ \overline{U}^2[AS^*]\ \omega\,([D^*]\ \overline{U}^2[AD^*])\,i\right)}$$

The superscript T represents the matrix transpose, and the "over-bar" stands for the Fourier conjugate transform for the formula above. Multiplying Equations 22.24 and 22.29 gives the following spectral density of generalized coordinates:

$$\begin{bmatrix} S_{\xi_1\xi_1} & \cdots & S_{\xi_1\xi_m} \\ S_{\xi_i\xi_1} & \cdots & S_{\xi_i\xi_m} \\ S_{\xi_m\xi_1} & \cdots & S_{\xi_m\xi_m} \end{bmatrix} = \overline{U}^4[G_1]\{f^*\}_b \begin{bmatrix} S_{\eta_1\eta_1} & S_{\eta_1\eta_2} \\ S_{\eta_2\eta_1} & S_{\eta_2\eta_2} \end{bmatrix} \{f^*\}_b^T[G_2]^T \tag{22.30}$$

where $S_{\eta i \eta j}$ = spectral density of normalized wind components. The mean square of the modal and physical displacements can be derived from their spectral densities. Once the displacement is known, the corresponding forces can be derived. The aerodynamic study should ascertain that no structural

member is over-stressed or over-deformed such that the strength and service limits are exceeded. For very long-span bridges, a comfort criterion must be fulfilled under buffeting vibration.

In order to include nonlinearities of structural and aerodynamic origins, time domain approach has been utilized for the analysis of flutter and buffeting response (Chen et al., 2000; Diana et al., 1998; Santos et al., 1993; Xiang et al., 1995). In Chen et al.'s approach, the unsteady forces are expressed in terms of the convolution integrals involving the aerodynamic impulse functions and the structural motions or wind fluctuations, which can be determined from experimentally derived flutter derivatives, admittance functions, and the spanwise coherence of aerodynamic forces.

22.4.6 Quasi-Static Divergence

Wind flowing against a structure exerts a pressure proportional to the square of the wind velocity. Wind pressure generally induces both forces and moments in a structure. At a critical wind velocity, the edge-loaded bridge may buckle "out-of-plane" under the action of a drag force or torsional diverge under a wind-induced moment that increases with a geometric twist angle. In reality, divergence involves an inseparable combination of lateral buckling and torsional divergence.

Consider a small rotation angle as shown in Figure 22.6, the torsional moment resulting from wind is (Simiu and Scanlan, 1996)

$$M_\alpha = \frac{1}{2}\rho U^2 B^2 C_M(\alpha\alpha = \frac{1}{2}\rho U^2 B^2\left[C_{M0} + \frac{dC_m}{d\alpha}_{\text{at } \alpha=0}\alpha\right] \tag{22.31}$$

When the torsional moment caused by wind exceeds the resisting torsional capacity, the displacement of the bridge diverges. Equating the aerodynamic force to the internal structural capacity gives

$$k_\alpha \alpha - \frac{1}{2}\rho U^2 B^2\left[C_M 0 + \frac{dC_m}{d\alpha}_{\text{at } \alpha=0}\alpha\right] = 0 \tag{22.32}$$

where k_α = spring constant of torsion. For an infinite α, we have the critical wind velocity for torsional divergence as

$$U_{cr} = \sqrt{\frac{2k_\alpha}{\rho B^2 \frac{dC_m}{d\alpha}_{\text{at } \alpha=0}}} \tag{22.33}$$

22.4.7 Cable Vibration

A common wind-induced problem in long-span bridges is cable vibration. There are a number of wind-induced vibrations in cables, individually or as a group, such as vortex excitation, wake galloping, excitation of a cable by imposed movement of its extremities, rain/wind and ice/wind-induced vibrations, and buffeting of cables in strong turbulent winds.

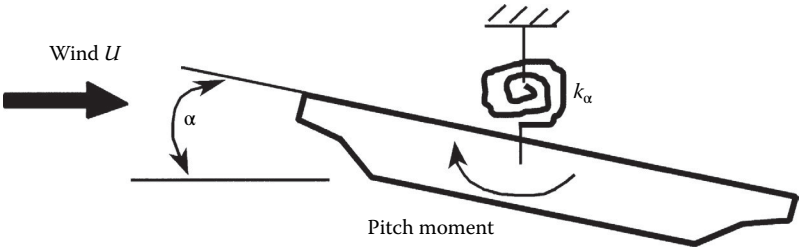

FIGURE 22.6 Explanation of torsional divergence.

The rain-wind-induced vibration of long stay cables of long-span cable-stayed bridges has drawn intensive research efforts since the 1980s when it was first recognized. Hikami and Shiraishi (1988) first noticed that the primary reasons for rain-wind-induced vibrations of cables for cable-stayed bridges were the formulation of water rivulets caused by rainfall on the smooth surface of the cable under the axial flow in the rear wake. Based on series of wind tunnel tests, the rain-wind-induced vibration of cables were classified in three types, that is, "galloping" type, vortex-shedding type and their mixed type (Matsumoto et al., 1995). Experiments or full scale measurements were carried out in order to investigate the mechanism and find appropriate mitigation methods (Main and Jones, 1999; Chen et al., 2004; Gu and Du, 2005).

Although the causes of the cable vibrations are different from each other and the theoretical solutions complicated, some mitigating measures for these cable vibrations are as common as the following:

1. Raise damping: It is an effective way for all kinds of cable vibrations. The cables are usually flexible and inherently low in damping. Therefore, an addition of relatively small damping (usually at the cable ends) to the cable can dramatically reduce the vibration.
2. Raise natural frequency: The natural frequency depends on the cable length, the tension force, and the mass. Since the cable force and the mass are determined from the structural design, commonly the cable length is reduced by using spacers or cross cables.
3. Change cable shape: A change in the cable shape characteristics by increasing the surface roughness or adding protrusions to the cable surface reduces the rain/wind and ice/wind-induced vibrations.
4. Other techniques: Rearranging the cables or raising the cable mass density can also be used, but these are usually limited by other design constraints. Raising the mass may reduce the natural frequency, but it increases the damping and Scruton number ($m\zeta/\rho D^2$), and overall is beneficial.

22.5 Practical Applications

22.5.1 Wind Climate at Bridge Sites

The future wind climate at a particular bridge site is usually not available, but it is commonly decided according to the historical wind data of the nearest airport. The wind data is then analyzed considering the local terrain features of the bridge site to obtain the necessary information such as the maximum wind velocity, dominant direction, turbulence intensity, and wind spectrum. For large bridges, an anemometer can be installed on the site for a few months to get the characteristics of the wind on the site itself. The most important quantity is the maximum wind velocity, which is dependent on the bridge-design period.

The bridge-design period is decided upon considering a balance between the cost and safety. For the strength design of a completed bridge, a design period of 50 or 100 years is usually used. Since the construction of a bridge lasts a relatively short period, a 10-year period can be used for construction strength checking. This is equivalent to keeping the same design period but reducing the safety factor during construction.

Flutter is an instability phenomenon. Once it occurs, its probability of failure is assumed to be 100%. A failure probability of 10^{-5} per year for completed bridges represents an acceptable risk, which is equivalent to a design period of 100,000 years. Similarly, the design period of flutter during construction can be reduced to, say 10,000 years. It should be noted that the design period does not represent the bridge's service life, but a level of failure risk.

Once the design period has been decided upon, the maximum wind velocity is determined. Increasing the design period by one order of magnitude usually raises the wind velocity only by a few percent, depending on the wind characteristics. Wind velocity for flutter (stability) design is usually about 20% larger than that for buffeting (strength) design, although the design period for the former is several orders higher. Once wind characteristics and design velocity are available, a wind tunnel/analytical investigation is conducted.

22.5.2 Design Consideration

The aerodynamic behavior of bridges depends mainly on four parameters: structural form, stiffness, cross-section shape and its details, and damping. Any significant changes that may affect these parameters need to be evaluated by a wind specialist.

1. Structural form: Suspension bridges, cable-stayed bridges, arch bridges, and truss bridges, because of the increase of rigidity in this order, have generally aerodynamic behaviors from worst to best. A truss-stiffened section, because it blocks less wind, is more favorable than a girder-stiffened one. But a truss-stiffened bridge is generally less stiff in torsion.
2. Stiffness: For long-span bridges, it is not economical to add more material to increase the stiffness. However, changing the boundary conditions, such as deck and tower connections in cable-stayed bridges, may significantly improve the stiffness. Cable-stayed bridges with "A" or inverted "Y" shape towers have higher torsional frequency than the bridges of "H" shape towers.
3. Cross-section shape and its details: A streamlined section blocks less wind thus has better aerodynamic behavior than a bluff section. Small changes in section details may significantly affect the aerodynamic behavior.
4. Damping: Concrete bridges have higher damping ratios than steel bridges. Consequently, steel bridges have more wind-induced problems than concrete bridges. An increase of damping can reduce aerodynamic vibration significantly.

Major design parameters are usually determined in the preliminary design stage, and then the aerodynamic behavior is evaluated by a wind specialist. Even if the bridge responds poorly under aerodynamic excitation, it is undesirable to change the major design parameters for the reason of scheduling and funding. The common way to improve its behavior is to change the section details. For example, changing the solid parapet to a half-opened parapet, or make some venting slots (Ehsan et al., 1993) on the bridge deck may significantly improve the aerodynamic behavior. To have more choices on how to improve the aerodynamic behavior of long-span bridges, to avoid making delays in the schedule, and to achieve an economical design, aerodynamics should be considered from the beginning.

Although a streamlined section is always favorable for aerodynamic behavior, there have recently been many composite designs, because of their construction advantages, for long-span bridges. The composite section shapes, with the concrete deck on steel girders, are bluff and thus not good for aerodynamics, but can be improved by changing section details as shown in Figure 22.7 (Irwin and Stone, 1989).

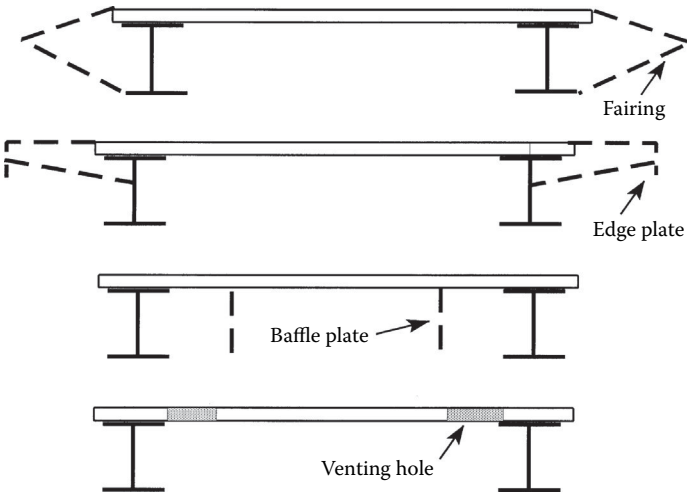

FIGURE 22.7 Typical aerodynamic modifications.

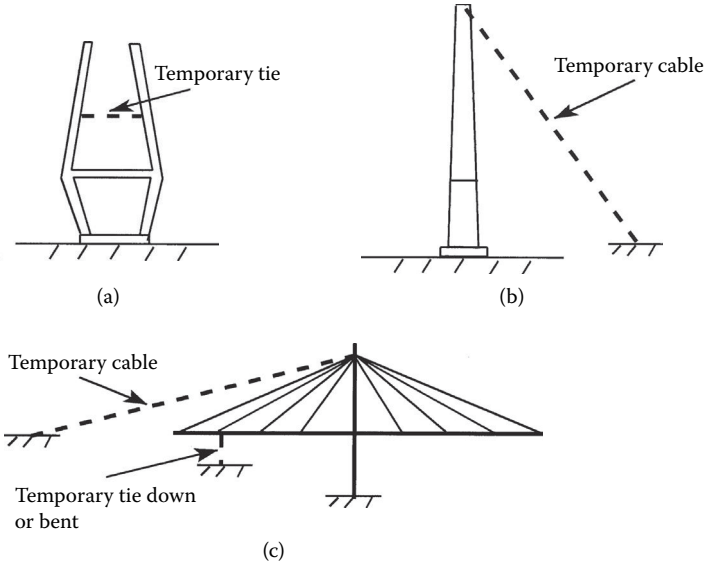

FIGURE 22.8 Typical construction stages. (a) Tower before completion; (b) completed tower; (c) stage with longest cantilever.

22.5.3 Construction Safety

The most common construction method for long-span bridges is segmental (staged) construction, such as balanced cantilever construction of cable stayed bridges, tie-back construction of arch bridges, and float-ins construction of suspended spans. These staged constructions result in different structural configurations during the construction time. Since some construction stages have lower stiffness and natural frequency than the completed bridges, construction stages are often more critical in terms of either strength of structural members or aerodynamic instability.

In the balanced cantilever construction of cable stayed bridges, three stages are usually identified as critical as shown in Figure 22.8. They are tower before completion, completed tower, and the stage with a longest cantilever arm. Reliable analytical solutions are not available yet, and wind tunnel testing is usually conducted to ensure safety. Temporary cables, tie-downs, and bents are common countermeasures during the construction stages.

22.5.4 Rehabilitation

Aerodynamic design is a relatively new consideration in structural design. Some existing bridges have experienced wind problems because aerodynamic design was not considered in the original design. There are many measures to improve their aerodynamic behavior, such as structural stiffening, section streamlining, and installation of damper or guide vanes. In the early days, structural stiffening was the major way for this purpose. For example, the girders of Golden Gate bridge were stiffened in 1950s, Deer Isle Bridge in Maine was stiffened since 1940s by adding stays, cross-bracings, and strengthening the girders, and guide vanes were installed on the Great Belt Bridge in 1998 to mitigate the vortex-induced oscillations. (Bosch, 1987; Kumarasena et al., 1991; Larsen et al., 2000).

Although the structural stiffening may have helped existing bridges survive many years' services, section streamlining is now commonly used. Streamlining the section is more efficient and less expensive than the structural stiffening. Figure 22.9 shows the streamlined section of Deer-Isle Bridge that has been proven to be very efficient (Cai, 1993; Bosch, 1987).

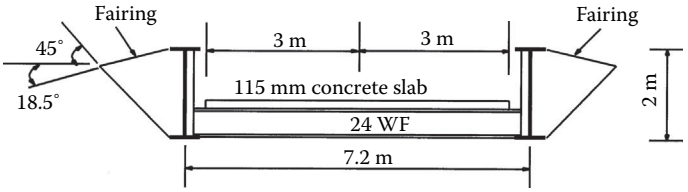

FIGURE 22.9 Deck section and fairings of Deer Isle Bridge.

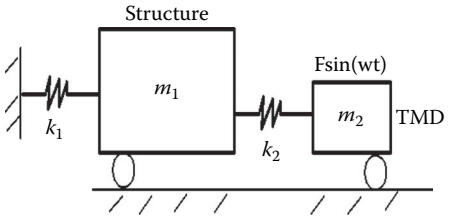

FIGURE 22.10 Explanation of tuned mass damper.

22.5.5 Structural Control

Another way to improve the aerodynamic behavior is to install either a passive or active control system on the bridges. A common practice in long-span bridges is the tuned mass damper (TMD). An example is the Normandy cable stayed bridge in France. This bridge has a main span of 856 m. To reduce the horizontal vibration during construction because of buffeting, a TMD was installed. Wind tunnel testing showed that the TMD reduced the vibration by 30% (Montens, 1997; Sorensen, 1995).

The basic principle of a passive TMD is explained with an example shown in Figure 22.10. A TMD with spring stiffness k_2 and mass m_2 is attached to a structural mass m_1, which is excited by an external sinusoidal force $F\sin(\omega t)$. The vibration amplitude of this two-mass system is

$$X_1 = \frac{F\omega_m^2(\omega_d^2 - \omega^2)}{(\omega_d^2 - \omega^2)[(k_1 + k_2)\omega_m^2 - k_1\omega^2] - k_2\omega_d^2\omega_m^2},$$
$$X_2 = \frac{F\omega_m^2\omega_d^2}{(\omega_d^2 - \omega^2)[(k_1 + k_2)\omega_m^2 - k_1\omega^2] - k_2\omega_d^2\omega_m^2} \tag{22.34}$$

where $\omega_m^2 = k_1/m_1$ and $\omega_d^2 = k_2/m_2$. It can be seen from Equation 22.34 that by selection of the stiffness k_2 and mass m_2 such that ω_d equals ω, then the structure vibration X_1 is reduced to zero. Since the wind is not a single-frequency excitation, the TMD can typically reduce the vibration of bridges, but not to zero.

The performance of the passive TMD system can be enhanced by the addition of an active TMD, which can be done by replacing the passive damper device with a servo actuator system. The basic principle of active TMD is the feedback concept as used in the modern control theory.

22.5.6 Structural Health Monitoring

Structural health monitoring (SHM) is used to produce a detailed assessment of the evolution of the structure's health condition and progressive damage during all its life. Using the periodically sampled dynamic response measurements from sensors, loads were estimated and damage features were extracted. Status of structural health can be monitored and an optimization of the maintenance intervention can be used to extend the life of the structures. To ensure the normal operation and safety of

long-span bridges, wind and SHM system has been installed at several long-span bridges, for example, the long-term measurement program for the Fred Hartman Bridge in Texas (Jones and Ozkan, 2002), the health monitoring system of Rion-Antirion Bridge in Greece (Diouron and Hovhanessian, 2005), and the Wind and Structural Health Monitoring System (WASHMS) installed for Stonecutters Bridge and Tsing Ma Bridge to monitor their performance and health status under various conditions (Chan et al., 2001, 2004, 2006).

22.5.7 Computational Fluid Dynamics

Computational Fluid Dynamics (CFD) uses numerical methods to solve the equations of the fluids including the Navior-Stokes equations. First of all, discretization methods, for instance, finite-difference method (FDM), finite volume method (FVM), finite element method (FEM), discrete vortex method (DVM), and so on, are used to divide the fluid into discrete meshes (Frandsen, 2001). The nonlinear governing equations of fluid dynamics can be solved numerically with appropriate boundary and initial conditions after using turbulence models to model the wide range of length and time scales. Typically used turbulence models include direct numerical simulation (DNS), Reynolds averaged Navier-Stokes (RANS), large eddy simulation (LES) and detached eddy simulation (DES). The basic measures for the selection and evaluation of turbulence models are based on the prediction accuracy and the computation time required (Murakami, 1997). With the aid of CFD, the analysis of wind problems for long-span bridges can be carried out earlier in the design cycle, and the risks can be lowered in the design process.

References

Adrian, R. J. 2005. Twenty years of particle image velocimetry. *Experiments in Fluids V39, No.2,* 159–69.

Berreby, D. 1992. The great bridge controversy. *Discover*,Vol 26, no. 1, 26–33.

Bosch, H. R. 1987. A wind tunnel investigation of the Deer Isle-Sedgwick bridge, *Report No. FHWA-RD-87-027*, Federal Highway Administration, McLean, Virginia.

Cai, C. S. 1993. *Prediction of long-span bridge response to turbulent wind*, PhD Dissertation, University of Maryland, College Park, USA.

Caracoglia, L. 2008. Recent investigations on long-span bridges aeroelasticity in the presence of turbulence fields with uncertain span-wise correlation. In: *BBAA VI International Colloquium on: Bluff Bodies Aerodynamic & Applications*. Milano, Italy.

Chan, T. H. T., Li, Z. X., and Ko, J. M. 2001. Fatigue analysis and life prediction of bridges with structural health monitoring data: Part II: Application. *International Journal of Fatigue*, 23, 55–64.

Chan, T. H. T., Li, Z. X., and Ko, J. M. 2004. Evaluation of typhoon induced fatigue damage using health monitoring data for the tsing ma bridge. *Structural Engineering and Mechanics*, 17, 655–670.

Chan, T. H. T., Yu, L., Tam, H. Y., Ni, Y. Q., Liu, S. Y., Chung, W. H., and Cheng, L. K. 2006. Fiber bragg grating sensors for structural health monitoring of tsing ma bridge: Background and experimental observation. *Engineering Structures*, 28, 648.

Chen, X., and Kareem, A. 2003. New frontiers in aerodynamic tailoring of long span bridges: An advanced analysis framework. *Journal of Wind Engineering and Industrial Aerodynamics*, 91, 1511–1528.

Chen, X., Matsumoto, M., and Kareem, A. 2000. Time domain flutter and buffeting response analysis of bridges. *Journal of Engineering Mechanics*, Vol 126, No. 1, pp. 7–16.

Chen, Z. Q., Wang, X. Y., Ko, J. M., and Ni, Y. Q. 2004. Mr damping system for mitigating wind-rain induced vibration on dongting lake cable-stayed bridge. *Wind & Structures*, 7, 293–304.

Diana, G., Bruni, S., Collina, A., and Zasso, A. 1998. Aerodynamic challenges in super long span bridges design. In: *Proceedings of International Sysmposium on Advances in Bridge Aerodynamics*. Copenhagen.

Diana, G., Cheli, F., Zasso, A., and Bocciolone, M. 1999. Suspension bridge response to turbulent wind: Comparison of new numerical simulation method results with full scale data. In: *Wind Engineering into the 21 Century*, Larsen et al. (eds.) Balkema, Rotterdam, The Netherlands, pp. 871–878.

Diouron, T. L., and Hovhanessian, G. 2005. The health monitoring system of rion-antirion bridge. In: *23rd Conference and Exposition on Structural Dynamics*. Curran Associates, Inc., Orlando, Florida, USA.

Ehsan, F., Jones, N. J., and Scanlan, R. H. 1993. Effect of sidewalk vents on bridge response to wind, *Journal of Structural Engineering*, ASCE, 119(2), 484–504.

Frandsen, J. B. 2001. Simultaneous pressures and accelerations measured full-scale on the great belt east suspension bridge. *Journal of Wind Engineering and Industrial Aerodynamics*, 89, 95–129.

Gu, M., and Du, X. 2005. Experimental investigation of rain-wind-induced vibration of cables in cable-stayed bridges and its mitigation. *Journal of Wind Engineering and Industrial Aerodynamics*, 93, 79–95.

Hikami, Y., and Shiraishi, N. 1988. Rain-wind induced vibrations of cables stayed bridges. *Journal of Wind Engineering and Industrial Aerodynamics*, 29, 409–418.

Holmes, J. D. 2007. *Wind Loading of Structures* (2nd Edition), Taylor & Francis, New York, NY.

Hui, M., and Yau, D. 2011. Major bridge development in Hong Kong—past, present and future. *Frontiers of Architecture and Civil Engineering in China,* Vol. 5, No. 4, pp 405–414.

Irwin, P. A., and Stone, G. K. 1989. Aerodynamic improvements for plate-girder bridges, *Proceedings, Structures Congress*, ASCE, San Francisco, CA, USA.

Jones, N. P., and Ozkan, E. 2002. Wind effects on long-span cable-stayed bridges—assessment and validation. In: *Proceedings of UNJR Panel on Wind and Seismic Effects*. Gaithesburg, MD.

Kareem, A. 2008. Numerical simulation of wind effects: A probabilistic perspective. *Journal of Wind Engineering and Industrial Aerodynamics,* 96, 1472–1497.

Kumarasena, T., Scanlan, R. H., and Ehsan, F. 1991. Wind-induced motions of Deer Isle bridge, *Journal of Structural Engineering*, ASCE, 117(11), 3356–3375.

Larsen, A., Esdahl, S., Andersen, J. E., and Vejrum, T. 2000. Storebaelt suspension bridge—vortex shedding excitation and mitigation by guide vanes. *Journal of Wind Engineering and Industrial Aerodynamics*, 88, 283.

Lin, Y. K., and Ariaratnam, S. T. 1980. Stability of bridge motion in turbulent winds. *Journal of Structural Mechanics*, 8(1), 1–15.

Lin, Y. K., and Li, Q.C. 1993. New stochastic theory for bridge stability in turbulent flow. *Journal of Engineering Mechanics*, 119, 113–127.

Main, J.A., and Jones, N.P. 1999. Full-scale measurements on a low-rise structure. 10th International Conference on Wind Engineering, Larsen (eds.) Copenhagen, Denmark, June 1999.

Matsuda, K., Cooper, K. R., Tanaka, H., Tokushige, M., and Iwasaki, T. 2001. An investigation of Reynolds number effects on the steady and unsteady aerodynamic forces on a 1:10 scale bridge deck section model. *Journal of Wind Engineering and Industrial Aerodynamics*, 89, 619–632.

Matsumoto, M., Saitoh, T., Kitazawa, M., Shirato, H., and Nishizaki, T. 1995. Response characteristics of rain-wind induced vibration of stay-cables of cable-stayed bridges. *Journal of Wind Engineering and Industrial Aerodynamics,* 57, 323–333.

Miyata, T. 2003. Historical view of long-span bridge aerodynamics. *Journal of Wind Engineering and Industrial Aerodynamics*, 91, 1393–1410.

Montens, S. 1997. Gusty wind action on balanced cantilever bridges. In: International Conference on *New Technologies in Structural Engineering*, Baptista, A.M. (ets.), Lisbon, Portugal.

Murakami, S. 1997. Current status and future trends in computational *wind engineering*, Journal of Wind Engineering and Industrial Aerodynamics, 67/68, 3–36

Namini, A., Albrecht, P., and Bosch, H. 1992. Finite element-based flutter analysis of cable-suspended bridges. *Journal of the Structural Division*, ASCE, 118(6), 1509–1526.

Raffel, M., Willert, C. E., and Kompenhans, J. 1998. *Particle image velocimetry, a practical guide*. Springer, Berlin.

Santos, J. C., Miyata, T., and Yamada, H. 1993. Gust response of a long span bridge by the time domain approach. In: *Proceedings of Third Asia Pacific Symposium on Wind Engineering*, Hong Kong, pp. 211–16.

Schewe, G., and Larsen, A. 1998. Reynolds number effects in the flow around a bluff bridge deck cross section. *Journal of Wind Engineering and Industrial Aerodynamics*, 74–76, 829–838.

Simiu, E., and Scanlan, R. H. 1996. *Wind Effects on Structures* (3rd Edition). John Wiley & Sons, New York, NY.

Scanlan, R. H. 1981. State-of-the-art methods for calculating flutter, vortex-induced, and buffeting response of bridge structures, *Report No. FHWA/RD-80/050*, Washington, DC.

Scanlan, R. H. 1988. On flutter and buffeting mechanisms in long-span bridges. *Probabilistic Engineering Mechanics*, 3, 22–27.

Scruton, C. 1981. *An Introduction to Wind Effects on Structures*. Oxford University Press. London, UK

Sorensen, L. 1995. The Normandy bridge, the steel main span. *Proceeding of the 12th Annual International Bridge Conference*, Pittsburgh, WV, USA.

Xiang, H., Liu, C. H., and Gu, M. 1995. Time domain analysis for coupled buffeting response of long span bridges. In: *The 9th International Conferences on Wind Engineering (ICWE)*. New Delhi, India.

Xiang, H., and Ge, Y. 2007. State-of-the-art of long-span bridge engineering in china. *Frontiers of Architecture and Civil Engineering in China*, 1, 379–388.

CIVIL ENGINEERING

Bridge Engineering Handbook

SECOND EDITION

FUNDAMENTALS

Over 140 experts, 14 countries, and 89 chapters are represented in the second edition of the **Bridge Engineering Handbook.** This extensive collection highlights bridge engineering specimens from around the world, contains detailed information on bridge engineering, and thoroughly explains the concepts and practical applications surrounding the subject.

Published in five books: **Fundamentals, Superstructure Design, Substructure Design, Seismic Design,** and **Construction and Maintenance,** this new edition provides numerous worked-out examples that give readers step-by-step design procedures, includes contributions by leading experts from around the world in their respective areas of bridge engineering, contains 26 completely new chapters, and updates most other chapters. It offers design concepts, specifications, and practice, as well as the various types of bridges. The text includes over 2,500 tables, charts, illustrations and photos. The book covers new, innovative, and traditional methods and practices, explores rehabilitation, retrofit, and maintenance, and examines seismic design, and building materials.

The first book, **Fundamentals** contains 22 chapters, and covers aesthetics, planning, design specifications, structural modeling, fatigue and fracture.

What's New in the Second Edition:

- Covers the basic concepts, theory and special topics of bridge engineering
- Includes seven new chapters: Finite Element Method, High Speed Railway Bridges, Concrete Design, Steel Design, Structural Performance Indicators for Bridges, High Performance Steel, and Design and Damage Evaluation Methods for Reinforced Concrete Beams under Impact Loading
- Provides substantial updates to existing chapters, including Conceptual Design, Bridge Aesthetics: Achieving Structural Art in Bridge Design, and Application of Fiber Reinforced Polymers in Bridges

This text is an ideal reference for practicing bridge engineers and consultants (design, construction, maintenance), and can also be used as a reference for students in bridge engineering courses.

K12391

ISBN: 978-1-4398-5207-1
90000
9 781439 852071

CRC Press
Taylor & Francis Group
an informa business
www.crcpress.com

6000 Broken Sound Parkway, NW
Suite 300, Boca Raton, FL 33487
711 Third Avenue
New York, NY 10017
2 Park Square, Milton Park
Abingdon, Oxon OX14 4RN, UK